frontiers | Research Topics

Organ cross talk and its impact on the clinical course in multiple trauma and critical illness

Edited by
Klemens Horst, Frank Hildebrand, Markus Huber-Lang and Tom E. Mollnes

Published in
Frontiers in Immunology

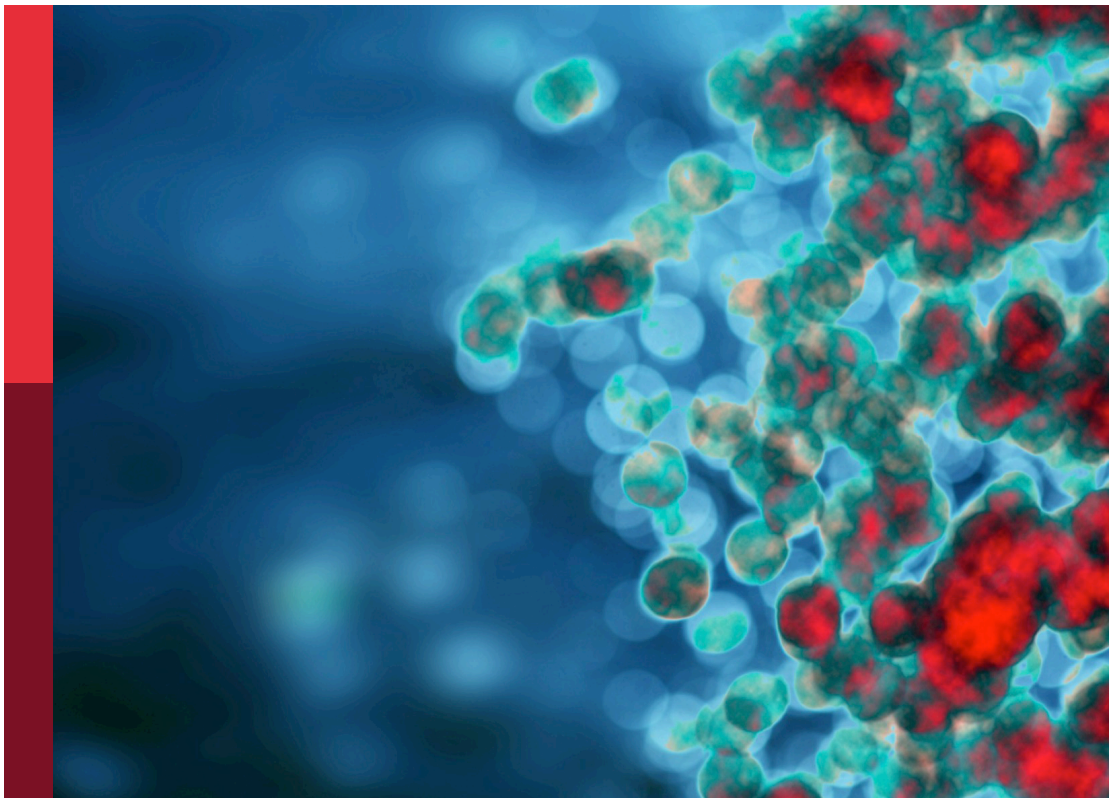

ISSN 1664-8714
ISBN 978-2-8325-2222-6
DOI 10.3389/978-2-8325-2222-6

About Frontiers

Frontiers is more than just an open access publisher of scholarly articles: it is a pioneering approach to the world of academia, radically improving the way scholarly research is managed. The grand vision of Frontiers is a world where all people have an equal opportunity to seek, share and generate knowledge. Frontiers provides immediate and permanent online open access to all its publications, but this alone is not enough to realize our grand goals.

Frontiers journal series

The Frontiers journal series is a multi-tier and interdisciplinary set of open-access, online journals, promising a paradigm shift from the current review, selection and dissemination processes in academic publishing. All Frontiers journals are driven by researchers for researchers; therefore, they constitute a service to the scholarly community. At the same time, the *Frontiers journal series* operates on a revolutionary invention, the tiered publishing system, initially addressing specific communities of scholars, and gradually climbing up to broader public understanding, thus serving the interests of the lay society, too.

Dedication to quality

Each Frontiers article is a landmark of the highest quality, thanks to genuinely collaborative interactions between authors and review editors, who include some of the world's best academicians. Research must be certified by peers before entering a stream of knowledge that may eventually reach the public - and shape society; therefore, Frontiers only applies the most rigorous and unbiased reviews. Frontiers revolutionizes research publishing by freely delivering the most outstanding research, evaluated with no bias from both the academic and social point of view. By applying the most advanced information technologies, Frontiers is catapulting scholarly publishing into a new generation.

What are Frontiers Research Topics?

Frontiers Research Topics are very popular trademarks of the *Frontiers journals series*: they are collections of at least ten articles, all centered on a particular subject. With their unique mix of varied contributions from Original Research to Review Articles, Frontiers Research Topics unify the most influential researchers, the latest key findings and historical advances in a hot research area.

Find out more on how to host your own Frontiers Research Topic or contribute to one as an author by contacting the Frontiers editorial office: frontiersin.org/about/contact

Organ cross talk and its impact on the clinical course in multiple trauma and critical illness

Topic editors

Klemens Horst — University Hospital RWTH Aachen, Germany
Frank Hildebrand — University Hospital RWTH Aachen, Germany
Markus Huber-Lang — Ulm University Medical Center, Germany
Tom E. Mollnes — University of Oslo, Norway

Citation

Horst, K., Hildebrand, F., Huber-Lang, M., Mollnes, T. E., eds. (2023). *Organ cross talk and its impact on the clinical course in multiple trauma and critical illness*. Lausanne: Frontiers Media SA. doi: 10.3389/978-2-8325-2222-6

Table of contents

frontiers | Frontiers in Immunology

TYPE Editorial
PUBLISHED 05 April 2023
DOI 10.3389/fimmu.2023.1195371

OPEN ACCESS

EDITED AND REVIEWED BY
Pietro Ghezzi,
University of Urbino Carlo Bo, Italy

*CORRESPONDENCE
Klemens Horst
khorst@ukaachen.de

SPECIALTY SECTION
This article was submitted to Inflammation, a section of the journal Frontiers in Immunology

RECEIVED 28 March 2023
ACCEPTED 30 March 2023
PUBLISHED 05 April 2023

CITATION
Horst K, Mollnes TE, Huber-Lang M and Hildebrand F (2023) Editorial: Organ cross talk and its impact on the clinical course in multiple trauma and critical illness.
Front. Immunol. 14:1195371.
doi: 10.3389/fimmu.2023.1195371

Editorial: Organ cross talk and its impact on the clinical course in multiple trauma and critical illness

Klemens Horst[1]*, Tom Eirik Mollnes[2,3], Markus Huber-Lang[4] and Frank Hildebrand[1]

[1]Department of Orthopaedics, Traumatology and Reconstructive Surgery, Rheinisch-Westfälische Technische Hochschule (RWTH) Aachen University, Aachen, Germany, [2]Department of Immunology, Oslo University Hospital and University of Oslo, Oslo, Norway, [3]Research Laboratory, Nordland Hospital Trust, Bodo, Norway, [4]Institute of Clinical and Experimental Trauma-Immunology, University Hospital of Ulm, Ulm, Germany

KEYWORDS

organ cross talk, multiple trauma, polytrauma, critical ill, clinical course

Editorial on the Research Topic
Organ cross talk and its impact on the clinical course in multiple trauma and critical illness

Communication between different body compartments that can also affect remote tissues has gained increasing interest. This so-called “organ-cross-talk” seems to be of major relevance after multiple trauma (MT) and critical illness (CI). In this context, systemic effects of injuries to different body compartments have been shown to be far greater than the sum of the isolated traumatic insults and posttraumatic dysfunction of primarily unaffected organs. This underscores the importance of a holistic research approach when studying the complex biology and pathophysiology in this field.

Posttraumatic and/or post-surgical inflammation have a substantial impact on patient outcome. Maleitzke et al. presented rare data on clinically relevant laboratory parameters in patients suffering from penetrating trauma. Aside from the injury severity score (ISS), the authors found that AST, CRP, erythrocyte count, pH, lactate, aPTT and K+ were useful for identifying patients at risk and adjusting surgical and ICU algorithms early on. Both detrimental and regenerative roles of inflammatory mediators have been described in numerous pre-clinical studies and experimental settings. For example, Ragipoglu et al. investigated the role of mast cells that have the potential to trigger local and systemic inflammation in bone repair in a murine model. The authors found that combined trauma resulted in compromised bone repair in mast-cell component mice. It was concluded that mast cells could represent a potential target for new treatment options to improve fracture healing in patients with multiple trauma. Another murine model, presented by Mkrtchian et al., investigated the role of extracellular vesicles (EVs) as potential mediators transferring information from the injured tissue to remote organs, including the brain. The authors concluded that surgical procedures alter the cargo of circulating EVs in the blood, thus regulating metabolic processes. Zhang et al. reported on systemic inflammatory consequences and focused on traumatic brain injury (TBI). As the brain and the spleen are connected *via* autonomic innervation and by soluble mediators, the authors hypothesized that

ethanol intoxication (EI), the most common comorbidity of TBI, influences the peripheral inflammatory response. They concluded that TBI induces rapid maturation of immunomodulatory functions of dendritic cells that is enhanced by EI prior to TBI.

Lackner et al. demonstrated cardiac alterations after hip fracture with enhanced myocardial expression of HMGB1, TLR2/4, TNF, IL1-β and NLRP3, as well as considerable alterations in the myocardial expression of glucose and fatty acid transporters (HFABP, GLUT4) in middle-aged (52-week-old) mice. Hemorrhagic shock (HS) and hypoperfusion influence the immunologic reaction in MT. As lung co-morbidities can aggravate tissue hypoxia *via* alveolar hypoxia, Wepler et al. hypothesized that glucocorticoid receptor (GR) function in mice and pre-traumatic cigarette smoke (CS) exposure would further impair hemodynamic stability and organ function after HS. As the authors were not able to explain whether the observed metabolic acidosis or increased lipolysis was responsible for the trend towards lower catecholamine requirements in CS-exposed mice, further studies are warranted. Halvachizadeh et al. studied the role of occult hypoperfusion (OH), defined by persistent lactic acidosis despite normalization of vital parameters. In a porcine model, the authors found that OH is associated with decreased local circulation and increased local inflammation in the injured soft tissue of the extremity in polytrauma, thus probably reflecting the severity of local soft tissue injuries and potentially guiding treatment strategies.

Following extensive trauma surgery, Teuben et al. recorded a shift in composition of the bone marrow (BM) neutrophil pool, which was associated with relative circulatory neutropenia in a porcine polytrauma model. Moreover, the authors reported that the $CXCR4^{high}$-neutrophil subset became overrepresented, possibly reflecting remigration of aged neutrophils into the BM. These findings may contribute to the development of novel interventions aimed at modifying the trauma-induced response in BM. Air embolism is a serious and underdiagnosed complication during invasive medical procedures. Storm et al. investigated the role of air embolism in a porcine model of thromboembolism. The authors described activation of complement mainly at the level of C3, with subsequent cytokine release, and concluded that C3-inhibition might represent a therapeutic approach to attenuate this response.

A feared complication in MT remains the development of sepsis and multi organ dysfunction syndrome (MODS). Nakanishi et al. focused on the prolonged physical dysfunction in MT patients and investigated the role of neutrophils in muscle atrophy in murine sepsis. They found that sepsis is causal for infiltration of neutrophils in muscles, leading to muscle atrophy and weakness. Of note, these findings were reversed by neutrophil depletion. Gray et al. also reported data from a murine sepsis model. The authors investigated the V-domain Immunoglobulin Suppressor of T cell Activation (VISTA) as it is a potential candidate for strategic targeting in sepsis. The group proposed a protective Treg-mediated role for VISTA by which inflammation-induced tissue injury is suppressed and improves survival in early-stage sepsis. The authors concluded that enhancing VISTA expression or adoptively transferring VISTA + Tregs in early-stage sepsis may represent a novel therapeutic approach to ameliorate inflammation-induced death. Patel et al. focused on macrophage migration inhibitory factor (MIF) in MT patients and a rat model of HS and the potential of MIF inhibitor ISO-1 to reduce MODS in this model. The authors described increased MIF levels in MT patients and HS rats. Whereas MIF caused organ injury and/or dysfunction and hypotension in rats, treatment with ISO-1 attenuated organ injury and dysfunction, and reduced the activation of NF-kB and NLRP3 pathways in the rat kidney and liver. Thus, the authors pointed out that MIF inhibitors may be used as a potential therapeutic approach for MODS after trauma and/or hemorrhage. Sulforaphane (SFN) was also reported to exert beneficial immunomodulatory effects in a murine model of HS and resuscitation as described by Liang et al. They proved that *in vivo* SFN treatment can decrease HS/resuscitation-induced hepatic ischemia-reperfusion injury and modulate the activity of Kupffer cells *via* an Nrf2-dependent pathway. To better understand the role of complement component 1 inhibitor (C1-INH), Nielsen et al. established a novel porcine model of ischemia-reperfusion injury (IRI) by cross-clamping the thoracic aorta. The authors evaluated the global changes occurring in organ function, systemic inflammatory response and organ damage with or without treatment with C1-INH-concentrate. Although C1-INH treatment did not have any significant effects, probably due to its low specificity and efficacy in inhibiting complement, the model itself was found to be valid for future testing of drugs to combat IRI.

Messerer et al. conducted a study to investigate possible drug effects in a porcine model of HS. The group investigated the role of the H2S donor sodium thiosulfate ($Na_2S_2O_3$, STS). As the authors had previously found beneficial effects in mice and pigs with co-morbidities such as coronary artery disease, they conducted a prospective, randomized, controlled, blinded experimental study to address the effects of STS in cardiovascular healthy pigs. However, $Na_2S_2O_3$ did not show any benefits in healthy organisms undergoing HS. Lupu et al. focused on complement activation and Toll-like-receptor signaling immediately after trauma. They assessed the efficacy of the combined inhibition therapy of complement factor C5 and TLR co-receptor CD14 on thrombo-inflammation and organ damage in a 72-h porcine model of MT and found that combined C5 and CD14 inhibition limited the catecholamine demand, the inflammatory response, and signs of organ damage after experimental polytrauma, which might indicate a promising therapeutic approach. Shah et al. focused on multi-system inflammation and organ dysfunction after trauma and HS in a murine model. By hypergraph analysis and principal component analysis of 20 proteins sampled from the heart, gut, lung, liver, spleen, kidney and systemic circulation, the authors found that IL-17A was present persistently in all tissues at all sampled time points (except for its absence in the plasma at 0.5 h) in the wild type strain compared to TLR4-null (TLR4 -/-) animals. The authors concluded that trauma and HS induced the efflux of Th17 cells from the circulation and into specific tissues, suggesting a complex, content-specific role for TLR4 and type 17 immunity following trauma and HS.

In conclusion, this Research Topic presents the latest scientific insights on immunological and cellular reactions among different organs after severe trauma or during the further clinical course of critically ill patients. The data presented will deepen our understanding of the underlying mechanisms in regard to organ-cross-talk as well as

potentially improving the treatment of patients post trauma or during intensive care. We thank all authors for their contribution.

Author contributions

KH, TM, MH-L, and FH defined the topic of this Research Topic. All authors contributed to the article and approved the submitted version.

Acknowledgments

The article was proofread by Proof-Reading-Service.com, Devonshire Business Centre, Works Road, Letchworth Garden City, SG6 1GJ, United Kingdom.

Conflict of interest

The authors declare that the research was conducted in the absence of any commercial or financial relationships that could be construed as a potential conflict of interest.

Publisher's note

frontiers in Immunology

ORIGINAL RESEARCH
published: 18 January 2022
doi: 10.3389/fimmu.2021.824696

Surgical Trauma in Mice Modifies the Content of Circulating Extracellular Vesicles

*Souren Mkrtchian[1], Anette Ebberyd[1], Rosanne E. Veerman[2], María Méndez-Lago[3], Susanne Gabrielsson[2], Lars I. Eriksson[1,4] and Marta Gómez-Galán[1]**

[1] Department of Physiology and Pharmacology, Section for Anesthesiology and Intensive Care Medicine, Karolinska Institutet, Stockholm, Sweden, [2] Department of Clinical Immunology and Transfusion Medicine and Division of Immunology and Allergy, Department of Medicine, Solna, Karolinska University Hospital and Karolinska Institutet, Stockholm, Sweden, [3] Genomics Core Facility, Institute of Molecular Biology gGmbH (IMB), Mainz, Germany, [4] Function Perioperative Medicine and Intensive Care, Karolinska University Hospital, Stockholm, Sweden

OPEN ACCESS

Edited by:
Klemens Horst, University Hospital RWTH Aachen, Germany

Reviewed by:
Sandra Kraemer, University Hospital RWTH Aachen, Germany
Johannes Greven, University Hospital RWTH Aachen, Germany

***Correspondence:**
Marta Gómez-Galán
marta.gomez@ki.se

Specialty section:
This article was submitted to Inflammation, a section of the journal Frontiers in Immunology

Received: *29 November 2021*
Accepted: *20 December 2021*
Published: *18 January 2022*

Citation:
Mkrtchian S, Ebberyd A, Veerman RE, Méndez-Lago M, Gabrielsson S, Eriksson LI and Gómez-Galán M (2022) Surgical Trauma in Mice Modifies the Content of Circulating Extracellular Vesicles. Front. Immunol. 12:824696. doi: 10.3389/fimmu.2021.824696

Surgical interventions rapidly trigger a cascade of molecular, cellular, and neural signaling responses that ultimately reach remote organs, including the brain. Using a mouse model of orthopedic surgery, we have previously demonstrated hippocampal metabolic, structural, and functional changes associated with cognitive impairment. However, the nature of the underlying signals responsible for such periphery-to-brain communication remains hitherto elusive. Here we present the first exploratory study that tests the hypothesis of extracellular vesicles (EVs) as potential mediators carrying information from the injured tissue to the distal organs including the brain. The primary goal was to investigate whether the cargo of circulating EVs after surgery can undergo quantitative changes that could potentially trigger phenotypic modifications in the target tissues. EVs were isolated from the serum of the mice subjected to a tibia surgery after 6, 24, and 72 h, and the proteome and miRNAome were investigated using mass spectrometry and RNA-seq approaches. We found substantial differential expression of proteins and miRNAs starting at 6 h post-surgery and peaking at 24 h. Interestingly, one of the up-regulated proteins at 24 h was α-synuclein, a pathogenic hallmark of certain neurodegenerative syndromes. Analysis of miRNA target mRNA and corresponding biological pathways indicate the potential of post-surgery EVs to modify the extracellular matrix of the recipient cells and regulate metabolic processes including fatty acid metabolism. We conclude that surgery alters the cargo of circulating EVs in the blood, and our results suggest EVs as potential systemic signal carriers mediating remote effects of surgery on the brain.

Keywords: circulating extracellular vesicles, surgery, proteomics, miRNA, alpha-synuclein

INTRODUCTION

There is a growing body of evidence that aseptic tissue injuries including surgery are closely associated with rapid onset of structural and functional changes within the brain, predominately in regions involved in cognitive processes, that are dependent on periphery-to-brain signaling pathways (1–4). Using an animal model of orthopedic surgery, we have previously shown a profound astrocytic response in the hippocampal area entailing morphological, metabolic, and functional alterations in neuronal circuits involved in cognitive processing, including synaptic transmission and plasticity (5, 6). However, the nature of the systemic signals traveling to the brain and triggering the aforementioned functional alterations remains largely unknown. We have suggested that the surgery-mediated activation of the innate immune system, which, within hours, orchestrates an adaptive systemic inflammatory response (7) might be responsible for such periphery-to-brain signaling. While such instantaneous activation of the immune system is suggested to produce rapid changes on the molecular and cellular levels in the brain, the periphery-to-brain communication pathways associated with more long-lasting cognitive and behavioral effects remain unknown.

Emerging evidence suggests an important role of extracellular vesicles (EVs) in inter-cellular-tissue communications including periphery-to-brain signaling (8–10). It may therefore be hypothesized that EV-dependent signaling provides an alternative pathway that is responsible for long-term changes in higher brain functions after surgery (5, 6).

Circulating EVs can be produced by a variety of tissues, however, one of the main sources is the blood immune cells. These EVs are suggested to serve as important modulators of innate and adaptive immune responses (11). In addition, several studies indicate that peripheral inflammation can modify the cargo of the immune cell-produced EVs that can in an endocrine-like manner regulate intracellular processes in the distant tissues, including the brain (12).

Here, in this first exploratory study, we have mapped the proteome and miRNAome of circulating EVs at different time points after mouse orthopedic surgery to establish a potential correlation/association with the temporal kinetics of the surgery-triggered systemic inflammatory response, brain dysfunction as previously described in a surgical animal model.

MATERIALS AND METHODS

Animals

14–16 weeks old male C57BL6 (Janvier, Germany) mice were housed five per cage under temperature- and humidity-controlled conditions in a 12 h light/dark cycle and fed standard rodent chow and water *ad libitum*.

All experiments were approved by the Local ethics Committee for Animal Research of Stockholm North and Karolinska Institutet in Sweden.

Surgery

The open stabilized tibia fracture was performed as previously described (5). Briefly, under the isoflurane anesthesia (2.1% inspired concentration in 0.30 FiO2) and analgesia (buprenorphine, 0.1 mg/kg, s.c.) a longitudinal incision was made on the left hind paw and the muscles were disassociated. A 0.38 mm stainless steel pin was then inserted in the intramedullary canal with the subsequent osteotomy. The wound was irrigated, sutured with 6-0 Prolene, and mice were allowed to recover in a warm box before returning to the home cage. The temperature was monitored and maintained at 37°C with the aid of a warming pad and temperature-controlled lights (Harvard Apparatus).

Animals from the surgery pool were randomly divided into three groups depending on the time point at which the blood sampling was performed: 6- (S6h), 24- (S24h), and 72 h (S72h) post-surgery. Each experimental group included 6 animals (in the mass spectrometry and NTA analysis the C6h group consisted of 7 animals). The S24h and S72h groups received a daily dose of analgesia to avoid possible effects of pain on the brain. Control mice received an equal volume of saline (s.c.). To avoid experimental variation over time, control animals from the same batch of animals were assigned to each of the groups (C6h and C24-72h) and received a daily injection of saline (s.c).

Serum Sampling

Animals were deeply anesthetized with pentobarbital (0.1 ml, ip) and blood was collected from the left ventricle of the heart with a 23-G needle attached to a 1 ml syringe and immediately transferred to a 1.5-ml Eppendorf tube. Blood was allowed to coagulate at room temperature for 45 min and posteriorly centrifuged at 3000 g for 10 minutes at 4°C. Supernatants (sera) were stored at -80°C until further use.

Isolation of Extracellular Vesicles

EVs were isolated using the commercial kit ExoQuick ULTRA (System Biosciences Inc., Mountain View, CA).

Following the manufacturer's protocol serum samples were cleared by centrifugation for 10 min at 12 000 g and transferred to a new tube. Immediately after that 67 µl of the ExoQuick buffer A was added to the 250 µl of the cleared serum, the mix was incubated for 30 min at 4°C and centrifuged at 3000 g for 10 min at 4°C. The supernatant was saved for further analyses as the EV-depleted serum (dEVs). EV-containing pellet was resuspended in the 200 µl of Buffer B and EVs were isolated using the purification columns from the kit in 500 µl of elution buffer. Both the EV isolated fraction and the dEV serum were stored at -80°C until further use.

We have submitted all relevant data of our experiments to the EV-TRACK knowledgebase (EV-TRACK ID: EV210383) (13).

Nanoparticle Tracking Analysis

The size and particle concentration of the serum EVs were determined by nanoparticle tracking analysis(NTA) using an LM10 platform with an sCMOS camera from NanoSight Ltd. The samples were diluted in sterile-filtered PBS to a particle

concentration of $5x10^8$ – $5x10^9$ particles/ml and analyzed with camera level 14 and detection threshold 3. For each sample, four consecutive videos were recorded in RT while injecting the sample with a syringe pump (speed 50).

The average from the four consecutive videos for each sample was calculated and posteriorly used for the visualization of the results as Concentration (particles/ml) vs. Particle Size (nm).

Due to a large number of samples (N=31), the NTA analysis was performed in two different sessions (run 1 and run 2). In run 1 we included the S6h (N=6) group together with its corresponding control group (C6h, N=7). In run 2 we included C24-72h (N=6), S24h (N=6), and S72h (N=6).

Negative Stain Transmission Electron Microscopy

Three microliters of the EV sample were applied on glow discharged carbon-coated and formvar stabilized 400 mesh copper grids (Ted Pella) and incubated for approximately 30s. Excess of the sample was blotted off and the grid was washed with MilliQ water prior to the negative staining using 2% uranyl acetate. Transmission electron microscopy (TEM) imaging was done using Hitachi HT7700 (Hitachi High-technologies) transmission electron microscope operated at 100 kV equipped with a 2kx2k Veleta CCD camera (Olympus Soft Imaging System).

Small RNA Sequencing

RNA isolation. RNA was isolated from all groups (N=6 in each group). Total RNA was extracted from the 200 µl of EVs fractions using the Exosomal RNA isolation kit from Norgen Biotek Corp. (Nordic BioSite AB, Täby, Sweden). RNA was eluted in a 25 µl of elution buffer and RNA concentrations were determined by Qubit 4 fluorometer (Invitrogen).

Library preparation. RNA quality was controlled with Agilent Bioanalyzer 2100 (Agilent, Palo Alto, CA) equipped with the small RNA chip. Small RNA libraries were constructed using the NEXTFLEX® Small RNA-Seq Kit v3 (Bioo Scientic Corp., Austin, Texas, USA) according to the manufacturer's protocol. Libraries were prepared with a starting amount of 2.3 ng of RNA and amplified in 22 PCR cycles. Amplified libraries were purified by running an 8% TBE gel and size-selected for insert sizes of 15-40 nt (library sizes of 143-168 bp).

Sequencing. All samples were pooled in equimolar ratio and sequenced on the Illumina NextSeq 500/550 high output flowcell, with a 75- cycle kit, single read for 84 cycles plus 7 cycles for the index read. Library construction, quality control, and sequencing were completed at the Genomics Core Facility, Institute of Molecular Biology GmbH (IMB), Mainz, Germany.

Bioinformatic analysis. The raw sequence reads in FastQ format were cleaned from adapter sequences and size-selected for 14-34 base-long inserts (plus 8 random adapter bases) using cutadaptv.2.4 (http://cutadapt.readthedocs.org) with parameters '-j 8 -a TGGAATTCTCGGGTGCCAAGG -m 22 -M 42' followed by quality checks with FastQC (https://www.bioinformatics.babraham.ac.uk/projects/fastqc). Read alignment to the mouse GRCm38/mm10 genome from Gencode release M25 (ftp://ftp.ebi.ac.uk/pub/databases/gencode/Gencode_mouse/release_M25) with concomitant trimming of the 8 random bases was performed using Bowtiev.1.2.2 (https://bowtie-bio.sourceforge.net).

For miRNA-focused analysis, the genome-aligned reads in SAM format were selected in the size range 20-24 bases using GNUAwkand Samtoolsv.1.10 (https://www.htslib.org), converted into sorted BAM files with Samtools, and read counts were summarized either per miRNA locus or per mature miRNA using featureCountsusing miRNA annotation either from Gencode M25 or from miRbase v.22 (ftp://mirbase.org/pub/mirbase/22/genomes/mmu.gff3). The miRbase annotation was converted from GFF3 into GTF format for use with featureCountsusing, the Bioconductor package rtracklayerin R v.3.6.0.

The expression of miRNAs was normalized as counts per million reads (CPM). The value of 10 CPM was chosen as a cut-off margin for filtering out the low-expression genes. Differential expression analysis was carried out with DESeq2 v.1.26.0 (https://bioconductor.org/packages/release/bioc/html/DESeq2.html) as implemented in the online tool iDEP (http://bioinformatics.sdstate.edu/idep) using a significance cut-off of 5% false discovery rate (FDR). Since no statistical difference was found between the two control groups (C6h and C24-72h), in order to simplify the miRNA differential expression analysis, only one set of controls (C6h, N=6) was selected and hereafter referred to as Control.

The fold change (FC) threshold for selecting differentially expressed genes was ≥1.5. Heat maps of differentially expressed genes and principal component analysis (PCA) using log2 normalized CPM expression values were generated using Qlucore Omics Explorer 3.2 (Qlucore, Lund, Sweden). Log2-transformed CPM values were used to generate Volcano plots (RStudio v 1.4.1717, PBC).

The miRNA sequencing data have been deposited in NCBI's Gene Expression Omnibus (14) and are accessible through GEO Series accession number GSE115440).

Liquid Chromatography-Tandem Mass Spectrometry–Based Proteome Analysis

Protein identification and quantification were carried out at the Proteomics Biomedicum core facility, Karolinska Institutet (https://ki.se/en/mbb/proteomics-biomedicum). Details of the sample preparation, peptide labeling with TMTpro mass tag reagent and subsequent separation of labeled peptides on EASY-Spray C18 column and mass spectra acquisition on Orbitrap Q Exactive HF mass spectrometer (ThermoFisher Scientific) are described in the **Supplementary File S1**. As the TMT-labeled experiments allow a maximum of 16 samples that could be analyzed simultaneously, the data were acquired from two independent runs, with C6h and S6h samples assigned for the first run, and the C24-72h, S24h and S72h samples assigned for the second run. Acquired raw data files were analyzed using Proteome Discoverer v2.4 (ThermoFisher Scientific) with Mascot Server v2.5.1 (Matrix Science Ltd., UK) search engine against mouse protein database (SwissProt). Initial search results

were filtered with 5% FDR using the Percolator node in Proteome Discoverer. Quantification was based on the reporter ion intensities, which were log2 and quantile normalized and analyzed for the differential expression of proteins with GraphPad Prism (v. 9.1.1) using multiple unpaired t-tests analysis with FDR set to 5%. Quantile normalized and log2-transformed protein abundances were used to generate Volcano plots (RStudio v 1.4.1717, PBC).

The mass spectrometry proteomics data have been deposited to the ProteomeXchange Consortium *via* the PRIDE (15) partner repository with the dataset identifier PXD030167

miRNA qPCR

TaqMan® Advanced miRNA Assays (Applied Biosystems, ThermoFisher Scientific) were used for validation of miRNA-seq results. cDNA templates from the selected EV total RNA samples were prepared using the TaqMan® Advanced miRNA cDNA Synthesis kit. The resulting cDNAs were amplified using 7500 Real-Time PCR System (Applied Biosystems, ThermoFisher Scientific) and the following TaqMan® Advanced miRNA Assays: mmu-miR-143-3p (assay ID, mmu480935_mir), mmu-miR-499-5p (mmu482780_mir), mmu-miR-375-3p (mmu48114_mir), mmu-miR-1a-3p (mmu482914_mir), mmu-miR-541-5p (mmu481211_mir).

All samples were amplified in triplicate. Mmu-miR-103-3p was chosen as the housekeeping miRNA based on the analysis of expression stability of several miRNAs using the RefFinder tool (https://www.heartcure.com.au/reffinder/). The relative abundance of each miRNA was estimated according to the $2^{-\Delta\Delta Ct}$ method.

Bead-Based Purification of EVs

Streptavidin-coated magnetic beads (SVMS-40-10, Spherotech) were coated with the biotinylated CD63 (clone MEM-259, BioSite Flow), CD9 (clone HI9a, Biolegend), and CD81 (clone M38, BioSite Flow) antibodies as it is described elsewhere (16). EVs (15 µg of total protein) from C24-72h and S24h groups were incubated overnight with antibody-coated beads. A sample with no EVs was included as a negative control. Beads were recovered on a magnetic stand, resuspended in RIPA buffer (Abcam) including protease and phosphatase inhibitors (Roche), sonicated, vortexed, and centrifugated at 10000 g. The supernatant containing EVs' proteins was collected for the α-synuclein immunodetection.

Western Blot

EVs, dEVs, and serum samples were solubilized with 2% SDS or RIPA buffer and thoroughly vortexed. Protein concentration was determined using the micro BCA Protein Assay Kit (Thermo Scientific) and samples containing equal amounts of protein (5 µg) were resolved by SDS-PAGE and transferred to a PVDF membrane (Invitrogen). Depending on the secondary antibodies (HRP- or IRDye-conjugated) protein bands were detected using either enhanced chemiluminescence reagents (GE Healthcare) and ChemiDoc MO analyzer (Bio-Rad) or Odyssey infrared fluorescence detection system (LI-COR, Lincoln, NE, USA).

The following primary antibodies were used at a 1:500 dilution: CD81 (sc-166029, Santa Cruz Biotechnology), HSP70 (ab181606, Abcam), CD63 (ab59479, Abcam), α-syn (610786, BD Bioscience).

Statistics

For the statistical analyses of miRNA qPCR experiments we have used ANOVA one-way test followed by Dunnett's multiple comparisons test (Graph Pad Prism v. v. 9.1.1). Data are presented as means ± SEM. $P<0.05$ was considered significant.

RESULTS

Characterization of EVs

EVs were isolated from the blood serum with further characterization of EVs and analyses of the EV cargo as schematically presented in **Figure 1**.

Isolated EVs were characterized using different approaches: transmission electron microscopy (TEM), Nanoparticle Tracking Analysis (NTA), and immunochemical detection of EV enriched proteins (western blot).

TEM was performed in C24-72h (N=4) and S24h (N=4) groups and no differences were observed regarding the number, morphology, and size of the detected particles (data not shown). **Figure 2A** shows a representative TEM image from a control mouse demonstrating the presence of particles ranging from 30 to 150 nm, which is a common pattern for the EVs isolated using the ExoQuick kit (17). In addition, these particles appear to be encircled by the membranous structures, identifying them as typical extracellular vesicles (**Figure 2A**, right panel).

NTA analysis, which determines the size distribution and the number of isolated particles (particles/ml), was performed on all samples but in two different sessions (run 1 or run 2; see Methods). The size distribution of the isolated EVs' particles was similar for all the experimental groups, independently of the assigned session. In all cases, the averaged particle size distribution ranged between 50-200 nm with the size of the most frequently detected particle (mode) close to 100 nm (**Figure 2B**). The average concentration of the particles was also similar between the control and surgical groups within the same session (run1: C6h vs S6h and run 2: C24-72h vs S24h and S72h). However, we found considerable differences in the number of particles detected during the different sessions (**Figure 2B**). This difference is probably due to the intrinsic high variability associated with the NTA method itself, which makes this method not suitable for the comparison of particle concentrations between the groups.

Finally, two EV enriched proteins, CD63 and CD81, known to be located on the surface of EVs, and an intra-vesicular protein, HSP70 were identified in the lysed EVs by western blot (**Figure 2C**). At the same time, the abundant serum protein, albumin was substantially depleted from the EV fraction (**Figure 2C**). It can be concluded that all the above-mentioned EV characteristics including the size and morphology of isolated particles, and the presence of EV enriched proteins are identical

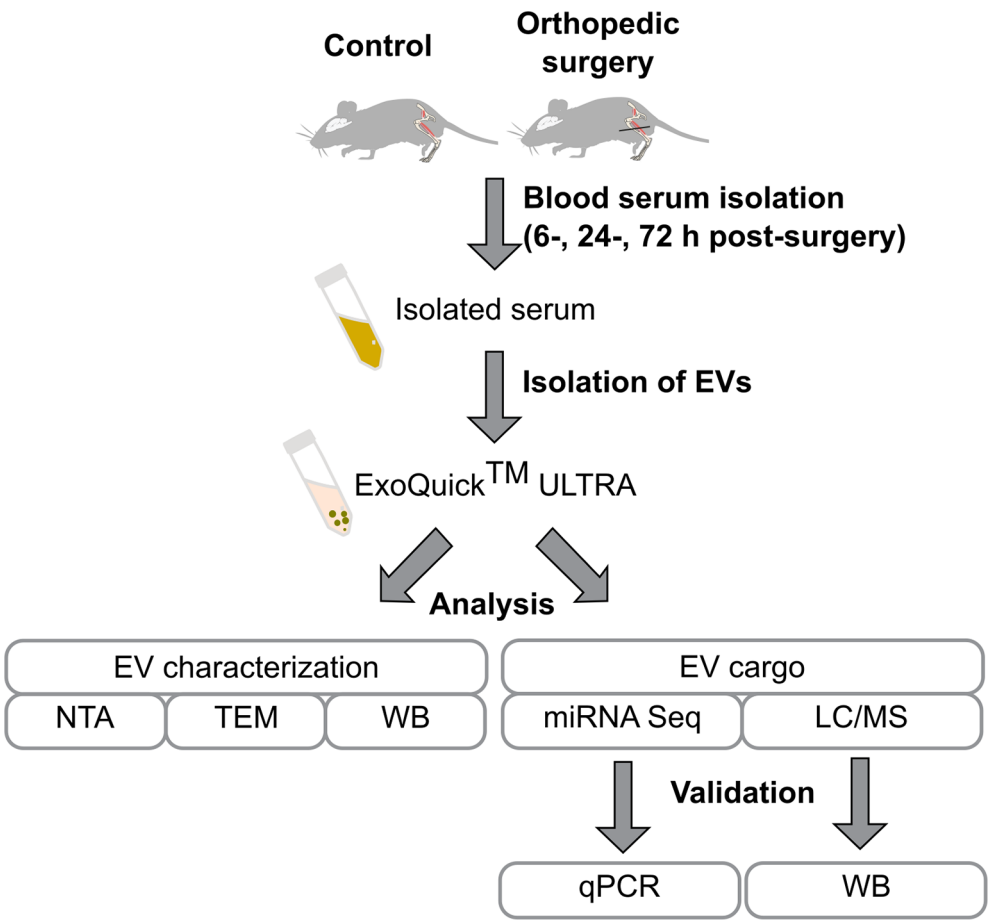

FIGURE 1 | Flowchart of the study design. Mice were subjected to tibia surgery, blood was collected from the control and surgery animals after 6, 24, and 72 h post-surgery. Isolated blood serum was used for the purification of EVs using the ExoQuick ULTRA kit. EVs were characterized by Nanoparticle Tracking Analysis (NTA), transmission electron microscopy (TEM), and identification of EV enriched proteins by western blot. EVs' proteome and miRNAome were investigated by LC/MS and RNA-seq and findings were validated by qPCR and western blot.

to the ones described by other groups using similar isolation methods (17).

Surgery Effects on the Proteome of Serum EVs

The EV proteome was investigated using the LC-Tandem Mass Spectrometry approach (for details see *Materials and Methods* and **Supplementary File S1**). Analysis of the acquired data identified 343 proteins in the samples from the first run (C6h and S6h) and 417 proteins in the samples from the second run (C24-72h, S24h and S72h) (see *Materials and Methods*) (**Supplementary Tables S1, S2**). Although several of them can be related to the pool of common serum proteins (albumin, apolipoproteins, and various chains of immunoglobulins), the gene ontology (GO) analysis identified many GO cellular component terms that can be specifically associated with EVs (**Table 1**). The most prominent EV-related groups are the late endosome lumen, blood microparticle, and the integrin alpha9-beta1 complex. The latter includes three integrins: Itgβ1, Itgβ3, and Itgα2b, characteristic EV surface proteins that facilitate the interaction of EVs with the extracellular matrix of the target tissues and even function as organotropic cues (18).

Comparison of the different experimental groups using the principal component analysis (PCA) demonstrates separation of the 6- and 24 h post-surgery group from the corresponding control samples, C6h and C24h-72h, respectively (**Figure 3**). Based on these data it was expected that most of the differentially expressed proteins would appear in the 24 h samples. Indeed, the expression levels of 12 proteins were found to be significantly different from the controls (FC>1.5, FDR<0.05) (**Figure 4A**, **Supplementary Table S3**). In addition, three different isoforms of glycogen phosphorylase (PYG) were also differentially expressed at 6 h post-surgery, of which the muscle isoform remains up-regulated even after 24 h (**Figure 4A** and **Supplementary Table S3**). These data can be better represented by the Volcano plots that enable quick visual identification of the up-and down-regulated proteins (**Figure 4B**). Interestingly, one of the top up-regulated proteins in the 24 h group was α-synuclein (α-syn), a protein whose

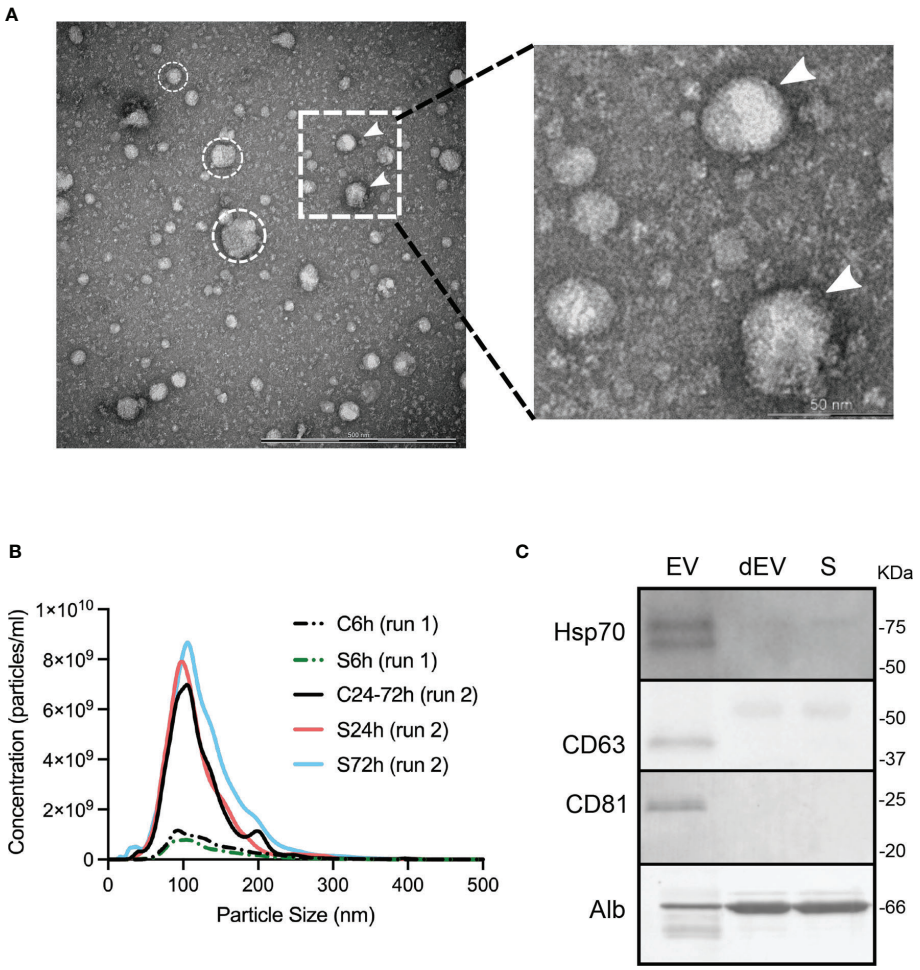

FIGURE 2 | Characterization of circulating EVs. **(A)** TEM image of the isolated particles, scale bar, 500 nm. Encircled are representative spherical particles. White arrows indicate putative lipid bilayers of EVs. The dotted insert is represented in higher magnification on the right panel. **(B)** Representative size distribution profile of isolated particles and their concentrations estimated by NTA. However, no differences in the control vs. S6h and the control vs, S24h and S72h comparisons were detected. **(C)** Western blot identification of EV enriched proteins and albumin. SDS-PAGE for CD63 western blot was run under non-reducing conditions. dEV, serum depleted of EVs, S, serum.

expression is largely associated with neural tissues (right panel in **Figures 4B, C**).

To confirm the EV origin of the α-syn we have analyzed serum, EVs, and dEVs samples from C24-72h and S24h groups by western blot. The α-syn signal was detected in the EV fraction from the 24 h surgical mouse, whereas it was absent in the serum and dEVs samples (**Figure 4D**). In the EVs from the control mouse, the signal was weak but detectable in all the samples. These data are complemented by yet another western blot analysis of the EVs that were additionally purified using magnetic beads coated with CD63, CD9, CD81 antibodies (see *Materials and Methods*). α-syn was identified in such enriched EVs from both control and 24 h surgical groups (**Supplementary Figure S1**). However, contrary to the MS data, we did not observe similar quantitative changes between the control and surgical mice. This is probably due to several reasons, such as the semiquantitative nature of the western blot and the difficulty to accurately quantify the low protein amounts after the EV enrichment.

Surgery Effects on the miRNAome of Serum EVs

Next-generation sequencing of small RNA libraries detected a mix of various RNA species including approximately 10% of mature miRNAs (**Figure 5A**). After removing miRNAs below the expression threshold (see *Materials and Methods*) the remaining 252 miRNAs were chosen for further analysis (**Supplementary Table S4**). PCA demonstrates clear separation of the control samples from the S24h and S72h groups, whereas the S6h group was clustered closer with the control samples (**Figure 5B**). At the same time, there is a partial overlap between the 24 and 72 h groups. Further analysis confirmed this trend, revealing the presence of 50 dysregulated miRNAs (FC>1.5, FDR<0.05) in the EVs from the S24h group (**Supplementary Table S5**). The surgery

TABLE 1 | Gene ontology (cellular component category) analysis of the differentially expressed EV proteins at 24 h post-surgery.

Gene onthology_cell component	Fold enrichment	FDR
late endosome lumen (GO:0031906)	54.02	3.83E-02
other organism part (GO:0044217)	54.02	3.79E-02
membrane attack complex (GO:0005579)	54.02	1.02E-07
fibrinogen complex (GO:0005577)	54.02	1.34E-06
myosin II filament (GO:0097513)	54.02	3.04E-03
integrin alpha9-beta1 complex (GO:0034679)	54.02	3.75E-02
blood microparticle (GO:0072562)	43.22	2.55E-08
spherical high-density lipoprotein particle (GO:0034366)	40.52	4.12E-06
intermediate-density lipoprotein particle (GO:0034363)	36.02	6.07E-04
proteasome core complex, alpha-subunit complex (GO:0019773)	33.77	8.03E-05
extrinsic component of external side of plasma membrane (GO:0031232)	30.01	1.19E-04

Proteins are ranked according to the fold enrichment of the corresponding cellular component term (http://geneontology.org/).

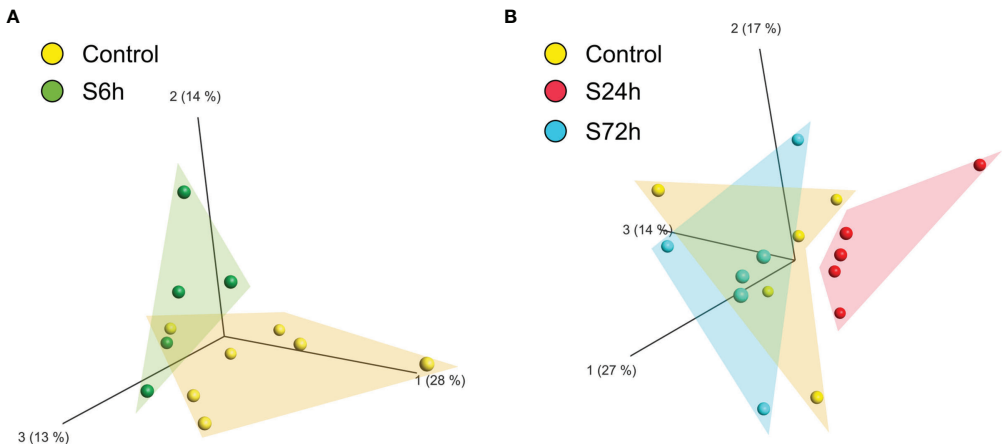

FIGURE 3 | Principal component analysis (PCA) of the proteomic data of circulating EVs. LC/MS produced quantitative proteomic data (protein abundances) were quantile normalized, log2-transformed, and used by Qlucore software for creating the PCA plots. **(A)** Control and 6 h post-surgery (S6h) experimental group form individual clusters. **(B)** Control and S24h groups are completely separated whereas the S72h group overlaps with the control samples.

effect declines after 72 h as judged by the lower number of dysregulated miRNAs (21) observed in the S72h group (**Figure 6A** and **Supplementary Table S5**). These data are graphically interpreted by the plot showing temporal kinetics of the fold changes of dysregulated miRNAs with peak values at 24 h, which decrease after 72 h almost to the baseline levels (**Figure 6B** and **Supplementary Table S5**), and by the corresponding Volcano plots (**Figure 6C**). Interestingly, only four out of 21 dysregulated miRNAs at 72 h post-surgery were not differentially expressed at 24 h (**Figure 6D**), which indicates the lasting, though declining effect of surgery on miRNA expression.

The heatmap presented in **Figure 6E** offers an even more nuanced view of the surgery effects. Thus, in addition to the already shown PCA clustering of control and experimental groups (control/C6h and S24h/S72h), the hierarchical clustering of miRNAs reveals two distinct clusters where cluster 1 includes down-regulated, and cluster 2, up-regulated at 24- and 72 h miRNAs.

miRNAs from circulating EVs are suggested to be involved in the post-transcriptional regulation in the target tissues (20). The miRNAs from both clusters were examined by the DIANA-miRPath online tool (21) that combines the prediction of miRNA target mRNAs (based on experimental data) with the analysis of the extent of enrichment of these genes in the different biological pathways. The bar graphs in **Figure 7A** show several KEGG pathways that are predicted to be regulated by the miRNAs from both clusters. A number of these pathways are involved in lipid metabolism, ECM-receptor interaction, gap junction, and various signal transduction pathways.

In order to validate the miRNA sequencing findings, we have estimated the expression of several differentially expressed miRNAs using the qPCR approach. Overall, the pattern of changes of the expression levels for the selected miRNAs was similar between the RNA-seq and qPCR analyses (**Supplementary Figure 2**).

Finally, it should be concluded that there is certainly a synergism in the temporal kinetics of the changes in the expression levels of both EV cargo molecules, proteins, and miRNA, as judged by the significant correlation between the numbers of both classes of dysregulated molecules at each post-surgery time point (**Figure 8**).

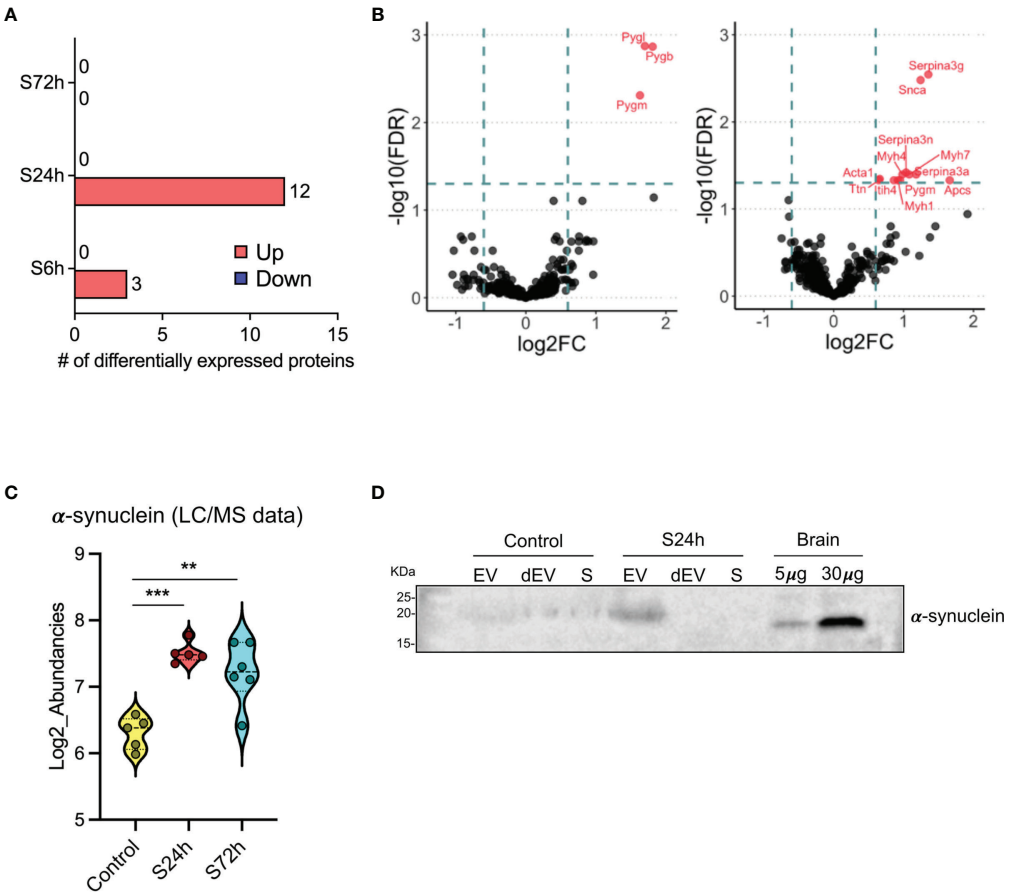

FIGURE 4 | Differential expression of proteins in the post-surgery circulating EVs. **(A)** Bar diagram representing the number of differentially expressed proteins in the 6, 24, and 72 h post-surgery groups compared to the control values as assessed by GraphPad Prism (v. 9.1.1) using multiple unpaired t-tests analysis with FDR < 0.05 and fold change (FC) > 1.5. (*Materials and Methods*). **(B)** Volcano plots showing the differentially expressed proteins at 6h (left) and 24h (right) post-surgery compared to their corresponding control groups (C6h and CS24-72h). Dotted lines represent FC > 1.5 threshold (log2-FC) and FDR <0.05 (-log10FDR), respectively. **(C)** Differential expression of α-synuclein in the EVs from S24h and S72h groups using log2-transformed LC/MS data. **(D)** α-synuclein expression validation by western blot. Mouse brain (hippocampus) homogenate was used as a positive control. SDS-PAGE was run under non-reducing conditions. dEV, serum depleted of EVs, S, serum. Snca in the 24h Volcano plot is the official gene symbol for α-synuclein (α-syn). **p < 0.005, ***p < 0.0005.

DISCUSSION

The principal aim of the present study was to determine whether surgical trauma, as represented by the mouse orthopedic surgery model is capable of modifying the cargo composition of circulating EVs, which would constitute a first step towards the elucidation of the potential role of EVs as active systemic mediators of surgery-induced periphery-to-brain communication.

We have, indeed, found statistically significant differences in the proteome and miRNAome of circulating EVs within the first 72 h after surgery. Their temporal appearance coincides with both the pattern of initiation and resolution of the systemic cellular and humoral inflammatory response and with the brain structural, metabolic, functional, and behavioral changes observed after orthopedic surgery in mice (5–7).

Proteomic profiling of the circulating EVs revealed that three proteins, i.e., brain, skeletal muscle, and liver isoforms of PYG, were rapidly up-regulated after surgery (**Figure 4B**). PYG is an enzyme involved in the breakdown of glycogen to glucose and as such essential for the maintenance of glucose homeostasis. The expression of PYG isozymes is not strictly tissue-specific (22), therefore it is difficult to pinpoint the precise tissue origin of EVs in our study.

Nevertheless, the surgery-injured muscles can be suggested as the most probable source of EVs carrying these proteins. Similarly, the increased levels of the same set of proteins were detected in the circulating EVs following yet another tissue injury (cardiac muscle) after the chemotherapy treatment (23). Therefore, the release of these EV-localized PYG isoforms appears to be an early indicator of tissue injury. In addition, the enrichment of EVs by PYGs might also occur due to the increased glycogenolysis in the muscle and liver, which is often observed during stress (24).

Alternatively, the increase of the brain isoform of PYG in the EVs may reflect the metabolic state of the brain after surgery.

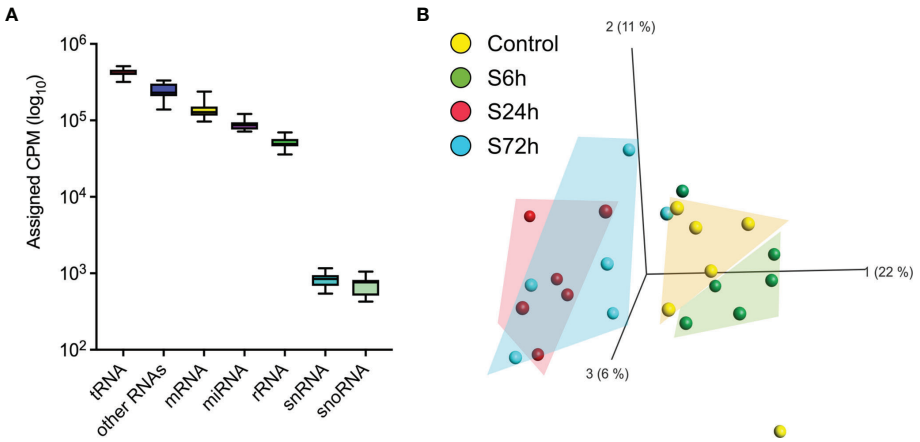

FIGURE 5 | RNA mapping and miRNA PCA. **(A)** The averaged RNA-seq data from the control samples were used to map RNA categories [sRNAbench webserver (19)]. **(B)** Principal component analysis of the circulating EVs' miRNA data. Normalized miRNA read counts [Counts Per Million reads (CPM)] were log2-transformed and used by Qlucore software to create a PCA plot. 24 h and 72 h post-surgery groups cluster together and are separated from the control whereas the 6 h group clusters with the control.

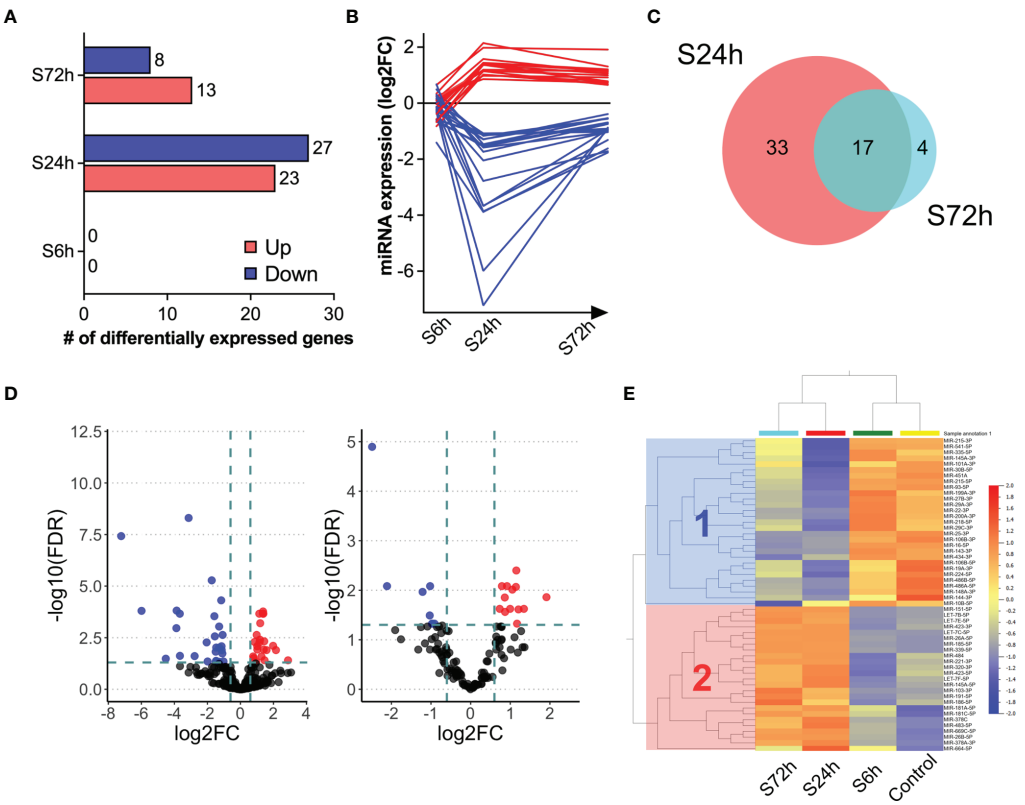

FIGURE 6 | Differential expression of miRNAs in the post-surgery circulating EVs. **(A)** Bar diagram representing the number of differentially expressed miRNAs in the 6, 24, and 72 h post-surgery groups compared to control values as assessed by DESeq2 analysis (FDR<0.05 and fold change (FC)>1.5; see *Materials and Methods*). **(B)** Post-surgery temporal kinetics of the differentially expressed miRNAs. Each line represents an individual differentially expressed miRNA. **(C)** Volcano plots showing the differentially expressed proteins at 24- (left) and 72 h (right) post-surgery compared to the control group (Control). The dotted lines represent FC > 1.5 threshold (log2-FC) and FDR <0.05 (-10logFDR), respectively. **(D)** Venn diagram showing the overlap between the differentially expressed miRNAs at 24 and 72 h post-surgery. **(E)** The log2-transformed CPM values of differentially expressed miRNAs at 24 and 72 h and the same miRNAs from the control and S6h groups were used to generate heatmap (Qlucore). Cluster 1 (blue) and cluster 2 (red) include down-regulated and up-regulated miRNAs at 24 and 72 h, respectively.

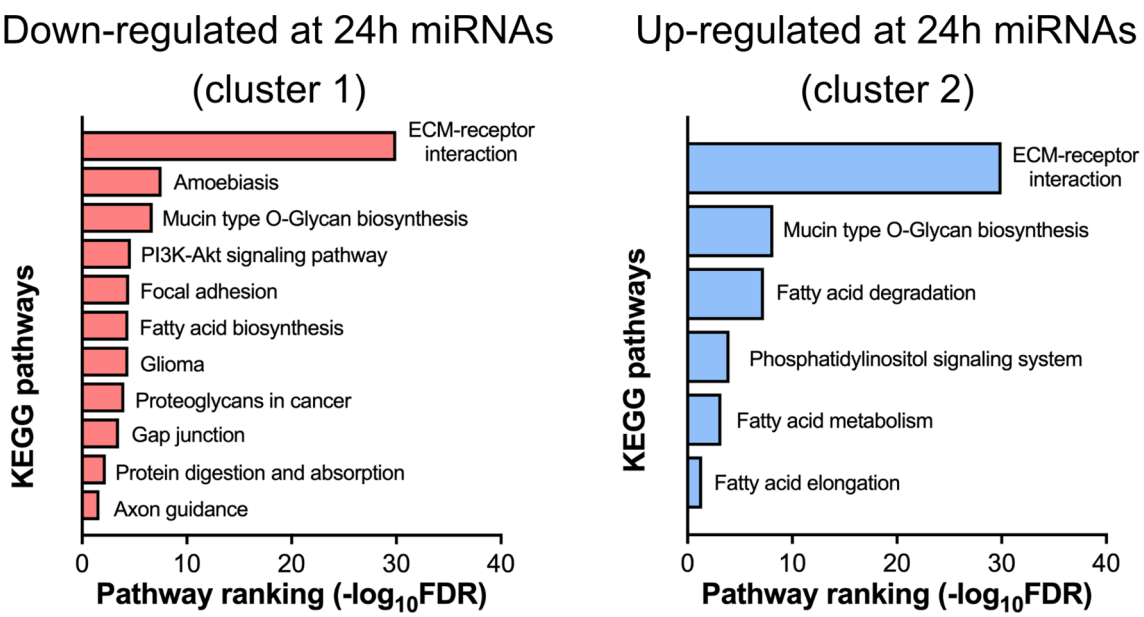

FIGURE 7 | Pathway analysis of differentially expressed miRNAs. Down- (cluster 1 from **Figure 6E**) and up-regulated (cluster 2 from **Figure 6E**) at 24 h post-surgery miRNAs were analyzed by the miRPath online tool (see *Materials and Methods*) that determines the miRNA target mRNAs (based on experimental data) and analyses the overrepresentation of these genes in the different KEGG pathways.

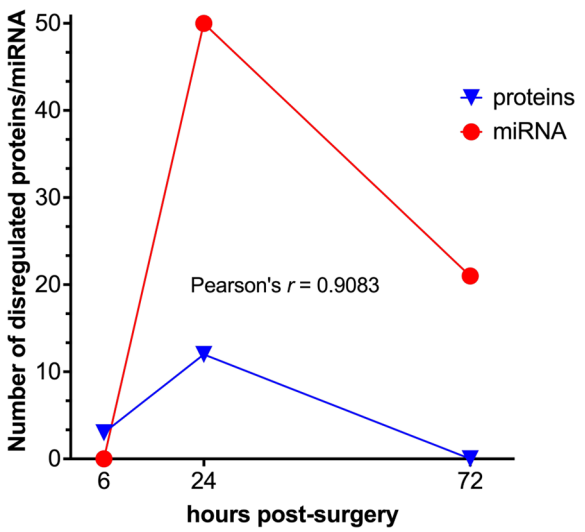

FIGURE 8 | Correlation analysis between the differentially expressed protein and miRNA data sets. Temporal kinetics of the differential expression of EVs' proteins and miRNAs demonstrates a high degree of correlation as to the Pearson's linear correlation coefficient (GraphPad Prism).

Indirect evidence confirming this hypothesis is our data on the modified glucose and glutamate metabolism in the hippocampus accompanied by changes in lactate levels at the same time points after surgery (6).

The most prominent changes in the EVs' protein cargo occur at 24 h post-surgery when 12 proteins were found up-regulated. Mining the functions and tissue expression profiles of these proteins allows conditional division of this group into two clusters: proteins related to the muscle structure and function [Myosin Heavy Chain 1, 4, and 7 (Myh1, Myh4, Myh7), PYGm, Titin (Ttn), Actin, Alpha Skeletal Muscle (Acta1)] and proteins involved in the acute-phase response to stress [Serpina3g, Serpina3n, Serpina3a, Serum Amyloid P-Component (Apcs), Inter-Alpha-Trypsin Inhibitor Heavy Chain H4 (Itih4)]. The

muscle-related cluster represents the same tendency that was detected already at the 6 h time point, that is the profound disruption of the surrounding tissues, including the muscle upon tibia surgery. Considering the known activation of the inflammatory response after surgery (25, 26) the elevation of levels of many acute-phase proteins from the second cluster is also not surprising. For instance, the circulating levels of Itih4 were found elevated after the surgical trauma as shown using yet another animal model of surgery (27). It can be therefore suggested that post-surgery EVs might also spread inflammatory signals to remote organs.

One of the differentially expressed proteins at 24 h post-surgery is α-syn, which cannot be categorized into either of these two subgroups. α-syn is expressed predominantly in neurons and mostly localizes at the presynaptic terminal where it regulates vesicle turnover (28). The aggregated form of α-syn is a hallmark of a group of neurodegenerative diseases, including PD and dementia with Lewy bodies (DLB) (29). However, α-syn is also expressed in peripheral tissues, including muscle cells (30) and blood cells, such as erythrocytes and platelets (31–33) whereas lesser amounts are found in peripheral blood mononuclear cells (PBMC) (34). This suggests potential source tissues of the α-syn found in the circulating EVs. One possibility is that it is released into EVs from the damaged muscles along with the abovementioned muscle proteins. It can also be hypothesized that PBMCs activated after surgery can shed "inflammatory" EVs carrying α-syn as one of the cargo molecules.

Up-regulation of α-syn in the circulating EVs after surgical trauma prompts an intriguing hypothesis that associates EV-born α-syn with acceleration and/or exacerbation of neurodegenerative diseases (35, 36) and the risk for late-onset dementia (37, 38) after surgery. Consistent with this hypothesis different preclinical and clinical studies demonstrated that α-syn bearing EVs are capable of amplifying and propagating PD-related pathology (39–42). In addition, it was also reported that LPS-induced peripheral inflammation may potentiate the delivery of erythrocyte-produced EVs containing α-syn across the BBB (43).

However, further detailed studies are certainly needed to explore this hypothesis and decipher possible clinical implications of α-syn up-regulation in the circulating EVs after surgery.

Whereas the protein fraction of EV cargo can potentially provide more information on the tissue origin of EVs, the miRNAs endowed with a strong post-transcriptional regulation potential are important for understanding and predicting the phenotypic changes of the recipient cells and tissues. It should be noted that despite the same temporal pattern of differential expression (**Figure 8**) the number of dysregulated miRNAs at 24 h post-surgery is significantly higher than the number of proteins at the same time point. Moreover, these changes do not completely subside as in the case with proteome but remain at a certain, albeit lower level at 72 h post-surgery, which might be indicative of a functionally more important role of EVs' miRNAs as compared to proteins, with a wider temporal window of action.

Analysis of the miRNA differential expression at 24 h post-surgery revealed an explicit pattern of biological pathways that these miRNAs (via their target mRNAs) may affect in the putative recipient tissue(s). Thus, the set of down-regulated miRNAs is involved in several pathways, the majority of which are unified by a common theme - regulation of extracellular matrix (ECM) (**Figure 7**). Interestingly, this set includes only few miRNAs out of 27 down-regulated miRNAs (mmu-miR-29c-3p, mmu-miR-145a-3p, mmu-miR-148a-3p, mmu-miR-29a-3p, mmu-miR-25-3p) (**Supplementary Figure S3**, left panel). Nearly the same set of miRNAs is also associated with a much broader scope pathway, the PI3K/AKT/mTOR signaling. The ECM components targeted by miRNAs are represented by a group of various collagens and their cell receptors, namely integrins. Notably, different members of the human miR-29 family that were found down-regulated in this study, are known to have anti-fibrotic properties (44) due to their capacity to interact with many mRNAs coding for ECM proteins. It can therefore be suggested that down-regulation of these miRNAs in the EVs could stimulate the synthesis of ECM proteins in the target tissue(s), a process that is closely associated with wound healing, especially at the initial stages (45). In line with this, it was reported that various cargo molecules of circulating EVs including miRNAs are capable of modulating this pathway (46), and therefore might facilitate healing at the injury site.

Such up-regulation of ECM components is reminiscent of ECM re-modeling upon the metastatic process when tumor EVs are preparing the "soil" for the arriving cancer cells - a metastatic niche formation (47, 48). Considering the involvement of the same set of miRNAs in the regulation of PI3K/AKT/mTOR pathway (**Supplementary Figure S3**, left panel) it is tempting to speculate that such "soiling" of the recipient tissue might represent an important first step facilitating the following activation of the PI3K/AKT/mTOR system with the very same miRNAs. However, due to the immense complexity of this pathway and uncertain target tissues of post-surgery EVs, it is difficult so far to predict specific miRNA-mediated effects *via* such a mechanism.

In addition to the 27 down-regulated EV miRNAs, 23 up-regulated miRNAs were found associated with several KEGG pathways. Again, it is just a few miRNAs in this group that are driving most of the regulatory functions. These are four different mmu-*let* miRNAs and mmu-miR-339-5p, mmu-miR-423-5p that are involved in several pathways linked to the fatty acid metabolism, along with yet another group of miRNAs (mmu-miR-181a-5p, mmu-miR-26b-5p, mmu-miR-26a-5p, mmu-miR-378a-3p, mmu-miR-181c-5p, mmu-miR-378c) that is connected with the phosphatidylinositol signaling system (**Supplementary Figure S3**, right panel). The same group of *let* miRNAs can also regulate the ECM (**Supplementary Figure S2**, right panel). Interestingly, the same pathway is targeted by down-regulated miRNAs (see above), however, *let* miRNAs can modulate translation of only a few collagen mRNAs, whereas the down-regulated miRNAs target many more ECM components including integrin receptors.

As indicated above, most pathways linked to the up-regulated miRNAs are related to the fatty acid metabolism and involve

mRNAs coding for both the enzymes participating in the fatty acid catabolism and the elongation and saturation of fatty acids. Therefore, it can be predicted that the overall effect of the miRNA up-regulation in the EVs would be the suppression of the fatty acid catabolism in the putative recipient tissue(s).

Interestingly, consistent with this prediction, unpublished hippocampal gene expression and metabolomic data from our laboratory indicate partial replacement of glucose as an energy source by fatty acids at 6 h post-surgery, whereas these changes were largely reversed 72 h after surgery and lipid catabolism was even decreased.

As in the case of down-regulated miRNAs, the group of up-regulated miRNAs is involved in the modulation of yet another complex multifunctional signal transduction pathway, phosphatidylinositol-dependent signaling. Similar to the PI3K/AKT/mTOR pathway, this signaling cascade is an active actor in many physiological and pathological intracellular events, which, on one hand, allows prediction of the active functional role of the post-surgery EVs in the various distant tissues, but, on the other hand, makes it equally difficult to envision any specific downstream effects.

In both up- and down-regulated miRNA groups, the miRPath pathway analysis tool singled out only a few dysregulated miRNAs that were considered to drive main metabolic effects. However, it cannot be ruled out that other differentially expressed miRNA might also modify gene expression in target cells. For instance, one of the top (FDR ranking) down-regulated at 24 h mmu-miR-143-3p is predicted to be involved in lipid and carbohydrate metabolism. Yet another top down-regulated mmu-mir-541-5p target is predicted to modify the MAPK signaling pathway (results not shown).

It should be mentioned that this study is not devoid of certain limitations. Thus, it is difficult to separate the effects of surgery and anesthesia without a corresponding experimental group of animals subjected only to anesthesia. We have previously demonstrated that the systemic immune activation in response to orthopedic surgery in mice is independent of the isoflurane anesthesia (7, 49). Nevertheless, it is still an open question if the modification of EVs composition under the same conditions is following the same pattern.

Another confounding factor is the use of only male animals in the study. We have unpublished yet data where we could not detect any sex differences in the behavioral experiments using the same tibia surgery model.

Proteomic data indicated α-synuclein as differentially expressed in the 24 h surgery samples. Western blot validation revealed a protein band slightly larger in size as compared to the brain positive control (**Figure 4D**). We believe that this size difference can be attributed to the different tissue sources of the protein and/or to the potential posttranslational modification(s) (50). However, more sensitive methods, such as immunoelectron microscopy might be needed to confirm the presence of the protein in the EVs.

Finally, there is an ongoing debate concerning the choice of the EV isolation method. The choice is largely dictated by the tissue type, available amounts, throughput options, suitability for various downstream applications, and the research question to be addressed. Taking all of these and also many comparative studies (17, 50–54) into account, we chose to use the commercial kit ExoQuick ULTRA. The ULTRA version enriches for EVs and has a relatively high yield, important for the small sample volumes obtained from mice. The disadvantage of using the ExoQuick, as well as similar precipitation methods is that it might produce certain amounts of contaminating proteins and also miRNAs associated with lipoproteins. However, whereas the gold standard EV isolation method, the ultracentrifugation could have provided with more refined EV fraction, it would had been not possible to apply using the minute amounts of mouse blood serum. The same reasoning can be applied to the other methods, such as size-exclusion chromatography (SEC), density gradient, affinity chromatography, *etc.* Interestingly, a comparison of SEC with the ExoQuick ULTRA using the identical serum volumes (250 µl) demonstrated the isolation of nearly the same set of EV-related proteins (17).

With the current study, we began to explore the hypothesis of circulatory EVs as potential mediators of the physiological effects of surgical trauma. The main question of the current project, whether the surgery is capable of modifying the expression of cargo molecules in circulating EVs, can be answered now positively. Moreover, differential expression of a specific set of miRNAs in the "surgical" EVs suggests that they can be involved in the regulation of several metabolic pathways, such as ECM-receptor interaction and lipid metabolism in the recipient tissues, which is consistent with our data on hippocampal metabolic and functional dysregulation after surgery (5, 6). Another interesting finding is the increased levels of α-syn in the circulating EVs after surgery, which might have potential long-term neurological consequences. We conclude that surgery alters the EV composition in the blood, which paves the way for further studies on the functional effects of these EVs on the brain.

DATA AVAILABILITY STATEMENT

The datasets presented in this study can be found in online repositories. The names of the repository/repositories and accession number(s) can be found below: NCBI GEO, accession no: GSE189972; PRIDE ProteomeXchange, accession no: PXD030167.

ETHICS STATEMENT

All experiments were reviewed and approved by the Local ethics Committee for Animal Research of Stockholm North and Karolinska Institutet in Sweden.

AUTHOR CONTRIBUTIONS

Conception and design: MG-G, SM. Methodology support: MM-L, RV. Acquisition data: MG-G, AE. Analysis and interpretation of the data: MG-G, SM. Funding acquisition: LE. Writing outline

of the manuscript: MG-G, SM. Reading and revision of the manuscript: all authors. All authors contributed to the article and approved the submitted version.

FUNDING

This work was funded by The Swedish Medical Research Council and The Swedish Brain Foundation.

ACKNOWLEDGMENTS

The authors thank Lars Haag and the electron microscopy unit (EMIl), Department of Laboratory Medicine, Karolinska Hospital Huddinge for the electron microscopy images; Genomics Core Facility at the Institute of Molecular Biology (IMB) Mainz, Germany for using the Illumina NextSeq500 (INST 247/870-1 FUGG), Hanna Lukas, Genomic Core Facility and Emil Karaulanov, Bioinformatics Core Facility, for assisting in RNA-seq and bioinformatics, respectively; Akos Vegvari at the Proteomics Biomedicum core facility, Karolinska Institutet, Stockholm. The authors also thank María Jesús Iglesias, Science for Life Laboratory, Department of Protein Science, CBH, KTH Royal Institute of Technology, Stockholm, Sweden for protein validation methodological support.

SUPPLEMENTARY MATERIAL

The Supplementary Material for this article can be found online at: https://www.frontiersin.org/articles/10.3389/fimmu.2021.824696/full#supplementary-material

REFERENCES

1. Moller JT, Cluitmans P, Rasmussen LS, Houx P, Rasmussen H, Canet J, et al. Long-Term Postoperative Cognitive Dysfunction in the Elderly ISPOCD1 Study. ISPOCD Investigators. International Study of Post-Operative Cognitive Dysfunction. *Lancet* (1998) 351:857–61. doi: 10.1016/S0140-6736(97)07382-0
2. Johnson T, Monk T, Rasmussen LS, Abildstrom H, Houx P, Korttila K, et al. Postoperative Cognitive Dysfunction in Middle-Aged Patients. *Anesthesiology* (2002) 96:1351–7. doi: 10.1097/00000542-200206000-00014
3. Monk TG, Weldon BC, Garvan CW, Dede DE, van der Aa MT, Heilman KM, et al. Predictors of Cognitive Dysfunction After Major Noncardiac Surgery. *Anesthesiology* (2008) 108:18–30. doi: 10.1097/01.anes.0000296071.19434.1e
4. Eckenhoff RG, Laudansky KF. Anesthesia, Surgery, Illness and Alzheimer's Disease. *Prog Neuropsychopharmacol Biol Psychiatry* (2013) 47:162–6. doi: 10.1016/j.pnpbp.2012.06.011
5. Terrando N, Gomez-Galan M, Yang T, Carlstrom M, Gustavsson D, Harding RE, et al. Aspirin-Triggered Resolvin D1 Prevents Surgery-Induced Cognitive Decline. *FASEB J* (2013) 27:3564–71. doi: 10.1096/fj.13-230276
6. Femenia T, Gimenez-Cassina A, Codeluppi S, Fernandez-Zafra T, Katsu-Jimenez Y, Terrando N, et al. Disrupted Neuroglial Metabolic Coupling After Peripheral Surgery. *J Neurosci* (2018) 38:452–64. doi: 10.1523/JNEUROSCI.1797-17.2017
7. Terrando N, Eriksson LI, Ryu JK, Yang T, Monaco C, Feldmann M, et al. Resolving Postoperative Neuroinflammation and Cognitive Decline. *Ann Neurol* (2011) 70:986–95. doi: 10.1002/ana.22664
8. Yanez-Mo M, Siljander PR, Andreu Z, Zavec AB, Borras FE, Buzas EI, et al. Biological Properties of Extracellular Vesicles and Their Physiological Functions. *J Extracell Vesicles* (2015) 4:27066. doi: 10.3402/jev.v4.27066
9. Zappulli V, Friis KP, Fitzpatrick Z, Maguire CA, Breakefield XO. Extracellular Vesicles and Intercellular Communication Within the Nervous System. *J Clin Invest* (2016) 126:1198–207. doi: 10.1172/JCI81134
10. Shi M, Sheng L, Stewart T, Zabetian CP, Zhang J. New Windows Into the Brain: Central Nervous System-Derived Extracellular Vesicles in Blood. *Prog Neurobiol* (2019) 175:96–106. doi: 10.1016/j.pneurobio.2019.01.005
11. Veerman RE, Gucluler Akpinar G, Eldh M, Gabrielsson S. Immune Cell-Derived Extracellular Vesicles - Functions and Therapeutic Applications. *Trends Mol Med* (2019) 25:382–94. doi: 10.1016/j.molmed.2019.02.003
12. Ridder K, Keller S, Dams M, Rupp AK, Schlaudraff J, Del Turco D, et al. Extracellular Vesicle-Mediated Transfer of Genetic Information Between the Hematopoietic System and the Brain in Response to Inflammation. *PloS Biol* (2014) 12:e1001874. doi: 10.1371/journal.pbio.1001874
13. Consortium E-T, Van Deun J, Mestdagh P, Agostinis P, Akay O, Anand S, et al. EV-TRACK: Transparent Reporting and Centralizing Knowledge in Extracellular Vesicle Research. *Nat Methods* (2017) 14:228–32. doi: 10.1038/nmeth.4185
14. Edgar R, Domrachev M, Lash AE. Gene Expression Omnibus: NCBI Gene Expression and Hybridization Array Data Repository. *Nucleic Acids Res* (2002) 30:207–10. doi: 10.1093/nar/30.1.207
15. Perez-Riverol Y, Csordas A, Bai J, Bernal-Llinares M, Hewapathirana S, Kundu DJ, et al. The PRIDE Database and Related Tools and Resources in 2019: Improving Support for Quantification Data. *Nucleic Acids Res* (2019) 47:D442–50. doi: 10.1093/nar/gky1106
16. Eldh M, Mints M, Hiltbrunner S, Ladjevardi S, Alamdari F, Johansson M, et al. Proteomic Profiling of Tissue Exosomes Indicates Continuous Release of Malignant Exosomes in Urinary Bladder Cancer Patients, Even With Pathologically Undetectable Tumour. *Cancers (Basel)* (2021) 13(13):3242. doi: 10.3390/cancers13133242
17. Veerman RE, Teeuwen L, Czarnewski P, Gucluler Akpinar G, Sandberg A, Cao X, et al. Molecular Evaluation of Five Different Isolation Methods for Extracellular Vesicles Reveals Different Clinical Applicability and Subcellular Origin. *J Extracell Vesicles* (2021) 10:e12128. doi: 10.1002/jev2.12128
18. Shimaoka M, Kawamoto E, Gaowa A, Okamoto T, Park EJ. Connexins and Integrins in Exosomes. *Cancers (Basel)* (2019) 11(11):106. doi: 10.3390/cancers11010106
19. Aparicio-Puerta E, Lebron R, Rueda A, Gomez-Martin C, Giannoukakos S, Jaspez D, et al. Srnabench and Srnatoolbox 2019: Intuitive Fast Small RNA Profiling and Differential Expression. *Nucleic Acids Res* (2019) 47:W530–5. doi: 10.1093/nar/gkz415
20. Bartel DP. Metazoan MicroRNAs. *Cell* (2018) 173:20–51. doi: 10.1016/j.cell.2018.03.006
21. Vlachos IS, Zagganas K, Paraskevopoulou MD, Georgakilas G, Karagkouni D, Vergoulis T, et al. DIANA-Mirpath V3.0: Deciphering microRNA Function With Experimental Support. *Nucleic Acids Res* (2015) 43:W460–6. doi: 10.1093/nar/gkv403
22. Schmid H, Pfeiffer-Guglielmi B, Dolderer B, Thiess U, Verleysdonk S, Hamprecht B. Expression of the Brain and Muscle Isoforms of Glycogen Phosphorylase in Rat Heart. *Neurochem Res* (2009) 34:581–6. doi: 10.1007/s11064-008-9825-3
23. Yarana C, Carroll D, Chen J, Chaiswing L, Zhao Y, Noel T, et al. Extracellular Vesicles Released by Cardiomyocytes in a Doxorubicin-Induced Cardiac Injury Mouse Model Contain Protein Biomarkers of Early Cardiac Injury. *Clin Cancer Res* (2018) 24:1644–53. doi: 10.1158/1078-0432.CCR-17-2046
24. Van Cromphaut SJ. Hyperglycaemia as Part of the Stress Response: The Underlying Mechanisms. *Best Pract Res Clin Anaesthesiol* (2009) 23:375–86. doi: 10.1016/j.bpa.2009.08.005
25. Forsberg A, Cervenka S, Jonsson Fagerlund M, Rasmussen LS, Zetterberg H, Erlandsson Harris H, et al. The Immune Response of the Human Brain to Abdominal Surgery. *Ann Neurol* (2017) 81:572–82. doi: 10.1002/ana.24909
26. Margraf A, Ludwig N, Zarbock A, Rossaint J. Systemic Inflammatory Response Syndrome After Surgery: Mechanisms and Protection. *Anesth Analg* (2020) 131:1693–707. doi: 10.1213/ANE.0000000000005175

27. Soler L, Garcia N, Unzueta A, Pineiro M, Alava MA, Lampreave F. Purification and Determination of C-Reactive Protein and Inter-Alpha-Trypsin Inhibitor Heavy Chain 4 in Dogs After Major Surgery Through Generation of Specific Antibodies. *Vet Immunol Immunopathol* (2016) 179:26–31. doi: 10.1016/j.vetimm.2016.07.010
28. Goedert M. Alpha-Synuclein and Neurodegenerative Diseases. *Nat Rev Neurosci* (2001) 2:492–501. doi: 10.1038/35081564
29. Lang AE, Lozano AM. Parkinson's Disease. First of Two Parts. *N Engl J Med* (1998) 339:1044–53. doi: 10.1056/NEJM199810083391506
30. Askanas V, Engel WK, Alvarez RB, Mcferrin J, Broccolini A. Novel Immunolocalization of Alpha-Synuclein in Human Muscle of Inclusion-Body Myositis, Regenerating and Necrotic Muscle Fibers, and at Neuromuscular Junctions. *J Neuropathol Exp Neurol* (2000) 59:592–8. doi: 10.1093/jnen/59.7.592
31. Li QX, Campbell BC, Mclean CA, Thyagarajan D, Gai WP, Kapsa RM, et al. Platelet Alpha- and Gamma-Synucleins in Parkinson's Disease and Normal Control Subjects. *J Alzheimers Dis* (2002) 4:309–15. doi: 10.3233/JAD-2002-4406
32. Michell AW, Luheshi LM, Barker RA. Skin and Platelet Alpha-Synuclein as Peripheral Biomarkers of Parkinson's Disease. *Neurosci Lett* (2005) 381:294–8. doi: 10.1016/j.neulet.2005.02.030
33. Barbour R, Kling K, Anderson JP, Banducci K, Cole T, Diep L, et al. Red Blood Cells are the Major Source of Alpha-Synuclein in Blood. *Neurodegener Dis* (2008) 5:55–9. doi: 10.1159/000112832
34. Pei Y, Maitta RW. Alpha Synuclein in Hematopoiesis and Immunity. *Heliyon* (2019) 5:e02590. doi: 10.1016/j.heliyon.2019.e02590
35. Glass CK, Saijo K, Winner B, Marchetto MC, Gage FH. Mechanisms Underlying Inflammation in Neurodegeneration. *Cell* (2010) 140:918–34. doi: 10.1016/j.cell.2010.02.016
36. Lage C, Gonzalez-Suarez A, Alcalde-Hierro MP, Sampedro-Gonzalez MI, Villanueva-Eguaras MA, Sanchez-Crespo MR, et al. Major Surgery Affects Memory in Individuals With Cerebral Amyloid-Beta Pathology. *J Alzheimers Dis* (2021) 79:863–74. doi: 10.3233/JAD-191229
37. Chen PL, Yang CW, Tseng YK, Sun WZ, Wang JL, Wang SJ, et al. Risk of Dementia After Anaesthesia and Surgery. *Br J Psychiatry* (2014) 204:188–93. doi: 10.1192/bjp.bp.112.119610
38. Eriksson LI, Lundholm C, Narasimhalu K, Sandin R, Jin YP, Gatz M, et al. Hospitalization, Surgery, and Incident Dementia. *Alzheimers Dement* (2019) 15:534–42. doi: 10.1016/j.jalz.2018.12.005
39. Emmanouilidou E, Melachroinou K, Roumeliotis T, Garbis SD, Ntzouni M, Margaritis LH, et al. Cell-Produced Alpha-Synuclein Is Secreted in a Calcium-Dependent Manner by Exosomes and Impacts Neuronal Survival. *J Neurosci* (2010) 30:6838–51. doi: 10.1523/JNEUROSCI.5699-09.2010
40. Grey M, Dunning CJ, Gaspar R, Grey C, Brundin P, Sparr E, et al. Acceleration of Alpha-Synuclein Aggregation by Exosomes. *J Biol Chem* (2015) 290:2969–82. doi: 10.1074/jbc.M114.585703
41. Stuendl A, Kunadt M, Kruse N, Bartels C, Moebius W, Danzer KM, et al. Induction of Alpha-Synuclein Aggregate Formation by CSF Exosomes From Patients With Parkinson's Disease and Dementia With Lewy Bodies. *Brain* (2016) 139:481–94. doi: 10.1093/brain/awv346
42. Ngolab J, Trinh I, Rockenstein E, Mante M, Florio J, Trejo M, et al. Correction to: Brain-Derived Exosomes From Dementia With Lewy Bodies Propagate Alpha-Synuclein Pathology. *Acta Neuropathol Commun* (2020) 8:123. doi: 10.1186/s40478-020-01006-4
43. Matsumoto J, Stewart T, Sheng L, Li N, Bullock K, Song N, et al. Transmission of Alpha-Synuclein-Containing Erythrocyte-Derived Extracellular Vesicles Across the Blood-Brain Barrier via Adsorptive Mediated Transcytosis: Another Mechanism for Initiation and Progression of Parkinson's Disease? *Acta Neuropathol Commun* (2017) 5:71. doi: 10.1186/s40478-017-0470-4
44. Kriegel AJ, Liu Y, Fang Y, Ding X, Liang M. The miR-29 Family: Genomics, Cell Biology, and Relevance to Renal and Cardiovascular Injury. *Physiol Genomics* (2012) 44:237–44. doi: 10.1152/physiolgenomics.00141.2011
45. Maquart FX, Monboisse JC. Extracellular Matrix and Wound Healing. *Pathol Biol (Paris)* (2014) 62:91–5. doi: 10.1016/j.patbio.2014.02.007
46. Rackov G, Garcia-Romero N, Esteban-Rubio S, Carrion-Navarro J, Belda-Iniesta C, Ayuso-Sacido A. Vesicle-Mediated Control of Cell Function: The Role of Extracellular Matrix and Microenvironment. *Front Physiol* (2018) 9:651. doi: 10.3389/fphys.2018.00651
47. Dos Anjos Pultz B, Andres Cordero Da Luz F, Socorro Faria S, Peixoto Ferreira De Souza L, Cristina Brigido Tavares P, Alonso Goulart V, et al. The Multifaceted Role of Extracellular Vesicles in Metastasis: Priming the Soil for Seeding. *Int J Cancer* (2017) 140:2397–407. doi: 10.1002/ijc.30595
48. Albacete-Albacete L, Navarro-Lerida I, Lopez JA, Martin-Padura I, Astudillo AM, Ferrarini A, et al. ECM Deposition Is Driven by Caveolin-1-Dependent Regulation of Exosomal Biogenesis and Cargo Sorting. *J Cell Biol* (2020) 219 (11):e202006178. doi: 10.1083/jcb.202006178
49. Terrando N, Monaco C, Ma D, Foxwell BM, Feldmann M, Maze M. Tumor Necrosis Factor-Alpha Triggers a Cytokine Cascade Yielding Postoperative Cognitive Decline. *Proc Natl Acad Sci USA* (2010) 107(47):20518–22. doi: 10.1073/pnas.1014557107
50. Burre J, Sharma M, Sudhof TC. Cell Biology and Pathophysiology of Alpha-Synuclein. *Cold Spring Harb Perspect Med* (2018) 8(3):a024091. doi: 10.1101/cshperspect.a024091
51. Kobayashi M, Morishita H, Sugiyama N, Yokochi K, Nakano M, Wada Y, et al. Mitochondrial Myopathy, Encephalopathy, Lactic Acidosis and Stroke-Like Episodes Syndrome and NADH-CoQ Reductase Deficiency. *J Inherit Metab Dis* (1986) 9:301–4. doi: 10.1007/BF01799670
52. Tang YT, Huang YY, Zheng L, Qin SH, Xu XP, An TX, et al. Comparison of Isolation Methods of Exosomes and Exosomal RNA From Cell Culture Medium and Serum. *Int J Mol Med* (2017) 40:834–44. doi: 10.3892/ijmm.2017.3080
53. Serrano-Pertierra E, Oliveira-Rodriguez M, Rivas M, Oliva P, Villafani J, Navarro A, et al. Characterization of Plasma-Derived Extracellular Vesicles Isolated by Different Methods: A Comparison Study. *Bioeng (Basel)* (2019) 6 (1):8. doi: 10.3390/bioengineering6010008
54. Brennan K, Martin K, Fitzgerald SP, O'sullivan J, Wu Y, Blanco A, et al. A Comparison of Methods for the Isolation and Separation of Extracellular Vesicles From Protein and Lipid Particles in Human Serum. *Sci Rep* (2020) 10:1039. doi: 10.1038/s41598-020-57497-7

Conflict of Interest: Author SG has a patent on B cell derived exosomes in immune therapy and is part of the Scientific Advisory Board of Anjarium Biosciences. RV is currently employed by Strike Pharma.

The remaining authors declare that the research was conducted in the absence of any commercial or financial relationships that could be construed as a potential conflict of interest.

Publisher's Note: All claims expressed in this article are solely those of the authors and do not necessarily represent those of their affiliated organizations, or those of the publisher, the editors and the reviewers. Any product that may be evaluated in this article, or claim that may be made by its manufacturer, is not guaranteed or endorsed by the publisher.

frontiers in Immunology

ORIGINAL RESEARCH
published: 10 February 2022
doi: 10.3389/fimmu.2022.822895

Sulforaphane Exerts Beneficial Immunomodulatory Effects on Liver Tissue *via* a Nrf2 Pathway-Related Mechanism in a Murine Model of Hemorrhagic Shock and Resuscitation

Weiqiang Liang[1,2†], Johannes Greven[1†], Kang Qin[1], Athanassios Fragoulis[3], Klemens Horst[1], Felix Bläsius[1], Christoph Wruck[3], Thomas Pufe[3], Philipp Kobbe[1], Frank Hildebrand[1] and Philipp Lichte[1]*

[1] Department of Orthopaedics, Trauma and Reconstructive Surgery, University Hospital Rheinisch-Westfälische Technische Hochschule (RWTH) Aachen, Aachen, Germany, [2] Department of Bone and Joint Surgery, The First Affiliated Hospital of Shandong First Medical University, Jinan, China, [3] Department of Anatomy and Cell Biology, Rheinisch-Westfälische Technische Hochschule (RWTH) Aachen University, Aachen, Germany

Our research explores the immunomodulatory effects of sulforaphane (SFN), a well-known nuclear factor erythroid 2-related factor 2 (Nrf2) pathway agonist, on the sterile inflammation of and ischemia-reperfusion injuries to the liver after hemorrhagic shock (HS) followed by resuscitation (R). Male C57/BL6 wild-type and transgenic ARE-*luc* mice were exposed to mean arterial pressure-controlled HS. Fluid resuscitation was performed after 90 min of HS, and SFN was administrated intraperitoneally after that. The animals were sacrificed at 6 h, 24 h, and 72 h after resuscitation, and their livers were extracted to perform H&E staining and myeloperoxidase (MPO) activity analysis. The Kupffer cells were isolated for cytokines profile measurements and Nrf2 immunofluorescence staining. Further, the ARE-*luc* mice were used to assess hepatic Nrf2 activity *in vivo*. We identified that SFN-activated Kupffer cells' Nrf2 pathway and modulated its cytokines expression, including TNF-α, MCP-1, KC/CXCL1, IL-6, and IL-10. Furthermore, SFN mitigated liver ischemia-reperfusion injury, as evidenced by the downregulation of the Suzuki score and the enhanced hepatic Nrf2 activity. The *in vivo* SFN treatment decreased neutrophils infiltration, as shown by the decreased MPO levels. Our study shows that SFN can decrease HS/R-induced hepatic ischemia-reperfusion injury and modulate the activity of Kupffer cells *via* an Nrf2-dependent pathway.

Keywords: hemorrhagic shock/resuscitation, liver, ischemia-reperfusion injury, cytokines, Kupffer Cells, sulforaphane, Nrf2, KEAP1

OPEN ACCESS

Edited by:
Christoph Thiemermann, Queen Mary University of London, United Kingdom

Reviewed by:
Martijn van Griensven, Maastricht University, Netherlands
Sura Al Zoubi, Al-Balqa Applied University, Jordan

***Correspondence:**
Kang Qin
kqin@ukaachen.de

†These authors have contributed equally to this work

Specialty section:
This article was submitted to Inflammation, a section of the journal Frontiers in Immunology

Received: *26 November 2021*
Accepted: *19 January 2022*
Published: *10 February 2022*

Citation:
Liang W, Greven J, Qin K, Fragoulis A, Horst K, Bläsius F, Wruck C, Pufe T, Kobbe P, Hildebrand F and Lichte P (2022) Sulforaphane Exerts Beneficial Immunomodulatory Effects on Liver Tissue via a Nrf2 Pathway-Related Mechanism in a Murine Model of Hemorrhagic Shock and Resuscitation. Front. Immunol. 13:822895. doi: 10.3389/fimmu.2022.822895

INTRODUCTION

Hemorrhagic shock (HS) remains one of the leading causes of death in traumatized patients (1) and negatively affects multiple organs of survivors by causing hypoxia, cell damage, and organ failure. This process is accompanied by a sterile inflammatory response that includes an overwhelming oxidative stress reaction (2). For the liver, as a central organ in homeostasis, a deficiency in blood supply may disrupt the hepatic cellular metabolism, leading to liver dysfunction and even failure, which is a fatal complication that leads to increased mortality rate. Hepatic Kupffer cells are well known to play a central role in these processes (3–5). As local resident macrophages, Kupffer cells serve as a major source of proinflammatory cytokines and reactive oxygen species (ROS), which are liberated during the early stages of HS (6).

The nuclear factor erythroid 2-related factor 2 (Nrf2) has been proven to exert hepatoprotective effects in case of toxin induced hepatitis. It belongs to the family of basic region leucine zipper (bZIP) transcription factors. In homeostatic conditions, Nrf2 is sequestered in the cytosol *via* the physical attachment of the N-terminal domain to the Kelch-like ECH-associated protein 1 (Keap1), which, in turn, causes the inhibition of Nrf2 activity (7). Upon the increased occurrence of oxidants, Nrf2 dissociates from Keap1 and translocate into the nucleus, interacts with the antioxidant response element (ARE), which is a DNA motif located in the upstream promoter regions, and, finally, mediates the expression of several antioxidant enzymes (8). Due to the aforementioned aspects, Nrf2 has been considered as a target for new therapeutic approaches in the treatment of several liver diseases (9).

Sulforaphane (SFN), a natural isothiocyanate, is a well-known Nrf2 pathway agonist (10). It has been reported that SFN activates Nrf2 activity in peritoneal macrophages and exerts anti-inflammatory effects *via* the inhabitation of TNF-α, IL-1β, COX-2, and iNOS expression in a murine model (11). In our previous publication, we reported the beneficial effects of *in vivo* SFN administration on lung ischemia-reperfusion damage and the systemic inflammatory response in an isolated murine HS/R model (12). It was indicated that SFN exerts anti-inflammatory effects by down-regulating multiple pro-inflammatory alveolar macrophages (AMs) generated cytokines, during which process accompanies AMs' Nrf2 pathway activation.

In this study, we investigated the effects of SFN on HS/R-induced liver damage because compared to other organs, the liver is actually well-protected from general ischemic injury due to its dual blood flow system. This system assures a rescue circulation since the blood received by the liver is shared between the portal vein and the hepatic artery (13, 14). Additionally, the highly permeable sinusoids of the liver allow increased oxygen diffusion to hepatocytes, increasing oxygen extraction to levels approaching 90% (15). However, the severe hypovolemia that occurs in the course of hemorrhagic shock can overcome even these robust supportive mechanisms and consequently damage the liver. This is of importance because the liver is the central organ of metabolism, and therefore a dysfunction of the hepatocytes has further serious consequences for the entire body. Because Nrf2 activity has been shown to be beneficial in a variety of liver injury models (9, 16–18) not only because of its cytoprotective and antioxidant properties but also because of its marked influence on metabolic pathways (19–21), the investigation of the effects of SFN-induced Nrf2 activity in our HS/R model was of great interest.

Our present study will elucidate the possible effects of SFN on liver inflammation after isolated HS/R and Nrf2-related mechanisms.

MATERIALS AND METHODS

With regard to the 3R-criteria by Russell and Burch (22), the presented results are taken from a larger project of which partial data have been published already (12).

Animal Care and Experimental Design

Our research was approved by the North Rhine-Westphalia Animal Welfare Committee (AZ 84-02.04.2017.A269). We selected male C57/BL6 wild-type (WT) mice (Charles Rivers Laboratories, Germany) and transgenic ARE-*luc* mice (Cgene, Oslo, Norway) that were 8–10 weeks old and weighed 20–30 g.

All the animals were kept for more than one week to prevent stressive factors from interfering with the stress/inflammation-related measurements. In total, 78 WT mice were divided into five groups (control, sham, HS/R, sham + SFN, and HS/R + SFN) and tested at three points of time (6 h, 24 h, and 72 h) after HS/R (**Table 1**). The number of animals was set by statistical power analysis *via* setting the confidence level at 95%, which ensured 6 animals per group was rational and statistically significant (http://powerandsamplesize.com/Calculators/Compare-k-Means/1-Way-ANOVA-Pairwise-1-Sided; https://clincalc.com/stats/samplesize.aspx). The control animals were sacrificed immediately to obtain samples, and the experimental mice were sacrificed at 6 h, 24 h, and 72 h post resuscitation. The sham animals were sacrificed at 6 h, 24 h, and 72 h post operation. Thoracotomy (with anesthesia using pentobarbital and desflurane) was performed, and the mice were exsanguinated *via* cardiac puncture. Liver tissues were collected from WT mice for myeloperoxidase (MPO) testing, hematoxylin and eosin (H&E) staining, and Suzuki score calculation. Kupffer cells were isolated and cultured for cytokine measurement. In total, 24 ARE-*luc* mice were allocated to each group (six per group) for testing the hepatic Nrf2 activity at 0 h (before surgical procedure), 6 h, and 24 h post HS/R and sham surgery. Each of ARE-*luc* mice was tested 3 times before sacrificed.

Anesthesia and Induction of HS/R

Analgesia was performed *via* preoperative (30 min) buprenorphine (Temgesic®, 0.05–0.1 mg/kg/body weight, s.c.) injection. The inhalation anesthesia was initiated with Desflurane (6%, MAC 50) in an induction box, and the anesthesia was maintained by inhalation anesthesia (1.5%, MAC 50). The mice were placed on a warming pad in a supine position. A unilateral incision of about 1 cm was made to expose

TABLE 1 | Groups distribution of WT and ARE-luc mice.

Termination post-intervention	Genotype	Control	Sham + vehicle	Sham + SFN	HS/R + vehicle	HS/R + SFN
0 h	C57/BL6 (WT)	6				
6 h	C57/BL6 (WT)		6	6	6	6
24 h	C57/BL6 (WT)		6	6	6	6
72 h	C57/BL6 (WT)		6	6	6	6
24 h	C57/BL6 (ARE-luc)		6	6	6	6

the femoral artery of the left femur, which was intubated with a sterile PE-10 polyethylene catheter (Braintree Scientific Inc., USA). Heparin (Baxter Healthcare Corporation, Deerfield, IL) (0.5 IU/g BW each) was used as an anticoagulant in the syringe during blood withdrawal and 90-min HS. The volume of blood withdrawal was shown in supplementary material (**Supplementary Table S1**). The catheter was connected to a digital blood pressure monitor (Digi-Med ®, Louisville, KY, USA), and the HS condition (MAP of 35–45 mmHg) was maintained for 90 min. The withdrawn blood was reinfused *via* infusion pump along with a 0.9% saline solution (two times the volume of the drawn blood) to perform resuscitation (0.2 ml/min). Protamine (0.5 IU/g BW each) was injected immediately after resuscitation *via* the catheter to counteract the heparin's effects. Finally, the PE catheter was removed, and the artery was ligated. Additional buprenorphine (0.05–0.1 mg/kg) was administered every 6–8 h post-surgery. The sham mice underwent the same surgical procedure without blood withdrawal.

SFN Administration

SFN (CAS registry number:142825-10-3) (50 mg/kg) was injected intraperitoneally after resuscitation in the Sham + SFN and HS/R + SFN groups. The solvent for SFN (0.9% saline) was used as the vehicle. The first SFN injection was 1.5h after hemorrhagic shock and resuscitation. In 6h and 24h groups, SFN was administrated once at 1.5h, while in 72h groups, SFN was injected 3 times at 1.5h, 24h and 48h.

Bioluminescence Imaging (BLI) of Hepatic Nrf2 Activity

The hepatic Nrf2 activity *in vivo* was evaluated with the male ARE-*luc* transgenic mice. The transcription of the luciferase gene is controlled by ARE, and the bioluminescence directly correlates with the Nrf2 activity. Measurements were performed three times for each mouse: Control measurements were performed before surgery for the determination of the baseline levels. Further measurements were performed at 6 h and 24 h after HS/R or sham surgery. A 200µl D-luciferin solution (containing 4 mg of D-luciferin; Synchem, Switzerland) was injected intraperitoneally under Desflurane inhalation anesthesia 10 min before testing, as described by Fet et al. (23). The front upper abdominal hepatic area was selected as the region of interest (ROI), and the images were recorded using a Xenogen Ivis® Lumina System. The Living Image Software 2.5 (Caliper Life Sciences, California) was used to quantify the photons emitted. The signal intensity was quantified as the sum of all photons counts per second within the ROI with reference to the background luminescence of the lower limbs. The results were presented as average radiance (photons/second/square centimeter/steradian: p/s/cm^2/sr).

Liver H&E Staining and Ischemia-Reperfusion Injury Evaluation

The right lateral lobes of the livers of the WT mice were excised under sterile conditions immediately after euthanasia and embedded in paraffin before H&E staining were performing. The liver tissues were sliced into 5–7 µm thick pieces using a microtome (Leica Biosystems, Heidelberger, Germany). Histological observation was performed using an optical microscope (Carl Zeiss, Jena, Germany) with a magnification of 200 times. Two independent researchers (WL and JG) assessed the acute liver injury scores according to the Suzuki standards (24).

MPO Testing

The accumulation of polymorphonuclear leukocytes in the livers was assessed by MPO activity. The left medial lobe of the livers from the WT mice were snap frozen in liquid nitrogen and stored at -80°C before MPO testing. The radioimmunoprecipitation (RIPA) assay buffer was used to prepare tissue homogenates by tissue lysis. An MPO-enzyme-linked immunosorbent assay (ELISA) kit (Hycultec GmbH, Beutelsbach, Germany) was used according to the manufacturer's instructions.

Isolation and Immunostaining of Kupffer Cells' Nuclear Nrf2 Translocation and Cyto-Plastic Keap1

The Kupffer cells were isolated with collagenase digestion and Percoll gradient centrifugation as previously described (25). The remaining lobes of the livers from the WT mice were perfused by HBSS (Thermo Fisher Scientific, USA) *via* the portal vein before removal. Thereafter, the liver tissues were incubated in a collagenase IV solution (Worthington, Lakewood) for 15 min at 37°C. Some of the isolated Kupffer cells was transferred to a six-well plate with a cell count of 5×10^5 per well and cultured in an incubator (37°C, 95% humidity, and 5% CO_2) for 24 h before the supernatant culture medium was stored at -80°C for ELISA testing.

The other two aliquots of Kupffer cells were immediately fixed with 4% paraformaldehyde Phosphate buffered saline (PBS) solution (pH = 7.4) at room temperature for immunofluorescence staining. The fixed Kupffer cells were then permeabilized with PBS containing 0.25% Triton X-100. After blocking with PBS containing 10% goat serum, the cells were incubated with anti-Nrf2 antibody (Abcam 137550,

England, 1:500) and anti-Keap1 antibody (Abcam 139729, London, England, 1:200) separately overnight. Then, the Kupffer cells were stained with goat anti-rabbit IgG H&L (DyLight1 488, Abcam 96895, 1:500) pre-adsorbed secondary antibodies for 1 h at room temperature. The nuclei were counter-stained with 4′,6-diamidino-2-phenylindole (DAPI). The subcellular localization of Nrf2 and cytoplastic Keap1 was observed in 20 microscopic fields (5–10 cells/field) by two independent researchers (WL and JG) with confocal fluorescence microscopy (Zeiss Axiovert 200M, Germany). Quantitative analyses of the mean density of fluorescence in the nuclei and cytoplasm were performed with the AxioVision Rel. 4.8 software (Carl Zeiss MicroImaging, LLC).

Assessment of Cytokines in Kupffer Cells' Culture Supernatant

The Kupffer cells' culture supernatant was tested for TNF-α, IL-6, human macrophage chemoattractant protein-1 (MCP-1), keratinocyte (KC), granulocyte macro-phage colony-stimulating factor (GM-CSF), and IL-10. These cytokine and chemokine levels were evaluated using mouse premixed multi-analyte kits (R&D System Inc., Minneapolis, MN, USA) according to the manufacturer's manuals.

Serum ALT and AST Levels

Serum ALT and AST levels were tested with auto-biochemical analyzer by a well-trained technician and were expressed as U/L.

Statistical Analysis

The Shapiro–Wilk test was used to determine the data distribution. Normally distributed data were expressed as mean ± SD. The interquartile range (IQR) was used if the data were non-normally distributed. Differences between the groups were determined by one-way ANOVA followed by Tukey's *post hoc* test for normally distributed data, and the non-normally distributed data were assessed using the Kruskal-Wallis test followed by Dunn's *post hoc* test. The statistical significance threshold for all analyses was set at $p < 0.05$. The statistical calculations were performed using SPSS (version 24.0.0; IBM, Armonk, NY, USA).

RESULTS

SFN's Effects on Hepatic Nrf2-ARE Activity

The BLI of the transgenic ARE-*luc* mice demonstrated that the average luminescence after HS/R was significantly increased from the baseline level of $1.2 \pm 0.3 \times 10^6$ p/s/cm^2/sr to a peak level of $7.2 \pm 0.9 \times 10^6$ p/s/cm^2/sr at 6 h post HS/R ($p < 0.01$). The SFN-treated HS/R mice showed enhanced hepatic Nrf2-ARE activity compared to the vehicle-treated mice, with a peak level being observed at 6 h after resuscitation ($23.9 \pm 3.1 \times 10^6$ p/s/cm^2/sr) ($p < 0.01$). The hepatic region of the sham animals also showed increased Nrf2-ARE activity after SFN treatment. However, the peak level of luminescence was much lower than that of the HS/R animals ($3.1 \pm 0.8 \times 10^6$ p/s/cm^2/sr) (**Figure 1**).

Effects of SFN on Nrf2 Translocation Into Kupffer Cells' Nuclei

The average fluorescence intensity of Nrf2 in the Kupffer cells' nuclei of the HS/R mice was significantly higher than that of the sham animals at 6 h ($p < 0.01$) and 24 h ($p < 0.05$) after HS/R.

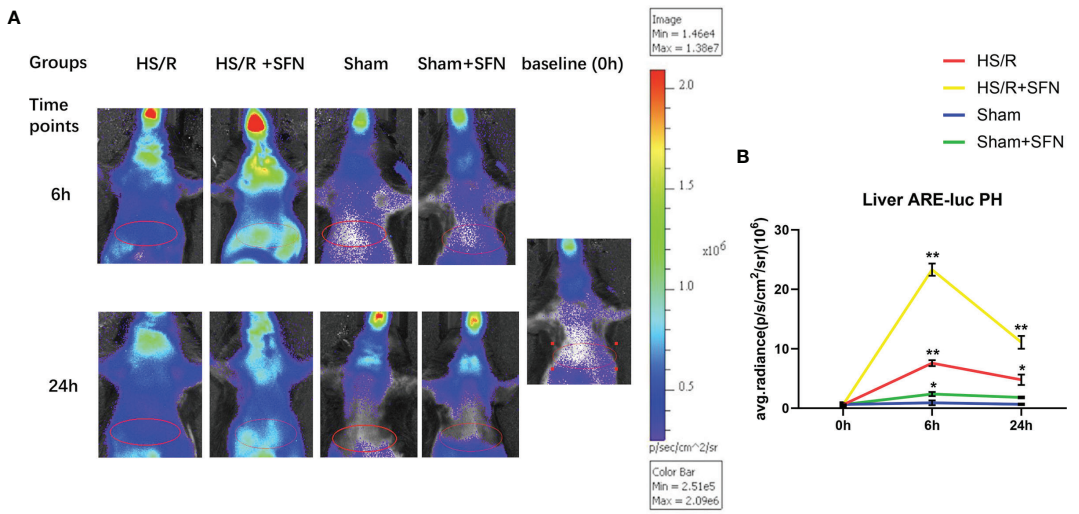

FIGURE 1 | Bioluminescence emission of the liver region of ARE-luc mice (n=6 in each group). The ARE-luc transgenic mice underwent an HS/R or sham operative procedure. The luciferase activity *in vivo* was measured *via* BLI after the intraperitoneal injection of luciferin preoperatively (0 h) and post operatively (6 h and 24 h). The red ellipses mark the selected ROIs used to evaluate signal intensity. **(A)** The representative animals for each group and time point. High signal intensities were also observed around the neck, chest, and the nasal and oral cavity. **(B)** The *in vivo* hepatic luciferase activity was recorded as the average radiance in photons per second per cm^2 per steradian (p/s/cm^2/sr), which represents the mean values for six animals and the standard deviation (*$p < 0.05$, **$p < 0.01$; One-way ANOVA followed by Tukey's *post hoc* test).

The highest Nrf2 nuclear accumulation for the HS/R animals was observed at 6 h post resuscitation. The SFN treatment significantly elevated the average fluorescence intensity of nuclear Nrf2 at 6 h ($p < 0.01$), 24 h ($p < 0.01$), and 72 h ($p < 0.05$). The Kupffer cells' average nuclear Nrf2 fluorescence intensity for the sham mice was not significantly affected by SFN treatment (**Figure 2**). Negative control of immunofluorescence is shown in supplementary material (**Supplementary Figure S1**).

Immunofluorescence Imaging of Kupffer Cells' Cytoplasmic Keap1

The average fluorescence density of the Kupffer cells' cytoplasmic Keap1 of the HS/R mice was significantly higher than that of the sham animals at 6 h ($p < 0.01$) post fluid resuscitation. SFN treatment after HS/R significantly up-regulated the average fluorescence density of cytoplasmic Keap1 at 6 h ($p < 0.01$), 24 h ($p < 0.01$), and 72 h ($p < 0.05$). The average fluorescence density of the Kupffer cells' cytoplasmic Keap1 of the sham mice was not modulated by SFN treatment (**Figure 3**).

SFN's Effects on the Cytokine Secretion of Kupffer Cells

HS/R led to significant enhancement in the Kupffer cell secretion of TNF-α, IL-6, MCP-1, KC, GM-CSF and IL-10 at three time points (6 h, 24 h, and 72 h) as compared to the sham group. The Kupffer cells of the mice that underwent *in vivo* SFN treatment after HS/R showed a significantly decreased expression of TNF-α (6 h), IL-6 (6 h and 24 h), MCP-1 (6 h), KC (6 h, 24 h, and 72 h), and IL-10 (24 h and 72h) compared to the vehicle-treated groups, while GM-CSF secretion was not significantly altered (**Figure 4**). The cytokine secretion of the sham mice was not influenced by SFN treatment.

SFN's Effects on Hepatic MPO Activity

The HS/R induced significantly elevated MPO activity at 6 h ($p < 0.05$), 24 h ($p < 0.01$), and 72 h ($p < 0.05$) post HS/R as compared to the sham animals. The *in vivo* SFN treatment was associated with a significant reduction in hepatic MPO activity as compared to the vehicle-treated animals at 6 h ($p < 0.01$) and 24 h ($p < 0.05$) post HS/R. The application of SFN had no significant effect on the MPO activity of the sham mice in our experiment (**Figure 5**).

Histological Analysis and Serum ALT and AST Level

Abnormal histological changes in the sham animals were minimal, with typical liver tissue sections that showed clear liver lobule structures. The HS/R animals showed varying degrees of inflammatory cell infiltration, loss of liver lobule tissue structure, including necrosis, steatosis, portal vein congestion, and interstitial edema, or haemorrhage. Overall, our research demonstrated a significantly higher acute liver Suzuki injury score in the HS/R animals than the sham animals (6 h, 24 h, and 72 h; $p < 0.01$). *In vivo* SFN administration is associated with a significant decrease in the

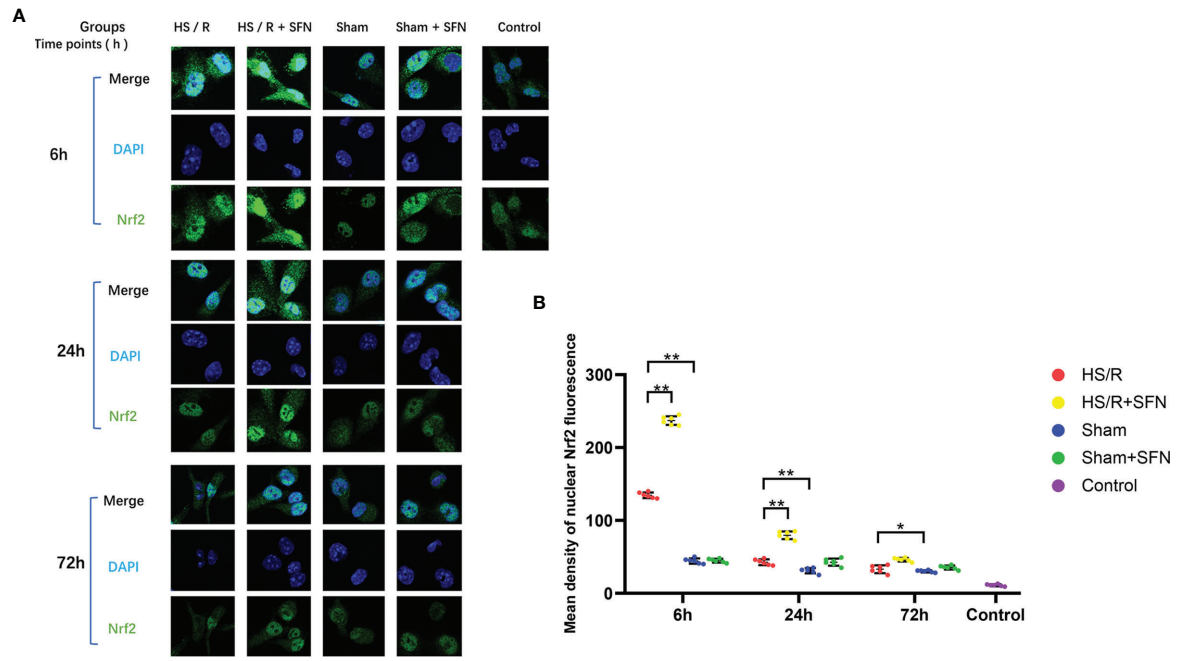

FIGURE 2 | Immunofluorescence analysis of Nrf2 nuclear translocation (n=6 in each group). **(A)** Kupffer cells were isolated from the WT mice that underwent the different experimental procedures and were fixed immediately. Nrf2 was probed with a primary anti-Nrf2 antibody and visualized with a goat anti-Rabbit DyLightH 488-conjugated secondary antibody. The nuclei were stained with DAPI. The images were taken using confocal fluorescence microscopy. **(B)** The quantitative analyses of the mean intensity of fluorescence (λ = 488nm) in the nuclei were performed with the AxioVision Rel. 4.8 software (Carl Zeiss Micro Imaging, LLC) (*$p < 0.05$, **$p < 0.01$; One-way ANOVA followed by Tukey's *post hoc* test).

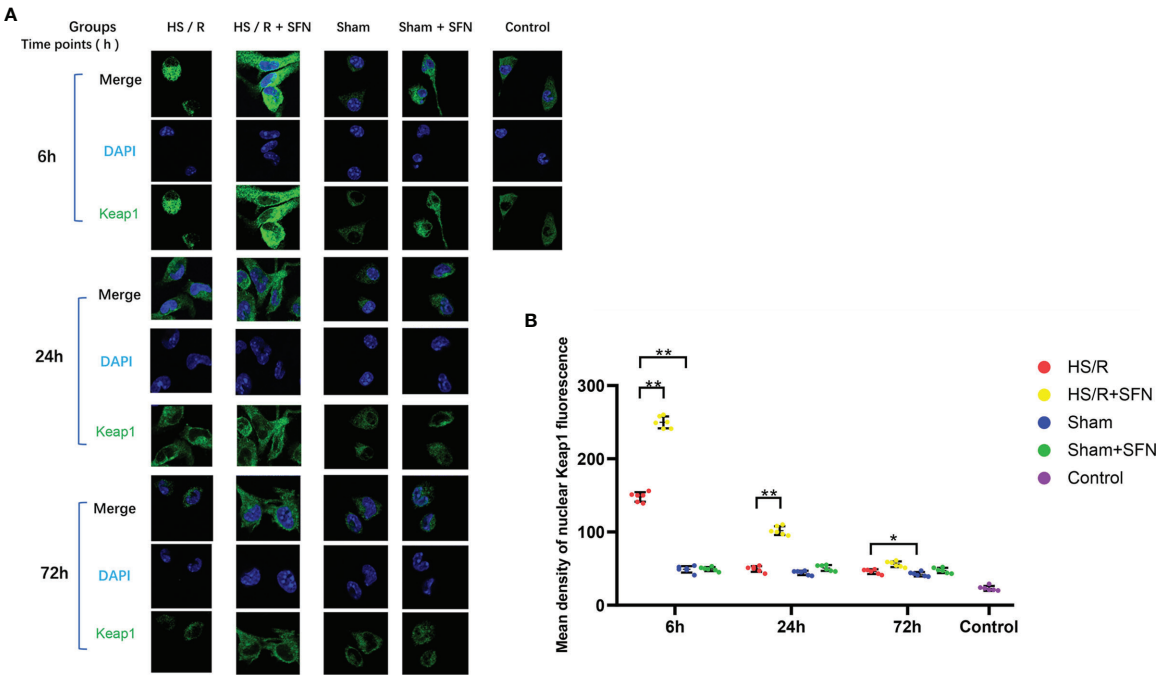

FIGURE 3 | Immunofluorescence analysis of cytoplasmic Keap1 (n=6 in each group). **(A)** Kupffer cells were isolated from the WT mice of different groups and fixed immediately. Keap1 was targeted with a primary anti-Keap1 antibody and visualized with a goat anti-Rabbit DyLightH 488-conjugated secondary antibody. The nuclei were stained with DAPI, and the images were taken using confocal fluorescence microscopy. **(B)** The quantitative analyses of the mean density of fluorescence in the nuclei were performed with the AxioVision Rel. 4.8 software (Carl Zeiss Micro Imaging, LLC) (*p < 0.05, **p < 0.01; One-way ANOVA followed by Tukey's *post hoc* test).

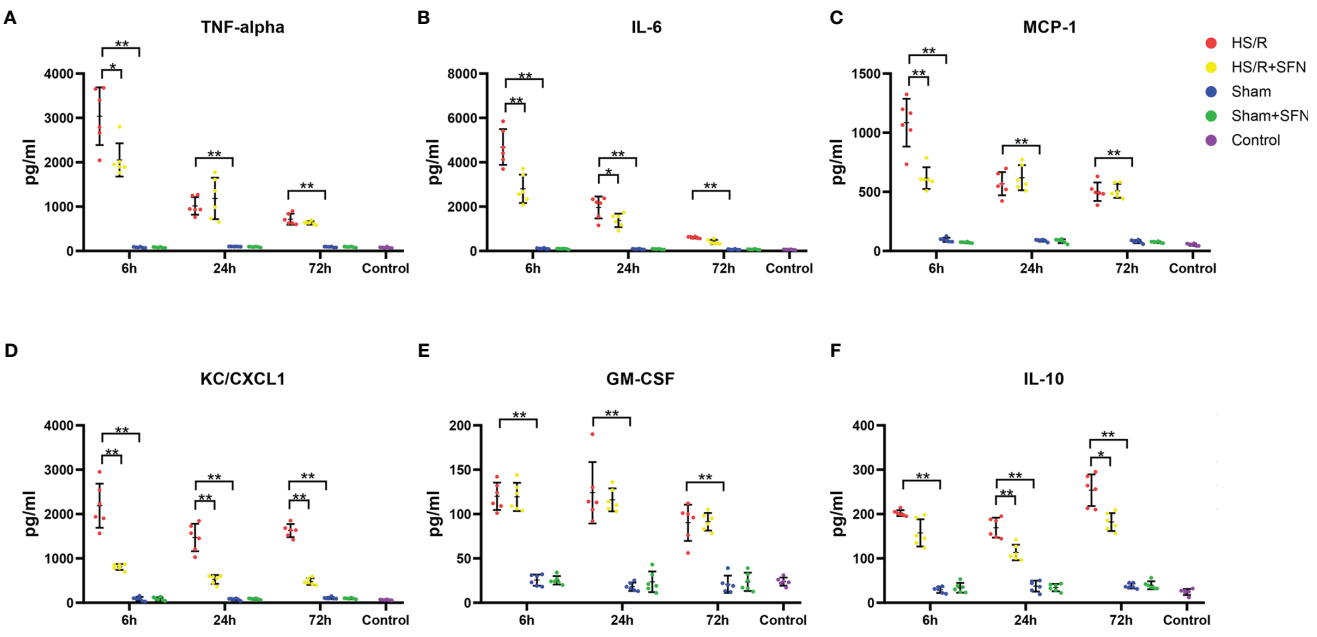

FIGURE 4 | Cytokines secreted by Kupffer cells (n=6 in each group). The TNF-α **(A)**, IL-6 **(B)**, MCP-1**(C)**, KC/CXCL1 **(D)**, GM-CSF **(E)**, and IL-10 **(F)** levels in C57/BL6 WT mouse plasma following HS/R or sham surgery with the HS/R + SFN group or sham + SFN group or without the administration of SFN (HS/R groups or sham groups). The results are expressed in pg/mL as mean ± SD. (*p < 0.05, **p < 0.01; the data of 6h group in graph **(A)** were analyzed by Kruskal-Wallis test followed by Dunn's *post hoc* test, and others were obtained with use of one-way ANOVA followed by Tukey's *post hoc* test).

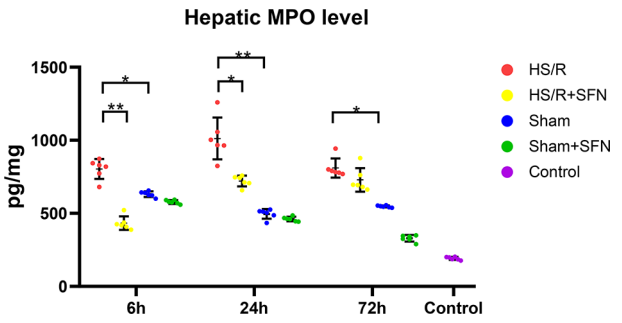

FIGURE 5 | Hepatic MPO activity (n=6 in each group). C57/BL6 WT mice following HS/R or sham surgery with HS/R + SFN or sham + SFN or without the administration of SFN (HS/R groups or sham groups). The results are expressed as pg/ml, data = mean ± SD (*p < 0.05, **p < 0.01; One-way ANOVA followed by Tukey's *post hoc* test).

Suzuki injury score at 72 h post-HS/R ($p < 0.01$) as compared to the HS/R animals that were treated with the vehicle (**Figures 6A, B**). The HS/R induced significantly elevated serum ALT level at 6 h, 24 h and 72 h (all $p < 0.01$) as compared to the sham groups. SFN treatment was associated with a significant reduction of serum ALT level as compared to the vehicle-treated animals at 6 h, 24 h and 72h (all $p < 0.01$) post HS/R. Serum AST significantly elevated at 6 h ($p < 0.01$), 24 h ($p < 0.05$) and 72 h ($p < 0.01$) post HS/R. SFN treatment down-regulated serum AST level as compared to the vehicle-treated animals at 72h ($p < 0.01$) post HS/R (**Figures 6C, D**).

DISCUSSION

HS is associated with an overwhelming formation of ROS, which promotes the liberation of multiple cytokines by hepatic localized Kupffer cells (26). Nrf2 is widely recognized as a key protective pathway against oxidative stress and hepatic inflammation (27). However, the potential beneficial effects of SFN, one of the most well-known Nrf2-ARE pathway agonists, for isolated HS/R-induced liver ischemia-reperfusion injury and sterile inflammation have not yet been sufficiently explored.

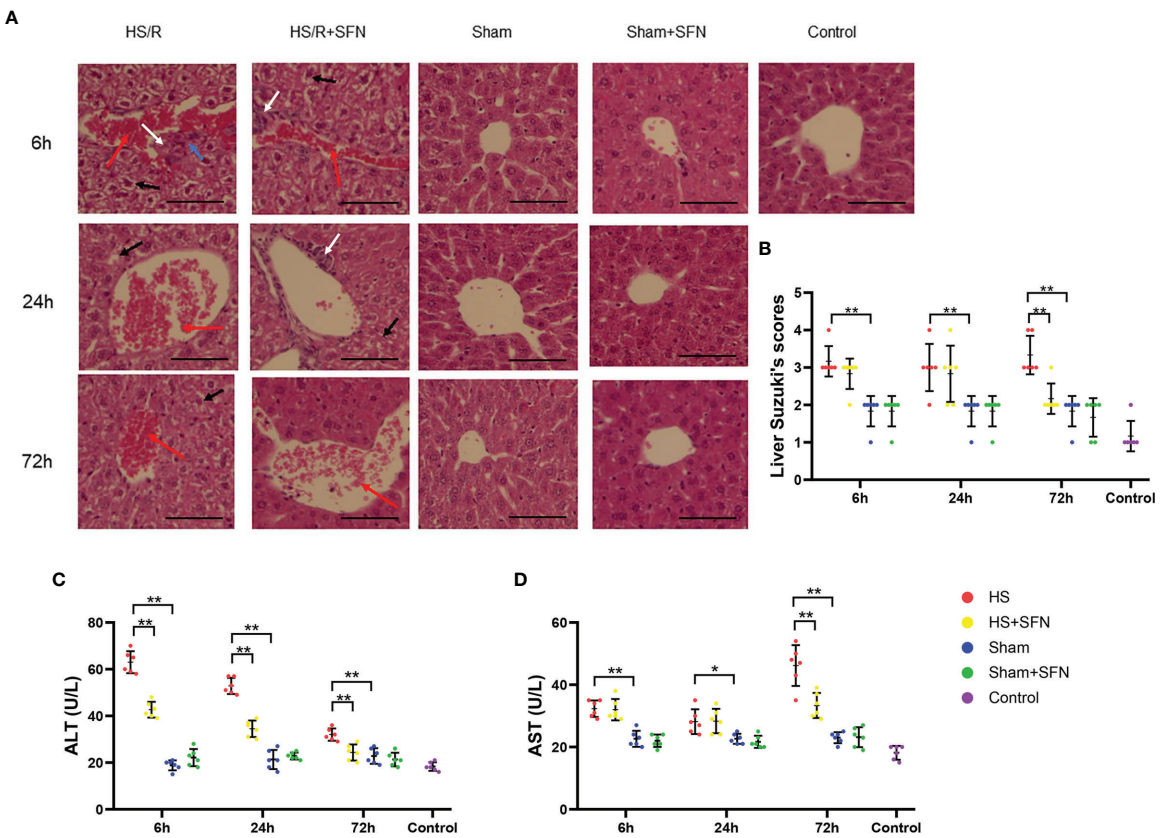

FIGURE 6 | **(A)** H&E staining liver (n=6 in each group; 200× magnification). H&E staining was performed to visualize cells and determine pathophysiological changes in them (blue arrows: hepatocyte necrosis; black arrows: hepatocyte vacuolation and steatosis; red arrows: portal vein congestion; white arrows: neutrophil infiltration). Scale bar = 50μm. **(B)** The liver injury score (according to the Suzuki standard). The liver injury score was calculated according to the scoring system that ranged from 0 to 5, as mentioned above. Every field of the sample was evaluated by two independent observers (*p < 0.05, **p < 0.01; Kruskal-Wallis test followed by Dunn's *post hoc* test). ALT **(C)** and AST **(D)** levels in C57/BL6 WT mouse plasma were expressed in U/L as mean ± SD. (n=6 in each group; *p < 0.05, **p < 0.01; One-way ANOVA followed by Tukey's *post hoc* test).

The main results of our study can be summarized as follows:

1. *In vivo* SFN administration significantly promotes hepatic Nrf2-ARE activity. After HS/R it contributes to both, Kupffer cells' cytoplasmic Nrf2-Keap1 disintegration and, in turn, Nrf2 translocation into their nuclei.
2. *In vivo* SFN treatment downregulates the isolated HS/R-induced proinflammatory cytokines, including TNF-α, MCP-1, IL-6, and KC as well as the anti-inflammatory cytokine IL-10 expressed by Kupffer cells.
3. *In vivo* SFN administration alleviates liver ischemia-reperfusion injury post HS/R and decreases MPO level.

Kudoh et al. (28) reported that the depletion of Nrf2 in mice aggravated hepatic inflammation and oxidative stress after ischemia and reperfusion (I/R), while the activation of Nrf2 significantly prevented hepatic damage. Accordingly, the results presented in the current study with increased Nrf2 activity after HS/R might be considered a compensative protective mechanism. The Kupffer cells' Nrf2 was most significantly translocated into the nucleus at 6 h post HS/R, while it showed reduced nucleus Nrf2 density later. Accordingly, the mean density of the cytoplastic Keap1 fluorescence showed a similar trend. This finding could be based on higher levels of possibly induced oxidative stress which might occur immediately after HS/R. Nevertheless, the observed natural Nrf2 activation seems to be insufficient to protect the liver from I/R damage. In fact, SFN promotes the expression of endogenous antioxidants, which are able to reduce oxidative stress. In this context, SFN has been shown to reduce oxidative stress and inflammation by activating Nrf2. Alam et al. and Fragoulis et al. (9, 29) demonstrated that SFN treatment modifies the Keap1 cysteine residues and promotes its disintegration with Nrf2, which, in turn, exerts potent Nrf2 pathway activating effects. The protective function of Nrf2 with regard to the oxidative stress on liver injuries is well described (30). In line with the current literature, we observed that *in vivo* SFN treatment promoted Kupffer cells' Nrf2 disintegration with Keap1. This was accompanied by an activated Kupffer cell Nrf2 pathway even beyond the very early phase (6 h after HS/R) and a decreased secretion of multiple proinflammatory cytokines, which may help attenuate I/R damage in the liver.

The local inflammatory status of the liver is profoundly affected by Kupffer cells. Previous studies reported that Nrf2 suppresses the macrophage-based inflammatory response by blocking proinflammatory cytokine transcription and acts as an upstream regulator of cytokine production (31). In this context, Kobayashi et al. (32) also found that Nrf2 interferes with the transcriptional upregulation of IL-6 *via* binding to the proximity of the gene and inhibits RNA Pol II recruitment in macrophages. This leads to a decreased secretion of IL-6, which is in line with the findings of this study.

It is well known that TNF-α activates cell-death pathways (33), and, therefore, the decrease in Kupffer cells' TNF-α expression of SFN-treated mice at 6 h post HS/R might be beneficial for alleviating hepatic necrosis. The Kupffer cells-produced IL-10 reached peak levels at 72 h post HS/R, while the proinflammatory cytokines' peak levels all occurred at 6 h. This may be interpreted as a classic counter balance mechanism, which was also demonstrated in polytrauma patients (SIRS/CARS) (34). Unexpectedly, we found not only pro- but also anti-inflammatory was down regulated by SFN. However, the ration of IL-6/IL-10 of HS/R group in 6h is 23.2, which is 17.8 of HS/R+SFN group. It showed that the degree of IL-6 decrease was much higher than that of IL-10 and indicated SFN exhibited anti-inflammatory properties for liver I/R injury. SFN did not show direct effects on IL-10 production at 6 h after HS/R but demonstrated a significant down-regulating effect on IL-10 at 24 h and 72 h. This could be caused directly by SFN itself or, more likely, could be driven by the lower proinflammatory trigger due to the decreased levels of proinflammatory cytokines. GM-CSF promotes inflammation in various inflammatory diseases and is generally assumed to be an efficient activator of M1 macrophage polarization (35). KC is a classical marker that indicates a potential transition from the alternative M2 to a more M1 proinflammatory phenotype (36). By contrast, IL-10 promotes reduced M1 macrophage activation and increased M2 macrophage activation (37). Thus, we can conclude that it is possible that sterile inflammation following isolated HS/R induces more Kupffer cells to polarize to the proinflammatory M1 phenotype and leads to the generation of more proinflammatory cytokines. Furthermore, Kupffer cell-produced GM-CSF may result in a positive feedback loop that augments M1 polarization (38). Nakasone et al. (31) found SFN to exert effects on the phenotypic differentiation of macrophages at non-cytotoxic concentration. SFN has the effect of shifting monocytes to specific M2-type macrophages or convert M1-polarized cells into M2 macrophages *via* a MAPK-related mechanism, which maybe another underlying explanation for our findings. Our findings indicate that SFN may yield the beneficial effects of promoting Kupffer cells' Nrf2 activation and modulating the expression of various cytokines that can potentially alleviate isolated HS/R-induced hepatic I/R injuries.

Oxidative stress and elevated inflammatory cytokines not only lead to harmful systemic effects but also potentially damage local organ tissue. Regarding the liver, inflammatory changes result in severe centrilobular congestion and hepatic dysfunction that are characterized by necrosis and vacuolization (39). Serum AST and ALT levels are the most useful indicators of liver cell injury (40). We observed significantly increase of ALT and AST post HS/R accompanying liver tissue injury as compared with sham animals.

In our study, SFN treatment for HS/R animals also led to significantly elevated Nrf2 activity of the liver tissues as compared to untreated animals. This was accompanied by significantly reduced Suzuki scores, MPO, ALT and AST levels post resuscitation. The alleviation of the liver injury may be closely related to possible lower levels of the oxidative stress which is indirectly indicated the determined higher Nrf2-ARE pathway activation, nevertheless not indicating the oxidative stress levels directly. Although MPO produced by both Kupffer cells and neutrophils, as document by literature, MPO is mainly derived from neutrophil infiltration following liver tissue injury

(41). In our present research, we found SFN exerts protective effect and attenuate necrosis, which may help reduce neutrophil infiltration and MPO level. The peak MPO level in the liver tissues at 6 h after HS/R may be also closely related to the elevated Kupffer cells' production of chemokines, especially MCP-1 and KC. We found SFN down-regulated Kupffer cells produced MCP-1 and KC, which may help reduce MPO level. Overwhelming oxidative stress promotes higher neutrophil infiltration in liver tissues as well. In addition, there is evidence showing that vascular endothelial function may be disrupted by neutrophil MPO *via* oxidative stress (42), which may be related to the severe portal venous congestion that we found in the HS/R mice. SFN administration decreased the liver MPO level at 6 h and 24 h after HS/R, which may also attribute to the Nrf2 pathway activation.

For the first time, SFN as a well-known Nrf2 pathway agonist, was applied to a rodent isolated HS/R model to observe its effects on Kupffer cells participating in hepatic sterile inflammation. Nevertheless, our study obtained positive results for SFN treatment of HS/R it underlies minor limitations. First, all operations are performed under general anesthesia in animals, which may cause regulation of cell damage. To avoid an unwanted bias, we included suitable sham and control groups in the experimental setup to be able to calculate and subtract possible shifts of the baseline from the data of the experimental groups. Furthermore, our research only studied the role of SFN in the early 72 hours post HS/R. The role of SFN in the late HS/R and the possibility of clinical application should be further confirmed. Finally, although designed to provide a clinically feasible setting, the complex injury pattern of our model is affected by many variables (such as drugs, infusions, diet, sample collection, etc.), and these variables may also affect the results.

CONCLUSION

In conclusion, our present study demonstrated that *in vivo* SFN treatment down-regulates the proinflammatory cytokines expressed by Kupffer cells after isolated HS/R. This might serve as a potential therapeutic way to protect the liver from overwhelming local sterile inflammation and ischemia-reperfusion damage induced by isolated HS/R. SFN's hepatic protective mechanism may be closely related with the Nrf2-ARE pathway activation of Kupffer cells and liver tissues. Further studies are required to elucidate the specific mechanisms and potential clinical applications of SFN.

DATA AVAILABILITY STATEMENT

The original contributions presented in the study are included in the article/**Supplementary Material**. Further inquiries can be directed to the corresponding author.

ETHICS STATEMENT

The animal study was reviewed and approved by North Rhine-Westphalia Animal Welfare Committee.

AUTHOR CONTRIBUTIONS

WL, JG, FH and PL conceived the ideas and designed the study. WL and KQ performed laboratory work. WL, JG, AF, CW, TP and PK performed the data collection. All authors analyzed data and/or provided samples and reagents. WL and KQ wrote the paper with contributions from JG, AF, KH, FB, CW, TP, PK, FH and PL. All authors contributed to the article and approved the submitted version.

FUNDING

This study was supported by the Braun Foundation (EMID: d2cd15afd6ed9f6d).

ACKNOWLEDGMENTS

We thank the Facility of the Interdisciplinary Center for Clinical Research (IZKF Aachen) for performing confocal microscopy.

SUPPLEMENTARY MATERIAL

The Supplementary Material for this article can be found online at: https://www.frontiersin.org/articles/10.3389/fimmu.2022.822895/full#supplementary-material

REFERENCES

1. Eastridge BJ, Holcomb JB, Shackelford S. Outcomes of Traumatic Hemorrhagic Shock and the Epidemiology of Preventable Death From Injury. *Transfusion* (2019) 59(S2):1423–8. doi: 10.1111/trf.15161
2. Chen H, Huang RS, Yu XX, Ye Q, Pan LL, Shao GJ, et al. Emodin Protects Against Oxidative Stress and Apoptosis in HK-2 Renal Tubular Epithelial Cells After Hypoxia/Reoxygenation. *Exp Ther Med* (2017) 14(1):447–52. doi: 10.3892/etm.2017.4473
3. Tomiyama K, Ikeda A, Ueki S, Nakao A, Stolz DB, Koike Y, et al. Inhibition of Kupffer Cell-Mediated Early Proinflammatory Response With Carbon Monoxide in Transplant-Induced Hepatic Ischemia/Reperfusion Injury in Rats. *Hepatology* (2008) 48(5):1608–20. doi: 10.1002/hep.22482
4. Kukan M, Vajdová K, Horecký J, Nagyová A, Mehendale HM, Trnovec T. Effects of Blockade of Kupffer Cells by Gadolinium Chloride on Hepatobiliary Function in Cold Ischemia-Reperfusion Injury of Rat Liver. *Hepatology* (1997) 26(5):1250–7. doi: 10.1002/hep.510260524
5. Song YK, Billiar TR, Lee YJ. Role of Galectin-3 in Breast Cancer Metastasis: Involvement of Nitric Oxide. *Am J Pathol* (2002) 160(3):1069–75. doi: 10.1016/s0002-9440(10)64927-9
6. Pinheiro D, Leirós L, Dáu JBT, Stumbo AC, Thole AA, Cortez EAC, et al. Cytokines, Hepatic Cell Profiling and Cell Interactions During Bone Marrow

Cell Therapy for Liver Fibrosis in Cholestatic Mice. *PloS One* (2017) 12(11): e0187970. doi: 10.1371/journal.pone.0187970
7. Battino M, Giampieri F, Pistollato F, Sureda A, de Oliveira MR, Pittalà V, et al. Nrf2 as Regulator of Innate Immunity: A Molecular Swiss Army Knife! *Biotechnol Adv* (2018) 36(2):358–70. doi: 10.1016/j.biotechadv.2017.12.012
8. Thimmulappa RK, Lee H, Rangasamy T, Reddy SP, Yamamoto M, Kensler TW, et al. Nrf2 is a Critical Regulator of the Innate Immune Response and Survival During Experimental Sepsis. *J Clin Invest* (2006) 116(4):984–95. doi: 10.1172/jci25790
9. Fragoulis A, Schenkel J, Herzog M, Schellenberg T, Jahr H, Pufe T, et al. Nrf2 Ameliorates DDC-Induced Sclerosing Cholangitis and Biliary Fibrosis and Improves the Regenerative Capacity of the Liver. *Toxicol Sci* (2019) 169 (2):485–98. doi: 10.1093/toxsci/kfz055
10. Zheng Y, Tao S, Lian F, Chau BT, Chen J, Sun G, et al. Sulforaphane Prevents Pulmonary Damage in Response to Inhaled Arsenic by Activating the Nrf2-Defense Response. *Toxicol Appl Pharmacol* (2012) 265(3):292–9. doi: 10.1016/j.taap.2012.08.028
11. Lin W, Wu RT, Wu T, Khor TO, Wang H, Kong AN. Sulforaphane Suppressed LPS-Induced Inflammation in Mouse Peritoneal Macrophages Through Nrf2 Dependent Pathway. *Biochem Pharmacol* (2008) 76(8):967–73. doi: 10.1016/j.bcp.2008.07.036
12. Liang W, Greven J, Fragoulis A, Horst K, Bläsius F, Wruck C, et al. Sulforaphane-Dependent Up-Regulation of NRF2 Activity Alleviates Both Systemic Inflammatory Response and Lung Injury After Hemorrhagic Shock/Resuscitation in Mice. *Shock* (2022) 57(2):221–9. doi: 10.1097/shk.0000000000001859
13. Reilly PM, Wilkins KB, Fuh KC, Haglund U, Bulkley GB. The Mesenteric Hemodynamic Response to Circulatory Shock: An Overview. *Shock* (2001) 15 (5):329–43. doi: 10.1097/00024382-200115050-00001
14. Spapen H. Liver Perfusion in Sepsis, Septic Shock, and Multiorgan Failure. *Anat Rec (Hoboken)* (2008) 291(6):714–20. doi: 10.1002/ar.20646
15. Lautt WW. Hepatic Vasculature: A Conceptual Review. *Gastroenterology* (1977) 73(5):1163–9. doi: 10.1016/S0016-5085(19)31879-7
16. Reisman SA, Buckley DB, Tanaka Y, Klaassen CD. CDDO-Im Protects From Acetaminophen Hepatotoxicity Through Induction of Nrf2-Dependent Genes. *Toxicol Appl Pharmacol* (2009) 236(1):109–14. doi: 10.1016/j.taap.2008.12.024
17. Taguchi K, Masui S, Itoh T, Miyajima A, Yamamoto M. Nrf2 Activation Ameliorates Hepatotoxicity Induced by a Heme Synthesis Inhibitor. *Toxicol Sci* (2019) 167(1):227–38. doi: 10.1093/toxsci/kfy233
18. Xu W, Hellerbrand C, Köhler UA, Bugnon P, Kan YW, Werner S, et al. The Nrf2 Transcription Factor Protects From Toxin-Induced Liver Injury and Fibrosis. *Lab Invest* (2008) 88(10):1068–78. doi: 10.1038/labinvest.2008.75
19. Yamamoto M, Kensler TW, Motohashi H. The KEAP1-NRF2 System: A Thiol-Based Sensor-Effector Apparatus for Maintaining Redox Homeostasis. *Physiol Rev* (2018) 98(3):1169–203. doi: 10.1152/physrev.00023.2017
20. Ramadori P, Drescher H, Erschfeld S, Schumacher F, Berger C, Fragoulis A, et al. Hepatocyte-Specific Keap1 Deletion Reduces Liver Steatosis But Not Inflammation During non-Alcoholic Steatohepatitis Development. *Free Radic Biol Med* (2016) 91:114–26. doi: 10.1016/j.freeradbiomed.2015.12.014
21. Wu KC, Cui JY, Klaassen CD. Effect of Graded Nrf2 Activation on Phase-I and -II Drug Metabolizing Enzymes and Transporters in Mouse Liver. *PloS One* (2012) 7(7):e39006. doi: 10.1371/journal.pone.0039006
22. Russell WMS, Burch RL. The Principles of Humane Experimental Technique. Wheathampstead: Universities Federation for Animal Welfare. (1959). Available at: https://scholar.google.com/scholar_lookup?title=The+Principles+of+Humane+Experimental+Technique&author=W+Russell&author=R+Burch&publication_year=1959&.
23. Fet N, Alizai PH, Fragoulis A, Wruck C, Pufe T, Tolba RH, et al. *In Vivo* Characterisation of the Inflammatory Reaction Following Mesh Implantation in Transgenic Mice Models. *Langenbecks Arch Surg* (2014) 399(5):579–88. doi: 10.1007/s00423-014-1192-8
24. Suzuki S, Toledo-Pereyra LH, Rodriguez FJ, Cejalvo D. Neutrophil Infiltration as an Important Factor in Liver Ischemia and Reperfusion Injury. Modulating Effects of FK506 and Cyclosporine. *Transplantation* (1993) 55(6):1265–72. doi: 10.1097/00007890-199306000-00011
25. Endo-Umeda K, Nakashima H, Komine-Aizawa S, Umeda N, Seki S, Makishima M. Liver X Receptors Regulate Hepatic F4/80 (+) CD11b(+) Kupffer Cells/Macrophages and Innate Immune Responses in Mice. *Sci Rep* (2018) 8(1):9281. doi: 10.1038/s41598-018-27615-7
26. Jaeschke H, Farhood A. Kupffer Cell Activation After No-Flow Ischemia Versus Hemorrhagic Shock. *Free Radic Biol Med* (2002) 33(2):210–9. doi: 10.1016/s0891-5849(02)00867-5
27. Shin SM, Yang JH, Ki SH. Role of the Nrf2-ARE Pathway in Liver Diseases. *Oxid Med Cell Longev* (2013) 2013:763257. doi: 10.1155/2013/763257
28. Kudoh K, Uchinami H, Yoshioka M, Seki E, Yamamoto Y. Nrf2 Activation Protects the Liver From Ischemia/Reperfusion Injury in Mice. *Ann Surg* (2014) 260(1):118–27. doi: 10.1097/sla.0000000000000287
29. Alam MB, Chowdhury NS, Sohrab MH, Rana MS, Hasan CM, Lee SH. Cerevisterol Alleviates Inflammation *via* Suppression of MAPK/NF-κb/AP-1 and Activation of the Nrf2/HO-1 Signaling Cascade. *Biomolecules* (2020) 10 (2):199. doi: 10.3390/biom10020199
30. Dinkova-Kostova AT, Fahey JW, Kostov RV, Kensler TW. KEAP1 and Done? Targeting the NRF2 Pathway With Sulforaphane. *Trends Food Sci Technol* (2017) 69(Pt B):257–69. doi: 10.1016/j.tifs.2017.02.002
31. Nakasone M, Nakaso K, Horikoshi Y, Hanaki T, Kitagawa Y, Takahashi T, et al. Preconditioning by Low Dose LPS Prevents Subsequent LPS-Induced Severe Liver Injury *via* Nrf2 Activation in Mice. *Yonago Acta Med* (2016) 59 (3):223–31.
32. Kobayashi EH, Suzuki T, Funayama R, Nagashima T, Hayashi M, Sekine H, et al. Nrf2 Suppresses Macrophage Inflammatory Response by Blocking Proinflammatory Cytokine Transcription. *Nat Commun* (2016) 7:11624. doi: 10.1038/ncomms11624
33. Li J, Ke W, Zhou Q, Wu Y, Luo H, Zhou H, et al. Tumour Necrosis Factor-α Promotes Liver Ischaemia-Reperfusion Injury Through the PGC-1α/Mfn2 Pathway. *J Cell Mol Med* (2014) 18(9):1863–73. doi: 10.1111/jcmm.12320
34. Wan S, Pan Q, Yang G, Kuang J, Luo S. Role of CYP4F2 as a Novel Biomarker Regulating Malignant Phenotypes of Liver Cancer Cells *via* the Nrf2 Signaling Axis. *Oncol Lett* (2020) 20(4):13. doi: 10.3892/ol.2020.11874
35. Benner B, Scarberry L, Suarez-Kelly LP, Duggan MC, Campbell AR, Smith E, et al. Generation of Monocyte-Derived Tumor-Associated Macrophages Using Tumor-Conditioned Media Provides a Novel Method to Study Tumor-Associated Macrophages *In Vitro*. *J Immunother Cancer* (2019) 7 (1):140. doi: 10.1186/s40425-019-0622-0
36. Martinez FO, Gordon S. The M1 and M2 Paradigm of Macrophage Activation: Time for Reassessment. *F1000Prime Rep* (2014) 6:13. doi: 10.12703/p6-13
37. Villalta SA, Rinaldi C, Deng B, Liu G, Fedor B, Tidball JG. Interleukin-10 Reduces the Pathology of Mdx Muscular Dystrophy by Deactivating M1 Macrophages and Modulating Macrophage Phenotype. *Hum Mol Genet* (2011) 20(4):790–805. doi: 10.1093/hmg/ddq523
38. Castro-Dopico T, Fleming A, Dennison TW, Ferdinand JR, Harcourt K, Stewart BJ, et al. GM-CSF Calibrates Macrophage Defense and Wound Healing Programs During Intestinal Infection and Inflammation. *Cell Rep* (2020) 32(1):107857. doi: 10.1016/j.celrep.2020.107857
39. Saafi EB, Louedi M, Elfeki A, Zakhama A, Najjar MF, Hammami M, et al. Protective Effect of Date Palm Fruit Extract (Phoenix Dactylifera L.) on Dimethoate Induced-Oxidative Stress in Rat Liver. *Exp Toxicol Pathol* (2011) 63(5):433–41. doi: 10.1016/j.etp.2010.03.002
40. Vasudevan AR, Hamirani YS, Jones PH. Safety of Statins: Effects on Muscle and the Liver. *Cleve Clin J Med* (2005) 72(11):990–3, 996-1001. doi: 10.3949/ccjm.72.11.990
41. Duval DL, Howard D, McCalden TA, Billings RE. The Determination of Myeloperoxidase Activity in Liver. *Life Sci* (1990) 47(24):Pl145–50. doi: 10.1016/0024-3205(90)90164-m
42. Xu J, Li Y, Zhang S, Jiang H, Wang N, Lin H. Identification of Tengfu Jiangya Tablet Target Biomarkers With Quantitative Proteomic Technique. *Evid Based Complement Alternat Med* (2017) 2017:7594805. doi: 10.1155/2017/7594805

Conflict of Interest: The authors declare that the research was conducted in the absence of any commercial or financial relationships that could be construed as a potential conflict of interest.

Publisher's Note: All claims expressed in this article are solely those of the authors and do not necessarily represent those of their affiliated organizations, or those of the publisher, the editors and the reviewers. Any product that may be evaluated in

this article, or claim that may be made by its manufacturer, is not guaranteed or endorsed by the publisher.

frontiers in Immunology

ORIGINAL RESEARCH
published: 24 February 2022
doi: 10.3389/fimmu.2022.824459

Fast Maturation of Splenic Dendritic Cells Upon TBI Is Associated With FLT3/FLT3L Signaling

Jin Zhang[1], Zhenghui Li[1,2], Akila Chandrasekar[1†], Shun Li[1], Albert Ludolph[1,3], Tobias Maria Boeckers[3,4], Markus Huber-Lang[5], Francesco Roselli[1,3,4‡] and Florian olde Heuvel[1‡]*

[1] Department of Neurology, Center for Biomedical Research (ZBMF), Ulm University, Ulm, Germany, [2] Department of Neurosurgery, Kaifeng Central Hospital, Kaifeng, China, [3] German Center for Neurodegenerative Diseases (DZNE) , Ulm, Germany, [4] Institute of Anatomy and Cell Biology, Ulm University, Ulm, Germany, [5] Institute of Clinical and Experimental Trauma-Immunology, University Hospital, Ulm, Germany

OPEN ACCESS

Edited by:
Katharina Schmidt-Bleek, Charité Universitätsmedizin Berlin, Germany

Reviewed by:
Kate Karelina, West Virginia University, United States
Mohammad Hossein Karimi, Shiraz University of Medical Sciences, Iran

***Correspondence:**
Florian olde Heuvel
florian.oldeheuvel@gmail.com

†Present address:
Akila Chandrasekar, Zoological Institute Braunschweig, Cellular Neurobiology - Biozentrum, Braunschweig

‡These authors share senior authorship

Specialty section:
This article was submitted to Inflammation, a section of the journal Frontiers in Immunology

Received: *29 November 2021*
Accepted: *31 January 2022*
Published: *24 February 2022*

Citation:
Zhang J, Li Z, Chandrasekar A, Li S, Ludolph A, Boeckers TM, Huber-Lang M, Roselli F and olde Heuvel F (2022) Fast Maturation of Splenic Dendritic Cells Upon TBI Is Associated With FLT3/FLT3L Signaling. Front. Immunol. 13:824459. doi: 10.3389/fimmu.2022.824459

The consequences of systemic inflammation are a significant burden after traumatic brain injury (TBI), with almost all organs affected. This response consists of inflammation and concurrent immunosuppression after injury. One of the main immune regulatory organs, the spleen, is highly interactive with the brain. Along this brain–spleen axis, both nerve fibers as well as brain-derived circulating mediators have been shown to interact directly with splenic immune cells. One of the most significant comorbidities in TBI is acute ethanol intoxication (EI), with almost 40% of patients showing a positive blood alcohol level (BAL) upon injury. EI by itself has been shown to reduce proinflammatory mediators dose-dependently and enhance anti-inflammatory mediators in the spleen. However, how the splenic immune modulatory effect reacts to EI in TBI remains unclear. Therefore, we investigated early splenic immune responses after TBI with and without EI, using gene expression screening of cytokines and chemokines and fluorescence staining of thin spleen sections to investigate cellular mechanisms in immune cells. We found a strong *FLT3*/*FLT3L* induction 3 h after TBI, which was enhanced by EI. The *FLT3L* induction resulted in phosphorylation of FLT3 in CD11c+ dendritic cells, which enhanced protein synthesis, maturation process, and the immunity of dendritic cells, shown by pS6, peIF2A, MHC-II, LAMP1, and CD68 by immunostaining and TNF-α expression by *in-situ* hybridization. In conclusion, these data indicate that TBI induces a fast maturation and immunity of dendritic cells which is associated with FLT3/FLT3L signaling and which is enhanced by EI prior to TBI.

Keywords: traumatic brain injury, spleen, FLT3, dendritic cell, ethanol

INTRODUCTION

Traumatic injury to the brain has acute, large-scale systemic consequences (1) that affect almost all organs and may lead to a compromised function of the heart, lung, gastrointestinal tract, liver, kidney, bones, lymphoid organs, and others, without direct systemic injury or infection (2, 3). The systemic response to TBI is characterized by inflammation and, at the same time, a net systemic

immunosuppression (4–6). Although brain injury results in a systemic increase of inflammatory mediators and cytokines in both patients (7–9) and rodent models of TBI (10–12), there remains ample evidence pointing toward systemic immunosuppression post-TBI, with a decrease in immune cells in the periphery (13–18). Generalized immunosuppression is highly relevant on clinical grounds, since it may contribute to an enhanced vulnerability to infections observed after severe tissue injury.

The spleen is one of the most important immune regulatory organs, involved not only in red blood cell clearance but also in the facilitation of interactions between antigen-presenting cells (APCs) and T and B lymphocytes (19). Prior investigation of the brain–spleen axis has revealed the interaction and regulation of splenic responses initiated by the central nervous system by either circulating mediators whose receptors are located on APCs (20) or by autonomic nerve fibers associated with splenic immune cells (21). There have been reports of sympathetic and parasympathetic fibers innervating dendritic cells (DCs) in the spleen (22). Furthermore, vagus nerve stimulation can reduce macrophage-induced TNF alpha release in the spleen through a so-called cholinergic anti-inflammatory pathway (23). However, it remains poorly understood whether the spleen is directly and rapidly involved in the early response to TBI.

Ethanol intoxication (EI) is a frequent comorbidity in brain injury, with almost 40% of patients showing a positive blood alcohol level (BAL) upon admission (24). Notably, the largest majority of patients showing EI in the context of TBI are not chronic alcohol consumers but rather young and often episodic weekend drinkers (the so-called "drink-and-drive" patients). Recent studies revealed that acute EI can have beneficial effects on the neuroimmunological response following experimental TBI (25–27), these findings have been supported by clinical evidence (28–30). However, some clinical studies have reported the opposite (31, 32). Animal models have demonstrated that high doses of EI reduce spleen size (33) and pro-inflammatory cytokines IL-1β and IL-6 but increase the anti-inflammatory cytokine IL-10 (34). Furthermore, EI has been shown to suppress antigen presentation by DCs (35), reflecting the immunosuppressive effects of ethanol intoxication on the spleen.

Is acute EI posited to interfere or rather to amplify the TBI-induced systemic immunoregulation, and in particular, is EI modulating TBI-induced immune reactions in the spleen? Given the high prevalence of EI in TBI patients, this question has direct clinical relevance. In this study, we investigated the effect of a single high-dose ethanol exposure prior to experimental TBI in adult mice with a focus on the immediate immunological responses in the spleen.

MATERIAL AND METHODS

Animals, Traumatic Brain Injury Model, and Ethanol Treatment

This study represents a *post-hoc* analysis of spleen samples obtained from previous studies (25, 26, 36, 37). Investigations with these samples have never been reported before, and this study was undertaken in accordance with the 3R principle, to reduce the number of mice in animal experimentation but increase the scientific output from animal sacrifice. These experiments have been approved by Ulm University Animal Experimentation Oversight Committee and by the Regierungspräsidium Tübingen (license number 1222). Male wild-type mice (B6-SJL) were bred locally under standard housing conditions (24°C, 60%–80% humidity, 12/12 light/dark cycle, with *ad libitum* access to food and water). TBI was performed on wild-type (WT) male mice aged p60–90, in agreement with epidemiological data in human TBI (38–40). Experimental TBI was performed as previously reported (25, 26, 36, 37). Briefly, mice were administered buprenorphine (0.1 mg/kg by subcutaneous injection) and anesthetized with sevoflurane (2.5% in 97.5% O_2), after which the mice were subjected to a closed head weight drop TBI model. Animals were positioned in the weight-drop apparatus, and the TBI was delivered by a weight of 333 g free falling from a height of 2 cm, targeting the parietal bone (41). Directly after the TBI, mice were administered 100% O_2, and apnea time was monitored. Control mice (sham group) had the same treatment and procedures (analgesia, anesthesia, skin incision, and handling), but without the trauma being administered. Ethanol treatment was performed as previously described (42, 43). Briefly, 100% synthesis grade ethanol was diluted in 0.9% NaCl saline to a final dilution of 32% volume/volume (32 µl of 100% ethanol and 68 µl of saline). Mice (20–25 g) were administered a volume of 400–500 µl of diluted ethanol (to obtain a concentration of 5 g/kg) by oral gavage 30 min before TBI. Four experimental groups were investigated: saline administered, subjected to sham surgery (saline-sham, SS); saline administered, subjected to TBI (saline-TBI, ST); ethanol administered, subjected to sham surgery (ethanol-sham, ES); and ethanol administered, subjected to TBI (ethanol-TBI, ET).

Tissue Isolation

Three hours post-trauma, mice were euthanized by cervical dislocation and organs were harvested for further processing. The spleen was dissected quickly and snap frozen in dry ice for further processing. Tissue was used for either RNA isolation and quantitative RT-PCR, for tissue sectioning and immunofluorescence staining.

RNA Isolation and Quantitative RT-PCR

RNA was isolated from the spleen using QIAzol (Qiagen, Germany) by disrupting and homogenizing the tissue in 1 ml QIAzol, after which 200 µl of chloroform was added and vortexed for 15 s. The samples were placed at RT for 10 min and centrifuged for 10 min 12,000×*g* at 4°C to achieve phase separation. The top layer (containing RNA) was moved to another tube and precipitated with the same amount of isopropanol. The samples were placed at RT for 10 min and centrifuged for 10 min 12,000×*g* at 4°C. The isopropanol was removed and 1 ml of 75% ethanol in DEPC-treated dH_2O was added and mixed. The samples were centrifuged for 10 min 8,000×*g* at 4°C, ethanol was removed, and the samples were air dried. The RNA pellet was redissolved in 20 µl RNAse-free

dH_2O. RNA concentration was determined by NanoDrop. Reverse transcription was performed by adding 5 µl random hexamers (Biomers, Germany) to 0.75µg RNA (total volume 40 µl diluted in dH_2O) and incubated for 10 min at 70°C. The samples were placed on ice and a master mix of 0.5µl reverse transcriptase (Promega, Germany), 0.5 µl RNase Inhibitor (RiboLock, Thermo Scientific, Germany), 2 µl dNTPs (Genaxxon, Germany), and 12 µl reverse transcriptase buffer (Promega, Germany). The samples were incubated for 10 min at RT and placed in a water bath for 45 min at 42°C. The samples were incubated for 3 min at 99°C, placed on ice, and frozen until further use.

The primers used in the present study were designed using the primer blast tool from NCBI (National Center for Biotechnology Information, USA), and sequences were found through the NCBI nucleotide search tool, GenBank. Sequences were copied into the primer blast tool and parameters were set to achieve the most optimal PCR product for the in-house lightcycler (Roche LightCycler 480 II). Briefly, the PCR product size was set from a minimum of 70 to a maximum of 140, the primer melting temperature (Tm) was set at 60°C ± 3°C, the exon junction span was set at no preference, and finally, the correct organism (*Mus musculus*) was set. The primer pair with the most optimal Tm, self-complementarity, and self-3′ complementarity was chosen. The chosen primer pairs were double-checked in the primer blast tool, to ensure specificity for the target gene. Primers were ordered from Biomers (Germany) and were validated, by performing a run on test samples together with the corresponding controls (samples without RNA and samples without reverse transcriptase) to verify the Ct value and thereby the selectivity and functioning of the primer before using them for the experiments. The detailed list of the primer sequences for each gene tested is reported in **Supplementary Table 1**.

qPCR was performed on the LightCycler 480 II (Roche) with the Power PCR TB green PCR master mix (Takara, Japan). Two microliters of sample cDNA was used in a total volume of 10 µl (3 µl primer mix and 5 µl of TB green) in a 96-well plate, all samples were duplicated, and the housekeeping gene GAPDH was used as a control (for a complete overview of cytokine sequences, see **Supplementary Table 1**). The Ct values obtained from the lightcycler were normalized according to the following equation: $2-\Delta Ct$ (ΔCt = Cttarget gene − CtGapdh) = relative mRNA.

Tissue Sectioning and Immunofluorescence Staining

Frozen spleen tissue was embedded in OCT (Tissue-Tek, The Netherlands), and 10 µm sections were cut with the cryostat and mounted on glass slides. Slides were stored for 24 h at −80°C and washed in 1× PBS, followed by a 10-min fixation step of the sections in 4% PFA. Target retrieval was performed in sodium citrate buffer pH 8.5, followed by blocking of the sections in blocking buffer (3% BSA, 0.3% Triton X-100; PBS) for 2 h at RT. The primary antibodies (for a complete overview of antibodies used, see **Supplementary Table 2**) were diluted in blocking buffer and incubated for 48 h at 4°C, followed by 3 × 30 min washes in PBS at RT. The secondary antibodies were diluted in blocking buffer and incubated for 2 h at RT, followed by 3 × 30 min washes in PBS, and the sections were mounted using Fluorogold prolong antifade mounting medium (Invitrogen, Germany).

Single mRNA *In-Situ* Hybridization

Fluorescence *in-situ* mRNA hybridization was used as previously reported (44) in agreement with the manufacturer's instructions (ACDBio, RNAscope, Newark, CA, USA fluorescence *in-situ* hybridization for fresh frozen tissue, all reagents and buffers were provided by ACDBio), with small modifications (25). Briefly, frozen spleen tissue was embedded in OCT (Tissue-Tek, the Netherlands), and 10 µm sections were cut with the cryostat and mounted on Superfrost Plus glass slides. Slides were stored for 24 h at −80°C and fixed for 10 min in 4% PFA at 4°C. Sections were covered by protease IV and incubated for 30 min at 40°C followed by 2 × 2 min washing in PBS. Both probes (TNF-α and ADRB2) were added and incubated for 4.5 h at 40°C followed by 2 × 2 min washing step with wash buffer. Then, amplification 1 was added to the sections and incubated for 30 min at 40°C followed by 2 × 2 min washing step with wash buffer. Next, amplification 2 was added to the sections and incubated for 15 min at 40°C followed by 2 × 2 min washing step with wash buffer. As a final amplification step, amplification 3 was added and incubated for 30 min at 40°C followed by 2 × 2 min washing step with wash buffer. Finally, the detection step was performed by adding detection reagent 4A to the sections and incubated for 45 min at 40°C followed by 2 × 2 min washing step with wash buffer, and then, the sections were blocked in blocking buffer (3% BSA, 0.3% Triton X-100; PBS) for 1 h at RT followed by an overnight incubation with primary antibodies diluted in blocking buffer. The sections were washed 3 × 30 min in PBST and incubated with secondary antibodies diluted in blocking buffer for 2 h at RT. A final washing step 3 × 30 min in PBST was performed and the sections were counterstained with DAPI and mounted using Fluorogold prolong antifade mounting medium (Invitrogen, Germany).

Image Acquisition and Image Analysis

Immunofluorescence staining was imaged with a Keyence BZ-X800 microscope (Keyence, Japan) equipped with a ×100 oil objective, and a single optical section with 3 × 3 tile scan was made spanning an area covering a splenic follicle and the red pulp. Acquisition parameters were set to avoid hyper- or hyposaturation and kept constant for each experimental set. Images were merged with the BZ-II analyzer software (Keyence, Japan) and analyzed using the ImageJ software. Fluorescence intensity was assessed by manually tracing the CD11c+ cells and measuring the mean gray value. Density was assessed by using the ImageJ plugin cell counter. The analyzed marker was assessed as high or low expressing, by thresholding the signal. Each picture was analyzed by making a ratio between total CD11c+/CD45+ cells and the imaged marker or the ratio between CD11c−/CD45+ cells and the imaged marker.

Single mRNA *in-situ* hybridization images were acquired using an LSM-710 (Carl Zeiss, Germany) microscope with a

×40 oil objective with optical thickness fitted to the optimum value. A z-stack of 8 images were acquired at 1,024 × 1,024 pixel resolution and 16-bit depth. Acquisition parameters were set to avoid over- and undersaturation and kept the same for each experimental set. TNF-α and beta-2 adrenergic receptor (ADRB2) mRNA density in CD11c+ cells were assessed by using the ImageJ plugin cell counter.

Statistical Analysis

Statistical analysis for the gene expression data sets (**Figures 1**, **2**) was performed using the IBM software suite, using a two-way multivariate ANOVA (with Wilk's λ parameter), because the experiment included multiple dependent variables (cytokines or chemokines) and two independent variables (TBI and ethanol treatment). The *post-hoc* comparisons were performed with

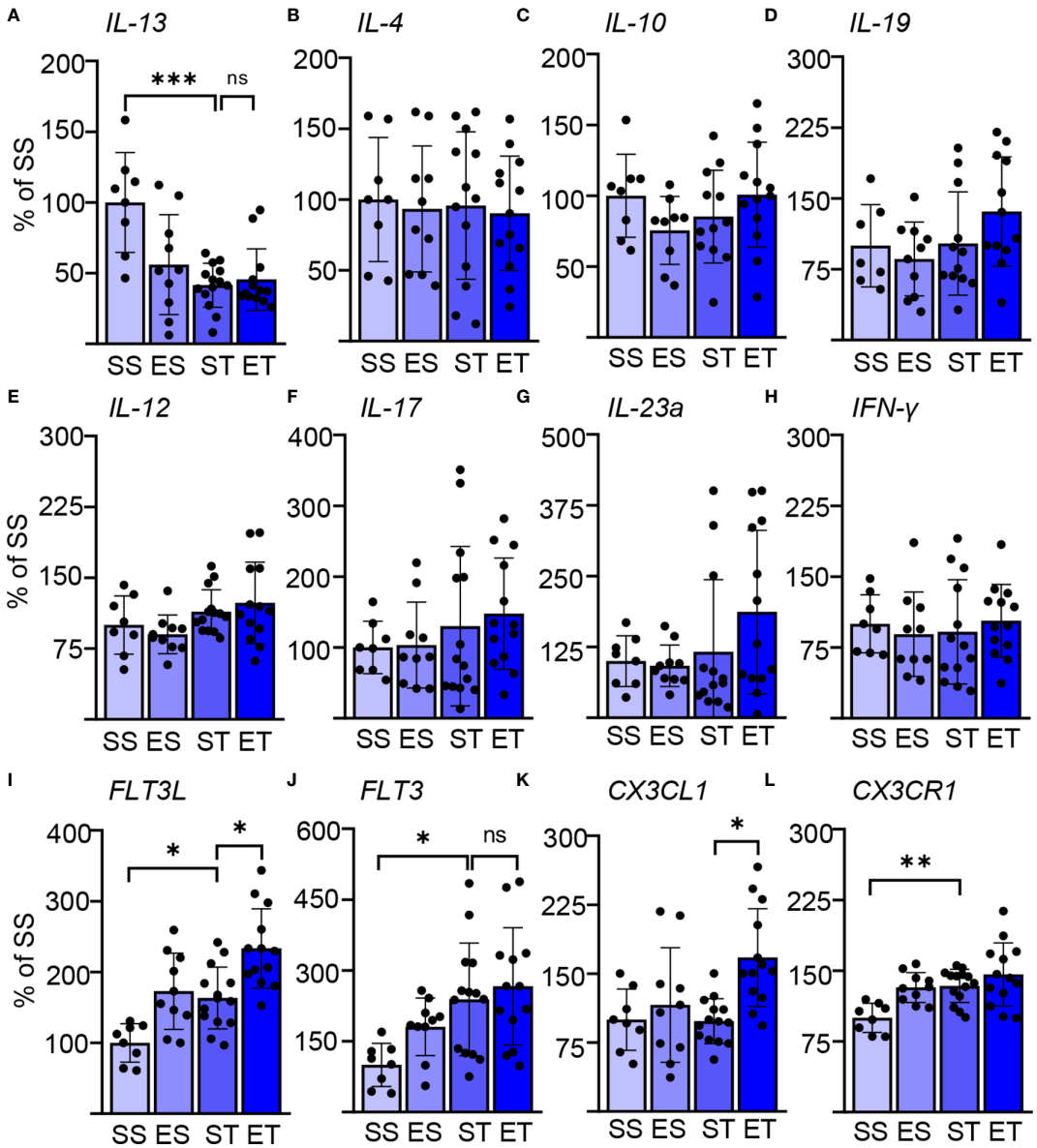

FIGURE 1 | Ethanol intoxication (EI) enhances the selective cytokine expression after traumatic brain injury (TBI). Cytokine expression screening in the spleen of saline sham (SS), ethanol sham (ES), saline TBI (ST), and ethanol TBI (ET)-treated mice 3 h after trauma. **(A–D)** Bar plots show the relative expression of Th2 cell and anti-inflammatory markers: *IL-13*, *IL-4*, *IL-10*, and *IL-19*. *IL-13* expression showed a significant downregulation after TBI (SS vs. ST; $p < 0.0005$); ethanol pretreatment did not alter the TBI-induced effect on *IL-13* (ST vs. ET; $p > 0.05$). *IL-4*, *IL-10*, and *IL-19* were not affected by any treatment. **(E–H)** Bar plots show the relative expression of Th1 cell and pro-inflammatory markers: *IL-12*, *IL-17*, *IL-23a*, and *IFN-γ*. TBI with or without ethanol pretreatment showed no significant differences. **(I–L)** Bar plots show the relative expression of dendritic cell (DC)–monocyte-specific mediators: *FLT3*, *FLT3R*, *CX3CL1*, and *CX3CR1*. TBI resulted in a significant increase of *FLT3* (SS vs. ST; $p < 0.037$), *FLT3L* (SS vs. ST; $p < 0.045$), and *CX3CR1* (SS vs. ST; $p < 0.01$). Ethanol pretreatment resulted in a further significant enhancement of *FLT3* (ST vs. ET; $p < 0.026$) and *CX3CL1* (ST vs. ET; $p < 0.006$). Data shown as bar plots and individual data points. Group size: SS N = 8, ES N = 10, ST N = 14, ET N = 13. *$p < 0.05$; **$p < 0.01$; ***$p < 0.001$; ns, not significant.

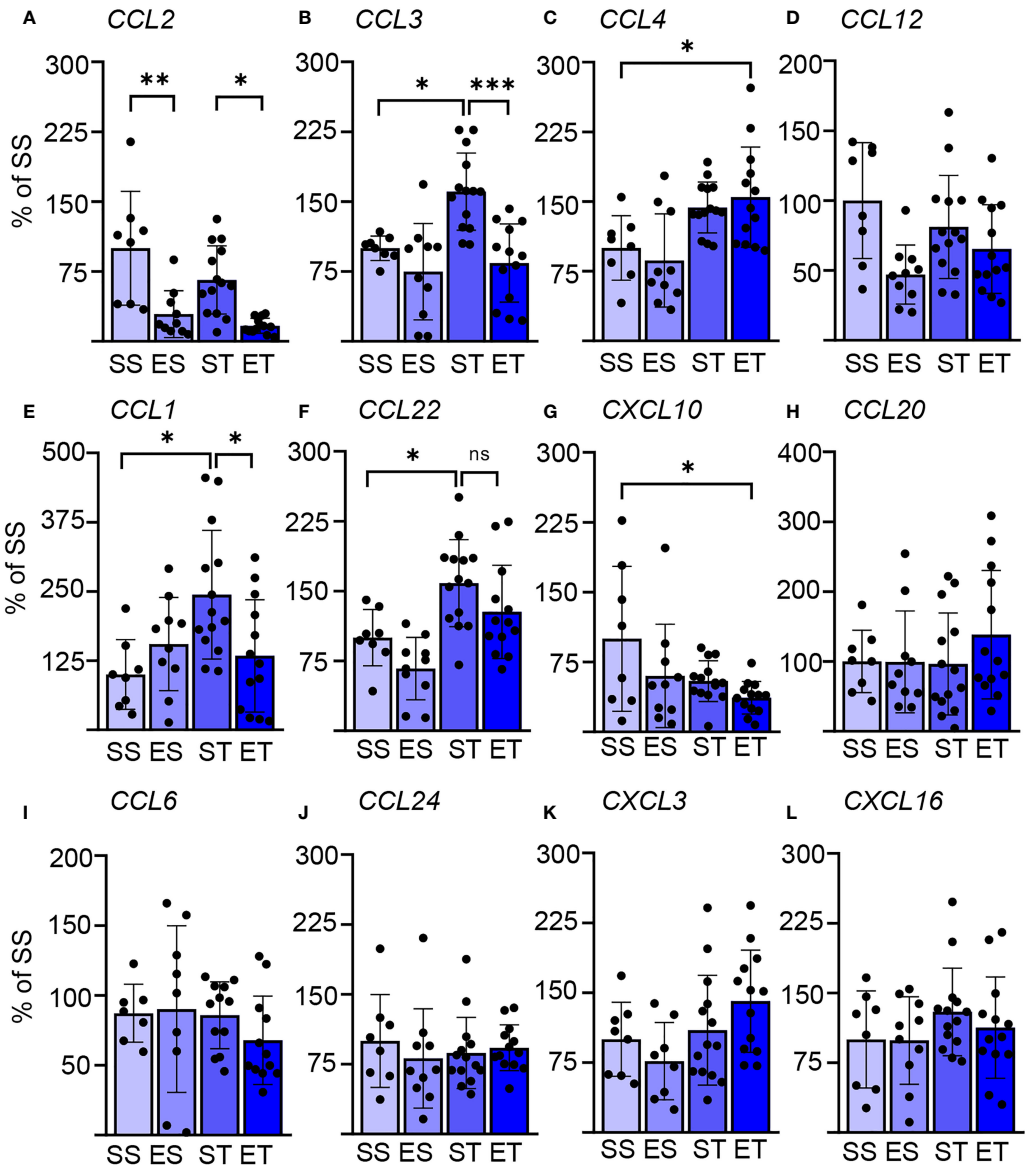

FIGURE 2 | Splenic chemokine expression shows a fast response to TBI and EI. Chemokine expression data in the spleen of saline sham (SS), ethanol sham (ES), saline TBI (ST), and ethanol TBI (ET)-treated mice 3 h after trauma. **(A–D)** Bar plots show the relative expression of modulators of DC biology: *CCL2*, *CCL3*, *CCL4*, and *CCL12*. TBI resulted in a significant upregulation of *CCL3* (SS vs. ST; $p = 0.028$), and ethanol pretreatment significantly reduced the TBI-induced *CCL3* expression (ST vs. ET; $p = 0.0006$). Ethanol by itself resulted in a significant downregulation of *CCL2*, independent of TBI (SS vs. ES, $p = 0.0021$; ST vs. ET, $p = 0.014$). ET resulted in a significant upregulation of *CCL4* compared with SS (SS vs. ET; $p = 0.042$). *CCL12* expression was not affected by any treatment. **(E–H)** Bar plots show the relative expression of modulators of Th cells: *CCL1*, *CCL22*, *CXCL10*, and *CCL20*. TBI resulted in a significant upregulation of *CCL1* (SS vs. ST; $p = 0.019$) and *CCL22* (SS vs. ST; $p = 0.039$), and ethanol pretreatment significantly reduced the TBI-induced *CCL1* expression (ST vs. ET; $p = 0.037$) but not for *CCL22* (ST vs. ET; $p = 0.35$). ET resulted in a significant downregulation of *CXCL10* compared with SS (SS vs. ET; $p = 0.014$). *CCL10* expression was not affected by any treatment. **(I–L)** Bar plots show the relative expression of modulators of leukocytes and NK cells: *CCL6*, *CCL24*, *CXCL3*, and *CXCL16*. TBI with or without ethanol pretreatment showed no significant differences. Data shown as bar plots and individual data points. Group size: SS $N = 8$, ES $N = 10$, ST $N = 14$, ET $N = 13$. $^{*}p < 0.05$; $^{**}p < 0.01$; $^{***}p < 0.001$.

two-way ANOVA with Tukey's *post-hoc* correction. All groups were tested for normality using the Shapiro–Wilk test. Correlation matrices of gene expression data were made with the Prism analysis suite (GraphPad Prism version 8), and Pearson r coefficient and p-values for every correlation were assessed. For the histological datasets, two-way ANOVA was performed with Tukey's *post-hoc* comparison, since two independent treatments were done (saline/ethanol and sham/

TBI). Statistical significance was set at $p < 0.05$ after multiple-comparison correction.

RESULTS

TBI Induces a Rapid and Selective Induction of Cytokine Upregulation in the Spleen, Enhanced by Concomitant EI

Systemic immune functions are quickly modulated by the occurrence of neurological conditions through pathways conceptualized as the "brain–spleen axis" (45–47). We set out to verify if any rapid modification in the splenic immune responses would take place upon mild/moderate TBI and, most importantly, if the comorbidity of EI would significantly interact with such responses.

As an entry point, we screened the induction of the mRNA of several cytokines (with the acknowledged limitation that mRNA levels may not directly represent protein levels) in whole-spleen extracts obtained 3 h after TBI (or sham surgery), pretreated (30 min) either with saline or with ethanol (5 g/kg).

We considered three sets of cytokines: prototypical Th1-cellular-immunity-directed, pro-inflammatory mediators (*IL-12*, *IL-17*, *IL-23a*, and *IFN-γ*); prototypical Th2-B-cell-directed, anti-inflammatory mediators (*IL-4*, *IL-10*, *IL-13*, and *IL-19*); and prototypical DC–monocyte mediators (*FLT3*, *FLT3L*, *CX3CL1*, and *CX3CR1*) (48–51). Surprisingly, we identified a significant effect of both the TBI itself and EI (two-way MANOVA; TBI: $F = 7.379$, Wilks' $\lambda = 0.253$, $p = 0.0001$; EI: $F = 4.599$, Wilks' $\lambda = 0.352$, $p = 0.0001$), and the interaction of the two parameters showed no significance in the two-way MANOVA ($F = 1.801$, Wilks' $\lambda = 0.581$, $p = 0.09$). This could be attributed (two-way ANOVA, Tukey corrected) to the significantly increased expression of *FLT3L* upon TBI alone ($F_{(3,\ 34)} = 9.771$; SS vs. ST; 100 ± 27 vs. 163 ± 44; $p = 0.045$; **Figure 1I**), *FLT3* ($F_{(3,\ 36)} = 4.266$; SS vs. ST; 100 ± 46 vs. 239 ± 119; $p = 0.037$; **Figure 1J**), and *CX3CR1* ($F_{(3,\ 41)} = 6.825$; SS vs. ST; 100 ± 16 vs. 134 ± 18; $p = 0.01$; **Figure 1L**), whereas *IL-13* was significantly downregulated ($F_{(3,\ 37)} = 7.499$; SS vs. ST; 100 ± 35 vs. 42 ± 16; $p = 0.0005$; **Figure 1A**). Ethanol intoxication before TBI resulted in a significant further enhancement of the expression of *FLT3L* (ST vs. ET; 163 ± 44 vs. 233 ± 56; $p = 0.026$; **Figure 1I**) and *CX3CL1* (ST vs. ET; 98 ± 25 vs. 168 ± 53; $p = 0.006$; **Figure 1K**), whereas *FLT3* and *CX3CR1* were unaltered in ET compared with ST (*FLT3*: ST vs. ET, 239 ± 119 vs. 266 ± 124, $p = 0.93$, **Figure 1J**; *CX3CR1*: ST vs. ET, 134 ± 18 vs. 146 ± 34, $p = 0.52$, **Figure 1L**). Most notably, no effect was observed on any of the other cytokines considered.

These screening data not only point toward a rapid activation of splenic immune cells upon TBI but also reveal a pattern compatible with a selective effect on innate immunity.

Rapid Modulation of the Splenic Chemokine Pattern by TBI and by EI/TBI

We sought to confirm and further extend the rapid effect of TBI on splenic immune cells, particularly on DCs. We assessed the expression of a set of chemokines known to be strong modulators of innate immune responses (52, 53). The focus was set, particularly on DC biology (and other APCs: *CCl2*, *CCL3*, *CCl4*, and *CCL12*) (54–56), Th cells (*CCL1*, *CCL20*, *CCL22*, and *CXCL10*) (57–60), or leukocytes and NK cells (*CCL6*, *CCl24*, *CXCL3*, and *CXCL16*) (61–64). We could identify a significant effect of TBI (two-way MANOVA: $F = 4.494$, Wilks' $\lambda = 0.357$, $p = 0.0001$) and EI ($F = 4.956$, Wilks' $\lambda = 0.335$, $p = 0.0001$), and the interaction of the two parameters showed no significant effect in the two-way MANOVA ($F = 1.776$, Wilks' $\lambda = 0.585$, $p = 0.099$). However, *post-hoc* analysis (Tukey corrected) showed that TBI alone significantly increased the expression of *CCL3* ($F_{(3,\ 37)} = 8.910$; SS vs. ST; 100 ± 13 vs. 161 ± 42; $p = 0.028$; **Figure 2B**), *CCL1* ($F_{(3,\ 39)} = 4.156$; SS vs. ST; 100 ± 63 vs. 244 ± 116; $p = 0.019$; **Figure 2E**), and *CCL22* ($F_{(3,\ 37)} = 7.483$; SS vs. ST; 100 ± 30 vs. 159 ± 47; $p = 0.039$; **Figure 2F**). On the other hand, concomitant EI significantly downregulated *CCL3* (ST vs. ET; 161 ± 42 vs. 84 ± 42; $p = 0.0006$; **Figure 2B**) and *CCL1* (ST vs. ET; 244 ± 116 vs. 134 ± 101; $p = 0.037$; **Figure 2E**), but *CCL22* was unaffected by EI and remained upregulated (ST vs. ET; 159 ± 47 vs. 128 ± 50; $p = 0.35$; **Figure 2F**). The ET group presented a distinct chemokine profile: a significant upregulation of *CCL4* was observed only in the ET group but not in the ST and ES groups alone ($F_{(3,\ 39)} = 6.093$; SS vs. ET, 100 ± 35 vs. 155 ± 54, $p = 0.042$; **Figure 2C**). Conversely, the ET group displayed the downregulation of *CXCL10* expression ($F_{(3,\ 41)} = 3.458$; SS vs. ET; 100 ± 78 vs. 37 ± 18; $p = 0.014$; **Figure 2G**). Finally, ethanol exposure alone caused a downregulation of *CCL2* in both sham and TBI groups ($F_{(3,\ 36)} = 9.679$; SS vs. ES, 100 ± 61 vs. 29 ± 25, $p = 0.0021$; ST vs. ET, 66 ± 37 vs. 17 ± 8, $p = 0.014$; **Figure 2A**).

As an additional exploration of the complex immunological interactions taking place in the spleen upon TBI with or without concomitant EI, we performed a cross-correlation analysis of the expression levels of the tested cytokines and chemokines (**Supplementary Data File 1**). We detected a significant correlation among the expression levels of *IL-17*, *IL-23*, *IL-19*, and *IFN-γ* (known to constitute a unified pathway) (65, 66) in ST and ET samples, underscoring the relevance of this cytokine module in TBI. Interestingly, *FLT3* and *FLT3L* expression was correlated in ET but not in ST samples. Furthermore, the expression levels of several chemokines (such as *CCL2*, *CCL3*, and *CCL4* vs. *CCL1*, *CCL20*, and *CCL24*) were significantly correlated in ET but not in ST samples, further underscoring the peculiar immunological milieu determined by the concomitant TBI and EI.

These data not only confirm the rapid engagement of the brain–spleen axis upon TBI but also show that EI displays a substantial modulatory effect on innate and adaptive immunity, particularly on APCs.

TBI Induces the Phosphorylation of FLT3 and Its Downstream Signaling Partner BTK in DCs, Which Are Both Enhanced by EI

Our expression screening indicated a possible upregulation of FLT3 signaling in association with a cytokine pattern compatible

with the involvement of DCs. Considering the well-known role of FLT3/FLT3L in regulating DC immunobiology (67), we sought direct confirmation of enhanced Flt3 engagement in splenic DCs upon TBI and ET. For this aim, we immunostained thin sections of the spleen from the four treatment groups for the pan-DC marker CD11c (21), for the pan-leukocyte marker CD45 (68), and phosphorylated FLT3 (pFLT3, Y589/591; **Figure 3A**). In agreement with the expression of CD45 in DC subpopulations (69), >95% of CD11c+ cells were also CD45+ (**Supplementary Figures 1D, E**). Phospho-FLT3 immunoreactivity was highly inhomogeneous in the spleen sections, with a comparatively small number of cells highly positive for pFLT3 localized around follicles and a minor number of cells with moderate pFLT3 immunoreactivity scattered in the parenchyma. Initial immunostainings revealed that CD11c density was not altered by TBI or concomitant EI (two-way ANOVA, $F_{(3,\ 12)} = 0.9360$; $p = 0.45$; **Supplementary Figures 1B, C**). Co-immunostaining with CD11c and CD45 revealed that nearly all the pFLT3^{high} cells (upon binning) were CD45+ (**Supplementary Figures 1F, G**). However, when investigating the density of pFLT3^{high} cells in CD45+/CD11c− subpopulations (labeling leukocytes other than DC), we found no significant difference among treatment groups (two-way ANOVA, $F_{(3,\ 12)} = 0.8446$; $p = 0.50$; **Supplementary Figures 1F, G**). Although the fluorescence intensity of pFLT3 in CD11c+ DCs was not altered across the four treatment groups (two-way ANOVA, $F_{(3,\ 588)} = 2.541$; $p = 0.06$; **Figure 3B**), the number of pFLT3^{high}/CD11c+ cells was significantly affected by TBI and treatment (two-way ANOVA, $F_{(3,\ 12)} = 45.84$; $p < 0.0001$), and *post-hoc* comparison (Tukey corrected) revealed a significant increase in pFLT3^{high}/CD11c+ cells after TBI alone (SS vs. ST; 20% ± 1% vs. 48% ± 4%; $p < 0.0001$; **Figure 3C**) and, interestingly, a substantial further enhancement in ET (ST vs. ET; 48 ± 4% vs. 65 ± 3%; $p = 0.0061$; **Figure 3C**), confirming that ST alone and, in particular, ET strongly induce FLT3 signaling in DCs. In order to verify that the phosphorylation of the FLT3 receptor corresponded to the functional engagement of signal transduction pathways, we monitored the phosphorylation of Bruton's tyrosine kinase (BTK), an established downstream target of FLT3 (70). Immunostaining of thin spleen sections for phosphorylated BTK (pBTK, Y223; **Figure 3D**) revealed a pattern closely resembling that of pFLT3. The fluorescence intensity of pBTK in CD11c+ cells showed a significant difference between treatment groups (two-way ANOVA, $F_{(3,\ 444)} = 123.5$; $p < 0.0001$), and a *post-hoc* comparison (Tukey corrected) showed a significant increase after TBI (SS vs. ST; 44 ± 9 vs. 48 ± 9; $p = 0.0008$; **Figure 3E**). ET resulted in a further increase of pBTK fluorescence intensity (ST vs. ET; 48 ± 9 vs. 62 ± 11; $p < 0.0001$; **Figure 3E**). Likewise, quantification of the number of pBTK^{high}/CD11c+ cells revealed a significant effect in the treatment groups (two-way ANOVA, $F_{(3,\ 12)} = 68.07$; $p < 0.0001$), due to the massive increase of pBTK^{high}/CD11c+ cells in the ST compared with the SS group (Tukey's *post-hoc*; SS vs. ST; 31% ± 6% vs. 58% ± 5%; $p < 0.0001$; **Figure 3F**), which was further increased in the ET group (ST vs. ET; 58% ± 5% vs. 67% ± 2%; $p = 0.022$; **Figure 3F**). Taken together, these data demonstrate that TBI causes fast (3 h) elevation of the phosphorylation of the FLT3 receptor (and its downstream target BTK) in splenic DCs and that this effect is substantially amplified by concomitant EI. Since CD11c+ cells were nearly always CD45+, we performed further investigations using the CD11c marker alone to identify DC.

TBI and Concomitant EI–TBI Strongly Induce Protein Synthesis in Splenic DCs

Activation of DCs is characterized by a substantial remodeling of their metabolic rates and is particularly associated with the upregulation of protein synthesis (71) which, in turn, brings about the long-term adaptation of the cellular metabolism to the immune function (72). Since FLT3 is a strong regulator of mTor (73), a major driver of protein synthesis, we set out to determine if the upregulation of FLT3 signaling observed upon TBI, and enhanced by ET, was accompanied by the activation-associated increase in protein synthesis. First, we considered the levels of phosphorylated S6 ribosomal protein (pS6), a proxy of mTOR activation directly involved in increasing ribosomal translation of mRNA. Immunostaining of thin spleen sections for phosphorylated-S6 (pS6, S235/236; **Figure 4A**) revealed a diffuse immunopositivity in the cytoplasm in nearly every cell; however, upon TBI, CD11c+ cells stood out for having a massive increase in pS6 immunofluorescence intensity (two-way ANOVA, $F_{(3,\ 465)} = 418.3$; $p < 0.0001$). The *post-hoc* comparison (Tukey corrected) showed a significant increase after TBI (SS vs. ST; 44 ± 6 vs. 70 ± 13; $p < 0.0001$; **Figure 4B**) and further enhanced in the ET group (ST vs. ET; 70 ± 13 vs. 98 ± 23; $p < 0.0001$; **Figure 4B**). This effect corresponded to the significant increase in the number of CD11c+ displaying high levels of pS6 (two-way ANOVA, $F_{(3,\ 12)} = 26.09$; $p < 0.0001$) due to the substantial elevation of pS6 occurring after TBI (Tukey's *post-hoc*; SS vs. ST; 32% ± 4% vs. 58% ± 8%; $p = 0.0002$; **Figure 4C**) but not further increased in ET compared with ST alone (ST vs. ET; 58% ± 8% vs. 65% ± 7%; $p = 0.34$; **Figure 4C**). Thus, ET magnifies the increased pS6 levels in all sensitive CD11c+ cells upon TBI but does not increase the number of cells responding to TBI itself.

Furthermore, the levels of the cellular stress-related phospho-eIF2A (71, 74) show a significant difference in fluorescence intensity in CD11c+ cells within treatment groups (two-way ANOVA, $F_{(3,\ 444)} = 8.553$; $p < 0.0001$, **Figure 4D**) due to a significant increase upon TBI (Tukey's *post-hoc*; SS vs. ST; 48 ± 10 vs. 54 ± 10; $p < 0.0001$; **Figure 4E**), again with no difference between ET and ST (ST vs. ET; 54 ± 10 vs. 52 ± 11; $p = 0.78$; **Figure 4E**). Colocalization of peIF2A^{high} cells with CD11c+ cells reveals a significant difference within treatment groups (two-way ANOVA, $F_{(3,\ 12)} = 40.50$; $p < 0.0001$). The *post-hoc* comparison (Tukey corrected) shows a significant increase after TBI (SS vs. ST; 39% ± 8% vs. 60% ± 4%; $p = 0.0001$; **Figure 4F**) with a further increase in ET compared with ST alone (ST vs. ET; 60% ± 4% vs. 67% ± 6%; $p = 0.01$; **Figure 4F**). Thus, TBI induces a substantial increase in protein synthesis, with some alteration of cap-dependent translation in DCs, and this effect is amplified by EI.

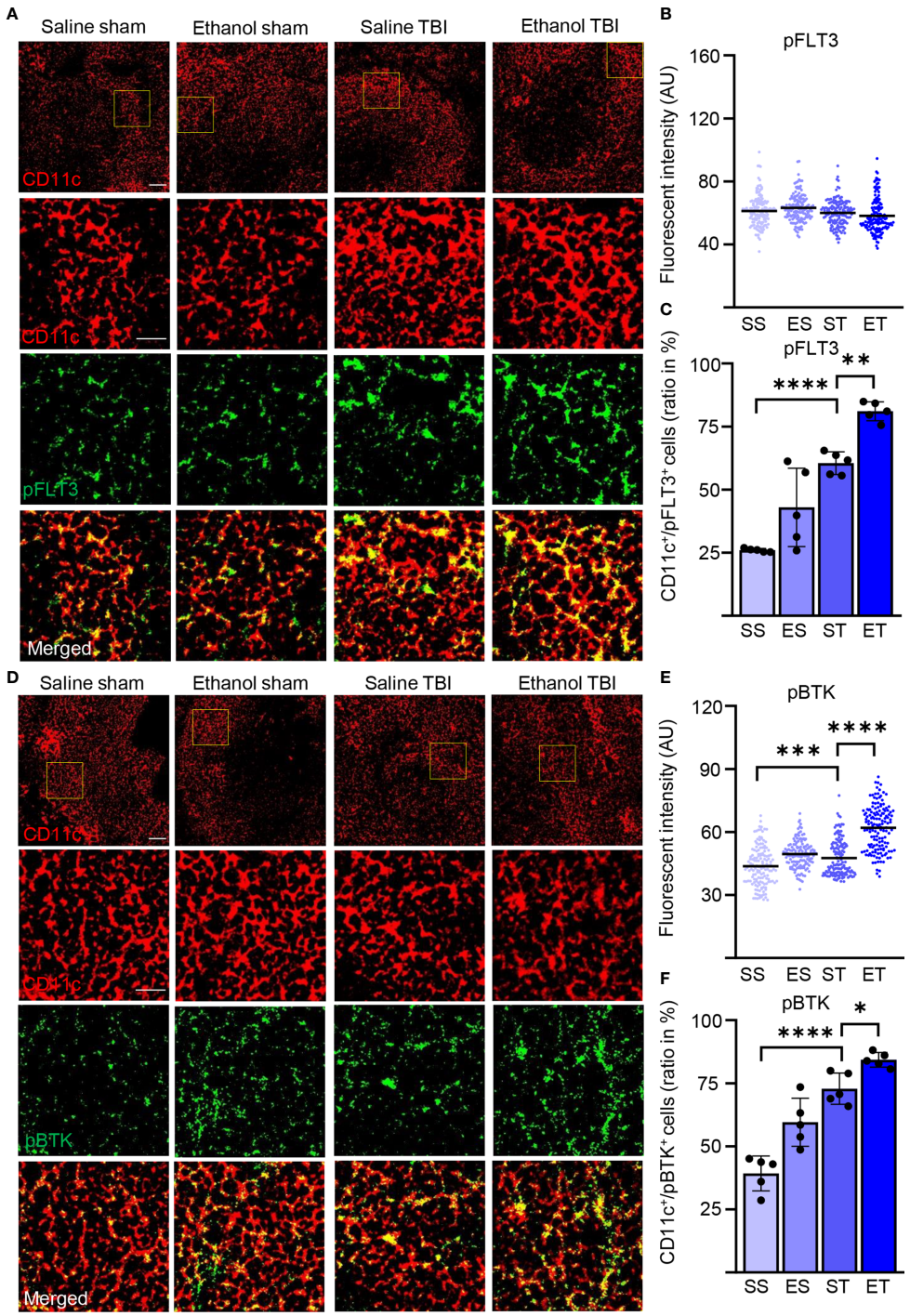

FIGURE 3 | TBI induced the phosphorylation of FLT3 and the downstream signaling partner BTK is further enhanced by EI. Immunofluorescence staining of pFLT3 and pBTK with DC marker CD11c on thin spleen sections of saline sham (SS), ethanol sham (ES), saline TBI (ST), and ethanol TBI (ET)-treated mice 3 h after trauma. **(A–C)** Immunofluorescence staining of pFLT3 colocalized with CD11c resulted in no significant difference in fluorescence intensity between treatment groups (p = 0.06). However, the amount of FLT3^{high}/CD11c+ cells revealed a significant increase after TBI (SS vs. ST; $p < 0.0001$) and a further significant enhancement in the ET group (ST vs. ET; $p = 0.006$). **(D–F)** Immunofluorescence staining of pBTK colocalized with CD11c resulted in a significant increase in fluorescence intensity upon TBI (SS vs. ST; $p = 0.0008$), with a further significant increase in the ET group (ST vs. ET; $p = 0.006$). Likewise, the number of BTK^{high}/CD11c+ cells revealed a significant increase after TBI (SS vs. ST; $p < 0.0001$) with a further significant increase after ET (ST vs. ET; $p < 0.0001$). Data shown as scatter plots or bar plots with individual data points. Group size: SS $N = 5$, ES $N = 5$, ST $N = 5$, ET $N = 5$. *$p < 0.05$; **$p < 0.01$; ***$p < 0.001$; ****$p < 0.0001$. Scale bar overview: 50 µm; scale bar insert: 20 µm.

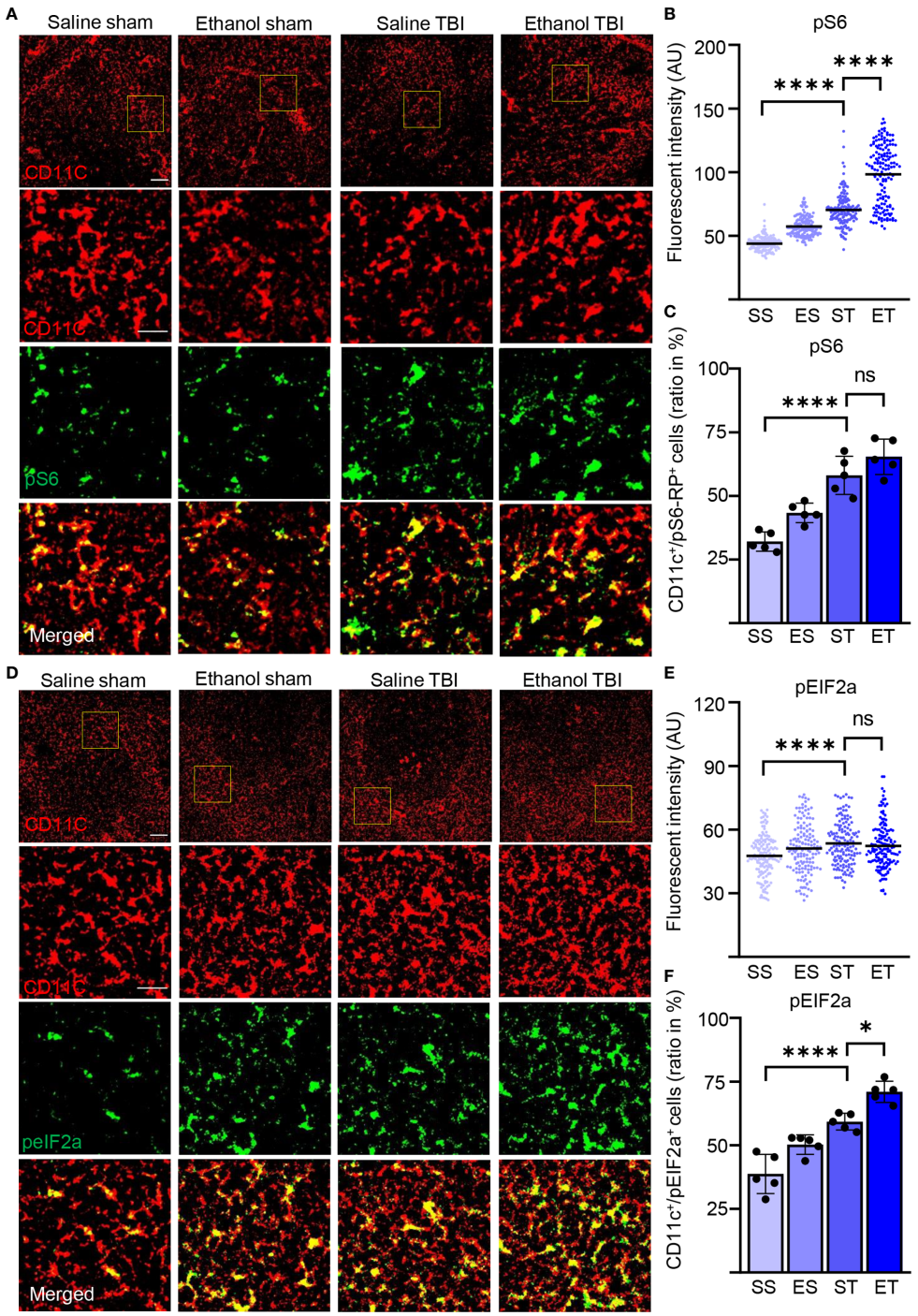

FIGURE 4 | TBI induced the metabolic rate and protein synthesis is further enhanced by EI. Immunofluorescence staining of pS6-RP and peIF2A with DC marker CD11c on thin spleen sections of saline sham (SS), ethanol sham (ES), saline TBI (ST), and ethanol TBI (ET)-treated mice 3 h after trauma. **(A–C)** Immunofluorescence staining of pS6-RP colocalized with CD11c resulted in a significant increase in fluorescence intensity upon TBI (SS vs. ST; $p < 0.0001$), with a significant enhancement in the ET group (ST vs. ET; $p < 0.0001$). The amount of pS6-RP^{high}/CD11c+ cells revealed a significant increase after TBI (SS vs. ST; $p < 0.0001$), but no significant difference in the ET group (ST vs. ET; $p = 0.34$). **(D–F)** Immunofluorescence staining of peIF2A colocalized with CD11c resulted in a significant increase in fluorescence intensity upon TBI (SS vs. ST; $p < 0.0001$), with no difference in the ET group (ST vs. ET; $p = 0.78$). The number of peIF2A^{high}/CD11c+ cells revealed a significant increase after TBI (SS vs. ST; $p = 0.0001$), with a further significant increase in the ET group (ST vs. ET; $p = 0.0107$). Data shown as scatter plots or bar plots with individual data points. Group size: SS $N = 5$, ES $N = 5$, ST $N = 5$, ET $N = 5$. *$p < 0.05$; ****$p < 0.0001$; ns, not significant. Scale bar overview: 50 µm; scale bar insert: 20 µm.

TBI and EI Cooperate to Enhance the Maturation of Splenic DCs

DC maturation occurs on stimulation with pathogen-associated molecular patterns or danger-associated molecular patterns (PAMPs or DAMPs) (75, 76). Maturation of DCs is accompanied by an increase of antigen presentation and by lysosomal activity. Antigen presentation of DCs (and macrophages) can be visualized by quantifying MHC-II expression in CD11c+ cells (77). Furthermore, enhanced antigen presentation in DC has been associated with increased phagocytic and lysosomal activity, and upregulation of lysosomal markers, including CD68 and LAMP1, has been associated with increased antigen presentation and induction of T-cell responses (78–81). We wondered if the signaling events and metabolic reprogramming observed in splenic DCs after TBI also corresponded to the appearance of a "mature" APC phenotype. Spleen sections were stained for MHC-II and CD11c (**Figure 5A**), which reveals a high amount of MHC-II in DCs upon TBI, resulting in a significant increase of fluorescence intensity within treatment groups (two-way ANOVA, $F_{(3,\ 444)} = 118.0$; $p < 0.0001$). *Post-hoc* analysis (Tukey corrected) indicated a significant increase after TBI (SS vs. ST; 26 ± 9 vs. 41 ± 11; $p < 0.0001$; **Figure 5B**) with a further increase in the ET group (ST vs. ET; 41 ± 11 vs. 45 ± 13; $p < 0.0001$; **Figure 5B**). Furthermore, when assessing the density of colocalizing MHC-II^{high} with CD11c+ cells, we found a significant increase within treatment groups (two-way ANOVA, $F_{(3,\ 12)} = 60.83$; $p < 0.0001$) due to a massive increase upon TBI (Tukey corrected; SS vs. ST; 44% ± 6% vs. 74% ± 5%; $p < 0.0001$; **Figure 5C**) and a further increase in the ET group (ST vs. ET; 74% ± 5% vs. 84% ± 4%; $p = 0.045$; **Figure 5C**). Thus, both the number of CD11c+ cells expressing MHC-II and the levels of such expression increase upon TBI and are further increased by EI.

We also assessed the lysosomal activity of splenic DCs by investigating CD68 and LAMP1 in our samples (82, 83). Immunostaining of CD68 and CD11c (**Figure 6A**) on spleen sections revealed a significant difference in intensity within treatment groups (two-way ANOVA, $F_{(3,\ 444)} = 79.68$; $p < 0.0001$) with a strong increase after TBI (Tukey corrected, SS vs. ST; 36 ± 13 vs. 51 ± 13; $p < 0.0001$; **Figure 6B**) and an even further enhancement in the ET group (ST vs. ET; 51 ± 13 vs. 63 ± 22; $p < 0.0001$; **Figure 6B**). When assessing the density of CD68^{high} cells colocalized with CD11c+ DCs, the treatment resulted in a significant difference within groups (two-way ANOVA, $F_{(3,\ 12)} = 41.25$; $p < 0.0001$) due to TBI which resulted in an increase in the amount of CD68^{high}/CD11c+ cells in the spleen (SS vs. ST; 25% ± 9% vs. 36% ± 6%; $p = 0.0007$; **Figure 6C**) and a further significant increase in ET (ST

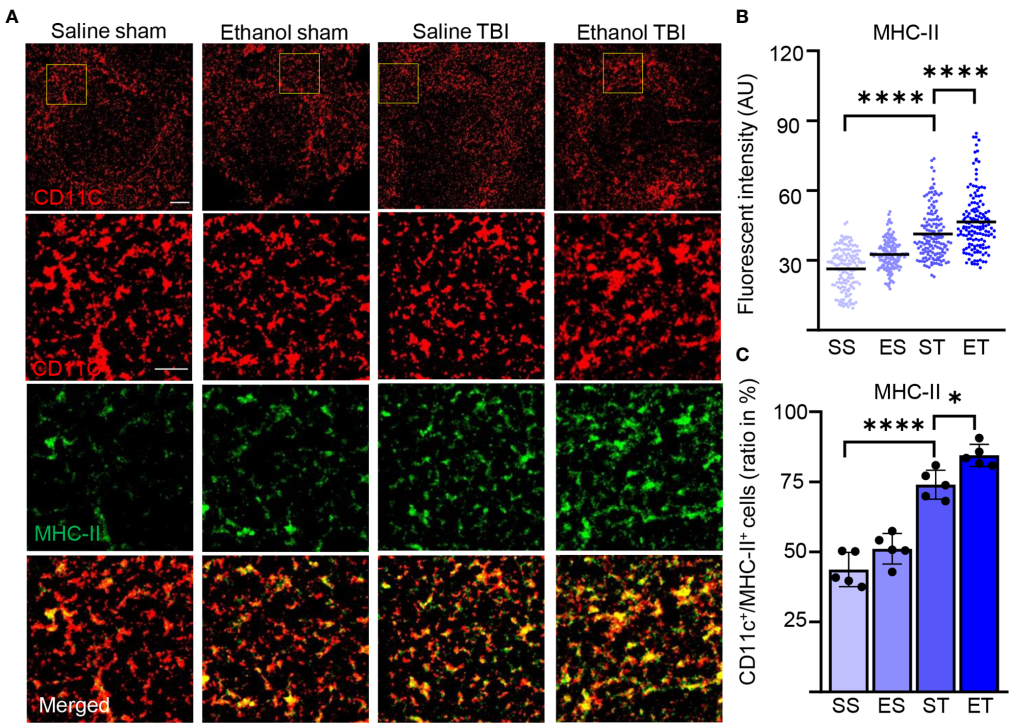

FIGURE 5 | TBI induces antigen presentation on DCs, which is further enhanced by EI. Immunofluorescence staining of MHC-II with DC marker CD11c on thin spleen sections of saline sham (SS), ethanol sham (ES), saline TBI (ST), and ethanol TBI (ET)-treated mice 3 h after trauma. **(A–C)** Immunofluorescence staining of MHC-II colocalized with CD11c resulted in a significant increase in fluorescence intensity upon TBI (SS vs. ST; $p < 0.0001$), with a significant enhancement in the ET group (ST vs. ET; $p < 0.0001$). Likewise, the amount of MHC-II^{high}/CD11c+ cells revealed a significant increase after TBI (SS vs. ST; $p < 0.0001$), with a significant enhancement in the ET group (ST vs. ET; $p = 0.045$). Data shown as scatter plots or bar plots with individual data points. Group size: SS $N = 5$, ES $N = 5$, ST $N = 5$, ET $N = 5$. *$p < 0.05$; ****$p < 0.0001$. Scale bar overview: 50 µm; scale bar insert: 20 µm.

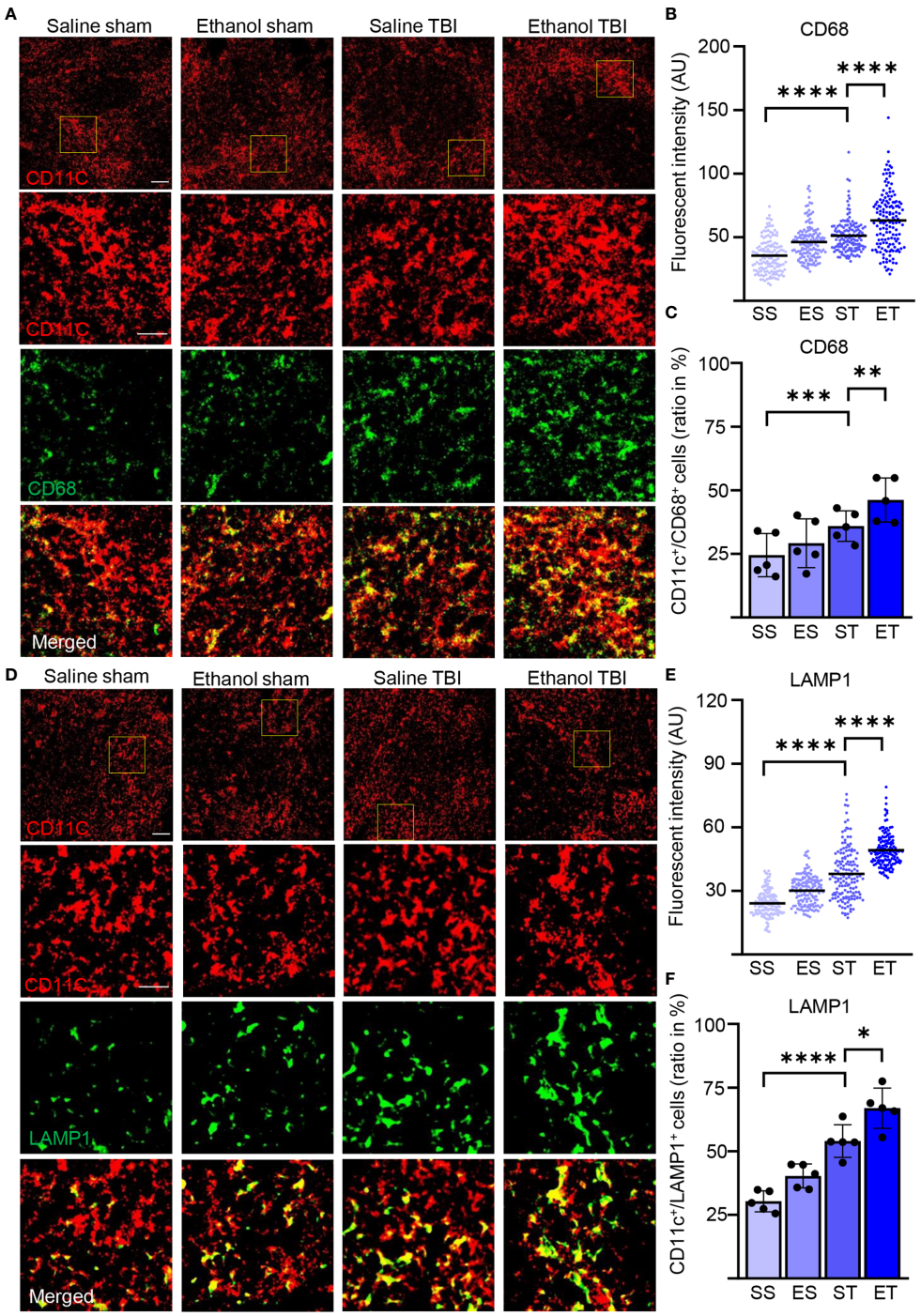

FIGURE 6 | Lysosomal activity in DCs is increased by TBI and further enhanced by EI. Immunofluorescence staining of CD68 and LAMP1 with DC marker CD11c on thin spleen sections of saline sham (SS), ethanol sham (ES), saline TBI (ST), and ethanol TBI (ET)-treated mice 3 h after trauma. **(A–C)** Immunofluorescence staining of CD68 colocalized with CD11c resulted in a significant increase in fluorescence intensity upon TBI (SS vs. ST; $p < 0.0001$), with a significant enhancement in the ET group (ST vs. ET; $p < 0.0001$). The amount of $CD68^{high}$/CD11c+ cells revealed a significant increase after TBI (SS vs. ST; $p = 0.0007$), with a significant enhancement in the ET group (ST vs. ET; $p = 0.002$). **(D–F)** Immunofluorescence staining of LAMP1 colocalized with CD11c resulted in a significant increase in fluorescence intensity upon TBI (SS vs. ST; $p < 0.0001$), with a significant increase in the ET group (ST vs. ET; $p < 0.0001$). The number of $LAMP1^{high}$/CD11c+ cells revealed a significant increase after TBI (SS vs. ST; $p = 0.0007$), with a further significant increase in the ET group (ST vs. ET; $p = 0.01$). Data shown as scatter plots or bar plots with individual data points. Group size: SS $N = 5$, ES $N = 5$, ST $N = 5$, ET $N = 5$. *$p < 0.05$; **$p < 0.01$; ***$p < 0.001$; ****$p < 0.0001$. Scale bar overview: 50 µm; scale bar insert: 20 µm.

vs. ET; 36% ± 6% vs. 46% ± 9%; $p = 0.002$; **Figure 6C**). Similarly, immunostaining of LAMP1 and CD11c (**Figure 6D**) on spleen sections revealed a significant effect on intensity within treatment groups (two-way ANOVA, $F_{(3,\ 444)} = 214.9$; $p < 0.0001$) due to a significant increase upon TBI (Tukey corrected; SS vs. ST; 24 ± 6 vs. 38 ± 12; $p < 0.0001$; **Figure 6E**), and a further significant increase was detected in the ET group (ST vs. ET; 38 ± 12.3 vs. 49.2 ± 7.6; $p < 0.0001$; **Figure 6E**). The density of LAMP1^{high} cells colocalized with CD11c+ cells exhibited a significant effect within the treatment groups (two-way ANOVA, $F_{(3,\ 12)} = 43.02$; $p < 0.0001$). The *post-hoc* comparison within the treatment groups (Tukey corrected) showed a strong significant upregulation after TBI (SS vs. ST; 30% ± 4% vs. 54% ± 6%; $p = 0.0007$; **Figure 6F**) and a further significant enhancement in ET (ST vs. ET; 54% ± 6% vs. 67% ± 8%; $p = 0.01$; **Figure 6F**). The convergence of MHC-II, LAMP1, and CD68 upregulation indicates that upon TBI, APC functions are upregulated in splenic DCs and they are further enhanced by concomitant EI.

TBI Strongly Induces the Immunogenic Function of Splenic DCs

The increased antigen presentation and lysosomal activity on CD11c+ DC, shown by the increase in MHC-II, CD68, and LAMP1, strongly suggest that TBI and EI induce a rapid maturation of splenic DC. However, the functional aspects of these mature DCs after TBI remain unclear. Initial evidence suggested that immature DCs are tolerogenic to T cells and mature DCs increase T-cell response and immunity (84, 85); however, other evidence points toward mature DCs with tolerogenic function (86, 87). To further explore the immunostimulatory phenotype of splenic DC in trauma, we assessed the expression levels of TNF-α in CD11c+ DCs. TNF-α is upregulated in DC by interaction with antigens and by stimulation of TLRs, and it is a major inducer of T-cell responses (88–90). We also considered the expression of the beta-2 adrenergic receptor, a marker associated with tolerogenic DC (91–93), under the hypothesis that expression of beta-2 adrenergic receptor and TNF-α should be inversely correlated. Fluorescence single mRNA *in-situ* hybridization was performed on spleen sections for ADRB2 and TNF-α (**Figure 7A**). Density analysis of single mRNA TNF-α in CD11c+ DCs revealed a significant difference within treatment groups (two-way ANOVA, $F_{(3,\ 267)} = 79.5$; $p < 0.0001$), due to a strong increase after TBI (Tukey corrected, SS vs. ST; 13 ± 6 vs. 22 ± 8; $p < 0.0001$; **Figure 7B**), with a further increase in the ET group (ST vs. ET; 22 ± 8 vs. 29 ± 10; $p < 0.0001$; **Figure 7B**). Furthermore, when assessing ADRB2 in CD11c+ DCs, density analysis revealed a significant difference within treatment groups (two-way ANOVA, $F_{(3,\ 267)} = 18.99$; $p < 0.0001$), due to a significant decrease after TBI (Tukey corrected, SS vs. ST; 14 ± 5 vs. 10 ± 4; $p < 0.0001$; **Figure 7C**). Interestingly, the ET group showed a strong increase in ADRB2 compared with the ST group (ST vs. ET; 10 ± 4 vs. 16 ± 7; $p < 0.0001$; **Figure 7C**). These data suggest that TBI induces an increase in immunogenic function of splenic DCs, shown by the increased TNF-α expression and decreased ADRB2 expression. Upon EI, the immunogenic function is further enhanced, shown by the increased TNF-α expression; however, the increase of ADRB2 suggests a simultaneous high sensitivity to adrenergic dampening of inflammation after EI.

DISCUSSION

Our data show that shortly (3 h) after TBI, splenic DCs undergo a maturation process that involves FLT3/FLT3L signaling, enhanced protein synthesis, increased phagocytotic and lysosome activity as well as upregulated expression of MHC-II, and finally, increased inflammatory properties, shown by TNF-α expression. Most notably, in the case of concomitant high-dose EI, the maturation process is enhanced, with increased expression of FLT3L and larger fractions of CD11c+ cells displaying elevated protein synthesis and signs of immune function activation, however with a simultaneous increased ADRB2 expression. Thus, not only does the TBI set in motion events that influence an important compartment of the systemic immune response, and even though concomitant EI is capable of substantially amplifying these cascades, it also simultaneously shows a rapid autonomic innervation.

Maturation of DCs is conceptualized as the phenotypic change from a state characterized by high endocytic capacity, low expression of co-stimulatory molecules and MHC-II, and weak induction of T-cell responses (immature dendritic cells) to a state of downregulated phagocytosis, high expression of MHC-I and MHC-II, and effective stimulation of naive T cells (77). Furthermore, maturation of DCs also involves a substantial remodeling of their metabolism, with increased mTOR-dependent protein synthesis (71, 73) and increased use of glycolytic pathways (94). DC maturation is also associated with a significant modification in the protein degradation flux, with upregulation of lysosomal markers such as LAMP3 (78) but reduced autophagy (95). Furthermore, the maturation process is intertwined with the upregulation of cytokine secretion such as TNF-α (88) and IL-12 (96). Therefore, with the demonstration of increased FLT3 phosphorylation, upregulation of protein synthesis markers, and increased expression of MHC-II and lysosomal proteins LAMP1 and CD68, we believe to provide substantial evidence to state that TBI induces a quick upregulation of the splenic DC maturation process, from steady-state cells to effective APCs. Several other markers are commonly applied to the study of DC maturation, such as CD40, CD80, and CD86 (97), which are often upregulated along with MHC-II [e.g., (98–100)]. These markers were not included in the present study and further characterization of the phenotype of splenic DC cells activated upon TBI may reveal their dynamics.

What drives such an induction of maturation? The maturation process of DCs is set in motion, among others, by PAMPs or DAMPs (75, 76), i.e., proteins released either by bacterial or viral pathogens, or by damaged tissue of the body. Indeed, the levels of brain tissue proteins and damaged markers are already elevated at 3 h in the serum of mice subject to TBI (including GFAP, NSE, S100B, and NFL) (37, 101). In particular,

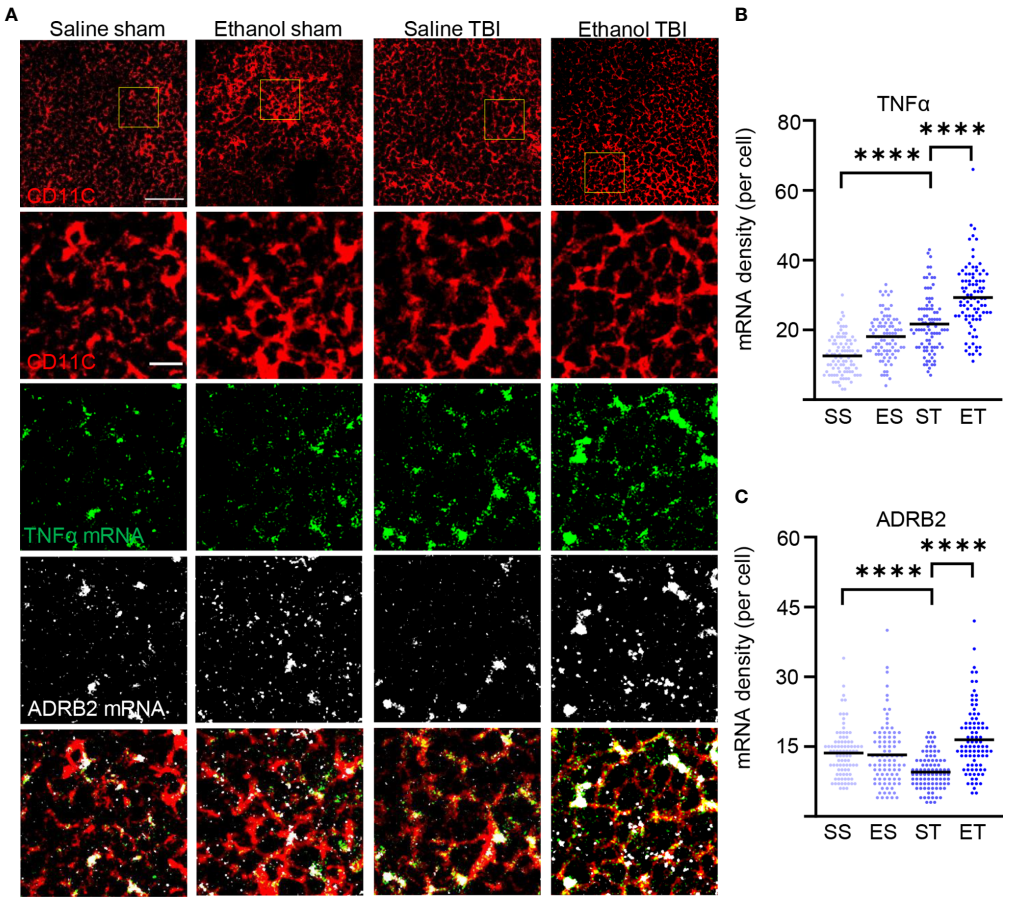

FIGURE 7 | TBI enhances TNF-α expression in splenic DCs and EI shows high sensitivity to adrenergic dampening. Fluorescence *in-situ* mRNA hybridization of TNF-α and beta-2 adrenergic receptor (ADRB2) with co-staining of DC marker CD11c on thin spleen sections of saline sham (SS), ethanol sham (ES), saline TBI (ST), and ethanol TBI (ET)-treated mice 3 h after trauma. **(A, B)** Fluorescence *in-situ* hybridization of TNF-α resulted in a significant increase in mRNA density upon TBI (SS vs. ST; $p < 0.0001$), with a significant enhancement in the ET group (ST vs. ET; $p < 0.0001$). **(A–C)** Fluorescence *in-situ* hybridization of ADRB2 resulted in a significant decrease in mRNA density upon TBI (SS vs. ST; $p < 0.0001$); however, ET shows a significant increase (ST vs. ET; $p < 0.0001$). Data shown as scatterplots. Group size: SS $N = 5$, ES $N = 5$, ST $N = 5$, ET $N = 5$. ****$p < 0.0001$. Scale bar overview: 50 µm; scale bar insert: 10 µm.

HMGB1, an alarmin located in the nucleus of neurons and glial cells and released upon brain tissue disruption (102, 103), is highly and rapidly elevated in serum after TBI (104, 105). Not only has HMGB1 been found to contribute to local neuroinflammation upon neurotrauma (106, 107), but also it is induced in non-cerebral tissues post-TBI and contributes to the subsequent systemic inflammation following TBI (10). Notably, HMGB1 is also a major inducer of DC maturation, an effect that appears to be relevant in the context of lung injury (through mTOR signaling) (108) and in liver injury (109). Nevertheless, recent evidence has demonstrated the strong involvement of the autonomic system in controlling splenic responses through adrenergic and cholinergic inputs (20, 22, 45, 110, 111). Moreover, the adrenergic activation of DCs is rather associated with limited expression of MHC-II and CD86 but strongly increases the secretion of IL-10 (112). Likewise, adrenergic stimulation of DCs substantially decreases the release of IL-12 and, in turn, suppresses the secretion of IFN-γ by Th1 lymphocytes (92). Thus, a role for the autonomic innervation in contributing to TBI-induced splenic DC maturation may take place along with the effect of systemic blood-borne cytokines.

What are the possible consequences of TBI-induced maturation of splenic DCs on local and systemic immune activation following brain injury? The net effect of the activation of the brain–spleen axis in TBI (either by circulating cytokines or by the dys-autonomia associated with TBI) seems to be detrimental, since immediate splenectomy results in an improved survival, reduced brain, and systemic cytokine response, ameliorated brain edema, and preservation of cognitive abilities in experimental rat TBI (4, 113). These effects were correlated with the decrease in NF-kB activation at the injury site (114). Similar beneficial effects of splenectomy have been reported in the context of spinal cord injury (SCI) (115) and stroke (20). However, the actual contribution of DC maturation may not necessarily be detrimental and may strongly depend on their activation status (immature, semi-mature, or

mature) (77). It was shown that DCs pulsed with myelin-basic protein could drive a protective T-cell response in SCI (116); on the other hand, autoimmune responses following TBI are associated with detrimental outcomes (117). Interestingly, DC maturation is impaired in SCI patients (118). Thus, our findings suggest that TBI causes a rapid recruitment of DCs in the spleen. Given the central role of these cells as APCs, they may be substantial contributors to the systemic imbalance of immune functions following TBI.

What is the contribution of EI-driven enhanced DC maturation upon TBI? EI has been reported to be dose-dependently associated with a reduced inflammatory response (with decreased cellular inflammation and altered cytokine pattern) at the injury site (25–27) in murine TBI models. Importantly, EI also rapidly (already at 3 h) dampens the systemic inflammatory response triggered by TBI. In particular, in murine TBI, the levels of HMGB1 and IL-6 are decreased in the liver of mice subject to ET compared with TBI alone (but IL-1β is upregulated) (10). In contrast, in the lungs, EI decreases the levels of HMGB1, IL-6, IL-1β, and TNF-α, while it moderately increases IL-10 (10). In line with this evidence, EI is associated with reduced systemic IL-6 levels and less pronounced leukocytosis in human TBI patients (119) and in patients after major traumas (including TBI) (120), as well as increased levels of IL-10 (121). Our findings suggest that EI results in an increased number of splenic DCs undergoing a maturation process, driven by increased FLT3 phosphorylation and demonstrated by the larger fraction of CD11c+ cells displaying upregulated protein synthesis (pS6) and lysosomal markers (LAMP1, CD68) as well as the induction of high levels of TNF-α mRNA. It must be stressed that our model takes into consideration an acute consumption of a high dose of ethanol ("binge"), and therefore, our findings are not directly comparable with the reports of reduced DC ability to stimulate T cells upon chronic ethanol exposure (122, 123). Nevertheless, the combination of *in-vitro* and *in-vivo* data about the effects of EI on trauma-associated inflammation suggests an overall immunosuppressive effect of EI, in agreement with the impact of chronic ethanol on DC function. If this extrapolation is sound, then the enhanced maturation of splenic DCs seen in EI/TBI samples may result in a DC phenotype with inflammation-resolution properties. This hypothesis is supported by the observed upregulation of the beta-2 adrenergic receptor in DC. Nevertheless, the combination of increased TNF-α and ADRB2 mRNA (not previously described) may correspond to a peculiar state of activation characterized by high immune-stimulatory properties and, at the same time, quick dampening from autonomic innervation. Thus, the impact of EI-driven expansion of DC maturation may ultimately contribute to the reduced systemic immune reactivity seen in TBI upon ethanol intoxication.

The present work is not without limitations. First, the ultimate evaluation of the DC function would require an active immunization protocol *in vivo* or an *ex-vivo* naive T-cell stimulation assay, which was beyond the technical scope of the present project. Second, the use of CD11c+ marker does not distinguish the subpopulation of myeloid DC or the plasmacytoid DC; we have nevertheless maintained a consistent selection of the region of interest in correspondence of the marginal zone (124).

In conclusion, our findings show that induction of maturation markers in splenic DC takes place rapidly after TBI and is highly correlated with the phosphorylation of FLT3; we further demonstrate that concomitant EI amplifies the maturation process of splenic DC post-TBI. Thus, our findings identify DC as a new player in the immunomodulation occurring upon EI in TBI.

DATA AVAILABILITY STATEMENT

The raw data supporting the conclusions of this article will be made available by the authors, without undue reservation.

ETHICS STATEMENT

The animal study was reviewed and approved by Regierungspräsidium Tübingen under licence number 1222.

AUTHOR CONTRIBUTIONS

FR and FoH conceived and designed the project. JZ, ZL, and SL performed the analysis of the spleen tissue. AC performed the TBI procedures. AL, TB, MH-L, FR, and FoH contributed to the analysis and the interpretation of the data. JZ, FR, MH-L, and FoH wrote the first draft of the manuscript. FR, FoH, JZ, ZL, SL, AL, TB, and MH-L contributed to the final version of the manuscript.

FUNDING

This work was supported by the Deutsche Forschungsgemeinschaft as part of the Collaborative Research Center 1149 "Danger Response, Disturbance Factors and Regenerative Potential after Acute Trauma" (DFG No. 251293561). JZ was supported by the Chinese Scholarship Council (ID No. 202108080183). FR was also supported by the ERANET-NEURON initiative "External Insults to the Nervous System" as part of the MICRONET consortium (funded by BMBF: FKZ 01EW1705A).

ACKNOWLEDGMENTS

We thank all the members of the CRC 1149 for their scientific input and discussion. We would like to thank Prof. Frank Kirchoff for the use of the confocal facility and Prof. Anita Ignatius for the access to the histology facility. Technical support by Thomas Lenk was highly appreciated.

SUPPLEMENTARY MATERIAL

The Supplementary Material for this article can be found online at: https://www.frontiersin.org/articles/10.3389/fimmu.2022.824459/full#supplementary-material

Supplementary Figure 1 | CD11c+ DC density is unaffected by TBI and EI. FLT3 phosphorylation remains unaltered in CD45+/CD11c- cells. Immunofluorescence staining of thin spleen sections of saline-sham (SS), ethanol-sham (ES), saline-TBI (ST) and ethanol-TBI (ET). **(A)** Immunofluorescence staining of CD11c in control groups reveals inhomogeneous distribution in thin spleen sections. With a high localisation around the follicles. **(B, C)** Density of CD11c+ cells remain unaltered 3h between treatment groups ($p = 0.45$). **(D, E)** Immunofluorescence staining of CD11c and CD45 shows that 95.3% of CD11c+ cells are CD45+. **(F, G)** immunofluorescence staining of CD45, CD11c and pFLT3 reveals unaltered phosphorylation levels of FLT3 in CD45+/CD11c- cells between treatment groups ($p = 0.50$). Data shown as barplots with individual data points. Group size: SS N = 5, ES N = 5, ST N = 5, ET N = 5. Scale bar overview A: 200 µm; scale bar insert A: 50 µm; scale bar overview B and D: 50 µm; scale bar insert D: 20 µm; scale bar overview B: 50 µm; scale bar insert F: 20 µm.

Supplementary Table 1 | Primer sequences used for gene expression analysis (RT-qPCR).

Supplementary Table 2 | Primary and secondary antibodies used for immunostaining (IF).

Supplementary Data File 1 | Correlation matrices corresponding to **Figures 1**, **2**. Correlation matrices to investigate possible correlation between cytokine and chemokine expression patterns within the treatment groups saline-sham (SS), ethanol-sham (ES), saline-TBI (ST) and ethanol-TBI (ET). A significant correlation in both ST and ET was detected between *IL-19* and *IL-17* (ST: $p < 0.0001$; ET: $p < 0.0001$), *IL-19* and *IL-23a* (ST: $p = 0.0011$; ET: $p < 0.0001$), *IL-19* and *IFN-y* (ST: $p < 0.0001$; ET: $p < 0.0001$), *IL-17* and *IL-23a* (ST: $p = 0.0002$; ET: $p < 0.0001$), *IL-17* and *IFN-y* (ST: $p < 0.0001$; ET: $p < 0.0004$) and between *IL-23a* and *IFN-y* (ST: $p = 0.0011$; ET: $p = 0.0011$). *FLT3L* was significantly correlated with *FLT3* in the ET group, but not in the ST group ($p = 0.0028$). A significant correlation only in ET, but not ST, was detected between *CCL2* and *CCL1* ($p = 0.012$), *CCL2* and *CCL20* ($p = 0.018$), *CCL3* and *CCL1* ($p = 0.0005$), *CCL3* and *CCL22* ($p = 0.049$), *CCL3* and *CCL20* ($p = 0.015$), *CCL4* and *CXCL10* ($p = 0.007$), *CCL4* and *CCL20* ($p = 0.044$), *CCL4* and *CCL24* ($p = 0.005$). Data shown as correlation matrices with Pearson r coefficient and p-values for every correlation individually.

REFERENCES

1. Sabet N, Soltani Z, Khaksari M. Multipotential and Systemic Effects of Traumatic Brain Injury. *J Neuroimmunol* (2021) 357:577619. doi: 10.1016/j.jneuroim.2021.577619
2. Rachfalska N, Putowski Z, Krzych ŁJ. Distant Organ Damage in Acute Brain Injury. *Brain Sci* (2020) 10:1–18. doi: 10.3390/brainsci10121019
3. Berthiaume L, Zygun D. Non-Neurologic Organ Dysfunction in Acute Brain Injury. *Crit Care Clin* (2006) 22:753–66. doi: 10.1016/j.ccc.2006.09.002
4. Huber-Lang M, Lambris JD, Ward PA. Innate Immune Responses to Trauma Review-Article. *Nat Immunol* (2018) 19:327–41. doi: 10.1038/s41590-018-0064-8
5. Hanscom M, Loane DJ, Shea-Donohue T. Brain-Gut Axis Dysfunction in the Pathogenesis of Traumatic Brain Injury. *J Clin Invest* (2021) 131(12): e143777. doi: 10.1172/JCI143777
6. McDonald SJ, Sharkey JM, Sun M, Kaukas LM, Shultz SR, Turner RJ, et al. Beyond the Brain: Peripheral Interactions After Traumatic Brain Injury. *J Neurotrauma* (2020) 37:770–81. doi: 10.1089/neu.2019.6885
7. Sun Y, Bai L, Niu X, Wang Z, Yin B, Bai G, et al. Elevated Serum Levels of Inflammation-Related Cytokines in Mild Traumatic Brain Injury are Associated With Cognitive Performance. *Front Neurol* (2019) 10:3389/fneur.2019.01120. doi: 10.3389/fneur.2019.01120
8. Di Battista AP, Rhind SG, Hutchison MG, Hassan S, Shiu MY, Inaba K, et al. Inflammatory Cytokine and Chemokine Profiles are Associated With Patient Outcome and the Hyperadrenergic State Following Acute Brain Injury. *J Neuroinflammation* (2016) 13:40. doi: 10.1186/s12974-016-0500-3
9. Rael LT, Bar-Or R, Mains CW, Slone DS, Levy AS, Bar-Or D. Plasma Oxidation-Reduction Potential and Protein Oxidation in Traumatic Brain Injury. *J Neurotrauma* (2009) 26:1203–11. doi: 10.1089/neu.2008.0816
10. Xu B, Chandrasekar A, Heuvel FO, Powerski M, Nowak A, Noack L, et al. Ethanol Intoxication Alleviates the Inflammatory Response of Remote Organs to Experimental Traumatic Brain Injury. *Int J Mol Sci* (2020) 21:1–15. doi: 10.3390/ijms21218181
11. Qian Y, Gao C, Zhao X, Song Y, Luo H, An S, et al. Fingolimod Attenuates Lung Injury and Cardiac Dysfunction After Traumatic Brain Injury. *J Neurotrauma* (2020) 37:2131–40. doi: 10.1089/neu.2019.6951
12. Villapol S, Kryndushkin D, Balarezo MG, Campbell AM, Saavedra JM, Shewmaker FP, et al. Hepatic Expression of Serum Amyloid A1 Is Induced by Traumatic Brain Injury and Modulated by Telmisartan. *Am J Pathol* (2015) 185:2641–52. doi: 10.1016/j.ajpath.2015.06.016
13. Kong XD, Bai S, Chen X, Wei HJ, Jin WN, Li MS, et al. Alterations of Natural Killer Cells in Traumatic Brain Injury. *Neurosci Bull* (2014) 30:903–12. doi: 10.1007/s12264-014-1481-9
14. Mrakovcic-Sutic I, Tokmadzic VS, Laskarin G, Mahmutefendic H, Lucin P, Zupan Z, et al. Early Changes in Frequency of Peripheral Blood Lymphocyte Subpopulations in Severe Traumatic Brain-Injured Patients. *Scand J Immunol* (2010) 72:57–65. doi: 10.1111/j.1365-3083.2010.02407.x
15. Schwulst SJ, Trahanas DM, Saber R, Perlman H. Traumatic Brain Injury-Induced Alterations in Peripheral Immunity. *J Trauma Acute Care Surg* (2013) 75:780–8. doi: 10.1097/ta.0b013e318299616a
16. Liao Y, Liu P, Guo F, Zhang ZY, Zhang Z. Oxidative Burst of Circulating Neutrophils Following Traumatic Brain Injury in Human. *PloS One* (2013) 8 (7):e68963. doi: 10.1371/journal.pone.0068963
17. Vermeij JD, Aslami H, Fluiter K, Roelofs JJ, Van Den Bergh WM, Juffermans NP, et al. Traumatic Brain Injury in Rats Induces Lung Injury and Systemic Immune Suppression. *J Neurotrauma* (2013) 30:2073–9. doi: 10.1089/neu.2013.3060
18. Ritzel RM, Doran SJ, Barrett JP, Henry RJ, Ma EL, Faden AI, et al. Chronic Alterations in Systemic Immune Function After Traumatic Brain Injury. *J Neurotrauma* (2018) 35(13):1419–36. doi: 10.1089/neu.2017.5399
19. Lewis SM, Williams A, Eisenbarth SC. Structure and Function of the Immune System in the Spleen. *Sci Immunol* (2019) 4(33):eaau6085. doi: 10.1126/sciimmunol.aau6085
20. Ajmo CT, Collier LA, Leonardo CC, Hall AA, Green SM, Womble TA, et al. Blockade of Adrenoreceptors Inhibits the Splenic Response to Stroke. *Exp Neurol* (2009) 218:47–55. doi: 10.1016/j.expneurol.2009.03.044
21. Hu D, Al-Shalan HAM, Shi Z, Wang P, Wu Y, Nicholls PK, et al. Distribution of Nerve Fibers and Nerve-Immune Cell Association in Mouse Spleen Revealed by Immunofluorescent Staining. *Sci Rep* (2020) 10 (1):9850. doi: 10.1038/s41598-020-66619-0
22. Takenaka MC, Guereschi MG, Basso AS. Neuroimmune Interactions: Dendritic Cell Modulation by the Sympathetic Nervous System. *Semin Immunopathol* (2017) 39:165–76. doi: 10.1007/s00281-016-0590-0
23. Wang H, Yu M, Ochani M, Amelia CA, Tanovic M, Susarla S, et al. Nicotinic Acetylcholine Receptor α7 Subunit is an Essential Regulator of Inflammation. *Nature* (2003) 421:384–8. doi: 10.1038/nature01339
24. Bjarkø VV, Skandsen T, Moen KG, Gulati S, Helseth E, Nilsen TIL, et al. Time of Injury and Relation to Alcohol Intoxication in Moderate-To-Severe Traumatic Brain Injury: A Decade-Long Prospective Study. *World Neurosurg* (2019) 122:e684–9. doi: 10.1016/j.wneu.2018.10.122
25. Olde Heuvel F, Holl S, Chandrasekar A, Li Z, Wang Y, Rehman R, et al. STAT6 Mediates the Effect of Ethanol on Neuroinflammatory Response in TBI. *Brain Behav Immun* (2019) 81:228–46. doi: 10.1016/j.bbi.2019.06.019
26. Chandrasekar A, olde Heuvel F, Palmer A, Linkus B, Ludolph AC, Boeckers TM, et al. Acute Ethanol Administration Results in a Protective Cytokine and Neuroinflammatory Profile in Traumatic Brain Injury. *Int Immunopharmacol* (2017) 51:66–75. doi: 10.1016/j.intimp.2017.08.002
27. Goodman MD, Makley AT, Campion EM, Friend LAW, Lentsch AB, Pritts TA. Preinjury Alcohol Exposure Attenuates the Neuroinflammatory

Response to Traumatic Brain Injury. *J Surg Res* (2013) 184:1053–8. doi: 10.1016/j.jss.2013.04.058
28. Brigode W, Cohan C, Beattie G, Victorino G. Alcohol in Traumatic Brain Injury: Toxic or Therapeutic? *J Surg Res* (2019) 244:196–204. doi: 10.1016/j.jss.2019.06.043
29. Raj R, Mikkonen ED, Siironen J, Hernesniemi J, Lappalainen J, Skrifvars MB. Alcohol and Mortality After Moderate to Severe Traumatic Brain Injury: A Meta-Analysis of Observational Studies. *J Neurosurg* (2016) 124:1684–92. doi: 10.3171/2015.4.JNS141746
30. Brennan JH, Bernard S, Cameron PA, Rosenfeld JV, Mitra B. Ethanol and Isolated Traumatic Brain Injury. *J Clin Neurosci* (2015) 22:1375–81. doi: 10.1016/j.jocn.2015.02.030
31. Shandro JR, Rivara FP, Wang J, Jurkovich GJ, Nathens AB, MacKenzie EJ. Alcohol and Risk of Mortality in Patients With Traumatic Brain Injury. *J Trauma - Inj Infect Crit Care* (2009) 66:1584–90. doi: 10.1097/TA.0b013e318182af96
32. Yue JK, Ngwenya LB, Upadhyayula PS, Deng H, Winkler EA, Burke JF, et al. Emergency Department Blood Alcohol Level Associates With Injury Factors and Six-Month Outcome After Uncomplicated Mild Traumatic Brain Injury. *J Clin Neurosci* (2017) 45:293–8. doi: 10.1016/j.jocn.2017.07.022
33. Liu X, Connaghan KP, Wei Y, Yang Z, Li MD, Chang SL. Involvement of the Hippocampus in Binge Ethanol-Induced Spleen Atrophy in Adolescent Rats. *Alcohol Clin Exp Res* (2016) 40:1489–500. doi: 10.1111/acer.13109
34. Liu X, Mao X, Chang SL. Altered Gene Expression in the Spleen of Adolescent Rats Following High Ethanol Concentration Binge Drinking. *Int J Clin Exp Med* (2011) 4:252–7.
35. Eken A, Ortiz V, Wands JR. Ethanol Inhibits Antigen Presentation by Dendritic Cells. *Clin Vaccine Immunol* (2011) 18:1157–66. doi: 10.1128/CVI.05029-11
36. Chandrasekar A, Aksan B, olde Heuvel F, Förstner P, Sinske D, Rehman R, et al. Neuroprotective Effect of Acute Ethanol Intoxication in TBI is Associated to the Hierarchical Modulation of Early Transcriptional Responses. *Exp Neurol* (2018) 302:34–45. doi: 10.1016/j.expneurol.2017.12.017
37. Chandrasekar A, Olde Heuvel F, Wepler M, Rehman R, Palmer A, Catanese A, et al. The Neuroprotective Effect of Ethanol Intoxication in Traumatic Brain Injury Is Associated With the Suppression of ERBB Signaling in Parvalbumin-Positive Interneurons. *J Neurotrauma* (2018) 35:2718–35. doi: 10.1089/neu.2017.5270
38. Faul M, Coronado V. Epidemiology of Traumatic Brain Injury. In: *Handb. Clin. Neurol.* London, England: Elsevier B.V. (2015). p. 3–13. doi: 10.1016/B978-0-444-52892-6.00001-5.
39. Peeters W, van den Brande R, Polinder S, Brazinova A, Steyerberg EW, Lingsma HF, et al. Epidemiology of Traumatic Brain Injury in Europe. *Acta Neurochir (Wien)* (2015) 157:1683–96. doi: 10.1007/s00701-015-2512-7
40. Iaccarino C, Carretta A, Nicolosi F, Morselli C. Epidemiology of Severe Traumatic Brain Injury. *J Neurosurg Sci* (2018) 62:535–41. doi: 10.23736/S0390-5616.18.04532-0
41. Flierl MA, Stahel PF, Beauchamp KM, Morgan SJ, Smith WR, Shohami E. Mouse Closed Head Injury Model Induced by a Weight-Drop Device. *Nat Protoc* (2009) 4:1328–37. doi: 10.1038/nprot.2009.148
42. Franz N, Dieteren S, Köhler K, Mörs K, Sturm R, Marzi I, et al. Alcohol Binge Reduces Systemic Leukocyte Activation and Pulmonary PMN Infiltration After Blunt Chest Trauma and Hemorrhagic Shock. *Inflammation* (2019) 42:690–701. doi: 10.1007/s10753-018-0927-z
43. Wagner N, Franz N, Dieteren S, Perl M, Mörs K, Marzi I, et al. Acute Alcohol Binge Deteriorates Metabolic and Respiratory Compensation Capability After Blunt Chest Trauma Followed by Hemorrhagic Shock—A New Research Model. *Alcohol Clin Exp Res* (2017) 41:1559–67. doi: 10.1111/acer.13446
44. Wang F, Flanagan J, Su N, Wang LC, Bui S, Nielson A, et al. RNAscope: A Novel *in Situ* RNA Analysis Platform for Formalin-Fixed, Paraffin-Embedded Tissues. *J Mol Diagn* (2012) 14:22–9. doi: 10.1016/j.jmoldx.2011.08.002
45. Zhang X, Lei B, Yuan Y, Zhang L, Hu L, Jin S, et al. Brain Control of Humoral Immune Responses Amenable to Behavioural Modulation. *Nature* (2020) 581:204–8. doi: 10.1038/s41586-020-2235-7
46. Carnevale D. Neural Control of Immunity in Hypertension: Council on Hypertension Mid Career Award for Research Excellence, 2019. *Hypertension* (2020) 76:622–8. doi: 10.1161/HYPERTENSIONAHA.120.14637
47. Wei Y, Chang L, Hashimoto K. Molecular Mechanisms Underlying the Antidepressant Actions of Arketamine: Beyond the NMDA Receptor. *Mol Psychiatry* (2021) 1–15. doi: 10.1038/s41380-021-01121-1
48. Guermonprez P, Helft J, Claser C, Deroubaix S, Karanje H, Gazumyan A, et al. Inflammatory Flt3l is Essential to Mobilize Dendritic Cells and for T Cell Responses During Plasmodium Infection. *Nat Med* (2013) 19:730–8. doi: 10.1038/nm.3197
49. Waskow C, Liu K, Darrasse-Jèze G, Guermonprez P, Ginhoux F, Merad M, et al. The Receptor Tyrosine Kinase Flt3 is Required for Dendritic Cell Development in Peripheral Lymphoid Tissues. *Nat Immunol* (2008) 9:676–83. doi: 10.1038/ni.1615
50. Papadopoulos EJ, Sassetti C, Saeki H, Yamada N, Kawamura T, Fitzhugh DJ, et al. Fractalkine, a CX3C Chemokine, is Expressed by Dendritic Cells and is Up-Regulated Upon Dendritic Cell Maturation. *Eur J Immunol* (1999) 29:2551–9. doi: 10.1002/(SICI)1521-4141(199908)29:08<2551::AID-IMMU2551>3.0.CO;2-T
51. Łyszkiewicz M, Witzlau K, Pommerencke J, Krueger A. Chemokine Receptor CX3CR1 Promotes Dendritic Cell Development Under Steady-State Conditions. *Eur J Immunol* (2011) 41:1256–65. doi: 10.1002/eji.201040977
52. Hughes CE, Nibbs RJB. A Guide to Chemokines and Their Receptors. *FEBS J* (2018) 285:2944–71. doi: 10.1111/febs.14466
53. Arolin DC, Palomino T, Avalheir LC. Marti, Chemokines and Immunity. *Einstein (Sao Paulo)* (2015) 13:469–73. doi: 10.1590/S1679-45082015RB3438
54. Castellino F, Huang AY, Altan-Bonnet G, Stoll S, Scheinecker C, Germain RN. Chemokines Enhance Immunity by Guiding Naive CD8+ T Cells to Sites of CD4+ T Cell-Dendritic Cell Interaction. *Nature* (2006) 440:890–5. doi: 10.1038/nature04651
55. Fujimura N, Xu B, Dalman J, Deng H, Aoyama K, Dalman RL. CCR2 Inhibition Sequesters Multiple Subsets of Leukocytes in the Bone Marrow. *Sci Rep* (2015) 5:1–13. doi: 10.1038/srep11664
56. Mikami N, Sueda K, Ogitani Y, Otani I, Takatsuji M, Wada Y, et al. Calcitonin Gene-Related Peptide Regulates Type IV Hypersensitivity Through Dendritic Cell Functions. *PloS One* (2014) 9:86367. doi: 10.1371/journal.pone.0086367
57. Barsheshet Y, Wildbaum G, Levy E, Vitenshtein A, Akinseye C, Griggs J, et al. CCR8+FOXp3+ Treg Cells as Master Drivers of Immune Regulation. *Proc Natl Acad Sci U S A* (2017) 114:6086–91. doi: 10.1073/pnas.1621280114
58. Yamazaki T, Yang XO, Chung Y, Fukunaga A, Nurieva R, Pappu B, et al. CCR6 Regulates the Migration of Inflammatory and Regulatory T Cells. *J Immunol* (2008) 181:8391–401. doi: 10.4049/jimmunol.181.12.8391
59. Piseddu I, Röhrle N, Knott MML, Moder S, Eiber S, Schnell K, et al. Constitutive Expression of CCL22 Is Mediated by T Cell–Derived GM-CSF. *J Immunol* (2020) 205:2056–65. doi: 10.4049/jimmunol.2000004
60. Wildbaum G, Netzer N, Karin N. Plasmid DNA Encoding IFN-γ-Inducible Protein 10 Redirects Antigen-Specific T Cell Polarization and Suppresses Experimental Autoimmune Encephalomyelitis. *J Immunol* (2002) 168:5885–92. doi: 10.4049/jimmunol.168.11.5885
61. Coelho AL, Schaller MA, Benjamim CF, Orlofsky AZ, Hogaboam CM, Kunkel SL. The Chemokine CCL6 Promotes Innate Immunity *via* Immune Cell Activation and Recruitment. *J Immunol* (2007) 179:5474–82. doi: 10.4049/jimmunol.179.8.5474
62. Li H, Meng YH, Shang WQ, Liu LB, Chen X, Yuan MM, et al. Chemokine CCL24 Promotes the Growth and Invasiveness of Trophoblasts Through ERK1/2 and PI3K Signaling Pathways in Human Early Pregnancy. *Reproduction* (2015) 150:417–27. doi: 10.1530/REP-15-0119
63. Sokulsky LA, Garcia-Netto K, Nguyen TH, Girkin JLN, Collison A, Mattes J, et al. A Critical Role for the CXCL3/CXCL5/CXCR2 Neutrophilic Chemotactic Axis in the Regulation of Type 2 Responses in a Model of Rhinoviral-Induced Asthma Exacerbation. *J Immunol* (2020) 205:2468–78. doi: 10.4049/jimmunol.1901350
64. Veinotte L, Gebremeskel S, Johnston B. CXCL16-Positive Dendritic Cells Enhance Invariant Natural Killer T Cell-Dependent Ifnγ Production and

Tumor Control. *Oncoimmunology* (2016) 5(6):e1160979. doi: 10.1080/2162402X.2016.1160979
65. Wang R, Maksymowych WP. Targeting the Interleukin-23/Interleukin-17 Inflammatory Pathway: Successes and Failures in the Treatment of Axial Spondyloarthritis. *Front Immunol* (2021) 12:3389/FIMMU.2021.715510. doi: 10.3389/FIMMU.2021.715510
66. Witte E, Kokolakis G, Witte K, Philipp S, Doecke WD, Babel N, et al. IL-19 is a Component of the Pathogenetic IL-23/IL-17 Cascade in Psoriasis. *J Invest Dermatol* (2014) 134:2757–67. doi: 10.1038/JID.2014.308
67. Cueto FJ, Sancho D. The Flt3l/Flt3 Axis in Dendritic Cell Biology and Cancer Immunotherapy. *Cancers (Basel)* (2021) 13(7):1525. doi: 10.3390/cancers13071525
68. Rheinländer A, Schraven B, Bommhardt U. CD45 in Human Physiology and Clinical Medicine. *Immunol Lett* (2018) 196:22–32. doi: 10.1016/j.imlet.2018.01.009
69. Merad M, Sathe P, Helft J, Miller J, Mortha A. The Dendritic Cell Lineage: Ontogeny and Function of Dendritic Cells and Their Subsets in the Steady State and the Inflamed Setting. *Annu Rev Immunol* (2013) 31:563–604. doi: 10.1146/ANNUREV-IMMUNOL-020711-074950
70. Oellerich T, Mohr S, Corso J, Beck J, Döbele C, Braun H, et al. FLT3-ITD and TLR9 Use Bruton Tyrosine Kinase to Activate Distinct Transcriptional Programs Mediating AML Cell Survival and Proliferation. *Blood* (2015) 125:1936–47. doi: 10.1182/blood-2014-06-585216
71. Lelouard H, Schmidt EK, Camosseto V, Clavarino G, Ceppi M, Hsu HT, et al. Regulation of Translation is Required for Dendritic Cell Function and Survival During Activation. *J Cell Biol* (2007) 179:1427–39. doi: 10.1083/JCB.200707166
72. Jovanovic M, Rooney MS, Mertins P, Przybylski D, Chevrier N, Satija R, et al. Dynamic Profiling of the Protein Life Cycle in Response to Pathogens. *Sci (80-)* (2015) 347(6226):1259038. doi: 10.1126/science.1259038
73. Sathaliyawala T, O'Gorman WE, Greter M, Bogunovic M, Konjufca V, Hou ZE, et al. Mammalian Target of Rapamycin Controls Dendritic Cell Development Downstream of Flt3 Ligand Signaling. *Immunity* (2010) 33:597–606. doi: 10.1016/j.immuni.2010.09.012
74. Mendes A, Gigan JP, Rodrigues CR, Choteau SA, Sanseau D, Barros D, et al. Proteostasis in Dendritic Cells is Controlled by the PERK Signaling Axis Independently of ATF4. *Life Sci Alliance* (2021) 4(2):e202000865. doi: 10.26508/LSA.202000865
75. Fang H, Ang B, Xu X, Huang X, Wu Y, Sun Y, et al. TLR4 is Essential for Dendritic Cell Activation and Anti-Tumor T-Cell Response Enhancement by DAMPs Released From Chemically Stressed Cancer Cells. *Cell Mol Immunol* (2014) 11:150–9. doi: 10.1038/cmi.2013.59
76. Oth T, Vanderlocht J, Van Elssen CHMJ, Bos GMJ, Germeraad WTV. Pathogen-Associated Molecular Patterns Induced Crosstalk Between Dendritic Cells, T Helper Cells, and Natural Killer Helper Cells Can Improve Dendritic Cell Vaccination. *Mediators Inflamm* (2016) 2016:5740373. doi: 10.1155/2016/5740373
77. Tan JKH, O'Neill HC. Maturation Requirements for Dendritic Cells in T Cell Stimulation Leading to Tolerance Versus Immunity. *J Leukoc Biol* (2005) 78:319–24. doi: 10.1189/jlb.1104664
78. De Saint-Vis B, Vincent J, Vandenabeele S, Vanbervliet B, Pin JJ, Aït-Yahia S, et al. A Novel Lysosome-Associated Membrane Glycoprotein, DC-LAMP, Induced Upon DC Maturation, is Transiently Expressed in MHC Class II Compartment. *Immunity* (1998) 9:325–36. doi: 10.1016/S1074-7613(00)80615-9
79. Trombetta ES, Ebersold M, Garrett W, Pypaert M, Mellman I. Activation of Lysosomal Function During Dendritic Cell Maturation. *Science* (2003) 299:1400–3. doi: 10.1126/SCIENCE.1080106
80. Arruda LB, Sim D, Chikhlikar PR, Maciel M, Akasaki K, August JT, et al. Dendritic Cell-Lysosomal-Associated Membrane Protein (LAMP) and LAMP-1-HIV-1 Gag Chimeras Have Distinct Cellular Trafficking Pathways and Prime T and B Cell Responses to a Diverse Repertoire of Epitopes. *J Immunol* (2006) 177:2265–75. doi: 10.4049/JIMMUNOL.177.4.2265
81. Bettiol E, Van De Hoef DL, Carapau D, Rodriguez A. Efficient Phagosomal Maturation and Degradation of Plasmodium-Infected Erythrocytes by Dendritic Cells and Macrophages. *Parasite Immunol* (2010) 32:389–98. doi: 10.1111/J.1365-3024.2010.01198.X
82. Chistiakov DA, Killingsworth MC, Myasoedova VA, Orekhov AN, Bobryshev YV. CD68/macrosialin: Not Just a Histochemical Marker. *Lab Investig* (2017) 97:4–13. doi: 10.1038/labinvest.2016.116
83. Saftig P, Klumperman J. Lysosome Biogenesis and Lysosomal Membrane Proteins: Trafficking Meets Function. *Nat Rev Mol Cell Biol* (2009) 10:623–35. doi: 10.1038/nrm2745
84. de Heusch M, Oldenhove G, Urbain J, Thielemans K, Maliszewski C, Leo O, et al. Depending on Their Maturation State, Splenic Dendritic Cells Induce the Differentiation of CD4(+) T Lymphocytes Into Memory and/or Effector Cells *In Vivo*. *Eur J Immunol* (2004) 34:1861–9. doi: 10.1002/EJI.200424878
85. Dhodapkar MV, Steinman RM, Krasovsky J, Munz C, Bhardwaj N. Antigen-Specific Inhibition of Effector T Cell Function in Humans After Injection of Immature Dendritic Cells. *J Exp Med* (2001) 193:233–8. doi: 10.1084/JEM.193.2.233
86. Menges M, Rößner S, Voigtländer C, Schindler H, Kukutsch NA, Bogdan C, et al. Repetitive Injections of Dendritic Cells Matured With Tumor Necrosis Factor Alpha Induce Antigen-Specific Protection of Mice From Autoimmunity. *J Exp Med* (2002) 195:15–21. doi: 10.1084/JEM.20011341
87. Stoitzner P, Holzmann S, McLellan AD, Ivarsson L, Stössel H, Kapp M, et al. Visualization and Characterization of Migratory Langerhans Cells in Murine Skin and Lymph Nodes by Antibodies Against Langerin/CD207. *J Invest Dermatol* (2003) 120:266–74. doi: 10.1046/J.1523-1747.2003.12042.X
88. Lehner M, Kellert B, Proff J, Schmid MA, Diessenbacher P, Ensser A, et al. Autocrine TNF Is Critical for the Survival of Human Dendritic Cells by Regulating BAK, BCL-2, and FLIP L. *J Immunol* (2012) 188:4810–8. doi: 10.4049/jimmunol.1101610
89. Durães FV, Carvalho NB, Melo TT, Oliveira SC, Fonseca CT. IL-12 and TNF-Alpha Production by Dendritic Cells Stimulated With Schistosoma Mansoni Schistosomula Tegument is TLR4- and MyD88-Dependent. *Immunol Lett* (2009) 125:72–7. doi: 10.1016/J.IMLET.2009.06.004
90. Doxsee CL, Riter TR, Reiter MJ, Gibson SJ, Vasilakos JP, Kedl RM. The Immune Response Modifier and Toll-Like Receptor 7 Agonist S-27609 Selectively Induces IL-12 and TNF-Alpha Production in CD11c+CD11b+CD8- Dendritic Cells. *J Immunol* (2003) 171:1156–63. doi: 10.4049/JIMMUNOL.171.3.1156
91. Helbig C, Weber F, Andreas N, Herdegen T, Gaestel M, Kamradt T, et al. The IL-33-Induced P38-/JNK1/2-Tnfα Axis is Antagonized by Activation of β-Adrenergic-Receptors in Dendritic Cells. *Sci Rep* (2020) 10(1):8152. doi: 10.1038/S41598-020-65072-3
92. Takenaka MC, Araujo LP, Maricato JT, Nascimento VM, Guereschi MG, Rezende RM, et al. Norepinephrine Controls Effector T Cell Differentiation Through β 2 -Adrenergic Receptor–Mediated Inhibition of NF-κb and AP-1 in Dendritic Cells. *J Immunol* (2016) 196:637–44. doi: 10.4049/jimmunol.1501206
93. Nijhuis LE, Olivier BJ, Dhawan S, Hilbers FW, Boon L, Wolkers MC, et al. Adrenergic β2 Receptor Activation Stimulates Anti-Inflammatory Properties of Dendritic Cells *In Vitro*. *PloS One* (2014) 9(1):e85086. doi: 10.1371/journal.pone.0085086
94. Everts B, Amiel E, Huang SCC, Smith AM, Chang CH, Lam WY, et al. TLR-Driven Early Glycolytic Reprogramming *via* the Kinases TBK1-Ikkε Supports the Anabolic Demands of Dendritic Cell Activation. *Nat Immunol* (2014) 15:323–32. doi: 10.1038/ni.2833
95. Sukhbaatar N, Hengstschläger M, Weichhart T. mTOR-Mediated Regulation of Dendritic Cell Differentiation and Function. *Trends Immunol* (2016) 37:778–89. doi: 10.1016/j.it.2016.08.009
96. Nagayama H, Sato K, Kawasaki H, Enomoto M, Morimoto C, Tadokoro K, et al. IL-12 Responsiveness and Expression of IL-12 Receptor in Human Peripheral Blood Monocyte-Derived Dendritic Cells. *J Immunol* (2000) 165:59–66. doi: 10.4049/jimmunol.165.1.59
97. Bhatia S, Edidin M, Almo SC, Nathenson SG. B7-1 and B7-2: Similar Costimulatory Ligands With Different Biochemical, Oligomeric and Signaling Properties. *Immunol Lett* (2006) 104:70–5. doi: 10.1016/J.IMLET.2005.11.019
98. Pollack KE, Meneveau MO, Melssen MM, Lynch KT, Koeppel AF, Young SJ, et al. Incomplete Freund's Adjuvant Reduces Arginase and Enhances Th1 Dominance, TLR Signaling and CD40 Ligand Expression in the Vaccine Site Microenvironment. *J Immunother Cancer* (2020) 8(1):e000544. doi: 10.1136/JITC-2020-000544

99. Wang C, Liu S, Xu J, Gao M, Qu Y, Liu Y, et al. Dissolvable Microneedles Based on Panax Notoginseng Polysaccharide for Transdermal Drug Delivery and Skin Dendritic Cell Activation. *Carbohydr Polym* (2021) 268:118211. doi: 10.1016/J.CARBPOL.2021.118211
100. Praveen C, Bhatia SS, Alaniz RC, Droleskey RE, Cohen ND, Jesudhasan PR, et al. Assessment of Microbiological Correlates and Immunostimulatory Potential of Electron Beam Inactivated Metabolically Active Yet Non Culturable (MAyNC) Salmonella Typhimurium. *PloS One* (2021) 16(4): e0243417. doi: 10.1371/JOURNAL.PONE.0243417
101. Li Z, Zhang J, Halbgebauer S, Chandrasekar A, Rehman R, Ludolph A, et al. Differential Effect of Ethanol Intoxication on Peripheral Markers of Cerebral Injury in Murine Blunt Traumatic Brain Injury. *Burns Trauma* (2021) 9: tkab027. doi: 10.1093/burnst/tkab027
102. Paudel YN, Shaikh MF, Chakraborti A, Kumari Y, Aledo-Serrano Á., Aleksovska K, et al. HMGB1: A Common Biomarker and Potential Target for TBI, Neuroinflammation, Epilepsy, and Cognitive Dysfunction. *Front Neurosci* (2018) 12:3389/fnins.2018.00628. doi: 10.3389/fnins.2018.00628
103. Parker TM, Nguyen AH, Rabang JR, Patil AA, Agrawal DK. The Danger Zone: Systematic Review of the Role of HMGB1 Danger Signalling in Traumatic Brain Injury. *Brain Inj* (2017) 31:2–8. doi: 10.1080/02699052.2016.1217045
104. Webster KM, Sun M, Crack PJ, O'Brien TJ, Shultz SR, Semple BD. Age-Dependent Release of High-Mobility Group Box Protein-1 and Cellular Neuroinflammation After Traumatic Brain Injury in Mice. *J Comp Neurol* (2019) 527:1102–17. doi: 10.1002/cne.24589
105. Au AK, Aneja RK, Bell MJ, Bayir H, Feldman K, Adelson PD, et al. Cerebrospinal Fluid Levels of High-Mobility Group Box 1 and Cytochrome C Predict Outcome After Pediatric Traumatic Brain Injury. *J Neurotrauma* (2012) 29:2013–21. doi: 10.1089/neu.2011.2171
106. Yang L, Wang F, Yang L, Yuan Y, Chen Y, Zhang G, et al. HMGB1 a-Box Reverses Brain Edema and Deterioration of Neurological Function in a Traumatic Brain Injury Mouse Model. *Cell Physiol Biochem* (2018) 46:2532–42. doi: 10.1159/000489659
107. Laird MD, Shields JS, Sukumari-Ramesh S, Kimbler DE, Fessler RD, Shakir B, et al. High Mobility Group Box Protein-1 Promotes Cerebral Edema After Traumatic Brain Injury *via* Activation of Toll-Like Receptor 4. *Glia* (2014) 62:26–38. doi: 10.1002/glia.22581
108. Li R, Zou X, Huang H, Yu Y, Zhang H, Liu P, et al. HMGB1/PI3K/Akt/mTOR Signaling Participates in the Pathological Process of Acute Lung Injury by Regulating the Maturation and Function of Dendritic Cells. *Front Immunol* (2020) 11:3389/fimmu.2020.01104. doi: 10.3389/fimmu.2020.01104
109. Chen Y, Zhang W, Bao H, He W, Chen L. High Mobility Group Box 1 Contributes to the Acute Rejection of Liver Allografts by Activating Dendritic Cells. *Front Immunol* (2021) 12:3389/fimmu.2021.679398. doi: 10.3389/fimmu.2021.679398
110. Kooijman S, Meurs I, van Beek L, Khedoe PPSJ, Giezekamp A, Pike-Overzet K, et al. Splenic Autonomic Denervation Increases Inflammatory Status But Does Not Aggravate Atherosclerotic Lesion Development. *Am J Physiol - Heart Circ Physiol* (2015) 309:H646–54. doi: 10.1152/ajpheart.00787.2014
111. Rosas-Ballina M, Tracey KJ. The Neurology of the Immune System: Neural Reflexes Regulate Immunity. *Neuron* (2009) 64:28–32. doi: 10.1016/j.neuron.2009.09.039
112. Wu H, Chen J, Song S, Yuan P, Liu L, Zhang Y, et al. β2-Adrenoceptor Signaling Reduction in Dendritic Cells is Involved in the Inflammatory Response in Adjuvant-Induced Arthritic Rats. *Sci Rep* (2016) 6:24548. doi: 10.1038/srep24548
113. Li M, Li F, Luo C, Shan Y, Zhang L, Qian Z, et al. Immediate Splenectomy Decreases Mortality and Improves Cognitive Function of Rats After Severe Traumatic Brain Injury. *J Trauma - Inj Infect Crit Care* (2011) 71:141–7. doi: 10.1097/TA.0b013e3181f30fc9
114. Chu W, Li M, Li F, Hu R, Chen Z, Lin J, et al. Immediate Splenectomy Down-Regulates the MAPKYNF-JB Signaling Pathway in Rat Brain After Severe Traumatic Brain Injury. *J Trauma Acute Care Surg* (2013) 74:1446–53. doi: 10.1097/TA.0b013e31829246ad
115. Blomster LV, Brennan FH, Lao HW, Harle DW, Harvey AR, Ruitenberg MJ. Mobilisation of the Splenic Monocyte Reservoir and Peripheral CX3CR1 Deficiency Adversely Affects Recovery From Spinal Cord Injury. *Exp Neurol* (2013) 247:226–40. doi: 10.1016/j.expneurol.2013.05.002
116. Hauben E, Gothilf A, Cohen A, Butovsky O, Nevo U, Smirnov I, et al. Vaccination With Dendritic Cells Pulsed With Peptides of Myelin Basic Protein Promotes Functional Recovery From Spinal Cord Injury. *J Neurosci* (2003) 23:8808–19. doi: 10.1523/jneurosci.23-25-08808.2003
117. Needham EJ, Stoevesandt O, Thelin EP, Zetterberg H, Zanier ER, Al Nimer F, et al. Complex Autoantibody Responses Occur Following Moderate to Severe Traumatic Brain Injury. *J Immunol* (2021) 207:90–100. doi: 10.4049/jimmunol.2001309
118. Picotto G, Morse LR, Nguyen N, Saltzman J, Battaglino R. TMEM176A and TMEM176B Are Candidate Regulators of Inhibition of Dendritic Cell Maturation and Function After Chronic Spinal Cord Injury. *J Neurotrauma* (2020) 37:528–33. doi: 10.1089/neu.2019.6498
119. Wagner N, Akbarpour A, Mörs K, Voth M, Störmann P, Auner B, et al. Alcohol Intoxication Reduces Systemic Interleukin-6 Levels and Leukocyte Counts After Severe TBI Compared With Not Intoxicated TBI Patients. *Shock* (2016) 46:261–9. doi: 10.1097/SHK.0000000000000620
120. Relja B, Menke J, Wagner N, Auner B, Voth M, Nau C, et al. Effects of Positive Blood Alcohol Concentration on Outcome and Systemic Interleukin-6 in Major Trauma Patients. *Injury* (2016) 47:640–5. doi: 10.1016/j.injury.2016.01.016
121. Wagner N, Dieteren S, Franz N, Köhler K, Perl M, Marzi I, et al. Alcohol-Induced Attenuation of Post-Traumatic Inflammation is Not Necessarily Liver-Protective Following Trauma/Hemorrhage. *Int J Mol Med* (2019) 44:1127–38. doi: 10.3892/ijmm.2019.4259
122. Fan J, Edsen-Moore MR, Turner LE, Cook RT, Legge KL, Waldschmidt TJ, et al. Mechanisms by Which Chronic Ethanol Feeding Limits the Ability of Dendritic Cells to Stimulate T-Cell Proliferation. *Alcohol Clin Exp Res* (2011) 35:47–59. doi: 10.1111/j.1530-0277.2010.01321.x
123. Siggins RW, Bagby GJ, Molina P, Dufour J, Nelson S, Zhang P. Alcohol Exposure Impairs Myeloid Dendritic Cell Function in Rhesus Macaques. *Alcohol Clin Exp Res* (2009) 33:1524–31. doi: 10.1111/j.1530-0277.2009.00980.x
124. Hey YY, O'Neill HC. Murine Spleen Contains a Diversity of Myeloid and Dendritic Cells Distinct in Antigen Presenting Function. *J Cell Mol Med* (2012) 16:2611–9. doi: 10.1111/j.1582-4934.2012.01608.x

Conflict of Interest: The authors declare that the research was conducted in the absence of any commercial or financial relationships that could be construed as a potential conflict of interest.

Publisher's Note: All claims expressed in this article are solely those of the authors and do not necessarily represent those of their affiliated organizations, or those of the publisher, the editors and the reviewers. Any product that may be evaluated in this article, or claim that may be made by its manufacturer, is not guaranteed or endorsed by the publisher.

frontiers in Immunology

ORIGINAL RESEARCH
published: 15 March 2022
doi: 10.3389/fimmu.2022.839632

Venous Air Embolism Activates Complement C3 Without Corresponding C5 Activation and Trigger Thromboinflammation in Pigs

Benjamin S. Storm[1,2,3,4], Judith K. Ludviksen[4], Dorte Christiansen[4], Hilde Fure[4], Kristin Pettersen[4], Anne Landsem[4], Bent Aksel Nilsen[1,3], Knut Dybwik[1], Tonje Braaten[3,5], Erik W. Nielsen[1,2,3,6] and Tom E. Mollnes[4,6,7,8,9]*

[1] Department of Anesthesia and Intensive Care Medicine, Nordland Hospital, Bodø, Norway, [2] Department of Clinical Medicine, Faculty of Health Sciences, UiT The Arctic University of Norway, Tromsø, Norway, [3] Faculty of Nursing and Health Sciences, Nord University, Bodø, Norway, [4] Research Laboratory, Nordland Hospital Trust, Bodø, Norway, [5] Department of Community Medicine, Faculty of Health Sciences, UiT The Arctic University of Norway, Tromsø, Norway, [6] Faculty of Medicine, Institute of Clinical Medicine, University of Oslo, Oslo, Norway, [7] Faculty of Health Sciences, KG. Jebsen TREC, UiT The Arctic University of Norway, Tromsø, Norway, [8] Department of Immunology, Oslo University Hospital, The University of Oslo, Oslo, Norway, [9] Centre of Molecular Inflammation Research, Norwegian University of Science and Technology, Trondheim, Norway

OPEN ACCESS

Edited by:
Mihály Józsi,
Eötvös Loránd University, Hungary

Reviewed by:
Janos Szebeni,
Semmelweis University, Hungary
Markus Bosmann,
Boston University, United States

***Correspondence:**
Benjamin S. Storm
Benjamin.storm@gmail.com

Specialty section:
This article was submitted to Inflammation, a section of the journal Frontiers in Immunology

Received: *20 December 2021*
Accepted: *21 February 2022*
Published: *15 March 2022*

Citation:
Storm BS, Ludviksen JK, Christiansen D, Fure H, Pettersen K, Landsem A, Nilsen BA, Dybwik K, Braaten T, Nielsen EW and Mollnes TE (2022) Venous Air Embolism Activates Complement C3 Without Corresponding C5 Activation and Trigger Thromboinflammation in Pigs. Front. Immunol. 13:839632. doi: 10.3389/fimmu.2022.839632

Introduction: Air embolism may complicate invasive medical procedures. Bubbles trigger complement C3-mediated cytokine release, coagulation, and platelet activation *in vitro* in human whole blood. Since these findings have not been verified *in vivo*, we aimed to examine the effects of air embolism in pigs on thromboinflammation.

Methods: Forty-five landrace pigs, average 17 kg (range 8.5-30), underwent intravenous air infusion for 300 or 360 minutes (n=29) or served as sham (n=14). Fourteen pigs were excluded due to e.g. infections or persistent foramen ovale. Blood was analyzed for white blood cells (WBC), complement activation (C3a and terminal C5b-9 complement complex [TCC]), cytokines, and hemostatic parameters including thrombin-antithrombin (TAT) using immunoassays and rotational thromboelastometry (ROTEM). Lung tissue was analyzed for complement and cytokines using qPCR and immunoassays. Results are presented as medians with interquartile range.

Results: In 24 pigs receiving air infusion, WBC increased from 17×10^9/L (10-24) to 28 (16-42) ($p<0.001$). C3a increased from 21 ng/mL (15-46) to 67 (39-84) ($p<0.001$), whereas TCC increased only modestly ($p=0.02$). TAT increased from 35 µg/mL (28-42) to 51 (38-89) ($p=0.002$). ROTEM changed during first 120 minutes: Clotting time decreased from 613 seconds (531-677) to 538 (399-620) ($p=0.006$), clot formation time decreased from 161 seconds (122-195) to 124 (83-162) ($p=0.02$) and α-angle increased from 62 degrees (57-68) to 68 (62-74) ($p=0.02$). In lungs from pigs receiving air compared to sham animals, C3a was 34 ng/mL (14-50) versus 4.1 (2.4-5.7) ($p<0.001$), whereas TCC was 0.3 CAU/mL (0.2-0.3) versus 0.2 (0.1-0.2) ($p=0.02$). Lung cytokines in pigs receiving air compared to sham animals were: IL-1β 302 pg/mL (190-437) versus 107 (66-120), IL-6 644 pg/mL (358-1094) versus

25 (23-30), IL-8 203 pg/mL (81-377) versus 21 (20-35), and TNF 113 pg/mL (96-147) versus 16 (13-22) (all p<0.001). Cytokine mRNA in lung tissue from pigs receiving air compared to sham animals increased 12-fold for IL-1β, 121-fold for IL-6, and 17-fold for IL-8 (all p<0.001).

Conclusion: Venous air embolism in pigs activated C3 without a corresponding C5 activation and triggered thromboinflammation, consistent with a C3-dependent mechanism. C3-inhibition might represent a therapeutic approach to attenuate this response.

Keywords: air embolism, porcine model, complement, inflammation, cytokines, coagulation, thromboinflammation

INTRODUCTION

Venous air embolism, a condition where air inadvertently enters the bloodstream, may complicate many medical and surgical interventions (1–3), or bubbles may form in the bloodstream during rapid decompression when diving (4). Animal studies and human case reports have shown that air embolism triggers acute pulmonary hypertension and hamper pulmonary gas exchange (5–7). Air may also transverse the pulmonary circulation, enter the arterial circulation, disrupt blood circulation, and cause organ ischemia and damage, such as acute myocardial infarction or stroke (6, 8, 9). Patient case reports have described prolonged severe inflammation after air embolism (6, 10), and one case report described a suspected link between perioperative air embolism and disseminated intravascular coagulation, albeit with an unknown pathophysiological mechanism (11). *In vitro* experiments in human serum and heparinized blood have shown that air activates C3 to C3(H_20), also termed iC3 (12–14), and *in vitro* studies in lepirudin anticoagulated human whole blood have shown that air emboli trigger a complement C3-driven thromboinflammation (15), which is attenuated by C3 inhibition (15). *Ex vivo* rat studies have shown how air emboli trigger a pulmonary inflammation involving both monocytes and granulocytes and complement (16), recent *in vivo* studies of divers suffering from decompression sickness have shown how microbubbles trigger an acute inflammation (17), and human *in vivo* and *in vitro* studies of bubble-oxygenators has shown that bubbles activate C3 in fully heparinized blood (12). Heparin anticoagulation, however, precludes detailed studies into thromboinflammation and is known to interact with complement in a dosage-dependent manner (18, 19). Despite the numerous *in vitro*, *ex vivo*, and *in vivo* studies on air emboli, the role of the complement system in the air-induced thromboinflammation has to our knowledge, not previously been examined in detail *in vivo* in minimally anticoagulated larger animals.

Measures for the prevention, detection, and immediate treatment of air embolism are well described (3). However, these measures only address the immediate emergency treatment and do not address the management of air-induced thromboinflammation. Based on our recent *in vitro* human whole blood study (15), we hypothesize that C3 activation plays a key role and that C3 inhibition can attenuate the detrimental thromboinflammatory effects of air embolism. Unfortunately, no C3 inhibitor shown to work in swine is available for therapeutic use in porcine studies. Thus, this hypothesis remains untested.

The aim of this exploratory study was to examine the effects of venous air embolism on the complement system, the cytokine network, and coagulation *in vivo* in a porcine model.

Abbreviations: CAU, complement activation units; CFT, clot formation time; IL, interleukin; IQR, interquartile range; NATEM, non-activated thromboelastometry test; NeF, nephritic factor; ROTEM, rotational thromboelastometry; TAT, thrombin-antithrombin complex; TCC, terminal complement complex; TNF, tumor necrosis factor.

MATERIALS AND METHODS

We developed a novel porcine model of venous air embolism based on previous animal studies by Durant, Oppenheimer, and Vik (5, 20, 21). The protocol was approved by The Norwegian Animal Research Authority (FOTS ID9466) and performed per the Norwegian Laboratory Animal Regulations and EU directive 2010/64/EU.

Anesthesia, Instrumentation, and Monitoring

We retrieved 45 Norwegian domestic landrace pigs weighing on average 17 kg (range 8.5-30 kg) from two local farms. Before retrieval, the animals were selected to undergo venous air infusion or serve as sham animals. The animals were anesthetized with azaperone 4 mg, ketamine 500 mg, and atropine 0.5 mg intramuscularly. An iv. cannula was placed in an ear vein, and anesthesia was maintained with a continuous infusion of morphine 2 mg/kg/h, midazolam 0.15 mg/kg/h, and pentobarbital 4 mg/kg/h. We endotracheally intubated the pigs with a Portex ID 6 mm endotracheal tube (Smiths Medical International Ltd, Kent, United Kingdom) and ventilated them with a tidal volume of 10-15 mL/kg, a respiratory rate of 20/minute, an inspired oxygen fraction of 21%, and a positive end-expiratory pressure of 0 cmH_2O using a Datex-Ohmeda Engström Carestation intensive care ventilator (GE Healthcare, Madison, WI).

We placed a pediatric 9T esophageal echo probe (General Electric, Horten, Norway) in the esophagus and connected it to a Vivid 7 pro echo doppler machine (General Electric). Using

sterile cut-down technique, we inserted a 4 Fr. 8 cm Leadercath arterial catheter (Vygon Ltd., Swindon, UK) in the right carotid artery, an 8 Fr. Avanti+ Vascular Sheath Introducer (Cordis, Santa Clara, CA), and a 7.5 Fr. Swan-Ganz CCOmbo pulmonary artery catheter (Edwards Lifesciences Corporation, Irvine, CA) in the right external jugular vein, a 4 Fr. 8 cm PiCCO thermodilution catheter (Pulsion/Getinge, Gothenburg, Sweden) in the femoral artery, and a suprapubic catheter with a temperature sensor in the bladder. The pulmonary artery catheter, sheath introducer, and arterial cannula were connected to a TruWave x3 T001660A Pressure Monitoring Set (Edwards Lifesciences Corporation), and the PiCCO catheter was connected to a PV8215 PiCCO Monitoring Kit (Pulsion). Both systems were connected to a pressurized 500 mL Ringer's acetate bag (Fresenius Kabi, Oslo, Norway) with 1250 IU Heparin (LEO Pharma AS, Oslo, Norway) added to a final concentration of 2.5 IU/mL. A continuous infusion of 3 mL/h of heparinized Ringer's acetate was delivered through each of the four pressure lines, i.e., 30 IU Heparin pr hour was administered to the animals. If flushing of the catheters was needed, normal saline was used. The catheters were not flushed with heparinized Ringer. After instrumentation, the animals were stabilized for thirty minutes before starting the air infusion or sham observation.

We recorded continuous invasive arterial, pulmonary, and venous blood pressures, ECG, plethysmographic arterial saturation (SpO_2), end-tidal expired CO_2 ($EtCO_2$), and hourly intermittent cardiac output by thermodilution using an Intellivue MP70 monitor (Philips Healthcare, Cambridge, CA) as per manufacture's instructions. Additionally, hourly intermittent and continuous cardiac output was measured using the Pulsion Pulsed index Continuous Cardiac Output PiCCO2 monitor (Pulsion) as per manufactures instructions. Before the experiments, we performed echocardiography, and throughout the experiments, cardiac function and buildup of air and thrombi in the pulmonary artery and systemic egress of air were monitored using continuous echocardiography.

Exclusion Criteria

Animals with infections, either observed upon retrieval or diagnosed at the post-mortem lung autopsy or defined as a white blood cell count or complement C3a level three standard derivations above mean baseline values, were excluded (**Figure 1**). Animals with persistent foramen ovale, detected by preoperative echocardiography with an agitated saline injection or by post-mortem autopsy, and animals with iatrogenic complications, such as ventricular fibrillation upon inflation of the pulmonary artery catheter or vessel injury due to cannulation, were excluded from the study. Also, one animal in the sham group was excluded due to severe volvulus, which became evident during the observation period, and one due to an unintended infusion of air through an unpurged intravenous line.

Air Infusion

After instrumentation and baseline blood sampling, we administered a continuous air infusion of 3-7 mL/kg/hour by syringe driver through an ear vein. The infusion rate was either maintained or increased with 1-2 mL/kg every sixty minutes for 300 minutes (21 pigs) or 360 minutes (3 pigs) or until the animals died (**Figure 2A**). The air infusion protocol was based on previous studies (5, 20, 21) and titrated to cause severe hemodynamic instability, but not systemic egress of air embolism or the death of the animals. Initially, a 360-minute

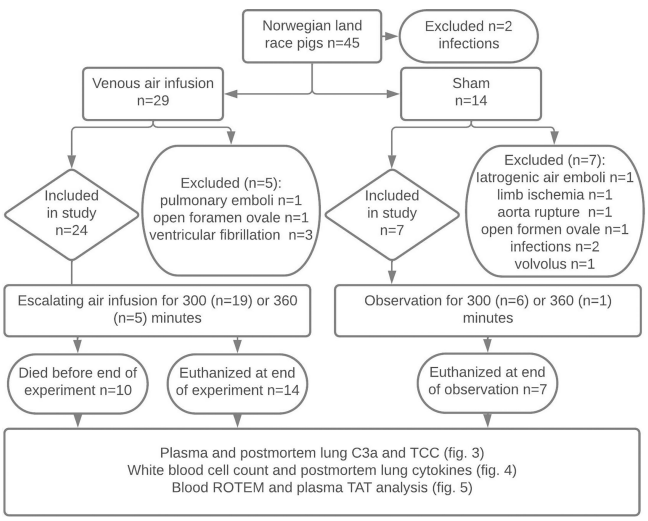

FIGURE 1 | Experimental flowchart. Forty-five Norwegian landrace pigs from two farms were selected by convenience sampling to undergo 300 or 360 minutes of titrated air infusion or serve as sham animals. Animals with infections, pulmonary emboli during animal preparation, persistent foramen ovale, ventricular fibrillation, iatrogenic venous air embolism, limb ischemia, or iatrogenic aortic rupture were excluded. Ten pigs receiving air infusion died due to the air infusion after a median infusion time of 243 minutes. Animals alive at the end of the experiments were euthanized. Blood was sampled at regular intervals throughout the experiments, and lung tissue was sampled post-mortem. Blood and lung samples were analyzed as detailed in the figure.

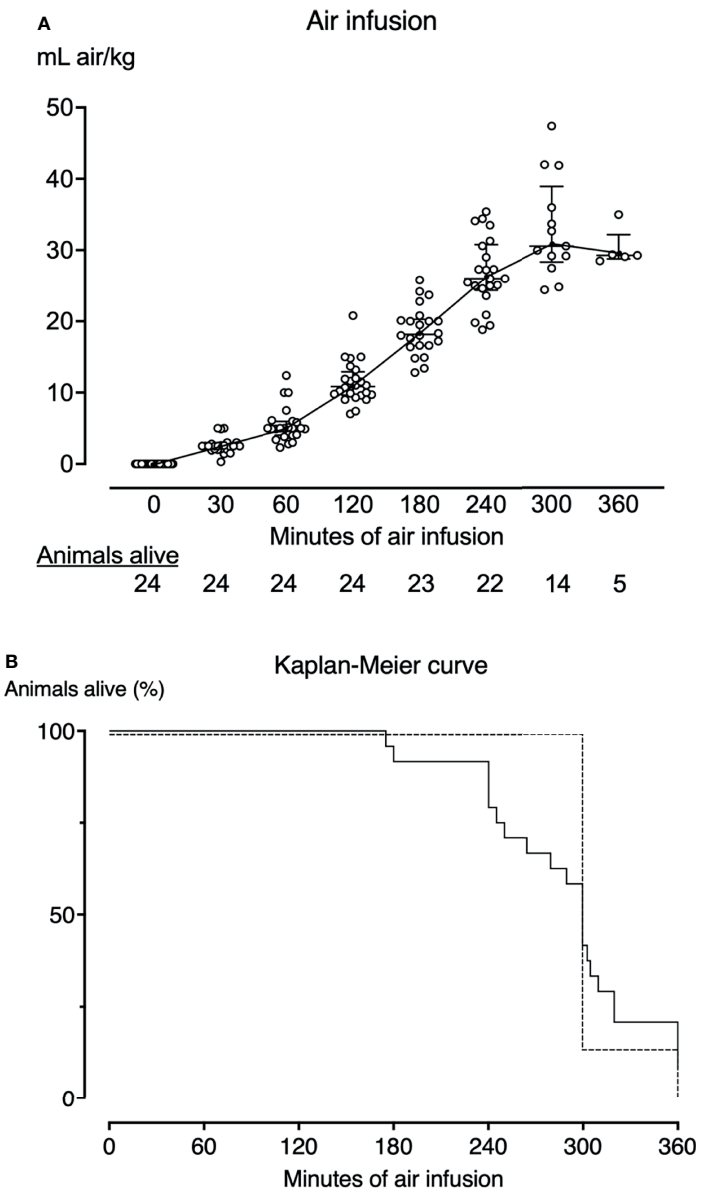

FIGURE 2 | Air infusion protocol and survival curves. **(A)** Twenty-four pigs received intravenous air infusion based on body weight. The infusion rate was increased hourly. Each point represents one pig. The horizontal lines indicate the median infusion rate. Error bars span the interquartile range. Animals are only included in the graph until death. Pigs alive at each sample point are listed below the graph. **(B)** Kaplan-Meier survival curve of the animals that received air infusion (solid line) and sham animals (dotted line). Pigs that received air infusions died after a median of 300 minutes (IQR 249-320). All sham animals lived until the end of the observation period of either 300 (n=6) or 360 minutes (n=1).

observation time was chosen to allow adequate time for the synthesis of cytokines. To reduce the preterm mortality of animals, this was reduced to 300 minutes after the initial experiments. We adjusted the respiratory tidal volume, respiratory rate, and inspired oxygen fraction throughout the experiments to maintain arterial pH 7.34-7.40 and SpO_2 above 90%. We infused 2-3 mL/kg/h of Ringer's acetate to compensate for insensible fluid losses. If mean arterial pressure dropped below 55 mmHg, we administered repeated boluses of 100 mL Ringer's acetate and infused noradrenaline (Abcur, Helsingborg, Sweden) in the range 0.01 to 0.8 μg/kg/minute. Animals still alive at the end of the experiment were euthanized by intravenous injection of 30-50 mmol potassium chloride (B. Braun, Melsungen, Germany).

Blood and Tissue Sampling and Analysis

We sampled arterial blood from the carotid artery at baseline (just before the air infusion was started at zero minutes), after 30, 60, 180, 240, and 300 minutes of air infusion, and at the end of the experiments. Approximately 100 mL of blood was sampled

from the animals throughout the experiments. The blood was sampled using a Vacutainer closed vacuum system, Vacuette EDTA tubes and 3.2% sodium-citrate tubes, and serum tubes with gel (all Vacuette, Greiner Bio-One GmbH Frickenhausen, Germany), and a safePICO heparinized blood gas syringe (Radiometer, Copenhagen, Denmark). To avoid unintended contamination of the samples with heparin from the line flush solution, 5 mL of blood was aspirated into a sterile syringe immediately before sampling. Additionally, after drawing blood into the heparinized blood gas syringe, 2 mL of blood was drawn and discarded before subsequent sampling. Blood drawn on heparinized syringes was analyzed immediately after drawing for lactate, pH, pO_2, and pCO_2 on the ABL80 Flex blood gas analyzer (Radiometer, Copenhagen, Denmark). A set of EDTA tubes were stored at room temperature for up to 8 hours and analyzed for white blood count using the ADVIA 2120i (Siemens Healthcare GmbH, Erlangen, Germany) or IDEXX ProCyte Dx (IDEXX Laboratories, Westbrook, ME). A set of EDTA tubes were immediately centrifuged at 4°C at 1500 g for 15 min and plasma isolated and frozen at -80°C for later analysis of complement and cytokines, as detailed below. PAXgene tubes were carefully tilted ten times, left at room temperature for a minimum of two hours, frozen at -20°C overnight, and then at -80°C until RNA extraction and cytokine mRNA analysis.

Post-mortem, we opened the thorax and sampled tissue from the lower lobe of the left lung. These samples were snap-frozen on dry ice in NUNC tubes (Thermo Scientific, Roskilde, Denmark) with no additive for further homogenization and analysis.

Homogenization of Lung Tissue

For cytokine mRNA analysis, approximately 20 mg of tissue was transferred to gentleMACS M-tubes (Miltenyi Biotec, Bergisch Gladbach, Germany), and 800 µL Trizol reagent (Thermo Fisher Scientific, MA) was added to the samples. The samples were homogenized using program 7 on the Dispomix homogenizer (Miltenyi Biotec). After homogenization, the samples were left at RT for 5 minutes, centrifuged at 1,400 *g* for two seconds, and transferred to 1.5 mL Eppendorf PCR Clean Safe-Lock Tubes (Eppendorf, Enfield, CT) and stored at -80°C for later mRNA isolation and PCR analysis.

For complement analysis, approximately 100 mg of tissue was transferred to gentleMACS M-tubes, and a mixture of 10 µL Protease Inhibitor Cocktail Set I (Merck KGAA, Darmstadt, Germany) and 1 mL CytoBuster Protein Extraction Reagent (Millipore Sigma, Burlington, MA) was added to the samples, and the samples were homogenized using program 7 on the Dispomix homogenizer (Miltenyi Biotec). After homogenization, the samples were incubated for 5 minutes on ice, centrifuged for 20 minutes at 2,500 *g* at 4°C, and the supernatant was transferred to 1 mL Matrix tubes (Thermo Fisher Scientific) and stored at -80°C for later analysis. Likely, receptor-bound C3a detached during the lysis process, making it available for subsequent ELISA detection.

Analysis of Complement in Plasma and Lung Tissue

We measured complement C3a using ELISA with porcine-specific C3a monoclonal antibodies as previously described in detail (22). The antibody binds to a neoepitope exposed when C3a is cleaved off C3, and the assay only detects free C3a in the fluid phase. We measured TCC using ELISA with the anti-human-C9 neoepitope antibody clone aE11 produced in-house as capture antibody and a porcine cross-reacting anti-human C6, Quidel (San Diego, CA) as detection antibody as described in detail (23, 24). We have previously documented that the aE11 cross-reacts with porcine TCC (23).

Analysis of Cytokines in Plasma

We analyzed EDTA plasma for the following cytokines using immunoassays: Tumor necrosis factor (TNF) and interleukin (IL)-6 using the Porcine TNF and IL-6 Quantikine sandwich ELISA kit (R&D Systems Inc.) with optical density measured by Infinite M200 Pro microplate reader (Tecan Trading AG, Switzerland); IL-1β, IL-6, and IL-8 using a porcine MILLIPLEX map Kit (Merck, EMD Millipore Corporation, Billerica, MA) and IL-10 using Invitrogen ProcartaPlex Multiplex Porcine Immunoassay (Bender MedSystems GmbH, Vienna, Austria), and the fluorescence intensity analyzed on a Bio-Plex 200 Multiplex Analyzer (Bio-Rad Laboratories). All analyses were performed in accordance with the manufacturer's instructions.

Analysis of Cytokines in Lung Tissue

We analyzed samples of homogenized lung tissue for IL-6 using the Milliplex map Kit (Merck) and IL-10 using Invitrogen ProcartaPlex Multiplex Immunoassay for Porcine assay (Bender MedSystems GmbH, Vienna, Austria). The fluorescence intensity was analyzed on a Bio-Plex 200 Multiplex Analyzer (Bio-Rad Laboratories). We analyzed the homogenized tissue for TNF, IL-1β, and IL-8 using Quantikine sandwich ELISA kits (R&D Systems Inc.) and measured the optical density using an Infinite M200 Pro microplate reader (Tecan Trading AG). All analyses were performed in accordance with the manufacturer's instructions. Results are given pr. mL homogenate.

Analysis of Cytokine mRNA in Lung Tissue

Paxgene blood, 1.5 mL, was transferred to 2 mL Eppendorf tubes (Eppendorf) and centrifuged at 5,000 *g*, 10 min. The supernatant was carefully poured from each tube, and the pellet was resuspended in 1 mL nuclease-free water. The RNA was re-pelleted by centrifugation at 5,000 *g* for 10 minutes. MagMAX for Stabilized Blood Tubes RNA Isolation Kit (Thermo Fisher Scientific) was used for total RNA isolation in accordance with the manufacturer's instructions. The extracted RNA was eluted in 50 µL of Elution Buffer, quantified using Thermo Scientific Nanodrop 2000 (Thermo Fisher Scientific), and controlled with the Agilent 2100 Bioanalyzer (Agilent Technologies Santa Clara, CA). The mean RNA Integrity Number was 9.6.

RNA was extracted from homogenized lung tissue using TRIzol Reagent and RNeasy MinElute Cleanup kit (Qiagen, Hilden, Germany) and subsequent DNase treatment (Thermo Fisher Scientific) as described previously (25). RNA was quantified using the NanoDrop 2000 and integrity controlled using the Agilent 2100 BioAnalyzer. The mean RNA integrity number was 8.1.

For gene expression studies, the TaqMan RNA-to-Ct 1-step Kit (Thermo Fisher Scientific) was used. The amount of input RNA was 25 ng in a total volume of 20 µL. Cycling conditions were set according to the kit insert, and qPCR was run in triplicates for each candidate gene in MicroAmp Fast 96-Well Reaction Plates (all reagents from Thermo Fisher Scientific) using QuantStudio 6 Flex Real-Time PCR System instrument (Thermo Fischer Scientific). Predeveloped TaqMan porcine gene expression assays (Thermo Fisher Scientific) for the following candidate genes were used: IL-1β (Ss03393804_m1), IL-8 (Ss03392437_m1), and TNF (Ss03391318_g1). IL-6 (PIG_IL6) was custom-made by Thermo Fisher Scientific. Ribosomal Protein S 18 (Ss03391029_g1) was used as endogenous control and was stably expressed in all samples. The relative quantification (RQ) of cytokine mRNA expression was calculated using the comparative cycle threshold ($2^{-\Delta\Delta Ct}$) method. All results are presented as fold change (RQ) compared to sham animals.

Analysis of Thrombin-Antithrombin Complex (TAT) in Plasma

We quantified the TAT in EDTA plasma using the human Enzygnost TAT micro (Siemens Healthcare Diagnostics Products GmbH, Marburg, Germany), documented to cross-react with porcine TAT (26) in accordance with the manufacturer's instructions. The optical density was measured using an Infinite M200 Pro microplate reader (Tecan Trading AG).

Whole Blood Rotational Thromboelastometry (ROTEM)

We used the ROTEM delta (Tem Innovations GmbH, Munich, Germany) to analyze the kinetic of the clot formation. Citrated blood sampled at 0, 30, 60, and 120 minutes of air infusion were incubated at 37°C for five minutes and analyzed using the non-activated thromboelastometry test (NATEM) according to the manufacturer's instructions. 300 µL citrated blood was added in a disposable cup with 20 µL star-TEM reagents containing $CaCl_2$ (Tem Innovations GmbH). The clot formation was detected by inhibition of the movement of the pin in the cup, and several parameters were measured or calculated. Clotting time (CT, in seconds), clot formation time (CFT, in seconds), α-angle (in degrees), and maximum clot formation (MCF, in millimeters) were analyzed in this study.

Data Analysis and Statistical Methods

All data was collected and organized, and missing values were imputed in Microsoft Excel for Mac version 16.54 (Microsoft Inc., Redmond, CA). In animals that died before 300 minutes of observation, missing data were imputed using the Last-Observation-Carried-Forward method. Changes from baseline were calculated for leukocytes, TAT, and ROTEM readouts, and RQ were calculated for cytokine mRNA qPCR in Microsoft Excel. Statistical analysis and data charting was done in Prism for macOS version 9.3.0 (Graphpad Software, La Jolla, CA). Results from post-mortem analysis of lung cytokines, cytokine mRNA, and complement in pigs receiving air infusion were compared with sham animals using the two-tailed Mann-Whitney U-test. Changes from baseline to time of death in plasma complement, TAT, and leukocytes and changes from baseline to 120 minutes of observation in whole blood ROTEM were analyzed using the Wilcoxon matched-pairs signed-rank test. All analyses were corrected for multiple comparisons using Benjamini and Hochberg's original false discovery rate (FDR) method with an FDR of 1%. A p-value <0.05 was considered significant. Results are presented as medians with interquartile range. Graphs of repeated samples are presented as changes from baseline. As our data did not follow a Gaussian, data are presented as medians with interquartile range. qPCR relative quantifications are presented as geometric means with 95% CI.

Five pigs had one or more plasma TCC results below the lower detection limit, and one pig had lung tissue TCC results below the lower detection limit. These missing values were imputed with a random number between 0.01 and the lower detection limit. Six pigs had lung cytokines results below the lower detection limit but with reliable results on the extrapolated standard curve. These results were included in the analysis. One lung tissue IL-8 analysis failed and yielded no result. This missing value was replaced with the median lung tissue IL-8 from all pigs. One pig had an erroneous ROTEM baseline reading due to a heparin bolus given shortly before the baseline sampling. The baseline ROTEM for this animal was imputed by averaging the ROTEM readings thirty minutes before and thirty minutes after baseline sampling.

RESULTS

Animals Included in the Study

Fourteen of 45 animals were excluded from the study due to infections, open foramen ovale, or perioperative adverse events (**Figure 1**). Twenty-four animals receiving air infusion and seven sham animals were included in the study. Baseline observations sampled after the initial instrumentation but before air infusion did not differ between pigs allocated to air infusion and sham animals (**Table 1**).

Despite careful titration of the air infusion, ten of the 24 animals (42%) receiving air infusion died before the end of the experiments with a clinical picture of acute right heart failure, after a median of 243 minutes (IQR 240-261) (**Figure 2B**). Fourteen of the 24 animals receiving air infusion, and all sham animals lived until the end of the experiments. The last observations were carried forward for the ten animals that died before 300 minutes of observation.

Complement in Plasma and Lung Tissue

In pigs receiving air infusion, baseline median plasma C3a was 21 ng/mL (IQR 15-46). Plasma C3a increased steadily after 120 minutes of air infusion and was 3.2-fold higher (67 ng/mL [IQR 39-84]) at death than at baseline (p<0.001) (**Figure 3A**). In sham animals, no C3a increase was observed during the observation period. In pigs receiving air infusion, baseline median plasma TCC was 0.8 CAU/mL (IQR 0.6-1.1). During the experiment, plasma TCC increased to a lesser extent and was 1.25-fold higher (1.0 CAU/mL [IQR 0.7-1.4]) at death than at baseline (p=0.02)

TABLE 1 | Characteristics of pigs included in the study at baseline[1].

		Pigs receiving air infusion (n=24) Median (IQR)	Sham animals (n=7) Median (IQR)	p[2]
Weight	kg	17 (10-24)	11 (9.5-22)	0.8
ROTEM				
Clotting time (CT)	seconds	613 (531-677)	519 (453-604)	0.2
Clot formation time (CFT)	seconds	161 (122-195)	133 (126-167)	0.6
α-angle	degrees	57 (62-68)	66 (59-68)	0.6
Maximum clot formation (MCF)	millimeter	64 (59-73)	65 (63-68)	0.6
Biochemistry				
White blood cell count (WBC)	$x10^9/L$	17 (10-24)	16 (11-18)	0.6
ELISA				
Thrombin-antithrombin complex (TAT)	µg/mL	35 (28-42)	23 (16-29)	0.2
C3a	ng/mL	21 (15-46)	12 (7.9-20)	0.2
TCC	CAU/mL	0.8 (0.6-1.1)	0.7 (0.3-0.8)	0.4

[1]*Sampled after 30 minutes after instrumentation, before air infusion (T0).* [2]*Wilcoxon signed-rank test. p values corrected for multiple comparisons using Benjamin and Hochberg's FDR method.*

(**Figure 3B**). In sham animals, no TCC increase was observed during the observation period.

In post-mortem lung tissue samples from pigs that received air infusion, median C3a was 34 ng/mL (IQR 14-50) versus 4.1 ng/mL (IQR 2.4-5.7) in sham animals (p<0.001) (**Figure 3C**), and median TCC was 0.3 CAU/mL (IQR 0.2-0.3) in pigs that received air infusion versus 0.2 CAU/mL (IQR 0.1-0.3) in the sham animals (p=0.02) (**Figure 3D**).

White Blood Cell Count

In pigs receiving air infusion, baseline median plasma white blood cell count was $17{\cdot}10^9$ cells/L (IQR 10-24). Plasma white blood cell count increased steadily after 120 minutes of air infusion and was 1.6-fold higher ($28{\cdot}10^9$ cells/L [IQR 16-42]) at death than at baseline (p<0.001) (**Figure 4A**). In sham animals, only a slight increase in white blood cell count was noted.

Cytokines in Plasma and Lung Tissue

During the experiments, no significant changes in plasma cytokines were observed in pigs receiving air infusion or sham animals. In contrast, in pigs receiving air infusion compared to sham animals, the post-mortem mean lung tissue cytokines mRNA expressions were increased: 12-fold for IL-1β, 121-fold for IL-6, and 17-fold for IL-8 (all p<0.001) (**Figure 4B**). The TNF mRNA expression did not differ between the groups. In line with the mRNA findings, the median lung tissue cytokines measured as protein in pigs receiving air infusion compared to sham animals were: IL-1β 302 pg/mL (IQR 190-437) versus 107 pg/mL (IQR 66-120), IL-6 644 pg/mL (IQR 358-1094) versus 25 pg/mL (IQR 23-30), IL-8 203 pg/mL (IQR 81-377) versus 21 pg/mL (IQR 20-35), and TNF 113 pg/mL (IQR 96-147) versus 16 pg/mL (IQR 13-22) (all p<0.001) (**Figure 4C**). Thus, TNF increased as measured by protein but not by mRNA.

Coagulation

In pigs that received air infusion, baseline median clotting time was 613 seconds (IQR 531-677) (**Figure 5A**), baseline median clot formation time was 161 seconds (IQR 122-195) (**Figure 5B**), and baseline median α-angle was 62 degrees (IQR 57-68) (**Figure 5C**). Already after 30 minutes of air infusion, clotting time and clot formation time had decreased and α-angle increased, and after 120 minutes of air infusion, both clotting time and clot formation time were significantly reduced compared to baseline, to 538 seconds (IQR 399-620) and 124 seconds (IQR 83-162) (p=0.006 and p=0.02, respectively). The α-angle significantly increased compared to baseline, to 68 degrees (IQR 62-74) (p=0.02). In contrast, in sham animals, neither clotting time, clot formation time, or α-angle changed significantly during the observation period (**Figures 5A–C**). The maximum clot formation did not change significantly during the experiments.

In pigs that received air infusion, baseline median TAT was 35 µg/mL (IQR 28-42). TAT increased after 180 minutes of air infusion and continued to increase throughout the experiments (**Figure 5D**). At the end of the experiments, median TAT was 1.5-fold higher (51 µg/mL [IQR 38-89]) than at baseline (p=0.002). In contrast, TAT remained at baseline in sham animals throughout the observation period.

DISCUSSION

In this study, we have shown *in vivo* in a porcine model how venous air embolism triggered a thromboinflammation with activation of the complement system, leukocytosis, release of proinflammatory cytokines, and activation of coagulation. Notably, air embolism triggered a relatively selective and robust C3 activation as measured by C3a, without a corresponding C5 activation, as measured by TCC.

The complement system is an integral part of the innate immune system, protecting the body against invading pathogens and endogenous cellular damage. The system consists of several plasma peptides, which bind to antibodies, lectins, or foreign surfaces, resulting in classical, lectin, or alternative pathway activation, respectively (27). It has previously been shown that air activates the complement system mainly through the alternative pathway (14, 15) by hydrolysis of C3 to generate C3 (H_2O), also termed C3b-like or iC3 (14). This initial alternative C3 activation generates the C3(H_2O)B, where factor B is cleaved by factor D to form Ba, which is released, and Bb, which together

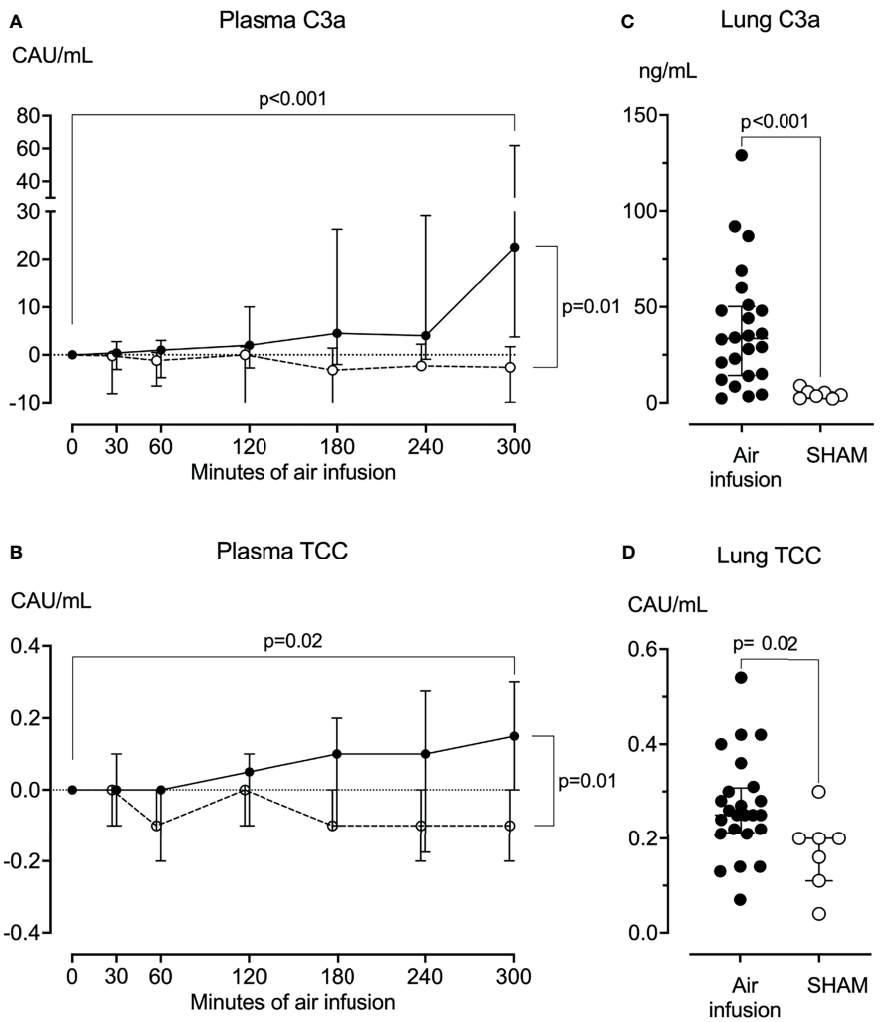

FIGURE 3 | Complement activation products in plasma and lung tissue. **(A)** Plasma C3a was measured at regular intervals throughout the experiments. C3a increased significantly from baseline in animals receiving air infusion (solid line) but not in sham animals (dotted line). **(B)** Plasma TCC measured at regular intervals throughout the experiments increased significantly from baseline in animals receiving air infusion (solid line) compared to the sham animals (dotted line). **(C)** In lung tissue sampled post-mortem, C3a was significantly higher in animals receiving air infusion than in sham animals. **(D)** In lung tissue sampled post-mortem, TCC was slightly but statistically significantly higher in animals receiving air infusion than sham animals. Dots in panels **(A, B)** and horizontal lines in panels **(C, D)** represent medians. Error bars span the interquartile range. Note Y-axis is split in panel **(A)** The two-tailed Mann-Whitney test was used between groups, and the Wilcoxon signed ranks test for within-group comparisons. P-values in panels **(A, B)** are corrected for multiple comparisons using Benjamin and Hochberg's FDR method.

with properdin (P) binds to C3(H_2O) and forms the first alternative C3 convertase, C3(H_2O)BbP. This convertase further activates C3 to be cleaved to C3b and C3a, and the final alternative pathway C3 convertase C3bBbP is formed. Under normal circumstances, C3bBbP forms the C5-convertase ($C3b_2BbP$), which catalyzes the formation of the terminal C5b-9 complement complex (TCC). Activated C3- and C5-split products have been shown to interact with thrombocytes and leukocytes (28, 29) and may potentially trigger a *thromboinflammation* involving both leukocytes, platelets, and coagulation. Interestingly, and in line with our previous *in vitro* findings in human whole blood (15), we discovered that air embolism predominantly activated C3 with only a minor C5 activation, contrary to what is otherwise observed in general when complement is activated, for example, by bacteria or damage or pathogen-associated molecular patterns. The C5a-C5aR axis is known to play an important role in complement-mediated thromboinflammation associated with a wide array of diseases (27, 30), and the monoclonal anti-C5 antibody eculizumab has been used clinically for many years to treat complement-driven diseases, such as paroxysmal nocturnal hemoglobinuria and atypical hemorrhagic uremic syndrome (31). C3a receptors have been shown on both platelets and activated astrocytes, neutrophils, and monocytes (32, 33), and we have previously shown how C3 inhibition attenuates air-induced thromboinflammation (15).

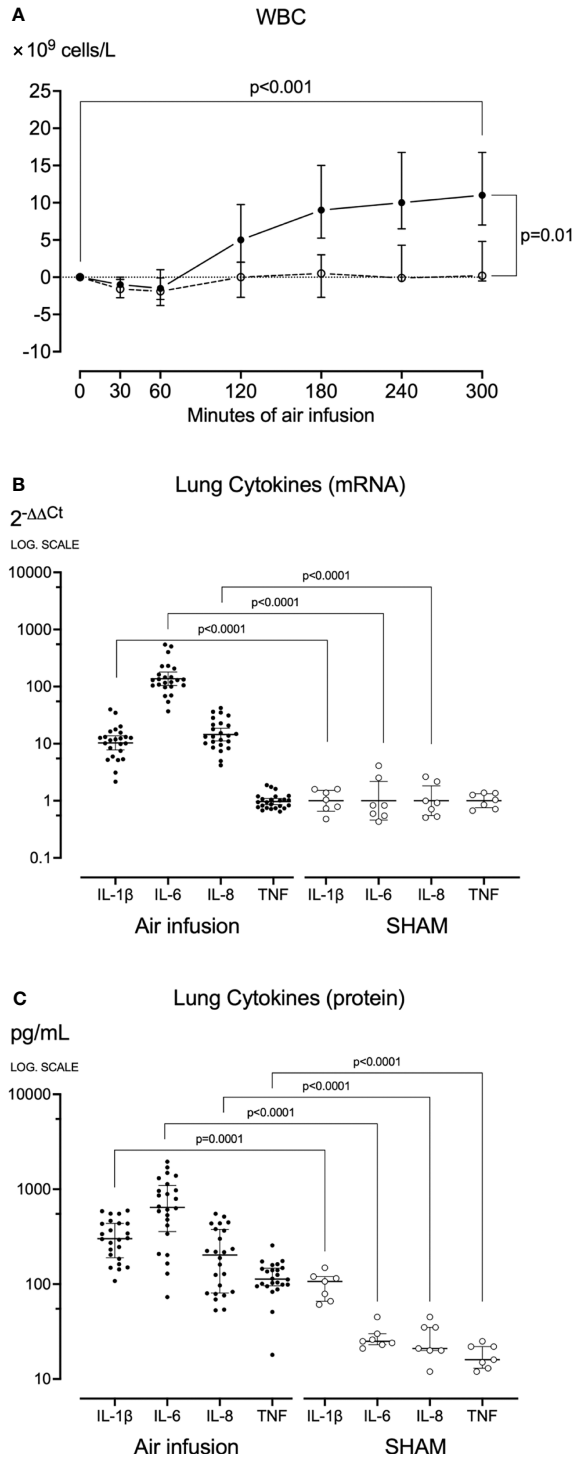

FIGURE 4 | Blood White Cell Count and Lung cytokines. **(A)** White blood cells were counted at regular intervals throughout the experiments. After sixty minutes of air infusion, white blood cells increased significantly from baseline in animals receiving air infusion (solid line) but not in sham animals (dotted line). **(B)** In lung tissue sampled post-mortem cytokine mRNA was analyzed using qPCR, and results were calculated using the $2^{-\Delta\Delta Ct}$ method. **(C)** In lung tissue sampled post-mortem, cytokines were measured using ELISA or multiplex. Animals receiving air infusion are represented as closed circles and solid lines, and sham animals as open circles and dotted lines. Circles in panel **(A)** and horizontal lines in panel **(C)** represent medians, and error bars span the interquartile range. The horizontal lines in panel **(B)** represent the geometric means, and error bars span the 95% CI of the mean.

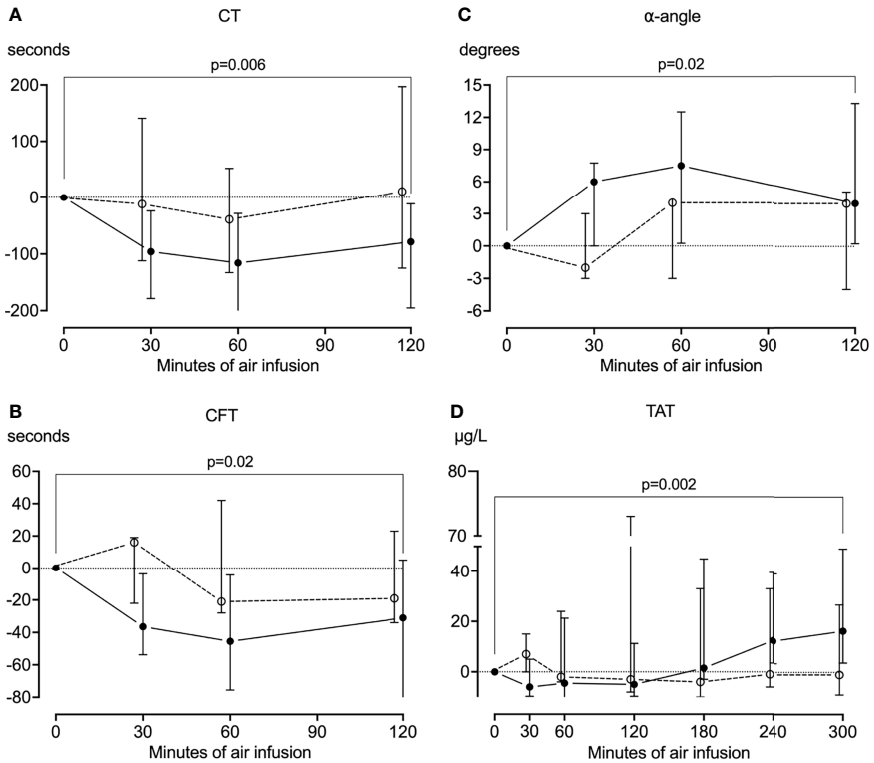

FIGURE 5 | Coagulation. Whole blood was drawn from the animals every half hour for the first two hours of the experiments, and the coagulation was analyzed using rotational thromboelastometry (ROTEM). In animals receiving air infusion, a significant reduction from baseline in the clotting time **(A)** and clot formation time **(B)** and a significant increase from baseline in the α-angle **(C)** was observed. These parameters mainly remained at baseline in sham animals, albeit with a pronounced heterogenicity. **(D)** Plasma was drawn from the animals throughout the experiments and analyzed for thrombin-antithrombin (TAT) using ELISA. TAT increased significantly from baseline in pigs receiving air infusion and remained at baseline in sham animals. Solid line represents pigs receiving air infusion. Dotted lines are sham animals. Circles represent medians, and error bars span the interquartile range.

Recently, a specific C3 inhibitor, pegcetacoplan (Empaveli, Apellis Pharmaceuticals, Waltham, MA), was approved to treat paroxysmal nocturnal hemoglobinuria (34), and further studies should evaluate if C3 inhibitors can be used to dampen thromboinflammation triggered by air embolism.

The aforementioned observed relative selective C3 activation without a corresponding C5 activation is most likely related to the mechanism by which air activates C3. The efficacy of the complement system convertases depends on whether the C3 activation occurs on the solid phase, where C3 binds to surfaces to generate a potent convertase, or in the fluid phase, where a less potent convertase is formed. As mentioned above, air bubbles have been shown to generate a fluid-phase C3 convertase *in vitro* in plasma experiments (14), and it is reasonable to assume that an identical fluid-phase convertase is formed *in vivo* in pigs with air embolism. The formation of a less efficient fluid-phase convertase could explain why the C5 convertase is insufficiently generated, which we documented with limited TCC formation compared to C3 activation. This contrasts the complement activation otherwise seen. For example, in a porcine study of polymicrobial sepsis (35), both C3a and TCC increased substantially, with C3a appearing first followed by TCC (22).

Another interesting imbalance between C3 and C5 convertase potency occurs when autoantibodies, nephritic factors (NeFs) form against the complement convertases, as recently reviewed (36). NeFs may bind to the C3, C4, or C5 convertase (C3NeF, C4Nef, and C5Nef, respectively). NeF binding stabilizes the convertases, resulting in pathological ongoing complement activation. As with air embolism, we have previously shown that some C3NeFs activate C3 without a corresponding C5 activation (37). NeFs cause an autoimmune kidney failure in patients, particularly if the C5 is activated (36).

The imbalance between C3 and C5 activation is important concerning the potential treatment of patients with air embolism. Most complement-mediated diseases involve the C5a or the C5b-9, and treatment involves inhibition of C5 to keep the C3 open for complement-driven bacterial defense. However, in the case of venous air embolism, C3 inhibition would be required to reduce the thromboinflammatory response effectively. It remains to be shown if other pathophysiological conditions are similarly mainly driven by C3 activation with only a modest activation of C5.

In our study, we measured C3a using an ELISA assay with a porcine-specific antibody (22) and TCC using a human assay

shown to work well in swine (23, 24), as no reliable porcine C5a assay is commercially available. This is a reasonable approach, as C5a and TCC (sC5b-9) are released in equimolar concentration in plasma. TCC has a plasma half-life of 50-60 minutes (38) compared to C5a with a half-life of one minute (23), making it a robust marker of terminal pathway activation. Further details on assays for the detection of complement activation products in humans and animals are reviewed in detail (39).

In pigs that received air infusion, but not in sham animals, we found increased levels of proinflammatory cytokines in lung tissue, increased circulating white blood cells, and coagulation system activation. Combined with our human *in vitro* findings (15), we have shed new light on the mechanisms for inflammation, coagulation, and the interplay between complement, inflammation, and coagulation. Our data suggest that complement activation played an important role mainly through the activation of C3. *In vitro*, we showed how selective inhibition of C3 reduced complement activation, cytokine release, and coagulation. Most of the inflammatory mediators were purely mediated by C3-activation, but a few were C5a dependent. The majority of mediators were abolished by C3 inhibition. Thus, there is a theoretical rationale for C3 inhibition as a treatment of air embolism *in vivo*. Unfortunately, as no inhibitor reacting with porcine C3 is currently available largescale for *in vivo* studies, we could not verify these findings in our porcine model.

The accumulation of C3a and increased cytokine concentrations in lung tissue of pigs with air embolism indicates the importance of the lungs in the pathophysiology of venous air embolism and air-induced thromboinflammation. Venous air emboli are transported with the bloodstream to the lung capillaries, where the air is absorbed into the alveoli and exhaled. However, large amounts of air may overwhelm the lung's filtering capacity, occlude the capillaries and obstruct blood flow, trigger a local inflammatory process, or transverse the lungs to the systemic circulation (7, 9, 40). In humans, air bubbles have been shown to activate the alternative complement pathway *in vivo, ex vivo*, and *in vitro* (12, 14, 15). We suggest that lodged air bubbles in the pig's lung capillaries activated C3 by a similar mechanism and subsequently triggered inflammation and coagulation alike in humans. This would explain the increase in lung tissue cytokines and circulating white blood cells observed in pigs receiving air infusion. The pulmonary inflammation may have triggered lung edema. The combination of air bubbles, thrombi, and edema may have further hampered blood flow and gas exchange, resulting in pulmonary hypertension, a drop in end-tidal CO_2, and acute right heart failure, as we and others have found in animals studies and human cases (6, 20, 41, 42).

In our study, air infusion triggered coagulation, measured by ROTEM and TAT. We recently showed *in vitro* in human whole blood that coagulation was activated through a complement-dependent mechanism, where C3 activation played a pivotal role, and through a complement-independent mechanism, which we did not identify in detail (15). We speculate that air embolism activated the coagulation through similar mechanisms *in vivo* in pigs. The ROTEM and TAT results were most likely diminished and underestimated, as we had to administer a heparin infusion of approximately 30 IU/h to avoid coagulation of arterial and venous lines and the buildup of thrombi on the pulmonary artery catheter. Additionally, in animals receiving air infusion, but not in sham animals, we also had to administer intermittent heparin boluses of approximately ten IU due to thrombi in the pulmonary artery catheter.

Despite many similarities between humans and pigs, human immunoassays may not reliably cross-react and work in pigs. In this study, we limited complement readouts to C3a and TCC, and we used only cytokine assays shown to work in pigs as detailed in (43). Many commercial immunological assays, including complement and cytokine assays, are marketed as working in pigs. Over the years, we have thoroughly tested most available complement assays, comparing them to the reliable C3a and TCC assays described above and in (22–24); disappointingly, in such comparisons, most assays failed to detect complement activation reliably. Likewise, we have recently studied porcine-specific cytokine assays, finding that many of these are also unreliable (43).

Our study has some limitations; it was a single-center, non-randomized, and non-blinded exploratory study. The animals were assigned to air infusion or to serve as sham animals at the examiner's discretion. However, we do not suggest that these limitations affected our results.

Despite careful titration of the air infusion, several animals died before the intended 300 minutes of air infusion, with most premature deaths occurring between 240 and 300 minutes of air infusion (**Figure 2**). These premature deaths could have been mitigated by using a less-aggressive air infusion protocol, for example, by not increasing the infusion rate after 180 minutes of air infusion or by terminating the experiments after 180 minutes of air infusion. However, we titrated the air infusion to maximize the effects of air embolism on the thromboinflammation to allow for complement production and time for the synthesis of cytokines. It is possible that reducing the air infusion or shortening the experiments would have reduced complement readouts and yielded lower post-mortem cytokine levels. However, we measured cytokines by mRNA and by protein quantification, enabling us to detect cytokines with high sensitivity. Cytokine mRNA forms rapidly before proteins are synthesized, but, as we observed concerning TNF and IL-1β, may also be downregulated and thus not detected by PCR when proteins are still present and detected by ELISA in the tissue. In our study, pigs that died prematurely were more inflammatory affected than animals surviving the experiment, and it is unlikely that premature death impacted our results negatively.

CONCLUSION

Venous air embolism triggered thromboinflammation *in vivo* in pigs, reflected by increased plasma complement C3 activation, leukocytosis, and coagulation. Furthermore, post-mortem pulmonary tissue homogenates revealed increased C3a and

cytokines IL-1β, IL-6, IL-10, and TNF, and increased synthesis of IL-1β, IL-6, IL-8, and IL-10 mRNA. A corresponding terminal pathway activation did not follow the C3 activation. These findings align with previous *in vitro* human whole blood studies, suggesting that C3-inhibition is relevant for further studies in the treatment of venous air embolism.

DATA AVAILABILITY STATEMENT

The raw data supporting the conclusions of this article will be made available by the authors upon request, without undue reservation.

ETHICS STATEMENT

The animal study was reviewed and approved by The Norwegian Animal Research Authority (FOTS ID9466) and performed perthe Norwegian Laboratory Animal Regulations and EU directive2010/64/EU.

AUTHOR CONTRIBUTIONS

BS, TM, and EN conceptualized and designed the study. BS, EN, BN, and KD conducted animal experiments. BS, DC, HF, JL, KP, and AL acquired and analyzed the biological materials. BS and TB conducted the statistical analyses. BS, EN, and TM drafted the manuscript. All authors critically revised the manuscript and approved the final version.

FUNDING

The study was funded by an unrestricted research grant from Northern Norway Regional Health Authority (Helse Nord RHF).

ACKNOWLEDGMENTS

We thank Chief Bioengineer Reidar Johansen, Department of Laboratory Medicine, Nordland Hospital, Gravdal, Norway, for valuable assistance with sample analysis, and Paul van Buren, Jr., and Sr., for proofreading the manuscript.

REFERENCES

1. Brull SJ, Prielipp RC. Vascular Air Embolism: A Silent Hazard to Patient Safety. *J Crit Care* (2017) 42:255–63. doi: 10.1016/j.jcrc.2017.08.010
2. Fromer IR, Horvath B, Prielipp RC, Kloesel B. Vascular Air Emboli During the Perioperative Period. *Curr Anesthesiol Rep* (2020) 10:436–48. doi: 10.1007/s40140-020-00407-4
3. Mirski MA, Lele AV, Fitzsimmons L, Toung TJK. Diagnosis and Treatment of Vascular Air Embolism. *Anesthesiology* (2007) 106:164–77. doi: 10.1097/00000542-200701000-00026
4. Lambrechts K, Pontier J-M, Mazur A, Buzzacott P, Morin J, Wang Q, et al. Effect of Decompression-Induced Bubble Formation on Highly Trained Divers Microvascular Function. *Physiol Rep* (2013) 1:10. doi: 10.1002/phy2.142
5. Oppenheimer MJ, Durant TM, Lynch P. Body Position in Relation to Venous Air Embolism and the Associated Cardiovascular-Respiratory Changes. *Am J Med Sci* (1953) 225:362–73. doi: 10.1097/00000441-195304000-00003
6. Storm BS, Andreasen S, Hovland A, Nielsen EW. Gas Embolism During Hysteroscopic Surgery?: Three Cases and a Literature Review. *Case Rep* (2017) 9:140–3. doi: 10.1213/XAA.0000000000000549
7. Vik A, Jenssen BM, Brubakk AO. Comparison of Haemodynamic Effects During Venous Air Infusion and After Decompression in Pigs. *Eur J Appl Physiol Occup Physiol* (1994) 68:127–33. doi: 10.1007/BF00244025
8. Rademaker BMP, Groenman FA, van der Wouw PA, Bakkum EA. Paradoxical Gas Embolism by Transpulmonary Passage of Venous Emboli During Hysteroscopic Surgery: A Case Report and Discussion. *Br J Anaesth* (2008) 101:230–3. doi: 10.1093/bja/aen138
9. Vik A, Brubakk AO, Hennessy TR, Jenssen BM, Ekker M, Slørdahl SA. Venous Air Embolism in Swine: Transport of Gas Bubbles Through the Pulmonary Circulation. *J Appl Physiol 1985* (1990) 69:237–44. doi: 10.1152/jappl.1990.69.1.237
10. Kapoor T, Gutierrez G. Air Embolism as a Cause of the Systemic Inflammatory Response Syndrome: A Case Report. *Crit Care* (2003) 7:R98–R100. doi: 10.1186/cc2362
11. Arstikyte K, Vitkute G, Traskaite-Juskeviciene V, Macas A. Disseminated Intravascular Coagulation Following Air Embolism During Orthotropic Liver Transplantation: Is This Just a Coincidence? *BMC Anesthesiol* (2021) 21:264. doi: 10.1186/s12871-021-01476-6
12. Pekna M, Nilsson L, Nilsson-Ekdahl K, Nilsson UR, Nilsson B. Evidence for Ic3 Generation During Cardiopulmonary Bypass as the Result of Blood-Gas Interaction. *Clin Exp Immunol* (1993) 91:404–9. doi: 10.1111/j.1365-2249.1993.tb05916.x
13. Gong J, Larsson R, Ekdahl KN, Mollnes TE, Nilsson U, Nilsson B. Tubing Loops as a Model for Cardiopulmonary Bypass Circuits: Both the Biomaterial and the Blood-Gas Phase Interfaces Induce Complement Activation in An*In Vitro* Model. *J Clin Immunol* (1996) 16:222–9. doi: 10.1007/BF01541228
14. Ekdahl KN, Nilsson B, Pekna M, Nilsson UR. Generation of Ic3 at the Interface Between Blood and Gas. *Scand J Immunol* (1992) 35:85–91. doi: 10.1111/j.1365-3083.1992.tb02837.x
15. Storm BS, Christiansen D, Fure H, Ludviksen JK, Lau C, Lambris J, et al. Air Bubbles Activate Complement and Trigger C3-Dependent Hemostasis and Cytokine Release Ex Vivo in Human Whole Blood. *J Immunol* (2021) 2021:2828–40. doi: 10.4049/jimmunol.2100308
16. Huang K-L. *The Role of Complement and Neutrophils in Air Bubble-induced Lung Injury*. Ann Abor, MI: University of Hawaii (1995). 189 p. ThesisUniversity of Hawaii. Lib. cat number 9604159.
17. Magri K, Eftedal I, Petroni Magri V, Matity L, Azzopardi CP, Muscat S, et al. Acute Effects on the Human Peripheral Blood Transcriptome of Decompression Sickness Secondary to Scuba Diving. *Front Physiol* (2021) 12:660402. doi: 10.3389/fphys.2021.660402
18. Mollnes TE, Brekke O-L, Fung M, Fure H, Christiansen D, Bergseth G, et al. Essential Role of the C5a Receptor in E Coli-Induced Oxidative Burst and Phagocytosis Revealed by a Novel Lepirudin-Based Human Whole Blood Model of Inflammation. *Blood* (2002) 100(5):1869–77.
19. Weiler JM, Edens RE, Linhardt RJ, Kapelanski DP. Heparin and Modified Heparin Inhibit Complement Activation *In Vivo*. *J Immunol* (1992) 1992:3210–5.
20. Durant TM, Long J, Oppenheimer MJ. Pulmonary (Venous) Air Embolism. *Am Heart J* (1947) 33:269–81. doi: 10.1016/0002-8703(47)90656-X
21. Vik A. *Vascular Gas Embolism During Air Infusion and After Decompression in Pigs. Hemodynamic Effects and Detection of Gas Emboli by Transesophagal Echocardiography*. Trondheim, Norway: NTNU (1993). Thesis.
22. Nilsson PH, Pettersen K, Oppermann M, Skjeflo EW, Fure H, Christiansen D, et al. Quantification of Porcine Complement Activation Fragment C3a by a Neoepitope-Based Enzyme-Linked Immunosorbent Assay. In: Roumenina LT,

editor. *The Complement System. Methods in Molecular Biology*. New York, NY: Springer US (2021). p. 51–9. doi: 10.1007/978-1-0716-1016-9_5
23. Mollnes TE, Lea T, Harboe M, Tschopp J. Monoclonal Antibodies Recognizing a Neoantigen of Poly(C9) Detect the Human Terminal Complement Complex in Tissue and Plasma. *Scand J Immunol* (1985) 22:183–95. doi: 10.1111/j.1365-3083.1985.tb01870.x
24. Jansen JH, Høgåsen K, Mollnes TE. Extensive Complement Activation in Hereditary Porcine Membranoproliferative Glomerulonephritis Type II (Porcine Dense Deposit Disease). *Am J Pathol* (1993) 143(5):1356–65.
25. Pischke SE, Hestenes S, Johansen HT, Fure H, Bugge JF, Espinoza A, et al. Sepsis Causes Right Ventricular Myocardial Inflammation Independent of Pulmonary Hypertension in a Porcine Sepsis Model. *PloS One* (2019) 14: e0218624. doi: 10.1371/journal.pone.0218624
26. Velik-Salchner C, Schnürer C, Fries D, Müssigang PR, Moser PL, Streif W, et al. Normal Values for Thrombelastography (ROTEM®) and Selected Coagulation Parameters in Porcine Blood. *Thromb Res* (2006) 117:597–602. doi: 10.1016/j.thromres.2005.05.015
27. Garred P, Tenner AJ, Mollnes TE. Therapeutic Targeting of the Complement System: From Rare Diseases to Pandemics. *Pharmacol Rev* (2021) 73:792–827. doi: 10.1124/pharmrev.120.000072
28. Markiewski MM, Nilsson B, Nilsson Ekdahl K, Mollnes TE, Lambris JD. Complement and Coagulation: Strangers or Partners in Crime? *Trends Immunol* (2007) 28:184–92. doi: 10.1016/j.it.2007.02.006
29. Barratt-Due A, Pischke SE, Nilsson PH, Espevik T, Mollnes TE. Dual Inhibition of Complement and Toll-Like Receptors as a Novel Approach to Treat Inflammatory Diseases—C3 or C5 Emerge Together With CD14 as Promising Targets. *J Leukoc Biol* (2017) 101:193–204. doi: 10.1189/jlb.3VMR0316-132R
30. Mannes M, Schmidt CQ, Nilsson B, Ekdahl KN, Huber-Lang M. Complement as Driver of Systemic Inflammation and Organ Failure in Trauma, Burn, and Sepsis. *Semin Immunopathol* (2021) 43(6):773–88. doi: 10.1007/s00281-021-00872-x
31. Thurman JM, Le Quintrec M. Targeting the Complement Cascade: Novel Treatments Coming Down the Pike. *Kidney Int* (2016) 90:746–52. doi: 10.1016/j.kint.2016.04.018
32. Sauter RJ, Sauter M, Reis ES, Emschermann FN, Nording H, Ebenhöch S, et al. Functional Relevance of the Anaphylatoxin Receptor C3aR for Platelet Function and Arterial Thrombus Formation Marks an Intersection Point Between Innate Immunity and Thrombosis. *Circulation* (2018) 138:1720–35. doi: 10.1161/CIRCULATIONAHA.118.034600
33. Gasque P, Singhrao SK, Neal JW, Wang P, Sayah S, Fontaine M, et al. The Receptor for Complement Anaphylatoxin C3a Is Expressed by Myeloid Cells and Nonmyeloid Cells in Inflamed Human Central Nervous System: Analysis in Multiple Sclerosis and Bacterial Meningitis. *J Immunol* (1998) 160(7):3543–54.
34. Mastellos DC, Ricklin D, Sfyroera G, Sahu A. From Discovery to Approval: A Brief History of the Compstatin Family of Complement C3 Inhibitors. *Clin Immunol* (2021) 235:108785. doi: 10.1016/j.clim.2021.108785
35. Skjeflo EW, Sagatun C, Dybwik K, Aam S, Urving SH, Nunn MA, et al. Combined Inhibition of Complement and CD14 Improved Outcome in Porcine Polymicrobial Sepsis. *Crit Care* (2015) 19(1). doi: 10.1186/s13054-015-1129-9
36. Corvillo F, Okrój M, Nozal P, Melgosa M, Sánchez-Corral P, López-Trascasa M. Nephritic Factors: An Overview of Classification, Diagnostic Tools and Clinical Associations. *Front Immunol* (2019) 10:886. doi: 10.3389/fimmu.2019.00886
37. Mollnes TE, Ng YC, Peters DK, Lea T, TSCHOPPt J, Harboe M. Effect of Nephritic Factor on C3 and on the Terminal Pathway of Complement *In Vivo* and *In Vitro*. *Clin Exp Immunol* (1986) 65(1):73–9.
38. Wagner JL, Hugli TE. Radioimmunoassay for Anaphylatoxins: A Sensitive Method for Determining Complement Activation Products in Biological Fluids. *Anal Biochem* (1984) 136:75–88. doi: 10.1016/0003-2697(84)90308-7
39. Harboe M, Thorgersen EB, Mollnes TE. Advances in Assay of Complement Function and Activation. *Adv Drug Deliv Rev* (2011) 63:976–87. doi: 10.1016/j.addr.2011.05.010
40. van Hulst RA, Klein J, Lachmann B. Gas Embolism: Pathophysiology and Treatment. *Clin Physiol Funct Imaging* (2003) 23:237–46. doi: 10.1046/j.1475-097X.2003.00505.x
41. Kyttä J, Randell T, Tanskanen P, Kajimoto Y, Rosenberg PH. Monitoring Lung Compliance and End-Tidal Oxygen Content for the Detection of Venous Air Embolism. *Br J Anaesth* (1995) 75:447–51. doi: 10.1093/bja/75.4.447
42. Storm BS, Halvorsen PS, Skulstad H, Dybwik K, Schjalm C, Christiansen D, et al. Open Chest and Pericardium Facilitate Transpulmonary Passage of Venous Air Emboli. *Acta Anaesthesiol Scand* (2021) 65:648–55. doi: 10.1111/aas.13796
43. Ueland NL, Ludvigsen JK, Hellerud BC, Mollnes TE, Skjeflo EW. Choice of Immunoassay to Evaluate Porcine Cytokine Levels. *Vet Immunol Immunopathol* (2020) 230:110129. doi: 10.1016/j.vetimm.2020.110129

Conflict of Interest: The authors declare that the research was conducted in the absence of any commercial or financial relationships that could be construed as a potential conflict of interest.

Publisher's Note: All claims expressed in this article are solely those of the authors and do not necessarily represent those of their affiliated organizations, or those of the publisher, the editors and the reviewers. Any product that may be evaluated in this article, or claim that may be made by its manufacturer, is not guaranteed or endorsed by the publisher.

frontiers in Immunology

ORIGINAL RESEARCH
published: 24 March 2022
doi: 10.3389/fimmu.2022.861670

Negative Immune Checkpoint Protein, VISTA, Regulates the CD4$^+$ T_{reg} Population During Sepsis Progression to Promote Acute Sepsis Recovery and Survival

*Chyna C. Gray[1,2], Bethany Biron-Girard[2], Michelle E. Wakeley[2], Chun-Shiang Chung[2], Yaping Chen[2], Yael Quiles-Ramirez[2], Jessica D. Tolbert[2] and Alfred Ayala[1,2]**

[1] Department of Molecular Biology, Cell Biology, and Biochemistry, Brown University, Providence, RI, United States,
[2] Division of Surgical Research, Department of Surgery, Brown University, Providence, RI, United States

OPEN ACCESS

Edited by:
Klemens Horst,
University Hospital RWTH Aachen, Germany

Reviewed by:
Tim-Philipp Simon,
RWTH Aachen University, Germany
Jan Tilmann Vollrath,
University Hospital Frankfurt, Germany

***Correspondence:**
Alfred Ayala
aayala@lifespan.org

Specialty section:
This article was submitted to Inflammation, a section of the journal Frontiers in Immunology

Received: 24 January 2022
Accepted: 25 February 2022
Published: 24 March 2022

Citation:
Gray CC, Biron-Girard B, Wakeley ME, Chung C-S, Chen Y, Quiles-Ramirez Y, Tolbert JD and Ayala A (2022) Negative Immune Checkpoint Protein, VISTA, Regulates the CD4$^+$ T_{reg} Population During Sepsis Progression to Promote Acute Sepsis Recovery and Survival. Front. Immunol. 13:861670. doi: 10.3389/fimmu.2022.861670

Sepsis is a systemic immune response to infection that is responsible for ~35% of in-hospital deaths and over 24 billion dollars in annual treatment costs. Strategic targeting of non-redundant negative immune checkpoint protein pathways can cater therapeutics to the individual septic patient and improve prognosis. B7-CD28 superfamily member V-domain Immunoglobulin Suppressor of T cell Activation (VISTA) is an ideal candidate for strategic targeting in sepsis. We hypothesized that immune checkpoint regulator, VISTA, controls T-regulatory cells (T_{reg}), in response to septic challenge, thus playing a protective role/reducing septic morbidity/mortality. Further, we investigated if changes in morbidity/mortality are due to a T_{reg}-mediated effect during the acute response to septic challenge. To test this, we used the cecal ligation and puncture model as a proxy for polymicrobial sepsis and assessed the phenotype of CD4$^+$ T_{regs} in VISTA-gene deficient (VISTA$^{-/-}$) and wild-type mice. We also measured changes in survival, soluble indices of tissue injury, and circulating cytokines in the VISTA$^{-/-}$ and wild-type mice. We found that in wild-type mice, CD4$^+$ T_{regs} exhibit a significant upregulation of VISTA which correlates with higher T_{reg} abundance in the spleen and small intestine following septic insult. However, VISTA$^{-/-}$ mice have reduced T_{reg} abundance in these compartments met with a higher expression of Foxp3, CTLA4, and CD25 compared to wild-type mice. VISTA$^{-/-}$ mice also have a significant survival deficit, higher levels of soluble indicators of liver injury (i.e., ALT, AST, bilirubin), and increased circulating proinflammatory cytokines (i.e., IL-6, IL-10, TNFα, IL-17F, IL-23, and MCP-1) following septic challenge. To elucidate the role of T_{regs} in VISTA$^{-/-}$ sepsis mortality, we adoptively transferred VISTA-expressing T_{regs} into VISTA$^{-/-}$ mice. This adoptive transfer rescued VISTA$^{-/-}$ survival to wild-type levels. Taken together, we propose a protective T_{reg}-mediated role for VISTA by which inflammation-induced tissue injury is suppressed and improves survival in early-stage murine sepsis. Thus, enhancing VISTA expression or adoptively transferring VISTA$^+$ T_{regs} in early-stage sepsis may provide a novel therapeutic approach to ameliorate inflammation-induced death.

Keywords: Vista, sepsis, regulatory T cells, cytokines, liver injury, Foxp3, CTLA4, CD25

1 INTRODUCTION

Despite exhaustive research on sepsis over the last 50 years (1) there remains no effective patho-physiological treatment options nor molecular methods of diagnosis. The incidence of sepsis has not improved, with sepsis accounting for ~35% of non-cardiac deaths during intensive care unit hospitalization, accounting for ~1 in 5 deaths worldwide (2), and it was the consensus cause of death assigned to those dying from COVID-19 infection (3). At >24 billion dollars in annual treatment costs, sepsis presents an economic as well as a healthcare burden (4). Historically, sepsis clinical trials have targeted the initial pro-inflammatory response by inhibiting cytokines in septic patients (5, 6). Efficacy was not universal, and treatment predisposed patients to fatal secondary infections (7).

Immune checkpoint blockade (ICB) has been used to ameliorate disease pathology with greater precision and success than many immune-directed therapies (8). Our laboratory, among others, has demonstrated that negative checkpoint regulator (NCR) targeting improves survival in preclinical sepsis models, but success has been limited in clinical trials (9–15). Strategic targeting of non-redundant NCR pathways has the potential to cater therapeutics to the individual septic patient and improve prognosis (16–18).

B7-CD28 superfamily member V-domain Immunoglobulin Suppressor of T cell Activation (VISTA) is an ideal candidate for such potential strategic targeting in sepsis (18, 19). VISTA is a 55–65-kDa type 1 transmembrane protein and has unique biology that set it apart from all other NCRs (20, 21).

VISTA can act as a receptor or a ligand binding in VISTA : VISTA interactions, with VSIG-3, or with PSGL-1 depending on the cell it is expressed on (22, 23). VISTA regulation is also temporally distinct, acting as the earliest NCR of peripheral tolerance. Under steady-state conditions, VISTA promotes quiescence of naïve $CD4^+$ T cells to prevent self-reactivity (24). Under inflammatory conditions, VISTA suppresses effector $CD4^+$ T cell function (17, 20), maintains the T regulatory cell (T_{reg}) pool size, and promotes induced T_{reg} (iT_{reg}) generation (25). This $CD4^+$ T cell-specific modularity makes VISTA a specific and non-redundant regulator of the acute T cell response (24–27).

Septic patients experience a reduced number/frequency of splenic and thymic T cells, decreased cytokine production, and increased expression of exhaustion markers (28, 29). In murine sepsis models, there is a significant loss of $CD4^+$ T cell frequency which impacts survival (30). Our laboratory, among others, has demonstrated that T_{regs} play an indispensable role in the acute septic response, resolving inflammatory tissue damage and improving survival (31–34).

Based on the findings from our laboratory and others, we set out to determine if the immune checkpoint regulator VISTA controls T-regulatory cells (T_{reg}), in response to septic challenge, thus playing a protective role and reducing septic morbidity/mortality. Further, we investigated if changes in morbidity/mortality were due to a T_{reg}-mediated effect during the acute response to a septic challenge.

2 MATERIAL AND METHODS

2.1 Mice

Male C57BL/6 mice were purchased from Jackson Laboratories (Bar Harbor, ME, USA). Animals obtained from our outside vendor were acclimated no less than 7 days, and often longer [maximum ~5 weeks], prior to utilizing these animals in the studies described here. During this period, they were housed in the Rhode Island Hospital (RIH) rodent facility (12-h: 12-h light/dark cycle, 23°C–25°C, 30%–70% humidity) where they received standard care and diet (standard rodent chow)/water *ad libitum*. All protocols were carried out in the morning (8–11 a.m.) and were performed in accordance with the National Institutes of Health guidelines and as approved by the Animal Use Committee of Rhode Island Hospital (AWC# 5064-18 & 5054-21). $VISTA^{-/-}$ mice were produced at the Brown University Transgenic Facility using CRISPR/Cas9 technology. Guide RNA sequences for the 5′ deletion site:

395_Vsir_ex2upsgRNA1: CTTAGTAACAAGACCCACAT

396_Vsir_ex2upsgRNA2: GCTTAGTAACAAGACCCACA

Guide RNA sequences for the 3′ deletion site:

398_Vsir_ex7sgRNA1: ATGTGCACTTGATCTATGGC (18-mer)

399_Vsir_ex7sgRNA2: GTGCCTAAAAGACTGTCCAA

The initial genotyping strategy and PCR results for G1 and F0 generations are described in **Supplemental Figure 1**. A routine genotyping of $VISTA^{-/-}$ mice was performed on tail biopsy samples collected after weaning. Tail samples were processed for PCR and treated with custom 25-nmol DNA oligos from Integrated DNA Technologies (Coralville, IA, USA). Following PCR amplification, samples were run on an SDS-Page gel and imaged for gene deletion analysis and validation. Male mice with appropriate base-pair deletion were used for downstream studies. All mice were housed, bred, and maintained at the Rhode Island Hospital Central Research Facilities.

2.2 Patients

Septic/critically ill patients who were admitted to trauma and surgical intensive care units, between July of 2018 and February of 2020, were enrolled in this study per institutional review board approval at Rhode Island Hospital (IRB study # 413013). Inclusion criteria for the study were trauma or sepsis-related critical illness requiring ICU admission. Patients were excluded from the study if they were pregnant or had previous lymphoma or leukemia diagnosis. Patient demographics from the day of blood draw were used to calculate the Acute Physiology of Chronic Health Evaluation II (APACHE II) score (**Table 1**). Healthy volunteers (age- and sex-matched) were enrolled in this study to serve as the control group.

2.3 CLP Model

Cecal ligation and puncture (CLP) as described previously (35–37) was performed on wild-type C57BL/6 and $VISTA^{-/-}$ male mice aged 8–10 weeks. Following midline laparotomy, the cecum was ligated ~1 cm above the cecal tip and punctured twice with a 22-G needle. Cecal contents were extruded into the

TABLE 1 | Patient demographics.

	Healthy Controls	Patients	p-value
Number	8	8	–
Age	48.5 +/- 17.2	58.8 +/- 16.6	0.25
Male gender	5 (62.5%)	6 (75%)	0.62
WBC	–	10.8 +/- 5.0 × 10^6/ml	–
APACHE II score	–	19.9 +/- 5.2	–
Mortality	–	2 (25%)	–
Active infection	–	7 (87.5%)	–

intraperitoneal cavity. The abdomen was closed using a sterile PDO suture. Mice were treated with lidocaine on the muscle layer and a subcutaneous injection of 1 ml Lactated Ringer's solution. The choice of male animals was made to maximize our ability to initially see an experimental difference septic response based on previous reports that male mice did poorer in response to these experimental stressors of septic (CLP) challenge than pro-estrus stratified female mice (38, 39). Mice were euthanized 24 h post procedure (based on the experiment as described in **Figure 1**), and tissues were harvested for downstream studies.

2.4 Flow Cytometry

2.4.1 Mouse Cell Phenotyping

The spleen, thymus, and intestine were harvested from mice 24 h following sham or CLP procedure. The spleen and thymus tissues were homogenized using frosted slides, and red blood cells were lysed using a Na^+Cl^- gradient. Small intestinal tissue was processed using the Lamina Propria Dissociation Kit (Miltenyi Biotec, Bergisch Gladbach, Germany: cat# 130-097-410) according to the manufacturer protocol. The total cell number from each sample was assessed using Trypan blue stain and

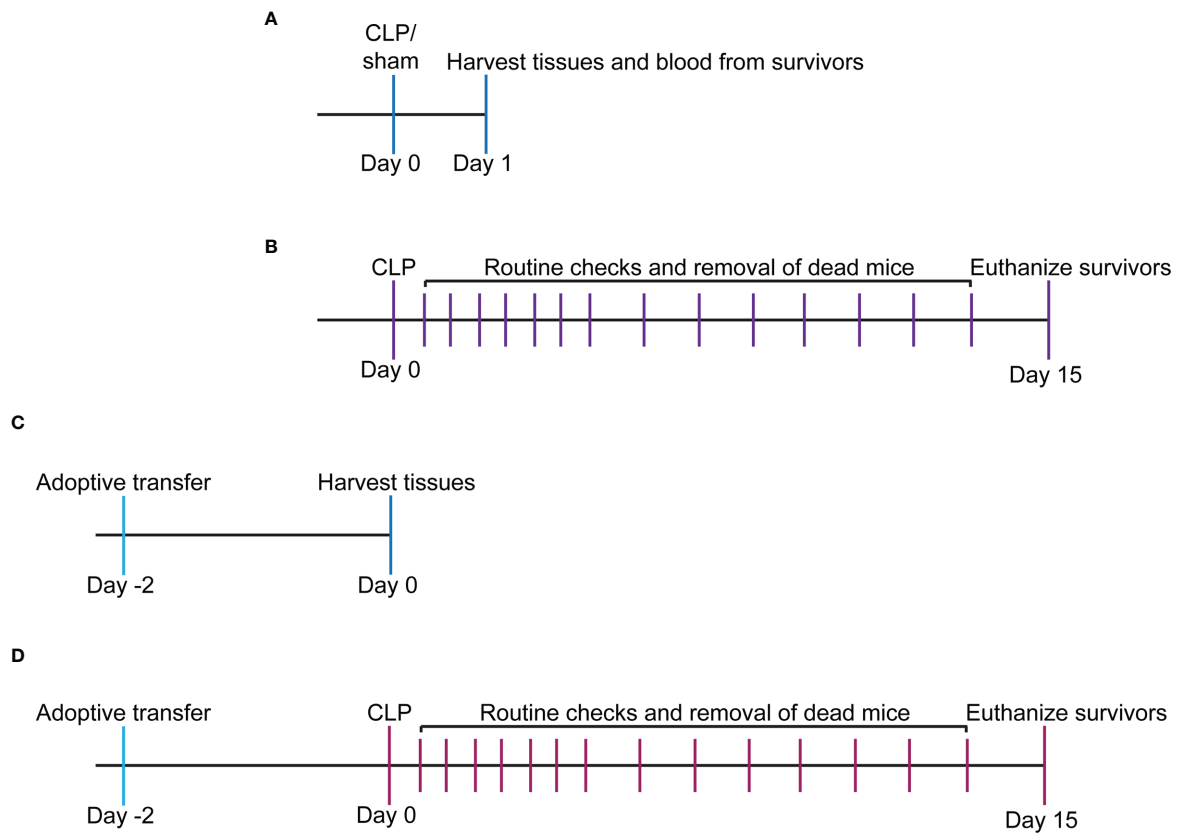

FIGURE 1 | Experimental timeline for study. **(A)** WT and VISTA$^{-/-}$ mice underwent sham or CLP procedure, and tissues/blood were harvested for downstream analysis *via* flow cytometry or spectrophotometry. **(B)** WT and VISTA$^{-/-}$ mice underwent a CLP procedure, and survival was tallied for 14 days. Surviving mice were euthanized on the 15th day. **(C)** WT mice were injected with Jurkat T_{regs}, and tissues were harvested 2 days postinjection for downstream analysis and validation of adoptive transfer *via* flow cytometry. **(D)** VISTA$^{-/-}$ mice were injected with Jurkat T_{regs} then underwent CLP 2 days postinjection, and survival was tallied for 14 days. Surviving mice were euthanized on the 15th day.

hemacytometer counting at ×10 magnification. Samples were diluted to 10^6 cells/ml in FACS buffer (2 mM EDTA, 0.5% BSA, PBS), Fc blocked, and stained with the following monoclonal anti-mouse antibodies: CD4-BV421 (BioLegend, San Diego, CA, USA, Cat# 100438, RRID : AB_11203718), CD8a-BV510 (BioLegend Cat# 100752, RRID : AB_2563057), CD69-FITC (Miltenyi Biotec Cat# 130-103-950, RRID : AB_2659081), PD-1H/VISTA-PE (BioLegend Cat# 143708, RRID : AB_11150599), CD25-PE/Cyanine7 (BioLegend Cat# 101916, RRID : AB_2616762), and CD152/CTLA-4-PerCP/Cyanine5.5 (BioLegend Cat# 106316, RRID : AB_2564474). Following initial staining, cells were fixed using 4% paraformaldehyde and permeabilized using the True Nuclear Transcription Buffer Set (BioLegend: cat# 424401) according to the manufacturer's protocol. Permeabilized cells were stained with anti-mouse FOXP3-Alexa Fluor 647 (BioLegend: cat# 126408). To compensate for spectral overlap, UltraComp eBeads Plus Compensation Beads (Thermo Fisher Scientific, Waltham, MA, USA: cat# 01-3333-41) were used according to the manufacturer's protocol. Fluorescence minus one (FMO) controls were used to determine positive expression gates during analysis using FlowJo software.

2.4.2 Human Cell Phenotyping

Whole blood was drawn from patients and healthy controls, collected in heparin-treated tubes, treated with Ficoll Histopaque-1077, and centrifuged to isolate leukocytes. The leukocyte layer was isolated, washed with PBS, and centrifuged. Cells were counted using a hemacytometer and Trypan blue then diluted to 10^6 cells/ml in FACS buffer (2 mM EDTA, 0.5% BSA, PBS). Cells were Fc blocked and stained with the following monoclonal anti-human antibodies: CD3-VioBlue (Miltenyi Biotec: Cat# 130-113-133, RRID : AB_2725961) and VISTA-APC (Thermo Fisher Scientific: Cat# 17-1088-42, RRID : AB_2744704). Fluorescence minus one (FMO) control was used to determine positive expression gates during analysis using FlowJo software.

2.4.3 Adoptive Transfer Validation

For adoptive transfer, the pMSCV-mouse Foxp3-EF1α-GFP-T2A-puro stable Jurkat cell line (System Biosciences, Palo Alto, CA, USA: cat# TCL110C-1), referred to as Jurkat T_{regs}, was harvested from culture, pelleted *via* centrifugation, and resuspended in HBSS (Thermo Fisher: cat# 24020117) at 2×10^6 cells/400 µl. 400 µl of Jurkat T_{reg} suspension or HBSS vehicle control was loaded into a syringe and administered to mouse *via* intraperitoneal injection. Spleen, thymus, and small intestine samples were harvested 48 h post adoptive transfer and processed as described in the previous section. Cells were stained with CD4-BV421 (BioLegend: Cat# 100438, RRID : AB_11203718) and VISTA/PD-1H-APC (BioLegend: Cat# 143709, RRID : AB_11219607). A FMO control was used to determine VISTA-positive expression gates during analysis using FlowJo software.

2.5 Colorimetric Assays for Morbidity Study

To assess indices of tissue injury, blood was collected from mice 24 h following sham or CLP procedure *via* cardiac puncture using a heparin-coated syringe. Blood sample was centrifuged at 10,000 rpm, and supernatant (plasma) was collected and stored at -80°C. For tissue injury assays, plasma was analyzed using the following kits according to the manufacturer's protocol: Urea Nitrogen (BUN) Colorimetric Detection Kit (Invitrogen, Carlsbad, CA, USA, cat# EIABUN), Creatine Kinase Activity Assay Kit (Sigma-Aldrich, St. Louis, MO, USA: cat# MAK116), Alanine Aminotransferase (ALT) Activity Assay Kit (Sigma-Aldrich: cat# MAK052), Aspartate Aminotransferase (AST) Activity Assay Kit (Sigma-Aldrich: cat# MAK055), Amylase Assay Kit (Colorimetric) (Abcam, Cambridge, MA, USA: cat# ab102523), and Bilirubin Assay Kit (Direct Colorimetric) (Abcam: cat# ab235627).

2.6 Multiplex Cytokine Analysis

Plasma samples were collected and stored as described in the previous section. To assess the cytokine concentration in plasma samples, the following multiplex kits were used according to the manufacturer's instruction: LEGENDplex Mouse Inflammation Panel (13-plex) with a V-bottom plate (BioLegend, cat# 740446) and LEGENDplex MU Th Cytokine Panel (12-plex) with VbP VO3 (BioLegend, cat# 741044). Multiplex experiments were carried out using MACSQuant Analyzer 10 (Miltenyi Biotec). Data were analyzed using the LEGENDplex software suite (BioLegend).

2.7 *In Vitro* Viability Assay

Jurkat T_{regs} were cultured in RPMI complete medium with 13F3 (Bio X Cell, Lebanon, NH, USA, Cat# BE0310, RRID : AB_2736990) or Ig control (Bio X Cell Cat# BE0091, RRID : AB_1107773) for 30 min at 37°C, 5% CO_2 then stained with alamarBlue (Bio-Rad, Hercules, CA, USA: product code BUF012A) according to the manufacturer's protocol. Sample absorbance was measured every 24 h for 7 days using the Bio-Rad spectrophotometer. Viability was calculated according to the manufacturer's protocol.

2.8 *In Vitro* Cytokine Analysis

Jurkat T_{regs} were cultured in RPMI complete medium with 13F3 (Bio X Cell Cat# BE0310, RRID : AB_2736990) or Ig control (Bio X Cell Cat# BE0091, RRID : AB_1107773) overnight at 37°C, 5% CO_2. Treated cells were then stimulated with 5 µl of plasma from CLP mouse for 2 h prior to harvest from culture. Cells were centrifuged, and supernatant was collected for multiplex analysis using LEGENDplex MU Th Cytokine Panel (12-plex) with VbP VO3 (BioLegend: cat# 741044) according to the manufacturer's protocol. Multiplex experiments were carried out using MACSQuant Analyzer 10 (Miltenyi Biotec). Data were analyzed using LEGENDplex software suite (BioLegend).

2.9 Statistical Analysis

Statistical significance between two groups was determined using either a two-tailed Student's unpaired *t* test for parametric data or the Mann–Whitney U test for the non-parametric test. Statistical significance between multiple groups was determined using either an ordinary one-way ANOVA for parametric data or the Kruskal–Wallis test for non-parametric data. Alpha was set

to 0.05 as the cutoff for statistical significance using Prism 9.3.0 (GraphPad Software) statistical software.

3 RESULTS

3.1 VISTA Expression Inversely Correlates With T-Cell Population Abundance in Septic Mice and Critically Ill Patients

Several research groups have shown that during acute sepsis progression there is a significant loss in T cell abundance in the spleen and thymus in both the murine CLP model (29, 40–42) and septic patients (43–46). In this study, we found that C57BL/6 wild-type (WT) mice exhibited a higher VISTA expression on $CD4^+$ T cells (**Figure 2A**) and reduced $CD4^+$ T cell population abundance (**Figure 2B**) in the spleen following septic challenge.

We enrolled a total of 8 critically ill patients from the trauma and surgical ICUs at a single level-1 trauma center. There was no significant difference between patients and healthy controls regarding gender or age. 87.5% of patients had an active ongoing source of infection at the time of draw, 62.5% required mechanical ventilation, and 37.5% were actively on vasopressor at the time of draw. 25% required dialysis due to critical illness. The average APACHE II score for the population was 19.9 (**Table 1**). Sources of infection included necrotizing soft tissue infections of the lower extremities, intra-abdominal abscesses after perforated hollow viscus injuries, and bacteremia. 75% of enrolled patients met systemic inflammatory response syndrome (SIRS) criteria, 63% met sepsis criteria, and 38% met septic shock criteria (47).

We found that critically ill patients experience a higher VISTA expression on circulating $CD3^+$ T cells (**Figure 2C**) despite reduced $CD3^+$ T cell population abundance (**Figure 2D**) in circulation. These results suggest that the relationship between VISTA expression and T-cell abundance observed in our murine model of sepsis appear to have a potential correlate in the critically ill septic patient. To further explore the role of VISTA in the sepsis-induced T-cell response and better understand its potential contribution to septic morbidity, we created a global VISTA gene-deficient ($VISTA^{-/-}$) mouse strain using CRISPR/Cas9 technology that could be examined to address this question (**Figures 2E, F**).

Le Tulzo et al. found that T cells become polarized into functionally distinct helper T-cell subsets in sepsis (44), and it is well documented that the regulatory T-cell (T_{reg}) subset increases during the acute septic response (46, 48, 49). In light of this, we chose to initially determine how VISTA impacted sepsis-induced T_{reg} polarization by comparing the $CD4^+Foxp3^+$ T_{reg} populations in WT as opposed to $VISTA^{-/-}$ mice *via* flow cytometry (**Supplementary Figure 2**).

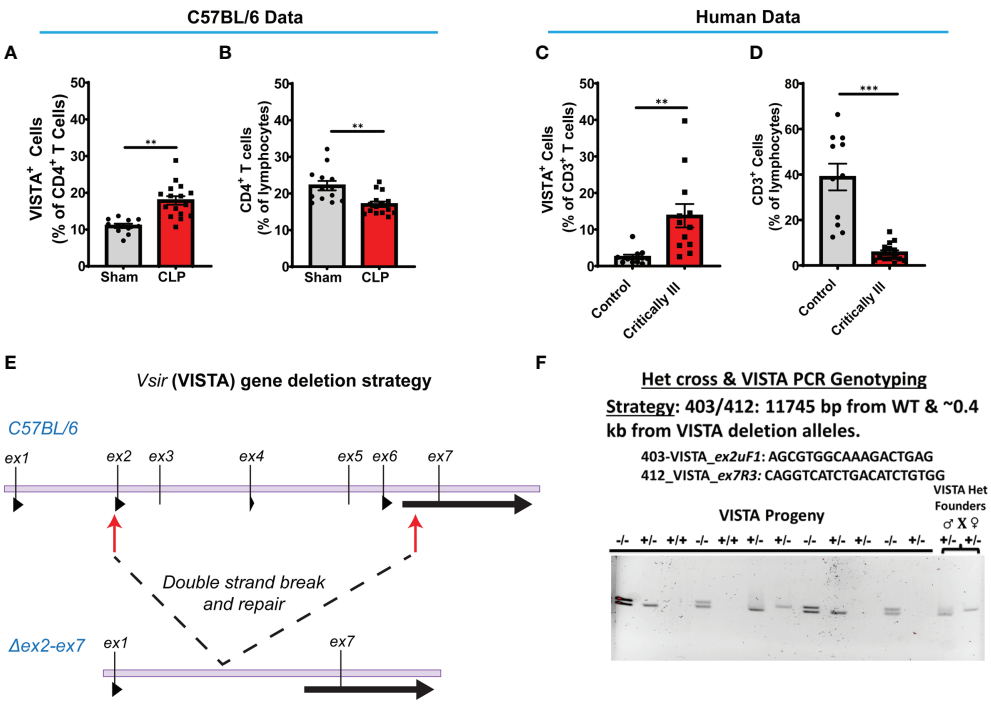

FIGURE 2 | $VISTA^+CD4^+$ T cells in mouse splenocytes and $VISTA^+CD3^+$ lymphocytes in patient blood increase following experimental or clinical sepsis. **(A)** Summary graph of $VISTA^+$ $CD4^+$ T cells in the wild-type mouse spleen. **(B)** Summary graph of $CD4^+$ T cell frequency in the wild-type mouse spleen. **(C)** Summary graph of $VISTA^+$ $CD3^+$ T cell frequency in the peripheral blood lymphocytes. **(D)** Summary graph of CD3+ T cell frequency in the peripheral blood. **(A–D)** Summary graphs show mean ± SEM [WT-sham: *n = 13*, WT-CLP: *n = 16*]; significance $^{**}p < 0.01$, $^{***}p < 0.001$. **(E)** Initial process (Strategy) for producing embryos deficient in the ~11.3-kb region containing exon (ex) 2 to exon 7 of the VISTA gene on mouse chromosome 10 with CRISPR/Cas9 followed by NHEJ-mediated repair. **(F)** Results of initial heterozygous cross of $VISTA^{-/+}$ founder mice resulting from CRISPR/Cas9 technology that produced homozygous $VISTA^{-/-}$ mice for breeding (PCR genotyping strategy: 403/412: 11,745 bp from WT and ~0.4 kb from VISTA deletion alleles).

3.2 CD4$^+$ T_{reg} Abundance Increases Following Septic Challenge, But the CD4$^+$ T_{reg} Population Is Significantly Smaller in Peripheral T-Cell Compartments of VISTA$^{-/-}$ Mice Compared to WT Mice

We found that in the WT spleen, there is a significant increase in total proportion of CD4$^+$ T_{regs} and VISTA$^+$CD4$^+$ T_{regs} following CLP (**Figures 3A–C**). VISTA$^{-/-}$ mice exhibit decreased abundance of total CD4$^+$ T_{regs} in the spleen (**Figures 3B, C**). In the thymus, we observe no change in VISTA expression on the T_{reg} populations between sham and CLP WT mice (**Supplementary Figures 3A, D**); however, VISTA$^{-/-}$ mice have higher total abundance of CD4$^+$ T_{regs} and CD4$^+$CD8$^+$ T_{regs} compared to WT mice (**Supplementary Figures 3B, E**). In the intraepithelial compartment of the small intestine, the frequency of VISTA$^+$CD4$^+$ T_{regs} increases significantly following CLP (**Figure 4A**) and VISTA$^{-/-}$ mice have less CD4$^+$ T_{regs} under steady-state (sham) and inflammatory (CLP) conditions compared to WT mice (**Figures 4B, C**). We did not observe any trends in the lamina propria compartment of the small intestine (**Supplementary Figure 4**).

3.3 CD4$^+$ T_{regs} Demonstrate Compensatory Upregulation of Several Checkpoint Proteins and Suppressive Factors in VISTA$^{-/-}$ Mice

The loss in CD4$^+$ T_{regs} in VISTA$^{-/-}$ mice lead us to ask if the cell-surface expression signature, as it related to suppressive function of these cells, was altered by CLP. In the spleen, Foxp3, CTLA4, and CD25, but not CD69, are significantly upregulated on CD4$^+$ T_{regs} in VISTA$^{-/-}$ mice compared to WT mice under steady-state and inflammatory conditions (**Figures 5A–D**). In the thymus (**Figures 6A–G**), CD25 is significantly upregulated on CD4$^+$ T_{regs} in VISTA$^{-/-}$ mice compared to WT mice under steady state and inflammatory conditions (**Figure 6C**). CD4$^+$ T_{regs} upregulate CD69 following CLP in WT and VISTA$^{-/-}$ mice (**Figure 6D**). We also found that Foxp3, CTLA4, and CD25 are significantly upregulated on CD4$^+$CD8$^+$ T_{regs} in WT mice compared to VISTA$^{-/-}$ mice under steady-state and inflammatory conditions (**Figures 6E–G**). In the lamina propria compartment, we observe a significant upregulation of CTLA4 on CD4$^+$ T_{regs} in VISTA$^{-/-}$ mice (**Supplementary Figure 5B**). However, this trend is not observed in the small intestinal intraepithelial compartment (**Supplementary Figure 6**).

3.4 VISTA$^{-/-}$ Mice Have Higher Th17-Related Cytokine Production Compared to WT Mice Following Septic Challenge

To expand from the T_{reg} phenotyping described above, we sought to measure the abundance of several cytokines in circulation implicated in the helper T cell response (**Figures 7A–J**). We found that VISTA$^{-/-}$ mice have significantly higher circulating IL-17F and IL-23 compared to WT mice post CLP (**Figures 7G, I**).

3.5 Compensatory Upregulation of Foxp3, CTLA4, and CD25 on Peripheral T_{reg} Populations Correlates With Decreased Survival in VISTA$^{-/-}$ Mice

Based on the apparent compensatory upregulation of suppressive T_{reg} mediators, we decided to compare the mortality and morbidity of VISTA$^{-/-}$ as opposed to WT mice when subjected

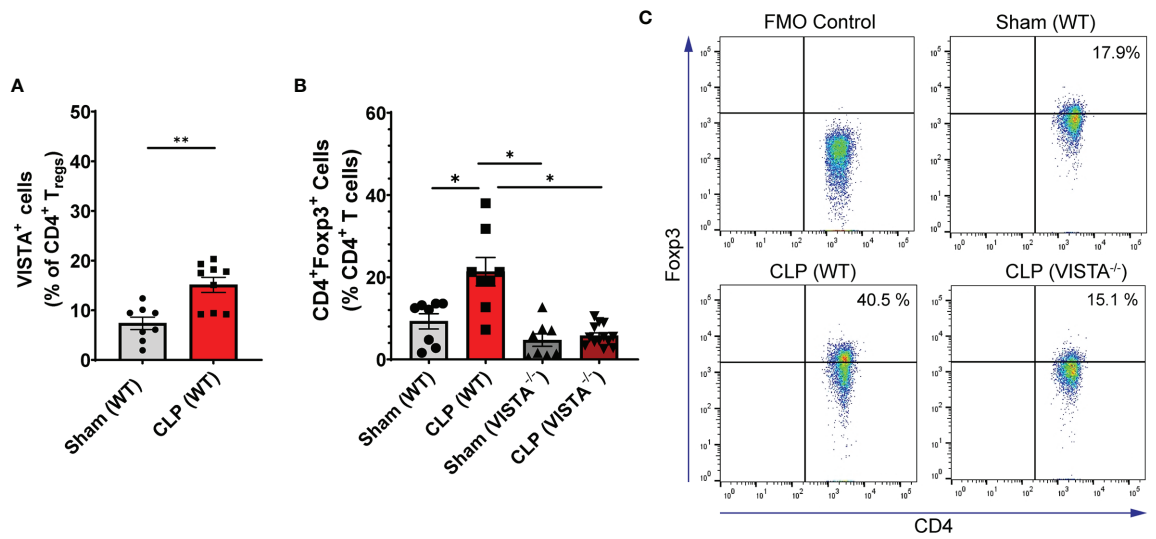

FIGURE 3 | VISTA expression correlates with CD4$^+$ T_{reg} population increase following CLP and VISTA$^{-/-}$ mice fail to expand the CD4$^+$$T_{reg}$ population in the spleen. **(A)** Summary graph of VISTA$^+$ CD4$^+$ T_{reg} frequency in the spleen. **(B)** Summary graph of CD4$^+$ T_{reg} frequency in the spleen and **(C)** representative flow cytometry plots comparing fluorescence minus one (FMO) control, sham (WT), CLP (WT), and CLP (VISTA$^{-/-}$) samples. Summary graphs show mean ± SEM [WT-sham: *n = 8*, WT-CLP: *n = 8*, VISTA$^{-/-}$sham: *n = 8*, VISTA$^{-/-}$ -CLP: *n = 13*]; significance *p < 0.05; **p < 0.01.

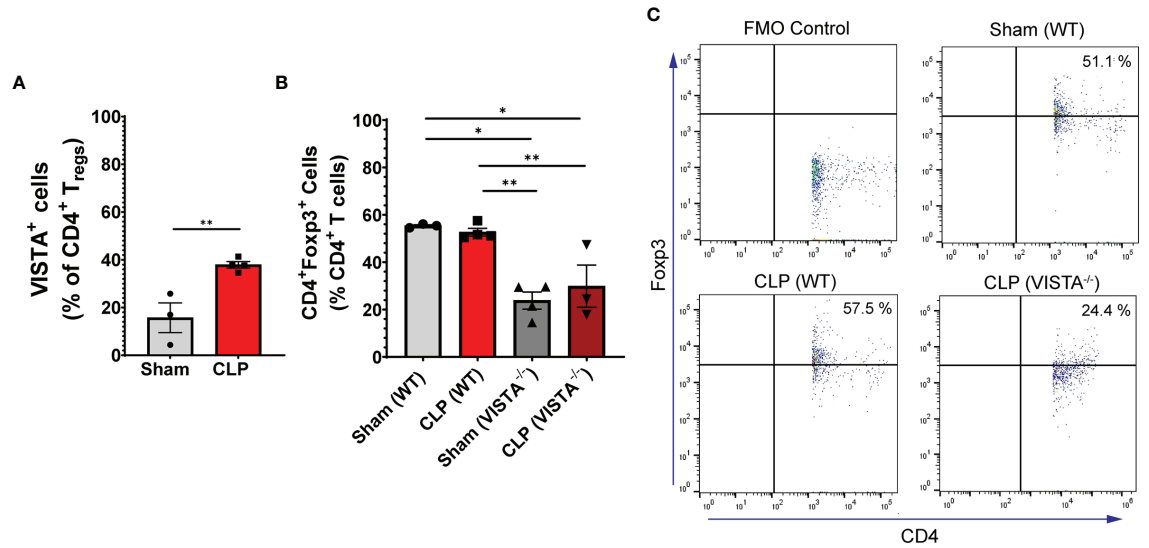

FIGURE 4 | VISTA expression correlates with CD4$^+$ T_{reg} population increase following CLP and VISTA$^{-/-}$ mice fail to expand the CD4$^+$ T_{reg} population in the intestinal intraepithelial compartment. **(A)** Summary graph of VISTA$^+$ CD4$^+$ T_{reg} frequency in the small intestine. **(B)** Summary graph of CD4$^+$ T_{reg} frequency in the small intestine and **(C)** representative flow cytometry plots comparing fluorescence minus one (FMO) control, sham (WT), CLP (WT), and CLP (VISTA$^{-/-}$) samples. Summary graphs show mean ± SEM [WT-sham: *n = 3*, WT-CLP: *n = 3*, VISTA$^{-/-}$sham: *n = 4*, VISTA$^{-/-}$ -CLP: *n = 4*]; significance *p < 0.05; **p < 0.01.

to CLP (**Figures 8A–J**). We found that VISTA$^{-/-}$ mice had significantly decreased survival, which coincided with increased blood bilirubin, ALT, and AST 24 h following CLP (**Figures 8A, D–G**). VISTA$^{-/-}$ mice also present a more proinflammatory systemic cytokine profile (**Figures 9A–J**). These mice exhibit higher circulating IL-6, IL-10, TNF-α, and MCP-1 compared to WT mice post CLP (**Figures 9C, D, G, I**).

3.6 Adoptive Transfer of VISTA-Expressing T_{regs} to VISTA$^{-/-}$ Mice Rescues Survival to WT Levels Following CLP

To establish the contribution of VISTA$^+$ T_{regs} to survival in murine sepsis, we chose to adoptively transfer pMSCV-mouse Foxp3-EF1α-GFP-T2A-puro stable Jurkat cells, hereby referred to as Jurkat T_{regs}, into VISTA$^{-/-}$ mice prior to CLP. 48 h post adoptive transfer, Jurkat T_{regs} accumulate in the spleen, thymus, and small intestine (**Supplementary Figures 7A–D**) and express high levels of VISTA (**Supplementary Figures 7E–H**). Based on these results, we performed the adoptive transfer 48 h before CLP and then subsequently assessed overall survival. We found that, following Jurkat T_{reg} adoptive transfer, VISTA$^{-/-}$ mice had comparable survival to WT mice post CLP (**Figure 10A**).

3.7 *In Vitro*, VISTA Blockade Reduces Jurkat T_{reg} Viability and Cytokine Production

In addition to establishing the relevance of VISTA-expressing T_{regs} in septic mouse morbidity/mortality, we wanted to uncover how VISTA expression/ligation might be directly impacting T_{reg} function. To do this, we again utilized the Jurkat T_{reg} cell line for mechanistic *in vitro* studies. Jurkat T_{regs} were pretreated with a commercially available VISTA-neutralizing antibody, 13F3, or antibody control then stained with alamarBlue. alamarBlue is a redox indicator used to measure metabolic activity as a readout for viability. The concentration of alamarBlue was assessed *via* a spectrophotometer every 24 h for 7 days. We found that there was a significant reduction in viability following treatment and this reduction was maintained for 7 days without additional 13F3 treatment (**Figure 10B**). Upon *in vitro* acute stimulation of Jurkat T_{regs} with plasma from septic mice, these cells produce several helper T cell-related cytokines (**Figures 10C–I**) but failed to produce IFN-γ, IL-4, or IL-17A (**Supplementary Figure 8**). Interestingly, 13F3-treated Jurkat T_{regs} produce lower levels of IL-9, IL-10, and IL-17F following acute stimulation (**Figures 10E, F, H**).

4 DISCUSSION

Since its initial discovery, VISTA has been implicated in diverse immune-related pathologies driven by both innate and adaptive cells (20–27, 50–54). In a preliminary study, we found that septic mice and critically ill patients exhibit a higher proportion of VISTA$^+$ T cells as compared to healthy controls. Based on these results, we set out to determine the impact of VISTA expression on regulatory T cells (T_{regs}) in murine sepsis. The CD4$^+$ T_{reg} plays a vital role in peripheral tolerance, regulation of effector cells, and prevention of bystander tissue damage under inflammatory and steady-state conditions as reviewed by Corthay (55). In sepsis, peripheral T_{regs} increase significantly

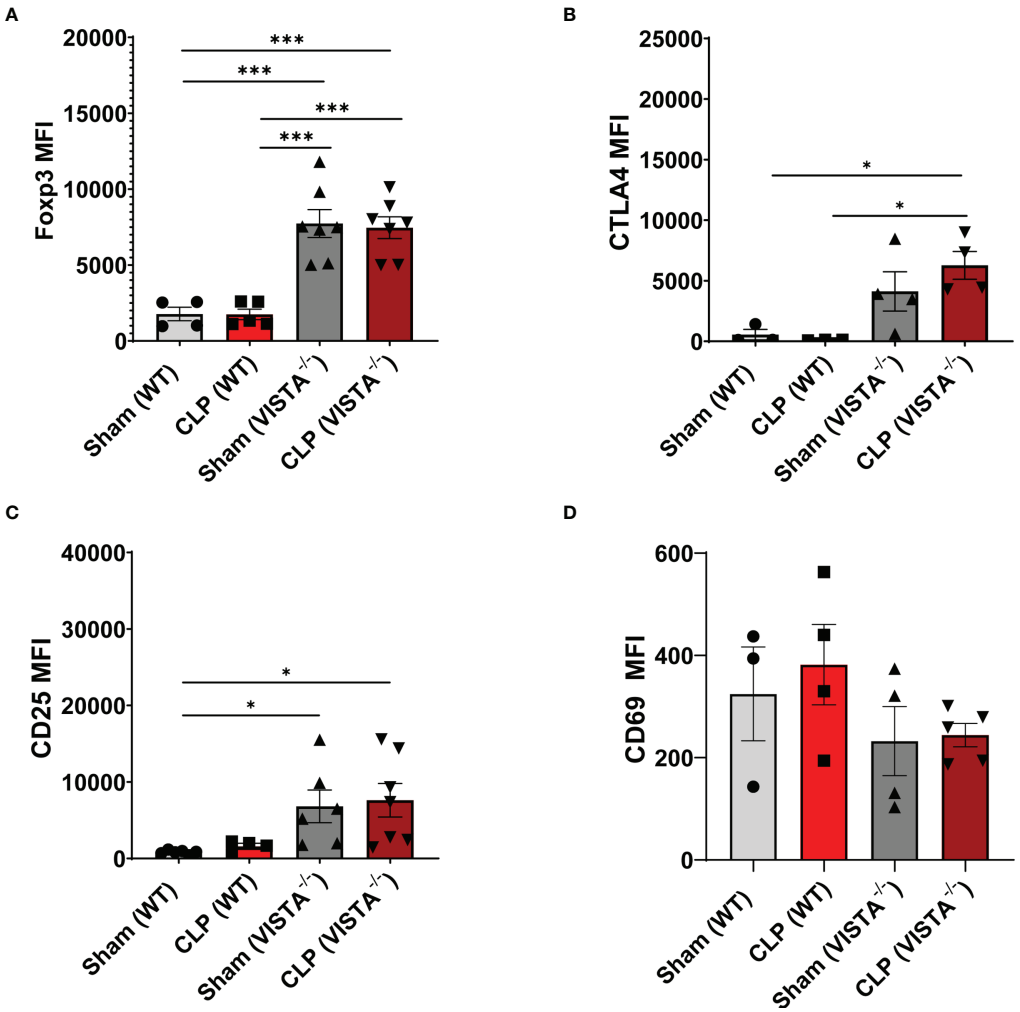

FIGURE 5 | Expression of suppressive markers is upregulated on CD4$^+$ T_{regs} in the spleen of VISTA$^{-/-}$ mice. Median fluorescence intensity (MFI) of **(A)** Foxp3, **(B)** CTLA4, **(C)** CD25, and **(D)** CD69 on CD4$^+$ T_{regs} in the spleen. Summary graphs show mean ± SEM [WT-sham: *n = 3*, WT-CLP: *n = 3*, VISTA$^{-/-}$sham: *n = 4*, VISTA$^{-/-}$ -CLP: *n = 4*]; significance *p < 0.05; ***p < 0.001.

and correlate with patient outcomes and lymphoproliferative pathology as reviewed by Jiang et al. (56, 57).

4.1 The T_{reg} Population Is Composed of Several Subpopulations That Arise From Diverse Stimuli and Developmental Programs

The T_{reg} classification as a distinct T cell lineage has been a point of contention due to the inherent plasticity of T_{regs} and the lack of a definitive "T_{reg}" marker as effector T cells can transiently express T_{reg} markers upon activation. Forkhead/winged-helix transcription factor box P3 (Foxp3) is arguably the most reliable T_{reg} marker in mice and was used to delineate effector T cells and T_{regs} in this study (55, 58, 59). CD4$^+$Foxp3$^+$ T cells are potent suppressors of effector CD4$^+$ T cells, CD8$^+$ T cells, natural killer (NK) cells, dendritic cells (DCs), and B cells under inflammatory conditions (55).

4.2 VISTA Plays a Role in T-Cell Polarizing Cytokine Production and CD4$^+$ T_{reg} Abundance in Sepsis

In this study, we found that VISTA expression and total CD4$^+$ T_{reg} abundance increase significantly during the acute septic response. Further, this increase in peripheral T_{reg} abundance is dependent on VISTA expression. We also found that VISTA expression plays a role in orchestrating the cytokine response to septic challenge. Cytokines provide contextual immunologic cues that shape cell lineage determination and plasticity. Higher levels of IL-17F, IL-6, and IL-23 promote CD4$^+$ T cell polarization toward a Th17 phenotype, and higher concentrations of these cytokines may explain the reduced T_{reg} abundance observed in VISTA$^{-/-}$ mice (60, 61). Previous studies found that VISTA regulated the T_{reg}–Th17 polarization axis in mice (25), further supporting our results in the context of sepsis.

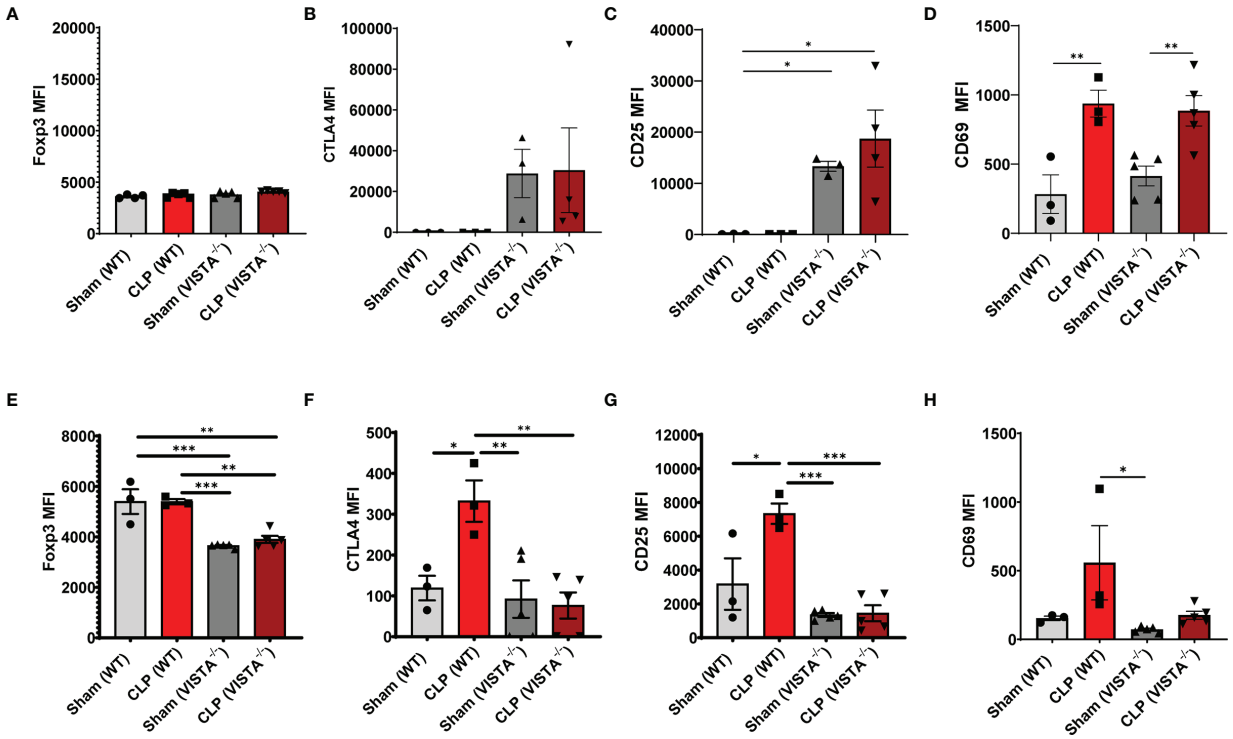

FIGURE 6 | Expression of suppressive markers is upregulated on $CD4^+$ T_{regs} and is downregulated on $CD4^+CD8^+$ T_{regs} in the thymus of $VISTA^{-/-}$ mice. Median fluorescence intensity (MFI) of **(A)** Foxp3, **(B)** CTLA4, **(C)** CD25, and **(D)** CD69 on $CD4^+$ T_{regs} in the thymus. Median fluorescence intensity (MFI) of **(E)** Foxp3, **(F)** CTLA4, **(G)** CD25, and **(H)** CD69 on $CD4^+CD8^+$ T_{regs} in the thymus. Summary graphs show mean ± SEM [WT-sham: *n = 3*, WT-CLP: *n = 3*, $VISTA^{-/-}$sham: *n = 4*, $VISTA^{-/-}$ -CLP: *n = 4*]; significance *p < 0.05; **p < 0.01; ***p < 0.001.

4.3 $VISTA^{-/-}$ Mice Experience Compensatory Upregulation of Several Endogenous Mediators of T_{reg} Suppression Such as CTLA4, Foxp3, and CD25 Under Steady-State Conditions

Interestingly, CTLA4 expression regulates the turnover and maintenance of T_{regs} at steady state while Foxp3 regulates T_{reg} function and lineage commitment (62–64). A steady-state T_{reg} pool is requisite for preventing autoimmune lymphoproliferative pathology (65). Several groups have shown that $VISTA^{-/-}$ mice do not exhibit overt autoimmune pathologies under tolerogenic conditions (26, 53, 66). Therefore, we posit that the higher baseline expression of CTLA4, Foxp3, and CD25 in VISTA-deficient $CD4^+$ T_{regs} represents an inherent compensatory mechanism to sustain peripheral tolerance under tolerogenic conditions.

4.4 In the Acute Immune Response to Infection, as Observed With Our Murine Model of Sepsis, Compensatory Upregulation of CTLA4, Foxp3, and CD25 by $CD4^+$ T_{regs} Is Insufficient

An explanation may lie in the efficacy of CTLA4, Foxp3, and/or CD25-mediated suppression in our model. $CD4^+$ T_{regs} utilize diverse contact-dependent and independent mechanisms to exert immune suppression (35–37, 67, 68). For example, CTLA4-expressing T_{regs} bind to B7-1/2 on antigen-presenting DCs, promoting trans-endocytosis of B7-1/2 and preventing DC-mediated activation of effector T cells. CD25 scavenges IL-2 from the environment, reduces IL-2 activation of effector T cells *via* competitive inhibition, and regulates the function of mature DCs (69).

Another mechanism by which T_{regs} exert immune suppression is by directly polarizing the monocyte lineage commitment from M1 to M2 macrophages (69, 70). M1 macrophages produce proinflammatory cytokines and exacerbate inflammation-derived tissue injury in sepsis (71). Two potent M1 cytokines, IL-6 and MCP-1, are highly upregulated in $VISTA^{-/-}$ mice following septic challenge. M1-mediated pathology is particularly profound in the liver during infection (72), which may explain the increased acute liver injury observed in septic $VISTA^{-/-}$ mice.

4.5 Higher M1-Associated Cytokines and Apparent Liver Injury in $VISTA^{-/-}$ Mice Represents a Possible Lapse in the Suppressive Capacity of $VISTA^{-/-}$ T_{regs} Despite Compensatory Upregulation of CTLA4, Foxp3, and CD25

To determine if $VISTA^{-/-}$ T_{regs} contribute to the survival deficit observed in $VISTA^{-/-}$ mice, we adoptively transferred VISTA-

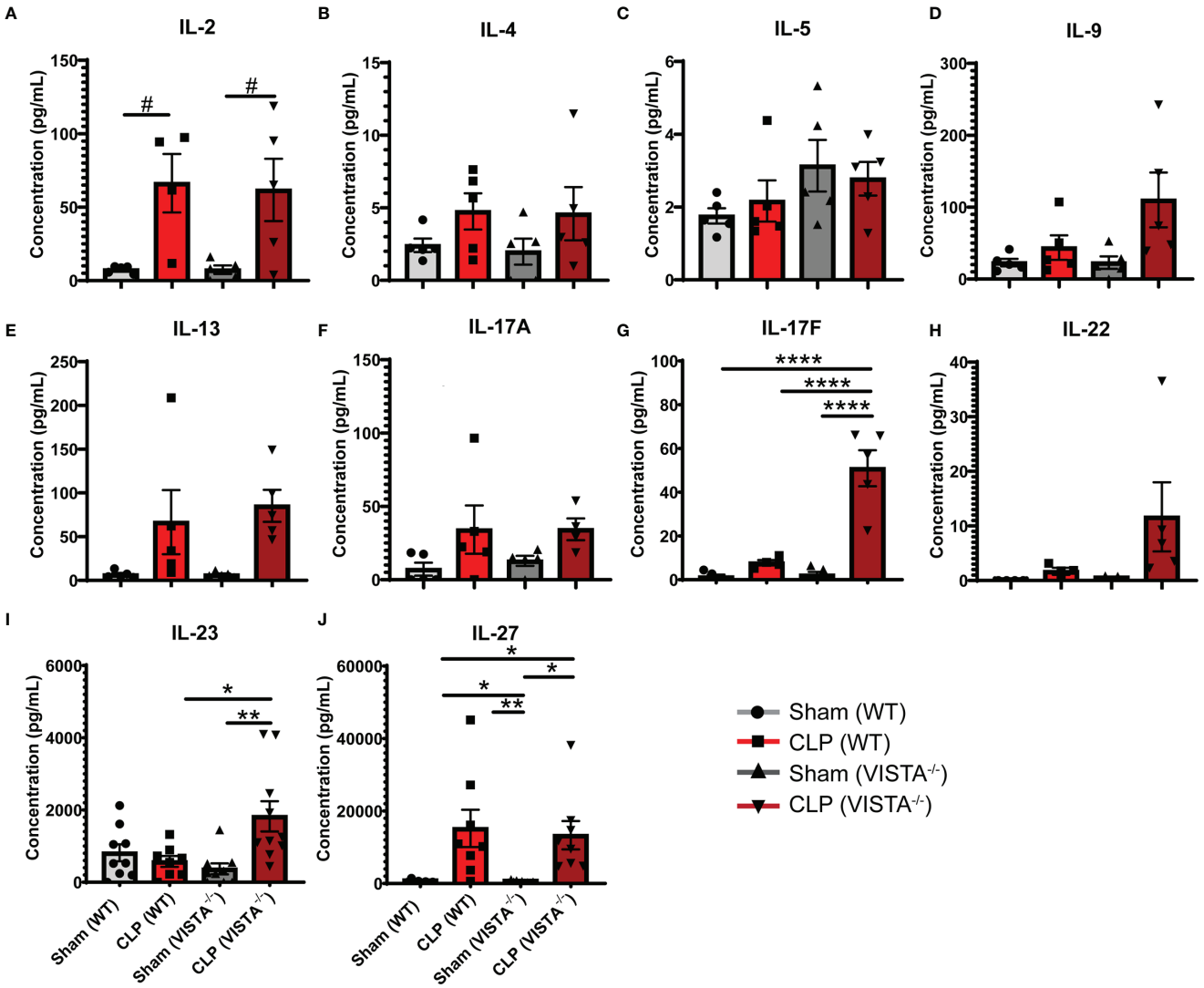

FIGURE 7 | VISTA$^{-/-}$ mice have significantly higher levels of several Th17 cytokines following septic challenge. **(A–J)** Plasma cytokine concentration of wild-type and VISTA$^{-/-}$ mice. Summary graphs show mean ± SEM [WT-sham: *n = 5*, WT-CLP: *n = 5*, VISTA$^{-/-}$sham: *n = 5*, VISTA$^{-/-}$ -CLP: *n=5*]; significance $^{\#}p = 0.05$; $^{*}p < 0.05$; $^{**}p < 0.01$; $^{****}p < 0.0001$.

overexpressing Jurkat T_{regs} into VISTA$^{-/-}$ mice prior to septic challenge. We found that addition of Jurkat T_{regs} into VISTA$^{-/-}$ mice rescues survival to wild-type levels. Upon VISTA blockade *in vitro*, the Jurkat T_{regs} exhibited reduced proliferative capacity and production of IL-9 and IL-10. T_{reg}-derived IL-9 plays a significant role in recruiting other suppressive immune cells, such as mast cells, to suppress bystander tissue damage as observed in a murine nephrotoxic serum nephritis model (73). T_{reg}-derived IL-10 is required to regulate effector T cells during acute inflammation (74, 75).

A recent study was published demonstrating a survival benefit upon VISTA antibody blockade prior to CLP (76). Importantly, in the Tao et al. study they utilized WT mice. However, it has also been shown that VISTA-gene-deficient mice have a predisposition to proinflammatory immune activation in several disease contexts (17, 20, 26, 66). Based on prior studies and our results, we believe that the VISTA-gene-deficient mice develop a predisposition to proinflammatory tissue injury that is exacerbated by CLP, thus resulting in a survival deficit. Consequently, acute VISTA blockade with an exogenous antibody in a developmentally normal WT mouse, as used in the Tao et al. study, might yield different results than observed in VISTA$^{-/-}$ mice in our study.

In conclusion, we found that WT mice have increased VISTA^{+}CD4^{+} T_{regs} and increased total CD4^{+} T_{regs} in the spleen and small intestine post CLP. This increase in total CD4^{+} T_{reg} abundance is lost in VISTA$^{-/-}$ mice; however, VISTA$^{-/-}$ CD4^{+} T_{regs} have a higher expression of Foxp3,

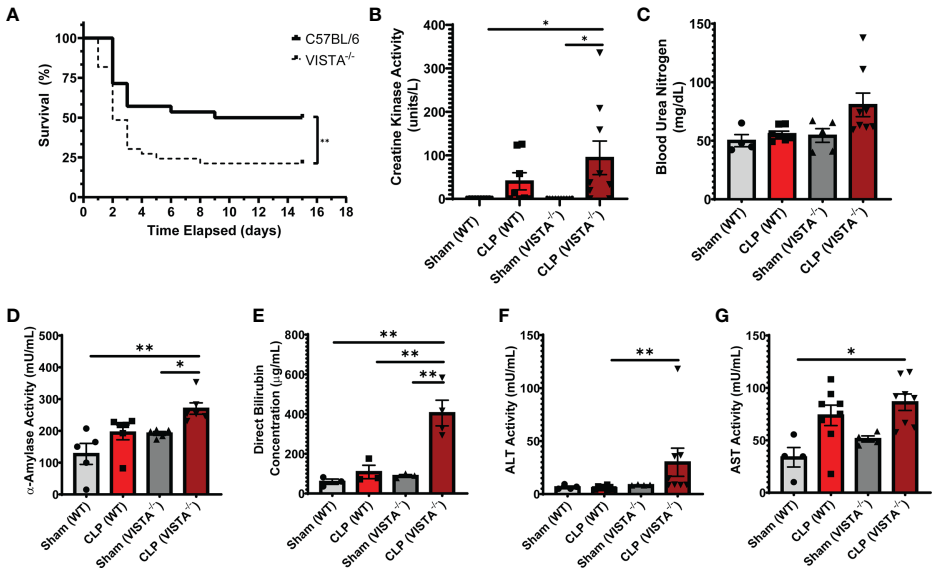

FIGURE 8 | VISTA$^{-/-}$ mice have significantly worse survival and morbidities following septic challenge. **(A)** 14-day survival following CLP [WT: *n = 28*, VISTA$^{-/-}$: *n = 26*]. **(B)** Creatine kinase activity [WT-sham: *n = 9*, WT-CLP: *n = 9*, VISTA$^{-/-}$sham: *n = 10*, VISTA$^{-/-}$ -CLP: *n = 10*]. **(C)** blood urea nitrogen [WT-sham: *n = 4*, WT-CLP: *n = 9*, VISTA$^{-/-}$sham: *n = 5*, VISTA$^{-/-}$ -CLP: *n = 8*]. **(D)** α-Amylase activity [WT-sham: *n = 5*, WT-CLP: *n = 6*, VISTA$^{-/-}$sham: *n = 5*, VISTA$^{-/-}$ -CLP: *n = 6*]. **(E)** Direct bilirubin concentration [WT-sham: *n = 3*, WT-CLP: *n = 3*, VISTA$^{-/-}$sham: *n = 3*, VISTA$^{-/-}$ -CLP: *n = 4*]. **(F)** alanine aminotransferase activity [WT-sham: *n = 4*, WT-CLP: *n = 8*, VISTA$^{-/-}$sham: *n = 4*, VISTA$^{-/-}$ -CLP: *n = 8*]. **(G)** Aspartate aminotransferase activity [WT-sham: *n = 4*, WT-CLP: *n = 8*, VISTA$^{-/-}$sham: *n = 4*, VISTA$^{-/-}$ -CLP: *n = 8*] from plasma samples of wild-type and VISTA$^{-/-}$ mice. **(B–G)** Summary graphs show mean ± SEM; significance *p < 0.05; **p < 0.01.

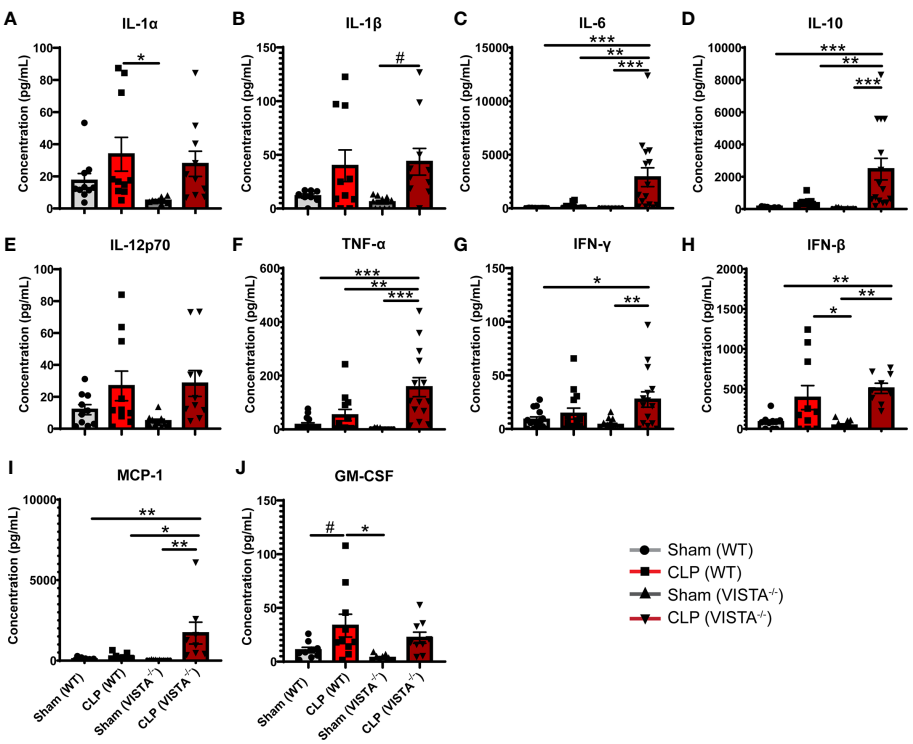

FIGURE 9 | VISTA$^{-/-}$ mice have significantly higher levels of several proinflammatory cytokines following septic challenge. **(A–J)** Plasma cytokine concentration of wild-type and VISTA$^{-/-}$ mice. Summary graphs show mean ± SEM [WT-sham: *n = 10*, WT-CLP: *n = 10*, VISTA$^{-/-}$sham: *n = 10*, VISTA$^{-/-}$ -CLP: *n = 10*]; significance $^{\#}$p = 0.05; *p < 0.05; **p < 0.01; ***p < 0.001.

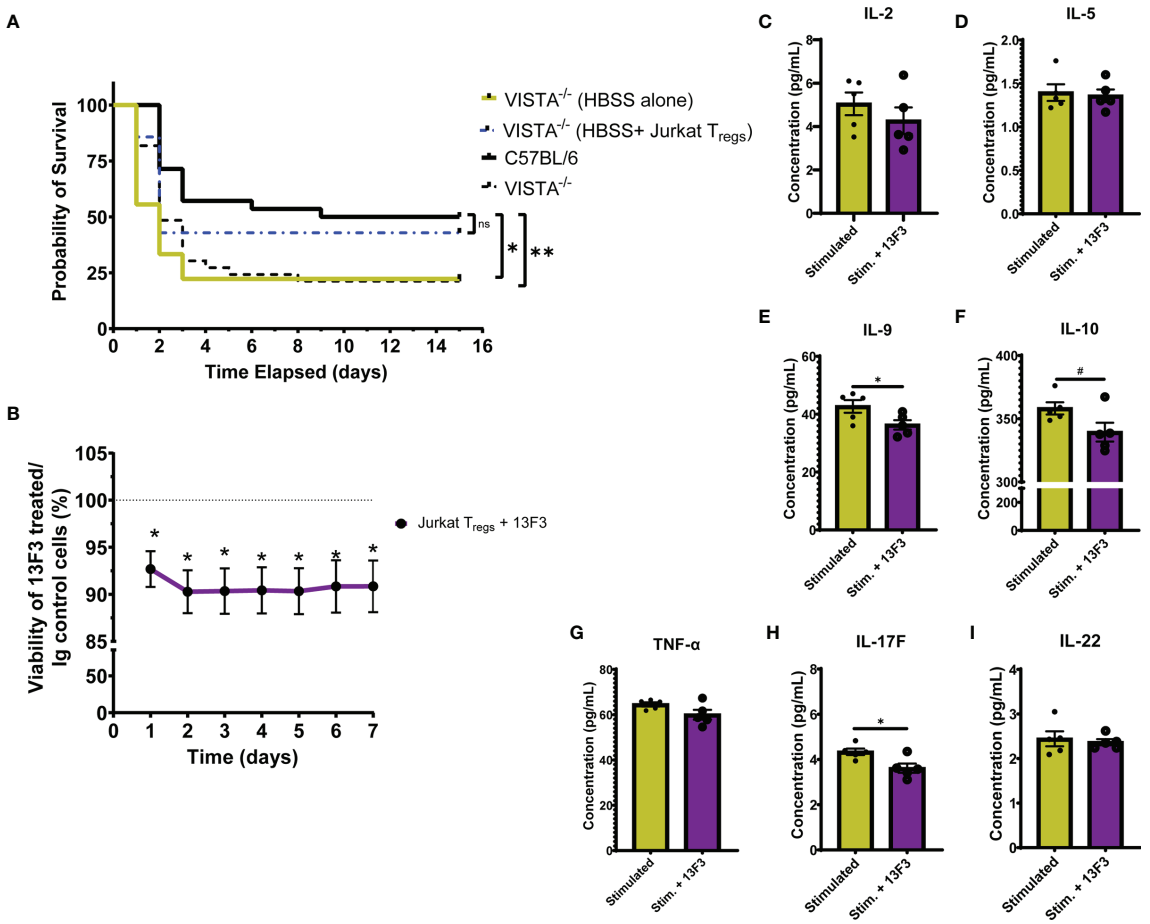

FIGURE 10 | Adoptive transfer of Jurkat T_{regs} improves survival of VISTA$^{-/-}$ mice post CLP. Blockade of VISTA in Jurkat T_{regs} *in vitro* reduces viability and cytokine production. **(A)** 14-day survival following adoptive transfer and CLP [VISTA$^{-/-}$(HBSS alone): *n = 11*, VISTA$^{-/-}$(HBSS+ Jurkat T_{regs}): *n = 10*]. **(B)** Alamar Blue viability assay of Jurkat T_{regs} following treatment with Ig control or 13F3. **(C–I)** Supernatant cytokine concentration of Jurkat T_{regs} following treatment with plasma from septic mouse (stimulated) or plasma and 13F3 (stim. + 13F3). Summary graphs show mean ± SEM; not significant ^{ns}; significance $^{\#}p = 0.05$; $^{*}p < 0.05$; $^{**}p < 0.01$.

CTLA4, and CD25 relative to WT mice. VISTA$^{-/-}$ mice also have an altered cytokine profile including higher IL-6, IL-10, TNF-a, IL-17F, IL-23, and MCP-1 relative to WT mice. VISTA$^{-/-}$ mice have higher indices of acute liver injury (i.e., bilirubin, ALT, and AST) and reduced survival post CLP compared to WT mice. Interestingly, we were able to rescue VISTA$^{-/-}$ survival to WT levels by adoptively transferring VISTA-expressing Jurkat T_{regs} into VISTA$^{-/-}$ mice prior to CLP. In addition, treating Jurkat T_{regs} with a VISTA-neutralizing antibody *in vitro*, reduced viability and cytokine production. We can conclude from these experiments that VISTA expression plays a pivotal role in promoting acute CD4^{+} T_{reg} survival/stability and regulating the cytokine milieu in acute sepsis to confer a survival benefit.

4.6 Future Considerations

This study has raised questions as to the mechanism by which VISTA promotes T_{reg} survival. Interestingly, Foxp3 and VISTA are both under the transcriptional regulation of p53 and HIF-1α. In fact, p53-Foxp3 and HIF1α-Foxp3 induction are indispensable for protective T_{reg} suppression under inflammatory conditions (24, 77–79). The tentative relationship between VISTA and Foxp3 expression provide an additional line of query regarding T_{reg} plasticity.

Another area for further investigation concerns the effector immune cells that are non-redundantly regulated by VISTA^{+} T_{regs}. Based on results from this study, VISTA may act as a non-redundant marker for the T_{reg} subset responsible for regulating M1/M2 polarization and limiting acute liver injury in sepsis. More work must be done to fully elucidate these mechanisms; however, we think this study contributes a novel perspective on checkpoint regulator, VISTA, in the acute sepsis response.

DATA AVAILABILITY STATEMENT

The original contributions presented in the study are included in the article/**Supplementary Material**. Further inquiries can be directed to the corresponding author.

ETHICS STATEMENT

The studies involving human participants were reviewed and approved by institutional review board approval at Rhode Island Hospital (IRB study # 413013). The patients/participants provided their written informed consent to participate in this study. All protocols were performed in accordance with the National Institutes of Health guidelines and as approved by the Animal Use Committee of Rhode Island Hospital (AWC# 5064-18 and 5054-21).

AUTHOR CONTRIBUTIONS

CG provided substantial contribution to the conception of this project, experiment design, data acquisition, and data analysis. CG also wrote the initial draft of the manuscript and participated in the revision steps of the manuscript. BB-G provided initial contribution to the conception of this project. MW enrolled patients and healthy controls, collected samples, and acquired human data. C-SC aided in small intestine sample isolation for flow cytometry studies. YC performed the initial survival study of VISTA$^{-/-}$ and WT mice and performed routine genotyping and husbandry of VISTA$^{-/-}$ mice. YQ-R performed initial ELISAs that supported multiplex experiments and results. JT generated preliminary data that contributed to the initial conception of this project. AA provided guidance throughout the conception and execution of this project. All authors reviewed this manuscript. All authors contributed to the article and approved the submitted version.

FUNDING

This study was supported by the National Institutes of Health (R35 GM118097 [provided for costs of supplies/animals/reagents, and portions of salary for AA, CG], R25 GM083270 [provided for a portion salary for CG], T32 GM065085 [provided fellowship support for MW], T32 HL134625 [provided fellowship support for BB-G], T35 HL67704 [provided fellowship support for YQ-R, JDT]).

ACKNOWLEDGMENTS

The VISTA$^{-/-}$ mouse model was created at the Brown University Mouse Transgenic and Gene Targeting Facility that is supported by a grant from the National Institute of General Medical Sciences (P30 GM103410) from the National Institutes of Health.

SUPPLEMENTARY MATERIAL

The Supplementary Material for this article can be found online at: https://www.frontiersin.org/articles/10.3389/fimmu.2022.861670/full#supplementary-material

REFERENCES

1. Kadri SS, Rhee C, Strich JR, Morales MK, Hohmann S, Menchaca J, et al. Estimating Ten-Year Trends in Septic Shock Incidence and Mortality in United States Academic Medical Centers Using Clinical Data. *Chest* (2017) 151(2):278–85. doi doi: 10.1016/j.chest.2016.07.010
2. Rudd KE, Johnson SC, Agesa KM, Shackelford KA, Tsoi D, Kievlan DR, et al. Global, Regional, and National Sepsis Incidence and Mortality, 1990-2017: Analysis for the Global Burden of Disease Study. *Lancet* (2020) 395 (10219):200–11. doi: 10.1016/S0140-6736(19)32989-7
3. Zhou F, Yu T, Du R, Fan G, Liu Y, Liu Z, et al. Clinical Course and Risk Factors for Mortality of Adult Inpatients With COVID-19 in Wuhan, China: A Retrospective Cohort Study. *Lancet* (2020) 395(10229):1054–62. doi: 10.1016/S0140-6736(20)30566-3
4. Rhee C, Dantes R, Epstein L, Murphy DJ, Seymour CW, Iwashyna TJ, et al. Incidence and Trends of Sepsis in US Hospitals Using Clinical vs Claims Data, 2009-2014. *JAMA* (2017) 318(13):1241–9. doi: 10.1001/jama.2017.13836
5. Hotchkiss RS, Monneret G, Payen D. Sepsis-Induced Immunosuppression: From Cellular Dysfunctions to Immunotherapy. *Nat Rev Immunol* (2013) 13 (12):862–74. doi: 10.1038/nri3552
6. Xiao W, Mindrinos MN, Seok J, Cuschieri J, Cuenca AG, Gao H, et al. A Genomic Storm in Critically Injured Humans. *J Exp Med* (2011) 208 (13):2581–90. doi: 10.1084/jem.20111354
7. Boomer JS, To K, Chang KC, Takasu O, Osborne DF, Walton AH, et al. Immunosuppression in Patients Who Die of Sepsis and Multiple Organ Failure. *JAMA* (2011) 306(23):2594–605. doi: 10.1001/jama.2011.1829
8. Li X, Shao C, Shi Y, Han W. Lessons Learned From the Blockade of Immune Checkpoints in Cancer Immunotherapy. *J Hematol Oncol* (2018) 11(1):31. doi: 10.1186/s13045-018-0578-4
9. Young WA, Fallon EA, Heffernan DS, Efron PA, Cioffi WG, Ayala A. Improved Survival After Induction of Sepsis by Cecal Slurry in PD-1 Knockout Murine Neonates. *Surgery* (2017) 161(5):1387–93. doi: 10.1016/j.surg.2016.11.008
10. Monaghan SF, Thakkar RK, Heffernan DS, Huang X, Chung CS, Lomas-Neira J, et al. Mechanisms of Indirect Acute Lung Injury: A Novel Role for the Coinhibitory Receptor, Programmed Death-1. *Ann Surg* (2012) 255(1):158–64. doi: 10.1097/SLA.0b013e31823433ca
11. Huang X, Chen Y, Chung CS, Yuan Z, Monaghan SF, Wang F, et al. Identification of B7-H1 as a Novel Mediator of the Innate Immune/Proinflammatory Response as Well as a Possible Myeloid Cell Prognostic Biomarker in Sepsis. *J Immunol* (2014) 192(3):1091–9. doi: 10.4049/jimmunol.1302252
12. Wakeley ME, Shubin NJ, Monaghan SF, Gray CC, Ayala A, Heffernan DS. Herpes Virus Entry Mediator (HVEM): A Novel Potential Mediator of Trauma-Induced Immunosuppression. *J Surg Res* (2020) 245:610–8. doi: 10.1016/j.jss.2019.07.009
13. Xu S, Yang Q, Bai J, Tao T, Tang L, Chen Y, et al. Blockade of Endothelial, But Not Epithelial, Cell Expression of PD-L1 Following Severe Shock Attenuates the Development of Indirect Acute Lung Injury in Mice. *Am J Physiol Lung Cell Mol Physiol* (2020) 318(4):L801–L12. doi: 10.1152/ajplung.00108.2019
14. Hutchins NA, Wang F, Wang Y, Chung CS, Ayala A. Kupffer Cells Potentiate Liver Sinusoidal Endothelial Cell Injury in Sepsis by Ligating Programmed Cell Death Ligand-1. *J Leukoc Biol* (2013) 94(5):963–70. doi: 10.1189/jlb.0113051
15. Wu Y, Chung CS, Chen Y, Monaghan SF, Patel S, Huang X, et al. A Novel Role for Programmed Cell Death Receptor Ligand-1 (PD-L1) in Sepsis-Induced Intestinal Dysfunction. *Mol Med* (2017) 22:830–40. doi: 10.2119/molmed.2016.00150
16. Hotchkiss RS, Monneret G, Payen D. Immunosuppression in Sepsis: A Novel Understanding of the Disorder and a New Therapeutic Approach. *Lancet Infect Dis* (2013) 13(3):260–8. doi: 10.1016/S1473-3099(13)70001-X

17. Flies DB, Han X, Higuchi T, Zheng L, Sun J, Ye JJ, et al. Coinhibitory Receptor PD-1H Preferentially Suppresses CD4(+) T Cell-Mediated Immunity. *J Clin Invest* (2014) 124(5):1966–75. doi: 10.1172/JCI74589
18. Deng J, Le Mercier I, Kuta A, Noelle RJ. A New VISTA on Combination Therapy for Negative Checkpoint Regulator Blockade. *J Immunother Cancer* (2016) 4:86. doi: 10.1186/s40425-016-0190-5
19. Kondo Y, Ohno T, Nishii N, Harada K, Yagita H, Azuma M. Differential Contribution of Three Immune Checkpoint (VISTA, CTLA-4, PD-1) Pathways to Antitumor Responses Against Squamous Cell Carcinoma. *Oral Oncol* (2016) 57:54–60. doi: 10.1016/j.oraloncology.2016.04.005
20. Wang L, Rubinstein R, Lines JL, Wasiuk A, Ahonen C, Guo Y, et al. VISTA, a Novel Mouse Ig Superfamily Ligand That Negatively Regulates T Cell Responses. *J Exp Med* (2011) 208(3):577–92. doi: 10.1084/jem.20100619
21. Mehta N, Maddineni S, Mathews II, Andres Parra Sperberg R, Huang PS, Cochran JR. Structure and Functional Binding Epitope of V-Domain Ig Suppressor of T Cell Activation. *Cell Rep* (2019) 28(10):2509–16 e5. doi: 10.1016/j.celrep.2019.07.073
22. Johnston RJ, Su LJ, Pinckney J, Critton D, Boyer E, Krishnakumar A, et al. VISTA Is an Acidic pH-Selective Ligand for PSGL-1. *Nature* (2019) 574 (7779):565–70. doi: 10.1038/s41586-019-1674-5
23. Wang J, Wu G, Manick B, Hernandez V, Renelt M, Erickson C, et al. VSIG-3 as a Ligand of VISTA Inhibits Human T-Cell Function. *Immunology* (2019) 156(1):74–85. doi: 10.1111/imm.13001
24. ElTanbouly MA, Zhao Y, Nowak E, Li J, Schaafsma E, Le Mercier I, et al. VISTA Is a Checkpoint Regulator for Naive T Cell Quiescence and Peripheral Tolerance. *Science* (2020) 367(6475):eaay0534. doi: 10.1126/science.aay0524
25. Wang Q, He J, Flies DB, Luo L, Chen L. Programmed Death One Homolog Maintains the Pool Size of Regulatory T Cells by Promoting Their Differentiation and Stability. *Sci Rep* (2017) 7(1):6086. doi: 10.1038/s41598-017-06410-w
26. Liu J, Yuan Y, Chen W, Putra J, Suriawinata AA, Schenk AD, et al. Immune-Checkpoint Proteins VISTA and PD-1 Nonredundantly Regulate Murine T-Cell Responses. *Proc Natl Acad Sci USA* (2015) 112(21):6682–7. doi: 10.1073/pnas.1420370112
27. Lines JL, Pantazi E, Mak J, Sempere LF, Wang L, O'Connell S, et al. VISTA Is an Immune Checkpoint Molecule for Human T Cells. *Cancer Res* (2014) 74 (7):1924–32. doi: 10.1158/0008-5472.CAN-13-1504
28. Boomer JS, Shuherk-Shaffer J, Hotchkiss RS, Green JM. A Prospective Analysis of Lymphocyte Phenotype and Function Over the Course of Acute Sepsis. *Crit Care* (2012) 16(3):R112. doi: 10.1186/cc11404
29. Unsinger J, McDonough JS, Shultz LD, Ferguson TA, Hotchkiss RS. Sepsis-Induced Human Lymphocyte Apoptosis and Cytokine Production in "Humanized" Mice. *J Leukoc Biol* (2009) 86(2):219–27. doi: 10.1189/jlb.1008615
30. Sharma A, Yang WL, Matsuo S, Wang P. Differential Alterations of Tissue T-Cell Subsets After Sepsis. *Immunol Lett* (2015) 168(1):41–50. doi: 10.1016/j.imlet.2015.09.005
31. Tang L, Bai J, Chung CS, Lomas-Neira J, Chen Y, Huang X, et al. Active Players in Resolution of Shock/Sepsis Induced Indirect Lung Injury: Immunomodulatory Effects of Tregs and PD-1. *J Leukoc Biol* (2014) 96 (5):809–20. doi: 10.1189/jlb.4MA1213-647RR
32. Heuer JG, Zhang T, Zhao J, Ding C, Cramer M, Justen KL, et al. Adoptive Transfer of *In Vitro*-Stimulated CD4+CD25+ Regulatory T Cells Increases Bacterial Clearance and Improves Survival in Polymicrobial Sepsis. *J Immunol* (2005) 174(11):7141–6. doi: 10.4049/jimmunol.174.11.7141
33. Kuhlhorn F, Rath M, Schmoeckel K, Cziupka K, Nguyen HH, Hildebrandt P, et al. Foxp3+ Regulatory T Cells Are Required for Recovery From Severe Sepsis. *PloS One* (2013) 8(5):e65109. doi: 10.1371/journal.pone.0065109
34. Andrade MMC, Ariga SSK, Barbeiro DF, Barbeiro HV, Pimentel RN, Petroni RC, et al. Endotoxin Tolerance Modulates TREG and TH17 Lymphocytes Protecting Septic Mice. *Oncotarget* (2019) 10(37):3451–61. doi: 10.18632/oncotarget.26919
35. Hubbard WJ, Choudhry M, Schwacha MG, Kerby JD, Rue LW3rd, Bland KI, et al. Cecal Ligation and Puncture. *Shock* (2005) 24(Suppl 1):52–7. doi: 10.1097/01.shk.0000191414.94461.7e
36. Rittirsch D, Huber-Lang MS, Flierl MA, Ward PA. Immunodesign of Experimental Sepsis by Cecal Ligation and Puncture. *Nat Protoc* (2009) 4 (1):31–6. doi: 10.1038/nprot.2008.214
37. Remick DG, Ayala A, Chaudry IH, Coopersmith CM, Deutschman C, Hellman J, et al. Premise for Standardized Sepsis Models. *Shock* (2019) 51 (1):4–9. doi: 10.1097/SHK.0000000000001164
38. Wichmann MW, Ayala A, Chaudry IH. Male Sex Steroids are Responsible for Depressing Macrophage Immune Function After Trauma-Hemorrhage. *Am J Physiol* (1997) 273(4):C1335–40. doi: 10.1152/ajpcell.1997.273.4.C1335
39. Zellweger R, Wichmann MW, Ayala A, Stein S, DeMaso CM, Chaudry IH. Females in Proestrus State Maintain Splenic Immune Functions and Tolerate Sepsis Better Than Males. *Crit Care Med* (1997) 25(1):106–10. doi: 10.1097/00003246-199701000-00021
40. Hotchkiss RS, Swanson PE, Knudson CM, Chang KC, Cobb JP, Osborne DF, et al. Overexpression of Bcl-2 in Transgenic Mice Decreases Apoptosis and Improves Survival in Sepsis. *J Immunol* (1999) 162(7):4148–56.
41. Hotchkiss RS, Tinsley KW, Swanson PE, Chang KC, Cobb JP, Buchman TG, et al. Prevention of Lymphocyte Cell Death in Sepsis Improves Survival in Mice. *Proc Natl Acad Sci USA* (1999) 96(25):14541–6. doi: 10.1073/pnas.96.25.14541
42. Huang X, Venet F, Wang YL, Lepape A, Yuan Z, Chen Y, et al. PD-1 Expression by Macrophages Plays a Pathologic Role in Altering Microbial Clearance and the Innate Inflammatory Response to Sepsis. *Proc Natl Acad Sci USA* (2009) 106(15):6303–8. doi: 10.1073/pnas.0809422106
43. Hotchkiss RS, Tinsley KW, Swanson PE, Schmieg REJr., Hui JJ, Chang KC, et al. Sepsis-Induced Apoptosis Causes Progressive Profound Depletion of B and CD4+ T Lymphocytes in Humans. *J Immunol* (2001) 166(11):6952–63. doi: 10.4049/jimmunol.166.11.6952
44. Le Tulzo Y, Pangault C, Gacouin A, Guilloux V, Tribut O, Amiot L, et al. Early Circulating Lymphocyte Apoptosis in Human Septic Shock Is Associated With Poor Outcome. *Shock* (2002) 18(6):487–94. doi: 10.1097/00024382-200212000-00001
45. Heffernan DS, Monaghan SF, Thakkar RK, Machan JT, Cioffi WG, Ayala A. Failure to Normalize Lymphopenia Following Trauma Is Associated With Increased Mortality, Independent of the Leukocytosis Pattern. *Crit Care* (2012) 16(1):R12. doi: 10.1186/cc11157
46. Gouel-Cheron A, Allaouchiche B, Guignant C, Davin F, Floccard B, Monneret G, et al. Early Interleukin-6 and Slope of Monocyte Human Leukocyte Antigen-DR: A Powerful Association to Predict the Development of Sepsis After Major Trauma. *PloS One* (2012) 7(3):e33095. doi: 10.1371/journal.pone.0033095
47. Levy MM, Fink MP, Marshall JC, Abraham E, Angus D, Cook D, et al. 2001 SCCM/ESICM/ACCP/ATS/SIS International Sepsis Definitions Conference. *Crit Care Med* (2003) 31(4):1250–6. doi: 10.1097/01.CCM.0000050454.01978.3B
48. Monneret G, Debard AL, Venet F, Bohe J, Hequet O, Bienvenu J, et al. Marked Elevation of Human Circulating CD4+CD25+ Regulatory T Cells in Sepsis-Induced Immunoparalysis. *Crit Care Med* (2003) 31(7):2068–71. doi: 10.1097/01.CCM.0000069345.78884.0F
49. Leng FY, Liu JL, Liu ZJ, Yin JY, Qu HP. Increased Proportion of CD4(+)CD25(+)Foxp3(+) Regulatory T Cells During Early-Stage Sepsis in ICU Patients. *J Microbiol Immunol Infect* (2013) 46(5):338–44. doi: 10.1016/j.jmii.2012.06.012
50. Le Mercier I, Chen W, Lines JL, Day M, Li J, Sergent P, et al. VISTA Regulates the Development of Protective Antitumor Immunity. *Cancer Res* (2014) 74 (7):1933–44. doi: 10.1158/0008-5472.CAN-13-1506
51. Bharaj P, Chahar HS, Alozie OK, Rodarte L, Bansal A, Goepfert PA, et al. Characterization of Programmed Death-1 Homologue-1 (PD-1H) Expression and Function in Normal and HIV Infected Individuals. *PloS One* (2014) 9(10): e109103. doi: 10.1371/journal.pone.0109103
52. Nowak EC, Lines JL, Varn FS, Deng J, Sarde A, Mabaera R, et al. Immunoregulatory Functions of VISTA. *Immunol Rev* (2017) 276(1):66–79. doi: 10.1111/imr.12525
53. Han X, Vesely MD, Yang W, Sanmamed MF, Badri T, Alawa J, et al. PD-1h (VISTA)-Mediated Suppression of Autoimmunity in Systemic and Cutaneous Lupus Erythematosus. *Sci Transl Med* (2019) 11(522):eaax1159. doi: 10.1126/scitranslmed.aax1159
54. Lines JL, Sempere LF, Broughton T, Wang L, Noelle R. VISTA Is a Novel Broad-Spectrum Negative Checkpoint Regulator for Cancer Immunotherapy. *Cancer Immunol Res* (2014) 2(6):510–7. doi: 10.1158/2326-6066.CIR-14-0072
55. Corthay A. How Do Regulatory T Cells Work? *Scand J Immunol* (2009) 70 (4):326–36. doi: 10.1111/j.1365-3083.2009.02308.x

56. Venet F, Chung CS, Kherouf H, Geeraert A, Malcus C, Poitevin F, et al. Increased Circulating Regulatory T Cells (CD4(+)CD25 (+)CD127 (-)) Contribute to Lymphocyte Anergy in Septic Shock Patients. *Intensive Care Med* (2009) 35(4):678–86. doi: 10.1007/s00134-008-1337-8
57. Jiang LN, Yao YM, Sheng ZY. The Role of Regulatory T Cells in the Pathogenesis of Sepsis and Its Clinical Implication. *J Interferon Cytokine Res* (2012) 32(8):341–9. doi: 10.1089/jir.2011.0080
58. Fontenot JD, Gavin MA, Rudensky AY. Foxp3 Programs the Development and Function of CD4+CD25+ Regulatory T Cells. *Nat Immunol* (2003) 4 (4):330–6. doi: 10.1038/ni904
59. Fontenot JD, Rasmussen JP, Williams LM, Dooley JL, Farr AG, Rudensky AY. Regulatory T Cell Lineage Specification by the Forkhead Transcription Factor Foxp3. *Immunity* (2005) 22(3):329–41. doi: 10.1016/j.immuni.2005.01.016
60. Voo KS, Wang YH, Santori FR, Boggiano C, Wang YH, Arima K, et al. Identification of IL-17-Producing FOXP3+ Regulatory T Cells in Humans. *Proc Natl Acad Sci USA* (2009) 106(12):4793–8. doi: 10.1073/pnas.0900408106
61. Beriou G, Costantino CM, Ashley CW, Yang L, Kuchroo VK, Baecher-Allan C, et al. IL-17-Producing Human Peripheral Regulatory T Cells Retain Suppressive Function. *Blood* (2009) 113(18):4240–9. doi: 10.1182/blood-2008-10-183251
62. Tang AL, Teijaro JR, Njau MN, Chandran SS, Azimzadeh A, Nadler SG, et al. CTLA4 Expression Is an Indicator and Regulator of Steady-State CD4+ FoxP3+ T Cell Homeostasis. *J Immunol* (2008) 181(3):1806–13. doi: 10.4049/jimmunol.181.3.1806
63. Gavin MA, Rasmussen JP, Fontenot JD, Vasta V, Manganiello VC, Beavo JA, et al. Foxp3-Dependent Programme of Regulatory T-Cell Differentiation. *Nature* (2007) 445(7129):771–5. doi: 10.1038/nature05543
64. Josefowicz SZ, Rudensky A. Control of Regulatory T Cell Lineage Commitment and Maintenance. *Immunity* (2009) 30(5):616–25. doi: 10.1016/j.immuni.2009.04.009
65. Kim J, Lahl K, Hori S, Loddenkemper C, Chaudhry A, deRoos P, et al. Cutting Edge: Depletion of Foxp3+ Cells Leads to Induction of Autoimmunity by Specific Ablation of Regulatory T Cells in Genetically Targeted Mice. *J Immunol* (2009) 183(12):7631–4. doi: 10.4049/jimmunol.0804308
66. Wang L, Le Mercier I, Putra J, Chen W, Liu J, Schenk AD, et al. Disruption of the Immune-Checkpoint VISTA Gene Imparts a Proinflammatory Phenotype With Predisposition to the Development of Autoimmunity. *Proc Natl Acad Sci USA* (2014) 111(41):14846–51. doi: 10.1073/pnas.1407447111
67. Remick DG. Pathophysiology of Sepsis. *Am J Pathol* (2007) 170(5):1435–44. doi: 10.2353/ajpath.2007.060872
68. Osuchowski MF, Ayala A, Bahrami S, Bauer M, Boros M, Cavaillon JM, et al. Minimum Quality Threshold in Pre-Clinical Sepsis Studies (MQTiPSS): An International Expert Consensus Initiative for Improvement of Animal Modeling in Sepsis. *Shock* (2018) 50(4):377–80. doi: 10.1097/SHK.0000000000001212
69. Romano M, Fanelli G, Albany CJ, Giganti G, Lombardi G. Past, Present, and Future of Regulatory T Cell Therapy in Transplantation and Autoimmunity. *Front Immunol* (2019) 10:43. doi: 10.3389/fimmu.2019.00043
70. Tiemessen MM, Jagger AL, Evans HG, van Herwijnen MJ, John S, Taams LS. CD4+CD25+Foxp3+ Regulatory T Cells Induce Alternative Activation of Human Monocytes/Macrophages. *Proc Natl Acad Sci USA* (2007) 104 (49):19446–51. doi: 10.1073/pnas.0706832104
71. Cavaillon JM, Adib-Conquy M. Monocytes/macrophages and Sepsis. *Crit Care Med* (2005) 33(12 Suppl):S506–9. doi: 10.1097/01.ccm.0000185502.21012.37
72. Triantafyllou E, Woollard KJ, McPhail MJW, Antoniades CG, Possamai LA. The Role of Monocytes and Macrophages in Acute and Acute-On-Chronic Liver Failure. *Front Immunol* (2018) 9:2948. doi: 10.3389/fimmu.2018.02948
73. Eller K, Wolf D, Huber JM, Metz M, Mayer G, McKenzie AN, et al. IL-9 Production by Regulatory T Cells Recruits Mast Cells That Are Essential for Regulatory T Cell-Induced Immune Suppression. *J Immunol* (2011) 186 (1):83–91. doi: 10.4049/jimmunol.1001183
74. Uhlig HH, Coombes J, Mottet C, Izcue A, Thompson C, Fanger A, et al. Characterization of Foxp3+CD4+CD25+ and IL-10-Secreting CD4+CD25+ T Cells During Cure of Colitis. *J Immunol* (2006) 177(9):5852–60. doi: 10.4049/jimmunol.177.9.5852
75. Rubtsov YP, Rasmussen JP, Chi EY, Fontenot J, Castelli L, Ye X, et al. Regulatory T Cell-Derived Interleukin-10 Limits Inflammation at Environmental Interfaces. *Immunity* (2008) 28(4):546–58. doi: 10.1016/j.immuni.2008.02.017
76. Tao T, Bo L, Li T, Shi L, Zhang H, Ye B, et al. High-Affinity Anti-VISTA Antibody Protects Against Sepsis by Inhibition of T Lymphocyte Apoptosis and Suppression of the Inflammatory Response. *Mediators Inflammation* (2021) 2021:6650329. doi: 10.1155/2021/6650329
77. Kim JE, Shin JS, Moon JH, Hong SW, Jung DJ, Kim JH, et al. Foxp3 Is a Key Downstream Regulator of P53-Mediated Cellular Senescence. *Oncogene* (2017) 36(2):219–30. doi: 10.1038/onc.2016.193
78. Dang EV, Barbi J, Yang HY, Jinasena D, Yu H, Zheng Y, et al. Control of T(H) 17/T(reg) Balance by Hypoxia-Inducible Factor 1. *Cell* (2011) 146(5):772–84. doi: 10.1016/j.cell.2011.07.033
79. Clambey ET, McNamee EN, Westrich JA, Glover LE, Campbell EL, Jedlicka P, et al. Hypoxia-Inducible Factor-1 Alpha-Dependent Induction of FoxP3 Drives Regulatory T-Cell Abundance and Function During Inflammatory Hypoxia of the Mucosa. *Proc Natl Acad Sci USA* (2012) 109(41):E2784–93. doi: 10.1073/pnas.1202366109

Conflict of Interest: The authors declare that the research was conducted in the absence of any commercial or financial relationships that could be construed as a potential conflict of interest.

Publisher's Note: All claims expressed in this article are solely those of the authors and do not necessarily represent those of their affiliated organizations, or those of the publisher, the editors and the reviewers. Any product that may be evaluated in this article, or claim that may be made by its manufacturer, is not guaranteed or endorsed by the publisher.

frontiers | Frontiers in Immunology

ORIGINAL RESEARCH
published: 01 April 2022
doi: 10.3389/fimmu.2022.852119

A Novel Porcine Model of Ischemia-Reperfusion Injury After Cross-Clamping the Thoracic Aorta Revealed Substantial Cardiopulmonary, Thromboinflammatory and Biochemical Changes Without Effect of C1-Inhibitor Treatment

Erik Waage Nielsen[1,2,3,4*], *Yoav Miller*[2], *Ole-Lars Brekke*[5,6], *Joost Grond*[5], *Anh Hoang Duong*[7], *Hilde Fure*[5], *Judith Krey Ludviksen*[5], *Kristin Pettersen*[5], *Leon Reubsaet*[7], *Rigmor Solberg*[7], *Harald Thidemann Johansen*[7] *and Tom Eirik Mollnes*[5,6,8,9]

[1] Department of Anesthesia and Intensive Care Medicine, Nordland Hospital, Bodø, Norway, [2] Institute of Clinical Medicine, UiT The Arctic University of Norway, Tromsø, Norway, [3] Faculty of Nursing and Health Sciences, Nord University, Bodø, Norway, [4] Department of Immunology, Faculty of Medicine, University of Oslo, Oslo, Norway, [5] Research Laboratory, Nordland Hospital Trust, Bodø, Norway, [6] Faculty of Health Sciences, Kristian Gerhard (K.G.) Jebsen Thrombosis Research Center (TREC), UiT The Arctic University of Norway, Tromsø, Norway, [7] Department of Pharmacy, University of Oslo, Oslo, Norway, [8] Department of Immunology, University of Oslo and Oslo University Hospital, Oslo, Norway, [9] Centre of Molecular Inflammation Research, Norwegian University of Science and Technology, Trondheim, Norway

Ischemic injury worsens upon return of blood and innate immunity including the complement system play a central role in ischemia-reperfusion injury (IRI) as in thoracic aortic surgery. Complement component1 inhibitor (C1-INH) has been shown to reduce IRI and is a broad-acting plasma cascade inhibitor. We established a new porcine model of IRI by cross-clamping the thoracic aorta and evaluated the global changes occurring in organ function, systemic inflammatory response and organ damage with or without treatment with C1-INH-concentrate. Twenty-four piglets (8.8-11.1 kg) underwent 45 minutes clamping of the thoracic aorta at the Th8 level. Upfront 12 piglets received human saline and 12 received C1-INH (250 IU/kg) intravenously. Three sham animals received thoracic opening without clamping. Reperfusion lasted 5 hours. We studied ten cardiorespiratory markers, three hematologic markers, eleven inflammatory markers, and twelve organ damage markers over the whole experimental period. Postmortem tissue homogenates from seven organs were examined for inflammatory markers and analysed by two-way repeated-measures ANOVA, area under the curve or unpaired t-tests. By excluding sham and combining treated and untreated animals, the markers reflected a uniform, broad and severe organ dysfunction. The mean and range

OPEN ACCESS

Edited by:
Christoph Thiemermann, Queen Mary University of London, United Kingdom

Reviewed by:
Jordi Lopez Tremoleda, Queen Mary University of London, United Kingdom
Barbara Mara Klinkhammer, University Hospital RWTH Aachen, Germany

***Correspondence:**
Erik Waage Nielsen
erik.waage.nielsen@uit.no

Specialty section:
This article was submitted to Inflammation, a section of the journal Frontiers in Immunology

Received: *11 January 2022*
Accepted: *10 March 2022*
Published: *01 April 2022*

Citation:
Nielsen EW, Miller Y, Brekke O-L, Grond J, Duong AH, Fure H, Ludviksen JK, Pettersen K, Reubsaet L, Solberg R, Johansen HT and Mollnes TE (2022) A Novel Porcine Model of Ischemia-Reperfusion Injury After Cross-Clamping the Thoracic Aorta Revealed Substantial Cardiopulmonary, Thromboinflammatory and Biochemical Changes Without Effect of C1-Inhibitor Treatment. Front. Immunol. 13:852119. doi: 10.3389/fimmu.2022.852119

fold change from before cross-clamp onset to maximum change for the different groups of markers were: cardiorespiratory 1.4 (0.2-3.7), hematologic 1.9 (1.2-2.7), plasma inflammatory 19.5 (1.4-176) and plasma organ damage 2.9 (1.1-8.6). Treatment with C1-INH had only a marginal effect on the IRI-induced changes, reaching statistical significance only for the plasma complement activation product TCC (p=0.0083) and IL-4 (p=0.022) and INF-α (p=0.016) in the colon tissue. In conclusion, the present novel model of porcine global IRI is forceful with regards to central markers and could generally be applicable for pathophysiological studies. C1-INH treatment had no significant effect, but the model allows for future testing of other drugs attenuating IRI globally.

Keywords: complement - immunological terms, Kallikrein - kinin system, porcine (pig) model, C1-INH (C1 inhibitor), C1-INH concentrate, ischemi/reperfusion injury, ANOVA & factor analysis

INTRODUCTION

Ischemia-reperfusion injury (IRI) is tissue damage caused by returning blood to organs temporarily deprived of circulation. IRI arises in coronary and cerebral infarctions, trauma, surgery and transplantation. Global IRI have been studied by clamping the aorta in various rat, rabbit and dog models. The translational value to humans are limited from small animal models and could advantageously be studied in large animals, where pig is a highly relevant animal model.

Several porcine models of thoracic aortic clamping have been described. However, these models have focused on the effect of single organs and not taken into account the global IRI from all organs affected by the clamping. Studies are described for the effects on cardiac (1, 2), renal (3, 4), hepatic (5), limb (6), spinal cord (7), and pulmonary IRI (8).

We aimed to establish a new porcine model for thoracic aortic cross-clamping using light weight piglets to allow for a minimal use of costly experimental therapeutics, while preserving translational value of the model. Such a model is highly relevant since thoracic aortic aneurysm surgery often require clamping of aorta. We have shown that the inflammatory reaction in such patients is largely mediated through the lectin complement pathway (9).

In IRI, reactive oxygen species and innate inflammation exacerbate ischemic injury through e.g. increased complement activation (10). Complement 1 inhibitor (C1-INH) controls the physiological activity of both the classical and lectin pathway of complement, and several studies show that C1-INH reduces IRI in animal models and in patients (10). In addition, C1-INH is by far the most important suppressor of bradykinin production from the kallikrein-kinin system, and would inhibit bradykinin-mediated inflammation in pigs (11), capillary leakage and pain (12).

The aim of the present study was to establish a novel and clinically relevant IRI pig model of aortic clamping. Secondly, to investigate the effect of IRI on cardiovascular, hematologic, inflammatory and organ damage markers during ischemia and for a five hour observation period, and thirdly, how these effects were modified by supraphysiological amounts of human C1-INH administered before clamping.

MATERIALS AND METHODS

Animal Handling

This study was approved by the National Animal Research Authority (FOTS-ID-8197). We performed the experiments under the Norwegian Laboratory Animal Regulations and the EU directive 2010/63/EU. Animals were healthy Specific Pathogen Free Norwegian landrace pigs from one farm close to the University and the operation theatre. The study was led by well-trained staff with over 10 years of experience in porcine anaesthesia. In total, 27 Norwegian Landrace pigs (mean weight: 9.9 ± 0.6 kg), 2 females (one in each treatment group) and 25 males were included in the study. The pigs received intramuscular anaesthesia consisting of 500 mg ketamine, 40 mg azaperone and 0.5 mg atropine blended in a 20 ml injection set at the farm maintaining spontaneous respiration. They were weighed and received one intravenous line in each ear. Anaesthesia was deepened with intravenous ketamine 50-100 mg and continuous infusion of 1 mg/kg/h midazolam and 1.1 μg/kg/h remifentanil. Prior to 45 minutes of aortic clamping, 12 animals received a bolus of saline solution and 12 animals received human C1-INH (250 U/kg). The dose was based on our previous study on the amount C1-INH needed to inhibit the complement activation (13), and other *in vivo* studies (14). Three sham animals received thoracic opening without aortic clamping or infusion. Intravenous boluses of 2-100 ml nitroprusside (200 μg/ml) and 3-5 ml propofol (10 mg/ml) were administered to adjust mean arterial pressure (MAP). After release of the aortic cross-clamp remifentanil was switched to fentanyl 66 μg/kg/h.

Monitoring

In short, animals were endotracheally intubated and received an arterial line in the left carotid artery, a central venous catheter in the left external jugular vein, a pulmonary catheter in the right external jugular vein and a suprapubic catheter for monitoring and sample collection purposes.

Aortic Clamping

A mini thoracotomy at the level of Th8 was performed, ribs opened with a Finochietto Retractor and the descending thoracic aorta was exposed. After manual palpation, aorta was occluded

with a medium sized Satinsky vascular clamp. Surgery was followed by a stabilization period of 30 minutes. Prior to aortic clamping the MAP was reduced to 30-40 mmHg with help of sodium nitroprusside and propofol bolus doses. In order to complete this severe period of ischemia, it was necessary to use potent vasopressors and vasodilators with quick and large adjustments. After initiation of clamping, total ischemia of the lower extremities was confirmed with an ultrasound Doppler of the femoral artery. The immediate increase in MAP after initiation of clamping was stabilized at 80-100 mmHg during the 45-minute ischemic period using in average 80.8 mg propofol and 13.3 mg nitroprusside. Noradrenaline was initiated after 35 minutes of ischemia to elevate blood pressure before release of the aorta clamp. Tribonate® 30 ml was administered at the 45-minute ischemia mark in anticipation of a fall in pH. The cross-clamp was removed and replaced by digital pressure and both the surgeon and anaesthetist carefully monitored end-tidal CO_2-values, heart rate and blood pressure. The anaesthetist used noradrenaline bolus doses to control blood pressure at this crucial time. It normally took around 10 minutes before digital pressure could be fully released and vital signs stabilized. The aim at this point was to keep MAP above 50 mmHg. If the dose of noradrenaline infusion reached 3.2 μg/kg/min a continuous infusion of vasopressin was added at a concentration of 1 U/ml with a start rate of 0.5 ml/h. In average 13.35 mg noradrenaline and 7.83 U vasopressin were used. If pH-values dropped below 7.2 boluses of 10 ml Tribonate® were administered, in average 44.6 ml. The average amount of infused Ringer Acetate was 694 ml. Neither of the above mentioned regimens were statistically different between the two groups. Overall, the hemodynamic management was performed in accordance with clinical practice, although experimental treatment of pigs cannot fully mimic the clinical situation.

Hemodynamic and Respiratory Parameters

Heart rate (HR) and mean arterial pressure (MAP) were measured using an arterial catheter (Millar Instruments, Houston TX). Mean pulmonary artery pressure (MPAP) was measured using a pulmonary catheter (Edwards Lifesciences, Irvine, CA). Animals were ventilated using the Pulmonetic System® LTV 1000 ventilator (Pulmonetic Systems, Minneapolis, MN). Fraction of inspired oxygen (FiO_2), respiratory minute volume (MV) and peak respiratory pressure were adjusted to normal saturation, pH and end-tidal CO_2 ($ETCO_2$) values when possible. Registration of hemodynamic and respiratory values, as well as blood sampling were done at the following time-points relative to start of reperfusion: -75 minutes (baseline), -50 minutes (before cross-clamp onset), -5 minutes (gradual release of clamp), 0 minutes (start reperfusion), and 60, 120, 180, 240 and 300 minutes after start of reperfusion.

Blood Analyses

Arterial blood gases and lactate were analysed directly on site using an epoc® Blood Analysis System (Epocal, Ottowa, ON). Haematological parameters were analysed in EDTA-blood on the ADVIA® 2120i System (Siemens healthineers, Eschborn, Germany). Biochemical parameters were analysed in heparinized plasma on the ADVIA® 1800 Chemistry System (Siemens healthineers, Tarrytown, NY). For the analyses of inflammatory and coagulation parameters EDTA and citrated blood samples were cooled and centrifuged at 1500 x g for 15 minutes immediately after collection and the obtained plasma was frozen at -80°C. Cytokines were analysed in EDTA-plasma using a 9-plex assay (eBioscience, San Diego, CA). C3a was measured in EDTA-plasma as previously described in detail (15). Soluble Terminal Complement Complex (TCC) levels were measured in EDTA-plasma using an in-house ELISA (16). Kallikrein activity was measured as measured by cleavage of the peptide substrate S-2302 (Pro-Phe-Arg-pNA) and calculating the increase in O.D. at 405 nm in citrate plasma as previously described (17). PAI-1 was measured in citrate plasma by ELISA (Molecular Innovations, Novi, MI). TAT was measured in citrate plasma (Siemens Healthineers, Newark, DE).

Cytokines in Tissue Homogenates

After 300 minutes of reperfusion, animals were euthanized by intravenous injection of potassium chloride. Biopsies were harvested from the left ventricle, left lung, liver, left kidney, spleen, small intestine and colon. Biopsies were rinsed in ice-cold saline and snap-frozen on dry-ice prior to storage at -80°C. Biopsies were homogenized and prepared for analysis as described previously (18). Tumour necrosis factor (TNF), interleukin (IL)-1-β, IL-4, IL-6, IL-8, IL-10, IL-12p40, interferon (IFN)-α and IFN-γ-levels were analysed using 9-plex (eBioscience, San Diego, CA).

Statistical Analyses

GraphPad Prism 8.4.3 (San Diego, CA, USA) was used for result handling and statistical analyses. Longitudinal time data in graphs were expressed as median and interquartile range. Markers of physiological organ function, systemic inflammatory response and organ damage were analysed using two-way repeated measures ANOVA with Geisser-Greenhouse correction and mixed effects analysis in case of missing values, as well as with t-test of the area under the curve calculated in Excel. Cytokine values from tissue homogenates were log-transformed and analysed using independent t-tests. P-values < 0.05 were considered significant.

RESULTS

A broad panel of markers changed considerably from before cross-clamp onset and showed a uniform pattern in both C1-INH-treated and untreated animals. The variation in time course of each marker is shown. The only marker that was significantly reduced by C1-INH treatment was TCC. To show the magnitude of the total response, we present the fold change (FC) of the markers in treated and untreated animals combined, excluding sham animals. The change is from 50 minutes before the start of IRI (approximately 5 minutes before cross-clamp onset) until

maximal change of marker value during the following observation period. FC for each marker is mean of maximal values after clamping in all animals divided by mean value before clamping. Each marker´s name in the Figure panels is succeeded by the FC in parenthesis when meaningful.

Cardiorespiratory Markers

Twelve cardiorespiratory markers were investigated. The absolute values and time course of MAP, MPAP, HR, FiO_2, Resp Min Vol, and $ETCO_2$ are presented in **Figures 1A–F**. In addition, the fold change is presented as text in parenthesis after each marker´s name. Taken together, the mean with range fold change was 1.4(1–2). The temperature, pH, lactate, Base Excess, PaO2 and glucose are presented in **Figures 2A–F**. The fold change is in parenthesis. Taken together the mean with range fold change of these markers was 1.65 (0.2-3.7).

Hematologic Markers

The absolute values and time course of three hematologic markers are presented in **Figures 3A–C**. The fold change is in

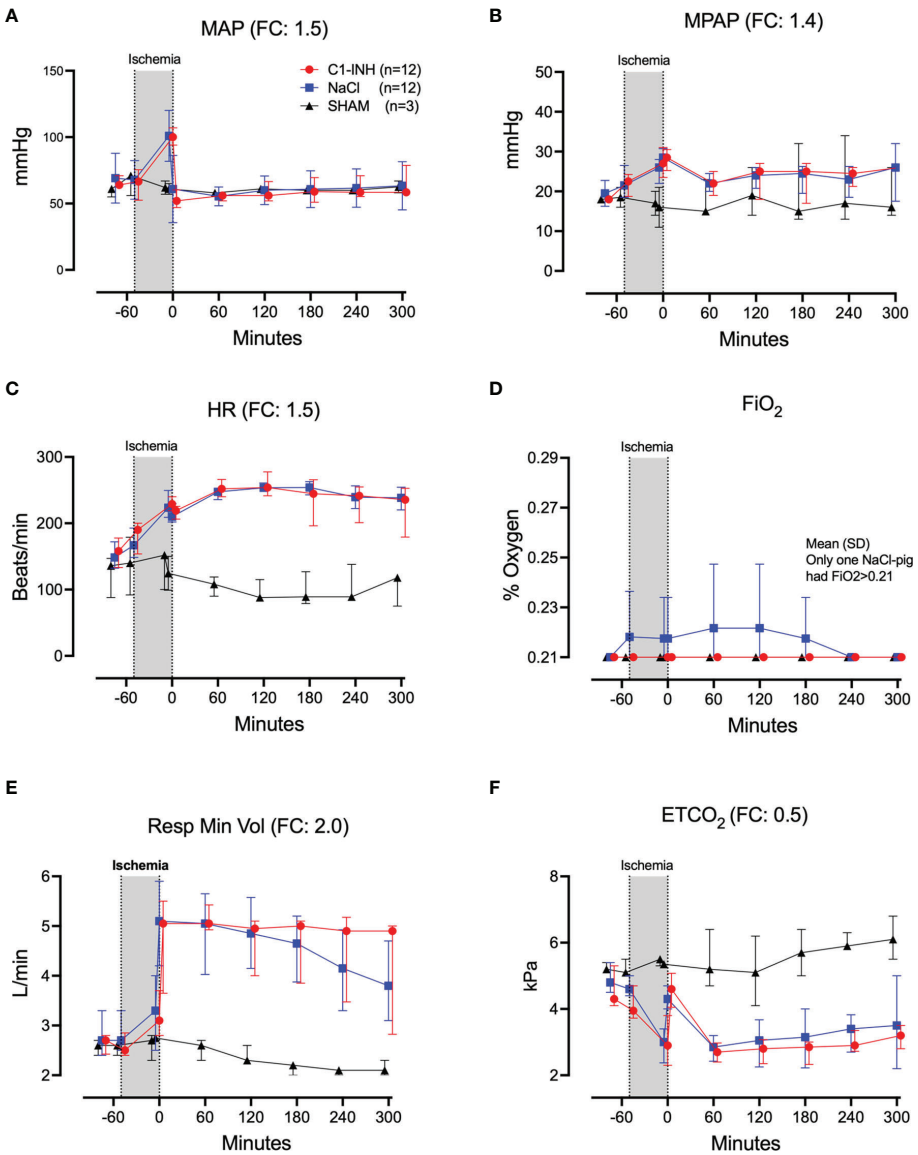

FIGURE 1 | Cardiorespiratory response I. **(A)** Mean arterial pressure (MAP), **(B)** mean pulmonary arterial pressure (MPAP), **(C)** heart rate (HR), **(D)** fraction of inspired oxygen (FiO_2), **(E)** respiratory minute volume (Resp Min Vol), and **(F)** end-tidal CO_2 ($ETCO_2$) were measured in 24 piglets undergoing 45 minutes of clamping of the thoracic aorta at the Th8 level. Upfront 12 piglets received human saline and 12 received C1-INH (250 IU/kg) intravenously, respectively. Three sham animals received thoracic opening without clamping. Reperfusion started at 0 minutes and lasted 5 hours. Longitudinal time data are expressed as median and interquartile range. "Ischemia" indicates the 45 minutes period of clamping. NaCl and C1-INH-groups were combined when there were no differences in the fold change (FC) calculation. FC is the change from before cross-clamp onset to maximum change.

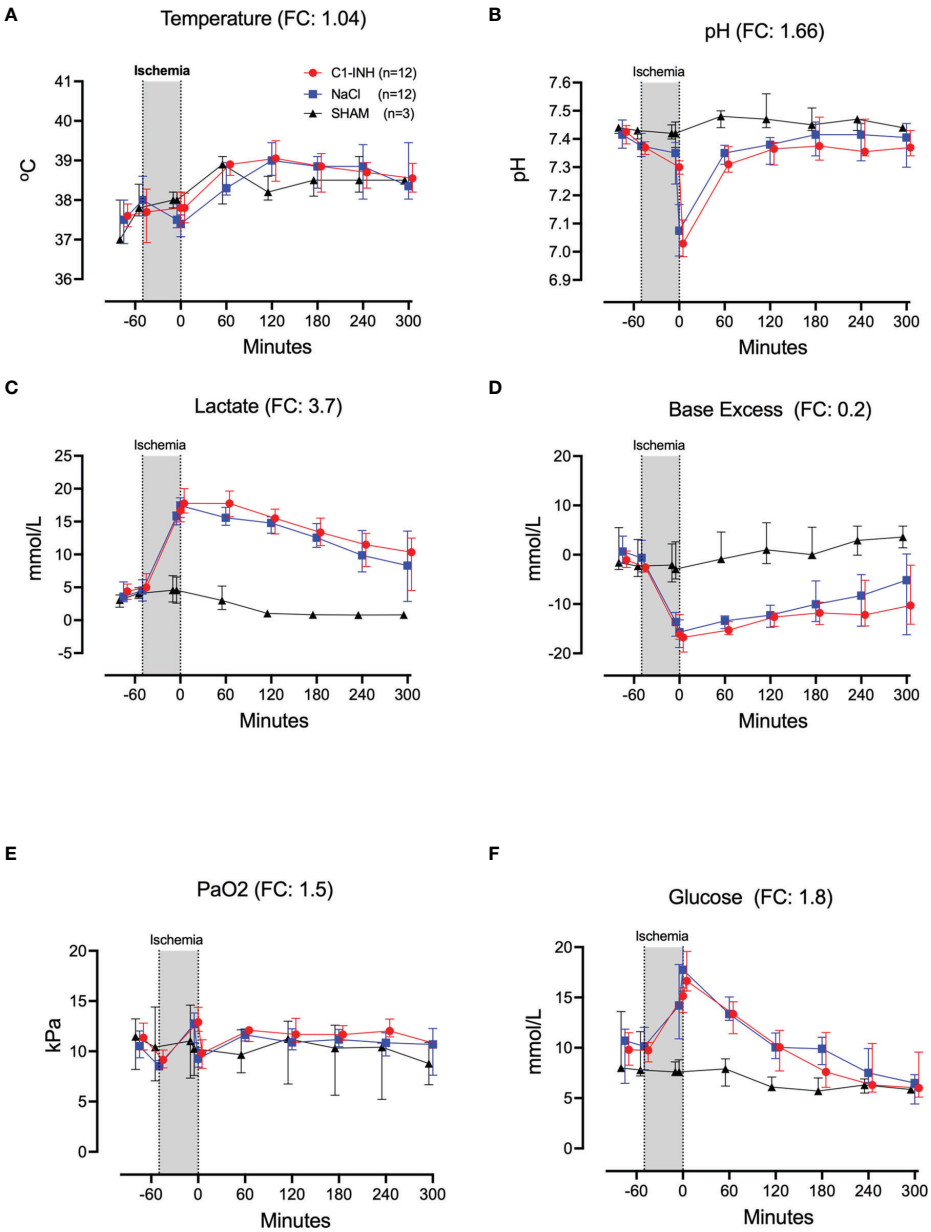

FIGURE 2 | Cardiorespiratory response II. **(A)** Temperature, **(B)** pH, **(C)** lactate, **(D)** Base Excess, **(E)** PaO2, and **(F)** Glucose were measured in 24 piglets undergoing 45 minutes of clamping of the thoracic aorta at the Th8 level. FC for Ph was calculated with absolute numbers of hydrogen ions. Upfront 12 piglets received human saline intravenously and 12 received C1-INH (250 IU/kg), respectively. Three sham animals received thoracic opening without clamping. Reperfusion started at 0 minutes and lasted 5 hours. Longitudinal time data are expressed as median and interquartile range. "Ischemia" indicates the 45 minutes period of clamping. NaCl and C1-INH-groups were combined when there were no differences in the fold change (FC) calculation. FC is the change from before cross-clamp onset to maximum change.

parenthesis. Taken together, hematocrit, white blood cells, and platelets had a mean and range fold change of 1.9 (1.2-2.7).

Inflammatory Markers

Eleven inflammatory markers were investigated. The absolute values and time course of complement activation measured by C3a, TCC and kallikrein activity are presented in **Figures 4A–C**. The fold change is in parenthesis. Taken together, the mean with range fold change of the inflammatory markers was 3.6 (2.5-4.4). The classical proinflammatory cytokines TNF, IL-1β, IL-6, and IL-8 are presented in **Figures 5A–D**. The fold change is in parenthesis. Except for IL-8, the mean and range fold change of these cytokines taken together was 4.3 (1.8-7.5). The regulatory cytokines and interferons, IL-10, IL-12p40, IFNα, and IFNγ are

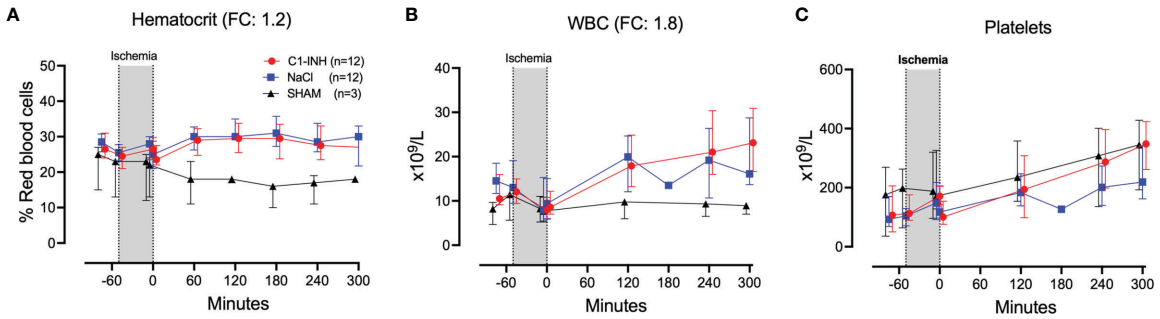

FIGURE 3 | Hematology. **(A)** Hematocrit, **(B)** white blood cells (WBC), and **(C)** platelets were measured in 24 piglets undergoing clamping of the thoracic aorta at the Th8 level. Upfront 12 piglets received human saline intravenously and 12 received C1-INH (250 IU/kg), respectively. Three sham animals received thoracic opening without clamping. Reperfusion started at 0 minutes and lasted 5 hours. Longitudinal time data are expressed as median and interquartile range. "Ischemia" indicates the 45 minutes period of clamping. NaCl and C1-INH-groups were combined when there were no differences in the fold change (FC) calculation. FC is the change from before cross-clamp onset to maximum change.

presented in **Figures 6A–D**. The fold change is in parenthesis. Taken together, the mean with range fold change was 3.7 (1.4-8.9).

Biochemical and Organ Damage Markers

Plasma proteins, kidney, and muscle markers were investigated. The absolute values and time course of total protein, albumin, creatinine, carbamide, myoglobulin, and CK are presented in **Figures 7A-F**. The fold change is in parenthesis. Taken together, the mean with range fold change was 2.5 (1.1-7.2). The following general and specific organ damage markers were measured: ALAT, ASAT, γGT, ALP, bilirubin, and lipase. The absolute values and time course are presented in **Figures 8A–F**. The fold change is in parenthesis. Taken together, the mean with range fold change was 3.2 (1.4-8.6).

Cytokines in Tissue Analysis

Eight organs were investigated for cytokines in postmortem biopsies. In seven organs there was no difference between the treated and untreated groups. In the colon, IL-4 and IFN-α showed a significant reduction in the C1-INH-treated group compared to the non-treated group (p=0.022 and 0.016, respectively) (**Figures 9A, B**).

DISCUSSION

The developed novel porcine model of ischemia-reperfusion injury after thoracic aorta cross-clamping produced robust results and proved to be a forceful and reliable model for the assessment of large scale IRI. The animals receiving thoracic aorta cross-clamping showed signs of severe large-scale ischemia with substantial lactic acidosis and, typical for porcine models, pulmonary hypertension. Keeping animals stable was challenging due to the severity of ischemia, but it was manageable. Despite severe hemodynamic changes, the animals in general responded in a uniform way. The effects of the IRI on

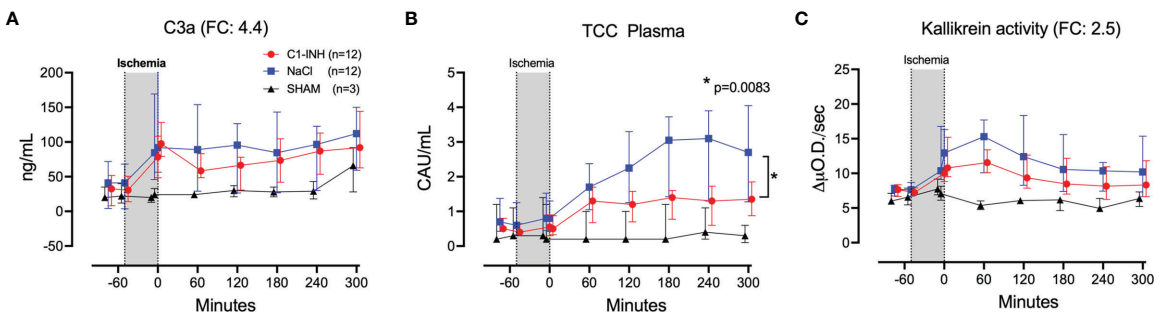

FIGURE 4 | Complement and kallikrein activation. **(A)** C3a, **(B)** terminal C5b-9 complement complex (TCC), and **(C)** kallikrein activity were measured in plasma of 24 piglets undergoing clamping of the thoracic aorta at the Th8 level. Upfront 12 piglets received human saline intravenously and 12 received C1-INH (250 IU/kg), respectively. Three sham animals received thoracic opening without clamping. Reperfusion started at 0 minutes and lasted 5 hours. Longitudinal time data are expressed as median and interquartile range. "Ischemia" indicates the 45 minutes period of clamping. NaCl and C1-INH-groups were combined when there were no differences in the fold change (FC) calculation. FC is the change from before cross-clamp onset to maximum change. * meaning: Probability of randomly seeing such a difference after C1-inhibitor treatment.

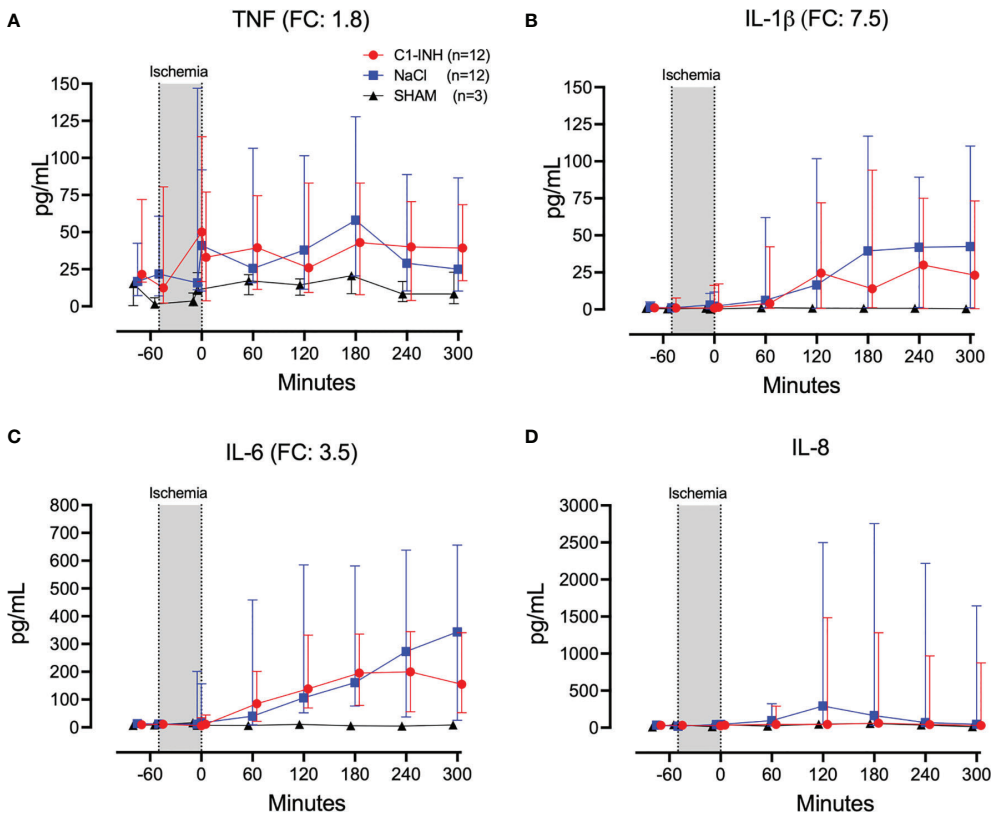

FIGURE 5 | Proinflammatory cytokines. **(A)** Tumour necrosis factor (TNF), **(B)** interleukin (IL)-1β, **(C)** IL-6, and **(D)** IL-8 were measured in plasma of 24 piglets undergoing clamping of the thoracic aorta at the Th8 level. Upfront 12 piglets received human saline intravenously and 12 received C1-INH (250 IU/kg), respectively. Three sham animals received thoracic opening without clamping. Reperfusion started at 0 minutes and lasted 5 hours. Longitudinal time data are expressed as median and interquartile range. "Ischemia" indicates the 45 minutes period of clamping. NaCl and C1-INH-groups were combined when there were no differences in the fold change (FC) calculation. FC is the change from before cross-clamp onset to maximum change.

blood and tissue markers also showed uniformity, supporting the value of the model and its potential for future testing of drugs aimed to restrict systemic IRI.

We did not see any significant effects of treatment with C1-INH on the damage from IRI in our model. Other animal studies have previously shown effect of C1-INH on IRI (19–22). These studies may not be fully comparable as few of them are in pigs, and most importantly do not involve a larger part of the body in a near systemic way. Our model is global and one of the most forceful models described, where all sub-diaphragmatic organs are virtually devoid of blood supply for 45 minutes. Therefore, the IRI in our model could be so severe that some inhibitors, including C1-INH, are inefficient.

Furthermore, blood in intercostal arteries and their branches could bypass the aortic clamping in some species. Also the aortic trifurcation in pigs could result in variable aortic retrograde flow compared to humans (23).Thus, interspecific differences could explain why human C1-INH did not improve outcome in our study. Finally, minor differences in the glycosylation of the C1-INH-protein could be of importance. An IRI study in mice found plasma-derived C1-INH, as we have used in the present study, inferior to recombinant human C1-INH (24). On the other hand, half-life of a recombinant human C1-Inhibitor produced in rabbits with a distinctive glycosylation (Ruconest, Pharming) had a shorter half-life in pigs than humans (14). However, the half-life of plasma-derived C1-inhibitor as we used in our study, administered both i.v. and subcutaneously to pigs had half-lives of more than 24 hours (25). Therefore C1-inhibitor levels are expected to remain high during our study period.

We have experienced in several *in vitro* studies that pharmacological inhibition of classical complement activation using C1-INH require extensively high doses, up to 20 times the physiological concentration (13). To the extent that the classical complement pathway plays an important role in IRI, this is in line with Ziccardi who 40 years ago found C1-INH to poorly inhibit when immunoglobulins were involved (26). Therefore, the dose of C1-INH per kg could have been insufficient to inhibit complement activation in severe IRI. Although some studies show effect of a lower (27) and some with higher doses up to 500 U/kg C1-INH (28), the reperfused organs were smaller, varying from skin flaps to kidneys and part of the heart. This makes a comparison of the studies difficult. In some models, researchers

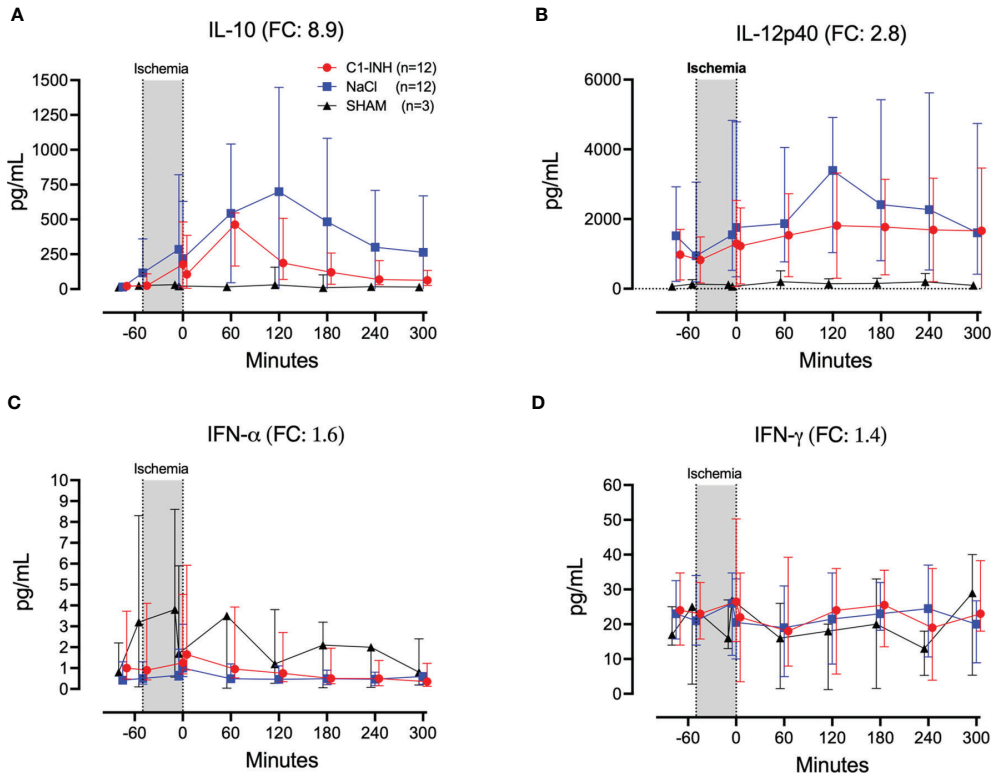

FIGURE 6 | Regulatory cytokines and interferons. **(A)** Interleukin (IL)-10, **(B)** IL-12p40, **(C)** interferon (IFN)-α, and **(D)** IFN-γ were measured in plasma of 24 piglets undergoing clamping of the thoracic aorta at the Th8 level. Upfront 12 piglets received human saline intravenously and 12 received C1-INH (250 IU/kg), respectively. Three sham animals received thoracic opening without clamping. Reperfusion started at 0 minutes and lasted 5 hours. Longitudinal time data are expressed as median and interquartile range. "Ischemia" indicates the 45 minutes period of clamping. NaCl and C1-INH-groups were combined when there were no differences in the fold change (FC) calculation. FC is the change from before cross-clamp onset to maximum change.

infuse C1-INH intra-arterially, directly into the targeted organs, increasing the dose pr kg tissue considerably. But even then, C1-INH can be inefficient. In a porcine infarction model Schreiber et al. found no effect of intracoronary infusion of 500 units C1-INH (29). However, the model by Schreiber et al. differed importantly from earlier models in that C1-INH was given after ischemia and during reperfusion. In our study C1-INH was infused prior to ischemia. Taken together, lack of effect in our global and forceful model due to too low C1-INH concentration cannot be totally excluded.

Supraphysiological doses of C1-INH have previously been reported to induce a procoagulant state which could have masked a positive effect by C1-INH (30). However, an *in vitro* study by our group found the opposite showing a dose-dependent anticoagulant effect of C1-INH in human whole blood (31). Our *in vivo* data from the present study also suggests a tendency towards an anticoagulatory effect, showing a non-significant tendency towards a reduction in TAT by C1-INH treatment. This could be explained by inactivation of FXII resulting in inhibition of the contact system by C1-INH, which could play a more significant role in IRI in this model. Cacci et al. suggested that thrombin inhibition by C1-INH might play a more important role in cases of severe inflammation as other major anticoagulatory systems are reduced in this state (32). Taken together, procoagulant effects of the C1-INH-infusion in the present study is an unlikely explanation for the observed lack of effect.

Publication biases could lead to overestimates of beneficial effects of C1-INH in IRI and underestimate negative results. According to Fanelli the proportion of positive results in the scientific literature in general increased to 85.9% in 2007 with a yearly increase of 6%, constant across most of the disciplines and countries (33). Therefore, our finding of limited effect of C1-INH in global ischemia is in our opinion an important contribution to the current literature. C1-INH is often placed on the list of complement inhibitors. Our study supports a general notion that C1-INH is not an efficient therapeutic, except for the reconstitution of patients with C1-INH deficiency. In our opinion, C1-INH should not be placed on the list of specific inhibitors for complement inhibition in the future, as we also have reviewed previously (34).

The present study raises the question which therapeutic targets could potentially reduce IRI.*in vivo* According to the danger model introduced by Matzinger, an inflammatory

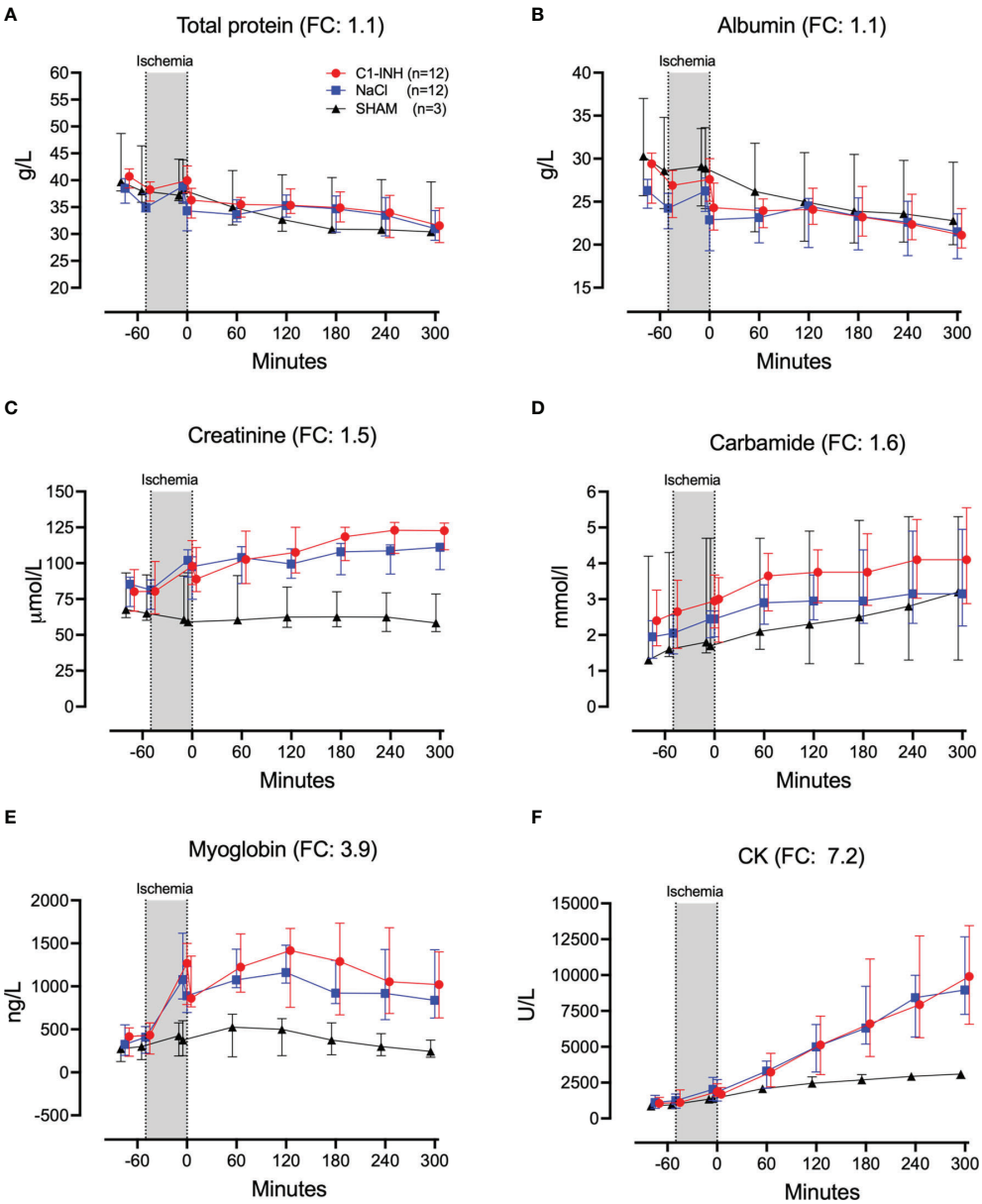

FIGURE 7 | Biochemical and organ damage markers I. **(A)** Total protein, **(B)** albumin, **(C)** creatinine, **(D)** carbamide, **(E)** myoglobin, and **(F)** creatine kinase (CK) were measured in serum of 24 piglet undergoing clamping of the thoracic aorta at the Th8 level. Upfront 12 piglets received human saline intravenously and 12 received C1-INH (250 IU/kg), respectively. Three sham animals received thoracic opening without clamping. Reperfusion started at 0 minutes and lasted 5 hours. Longitudinal time data are expressed as median and interquartile range. "Ischemia" indicates the 45 minutes period of clamping. NaCl and C1-INH-groups were combined when there were no differences in the fold change (FC) calculation. FC is the change from before cross-clamp onset to maximum change.

response involving innate immunity and complement can be expected in IRI (35). Therefore we anticipate a possible beneficial effect of combined inhibition of CD14 and complement C5 in IRI. In pediatric kidney transplant recipients, C5 inhibition with eculizumab prior to graft reperfusion was shown to improve early graft function, graft morphology and early graft survival indicating a reduction in IRI (36). There are also several other therapies available including highly specific complement inhibitors, as well as drugs targeting key upstream innate immune recognition molecules (34).

Our aim to establish a new porcine model for thoracic aortic cross-clamping using light weight piglets to allow for a minimal use of costly experimental therapeutics, while preserving translational value of the model is also a limitation of the study. The model is focused on the acute response and do not cover late complications.

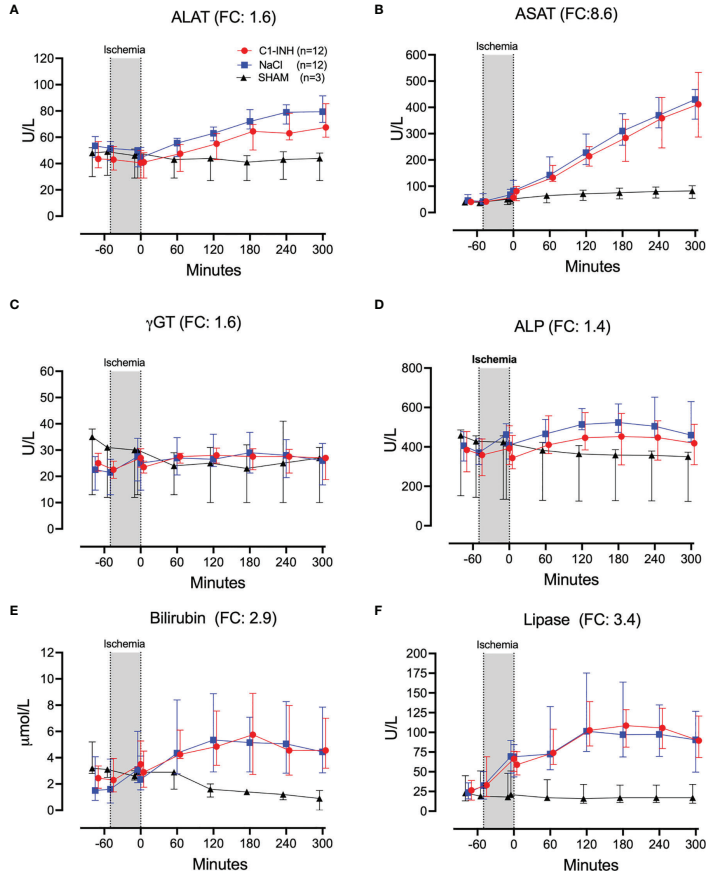

FIGURE 8 | Biochemical and organ damage markers II. **(A)** Alanine aminotransaminase (ALAT), **(B)** aspartate aminotransferase (ASAT), **(C)** gamma-glutamyl transferase (γGT), **(D)** alkaline phosphatase (ALP), **(E)** bilirubin, and **(F)** lipase were measured in serum of 24 piglets undergoing clamping of the thoracic aorta at the Th8 level. Upfront 12 piglets received human saline intravenously and 12 received C1-INH (250 IU/kg), respectively. Three sham animals received thoracic opening without clamping. Reperfusion started at 0 minutes and lasted 5 hours. Longitudinal time data are expressed as median and interquartile range. "Ischemia" indicates the 45 minutes period of clamping. NaCl and C1-INH-groups were combined when there were no differences in the fold change (FC) calculation. FC is the change from before cross-clamp onset to maximum change.

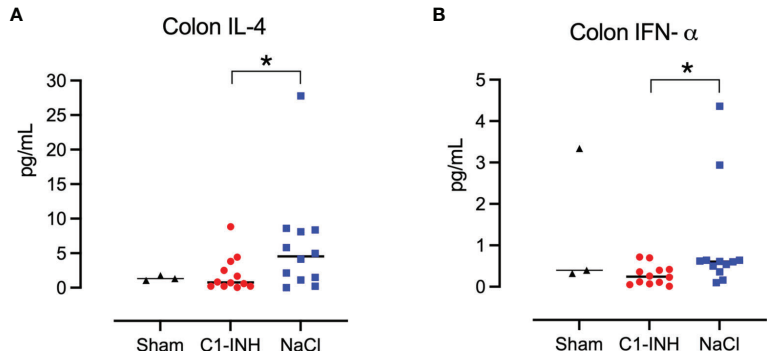

FIGURE 9 | Cytokines in tissue. Post mortem biopsies from seven organs were homogenised and analysed for cytokines by multiplex immunoassays. C1-INH-treatment had no effect on the tissue cytokines except for two cytokines in the colon tissue: **(A)** interleukin (IL)-4 and **(B)** interferon (IFN)-α. Asterisks mean p=0.022 and p=0.016, respectively.

CONCLUSION

This study describes a novel, forceful model of porcine IRI that did not respond significantly to adequate C1-INH treatment but should allow for future testing of other drugs that could attenuate global IRI.

DATA AVAILABILITY STATEMENT

The original contributions presented in the study are included in the article/supplementary files. Further inquiries can be directed to the corresponding author.

ETHICS STATEMENT

The animal study was reviewed and approved by Norwegian National Animal Research Authority (FOTS-ID-8197).

AUTHOR CONTRIBUTIONS

EN, YM, and TM designed the study. O-LB, JG, AD, HF, JL, KP, LR, RS and HJ planned and/or performed the experiments and analyses. EN and TM drafted the paper. EN and TM edited the draft. All authors critically revised the paper and approved the final draft.

REFERENCES

1. Pischke SE, Gustavsen A, Orrem HL, Egge KH, Courivaud F, Fontenelle H, et al. Complement Factor 5 Blockade Reduces Porcine Myocardial Infarction Size and Improves Immediate Cardiac Function. *Basic Res Cardiol* (2017) 112:1–14. doi: 10.1007/s00395-017-0610-9
2. Vento AE, Rämö OJ, Pesonen EJ, Heikkilä L, Nissinen E, Holopainen A, et al. The Effect of Nitecapone, a New Antioxidant, on Myocardial Function After Aortic Cross-Clamping in Experimental Heart Ischemia. *Int J Angiol Off Publ Int Coll Angiol Inc* (1999) 8:16–21. doi: 10.1007/BF01616836
3. Athanasiadis D, Kapelouzou A, Martikos G, Katsimpoulas M, Schizas D, Vasdekis SN, et al. Remote Ischemic Preconditioning May Attenuate Renal Ischemia-Reperfusion Injury in a Porcine Model of Supraceliac Aortic Cross-Clamping. *J Vasc Res* (2015) 52:161–71. doi: 10.1159/000439219
4. Hauser B, Gröger M, Ehrmann U, Albicini M, Brückner UB, Schelzig H, et al. The Parp-1 Inhibitor Ino-1001 Facilitates Hemodynamic Stabilization Without Affecting DNA Repair in Porcine Thoracic Aortic Cross-Clamping-Induced Ischemia/Reperfusion. *Shock Augusta Ga* (2006) 25:633–40. doi: 10.1097/01.shk.0000209561.61951.2e
5. Martikos G, Kapelouzou A, Peroulis M, Paspala A, Athanasiadis D, Machairas A, et al. Remote Ischemic Preconditioning Decreases the Magnitude of Hepatic Ischemia-Reperfusion Injury on a Swine Model of Supraceliac Aortic Cross-Clamping. *Ann Vasc Surg* (2018) 48:241–50. doi: 10.1016/j.avsg.2017.08.006
6. Abdelhafez MM, Shaw J, Sutter D, Schnider J, Banz Y, Jenni H, et al. Effect of C1-INH on Ischemia/Reperfusion Injury in a Porcine Limb *Ex Vivo* Perfusion Model. *Mol Immunol* (2017) 88:116–24. doi: 10.1016/j.molimm.2017.06.021
7. Maier C, Scheuerle A, Hauser B, Schelzig H, Szabó C, Radermacher P, et al. The Selective Poly(ADP)ribose-Polymerase 1 Inhibitor INO1001 Reduces Spinal Cord Injury During Porcine Aortic Cross-Clamping-Induced Ischemia/Reperfusion Injury. *Intensive Care Med* (2007) 33:845–50. doi: 10.1007/s00134-007-0585-3
8. Frick AE, Orlitová M, Vanstapel A, Ordies S, Claes S, Schols D, et al. A Novel Experimental Porcine Model to Assess the Impact of Differential Pulmonary Blood Flow on Ischemia-Reperfusion Injury After Unilateral Lung Transplantation. *Intensive Care Med Exp* (2021) 9:1–15. doi: 10.1186/s40635-021-00371-1
9. Fiane AE, Videm V, Lingaas PS, Heggelund L, Nielsen EW, Geiran OR, et al. Mechanism of Complement Activation and Its Role in the Inflammatory Response After Thoracoabdominal Aortic Aneurysm Repair. *Circulation* (2003) 108:849–56. doi: 10.1161/01.CIR.0000084550.16565.01
10. Duehrkop C, Rieben R. Ischemia/Reperfusion Injury: Effect of Simultaneous Inhibition of Plasma Cascade Systems Versus Specific Complement Inhibition. *Biochem Pharmacol.* (2014) 88(1):12–22. doi: 10.1016/j.bcp.2013.12.013
11. Seip KF, Evjenth B, Hovland A, Dybwik KG, Johansen HT, Fure H, et al. Bradykinin-Induced Shock Increase Exhaled Nitric Oxide, Complement Activation and Cytokine Production in Pigs. *J Cardiol Clin Res* (2016) 4:1–5.
12. Pirahanchi Y, Sharma S. Physiology, Bradykinin, in: *StatPearls* (2021). Treasure Island. FL: StatPearls Publishing. Available at: http://www.ncbi.nlm.nih.gov/books/NBK537187/ (Accessed August 2, 2021).
13. Nielsen EW, Waage C, Fure H, Brekke OL, Sfyroera G, Lambris JD, et al. Effect of Supraphysiologic Levels of C1-Inhibitor on the Classical, Lectin and Alternative Pathways of Complement. *Mol Immunol* (2007) 44:1819–26. doi: 10.1016/j.molimm.2006.10.003

14. Dalle Lucca JJ, Li Y, Simovic M, Pusateri AE, Falabella M, Dubick MA, et al. Effects of C1 Inhibitor on Tissue Damage in a Porcine Model of Controlled Hemorrhage. *Shock* (2012) 38(1):82–91. doi: 10.1097/SHK.0b013e31825a3522
15. Nilsson PH, Pettersen K, Oppermann M, Skjeflo EW, Fure H, Christiansen D, et al. Quantification of Porcine Complement Activation Fragment C3a by a Neoepitope-Based Enzyme-Linked Immunosorbent Assay. In: LT Roumenina, editor. *The Complement System: Innovative Diagnostic and Research Protocols. Methods in Molecular Biology*. New York, NY: Springer US (2021). p. 51–9. doi: 10.1007/978-1-0716-1016-9_5
16. Jansen JH, Høgåsen K, Mollnes TE. Extensive Complement Activation in Hereditary Porcine Membranoproliferative Glomerulonephritis Type II (Porcine Dense Deposit Disease). *Am J Pathol* (1993) 143:1356–65.
17. Gallimore MJ, Friberger P. Simple Chromogenic Peptide Substrate Assays for Determining Prekallikrein, Kallikrein Inhibition and Kallikrein "Like" Activity in Human Plasma. *ThrombRes* (1982) 25:293–8. doi: 10.1016/0049-3848(82)90248-1
18. Thorgersen EB, Pischke SE, Barratt-Due A, Fure H, Lindstad JK, Pharo A, et al. Systemic CD14-Inhibition Attenuates Organ Inflammation in Porcine Escherichia Coli-Sepsis. *Infect Immun* (2013) 81:3173–81. doi: 10.1128/IAI.00390-13
19. Panagiotou A, Trendelenburg M, Osthoff M. The Lectin Pathway of Complement in Myocardial Ischemia/Reperfusion Injury-Review of Its Significance and the Potential Impact of Therapeutic Interference by C1 Esterase Inhibitor. *Front Immunol* (2018) 9:1151. doi: 10.3389/fimmu.2018.01151
20. Fries CA, Villamaria CY, Spencer JR, Rasmussen TE, Davis MR. C1 Esterase Inhibitor Ameliorates Ischemia Reperfusion Injury in a Swine Musculocutaneous Flap Model. *Microsurgery* (2017) 37:142–7. doi: 10.1002/micr.30053
21. Simone S, Rascio F, Castellano G, Divella C, Chieti A, Ditonno P, et al. Complement-Dependent NADPH Oxidase Enzyme Activation in Renal Ischemia/Reperfusion Injury. *Free Radic Biol Med* (2014) 74:263–73. doi: 10.1016/j.freeradbiomed.2014.07.003
22. Castellano G, Melchiorre R, Loverre A, Ditonno P, Montinaro V, Rossini M, et al. Therapeutic Targeting of Classical and Lectin Pathways of Complement Protects From Ischemia-Reperfusion-Induced Renal Damage. *Am J Pathol* (2010) 176(4):1648–59. doi: 10.1016/j.molimm.2009.05.262
23. Papakostas JC, Matsagas MI, Toumpoulis IK, Malamou-Mitsi VD, Pappa LS, Gkrepi C, et al. Evolution of Spinal Cord Injury in a Porcine Model of Prolonged Aortic Occlusion. *J Surg Res* (2006) 133:159–66. doi: 10.1016/j.jss.2005.10.007
24. Mercurio D, Piotti A, Valente A, Oggioni M, Ponstein Y, Van Amersfoort E, et al. Plasma-Derived and Recombinant C1 Esterase Inhibitor: Binding Profiles and Neuroprotective Properties in Brain Ischemia/Reperfusion Injury. *Brain Behav Immun* (2021) 93:299–311. doi: 10.1016/j.bbi.2021.01.002
25. Jiang H, Zhang HM, Frank MM. Subcutaneous Infusion of Human C1 Inhibitor in Swine. *Clin Immunol* (2010) 136:323–8. doi: 10.1016/j.clim.2010.05.001
26. Ziccardi RJ. A New Role for C-1-Inhibitor in Homeostasis: Control of Activation of the First Component of Human Complement. *J Immunol* (1982) 128:2505–8.
27. Horstick G, Berg O, Heimann A, Gotze O, Loos M, Hafner G, et al. Application of C1-Esterase Inhibitor During Reperfusion of Ischemic Myocardium: Dose-Related Beneficial Versus Detrimental Effects. *Circulation* (2001) 104:3125–31. doi: 10.1161/hc5001.100835
28. Delpech P-O, Thuillier R, SaintYves T, Danion J, Le Pape S, van Amersfoort ES, et al. Inhibition of Complement Improves Graft Outcome in a Pig Model of Kidney Autotransplantation. *J Transl Med* (2016) 14:1–13. doi: 10.1186/s12967-016-1013-7
29. Schreiber C, Heimisch W, Schad H, Brkic A, Badiu C, Lange R, et al. C1-INH and its Effect on Infarct Size and Ventricular Function in an Acute Pig Model of Infarction, Cardiopulmonary Bypass, and Reperfusion. *ThoracCardiovascSurg* (2006) 54:227–32. doi: 10.1055/s-2006-923947
30. Arzneimittelkommission der Deutschen Aerzteschaft. Schwerwiegende Thrombenbildung Nach Berinert HS [Serious Thrombosis After Berinert Hs]. *Deutches Aerzteblatt* (2000) 97:B–864.
31. Landsem A, Fure H, Mollnes TE, Nielsen EW, Brekke OL. C1-Inhibitor Efficiently Delays Clot Development in Normal Human Whole Blood and Inhibits Escherichia Coli-Induced Coagulation Measured by Thromboelastometry. *Thromb Res* (2016) 143:63–70. doi: 10.1016/j.thromres.2016.04.024
32. Caccia S, Castelli R, Maiocchi D, Bergamaschini L, Cugno M. Interaction of C1 Inhibitor With Thrombin on the Endothelial Surface. *Blood Coagul Fibrinol Int J Haemost Thromb* (2011) 22:571–5. doi: 10.1097/MBC.0b013e3283494ba7
33. Fanelli D. Negative Results are Disappearing From Most Disciplines and Countries. *Scientometrics* (2012) 90:891–904. doi: 10.1007/s11192-011-0494-7
34. Garred P, Tenner AJ, Mollnes TE. Therapeutic Targeting of the Complement System: From Rare Diseases to Pandemics. *Pharmacol Rev* (2021) 73:792–827. doi: 10.1124/pharmrev.120.000072
35. Matzinger P. The Danger Model: A Renewed Sense of Self. *Science* (2002) 296:301–5. doi: 10.1126/science.1071059
36. Kaabak M, Babenko N, Shapiro R, Zokoyev A, Dymova O, Kim E. A Prospective Randomized, Controlled Trial of Eculizumab to Prevent Ischemia-Reperfusion Injury in Pediatric Kidney Transplantation. *Pediatr Transplant* (2018) 22:1–8. doi: 10.1111/petr.13129

Conflict of Interest: The authors declare that the research was conducted in the absence of any commercial or financial relationships that could be construed as a potential conflict of interest.

Publisher's Note: All claims expressed in this article are solely those of the authors and do not necessarily represent those of their affiliated organizations, or those of the publisher, the editors and the reviewers. Any product that may be evaluated in this article, or claim that may be made by its manufacturer, is not guaranteed or endorsed by the publisher.

frontiers | Frontiers in Immunology

ORIGINAL RESEARCH
published: 06 April 2022
doi: 10.3389/fimmu.2022.886421

Inhibition of Macrophage Migration Inhibitory Factor Activity Attenuates Haemorrhagic Shock-Induced Multiple Organ Dysfunction in Rats

Nikita M. Patel[1], Noriaki Yamada[1,2], Filipe R. M. B. Oliveira[3], Lara Stiehler[1,4], Elisabeth Zechendorf[4], Daniel Hinkelmann[4], Sandra Kraemer[4], Christian Stoppe[5], Massimo Collino[6], Debora Collotta[6], Gustavo Ferreira Alves[6], Hanna Pillmann Ramos[3], Regina Sordi[3], Ingo Marzi[7], Borna Relja[7,8], Gernot Marx[4], Lukas Martin[1,4*†] and Christoph Thiemermann[1†]*

[1] William Harvey Research Institute, Barts and The London School of Medicine and Dentistry, Queen Mary University of London, London, United Kingdom, [2] Gifu University Graduate School of Medicine, Department of Emergency and Disaster Medicine Gifu University Hospital Advanced Critical Care Center, Gifu, Japan, [3] Department of Pharmacology, Universidade Federal de Santa Catarina, Florianópolis, Brazil, [4] Department of Intensive Care and Intermediate Care, University Hospital RWTH Aachen, Aachen, Germany, [5] Department of Anesthesiology & Intensive Care Medicine, University Hospital Würzburg, Würzburg, Germany, [6] Department of Neurosciences "Rita Levi Montalcini", University of Turin, Turin, Italy, [7] Department of Trauma, Hand and Reconstructive Surgery, University Hospital Frankfurt, Goethe University, Frankfurt, Germany, [8] Experimental Radiology, Department of Radiology and Nuclear Medicine, Otto-von-Guericke University, Magdeburg, Germany

OPEN ACCESS

Edited by:
Tom E. Mollnes, University of Oslo, Norway

Reviewed by:
Roman Pfeifer, University Hospital Zürich, Switzerland
Philipp Mommsen, Hannover Medical School, Germany

***Correspondence:**
Lukas Martin
lmartin@ukaachen.de
Nikita M. Patel
n.m.patel@qmul.ac.uk

†These authors have contributed equally to this work and share senior authorship

Specialty section:
This article was submitted to Inflammation, a section of the journal Frontiers in Immunology

Received: *28 February 2022*
Accepted: *14 March 2022*
Published: *06 April 2022*

Citation:
Patel NM, Yamada N, Oliveira FRMB, Stiehler L, Zechendorf E, Hinkelmann D, Kraemer S, Stoppe C, Collino M, Collotta D, Alves GF, Ramos HP, Sordi R, Marzi I, Relja B, Marx G, Martin L and Thiemermann C (2022) Inhibition of Macrophage Migration Inhibitory Factor Activity Attenuates Haemorrhagic Shock-Induced Multiple Organ Dysfunction in Rats. Front. Immunol. 13:886421. doi: 10.3389/fimmu.2022.886421

Objective: The aim of this study was to investigate (a) macrophage migration inhibitory factor (MIF) levels in polytrauma patients and rats after haemorrhagic shock (HS), (b) the potential of the MIF inhibitor ISO-1 to reduce multiple organ dysfunction syndrome (MODS) in acute (short-term and long-term follow-up) HS rat models and (c) whether treatment with ISO-1 attenuates NF-κB and NLRP3 activation in HS.

Background: The MODS caused by an excessive systemic inflammatory response following trauma is associated with a high morbidity and mortality. MIF is a pleiotropic cytokine which can modulate the inflammatory response, however, its role in trauma is unknown.

Methods: The MIF levels in plasma of polytrauma patients and serum of rats with HS were measured by ELISA. Acute HS rat models were performed to determine the influence of ISO-1 on MODS. The activation of NF-κB and NLRP3 pathways were analysed by western blot in the kidney and liver.

Results: We demonstrated that (a) MIF levels are increased in polytrauma patients on arrival to the emergency room and in rats after HS, (b) HS caused organ injury and/or dysfunction and hypotension (post-resuscitation) in rats, while (c) treatment of HS-rats with ISO-1 attenuated the organ injury and dysfunction in acute HS models and (d) reduced the activation of NF-κB and NLRP3 pathways in the kidney and liver.

Conclusion: Our results point to a role of MIF in the pathophysiology of trauma-induced organ injury and dysfunction and indicate that MIF inhibitors may be used as a potential therapeutic approach for MODS after trauma and/or haemorrhage.

Keywords: haemorrhagic shock, ischaemia-reperfusion, ISO-1, macrophage migration inhibitory factor, multiple organ dysfunction syndrome, trauma

INTRODUCTION

Trauma is one of the leading causes of death and disability in young people aged under 44 and exceeds the number of deaths caused by HIV, tuberculosis and malaria combined (1). Globally, injuries are responsible for over 9% of all mortalities and annually there are approximately 6 million trauma-related deaths (1, 2). Trauma-associated haemorrhage and haemorrhagic shock (HS) account for nearly 40% of all trauma deaths and is a key driver of multiple organ dysfunction (MODS) (3–7).

Whilst the number of early post-injury deaths have decreased in recent years secondary to improved care in the pre-hospital setting, there has been an accompanying increase in deaths attributed to MODS during the late post-injury phase (4, 8, 9). The mechanisms contributing to MODS include (a) an excessive systemic inflammatory response secondary to the release of damage-associated molecular patterns (DAMPs) from extensive tissue damage and (b) ischaemia-reperfusion (I/R) injury (8, 10).

DAMPs activate the immune system, leading to the release of cytokines which can cause organ injury and dysfunction (11). Moreover, raised cytokine levels are linked to worse prognosis in critically ill patients (12–14). One such cytokine is macrophage migration inhibitory factor (MIF) which is pro-inflammatory and possesses chemokine-like properties by promoting the expression or production of several pro-inflammatory mediators including IL-1β, IL-2, IL-6, IL-8, IL-12, IFN-γ, nitric oxide, TNF-α, cyclooxygenase 2 and matrix metalloproteinases (15–23). Consequently, further leukocytes are directed to the site of injury and/or infection (24–26). MIF also has a role in counter-regulating the immunosuppressive and anti-inflammatory effects of glucocorticoids (27, 28).

It has previously been shown that MIF concentration in the plasma/serum of trauma patients was higher than that of healthy controls (29, 30) and serum MIF levels in blunt trauma patients with MODS were significantly greater than patients without MODS (31, 32). Currently, there are no specific pharmacological treatments which prevent the onset of MODS associated with HS. Therefore, the aim of this study was to investigate the effects of blocking MIF activity with the inhibitor ISO-1 [(S,R)-3-(4-hydroxyphenyl)-4,5-dihydro-5-isoxazole acetic acid methyl ester] on the HS-induced MODS in rats.

METHODS

MIF Gene Expression in Human Whole Blood

Original data was obtained under Gene Expression Omnibus (GEO) accession GSE36809, published by Xiao and colleagues (33). RNA was extracted from whole blood leukocytes of severe blunt trauma patients (n = 167) over the course of 28 days and healthy controls (n = 37) and hybridised onto an HU133 Plus 2.0 GeneChip (Affymetrix) according to the manufacturer's recommendations. The dataset was reanalysed for MIF gene expression.

Ethical Statement

Blood samples of 208 patients were collected after written informed consent was obtained from either the patient or a nominated legally authorised representative. Samples were collected between 2010-2014 from University Hospital Frankfurt of Goethe-University and approved by an institutional ethics committee (Number 312/10) in accordance with the declaration of Helsinki and following STROBE-guidelines (34).

For the short-term follow-up acute HS model, all animal procedures were approved by the Animal Welfare Ethics Review Board of Queen Mary University of London and by the Home Office (Licence number PC5F29685). For the long-term follow-up acute HS model, all animal procedures were approved by the Universidade Federal de Santa Catarina Institutional Committee for Animal Use in Research (Licence number 7396250219) in accordance with the Brazilian Government Guidelines for Animal Use in Research. All *in vivo* experiments are reported in accordance to ARRIVE guidelines.

Patient Study Population and Sample Collection

Blood samples from patients (18-80 years) with blunt or penetrating trauma and ISS ≥ 16 were obtained on Day 0 (arrival to the emergency room); Day 2; Day 5 and Day 7. Exclusion criteria were patient death in the emergency room or within 24 h of hospital admission, known pre-existing immunological disorders, treatment with immunosuppressive or anti-coagulant medication, burns, concomitant acute myocardial infarction and thromboembolic events. Blood samples were collected in pre-chilled ethylenediaminetetraacetic acid tubes (BD vacutainer, Becton Dickinson Diagnostics, Aalst, Belgium) and kept on ice. Blood was centrifuged at 2,000 g for 15 min at 4°C to separate serum and stored at −80°C for further analysis.

Experimental Design

Male Wistar rats (for short-term follow-up acute model: Charles River Laboratories Ltd., UK; for long-term follow-up acute model: Universidade Federal de Santa Catarina, Brazil) weighing 250-350 g were kept under standard laboratory

conditions and received a chow diet and water *ad libitum*. ISO-1 (25 mg/kg; Tocris, UK) was diluted in 5% DMSO + 95% Ringer's Lactate (vehicle) and rats were treated (i.v. in short-term follow-up and i.p. in long-term follow-up) upon resuscitation.

Acute Haemorrhagic Shock Model (Short-Term Follow-Up)

The pressure-controlled short-term follow-up acute HS model was performed as previously described (35–38). Briefly, forty rats were anaesthetised with sodium thiopentone (120 mg/kg i.p. initially and 10 mg/kg i.v. for maintenance as needed and randomised into four groups (n = 10 per group): Sham + vehicle; Sham + ISO-1 (25 mg/kg), HS + vehicle; HS + ISO-1 (25 mg/kg) using the GraphPad online random number generator. The investigator was blinded to the intervention (vehicle or ISO-1) and treatment group allocation was revealed following data analysis. Analgesia was not administered as the rats remain anaesthetised for the duration of the experiment (non-recovery procedure) and as such do not expect the animals to feel pain. Adequacy of anaesthesia was ascertained throughout the experiment by testing the pedal reflex. No animals died during the course of the study, thus all data have been included. Blood was withdrawn to achieve a fall in mean arterial pressure (MAP) to 35 ± 5 mmHg, which was maintained for 90 min. At 90 min after initiation of haemorrhage (or when 25% of the shed blood had to be reinjected to sustain MAP at 35 ± 5 mmHg), resuscitation was performed with the shed blood over a period of 5 min. At 4 h post-resuscitation, blood was collected for the measurement of biomarkers of organ injury/dysfunction (MRC Harwell Institute, Oxfordshire, UK) and organs for *ex vivo* analysis. Sham-operated rats were used as control and underwent identical surgical procedures, but without haemorrhage or resuscitation. Detailed description of the short-term follow-up model can be found in the supplemental (**Supplemental Figure 1A**).

Acute Haemorrhagic Shock Model (Long-Term Follow-Up)

The pressure-controlled long-term follow-up acute HS model was performed as previously described (36). Briefly, thirty rats were administered analgesia with tramadol (10 mg/kg i.p.) 15 min prior to anaesthesia induction with ketamine and xylazine (100 mg/kg and 10 mg/kg i.m. respectively) and randomised into three groups: Sham + vehicle (n = 6); HS + vehicle (n = 12); HS + ISO-1 (25 mg/kg; n = 12) using the GraphPad online random number generator. The investigator was blinded to the intervention (vehicle or ISO-1) and treatment group allocation was revealed following data analysis. Adequacy of anaesthesia throughout the experiment was ascertained by testing the pedal reflex. No animals died during the course of the study, thus all data have been included. Blood was withdrawn to achieve a fall in MAP to 40 ± 2 mmHg, which was maintained for 90 min. At 90 min after initiation of haemorrhage (or when 25% of the shed blood had to be reinjected to sustain MAP at 40 ± 2 mmHg), resuscitation was performed with the shed blood over a period of 5 min plus 1.5 mL/kg Ringer's lactate. At 24 h post-resuscitation, blood was collected for the measurement of organ injury/dysfunction parameters (Hospital Universitário Professor Polydoro Ernani de São Thiago, Brazil) and organs for *ex vivo* analysis. Sham-operated rats were used as control and underwent identical surgical procedures, but without haemorrhage or resuscitation. Detailed description of the long-term follow-up model can be found in the supplemental (**Supplemental Figure 1B**).

MIF ELISA

Human MIF plasma levels (R&D SYSTEMS Human MIF DuoSet) and rat MIF serum levels from the acute HS (short-term follow-up) model (Cusabio Biotech, Wuhan, China) were detected by commercially available ELISAs according to the manufacturer protocol. Detection occurred at 450 nm and 540 nm using iMark® microplate absorbance reader (BioRad). Further details can be found in the **Supplemental Table 1**.

Western Blot Analysis

Semi-quantitative immunoblot analysis was carried out in kidney and liver samples as previously described (36). Detailed description of the method can be found in the supplemental.

CD68 Immunohistochemical Staining

Lung tissue sections were deparaffinised and hydrated and stained for CD68. Detailed description of the method can be found in the supplemental.

Quantification of Myeloperoxidase Activity

Determination of myeloperoxidase activity in lung and liver tissue samples was performed as previously described (36). Detailed description of the method can be found in the supplemental.

Statistical Analysis

All figures are expressed as median with range of *n* observations, where *n* represents the number of animals/experiments/subjects studied. Measurements obtained from the vehicle and ISO-1 treated animal groups were analysed by one-way ANOVA followed by a Bonferroni's *post-hoc* test on GraphPad Prism 8.0 (GraphPad Software, Inc., La Jolla, CA, USA). The distribution of the data was verified by Shapiro-Wilk normality test, and the homogeneity of variances by Bartlett test. When necessary, values were transformed into logarithmic values to achieve normality and homogeneity of variances. To investigate the relationship between the variables, Pearson correlation *r* was performed. $P<0.05$ was considered statistically significant.

RESULTS

MIF Gene Expression Is Elevated in Trauma Patients

Xiao and colleagues (33) compared genome-wide expression in leukocytes from trauma patients against matched healthy controls. We reanalysed this dataset for MIF expression. When compared to healthy controls, MIF expression was significantly

elevated at all time points except Day 1 ($p<0.05$; **Supplemental Figure 2**). An initial increase was noted at 12 h followed by a later peak at Day 7. MIF expression remained elevated at Day 28, the latest timepoint measured.

MIF Gene Expression Does Not Differ Between Uncomplicated and Complicated Recovery Patient Groups

Xiao and colleagues (33) also stratified their trauma patient cohort into uncomplicated (recovery in <5 days) and complicated (recovery after 14 days, no recovery by Day 28 or death) to further identify genotypic differences. We reanalysed this dataset for MIF expression using this stratification. When comparing uncomplicated and complicated patients, there were no significant differences at any of the timepoints measured ($p>0.05$; **Supplemental Figure 3**).

Plasma MIF Levels Are Elevated in Polytrauma Patients and Associated With Longer Stay in ICU and Hospital

To investigate the role of MIF in trauma, 208 patients were included in the study. Detailed patient characteristics can be found in **Table 1**. Polytrauma patients showed significantly increased MIF levels on Day 0 (on arrival to the emergency room, 12398 ± 1262 pg/mL) compared to Day 2 (2866.9 ± 377.8 pg/mL), Day 5 (2335.7 ± 203.4 pg/mL) and Day 7 (2114.6 ± 165.3 pg/mL) (all $p<0.001$; **Figure 1A**). Furthermore, we found a weak positive correlation between MIF levels on Day 0 and both hospital ($r = 0.22$, $n = 199$, $p<0.01$; **Figure 1C**) and ICU ($r = 0.26$, $n = 198$, $p<0.01$; **Figure 1D**) stays. MIF levels on Day 0 were not correlated with baseline characteristics such as age ($r = -0.05$, $n = 200$, $p = 0.49$) and sex ($r = -0.07$, $n = 200$, $p = 0.3$) and only weakly correlated with ISS score ($r = 0.15$, $n = 177$, $p<0.05$) (**Figure 1B**).

MIF Levels Are Elevated in Serum of Rats After Induction of Acute HS (Short-Term Follow-Up)

Having found elevated plasma MIF levels in patients with trauma-haemorrhage, we investigated whether haemorrhage alone (in the absence of physical trauma) is sufficient to drive increases in MIF. To address this question, we used a model of severe haemorrhage followed by resuscitation in the rat. When compared to sham-operated rats, haemorrhage followed by resuscitation resulted in a significant increase in MIF levels ($p<0.001$; **Figure 2A**). Although ISO-1 has been reported to inhibit the effects, rather than the formation, of MIF *in vivo*, we report here that treatment of HS rats with ISO-1 resulted in a significantly lower MIF level when compared to HS rats treated with vehicle ($p<0.05$; **Figure 2A**). Administration of ISO-1 to sham-operated rats had no effect on MIF levels ($p>0.05$; **Figure 2A**).

TABLE 1 | Trauma patient clinical characteristics.

	Trauma (n = 208)
Age (year) (IQR)	47.0 (31-60)
Male sex (%)	156 (75.0)
SOFA (points) (IQR)	5.00 (1.0-7.0)
APACHE II (points) (IQR)	16.0 (6.0-22.0)
ISS score (points) (IQR)	23.0 (17.0-32.0)
LOS ICU (days) (IQR)	8.0 (4.0-15.0)
LOS In-hospital (days) (IQR)	19.0 (13.0-29.0)
MIF D0 [pg/ml] (IQR)	6839 (3713-14205)
MIF D2 [pg/ml] (IQR)	1598.0 (1080.0-2555.5)
MIF D5 [pg/ml] (IQR)	1137.0 (650.0-1960.0)
MIF D7 [pg/ml] (IQR)	1331.9 (814.2-2158.5)

Data are presented as n (%) or median (IQR). D0/2/5/7: Day 0/2/5/7; ICU, intensive care unit; IQR, interquartile ranges (Q1-Q3); LOS, length of stay.

Treatment With ISO-1 Improves HS-Induced Circulatory Failure in Acute HS (Short-Term Follow-Up)

To investigate the effects of ISO-1 on circulatory failure, MAP was measured from the completion of surgery to the termination of the experiment. Baseline MAP values were similar amongst all four groups. Rats subjected to HS demonstrated a decline in MAP which was ameliorated by resuscitation, but still remained lower than that of sham-operated rats during resuscitation (at the equivalent time points, **Figure 2B**). When compared to sham-operated rats, HS-rats treated with vehicle exhibited a more pronounced decrease in MAP over time post-resuscitation. In contrast, MAP of HS-rats treated with ISO-1 was significantly higher than HS-rats treated with vehicle 4 h post-resuscitation ($p<0.001$; **Figure 2B**).

Treatment With ISO-1 Attenuates HS-Induced Organ Damage in Acute HS (Short-Term Follow-Up)

Having demonstrated that treatment with ISO-1 improves HS-induced circulatory failure, we next explored whether ISO-1 attenuates MODS associated with HS in rats. When compared to sham-operated rats, rats subjected to HS and treated with vehicle displayed increases in serum urea ($p<0.001$; **Figure 3A**) and creatinine ($p<0.001$; **Figure 3B**) and a decrease in creatinine clearance ($p<0.001$; **Figure 3C**) indicating the development of renal dysfunction. When compared to sham-operated rats, vehicle treated HS-rats exhibited significant increases in both ALT ($p<0.001$; **Figure 3D**) and AST ($p<0.001$; **Figure 3E**) indicating the development of hepatic injury, while the increases in amylase ($p<0.001$; **Figure 3F**) and CK ($p<0.001$; **Figure 3G**) denote pancreatic and neuromuscular injury, respectively. The significant increase in LDH ($p<0.001$; **Figure 3H**) in HS-rats treated with vehicle confirmed tissue injury whilst the increase in lactate ($p<0.001$; **Figure 3I**) indicated decreased transport of oxygen to the tissues developing from the state of hypoperfusion. Treatment of HS-rats with ISO-1 significantly attenuated the renal dysfunction, hepatic injury, pancreatic injury, neuromuscular injury and general tissue damage caused by HS (all $p<0.05$; **Figures 3A–I**). As HS causes macrophage infiltration into the lungs, we measured $CD68^+$ positive cells as a marker for macrophage invasion. When compared to sham-operated rats (21.75 ± 2.29 per field), HS-rats treated with vehicle displayed a significant increase in macrophage count (47.33 ± 8.75 per field, $p<0.05$). Treatment with ISO-1 in HS-rats did not result in a significant decrease in macrophage count (35.90 ± 4.30 per field; **Supplemental Figure 4**).

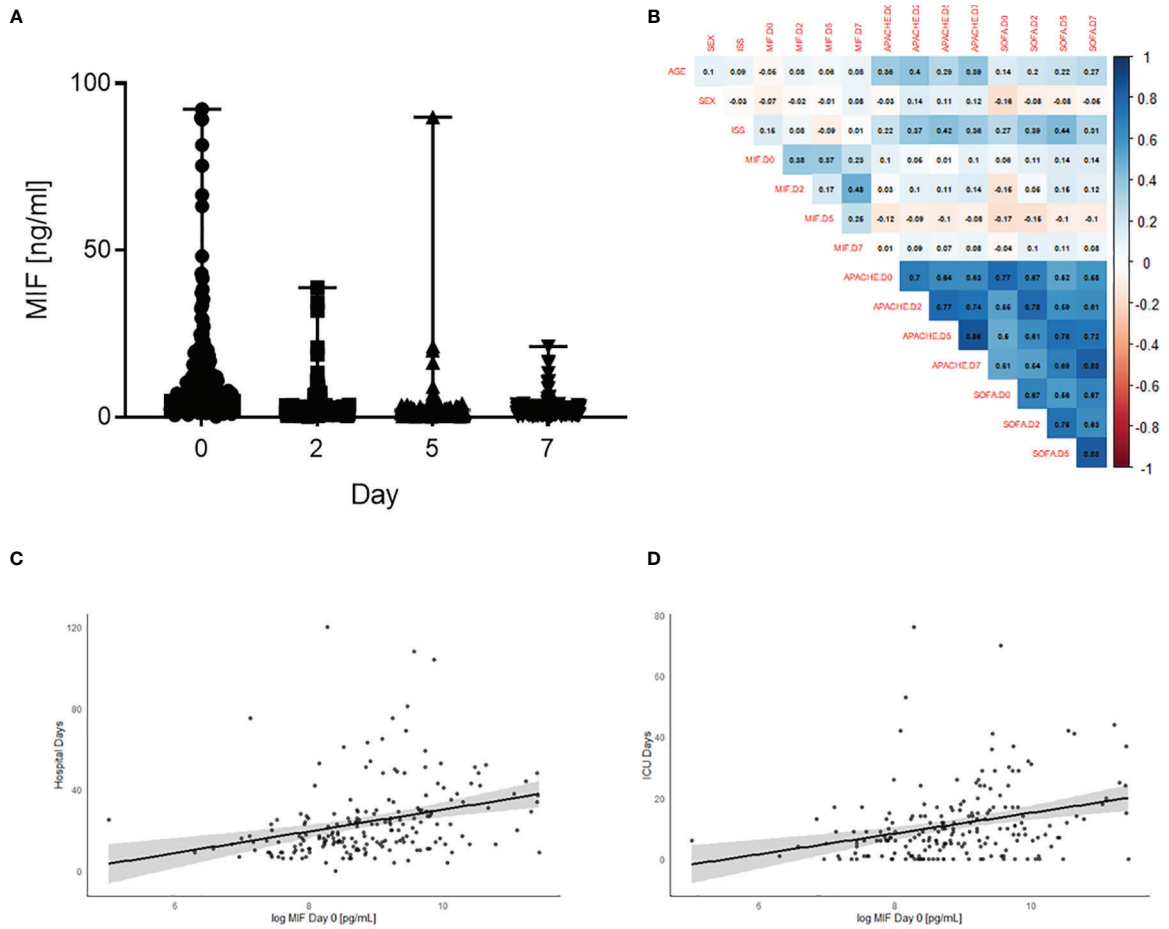

FIGURE 1 | Plasma MIF levels are elevated in polytrauma patients and associated with longer stay in ICU and hospital. **(A)** Plasma MIF levels in trauma patients (n = 208) at different time points: Day 0 (Emergency room), Day 2, Day 5 and Day 7. Data are expressed as median with range. **(B)** Heatmap for correlations between MIF levels and baseline characteristics sex, age, SOFA, ISS and APACHE score. Scatter plot for Day 0 MIF levels against **(C)** hospital stay and **(D)** intensive care unit (ICU) stay.

Serum MIF Levels Are Strongly Associated With Clinical Chemistry and MAP in Acute HS (Short-Term Follow-Up)

Having shown rats subjected to HS had elevated serum MIF levels, we wished to elucidate whether this observed increase correlates with clinical chemistry parameters (measured in serum collected 4 h post-resuscitation) and MAP (measured at 4 h post-resuscitation before sample collection). There was a positive correlation between MIF and all clinical chemistry parameters ($p<0.05$; **Supplemental Figure 5** shown in blue, r values range from 0.64 – 0.77), with the strongest correlations between AST (r = 0.77) and LDH (r = 0.72). There was a negative correlation between MIF and MAP ($p<0.05$; **Supplemental Figure 5** shown in red, r = -0.66).

Treatment With ISO-1 Attenuates Hepatic and Renal NF-κB Activation in Acute HS (Short-Term Follow-Up)

The effect of MIF inhibition on the activation of the signalling events leading to the activation of NF-κB, was investigated in the kidney and liver. When compared to sham-operated rats, HS-rats treated with vehicle had significant increases in the phosphorylation of IKKα/β at $Ser^{176/180}$ ($p<0.001$; **Figure 4A** and $p<0.001$; **Figure 4B**) and translocation of p65 to the nucleus ($p<0.001$; **Figure 4C** and $p<0.05$; **Figure 4D**). Treatment with ISO-1 significantly attenuated the increases in hepatic and renal phosphorylation of IKKα/β at $Ser^{176/180}$ ($p<0.001$; **Figure 4A** and $p<0.001$; **Figure 4B**) and the nuclear translocation of p65 ($p<0.001$; **Figure 4C** and $p<0.05$; **Figure 4D**).

Treatment With ISO-1 Attenuates Hepatic and Renal NLRP3 Inflammasome Activation in Acute HS (Short-Term Follow-Up)

Having discovered treatment with ISO-1 significantly reduced the activation of NF-κB in the kidney and liver of rats subjected to HS, we next analysed the potential involvement of the NLRP3 inflammasome. When compared to sham-operated rats, HS-rats treated with vehicle exhibited a significantly increased expression

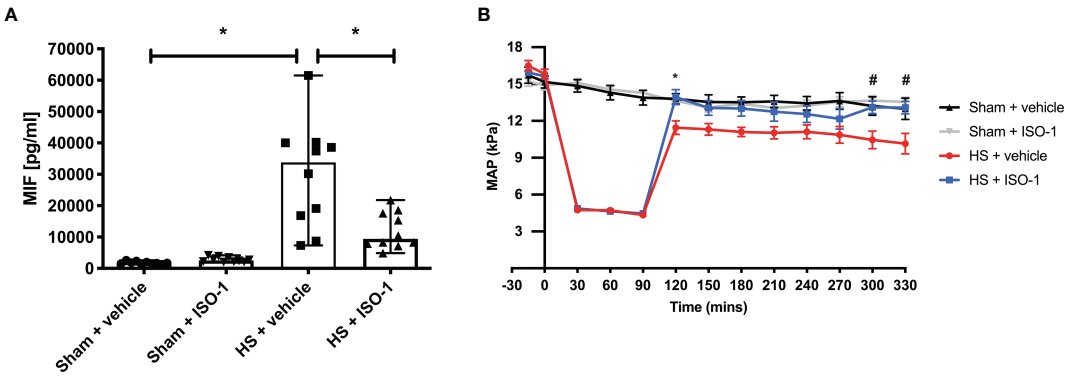

FIGURE 2 | Serum MIF levels are elevated in HS-rats and ISO-1 improves HS-induced circulatory failure in a short-term follow-up acute HS model. **(A)** Serum MIF levels were detected by ELISA in vehicle or ISO-1 treated rats. Data are expressed as median with range of ten animals per group. **(B)** Mean arterial pressure (MAP) was measured from the completion of surgery to the termination of the experiment for all groups. Statistical analysis was performed using one-way ANOVA followed by a Bonferroni's *post-hoc* test. *p < 0.05 Sham + vehicle vs. HS + vehicle; #p < 0.05 HS + vehicle vs. HS + ISO-1.

of the NLRP3 inflammasome (p<0.001; **Figure 4E** and p<0.001; **Figure 4F**) and cleavage of pro-caspase 1 to caspase 1 (p=0.008; **Figure 4G** and p<0.001; **Figure 4H**). Treatment with ISO-1 significantly inhibited the hepatic and renal expression of NLRP3 (p<0.001; **Figure 4E** and p<0.001; **Figure 4F**) and cleavage of pro-caspase 1 to caspase 1 (p=0.015; **Figure 4G** and p<0.001; **Figure 4H**).

Treatment With ISO-1 Improves HS-Induced Circulatory Failure in Acute HS (Long-Term Follow-Up)

Having demonstrated treatment with ISO-1 improved blood pressure in a short-term follow-up model, we wished to determine whether ISO-1 would still be effective in a model in which the resuscitation period is prolonged to 24 h. When compared to sham-operated rats, HS-rats treated with vehicle had significantly lower MAP values at 24 h post-resuscitation (p<0.001; **Figure 5A**); highlighting that either cardiovascular dysfunction or excessive hypotension was still present. In contrast, MAP of HS-rats treated with ISO-1 was significantly higher at 24 h than vehicle treated rats (p<0.05; **Figure 5A**). There were no significant differences in HR between any of the three groups investigated (p>0.05; **Figure 5B**).

Treatment With ISO-1 Attenuates HS-Induced Organ Damage and Myeloperoxidase Activity in Acute HS (Long-Term Follow-Up)

Having shown that treatment with ISO-1 ameliorated the MODS associated with HS in a short-term follow-up model, we examined whether this effect was sustained when the resuscitation period was extended to 24 h. As with the short-term follow-up model, when compared to sham-operated rats, rats subjected to HS with long-term follow-up and treated with vehicle displayed significant increases in serum urea (p<0.05; **Figure 6A**) and creatinine (p<0.001; **Figure 6B**) indicating the development of renal dysfunction. When compared to sham-operated rats, vehicle treated HS-rats exhibited significant increases in ALT (p<0.001; **Figure 6C**), AST (p<0.001; **Figure 6D**), lipase (p<0.05; **Figure 6E**) and LDH (p<0.05; **Figure 6F**). Treatment of HS-rats with ISO-1 significantly attenuated the renal dysfunction, hepatic injury and tissue damage caused by HS (all p<0.05; **Figures 6A–D, F**). Having demonstrated that treatment with ISO-1 reduced the cell infiltration in the lung in a short-term follow-up acute HS model, we measured myeloperoxidase (MPO) activity in the lung and liver as an indicator of neutrophil infiltration. When compared to sham-operated rats, HS-rats treated with vehicle showed a significant increase in MPO activity in the lung (p<0.001; **Figure 6G**) and liver (p<0.05; **Figure 6H**). Treatment with ISO-1 in HS-rats significantly attenuated these rises in MPO activity (p<0.001; **Figure 6G** and p<0.05; **Figure 6H**).

DISCUSSION

This study reports that inhibition of MIF activity attenuates organ injury/dysfunction and circulatory failure in acute short-term follow-up (**Figures 2**, **3**) and long-term follow-up (**Figures 5**, **6**) rat models of HS. Having shown that MIF gene expression is significantly elevated in leukocytes of trauma patients (**Supplemental Figure 2**) and plasma MIF levels are raised in polytrauma patients (**Figure 1**), we used a reverse translational approach to investigate whether pharmacological intervention with ISO-1 ameliorates the MODS associated with HS in a well-established rat model. Inhibition of MIF activity significantly attenuated the fall in blood pressure (**Figure 2** short-term follow-up and **Figure 5** long-term follow-up) and, hence, the delayed vascular decompensation caused by HS (39). Moreover, ISO-1 significantly attenuated the renal dysfunction, hepatic injury and neuromuscular injury caused by HS (**Figure 3** short-term follow-up and **Figure 6** long-term follow-up); highlighting the drug efficacy at both timepoints. Similarly, ISO-1 also reduces disease severity in animal models of sepsis

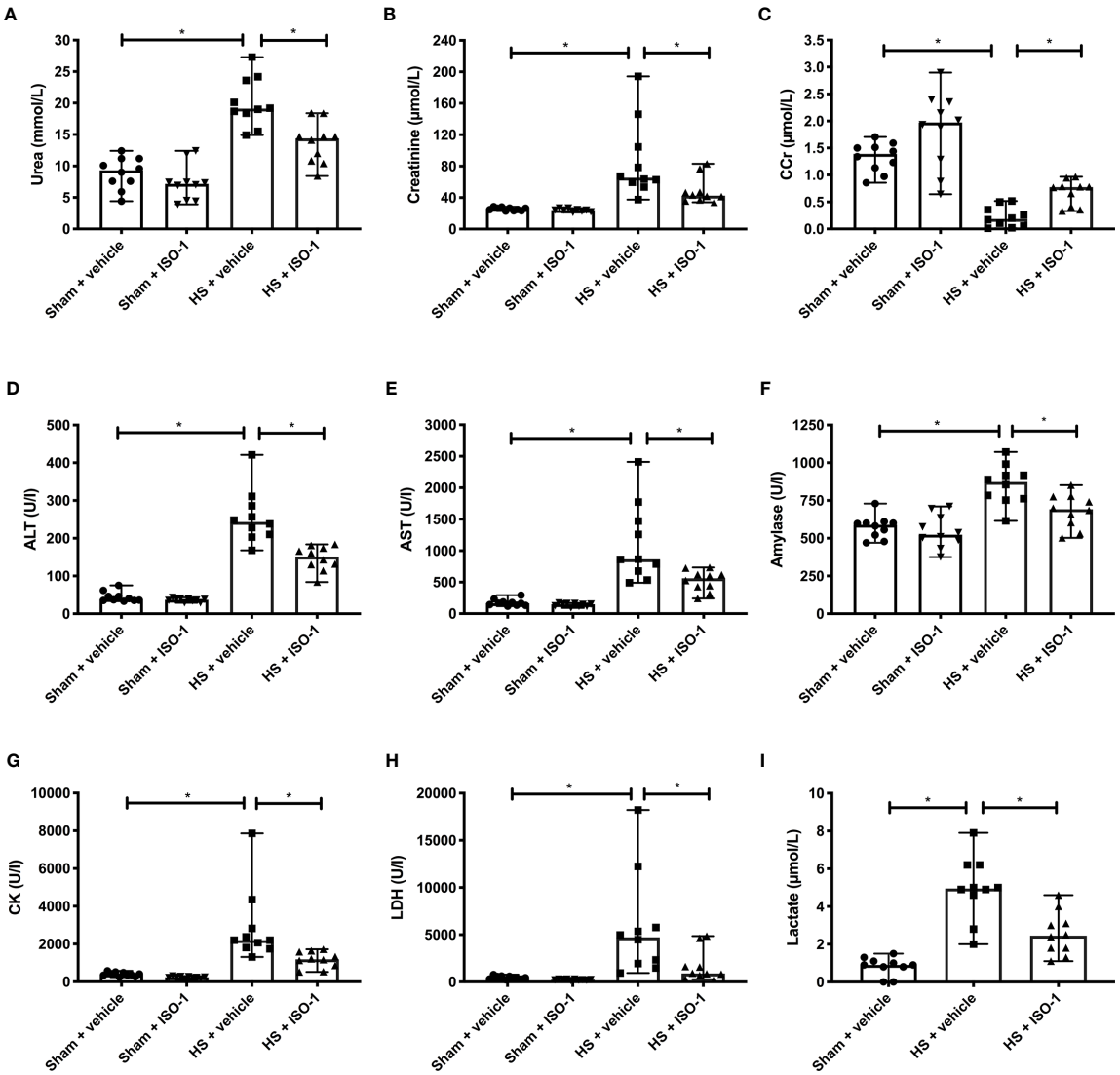

FIGURE 3 | Treatment with ISO-1 attenuates HS-induced organ damage in a short-term follow-up acute HS model. Rats were subjected to haemorrhagic shock (HS) and 4 h after resuscitation, levels of serum **(A)** urea, **(B)** creatinine, **(C)** creatinine clearance (CCr), **(D)** alanine aminotransferase (ALT), **(E)** aspartate aminotransferase (AST), **(F)** amylase, **(G)** creatine kinase (CK), **(H)** lactate dehydrogenase (LDH) and **(I)** lactate were determined. Sham-operated rats were used as control. Data are expressed as median with range of ten animals per group. Statistical analysis was performed using one-way ANOVA followed by a Bonferroni's *post-hoc* test. *$p < 0.05$ denoted statistical significance.

(40), acute pancreatitis (41–46), pneumonia (47), asthma (48), COPD (49), cystitis (50) and colitis (51).

We have illustrated that severe haemorrhage followed by resuscitation in the rat caused a significant increase in serum MIF levels, the magnitude of which was similar to the one seen in trauma patients. This finding implies that haemorrhage (rather than physical trauma) is the main driver for the observed increase in MIF in rats and possibly also in humans. Whilst the elevated plasma MIF levels in our cohort of polytrauma patients do not necessarily indicate an increase in synthesis, the increased gene expression measured by Xiao and colleagues (33) does suggest an associated rise in MIF production.

Post-traumatic complications can result in prolonged stays in ICU and in hospital. In the acute setting, there is a lack of diagnostic or risk stratification tools which allow the identification of the potential clinical outcome of trauma patients. We determined a significant positive correlation between elevated MIF levels in polytrauma patients and the overall length of ICU and hospital stays. These findings indicate that high plasma MIF levels at time of hospital admission are strongly predictive for a longer stay in ICU and hospital. Indeed, the human plasma MIF levels and gene expression data provide evidence supporting the role of MIF in trauma, as both gene expression and plasma levels increase following trauma. Most

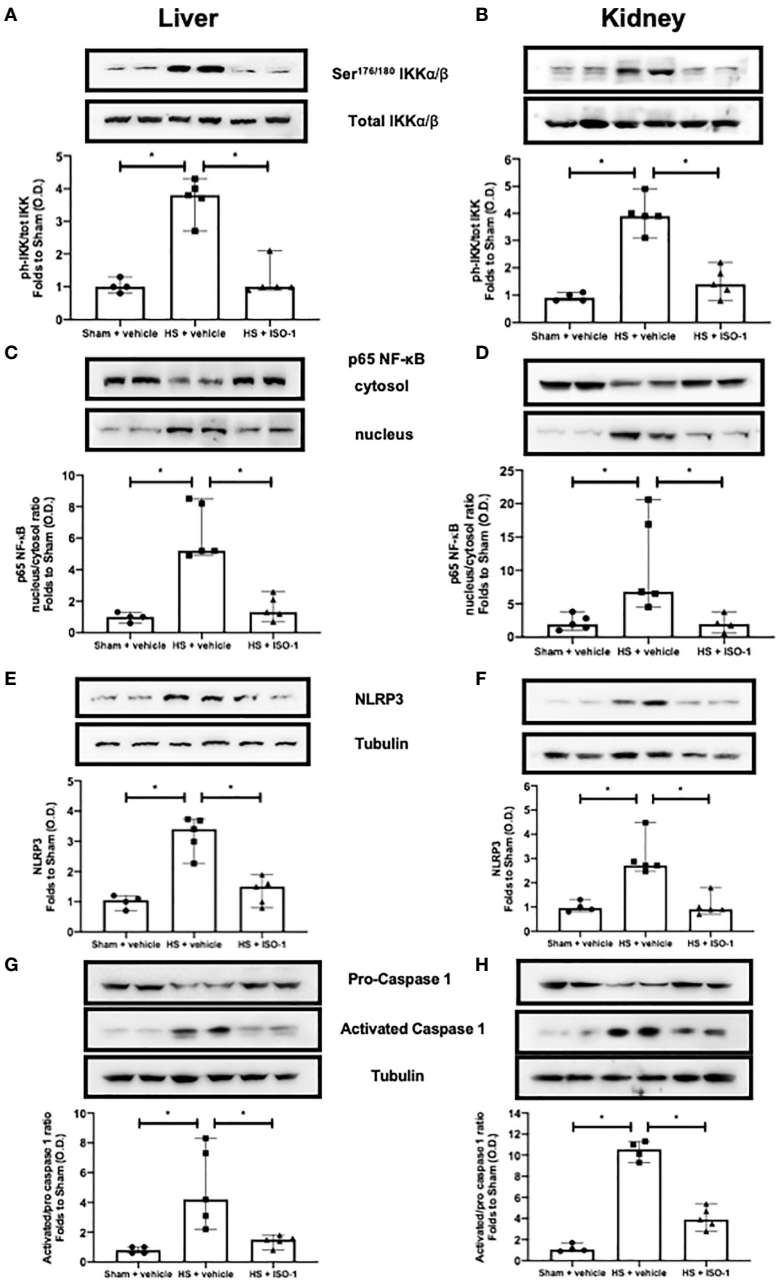

FIGURE 4 | Treatment with ISO-1 attenuates NF-κB and NLRP3 activation in a short-term follow-up acute HS model. **(A, B)** The phosphorylation of IKKα/β at $Ser^{176/180}$, **(C, D)** nuclear translocation of p65, **(E, F)** activation of NLRP3 and **(G, H)** cleavage of pro-caspase 1 of vehicle and ISO-1 treated rats were determined by western blot in the liver and kidney. Protein expression was measured as relative optical density (O.D.) and normalised to the sham band. Data are expressed as median with range of 4-5 animals per group. Statistical analysis was performed using one-way ANOVA followed by a Bonferroni's *post-hoc* test. *$p < 0.05$ denoted statistical significance.

notably, MIF was a better predictor of hospital stay than either ISS or SOFA scores. For every further increase of MIF on admission by 5000 pg/mL, the stay of patients in hospital is prolonged by ~1.2 days. Similarly, Cho and colleagues showed that trauma patients with elevated MIF levels had longer ICU stays than patients with lower or normal MIF levels (52).

Nevertheless, we found a weak positive but significant correlation between MIF levels on admission and ISS which supports the findings of Chuang and colleagues' study illustrating higher MIF levels were associated with worse clinical severity scores (APACHE II, RTS and TRISS) (30). Although clinical severity scores cannot be measured in rats,

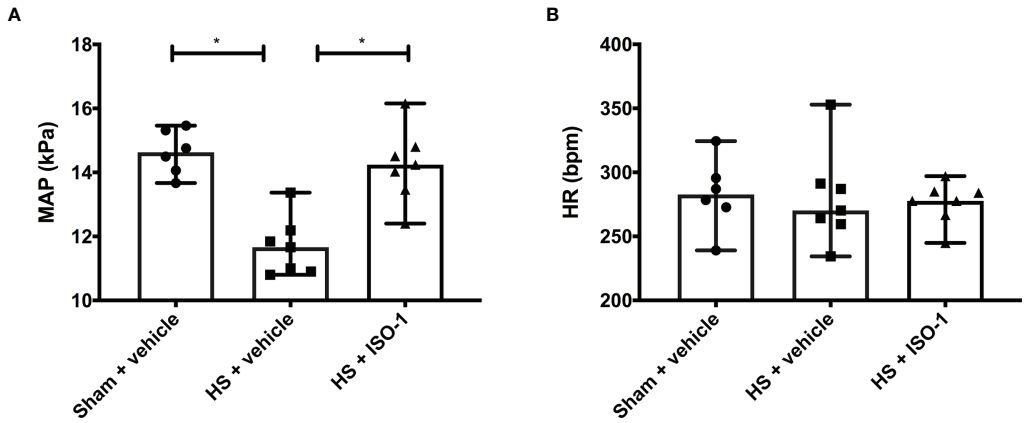

FIGURE 5 | Treatment with ISO-1 improves HS-induced cardiac dysfunction in a long-term follow-up acute HS model. **(A)** Mean arterial pressure (MAP) and **(B)** heart rate (HR) were measured 24 h post resuscitation for vehicle and ISO-1 treated rats. Data are expressed as median with range. Sham + vehicle (n = 6), HS + vehicle (n = 7) and HS + ISO-1 (n = 7). Statistical analysis was performed using one-way ANOVA followed by a Bonferroni's *post-hoc* test. *p < 0.05 denoted statistical significance.

we found significant positive correlations between serum MIF levels and clinical chemistry parameters and a significant negative correlation between MIF and MAP both of which can be considered as indicators organ function (**Supplementary Figure 5**).

What, then, are the mechanisms by which ISO-1 attenuates HS-associated organ injury/dysfunction? It is recognised that key signalling pathways, such as those leading to NF-κB activation, initiate the production of pro-inflammatory mediators such as cytokines, chemokines and enzymes (53). As part of a positive feedback mechanism, these inflammatory mediators can induce activation of NF-κB and its upstream signalling machinery, further amplifying and propagating the NF-κB-mediated inflammatory responses. This can result in a more permeable endothelium, hypoxic/hypoperfused tissues, tissue injury and ultimately MODS (54). Trauma has been shown to increase the translocation of NF-κB to the nucleus (35–38). Inhibition of MIF activity with ISO-1 reduced NF-κB activation in the kidney and liver of HS-rats (**Figure 4**). This may suggest that inhibiting NF-κB activation contributes to the observed protective effects of ISO-1 in HS. It should be noted that MIF has been shown to upregulate TLR4 expression, leading to increased translocation of NF-κB into the nucleus (55) and interact with thioredoxin-interacting protein to induce NF-κB activity (56).

Activation of the NLRP3 inflammasome stimulates IL-1β production which plays a crucial role in trauma-associated systemic inflammation and organ dysfunction/injury (36). Inhibition of MIF activity with ISO-1 reduced both the assembly and subsequent activation of the NLRP3 inflammasome in the kidney and liver of HS-rats (**Figure 4**). This may suggest that inhibiting NLRP3 inflammasome activation contributes to the observed beneficial effects of ISO-1 in HS by decreasing the pro-inflammatory effects related to increased IL-1β production and ensuing tissue inflammation (57). Of note, MIF has been proposed to play a role in the activation of the NLRP3 inflammasome (58, 59).

The sterile inflammation caused by HS is associated with increased recruitment of leukocytes to the tissues and is secondary to NF-κB and NLRP3 activation and their transcriptional regulation of pro-inflammatory cytokines (60–62). Furthermore, the leukocyte and endothelial cell surface expression of adhesion molecules is regulated by NF-κB and promotes leukocyte extravasation from the circulation to the injury site (63). We found a significant increase in $CD68^+$ cells in the lung (**Supplementary Figure 4**) and in pulmonary and hepatic MPO activity (**Figure 6**), markers of macrophage and neutrophil recruitment respectively, after induction of HS in rats. Treatment of HS-rats with ISO-1 did not significantly reduce the number of pulmonary $CD68^+$ cells and thus, macrophage infiltration into the lung. In contrast, administration of ISO-1 to HS-rats attenuated the rise in MPO activity related to increased neutrophil recruitment. Taken together, these results could imply that ISO-1 attenuates neutrophil, but not macrophage recruitment in HS. Indeed, an anti-MIF antibody was shown to attenuate the LPS-induced migration and accumulation of neutrophils in the lung (64). These observations can be explained by the chemokine-like properties of MIF, which facilitate the activation and recruitment of leukocytes during immune surveillance and inflammation (65, 66). Initially, MIF was eponymously described by its ability to inhibit random macrophage migration *in vitro* (67, 68). However, it is now known that MIF can mediate the recruitment of mononuclear cells in a number of disease states (69–72). A possible explanation as to why ISO-1 did not significantly reduce pulmonary macrophage invasion is that the presence of other inflammatory mediators, such as IL-1β, IL-6 and TNF-α, could have stimulated the migration of macrophages, but we would need to measure these mediators to confirm this theory.

LIMITATIONS

Although ISO-1 displayed some striking, beneficial effects in the acute HS models, there are study limitations which should be taken into consideration. In total, 208 patients were included in

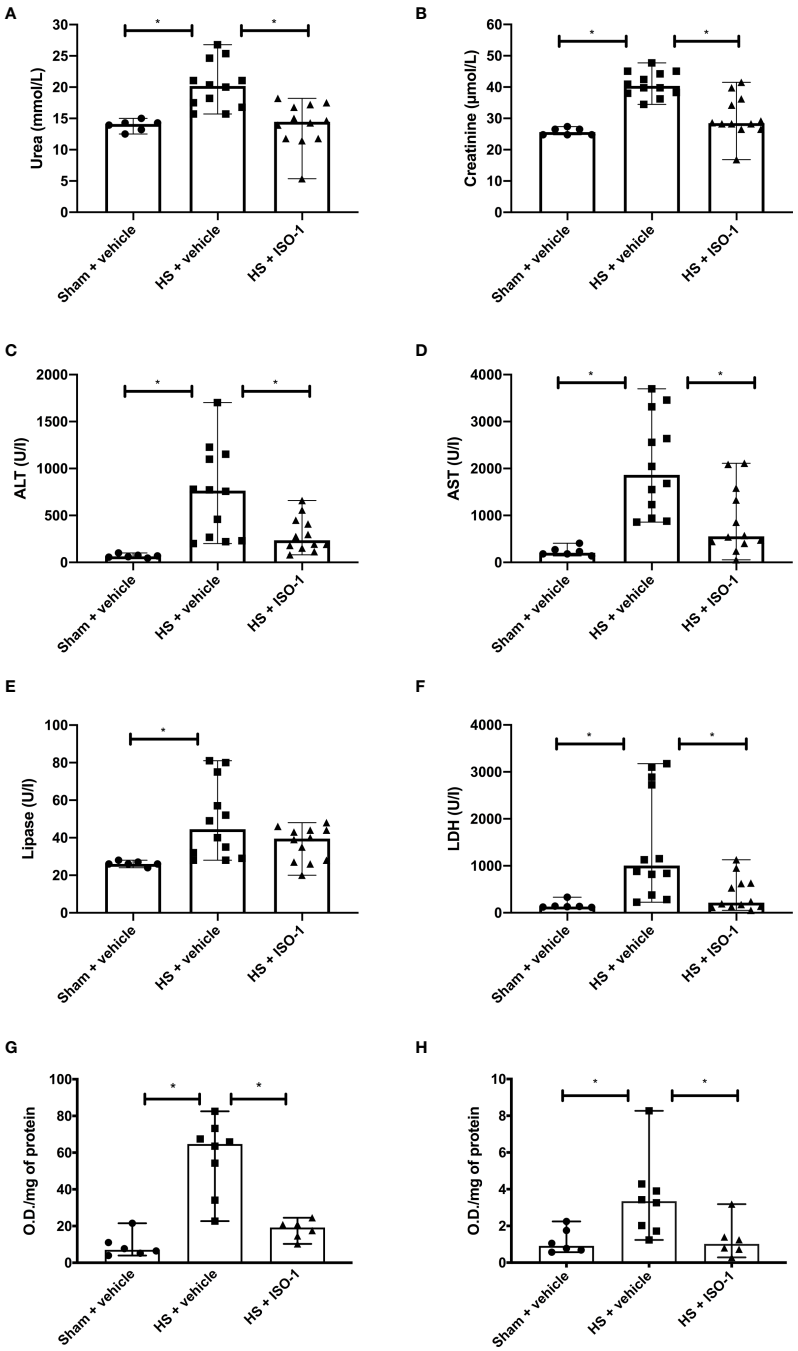

FIGURE 6 | Treatment with ISO-1 attenuates HS-induced organ damage and myeloperoxidase activity in a long-term follow-up acute HS model. Rats were subjected to haemorrhagic shock (HS) and 24 h after resuscitation, levels of serum **(A)** urea, **(B)** creatinine, **(C)** alanine aminotransferase, (ALT), **(D)** aspartate aminotransferase (AST), **(E)** lipase and **(F)** LDH were determined were determined in vehicle and ISO-1 treated rats. Sham-operated rats were used as control. Sham + vehicle (n = 6), HS + vehicle (n = 12) and HS + ISO-1 (n = 12). Myeloperoxidase activity in **(G)** lung and **(H)** liver were determined for vehicle and ISO-1 treated rats. Sham + vehicle (n = 6), HS + vehicle (n = 8) and HS + ISO-1 (n = 6). Data are expressed as median with range. Statistical analysis was performed using one-way ANOVA followed by a Bonferroni's *post-hoc* test. *p<0.05 denoted statistical significance.

the study, however, in some instances there were insufficient plasma volumes available for some of the measured timepoints. Therefore, some correlation analyses were performed with a reduced number of samples/patients. Following trauma, there is an increased inflammatory response, and we were able to measure elevated plasma MIF levels in polytrauma patients. However, we cannot exclude the possibility that the increased plasma levels are not exclusively associated with polytrauma. The

animal models used in our study do not encompass all aspects of trauma/HS and further long-term survival experiments are needed to verify that the observed early reduction in MODS does, indeed, translate to improved outcome and ultimately reduced mortality. Hence, caution must be exercised when interpreting the pre-clinical results and extrapolating to the clinical scenario. Additionally, future studies in larger animals/higher species may be useful to confirm efficacy and to further examine the mechanism(s) of action (e.g. microcirculatory effects and blood gas analysis) of ISO-1 in HS. It should be noted that only healthy young male rats were used and, hence, age and gender differences and the presence of co-morbidities were not investigated (but may well impact outcome). Moreover, clinical studies with larger cohorts of trauma patients are required to robustly examine the relationship between MIF activity, inhibition and clinical outcomes in humans. Whilst we did not measure the long-term stability of MIF in the patient samples collected between 2010-2014, we were able to demonstrate significant and time-related elevations in MIF in the blood of patients with trauma and haemorrhage. Indeed, the peak levels of MIF observed in patients on admission to the hospital (measured in samples that were several years old) were similar to the peak levels measured in rats with severe haemorrhage (that we measured within weeks of completing the experiments). Nevertheless, we cannot, however, entirely rule out that the levels of MIF in patients with trauma-haemorrhage would have been even higher if the MIF determinations would have been carried out earlier after the trauma occurred.

CONCLUSIONS

In conclusion, we demonstrate here for the first time that MIF levels are elevated in polytrauma patients on arrival to the emergency room and higher MIF levels are associated with longer stays in ICU and hospital overall. The finding that HS alone (in the absence of physical trauma) in rats resulted in a rise in MIF levels similar to that seen in polytrauma patients supports the view that haemorrhage is the main driver for the elevations in MIF. Furthermore, treatment with ISO-1 reduces the organ injury/dysfunction and circulatory failure caused by severe haemorrhage in the rat, highlighting a role of MIF in disease pathogenesis. Administration of ISO-1 attenuates the degree of NF-κB and NLRP3 inflammasome activation (measured in the kidney and liver), both of which are key drivers of local and systemic inflammation. Thus, we propose that MIF inhibitors may be used in trauma patients to lower the organ injury and inflammation caused by severe haemorrhage and resuscitation.

DATA AVAILABILITY STATEMENT

Publicly available datasets were analysed in this study. This data can be found here: https://www.ncbi.nlm.nih.gov/geo/query/acc.cgi?acc=gse36809.

ETHICS STATEMENT

The studies involving human participants were reviewed and approved by University Hospital Frankfurt of Goethe-University - Institutional Ethics Committee (Number 312/10). The patients/participants provided their written informed consent to participate in this study. The animal study was reviewed and approved by Animal Welfare Ethics Review Board of Queen Mary University of London and by the Home Office (Licence number PC5F29685) and Universidade Federal de Santa Catarina Institutional Committee for Animal Use in Research (Licence number 7396250219).

AUTHOR CONTRIBUTIONS

Conception and design: NMP, LM, and CT. Animal experiments: NY, NMP, FRMBO, HPR, and RS. Human sample analysis: LM, EZ, GM, IM, BR, DH, LS, and CS. Animal sample analyses: NY, NMP, LM, CT, LS, EZ, FRMBO, HPR, SK, DC, MC, GFA, and RS. Clinical study and patient data analyses: LM, EZ, CT, IM, BR, DH, LS, NMP, and CS. Statistical analyses: NY, NMP, DH, LM, and CT. Drafting the manuscript for important intellectual content: LS, LM, EZ, NMP, and CT. All authors reviewed and approved the manuscript.

FUNDING

NMP was funded by the William Harvey Research Foundation. HPR and FRMBO were funded by National Council for Scientific and Technological Development (CNPq) fellowship. This study was supported by the German Research Foundation to LM (DFG, MA 7082/3-1), to CS (DFG, STO 1099/8-1) and by an intramural grant to EZ (START 131/19), National Council for Scientific and Technological Development to RS (CNPq, Brazil, Grant 409018/2018-0).

ACKNOWLEDGMENTS

We would like to thank Dr. Ronald Tompkins and Dr. Wenzhong Xiao for their support in the human MIF gene expression data analysis.

SUPPLEMENTARY MATERIAL

The Supplementary Material for this article can be found online at: https://www.frontiersin.org/articles/10.3389/fimmu.2022.886421/full#supplementary-material

REFERENCES

1. World Health Organization. *Injuries and Violence: The Facts 2014* (2014). Available at: www.who.int/healthinfo/global_burden_disease/projections/en/.
2. Haagsma JA, Graetz N, Bolliger I, Naghavi M, Higashi H, Mullany EC, et al. The Global Burden of Injury: Incidence, Mortality, Disability-Adjusted Life Years and Time Trends From the Global Burden of Disease Study 2013. *Injury Prev* (2016) 22(1):3–18. doi: 10.1136/injuryprev-2015-041616
3. Curry N, Hopewell S, Dorée C, Hyde C, Brohi K, Stanworth S. The Acute Management of Trauma Hemorrhage: A Systematic Review of Randomized Controlled Trials. *Crit Care* (2011) 15(2):1–10. doi: 10.1186/cc10096
4. Dewar D, Moore FA, Moore EE, Balogh Z. Postinjury Multiple Organ Failure. *Injury* (2009) 40:912–8. doi: 10.1016/j.injury.2009.05.024
5. Geeraedts LMG, Kaasjager HAH, van Vugt AB, Frölke JPM. Exsanguination in Trauma: A Review of Diagnostics and Treatment Options. *Injury* (2009) 40 (1):11–20. doi: 10.1016/j.injury.2008.10.007
6. Dutton RP, Stansbury LG, Leone S, Kramer E, Hess JR, Scalea TM. Trauma Mortality in Mature Trauma Systems: Are We Doing Better? An Analysis of Trauma Mortality Patterns, 1997-2008. *J Trauma - Injury Infect Crit Care* (2010) 69(3):620–6. doi: 10.1097/TA.0b013e3181bbfe2a
7. Teixeira PGR, Inaba K, Hadjizacharia P, Brown C, Salim A, Rhee P, et al. Preventable or Potentially Preventable Mortality at a Mature Trauma Center. *J Trauma* (2007) 63(6):1338–47. doi: 10.1097/TA.0b013e31815078ae
8. Lord JM, Midwinter MJ, Chen YF, Belli A, Brohi K, Kovacs EJ, et al. The Systemic Immune Response to Trauma: An Overview of Pathophysiology and Treatment. *Lancet* (2014) 384:1455–65. Lancet Publishing Group. doi: 10.1016/S0140-6736(14)60687-5
9. Sauaia A, Moore EE, Johnson JL, Chin TL, Banerjee A, Sperry JL, et al. Temporal Trends of Postinjury Multiple-Organ Failure: Still Resource Intensive, Morbid, and Lethal. *J Trauma Acute Care Surg* (2014) 76(3):582. doi: 10.1097/TA.0000000000000147
10. Relja B, Mörs K, Marzi I. Danger Signals in Trauma. *Eur J Trauma Emergency Surg* (2018) 44(3):301. doi: 10.1007/s00068-018-0962-3
11. Chen GY, Nuñez G. Sterile Inflammation: Sensing and Reacting to Damage. *Nat Rev Immunol* (2010) 10:826–37. NIH Public Access. doi: 10.1038/nri2873
12. Halbgebauer R, Braun CK, Denk S, Mayer B, Cinelli P, Radermacher P, et al. Hemorrhagic Shock Drives Glycocalyx, Barrier and Organ Dysfunction Early After Polytrauma. *J Crit Care* (2018) 44:229–37. doi: 10.1016/j.jcrc.2017.11.025
13. Manson J, Thiemermann C, Brohi K. Trauma Alarmins as Activators of Damage-Induced Inflammation. *Br J Surg* (2012) 99:12–20. doi: 10.1002/bjs.7717
14. Jackman RP, Utter GH, Muench MO, Heitman JW, Munz MM, Jackman RW, et al. Distinct Roles of Trauma and Transfusion in Induction of Immune Modulation After Injury. *Transfusion* (2012) 52(12):2533–50. doi: 10.1111/j.1537-2995.2012.03618.x
15. Calandra T, Bernhagen J, Metz CN, Spiegel LA, Bacher M, Donnelly T, et al. MIF as a Glucocorticoid-Induced Modulator of Cytokine Production. *Nature* (1995) 377(6544):68–71. doi: 10.1038/377068a0
16. Bacher M, Metz CN, Calandra T, Mayer K, Chesney J, Lohoff M, et al. An Essential Regulatory Role for Macrophage Migration Inhibitory Factor in T-Cell Activation. *Proc Natl Acad Sci USA* (1996) 93(15):7849. doi: 10.1073/pnas.93.15.7849
17. Donnelly SC, Bucala R. Macrophage Migration Inhibitory Factor: A Regulator of Glucocorticoid Activity With a Critical Role in Inflammatory Disease. *Mol Med Today* (1997) 3:502–7. doi: 10.1016/S1357-4310(97)01133-7
18. Bozza M, Satoskar AR, Lin G, Lu B, Humbles AA, Gerard C, et al. Targeted Disruption of Migration Inhibitory Factor Gene Reveals its Critical Role in Sepsis. *J Exp Med* (1999) 189(2):341–6. doi: 10.1084/jem.189.2.341
19. Mitchell RA, Liao H, Chesney J, Fingerle-Rowson G, Baugh J, David J, et al. Macrophage Migration Inhibitory Factor (MIF) Sustains Macrophage Proinflammatory Function by Inhibiting P53: Regulatory Role in the Innate Immune Response. *Proc Natl Acad Sci* (2002) 99:345–50. doi: 10.1073/pnas.012511599
20. Calandra T, Roger T. Macrophage Migration Inhibitory Factor: A Regulator of Innate Immunity. *Nat Rev Immunol* (2003) 30:S27–35. doi: 10.1002/0471203076.emm0331
21. Rodríguez-Sosa M, Rosas LE, David JR, Bojalil R, Satoskar AR, Terrazas LI. Macrophage Migration Inhibitory Factor Plays a Critical Role in Mediating Protection Against the Helminth Parasite Taenia Crassiceps. *Infection Immun* (2003) 71(3):1247. doi: 10.1128/IAI.71.3.1247-1254.2003
22. Onodera S, Kaneda K, Mizue Y, Koyama Y, Fujinaga M, Nishihira J. Macrophage Migration Inhibitory Factor Up-Regulates Expression of Matrix Metalloproteinases in Synovial Fibroblasts of Rheumatoid Arthritis. *J Biol Chem* (2000) 275(1):444–50. doi: 10.1074/jbc.275.1.444
23. Onodera S, Nishihira J, Iwabuchi K, Koyama Y, Yoshida K, Tanaka S, et al. Macrophage Migration Inhibitory Factor Up-Regulates Matrix Metalloproteinase-9 and -13 in Rat Osteoblasts: Relevance To Intracellular Signaling Pathways. *J Biol Chem* (2002) 277(10):7865–74. doi: 10.1074/jbc.M106020200
24. Calandra T, Bernhagen J, Mitchell RA, Bucala R. The Macrophage is an Important and Previously Unrecognized Source of Macrophage Migration Inhibitory Factor. *J Exp Med* (1994) 179(6):1895–902. doi: 10.1084/jem.179.6.1895
25. Calandra T, Echtenacher B, le Roy D, Pugin J, Metz CN, Hültner L, et al. Protection From Septic Shock by Neutralization of Macrophage Migration Inhibitory Factor. *Nat Med* (2000) 6(2):164–70. doi: 10.1038/72262
26. Benigni F, Atsumi T, Calandra T, Metz C, Echtenacher B, Peng T, et al. The Proinflammatory Mediator Macrophage Migration Inhibitory Factor Induces Glucose Catabolism in Muscle. *J Clin Invest* (2000) 106(10):1291. doi: 10.1172/JCI9900
27. Baugh JA, Bucala R. Macrophage Migration Inhibitory Factor. *Crit Care Med* (2002) 30(1 Suppl):S27–35. doi: 10.1097/00003246-200201001-00004
28. Calandra T, Bucala R. Macrophage Migration Inhibitory Factor: A Counter-Regulator of Glucocorticoid Action and Critical Mediator of Septic Shock. *J Inflammation* (1995) 47(1–2):39–51.
29. Joshi PC, Poole GV, Sachdev V, Zhou X, Jones Q. Trauma Patients With Positive Cultures Have Higher Levels of Circulating Macrophage Migration Inhibitory Factor (MIF). *Res Commun Mol Pathol Pharmacol* (2000) 107(1–2):13–20.
30. Chuang C-C, Hung C-J, Tsai M-C, Yeh T-M, Chuang Y-C. High Concentrations of Circulating Macrophage Migration Inhibitory Factor in Patients With Severe Blunt Trauma: Is Serum Macrophage Migration Inhibitory Factor Concentration a Valuable Prognostic Factor? *Crit Care Med* (2004) 32(3):734–9. doi: 10.1097/01.CCM.0000117170.13320.F4
31. Hayakawa M, Katabami K, Wada T, Minami Y, Sugano M, Shimojima H, et al. Imbalance Between Macrophage Migration Inhibitory Factor and Cortisol Induces Multiple Organ Dysfunction in Patients With Blunt Trauma. *Inflammation* (2010) 34(3):193–7. doi:10.1007/s10753-010-9223-2
32. Shih HC, Huang MS, Lee CH. Polymorphonuclear Cell Priming Associated With NF-kB Activation in Patients With Severe Injury is Partially Dependent on Macrophage Migration Inhibitory Factor. *J Am Coll Surgeons* (2010) 211 (6):791–7. doi: 10.1016/j.jamcollsurg.2010.07.028
33. Xiao W, Mindrinos MN, Seok J, Cuschieri J, Cuenca AG, Gao H, et al. A Genomic Storm in Critically Injured Humans. *J Exp Med* (2011) 208(13):2581. doi: 10.1084/jem.20111354
34. von Elm E, Altman DG, Egger M, Pocock SJ, Gøtzsche PC, Vandenbroucke JP. The Strengthening the Reporting of Observational Studies in Epidemiology (STROBE) Statement: Guidelines for Reporting Observational Studies. *Lancet (London England)* (2007) 370(9596):1453–7. doi: 10.1016/S0140-6736(07)61602-X
35. Sordi R, Chiazza F, Collotta D, Migliaretti G, Colas RA, Vulliamy P, et al. Resolvin D1 Attenuates the Organ Injury Associated With Experimental Hemorrhagic Shock. *Ann Surg* (2021) 273(5):1012–21. doi: 10.1097/SLA.0000000000003407
36. Patel NM, Oliveira FRMB, Ramos HP, Aimaretti E, Alves GF, Coldewey SM, et al. Inhibition of Bruton's Tyrosine Kinase Activity Attenuates Hemorrhagic Shock-Induced Multiple Organ Dysfunction in Rats. *Ann Surg* (2021). doi: 10.1097/SLA.0000000000005357
37. Sordi R, Nandra KK, Chiazza F, Johnson FL, Cabrera CP, Torrance HD, et al. Artesunate Protects Against the Organ Injury and Dysfunction Induced by Severe Hemorrhage and Resuscitation. *Ann Surg* (2017) 265:408–17. doi: 10.1097/SLA.0000000000001664
38. Yamada N, Martin LB, Zechendorf E, Purvis GSD, Chiazza F, Varrone B, et al. Novel Synthetic, Host-Defense Peptide Protects Against Organ Injury/Dysfunction in a Rat Model of Severe Hemorrhagic Shock. *Ann Surg* (2018) 268:348–56. doi: 10.1097/SLA.0000000000002186
39. Thiemermann C, Szabo C, Mitchell JA, Vane JR. Vascular Hyporeactivity to Vasoconstrictor Agents and Hemodynamic Decompensation in Hemorrhagic Shock is Mediated by Nitric Oxide. *Proc Natl Acad Sci USA* (1993) 90(1):267–71. doi: 10.1073/pnas.90.1.267

40. Al-Abed Y, Dabideen D, Aljabari B, Valster A, Messmer D, Ochani M, et al. ISO-1 Binding to the Tautomerase Active Site of MIF Inhibits its Pro-Inflammatory Activity and Increases Survival in Severe Sepsis. *J Biol Chem* (2005) 280:36541–4. doi: 10.1074/jbc.C500243200
41. Wang B, Zhao K, Hu W, Ding Y, Wang W. Protective Mechanism of MIF Inhibitor ISO-1 on Intrahepatic Bile Duct Cells in Rats With Severe Acute Pancreatitis. *Digestive Dis Sci* (2021) 66(10):3415–26. doi: 10.1007/s10620-020-06674-9
42. Li M, Yu J, Zhao L, Mei F-C, Zhou Y, Hong Y-P, et al. Inhibition of Macrophage Migration Inhibitory Factor Attenuates Inflammation and Fetal Kidney Injury in a Rat Model of Acute Pancreatitis in Pregnancy. *Int Immunopharmacol* (2019) 68:106–14. doi: 10.1016/j.intimp.2018.12.068
43. Zhou Y, Zhao L, Mei F, Hong Y, Xia H, Zuo T, et al. Macrophage Migration Inhibitory Factor Antagonist (S,R)3-(4-hydroxyphenyl)-4,5-dihydro-5-isoxazole Acetic Acid Methyl Ester Attenuates Inflammation and Lung Injury in Rats With Acute Pancreatitis in Pregnancy. *Mol Med Rep* (2018) 17(5):6576–84. doi: 10.3892/mmr.2018.8672
44. Liu Y, Liu Y, Wang Q, Song Y, Chen S, Cheng B, et al. MIF Inhibitor ISO-1 Alleviates Severe Acute Pancreatitis-Associated Acute Kidney Injury by Suppressing the NLRP3 Inflammasome Signaling Pathway. *Int Immunopharmacol* (2021) 96:107555. doi: 10.1016/j.intimp.2021.107555
45. Guo ZD, Zhao L, Wang P, Deng WH, Shi Q, Zuo T, et al. Fetal Liver Injury Ameliorated by Migration Inhibitory Factor Inhibition in a Rat Model of Acute Pancreatitis in Pregnancy. *J Obstetrics Gynaecol Res* (2018) 44(3):374–83. doi: 10.1111/jog.13538
46. Zhu C, Liu Y, Song Y, Wang Q, Liu Y, Yang S, et al. Deletion of Macrophage Migration Inhibitory Factor Ameliorates Inflammation in Mice Model Severe Acute Pancreatitis. *Biomedicine Pharmacotherapy = Biomedecine pharmacotherapie* (2020) 125:109919. doi: 10.1016/j.biopha.2020.109919
47. Hou XQ, Gao YW, Yang ST, Wang CY, Ma ZY, Xia XZ. Role of Macrophage Migration Inhibitory Factor in Influenza H5N1 Virus Pneumonia. *Acta Virologica* (2009) 53(4):225–31. doi: 10.4149/av_2009_04_225
48. Chen PF, Luo YL, Wang W, Wang JX, Lai WY, Hu SM, et al. ISO-1, a Macrophage Migration Inhibitory Factor Antagonist, Inhibits Airway Remodeling in a Murine Model of Chronic Asthma. *Mol Med* (2010) 16(9–10):400–8. doi: 10.2119/molmed.2009.00128
49. Russell KE, Chung KF, Clarke CJ, Durham AL, Mallia P, Footitt J, et al. The MIF Antagonist ISO-1 Attenuates Corticosteroid-Insensitive Inflammation and Airways Hyperresponsiveness in an Ozone-Induced Model of COPD. *PloS One* (2016) 11(1):e0146102. doi: 10.1371/journal.pone.0146102
50. Vera PL, Iczkowski KA, Howard DJ, Jiang L, Meyer-Siegler KL. Antagonism of Macrophage Migration Inhibitory Factor Decreases Cyclophosphamide Cystitis in Mice. *Neurourology Urodynamics* (2010) 29(8):1451–7. doi: 10.1002/nau.20878
51. Shah YM, Ito S, Morimura K, Chen C, Yim SH, Haase VH, et al. Hypoxia-Inducible Factor Augments Experimental Colitis Through a MIF-Dependent Inflammatory Signaling Cascade. *Gastroenterology* (2008) 134(7):2036. doi: 10.1053/j.gastro.2008.03.009
52. Cho YD, Choi SH, Kim JY, Park SJ, Yoon YH, Cho HJ, et al. Macrophage Migration Inhibitory Factor Levels Correlate With an Infection in Trauma Patients. *Ulusal travma ve acil cerrahi dergisi = Turkish J Trauma Emergency surgery: TJTES* (2017) 201723(3):193–8. doi: 10.5505/tjtes.2016.04780
53. Senftleben U, Karin M. The IKK/NF-Kappa B Pathway. *Crit Care Med* (2002) 30:S18–26. doi: 10.1097/00003246-200201001-00003
54. Liu SF, Malik AB. NF-κb Activation as a Pathological Mechanism of Septic Shock and InflammationAmerican Journal of Physiology - Lung Cellular and Molecular Physiology. *Am J Physiol Lung Cell Mol Physiol* (2006) 290:L622–45. doi: 10.1152/ajplung.00477.2005.
55. Roger T, David J, Glauser MP, Calandra T. MIF Regulates Innate Immune Responses Through Modulation of Toll-Like Receptor 4. *Nature* (2001) 414 (6866):920–4. doi: 10.1038/414920a
56. Kim MJ, Kim WS, Kim DO, Byun JE, Huy H, Lee SY, et al. Macrophage Migration Inhibitory Factor Interacts With Thioredoxin-Interacting Protein and Induces NF-κb Activity. *Cell signalling* (2017) 34:110–20. doi: 10.1016/j.cellsig.2017.03.007
57. Dinarello CA. Biologic Basis for Interleukin-1 in Disease. *Blood* (1996) 87:2095–147. American Society of Hematology. doi: 10.1182/blood.V87.6.2095.bloodjournal8762095
58. Lang T, Lee JPW, Elgass K, Pinar AA, Tate MD, Aitken EH, et al. Macrophage Migration Inhibitory Factor is Required for NLRP3 Inflammasome Activation. *Nat Commun* (2018) 9(1):1–15. doi: 10.1038/s41467-018-04581-2
59. Shin MS, Kang Y, Wahl ER, Park HJ, Lazova R, Leng L, et al. Macrophage Migration Inhibitory Factor Regulates U1 Small Nuclear RNP Immune Complex-Mediated Activation of the NLRP3 Inflammasome. *Arthritis Rheumatol (Hoboken NJ)* (2019) 71(1):109–20. doi: 10.1002/art.40672
60. Chen CC, Manning AM. Transcriptional Regulation of Endothelial Cell Adhesion Molecules: A Dominant Role for NF-κb. *Agents Actions Suppl* (1995) 47:135–41. doi: 10.1007/978-3-0348-7343-7_12
61. Collins T, Read MA, Neish AS, Whitley MZ, Thanos D, Maniatis T. Transcriptional Regulation of Endothelial Cell Adhesion Molecules: NF-κb and Cytokine-Inducible Enhancers. *FASEB J* (1995) 9(10):899–909. doi: 10.1096/fasebj.9.10.7542214
62. Campbell SJ, Anthony DC, Oakley F, Carlsen H, Elsharkawy AM, Blomhoff R, et al. Hepatic Nuclear Factor κb Regulates Neutrophil Recruitment to the Injured Brain. *J Neuropathology Exp Neurol* (2008) 67(3):223–30. doi: 10.1097/NEN.0b013e3181654957
63. Hayden MS, Ghosh S. NF-κb in Immunobiology. *Cell Res* (2011) 21(2):223–44. doi: 10.1038/cr.2011.13
64. Makita H, Nishimura M, Miyamoto K, Nakano T, Tanino Y, Hirokawa J, et al. Effect of Anti-Macrophage Migration Inhibitory Factor Antibody on Lipopolysaccharide-Induced Pulmonary Neutrophil Accumulation. *Am J Respir Crit Care Med* (1998) 158(2):573–9. doi: 10.1164/ajrccm.158.2.9707086
65. Bernhagen J, Krohn R, Lue H, Gregory JL, Zernecke A, Koenen RR, et al. MIF is a Noncognate Ligand of CXC Chemokine Receptors in Inflammatory and Atherogenic Cell Recruitment. *Nat Med* (2007) 13(5):587–96. doi: 10.1038/nm1567
66. Gregory JL, Leech MT, David JR, Yang YH, Dacumos A, Hickey MJ. Reduced Leukocyte–Endothelial Cell Interactions in the Inflamed Microcirculation of Macrophage Migration Inhibitory Factor–Deficient Mice. *Arthritis Rheumatism* (2004) 50(9):3023–34. doi: 10.1002/art.20470
67. David JR. Delayed Hypersensitivity *In Vitro*: Its Mediation by Cell-Free Substances Formed by Lymphoid Cell-Antigen Interaction. *Proc Natl Acad Sci* (1966) 56(1):72–7. doi: 10.1073/pnas.56.1.72
68. Bloom BR, Bennett B. Mechanism of a Reaction in Vitro Associated With Delayed-Type Hypersensitivity. *Science* (1966) 153(3731):80–2. doi: 10.1126/science.153.3731.80
69. Leech M, Metz C, Santos L, Peng T, Holdsworti-I SR, Bucala R, et al. Involvement of Macrophage Migration Inhibitory Factor in the Evolution of Rat Adjuvant Arthritis. *Arthritis Rheumatism* (1998) 41(5):910–7. doi: 10.1002/1529-0131(199805)41:5<910::AID-ART19>3.0.CO;2-E
70. Burger-Kentischer A, Göbel H, Kleemann R, Zernecke A, Bucala R, Leng L, et al. Reduction of the Aortic Inflammatory Response in Spontaneous Atherosclerosis by Blockade of Macrophage Migration Inhibitory Factor (MIF). *Atherosclerosis* (2006) 184(1):28–38. doi: 10.1016/j.atherosclerosis.2005.03.028
71. Schober A, Bernhagen J, Thiele M, Zeiffer U, Knarren S, Roller M, et al. Stabilization of Atherosclerotic Plaques by Blockade of Macrophage Migration Inhibitory Factor After Vascular Injury in Apolipoprotein E-Deficient Mice. *Circulation* (2004) 109(3):380–5. doi: 10.1161/01.CIR.0000109201.72441.09
72. Gregory JL, Morand EF, McKeown SJ, Ralph JA, Hall P, Yang YH, et al. Macrophage Migration Inhibitory Factor Induces Macrophage Recruitment *via* CC Chemokine Ligand 2. *J Immunol* (2006) 177(11):8072–9. doi: 10.4049/jimmunol.177.11.8072

Conflict of Interest: The authors declare that the research was conducted in the absence of any commercial or financial relationships that could be construed as a potential conflict of interest.

frontiers | Frontiers in Immunology

ORIGINAL RESEARCH
published: 26 April 2022
doi: 10.3389/fimmu.2022.883707

Mast Cells Drive Systemic Inflammation and Compromised Bone Repair After Trauma

Deniz Ragipoglu[1], Jasmin Bülow[1], Kristin Hauff[1], Martin Voss[2], Melanie Haffner-Luntzer[1], Anne Dudeck[2], Anita Ignatius[1] and Verena Fischer[1]**

[1] Institute of Orthopedic Research and Biomechanics, Trauma Research Center Ulm (ZTF), Ulm University Medical Center, Ulm, Germany, [2] Medical Faculty, Institute for Molecular and Clinical Immunology, Otto-von-Guericke University Magdeburg, Magdeburg, Germany

There is evidence that mast cells contribute to inflammation induced by hemorrhagic shock, severe tissue injury or sepsis. Mast cells are highly responsive to alarm signals generated after trauma, and release many inflammatory mediators including interleukin-6, a key mediator of posttraumatic inflammation. An overwhelming posttraumatic inflammation causes compromised bone healing; however, the underlying cellular and molecular mechanisms are poorly understood. Recently, we found that mast cells trigger local and systemic inflammation after isolated fracture leading to uneventful bone repair. Here, we investigated whether mast cells critically contribute to trauma-induced compromised bone healing. Male Mcpt5-Cre$^+$ R-DTA mice, which lack connective tissue type mast cells, and their mast cell-competent Cre$^-$ littermates underwent a femur fracture with/without thoracic trauma. Posttraumatic systemic and local inflammation and bone repair were assessed 3 h and 21 d post injury. Both, the systemic and pulmonary inflammation was significantly increased in mast cell-competent mice upon combined trauma compared to isolated fracture. In mast cell-deficient mice, the increase of inflammatory mediators in the circulation induced by the severe trauma was abolished. In the bronchoalveolar lavage fluid, the trauma-induced increase of inflammatory cytokines was not reduced, but the neutrophil invasion into the lungs was significantly diminished in the absence of mast cells. Locally in the fracture hematoma, mast cell-competent mice displayed reduced inflammatory mediator concentrations after combined trauma compared to isolated fracture, which was abolished in mast cell-deficient mice. Notably, while combined trauma resulted in compromised bone repair in mast cell-competent mice, indicated by significantly reduced bone and increased cartilage fracture callus contents, this was abolished in Mcpt5-Cre$^+$ R-DTA mice. Therefore, mast cells contribute to trauma-induced compromised bone repair and could be a potential target for new treatment options to improve fracture healing in multiply injured patients.

Keywords: mast cells, posttraumatic inflammation, fracture healing, trauma, interleukin-6

OPEN ACCESS

Edited by:
Klemens Horst, University Hospital RWTH Aachen, Germany

Reviewed by:
Dirk Henrich, University Hospital Frankfurt, Germany
Elizabeth R. Balmayor, Maastricht University, Netherlands

****Correspondence:***
Anita Ignatius
anita.ignatius@uni-ulm.de
Verena Fischer
verena.fischer@uni-ulm.de

Specialty section:
This article was submitted to Inflammation, a section of the journal Frontiers in Immunology

Received: *25 February 2022*
Accepted: *31 March 2022*
Published: *26 April 2022*

Citation:
Ragipoglu D, Bülow J, Hauff K, Voss M, Haffner-Luntzer M, Dudeck A, Ignatius A and Fischer V (2022) Mast Cells Drive Systemic Inflammation and Compromised Bone Repair After Trauma. Front. Immunol. 13:883707. doi: 10.3389/fimmu.2022.883707

INTRODUCTION

One of the most common forms of injuries in multi-trauma patients are extremity fractures. Depending on trauma severity, the risk for fracture malunion increases up to 50% (1, 2). Tissue trauma induces a systemic posttraumatic immune response triggered by damage-associated molecular patterns (DAMPs) being released from injured tissues (3). In multiply injured patients, the blunt chest trauma is clinically highly relevant, as it represents one of the most critical injures and is regarded as an important trigger of the systemic inflammatory response (3–5). Furthermore, 50% of patients with blunt chest trauma are additionally affected by fractures (6). The systemic hyper-inflammation after trauma is characterized by immune cell activation and a storm of pro-inflammatory mediators (3), which might negatively interfere with the inflammation and regenerative processes locally at the fracture site (7–10). In this line, it was demonstrated that the immune cell composition in the fracture hematoma was altered in a murine model of combined fracture and thoracic trauma, with a significantly higher number of neutrophils and a decreased number of macrophages (11, 12). In pigs, the levels of inflammatory mediators including interleukin-6 (IL-6), IL-8, IL-10 and the alarmin high-mobility-group-protein B-1 were altered in the fracture hematoma after an additional chest or polytrauma (13, 14). In humans, impaired bone healing was associated with altered leucocyte kinetics in multi-trauma patients (15). Furthermore, the blockade of posttraumatic inflammation appears to improve fracture healing after severe trauma. For example, it was demonstrated that IL-6, a key inflammatory cytokine in the posttraumatic immune response (16), may play a critical role in trauma-induced compromised fracture healing, because the selective blockade of IL-6 trans-signaling attenuated the deleterious effects of an additional blunt chest trauma on bone repair in mice (17). Similarly, the blockade of the complement anaphylatoxin receptor C5aR1 reduced the systemic immune response and ameliorated trauma-induced impaired fracture healing (18). In summary, these studies suggest that disturbed inflammatory processes and immune cell functions play an essential role in compromised bone healing after trauma; however, the underlying mechanisms remain poorly understood.

Mast cells store and *de novo* synthesize numerous mediators, including IL-6, tumor necrosis factor (TNF), histamine, heparin, enzymes, and growth factors. Acting as immunological guards, these cells are mainly located in tissues exposed to the external environment, including skin, intestines, and lungs but also in the bone marrow (19, 20). Because mast cells are highly responsive to early alarm signals that are generated after trauma including DAMPs and complement anaphylatoxins (19), they may be one of the critical drivers in posttraumatic inflammation and trauma-induced compromised fracture healing. Supporting this, some authors demonstrated that mast cells contribute to the inflammatory response induced by hemorrhagic shock, severe tissue injury, or ischemia-reperfusion injury (21–23). For example, the inhibition of mast cell degranulation with the mast cell-stabilizer cromolyn ameliorated severe consequences of ischemia-reperfusion injury in rodents (24). Moreover, the inflammatory response and multiple organ injury were attenuated after hemorrhagic shock in mast cell-deficient mice compared to wildtype mice (21), and after mast cell stabilization using ketotifen and cromolyn in rats (25).

Mast cells appear to also play an important role in fracture healing (26–28). Our group demonstrated that bone resident mast cells trigger local and systemic inflammatory processes after an isolated fracture, a model for undisturbed bone repair. In mast cell-deficient Mcpt5-Cre R-DTA mice, which lack connective tissue mast cells, the levels of proinflammatory cytokines, including IL-6, IL-1β, and interferon-γ, and the number of neutrophils and macrophages were significantly reduced in the fracture hematoma. In addition, systemic levels of pro-inflammatory cytokines were also reduced in the absence of mast cells (26). Moreover, mast cells might contribute to bone formation and callus remodeling during bone repair (27, 28), because they were shown, for example, to stimulate osteoclast formation and activity during fracture callus resorption (26). Recently, we additionally revealed that mast cells were responsible for the increased fracture-induced systemic and local inflammatory response and for compromised healing in osteoporotic bone (29, 30). These data suggest that mast cells regulate inflammation and repair during bone fracture healing. However, their role in compromised fracture healing after severe trauma has, to date, not been elucidated.

The present study aimed to investigate, whether mast cells critically contribute to trauma-induced compromised bone repair. To this end, we exposed mast cell-deficient Mcpt5-Cre R-DTA mice to an isolated femur fracture, which heals uneventfully, or to combined fracture and thoracic trauma, inducing more severe inflammation and compromised fracture healing. We demonstrated, that mast cell-deficient mice displayed a balanced systemic and local inflammatory response and were protected from compromised bone healing after severe trauma. Therefore, this study implies that mast cells could be a target for new therapeutic strategies to improve bone repair in multiply injured patients.

MATERIALS AND METHODS

Study Design

The experiments were performed in male Mcpt5-Cre R-DTA mice (C57BL/6J background). These mice express diphtheria toxin (DT) under the control of the Mcpt5 promoter, which is specific for connective tissue type mast cells and drives Cre-specific mast cell ablation in these mice (mast cell-deficient). Male Mcpt5-Cre$^-$ R-DTA littermates were used as mast cell-competent controls. Mice were bred as described previously (31, 32). The animals were housed in groups of two to five mice under standard rodent conditions. When aged 12 weeks, the mice were randomly assigned to the different treatment groups either subjected to isolated femur fracture (Fx) or a combined fracture and thoracic trauma (Fx + TxT). Mice were euthanized 3 h, 6 h and 21 d after injury (n = 3–8 per group and time point) using isoflurane overdose. Blood, bronchoalveolar

lavage (BAL) fluids and tissues (fracture hematoma, femur, lung, liver) were harvested for multiplex analysis (blood, BAL), tissue histology (lung, femur), gene expression analysis (liver), and μCT and biomechanical testing (femur). Samples were allocated in a blinded manner to the different analyses, which were performed only on a subset of tissue specimens due to technical reasons. All animal experiments were performed in compliance with international regulations for the care and use of laboratory animals (ARRIVE guidelines and EU Directive 2010/63/EU for animal experiments) with the approval of the Local Ethical Committee (no. 1386, Regierungspraesidium Tuebingen, Germany).

Femur Osteotomy and Thoracic Trauma

When aged 12 weeks, all mice were subjected to a standardized unilateral femur osteotomy as described previously (33). Briefly, under general anesthesia with 2% isoflurane, an osteotomy gap (gap size: 0.44 mm) was created at the mid-shaft of the femur using a 0.44 mm Gigli wire saw (RISystem, Davos, Switzerland) that was stabilized with an external fixator (axial stiffness 3 N/mm, RISystem). The external fixator prevents torsional stability, which results in defined and standardized biomechanical conditions that greatly influence the fracture healing process, and does not impede with biological reactions at the fracture site (33, 34). Prior to the surgery the mice received one subcutaneous injection of the antibiotic clindamycin-2-dihydrogenphosphate (45 mg/kg, Ratiopharm, Ulm, Germany). Half of the mast cell-competent and mast cell-deficient mice received an additional thoracic trauma immediately after the fracture while the mice were still under general anesthesia as previously described (11, 17). Briefly, using a blast-wave generator, a single blast wave was applied to the middle of the thorax, which produces a standardized bilateral, isolated lung contusion. For pain treatment, all mice received tramadol hydrochloride (25 mg/l) in the drinking water starting 1 d pre-surgery until 3 d post-surgery.

Multiplex Cytokine Analysis and ELISA

To assess the systemic and local inflammation, serum, BAL, and hematoma were obtained 3 h post-fracture. The lungs were flushed with ice-cold phosphate-buffered saline, and BAL fluids were centrifuged at 300 × *g* for 15 min (35). The fracture hematoma was harvested and lysed as previously described (17). A customized mouse Multiplex Cytokine Kit (ProcartaPlex, eBioscience, Frankfurt, Germany) was used to determine blood serum, BAL, and hematoma concentrations of the following inflammatory cytokines and chemokines using the Bio-Plex 200 System (Bio-Rad Laboratories, Hercules, CA, USA): IL-6, IL-5, C-X-C motif chemokine-10 (CXCL-10), monocyte chemoattractant protein-1 (MCP-1), MCP-3, eotaxin, CXCL-1, IL-10, IL-9, and IL-3. Instrument validation was performed monthly using the Bio-Plex Validation Kit (Bio-Rad Laboratories) and calibration was performed prior to sample measurement using the Bio-Plex Calibration Kit (Bio-Rad Laboratories) according to the manufacturers protocol, respectively. Total protein concentration of the fracture hematoma was determined with the Pierce™ BCA Protein Assay Kit and the cytokine concentrations were normalized to total protein.

Liver Homogenates and Real-Time PCR

Liver lobes were harvested 3 h after surgery, immediately frozen in liquid nitrogen, and stored at −80°C until homogenates were prepared. A small piece was taken from each frozen liver sample, and homogenized in Trizol, using a homogenisator (MICCRA D-9, MICCRA GmbH, Müllheim, Germany), and incubated for 5 min at room temperature (RT). Subsequently, 200 μl chloroform were added and vigorously vortexed before centrifugation at 12,000 × *g* for 30 min. Following centrifugation, the supernatants were collected, and the RNA was isolated using the PureLink® Mini Kit (Thermo Fisher Scientific, Waltham, MA, USA) according to the manufacturer's recommendations. The isolated RNA was diluted in RNase-free water after DNase digestion. Further processing and qPCR analysis were performed as previously described (36, 37). Glyceraldehyde 3-phosphate dehydrogenase (*Gapdh*) served as a housekeeping gene (F: 5′-ACC CAG AAG ACT GTG GAT GG-3′, R: 5′-GGA TGC AGG GAT GAT GTT CT-3′). The expression of chemokines and acute-phase proteins was determined using specific primers for *Cxcl-1* (F: 5′-TCT CCG TTA CTT GGG GAC AC-3′, R: 5′-CCA CAC TCA AGA ATG GTC GC-3′), and C-reactive protein (*Crp)* (F: 5′-ATC CCA GCA GCA TCC ATA GC-3′, R: 5′-AAC ATG TCT TCA TGA CCA AAA GTC C-3′). Relative gene expression was calculated by normalizing to the house keeping gene *Gapdh* using the delta-delta CT method.

Lung Histomorphometry and Immunohistochemistry

Lungs harvested after 3 h and 6 h were fixed in 4% paraformaldehyde for 48 h and embedded in paraffin. For morphological analysis of lung injury, paraffin-embedded lung sections harvested 3 h after surgery were stained with hematoxylin and eosin. Neutrophil granulocytes and mucosal mast cells were stained using Ly6G antibody (1:200, BioLegend, CA, USA) and Mcpt-1 antibody (1:100, Invitrogen, MA, USA), 3 h and 6 h after surgery, respectively. To this end, lung sections were deparaffinized in xylene, rehydrated in descending ethanol gradient, and boiled in sodium citrate buffer for antigen retrieval. Sections were blocked with 5% goat serum for 1h at RT and incubated with the primary antibodies. Species-specific IgG was used as negative control for Ly6G staining and rabbit serum for Mcpt-1 staining. As secondary antibody, goat anti-rat IgG-biotin (1:200 and 1:100 (Life Technologies, Carlsbad, CA, USA), respectively, for Mcpt-1 and Ly6G staining) was used and incubated at RT for 1 h (Mcpt-1) or 30 min (Ly6G). For signal detection, the Vectastain Elite ABC kit and Vector NovaRed substrate (both Vector laboratories Inc., Burlingame, USA) were used according to the manufacturer's instructions. Sections were counterstained with hematoxylin and analyzed by light microscopy (Leica DMI600B, Leica, Wetzlar, Germany).

Biomechanical Testing

To evaluate the mechanical competence of healed femurs explanted on d 21, a non-destructive three-point bending test

was performed as described previously (33). In brief, the external fixator was removed and femurs were fixed with aluminum cylinders into a material testing machine (Zwick Roell, Ulm, Germany). An axial load with a maximum of 2 N was applied to the top of the fracture callus at the midshaft of the femur and the load and deflection were recorded. The bending stiffness of the fractured bone was calculated from the slope of the load-deflection curve.

Micro-Computed Tomography (μCT) Analysis

Following biomechanical testing, fractured femurs were fixed in 4% paraformaldehyde for 48 h. Femurs were scanned using a μCT device (Skyscan 1172; Bruker, Kontrich, Belgium) to evaluate the structural properties of the fracture calli at an isotropic voxel resolution of 8 μm using a voltage of 50 kV and 200 mA. Two phantoms with a defined hydroxyapatite (HA) content were used for calibration and the assessment of bone mineral density (250 and 750 mgHA/cm^3). The volume of interest comprised the entire periosteal callus between the two inner pin-holes. A global threshold for mineralized tissue was set at 642 mgHA/cm^3 and data were analyzed according to Bouxsein et al. (38).

Fracture Calli Histomorphometry and Immunohistochemistry

Histological analysis was performed on fracture calli on d 21 post-fracture. Following μCT analysis, fractured bones were decalcified using 20% ethylenediamine tetraacetic acid (pH 7.2–7.4) and embedded in paraffin. Sections of 7 μm were stained with Safranin O (Sigma Aldrich, St. Louis, MO, USA) and the relative amounts of bone, cartilage and soft tissue were evaluated by image analysis (Software MMAF 1.4.0 MetaMorph, Leica) using a light microscope (Leica DMI600B, Leica). The fracture gap was defined as a region of interest. Osteoblasts were counted in Toluidine blue-stained sections and osteoclasts in sections stained for tartrate-resistant acid phosphatase in a rectangular area (650 × 450 μm) in the middle of the fracture callus.

For immunofluorescence staining, 4 μm thick sections of the fracture calli on d 21 post-fracture were prepared and Avidin Texas Red conjugated antibody (Thermo Fisher Scientific, MA, USA) was used to detect connective tissue type mast cells. Bone sections were deparaffinized, rehydrated, and antigen retrieval was performed using sodium citrate buffer boiling, followed by blocking with 5% bovine serum albumin and incubation with the Avidin Texas Red antibody (1:300) for 1 h at RT. Mast cell-deficient mice were used as negative controls. For signal detection, a spectrum with excitation and emission maxima of ~595/615 nm was used. Hoechst (1:2000) was used for counterstaining and sections were analyzed by light microscopy (Leica DMI600B, Leica). Mast cells were counted in the entire periosteal callus and the bone marrow between the two inner pinholes.

Statistical Analysis

In all figures, data are presented as box-and-whisker plots (with the median and interquartile range) from maximum to minimum, showing all data points. Data in tables are presented as mean ± standard deviation. Data were tested for normal distribution using Shapiro-Wilk normality test. Comparisons between two groups were either performed by two-tailed Student's t-test in the case of normal distribution or Mann-Whitney U test if data were not normally distributed. Comparisons between more than two groups were either performed by one way analysis of variance (ANOVA) and Fishers LSD *post hoc* test in the case of normal distribution or Kruskal-Wallis and Dunn's *post hoc* test if data were not normally distributed. Statistical analysis was performed using GraphPad Prism 9.0 software (GraphPad Software, La Jolla, CA, USA). The level of significance was set at $p<0.05$. The sample numbers are indicated in the figures.

RESULTS

No animals were lost during anaesthesia, however, 3 animals died after thoracic trauma. Furthermore, we excluded 4 animals due to post-surgery complications (sample handling, fracture gap size), which resulted in a total complication rate of 10%. All animals tolerated the external fixator well and showed normal and physiological limb loading few days after fracture.

Mast Cell-Deficiency Attenuates Trauma-Induced Systemic Inflammation

To investigate the relevance of mast cells in compromised bone repair after severe trauma, we subjected mast cell-competent and -deficient mice to an isolated femur fracture or combined fracture and thoracic trauma. Confirming our previous studies, in mast cell-competent control mice, the additional thoracic trauma led to an increased inflammatory response 3 h after fracture, as indicated by significantly increased serum IL-6, IL-5, CXCL-10, MCP-3, and eotaxin levels compared to mice with an isolated fracture (**Figures 1A–E**). There were no significant differences in MCP-1 levels between the groups detectable (**Figure 1F**). In **Table 1** all other inflammatory mediators are displayed that were detectable in the serum. Notably, mast cell-deficient mice did not display increased serum concentrations of inflammatory cytokines after combined trauma, with the exception of CXCL-10, the levels of which were significantly increased compared to isolated fracture (**Figures 1A–E**). However, serum IL-6 and CXCL-10 levels were significantly reduced compared to mast cell-competent mice after additional thoracic trauma (**Figures 1A, B**).

Furthermore, the systemic hepatic acute-phase response was strongly reduced in the absence of mast cells after isolated fracture, as well as after combined fracture with thoracic trauma, as indicated by significantly reduced *Crp* and *Cxcl-1* gene expression compared to the respective mast cell-competent groups (**Figures 2A, B**). In summary, mast cell-deficiency attenuated the early trauma-induced systemic inflammation.

Mast Cell-Deficiency Only Marginally Influences Trauma-Induced Lung Inflammation

In the lungs, the combined trauma significantly increased the levels of inflammatory mediators in BAL fluids of mast cell-competent mice after 3 h, including IL-6, IL-5, MCP-3, eotaxin and MCP-1, compared to the isolated fracture (**Figures 3A, C–F**).

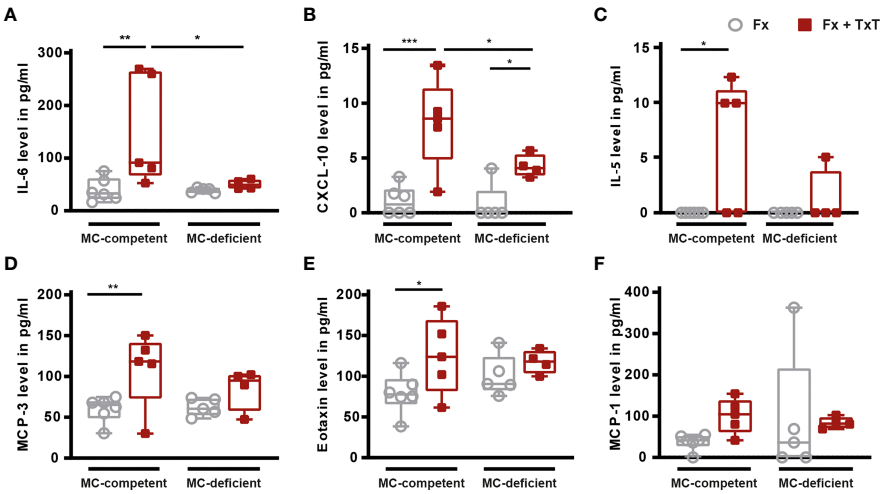

FIGURE 1 | Inflammatory mediator concentrations in serum of mast cell (MC)-competent and MC-deficient mice 3 h after isolated fracture (Fx) and combined fracture and thoracic trauma (Fx + TxT). Serum **(A)** interleukin-6 (IL-6), **(B)** C-X-C motif chemokine ligand 10 (CXCL-10), **(C)** IL-5, **(D)** monocyte chemoattractant protein-3 (MCP-3), **(E)** eotaxin, and **(F)** MCP-1 levels. Gray boxes represent Fx mice, red boxes represent Fx + TxT mice. Data are shown as box-and-whisker plots (with median and interquartile range) from maximum to minimum, showing all data points. *p<0.05; **p<0.01; ***p<0.001. The p values were determined using one-way ANOVA with *post hoc* Fisher's LSD in the case of normal distribution or with Kruskal-Wallis with *post hoc* Dunn's test if data were not normally distributed.

BAL CXCL-10 levels were also tendentially increased in mast cell-competent mice in the combined trauma group (**Figure 3B**). Other measured inflammatory mediators in BAL fluids are presented in **Table 1**. Notably, pro-inflammatory mediator concentrations in BAL fluids were not significantly reduced in the absence of connective tissue type mast cells (**Figures 3A–F**), with the exception of IL-13 and IL-9, the levels of which were significantly lower in mast cell-deficient mice after combined trauma (**Table 1**).

Furthermore, the combined trauma caused lung tissue damage and inflammation in mast cell-competent mice, as indicated by the presence of thicker alveolar walls and blood clots 3 h after fracture (**Figure 4C**). This effect was not obviously affected by the absence of connective tissue type mast cells (**Figure 4C**). However, the neutrophil infiltration into the lung was significantly increased only in mast cell-competent mice after combined trauma, but markedly reduced in mast cell-deficient mice (**Figures 4A, D**). Lungs of mast cell-competent and mast cell-deficient mice contained mucosal type mast cells 6 h after trauma (**Figures 4B, E**), but there were no differences visible between the isolated fracture and the fracture and thoracic trauma groups, which was probably influenced by the small sample size and high standard deviations.

Mast Cell-Deficiency Alters Local Inflammation at the Fracture Site After Trauma

To investigate the local inflammation at the fracture site, we determined inflammatory cytokine and chemokine concentrations in the fracture hematoma after 3 h. The combined trauma significantly reduced local levels of inflammatory mediators in the fracture hematoma of mast cell-competent mice, including IL-6, IL-

TABLE 1 | Inflammatory mediator levels in serum and BAL fluids.

	MC-Competent		MC-Deficient	
	Fx	Fx + TxT	Fx	Fx + TxT
Serum				
IL-17a	3.9 ± 4.0	7.4 ± 14.0	0.6 ± 0.8	0.7 ± 0.8
CXCL-1	266.5 ± 182.3	420.6 ± 207.7	126.4 ± 124.8	269.1 ± 205.7
BAL				
CXCL-1	3.4 ± 7.2	51.0 ± 83.0	1.8 ± 4.1	40.1 ± 50.1
IL-10	17.7 ± 16.8	17.1 ± 13.5	18.1 ± 11.7	2.2 ± 3.2
IL-13	3.7 ± 2.5	3.9 ± 2.8	5.0 ± 4.1	0.8 ± 1.2*
IL-9	58.7 ± 56.4	38.7 ± 55.3	79.8 ± 80.6	0.0 ± 0.0*

Significantly different (p<0.05) compared to the Fx group, one-way ANOVA with post hoc Fisher's LSD in the case of normal distribution or with Kruskal-Wallis with post hoc Dunn's test if data were not normally distributed. MC, mast cell; Fx, isolated fracture; Fx + TxT, fracture and additional thoracic trauma; IL, Interleukin; CXCL, C-X-C motif chemokine ligand; BAL, bronchoalveolar lavage.

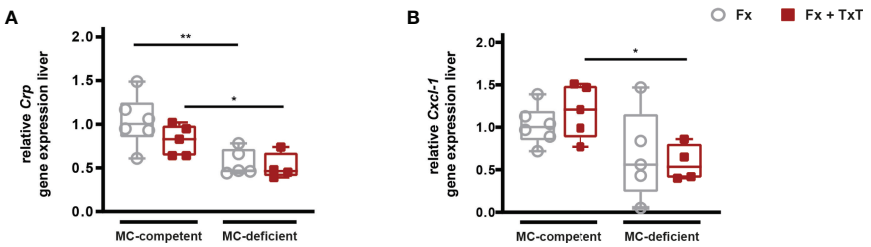

FIGURE 2 | Hepatic acute-phase reaction in mast cell (MC)-competent and MC-deficient mice 3 h after fracture (Fx) and combined fracture and thoracic trauma (Fx + TxT). Relative gene expression of **(A)** C-reactive protein (*Crp*) and **(B)** C-X-C motif chemokine ligand 1 (*Cxcl-1*) in the liver. Relative gene expression was calculated by normalizing to the house keeping gene *Gapdh*. Gray boxes represent Fx mice, red boxes represent Fx + TxT mice. Data are shown as box-and-whisker plots (with median and interquartile range) from maximum to minimum, showing all data points. *p<0.05; **p<0.01. The p values were determined using one-way ANOVA with *post hoc* Fisher's LSD.

5, CXCL-1, and MCP-1 and -3 (**Figures 5A, C–F**). Additionally, hematoma CXCL-10 levels were tendentially reduced in mast cell-competent mice (**Figure 5B**). Notably, these mediators were not reduced in the fracture hematoma of mast cell-deficient mice after combined trauma, with the exception of IL-6, the levels of which were also significantly reduced in mast cell-deficient mice (**Figure 5A**).

Mast Cell-Deficiency Attenuates Compromised Fracture Healing After Trauma

On d 21 after fracture, bone repair was assessed by biomechanical testing, µCT, and histomorphometric analyses. In mast cell-competent mice, the combined trauma significantly impaired fracture healing compared to isolated fracture (**Figures 6A–D**), as indicated by a slightly reduced bending stiffness of the fractured bones, and a significantly reduced bone volume to tissue volume (BV/TV) of the callus as assessed by µCT analysis (**Figures 6B, D**). Histomorphometric evaluation revealed that the callus size was significantly increased in mast cell-competent mice after combined trauma (**Figures 7A, F**). Furthermore, the combined fracture and thoracic trauma led to a significant reduction of the amount of newly formed bone and a significant increase of the amount of cartilage in the callus of mast cell-competent mice (**Figures 7B, C, F**). The amount of soft tissue was unaffected (**Figures 7D, F**). Notably, mast cell-deficient mice did not display compromised bone healing after combined trauma, because the bone and cartilage contents did not differ compared to mast cell-

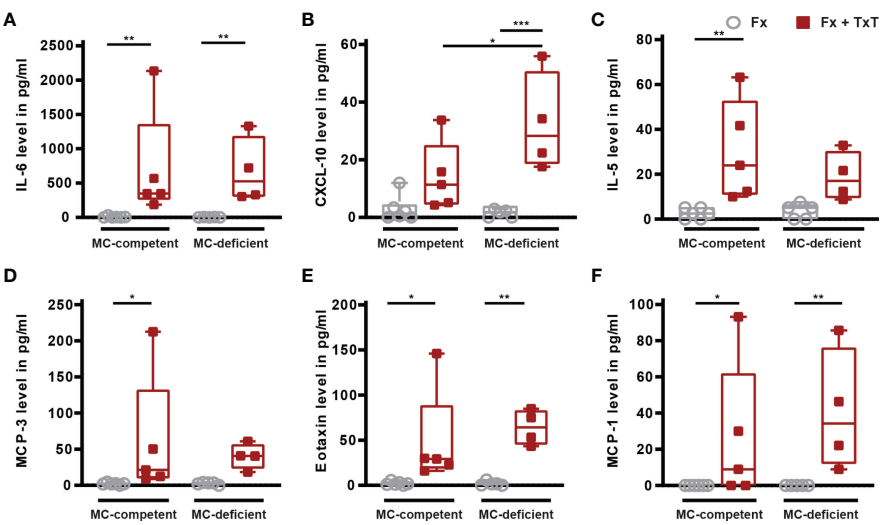

FIGURE 3 | Inflammatory mediator concentrations in bronchoalveolar lavage (BAL) fluid samples of mast cell (MC)-competent and MC-deficient mice 3 h after isolated fracture (Fx) and combined fracture and thoracic trauma (Fx + TxT). BAL fluids **(A)** interleukin-6 (IL-6), **(B)** C-X-C motif chemokine ligand 10 (CXCL-10), **(C)** IL-5, **(D)** monocyte chemoattractant protein-3 (MCP-3), **(E)** eotaxin, and **(F)** MCP-1 levels. Gray boxes represent Fx mice, red boxes represent Fx + TxT mice. Data are shown as box-and-whisker plots (with median and interquartile range) from maximum to minimum, showing all data points. *p<0.05; **p<0.01; ***p<0.001. The p values were determined using one-way ANOVA with *post hoc* Fisher's LSD in the case of normal distribution or with Kruskal-Wallis with *post hoc* Dunn's test if data were not normally distributed.

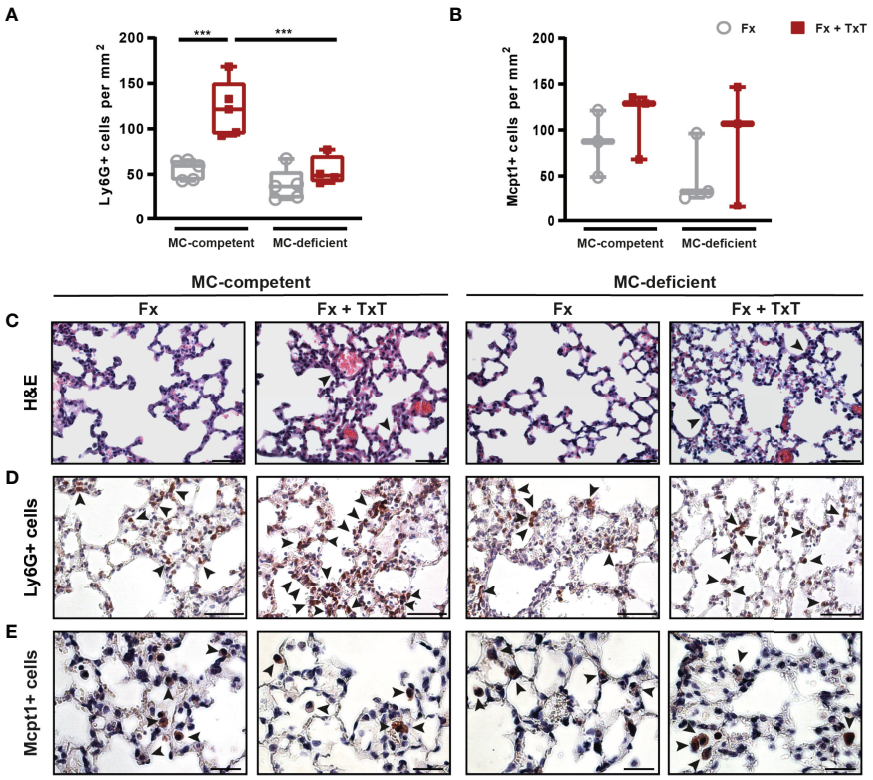

FIGURE 4 | Pulmonary inflammation in mast cell (MC)-competent and MC-deficient mice 3 and 6 h after isolated fracture (Fx) and combined fracture and thoracic trauma (Fx + TxT). **(A)** Number of Ly6G+ cells (neutrophils) in the lung of MC-competent and MC-deficient mice after 3 h. **(B)** Number of Mcpt1+ cells (mucosal mast cells) in the lung of MC-competent and MC-deficient mice after 6 h. **(C)** Representative images of hematoxylin and eosin (H&E) stained lungs of MC-competent and MC-deficient mice. Arrowheads indicate wall thickening. Scale bar = 50 µm. **(D)** Representative images of lungs stained for neutrophils (Ly6G+). Arrowheads indicate positively stained neutrophils. Scale bar = 50 µm. **(E)** Representative images of lungs stained for mucosal mast cells in MC-competent and MC-deficient mice after 6 h. Arrowheads indicate positively stained mast cells (Mcpt-1+). Scale bar = 25µm. Gray boxes represent Fx mice, red boxes represent Fx + TxT mice. Data are shown as box-and-whisker plots (with median and interquartile range) from maximum to minimum, showing all data points. ***p<0.001. The p values were determined using one-way ANOVA with *post hoc* Fisher's LSD.

competent mice with isolated fracture (**Figure 7**), suggesting that mast cells contribute to compromised bone repair after trauma.

In the fracture callus on d 21, osteoclast numbers were significantly reduced in mast cell-deficient mice with isolated fracture and with the combined trauma compared to the respective mast cell-competent mice (**Figures 8A, D**). By contrast, osteoblast numbers did not differ between mast cell-competent and mast cell-deficient mice of both the isolated fracture and combined trauma groups (**Figure 8B**). Interestingly, in mast cell-competent mice with an additional thoracic trauma, the number of connective tissue type mast cells was significantly increased in the fracture callus on d 21 (**Figures 8C, E**). As expected, in mast cell-deficient mice, there were no connective tissue type mast cells detectable in both groups (**Figures 8C, E**).

DISCUSSION

The present study investigated the role of mast cells in the pathology of compromised bone fracture healing after severe trauma. Using mast cells-deficient Mcpt5-Cre R-DTA mice that lack connective tissue type mast cells (31), we showed that mast cells contribute to the increased systemic posttraumatic inflammation after severe trauma and a dysregulated early immune response locally at the fracture site, which results in trauma-induced compromised bone repair. These results implicate that mast cells could be a target for new therapeutic strategies to improve bone repair in multiply injured patients.

Mast cells may be the first line of cellular defense after trauma because of their high responsiveness to alarm signals generated after injury such as complement anaphylatoxins or DAMPs, and their release of pre-formed and *de novo* synthesized inflammatory mediators (19). However, nothing is known about their involvement in trauma-induced compromised bone repair, which is frequently observed in multiply injured patients (2). Thereby, we focused on the early inflammatory phase, which is strongly affected by the additional trauma, and on the later repair phase, which serves as a read-out for successful fracture healing, and where mast cells were already shown to play an important role during fracture repair (26, 29). In agreement with

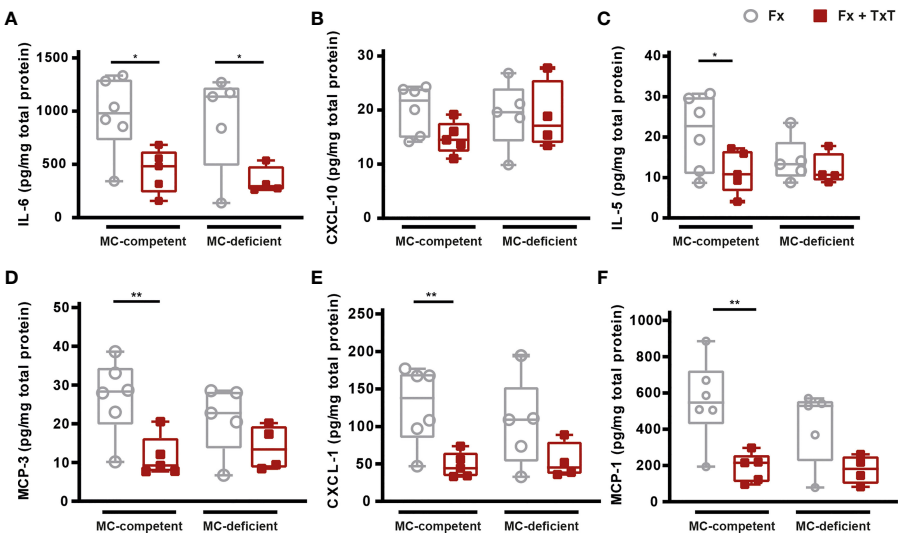

FIGURE 5 | Local inflammation in the fracture hematoma of mast cell (MC)-competent and MC-deficient mice 3 h after isolated fracture (Fx) and combined fracture and thoracic trauma (Fx + TxT). Hematoma **(A)** interleukin-6 (IL-6), **(B)** C-X-C motif chemokine ligand 10 (CXCL-10), **(C)** IL-5, **(D)** monocyte chemoattractant protein-3 (MCP-3), **(E)** CXCL-1, and **(F)** MCP-1 levels. Gray boxes represent Fx mice, red boxes represent Fx + TxT mice. Data are shown as box-and-whisker plots (with median and interquartile range) from maximum to minimum, showing all data points. *p<0.05; **p<0.01. The p values were determined using one-way ANOVA with *post hoc* Fisher's LSD in the case of normal distribution or with Kruskal-Wallis with *post hoc* Dunn's test if data were not normally distributed.

previous experimental studies (7, 11, 13, 17, 26, 39–42), the model of combined fracture and thoracic trauma used in the present study induced an increased systemic inflammation after 3 h in mast cell-competent mice as indicated by elevated serum IL-6, CXCL-10, MCP-3, IL-5 and eotaxin levels. IL-6 is one of the key cytokines of posttraumatic inflammation and its level correlates with injury severity and mortality in trauma patients (16, 30, 43). The chemokine CXCL-10 drives leukocyte recruitment and activation (44), whereas IL-5 and eotaxin are key mediators of eosinophil activation (45, 46). MCP-1 is a chemoattractant for monocytes (47), and MCP-3 recruits distinct leukocyte subtypes to injured tissues (48). Moreover, the concomitant thoracic trauma induced pulmonary inflammation, indicated by lung damage, increased inflammatory mediators in the BAL fluids, including IL-6, IL-5, eotaxin, MCP-3, and MCP-1, and increased neutrophil infiltration into the lungs in mast cell-competent mice. These findings are in agreement with previous investigations of trauma models in mice (11, 12, 17, 35) and pigs (14). In the fracture hematoma, the concomitant thoracic trauma significantly reduced the levels of inflammatory mediators in mast cell-competent mice after 3 h. Supporting our data, Horst et al. also found lower IL-6 and IL-8 concentrations locally in the fracture hematoma of pigs after a combined trauma compared to an isolated fracture (42). The deficiency of critical pro-inflammatory mediators during the early inflammatory phase of bone repair was proposed to hamper effective mesenchymal stem cell recruitment and, consequently, bone regeneration (49). Fracture hematoma mediator concentrations are highly dynamic and change rapidly after trauma (13, 42), which is why results might differ at later observation time points. However, as a limitation of our study, we did not include later observation time points during the inflammatory phase. Confirming previous data (11, 12, 17), mast cell-competent mice of the combined trauma group displayed compromised fracture healing at d 21 as indicated by a reduced bone content and increased cartilage residuals in the fracture callus. Interestingly, mast cell numbers were significantly increased in the callus of mast cell-competent mice after combined trauma. This further indicates a direct pathological role of these cells in this context.

Confirming this hypothesis, our study revealed that mast cell-deficient mice displayed a diminished systemic inflammatory response, an altered immune response in the fracture hematoma and uneventful bone repair after combined trauma, indicating that mast cells might contribute to trauma-induced compromised bone repair. Supporting our findings, others previously revealed that mast cell-deficiency increased survival rates after acute sepsis (50). In hemorrhagic shock, mast cell stabilization using cromolyn or doxantrazole, respectively, improved cardiac contractility (25), and the outcome of gut and lung injury in mice (51). Here, we found that mast cell-deficient mice displayed reduced systemic IL-6 and CXCL-10 levels compared to mast cell-competent mice after combined injury. Consequently, mast cells might contribute to posttraumatic inflammation after combined fracture and thoracic trauma by the release of the mentioned factors. Mast cells store considerable amounts of IL-6 and can rapidly *de novo* synthesize IL-6 after activation (52, 53). *In vitro*, mast cells were shown to release IL-6 in response to lipopolysaccharide stimulation (54). In sepsis, mast cells are a critical source for IL-6, because mice with a mast cell-specific IL-6 depletion displayed diminished survival and bacterial clearance in a cecal ligation and puncture model (55). Supporting our findings, systemic cytokine concentrations,

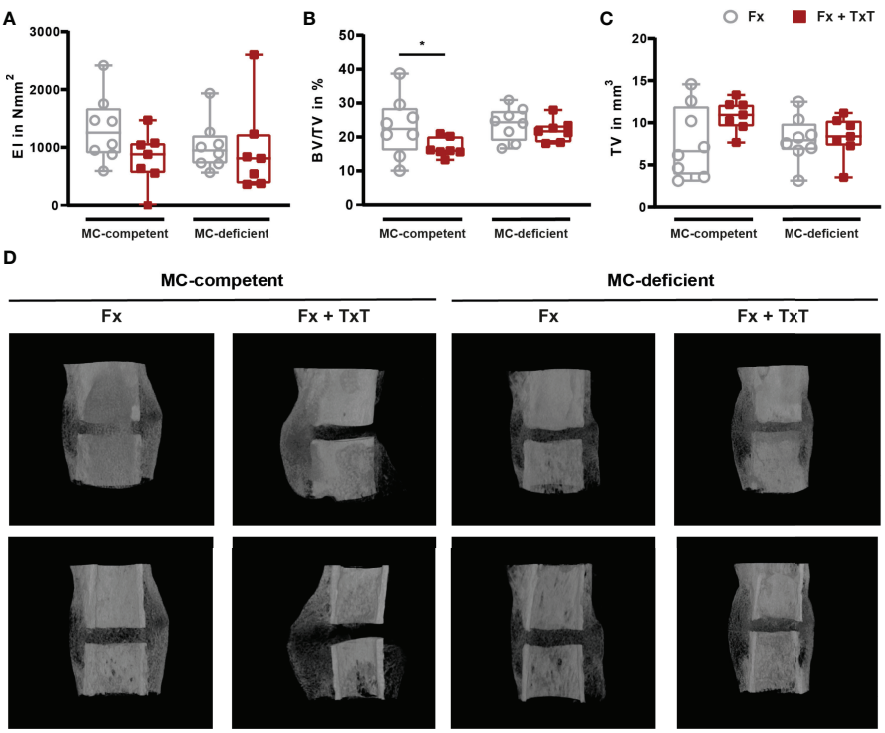

FIGURE 6 | Biomechanical and µCT analyses from fractured femurs of mast cell (MC)-competent and MC-deficient mice 21 d after isolated fracture (Fx) and combined fracture and thoracic trauma (Fx + TxT). **(A)** Bending stiffness (EI) of fractured femurs. **(B)** Bone volume to tissue volume (BV/TV) in the periosteal fracture callus. **(C)** Tissue volume (TV) of the periosteal fracture callus. **(D)** Representative images from µCT three-dimensional reconstructions of the fracture area recorded at similar settings. Gray boxes represent Fx mice, red boxes represent Fx + TxT mice. Data are shown as box-and-whisker plots (with median and interquartile range) from maximum to minimum, showing all data points. *p<0.05. The p values were determined using one-way ANOVA with *post hoc* Fisher's LSD.

including IL-6 levels, were reduced in mast cell-deficient mice after hemorrhagic shock and multiple organ injury was improved (21). Furthermore, mast cell-deficient mice displayed diminished IL-6 levels and improved coronary inflammation in response to stress-induced trauma (56). In addition, systemic inflammatory mediator levels, including IL-6 and CXCL-10, were reduced in mast cell-deficient mice during regular and ovariectomy-induced compromised bone repair, indicating that mast cells contribute to fracture-induced inflammation (26, 29). Mast cell stabilization using cromolyn in mice improved the outcome of ischemic-reperfusion injury associated with reduced blood IL-6 and TNF levels (24). IL-6 is a strong inducer of the hepatic acute-phase response (57), which is initiated after tissue injury or inflammation (58). Interestingly, the posttraumatic liver *Crp* and *Cxcl-1* expression was considerably reduced in mast cell-deficient mice after combined trauma, suggesting that mast cell-released IL-6 might critically regulate the acute-phase response after trauma. Moreover, mast cells are able to produce CXCL-10 (59), which was recently also shown by our group *in vitro* and *in vivo* to be present in the murine fracture callus (29). Supporting this, *in vitro* data showed that mast cells release CXCL-10 upon respiratory virus infection (60), and stimulate airway muscle cells to produce CXCL-10 (61). Furthermore, mast cell numbers correlated with CXCL-10 expression in asthma (62). The IL-5, MCP-3, and eotaxin levels were also significantly reduced in mast cell-deficient mice after combined trauma. It was shown that mast cells produce and release IL-5 in asthma (63), and that mast cell-released IL-5 contributes to intestinal inflammatory disease (64). Both Eotaxin and MCP-3 are produced by mast cells (59), however, nothing is known about the involvement of mast cell-released eotaxin or MCP-3 in other trauma settings. Concluding, our results suggest that mast cell-released inflammatory mediators contribute to trauma-induced systemic inflammation after concomitant thoracic trauma.

In the lungs, MC-deficient mice also displayed an increased pulmonary inflammation in response to the combined trauma, because BAL fluid IL-6, CXCL-10 and MCP-1 levels were elevated. Importantly, the lungs of mice contain both, connective tissue and mucosal mast cells (65, 66). It was previously shown, and is also supported by our findings in the lung, that Mcpt5-Cre R-DTA mice display mucosal mast cells (31), which might explain the increased pulmonary inflammation observed after trauma in both groups. Moreover, other immune cells secrete inflammatory cytokines after lung injury, including tissue-resident macrophages and T cells (67), and could thereby contribute to pulmonary inflammation in our model. However, our study was limited in that we did not investigate further immune cell populations, except

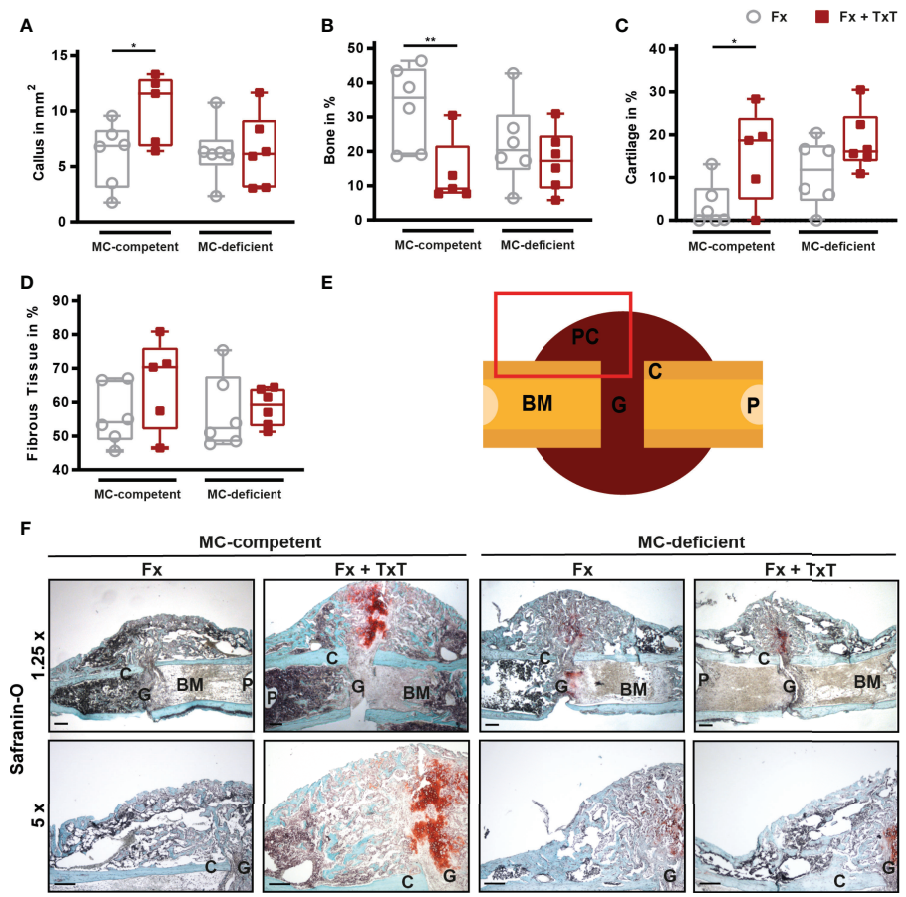

FIGURE 7 | Histomorphometrical analysis from fractured femurs of mast cell (MC)-competent and MC-deficient mice 21 d after isolated fracture (Fx) and combined fracture and thoracic trauma (Fx + TxT). Sections of fractured femurs were stained with Safranin O and **(A)** callus size, **(B)** relative bone area, **(C)** relative cartilage area, and **(D)** relative fibrous tissue area were determined by histomorphometric analysis. **(E)** Schematic illustration of the area (red rectangle) of the fracture callus that was illustrated in F bottom. C = cortex, G = gap, P = pin hole, PC = periosteal callus, BM = bone marrow. **(F)** Representative images from the periosteal fracture callus stained with Safranin O in 1.25 x (top) and 5 x (bottom). Scale bar (top) = 500 µm; scale bar (bottom) = 200 µm. Gray boxes represent Fx mice, red boxes represent Fx + TxT mice. Data are shown as box-and-whisker plots (with median and interquartile range) from maximum to minimum, showing all data points. *p<0.05; **p<0.01. The p values were determined using one-way ANOVA with post-hoc Fisher's LSD.

neutrophils, in the lungs of our mice. Interestingly, neutrophil infiltration in the lung was reduced in mast cell-deficient mice compared to mast cell competent-mice after thoracic trauma. One possible explanation for this might be that the systemically reduced chemokine concentrations of CXCL-10, eotaxin and MCP-1 in mast cell-deficient mice attenuated neutrophil recruitment from the bone marrow to the inflamed lung (68–70). Supporting this hypothesis, liver *Cxcl-1* expression was significantly reduced in mast cell-deficient mice compared to -competent mice after combined trauma. Alternatively, this might indicate a special role of lung connective tissue type mast cells for neutrophil recruitment into the lung after thoracic trauma. Supporting this, mast cells have been demonstrated to recruit neutrophils, for example, *via* CXCL-1 during tissue inflammation, or IL-1β in urticaria (71, 72). Concluding, while mast cell-deficiency did not abolish trauma-induced lung inflammation, it did influence it.

In contrast to mast cell-competent fracture hematoma, the inflammatory mediators were not reduced in mast cell-deficient mice 3 h after combined fracture and thoracic trauma indicating that mast cells regulate local immune responses at the fracture site after severe injury. Only local IL-6 levels were similarly diminished in mast cell-deficient mice upon the combined trauma, which could be explained by the 3 h observation time point, and the fact that IL-6 is mainly *de novo* synthesized by mast cells, which takes some time (53). Mast cell-specific knockout models could further clarify the role of distinct mast cell-released mediators during uneventful and trauma-induced compromised fracture healing. Furthermore, mast cells are not the single source of IL-6 in the fracture hematoma, because, for example, neutrophils and bone-resident osteoblasts also produce IL-6 locally (12, 36). As a limitation of our study, we did not investigate the immune cell composition in the early fracture hematoma, which would provide additional insights into the

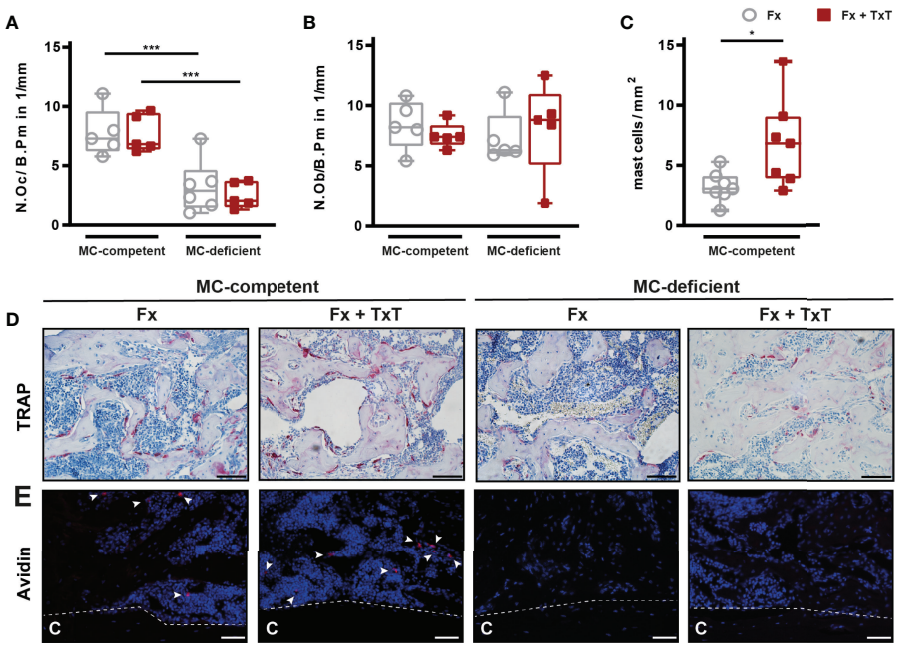

FIGURE 8 | Cellular composition of the fracture callus of mast cell (MC)-competent and MC-deficient mice 21 d after isolated fracture (Fx) and combined fracture and thoracic trauma (Fx + TxT). **(A)** Number of osteoclasts per bone perimeter (N.Oc/B.Pm), **(B)** number of osteoblasts per bone perimeter (N.Ob/B.Pm) and **(C)** number of mast cells per mm^2. **(D)** Representative images from an area within the periosteal fracture callus stained for TRAP. Scale bar = 100 µm. **(E)** Representative images of mast cell (arrowheads) staining from an area within the periosteal callus. Scale bar = 75 µm. Gray boxes represent Fx mice, red boxes represent Fx + TxT mice, C = cortex. Data are shown as box-and-whisker plots (with median and interquartile range) from maximum to minimum, showing all data points. *p<0.05; ***p<0.001. The p values were determined using one-way ANOVA with post-hoc Fisher's LSD.

interaction of mast cells and other immune cells, including neutrophils, whose numbers are locally increased after severe trauma (11, 17, 40). Regarding this, we previously showed that in regular fracture healing, the neutrophil and macrophage numbers were reduced in the hematoma of mast cell-deficient mice (26). Nevertheless, our present data showed that a balanced local immune response in mast cell-deficient mice resulted in improved bone regeneration 21 days after fracture by enhancing the fracture callus bone content. However, we did not observe any differences in fracture callus osteoblast numbers between mast cell-competent and -deficient mice. Therefore, the improved healing might be a result of an accelerated cartilage-to-bone transition, because the cartilage content was not increased in mast cell-deficient mice with concomitant thoracic trauma. However, limiting our study, we did not investigate an intermediate time point covering the phase of endochondral bone formation, nor a very late time point after fracture, which might have completed the picture of the mechanistic role of mast cells in trauma-induced compromised bone repair. Confirming previous studies, osteoclast numbers did not differ between isolated fracture and the combined trauma groups (35), but osteoclasts were significantly reduced in mast cell-deficient mice of both groups, thereby confirming our previous findings that mast cells play a role in the regulation of osteoclastogenesis during callus remodeling (26, 29). Concluding, our results demonstrated that trauma-induced compromised fracture healing was abolished in mast-cell deficient mice.

In conclusion, the present study demonstrated for the first time that mast cells are involved in the pathomechanisms of compromised bone repair after severe trauma by regulating posttraumatic systemic and local inflammatory reactions. However, additional investigations are needed to elucidate the crosstalk of mast cells and other immune cells, as well as the underlying molecular mechanisms. Nevertheless, our results imply that mast cells could be a target for the development of new therapeutic strategies to improve bone repair in multiply injured patients.

DATA AVAILABILITY STATEMENT

The original contributions presented in the study are included in the article/supplementary material. Further inquiries can be directed to the corresponding authors.

ETHICS STATEMENT

The animal study was reviewed and approved by Regierungspräsidium Tübingen.

AUTHOR CONTRIBUTIONS

DR: conceptualization, investigation, data curation and interpretation, formal analysis, visualization, and writing-original draft. JB: investigation, data curation. KH: investigation, data curation. MV: data curation. MH-L: conceptualization, funding acquisition, methodology, data interpretation, supervision. AD: conceptualization, methodology, data interpretation, supervision, funding aquisition. AI: conceptualization, data interpretation, funding acquisition, writing-original draft, writing-review and editing, supervision. VF: conceptualization, formal analysis, visualization, data curation and interpretation, writing-original draft, writing-review and editing. All authors contributed to the article and approved the submitted version.

FUNDING

This research was supported by the German Research Foundation, within the context of the Collaborative Research Center 1149 "Danger Response, Disturbance Factors and Regenerative Potential after Acute Trauma" (Project-ID 251293562, C01 INST 40/491-2), and by grant 361210922/RTG 2408 of the German Research Foundation.

ACKNOWLEDGMENTS

We thank Iris Baum, Bettina Herde, Tina Hieber, Andrea Böhmler and Kathleen Baumgart for excellent technical assistance.

REFERENCES

1. Zura R, Xiong Z, Einhorn T, Watson JT, Ostrum RF, Prayson MJ, et al. Epidemiology of Fracture Nonunion in 18 Human Bones. *JAMA Surg* (2016) 151(11):e162775. doi: 10.1001/jamasurg.2016.2775
2. Bhandari M, Tornetta P, Sprague S, Najibi S, Petrisor B, Griffith L, et al. Predictors of Reoperation Following Operative Management of Fractures of the Tibial Shaft. *J Orthop Trauma* (2003) 17(5):353–61. doi: 10.1097/00005131-200305000-00006
3. Huber-Lang M, Lambris JD, Ward PA. Innate Immune Responses to Trauma. *Nat Immunol* (2018) 19(4):327–41. doi: 10.1038/s41590-018-0064-8
4. Veysi VT, Nikolaou VS, Paliobeis C, Efstathopoulos N, Giannoudis PV. Prevalence of Chest Trauma, Associated Injuries and Mortality: A Level I Trauma Centre Experience. *Int Orthop* (2009) 33(5):1425–33. doi: 10.1007/s00264-009-0746-9
5. Stellin G. Survival in Trauma Victims With Pulmonary Contusion. *Am Surg* (1991) 57(12):780–4.
6. Shorr RM, Crittenden M, Indeck M, Hartunian SL, Rodriguez A. Blunt Thoracic Trauma. Analysis of 515 Patients. *Ann Surg* (1987) 206(2):200–5. doi: 10.1097/00000658-198708000-00013
7. Bastian O, Pillay J, Alblas J, Leenen L, Koenderman L, Blokhuis T. Systemic Inflammation and Fracture Healing. *J Leukoc Biol* (2011) 89(5):669–73. doi: 10.1189/jlb.0810446
8. Claes L, Recknagel S, Ignatius A. Fracture Healing Under Healthy and Inflammatory Conditions. *Nat Rev Rheumatol* (2012) 8(3):133–43. doi: 10.1038/nrrheum.2012.1
9. Loi F, Cordova LA, Pajarinen J, Lin TH, Yao Z, Goodman SB. Inflammation, Fracture and Bone Repair. *Bone* (2016) 86:119–30. doi: 10.1016/j.bone.2016.02.020
10. Pape HC, Marcucio R, Humphrey C, Colnot C, Knobe M, Harvey EJ. Trauma-Induced Inflammation and Fracture Healing. *J Orthop Trauma* (2010) 24(9):522–5. doi: 10.1097/BOT.0b013e3181ed1361
11. Kemmler J, Bindl R, McCook O, Wagner F, Groger M, Wagner K, et al. Exposure to 100% Oxygen Abolishes the Impairment of Fracture Healing After Thoracic Trauma. *PloS One* (2015) 10(7):e0131194. doi: 10.1371/journal.pone.0131194
12. Kovtun A, Bergdolt S, Wiegner R, Radermacher P, Huber-Lang M, Ignatius A. The Crucial Role of Neutrophil Granulocytes in Bone Fracture Healing. *Eur Cells Mater* (2016) 32:152–62. doi: 10.22203/eCM.v032a10
13. Horst K, Eschbach D, Pfeifer R, Hubenthal S, Sassen M, Steinfeldt T, et al. Local Inflammation in Fracture Hematoma: Results From a Combined Trauma Model in Pigs. *Mediators Inflamm* (2015) 2015:126060. doi: 10.1155/2015/126060
14. Horst K, Simon TP, Pfeifer R, Teuben M, Almahmoud K, Zhi Q, et al. Characterization of Blunt Chest Trauma in a Long-Term Porcine Model of Severe Multiple Trauma. *Sci Rep* (2016) 6:39659. doi: 10.1038/srep39659
15. Bastian OW, Kuijer A, Koenderman L, Stellato RK, van Solinge WW, Leenen LP, et al. Impaired Bone Healing in Multitrauma Patients Is Associated With Altered Leukocyte Kinetics After Major Trauma. *J Inflamm Res* (2016) 9:69–78. doi: 10.2147/JIR.S101064
16. Frink M, van Griensven M, Kobbe P, Brin T, Zeckey C, Vaske B, et al. Il-6 Predicts Organ Dysfunction and Mortality in Patients With Multiple Injuries. *Scand J Trauma Resusc Emerg Med* (2009) 17:49. doi: 10.1186/1757-7241-17-49
17. Kaiser K, Prystaz K, Vikman A, Haffner-Luntzer M, Bergdolt S, Strauss G, et al. Pharmacological Inhibition of Il-6 Trans-Signaling Improves Compromised Fracture Healing After Severe Trauma. *Naunyn Schmiedebergs Arch Pharmacol* (2018) 391(5):523–36. doi: 10.1007/s00210-018-1483-7
18. Recknagel S, Bindl R, Kurz J, Wehner T, Schoengraf P, Ehrnthaller C, et al. C5ar-Antagonist Significantly Reduces the Deleterious Effect of a Blunt Chest Trauma on Fracture Healing. *J Orthop Res* (2012) 30(4):581–6. doi: 10.1002/jor.21561
19. Wernersson S, Pejler G. Mast Cell Secretory Granules: Armed for Battle. *Nat Rev Immunol* (2014) 14(7):478–94. doi: 10.1038/nri3690
20. Ragipoglu D, Dudeck A, Haffner-Luntzer M, Voss M, Kroner J, Ignatius A, et al. The Role of Mast Cells in Bone Metabolism and Bone Disorders. *Front Immunol* (2020) 11:163. doi: 10.3389/fimmu.2020.00163
21. Cai C, Cao Z, Loughran PA, Kim S, Darwiche S, Korff S, et al. Mast Cells Play a Critical Role in the Systemic Inflammatory Response and End-Organ Injury Resulting From Trauma. *J Am Coll Surg* (2011) 213(5):604–15. doi: 10.1016/j.jamcollsurg.2011.08.009
22. Shiota N, Nishikori Y, Kakizoe E, Shimoura K, Niibayashi T, Shimbori C, et al. Pathophysiological Role of Skin Mast Cells in Wound Healing After Scald Injury: Study With Mast Cell-Deficient W/W(V) Mice. *Int Arch Allergy Immunol* (2010) 151(1):80–8. doi: 10.1159/000232573
23. Strbian D, Kovanen PT, Karjalainen-Lindsberg ML, Tatlisumak T, Lindsberg PJ. An Emerging Role of Mast Cells in Cerebral Ischemia and Hemorrhage. *Ann Med* (2009) 41(6):438–50. doi: 10.1080/07853890902887303
24. El-Shitany NA, El-Desoky K. Cromoglycate, Not Ketotifen, Ameliorated the Injured Effect of Warm Ischemia/Reperfusion in Rat Liver: Role of Mast Cell Degranulation, Oxidative Stress, Proinflammatory Cytokine, and Inducible Nitric Oxide Synthase. *Drug Des Devel Ther* (2015) 9:5237–46. doi: 10.2147/DDDT.S88337
25. Santone DJ, Shahani R, Rubin BB, Romaschin AD, Lindsay TF. Mast Cell Stabilization Improves Cardiac Contractile Function Following Hemorrhagic Shock and Resuscitation. *Am J Physiol Heart Circ Physiol* (2008) 294(6):H2456–64. doi: 10.1152/ajpheart.00925.2007
26. Kroner J, Kovtun A, Kemmler J, Messmann JJ, Strauss G, Seitz S, et al. Mast Cells Are Critical Regulators of Bone Fracture-Induced Inflammation and Osteoclast Formation and Activity. *J Bone Miner Res* (2017) 32(12):2431–44. doi: 10.1002/jbmr.3234
27. Behrends DA, Cheng L, Sullivan MB, Wang MH, Roby GB, Zayed N, et al. Defective Bone Repair in Mast Cell Deficient Mice With C-Kit Loss of Function. *Eur Cell Mater* (2014) 28:209–21. doi: 10.22203/ecm.v028a14
28. Ramirez-GarciaLuna JL, Chan D, Samberg R, Abou-Rjeili M, Wong TH, Li A, et al. Defective Bone Repair in Mast Cell-Deficient Cpa3cre/+ Mice. *PloS One* (2017) 12(3):e0174396. doi: 10.1371/journal.pone.0174396
29. Fischer V, Ragipoglu D, Diedrich J, Steppe L, Dudeck A, Schutze K, et al. Mast Cells Trigger Disturbed Bone Healing in Osteoporotic Mice. *J Bone Miner Res* (2022) 37(1):137–51. doi: 10.1002/jbmr.4455

30. Gebhard F, Pfetsch H, Steinbach G, Strecker W, Kinzl L, Bruckner UB. Is Interleukin 6 an Early Marker of Injury Severity Following Major Trauma in Humans? *Arch Surg* (2000) 135(3):291–5. doi: 10.1001/archsurg.135.3.291
31. Dudeck A, Dudeck J, Scholten J, Petzold A, Surianarayanan S, Kohler A, et al. Mast Cells Are Key Promoters of Contact Allergy That Mediate the Adjuvant Effects of Haptens. *Immunity* (2011) 34(6):973–84. doi: 10.1016/j.immuni.2011.03.028
32. Peschke K, Dudeck A, Rabenhorst A, Hartmann K, Roers A. Cre/Loxp-Based Mouse Models of Mast Cell Deficiency and Mast Cell-Specific Gene Inactivation. *Methods Mol Biol* (2015) 1220:403–21. doi: 10.1007/978-1-4939-1568-2_25
33. Rontgen V, Blakytny R, Matthys R, Landauer M, Wehner T, Gockelmann M, et al. Fracture Healing in Mice Under Controlled Rigid and Flexible Conditions Using an Adjustable External Fixator. *J Orthop Res* (2010) 28 (11):1456–62. doi: 10.1002/jor.21148
34. Claes L. Improvement of Clinical Fracture Healing - What Can Be Learned From Mechano-Biological Research? *J Biomech* (2021) 115:110148. doi: 10.1016/j.jbiomech.2020.110148
35. Kovtun A, Bergdolt S, Hagele Y, Matthes R, Lambris JD, Huber-Lang M, et al. Complement Receptors C5ar1 and C5ar2 Act Differentially During the Early Immune Response After Bone Fracture But Are Similarly Involved in Bone Repair. *Sci Rep* (2017) 7(1):14061. doi: 10.1038/s41598-017-14444-3
36. Prystaz K, Kaiser K, Kovtun A, Haffner-Luntzer M, Fischer V, Rapp AE, et al. Distinct Effects of Il-6 Classic and Trans-Signaling in Bone Fracture Healing. *Am J Pathol* (2018) 188(2):474–90. doi: 10.1016/j.ajpath.2017.10.011
37. Haffner-Luntzer M, Heilmann A, Rapp AE, Beie S, Schinke T, Amling M, et al. Midkine-Deficiency Delays Chondrogenesis During the Early Phase of Fracture Healing in Mice. *PloS One* (2014) 9(12):e116282. doi: 10.1371/journal.pone.0116282
38. Bouxsein ML, Boyd SK, Christiansen BA, Guldberg RE, Jepsen KJ, Muller R. Guidelines for Assessment of Bone Microstructure in Rodents Using Micro-Computed Tomography. *J Bone Miner Res* (2010) 25(7):1468–86. doi: 10.1002/jbmr.141
39. Recknagel S, Bindl R, Kurz J, Wehner T, Ehrnthaller C, Knoferl MW, et al. Experimental Blunt Chest Trauma Impairs Fracture Healing in Rats. *J Orthop Res* (2011) 29(5):734–9. doi: 10.1002/jor.21299
40. Bergdolt S, Kovtun A, Hagele Y, Liedert A, Schinke T, Amling M, et al. Osteoblast-Specific Overexpression of Complement Receptor C5ar1 Impairs Fracture Healing. *PloS One* (2017) 12(6):e0179512. doi: 10.1371/journal.pone.0179512
41. Fitschen-Oestern S, Lippross S, Klueter T, Weuster M, Varoga D, Tohidnezhad M, et al. A New Multiple Trauma Model of the Mouse. *BMC Musculoskelet Disord* (2017) 18(1):468. doi: 10.1186/s12891-017-1813-9
42. Horst K, Greven J, Luken H, Zhi Q, Pfeifer R, Simon TP, et al. Trauma Severity and Its Impact on Local Inflammation in Extremity Injury-Insights From a Combined Trauma Model in Pigs. *Front Immunol* (2019) 10:3028. doi: 10.3389/fimmu.2019.03028
43. Alper B, Erdogan B, Erdogan MO, Bozan K, Can M. Associations of Trauma Severity With Mean Platelet Volume and Levels of Systemic Inflammatory Markers (Il1beta, Il6, Tnfalpha, and Crp). *Mediators Inflamm* (2016) 2016:9894716. doi: 10.1155/2016/9894716
44. Gasper NA, Petty CC, Schrum LW, Marriott I, Bost KL. Bacterium-Induced Cxcl10 Secretion by Osteoblasts Can Be Mediated in Part Through Toll-Like Receptor 4. *Infect Immun* (2002) 70(8):4075–82. doi: 10.1128/iai.70.8.4075-4082.2002
45. Takatsu K. Interleukin-5 and Il-5 Receptor in Health and Diseases. *Proc Jpn Acad Ser B Phys Biol Sci* (2011) 87(8):463–85. doi: 10.2183/pjab.87.463
46. Jose PJ, Griffiths-Johnson DA, Collins PD, Walsh DT, Moqbel R, Totty NF, et al. Eotaxin: A Potent Eosinophil Chemoattractant Cytokine Detected in a Guinea Pig Model of Allergic Airways Inflammation. *J Exp Med* (1994) 179 (3):881–7. doi: 10.1084/jem.179.3.881
47. Deshmane SL, Kremlev S, Amini S, Sawaya BE. Monocyte Chemoattractant Protein-1 (Mcp-1): An Overview. *J Interferon Cytokine Res* (2009) 29(6):313–26. doi: 10.1089/jir.2008.0027
48. Menten P, Wuyts A, Van Damme J. Monocyte Chemotactic Protein-3. *Eur Cytokine Netw* (2001) 12(4):554–60.
49. Schmidt-Bleek K, Kwee BJ, Mooney DJ, Duda GN. Boon and Bane of Inflammation in Bone Tissue Regeneration and Its Link With Angiogenesis. *Tissue Eng Part B Rev* (2015) 21(4):354–64. doi: 10.1089/ten.TEB.2014.0677
50. Dahdah A, Gautier G, Attout T, Fiore F, Lebourdais E, Msallam R, et al. Mast Cells Aggravate Sepsis by Inhibiting Peritoneal Macrophage Phagocytosis. *J Clin Invest* (2014) 124(10):4577–89. doi: 10.1172/JCI75212
51. Fishman JE, Sheth SU, Levy G, Alli V, Lu Q, Xu D, et al. Intraluminal Nonbacterial Intestinal Components Control Gut and Lung Injury After Trauma Hemorrhagic Shock. *Ann Surg* (2014) 260(6):1112–20. doi: 10.1097/SLA.0000000000000631
52. Conti P, Kempuraj D, Di Gioacchino M, Boucher W, Letourneau R, Kandere K, et al. Interleukin-6 and Mast Cells. *Allergy Asthma Proc* (2002) 23(5):331–5.
53. Kruger-Krasagakes S, Moller A, Kolde G, Lippert U, Weber M, Henz BM. Production of Interleukin-6 by Human Mast Cells and Basophilic Cells. *J Invest Dermatol* (1996) 106(1):75–9. doi: 10.1111/1523-1747.ep12327815
54. Caslin HL, Abebayehu D, Abdul Qayum A, Haque TT, Taruselli MT, Paez PA, et al. Lactic Acid Inhibits Lipopolysaccharide-Induced Mast Cell Function by Limiting Glycolysis and Atp Availability. *J Immunol* (2019) 203(2):453–64. doi: 10.4049/jimmunol.1801005
55. Sutherland RE, Olsen JS, McKinstry A, Villalta SA, Wolters PJ. Mast Cell Il-6 Improves Survival From Klebsiella Pneumonia and Sepsis by Enhancing Neutrophil Killing. *J Immunol* (2008) 181(8):5598–605. doi: 10.4049/jimmunol.181.8.5598
56. Huang M, Pang X, Karalis K, Theoharides TC. Stress-Induced Interleukin-6 Release in Mice Is Mast Cell-Dependent and More Pronounced in Apolipoprotein E Knockout Mice. *Cardiovasc Res* (2003) 59(1):241–9. doi: 10.1016/s0008-6363(03)00340-7
57. Schmidt-Arras D, Rose-John S. Il-6 Pathway in the Liver: From Physiopathology to Therapy. *J Hepatol* (2016) 64(6):1403–15. doi: 10.1016/j.jhep.2016.02.004
58. Moshage H. Cytokines and the Hepatic Acute Phase Response. *J Pathol* (1997) 181(3):257–66. doi: 10.1002/(SICI)1096-9896(199703)181:3<257::AID-PATH756>3.0.CO;2-U
59. Mukai K, Tsai M, Saito H, Galli SJ. Mast Cells as Sources of Cytokines, Chemokines, and Growth Factors. *Immunol Rev* (2018) 282(1):121–50. doi: 10.1111/imr.12634
60. Al-Afif A, Alyazidi R, Oldford SA, Huang YY, King CA, Marr N, et al. Respiratory Syncytial Virus Infection of Primary Human Mast Cells Induces the Selective Production of Type I Interferons, Cxcl10, and Ccl4. *J Allergy Clin Immunol* (2015) 136(5):1346–54.e1. doi: 10.1016/j.jaci.2015.01.042
61. Alkhouri H, Cha V, Tong K, Moir LM, Armour CL, Hughes JM. Human Lung Mast Cell Products Regulate Airway Smooth Muscle Cxcl10 Levels. *J Allergy (Cairo)* (2014) 2014:875105. doi: 10.1155/2014/875105
62. Gauthier M, Chakraborty K, Oriss TB, Raundhal M, Das S, Chen J, et al. Severe Asthma in Humans and Mouse Model Suggests a Cxcl10 Signature Underlies Corticosteroid-Resistant Th1 Bias. *JCI Insight* (2017) 2(13):1–17. doi: 10.1172/jci.insight.94580
63. Bradding P, Roberts JA, Britten KM, Montefort S, Djukanovic R, Mueller R, et al. Interleukin-4, -5, and -6 and Tumor Necrosis Factor-Alpha in Normal and Asthmatic Airways: Evidence for the Human Mast Cell as a Source of These Cytokines. *Am J Respir Cell Mol Biol* (1994) 10(5):471–80. doi: 10.1165/ajrcmb.10.5.8179909
64. Lorentz A, Schwengberg S, Mierke C, Manns MP, Bischoff SC. Human Intestinal Mast Cells Produce Il-5 in Vitro Upon Ige Receptor Cross-Linking and in Vivo in the Course of Intestinal Inflammatory Disease. *Eur J Immunol* (1999) 29(5):1496–503. doi: 10.1002/(SICI)1521-4141(199905)29:05<1496::AID-IMMU1496>3.0.CO;2-5
65. Xing W, Austen KF, Gurish MF, Jones TG. Protease Phenotype of Constitutive Connective Tissue and of Induced Mucosal Mast Cells in Mice Is Regulated by the Tissue. *Proc Natl Acad Sci USA* (2011) 108(34):14210–5. doi: 10.1073/pnas.1111048108
66. Gurish MF, Austen KF. Developmental Origin and Functional Specialization of Mast Cell Subsets. *Immunity* (2012) 37(1):25–33. doi: 10.1016/j.immuni.2012.07.003
67. Kumar V. Pulmonary Innate Immune Response Determines the Outcome of Inflammation During Pneumonia and Sepsis-Associated Acute Lung Injury. *Front Immunol* (2020) 11:1722. doi: 10.3389/fimmu.2020.01722
68. Menzies-Gow A, Ying S, Sabroe I, Stubbs VL, Soler D, Williams TJ, et al. Eotaxin (Ccl11) and Eotaxin-2 (Ccl24) Induce Recruitment of Eosinophils, Basophils, Neutrophils, and Macrophages as Well as Features of Early- and Late-Phase Allergic Reactions Following Cutaneous Injection in Human

Atopic and Nonatopic Volunteers. *J Immunol* (2002) 169(5):2712–8. doi: 10.4049/jimmunol.169.5.2712
69. Jin L, Ghimire L, Paudel S, Cai S, Rangasamy T, Jeyaseelan S. Mcp-1 Plays a Critical Role in Neutrophil Function and Pyroptosis During Carbapenemf-Resistant Klebsiella Pneumoniae. *J Immunol* (2018) 200(1 Supplement):46.17–7.
70. Ichikawa A, Kuba K, Morita M, Chida S, Tezuka H, Hara H, et al. Cxcl10-Cxcr3 Enhances the Development of Neutrophil-Mediated Fulminant Lung Injury of Viral and Nonviral Origin. *Am J Respir Crit Care Med* (2013) 187 (1):65–77. doi: 10.1164/rccm.201203-0508OC
71. De Filippo K, Dudeck A, Hasenberg M, Nye E, van Rooijen N, Hartmann K, et al. Mast Cell and Macrophage Chemokines Cxcl1/Cxcl2 Control the Early Stage of Neutrophil Recruitment During Tissue Inflammation. *Blood* (2013) 121(24):4930–7. doi: 10.1182/blood-2013-02-486217
72. Nakamura Y, Kambe N, Saito M, Nishikomori R, Kim YG, Murakami M, et al. Mast Cells Mediate Neutrophil Recruitment and Vascular Leakage Through the Nlrp3 Inflammasome in Histamine-Independent Urticaria. *J Exp Med* (2009) 206(5):1037–46. doi: 10.1084/jem.20082179

Conflict of Interest: The authors declare that the research was conducted in the absence of any commercial or financial relationships that could be construed as a potential conflict of interest.

Publisher's Note: All claims expressed in this article are solely those of the authors and do not necessarily represent those of their affiliated organizations, or those of the publisher, the editors and the reviewers. Any product that may be evaluated in this article, or claim that may be made by its manufacturer, is not guaranteed or endorsed by the publisher.

frontiers | Frontiers in Immunology

ORIGINAL RESEARCH
published: 17 May 2022
doi: 10.3389/fimmu.2022.883863

Shift of Neutrophils From Blood to Bone Marrow Upon Extensive Experimental Trauma Surgery

*Michel P. J. Teuben[1,2,3], Marjolein Heeres[1,2], Taco Blokhuis[4], Roy Spijkerman[1,5], Eric Knot[1], Nienke Vrisekoop[2,5], Roman Pfeifer[3], Hans-Christoph Pape[3], Leo Koenderman[2,5] and Luke P. H. Leenen[1]**

[1] Department of Trauma, University Medical Centre Utrecht, Utrecht, Netherlands, [2] Center for Translational Immunology, University Medical Centre Utrecht, Utrecht, Netherlands, [3] Department of Traumatology, University Hospital Zürich, Zürich, Switzerland, [4] Department of Surgery, Maastricht University Medical Center, Maastricht, Netherlands, [5] Department of Respiratory Medicine, University Medical Center Utrecht, Utrecht, Netherlands

OPEN ACCESS

Edited by:
Klemens Horst,
University Hospital RWH Aachen, Germany

Reviewed by:
Matthias Weuster,
Lutheran Diakonissenanstalt to Felnsburg, Germany
Philipp Störmann,
University Hospital Frankfurt, Germany

***Correspondence:**
Luke P. H. Leenen
l.p.h.leenen@umcutrecht.nl

Specialty section:
This article was submitted to Inflammation, a section of the journal Frontiers in Immunology

Received: 25 February 2022
Accepted: 29 March 2022
Published: 17 May 2022

Citation:
Teuben MPJ, Heeres M, Blokhuis T, Spijkerman R, Knot E, Vrisekoop N, Pfeifer R, Pape H-C, Koenderman L and Leenen LPH (2022) Shift of Neutrophils From Blood to Bone Marrow Upon Extensive Experimental Trauma Surgery. Front. Immunol. 13:883863. doi: 10.3389/fimmu.2022.883863

Introduction: Extensive trauma surgery evokes an immediate cellular immune response including altered circulatory neutrophil numbers. The concurrent bone marrow (BM) response however is currently unclear. We hypothesize that these BM changes include (1) a relative reduction of the bone marrow neutrophil fraction and (2) increasing heterogeneity of the bone marrow neutrophil pool due to (3) the appearance of aged/returning neutrophils from circulation into the BM-compartment.

Materials and Methods: Eight pigs were included in a standardized extensive trauma surgery model. Blood and bone marrow samples were collected at baseline and after 3 hours of ongoing trauma surgery. Leukocyte and subtype counts and cell surface receptor expression levels were studied by flow cytometry.

Results: All animals survived the interventions. A significant drop in circulating neutrophil counts from 9.3 to 3.2x10^6 cells/ml (P=0.001) occurred after intervention, whereas circulatory neutrophil cell surface expression of CD11b increased. The concurrent bone marrow response included an increase of the BM neutrophil fraction from 63 ± 3 to 71 ± 3 percent (P<0.05). Simultaneously, the BM neutrophil pool became increasingly mature with a relative increase of a CXCR4^{high}-neutrophil subtype that was virtually absent at baseline.

Conclusion: The current study shows a shift in composition of the BM neutrophil pool during extensive trauma surgery that was associated with a relatively circulatory neutropenia. More specifically, under these conditions BM neutrophils were more mature than under homeostatic conditions and a CXCR4^{high}-neutrophil subset became overrepresented possibly reflecting remigration of aged neutrophils to the BM. These findings may contribute to the development of novel interventions aimed to modify the trauma-induced immune response in the BM.

Keywords: trauma, neutrophil, subsets, bone marrow, porcine model

INTRODUCTION

Trauma and subsequent surgery induce acute systemic inflammation and trigger activation of innate immune cells (1–3). Extensive ongoing trauma surgery is associated with an increased activation state of circulatory neutrophils and enhanced neutrophil migration to the tissue (4, 5). Furthermore, a prompt decline in circulatory neutrophil numbers upon insult has been described in specific cases (4–7) and linked to the development of inflammatory complications (4, 5). To maintain homeostasis of circulatory neutrophils, compensatory mobilization of cells originating from the bone marrow (BM) occurs. Consequently, drastic shifts in the constitution of the blood neutrophil pool during systemic inflammation has been reported (8, 9).

Enhanced mobilization of BM-neutrophils is considered to alter the content of the BM immune cell pool as well. To restore bone marrow immune reserves, enhanced hematopoiesis is mandated (10). Granulopoiesis is, however, considered a time-consuming process as maturation in the post-mitotic pool takes >4 days (11, 12). The compensation mechanisms in the BM and kinetics in response to increased cell demands are poorly understood (10, 13).

Profound inflammatory conditions have further been linked to the ′empty bone-marrow′ phenomenon (14, 15). This BM-condition is defined as a deficit of both post-mitotic neutrophils and their progenitors. An empty bone marrow has been reported at least 24 hours post-insult after trauma due to a mismatch between circulatory demand and bone marrow synthesis capacity (14–16). In addition to liberation of neutrophils from the bone marrow, remigration of relatively aged neutrophils from circulation into the bone marrow compartment has also been suggested (17, 18). The role of this phenomenon during a decrease in circulatory neutrophils during extensive surgery has not been studied before. To date, the exact interplay between changes of circulatory neutrophils after an acute trauma-induced inflammatory insult and the early bone marrow neutrophil-response has yet to be elucidated.

The hypothesis that is tested predicts that acute trauma-evoked depletion of systemic neutrophils is associated with altered composition of the bone marrow neutrophil pool. Such changes are characterized by (1) relative enhancement of the bone marrow neutrophil fraction and (2) increasing heterogeneity of the bone marrow neutrophil pool due to (3) the appearance of aged/returning neutrophils from circulation into the BM-compartment.

In order to test this hypothesis, a standardized porcine trauma model of extensive trauma surgery was utilized. The porcine model was chosen as this model allows for standardization of severe trauma and subsequent surgical interventions. Furthermore, porcine models have superior translational properties, as pigs are more closely related to humans in terms of their dimensions, anatomy, genetics, physiology and immunology compared to alternative non-primate animal models (19, 20).

MATERIALS AND METHODS

All experiments were performed in accordance with the guidelines of the Institutional Animal Care and Use. The study protocol was approved by the Saarland University Hospital Animal Care Committee.

Experimental Animals

All experiments were performed as described in the application and *Female Landrace* pigs were utilized (50-60 kilograms).

Experimental Procedure

Premedication included intramuscular midazolam (1mg/kg), ketamin (20mg/kg) and atropine (50ug/kg). Intubation was performed following 2 minutes of pre-oxygenation with 100 percent Oxygen at 10L/min. A volume-controlled ventilation protocol was utilized. Maintenance of anesthesia was achieved by Isoflurane 0,25-0,50%, continuous midazolam infusion (0,6 mg/kg/hour), and sufentanil infusion (15ug/kg/hour). Ventilation rates were guided by end tidal CO_2-values and FiO_2 of 0.3, Positive end-expiratory pressure of 0cm H_2O and an I:E-ratio of 1:2 was preferred and aimed for in all animals. Frequent arterial blood gas analyses were performed to check ventilator and metabolic status. Antibiotics were not applied and hypothermia was prevented by altering room temperature. In accordance with the treatment concepts of the Definitive Surgical Trauma Care (DSTC^{TM})-course (21), hypovolemia was corrected by additional sodium chloride 0.9% fluid resuscitation. Continuous arterial line blood pressure measurements were available. All animals were exposed to standardized extensive trauma surgery. The protocol has been described previously (22). In short, the following injuries were induced: liver laceration, 5 small bowel injuries, diaphragm injury, stomach, spleen, pancreas, left kidney. Furthermore, a thoracotomy was performed, and a cardiac injury was induced. Additionally, the left lung was injured and treated through hilar clamping and resection. Finally, the infrarenal inferior vena cava and right kidney were lacerated. All standardized injuries were treated by experienced trauma surgeons and anaesthetists and in line with treatment concepts of the DSTC^{TM}-protocols for trauma care (21). The sequence and execution of injury induction and surgical care were standardized and performed according to a standardized time-schedule. Animals were euthanized after 3 hours of ongoing surgery by pentobarbital infusion.

Sampling

Blood and bone marrow samples were obtained at baseline and after 3 hours (immediately prior to euthanization). For blood neutrophil analysis, 9 mL of peripheral blood were collected from a central venous catheter in ethylenediaminetetraacetic acid (EDTA)-anticoagulated Vacutainers at baseline and directly after the animals were exposed to the final injury and subsequent therapy. An ice-cold isotonic NH_4CL-lysis buffer was utilized twice for the lysis of erythrocytes and cells were washed in between with FACS-buffer (Dulbecco phosphate buffered saline supplemented with 2% heat inactivated fetal calf serum, 5mM EDTA). White blood cell numbers for staining have been standardized by the utilization of a Neubauer Chamber to calculate the appropriate dilution factor. Antibody mixes were added, and samples were incubated in dark conditions for 45 minutes on 4°C. Then, samples were washed twice with PBS2+ (phosphate-buffered saline with added sodium citrate [0.38% wt/

vol] and pasteurized plasma proteins [10% vol/vol; Sanquin, Amsterdam, The Netherlands]. Following the final wash steps, cells were fixed with BD Cellfix (BD, Mountain View, CA, USA), a premixed fixing concentrate containing 1% formaldehyde and 0,1% sodium azide. Prior to the experiments the stability of all antibodies was tested and validated. All fixed samples were analyzed within 24 hours with a FACS Canto II flowcytometer (BD, Mountain View, CA, USA). Data from individual experiments are depicted as fluorescence intensity as the median fluorescence intensity (MFI). A minimum of 20,000 neutrophils per sample was analyzed. Populations not expressing the used markers were used to set background fluorescence levels and compensation matrixes were composed by using beads and the automated setup system for compensation in BD FACSDiva software version 6.1.3 (BD, Mountain View, CA, USA).

Bone marrow material was harvested in accordance with recommendations for humans (23, 24). In short, the pig was placed in the supine position with both legs fixed. The appropriate extremity was prepared with antiseptic, scrubbed and draped, only exposing the site to be sampled. A 1.5cm longitudinal skin incision was made and bone-covering soft tissue was removed. Thereafter a 2 mm unicortical entry point was drilled with a sterile hand drill at the anterior-medial aspect of the proximal tibial metaphysis (10cm distal from the knee joint). Thereafter, an EDTA-coated 50 milliliter syringe with 1ml and a 25-Gauge needle were used to aspirate BM-content from the cavity.

After collection, BM-samples were directly and simultaneously processed with corresponding blood samples. At baseline, material was collected from the left tibia, whereas after intervention cells were gathered from the right tibia. In our model no extremity trauma was applied.

Flowcytometry Analysis of Porcine Peripheral Blood Samples

A previously validated gating strategy was applied to distinguish between circulatory leukocyte subtypes. First, nucleated, viable singlet leukocytes ($CD45^+$-cells) were included (see **Figures 1A–C**). Thereafter, forward/sideward scatter (FSC/SSC) profiles were utilized to identify different leukocyte subtypes, as previously described (25, 26). Neutrophils were identified through typical high sideward scatter profiles as observed both in human and porcine blood samples (25–29). Furthermore, SWC 1 negative cells were excluded as this marker is expressed on porcine neutrophils and not on porcine eosinophils (29). A representative example of the gating strategy of blood leukocytes is shown in **Figure 1**. To obtain leukocyte populations for determination of reference values, monocytes as well as lymphocytes and blasts (pooled) were gated as well. CountBright counting beads (Invitrogen, Waltham, Massachusetts, USA) were utilized to count and compare absolute cell numbers over time.

Determination of Bone Marrow Leukocyte Subtypes and the Neutrophil Fraction

The bone marrow neutrophil fraction was defined as the proportion of marrow immune cells ($CD45^+$) belonging to the neutrophil category, which was determined with flow studies (27–29). More specifically, bone marrow immune cells were identified by a multistep gating protocol. A representative example of this gating strategy is shown in **Figure 2**. First, vital BM-$CD45^+$-cells were selected, and debris and doublets were excluded (see **Figures 2A–C**). Thereafter, a SSC/CD45 gate was used to select bone marrow granulocytes (see **Figure 2D**). Basophils were gated out based on their lower SSC signal. This is an established gating strategy for both porcine and human bone marrow analysis (27–29). Thereafter, SWC 1-positive cells were selected as this marker is exclusively expressed on porcine neutrophils and not on eosinophils (see **Figure 2E**) (29). This gating strategy has been validated by co-expression analysis of different leukocyte subtypes. Furthermore, validation experiments including cell sorting studies with morphologic analysis demonstrated a neutrophil purity over 99%. The BM-neutrophil fraction was determined by calculating the percentage of BM-neutrophils among all BM-immune cells.

Monoclonal Antibodies and Flow Cytometry Measurements

For the flow cytometry analysis of neutrophil receptor expression, the following commercially available anti-pig monoclonal antibodies were obtained and when indicated conjugated by validated and commercially available antibody conjugation kits: SWC 1 (clone K263.3d7, Novus Biol, Centennial, Colorado, USA), SWC 3 (clone 74-22-15, Accurate Chemical, Westbury, New York, USA), SWC 8 (MIL-1, Abd Serotec, Kidlington, UK), CD11b (clone 2F4/11, Abd Serotec, Kidlington, UK), CD16 (clone G7, Abd Serotec, Kidlington, UK), CD29 (clone NaM160-1A3, BD, Mountain View, CA, USA), CD45 (clone K252.1E4, Abd Serotec, Kidlington, UK), CD45Ra (clone MIL-13, GenWay Biotech, San Diego, CA, USA), CD49D (clone L25, BD, Mountain View, CA, USA), CD184 (clone H-118, Santa Cruz Biotechnol, Santa Cruz, CA, USA). Lightning Link conjugation kits (Novus Biol, Centennial, Colorado, USA). A viability staining Vivid (Invitrogen, Waltham, USA) was added to exclude dead cells.

Data Analysis and Statistics

Data was analyzed using software programs SPSS version 21.0 (SPSS Inc., Chicago, IL, USA), GraphPad Prism 8.0 (GraphPad Software Inc., La Jolla, CA, USA) and FlowJo Version 10 (*De Novo* Software, Glendale, CA, USA). Results were expressed as means (SEM) unless otherwise mentioned. For comparisons, Student's T-tests, Paired T-testing or Mann Whitney U-tests were applied as appropriate. Equality of variance was tested using Lavene's test. A p-value < 0.05 was considered statistically significant.

RESULTS

All subjects survived the interventions, and respiratory complications were not diagnosed. Bone marrow sampling was not successful in one experimental animal and, therefore, bone marrow analysis was not performed on cells from this animal. All other samples provided sufficient material for analysis.

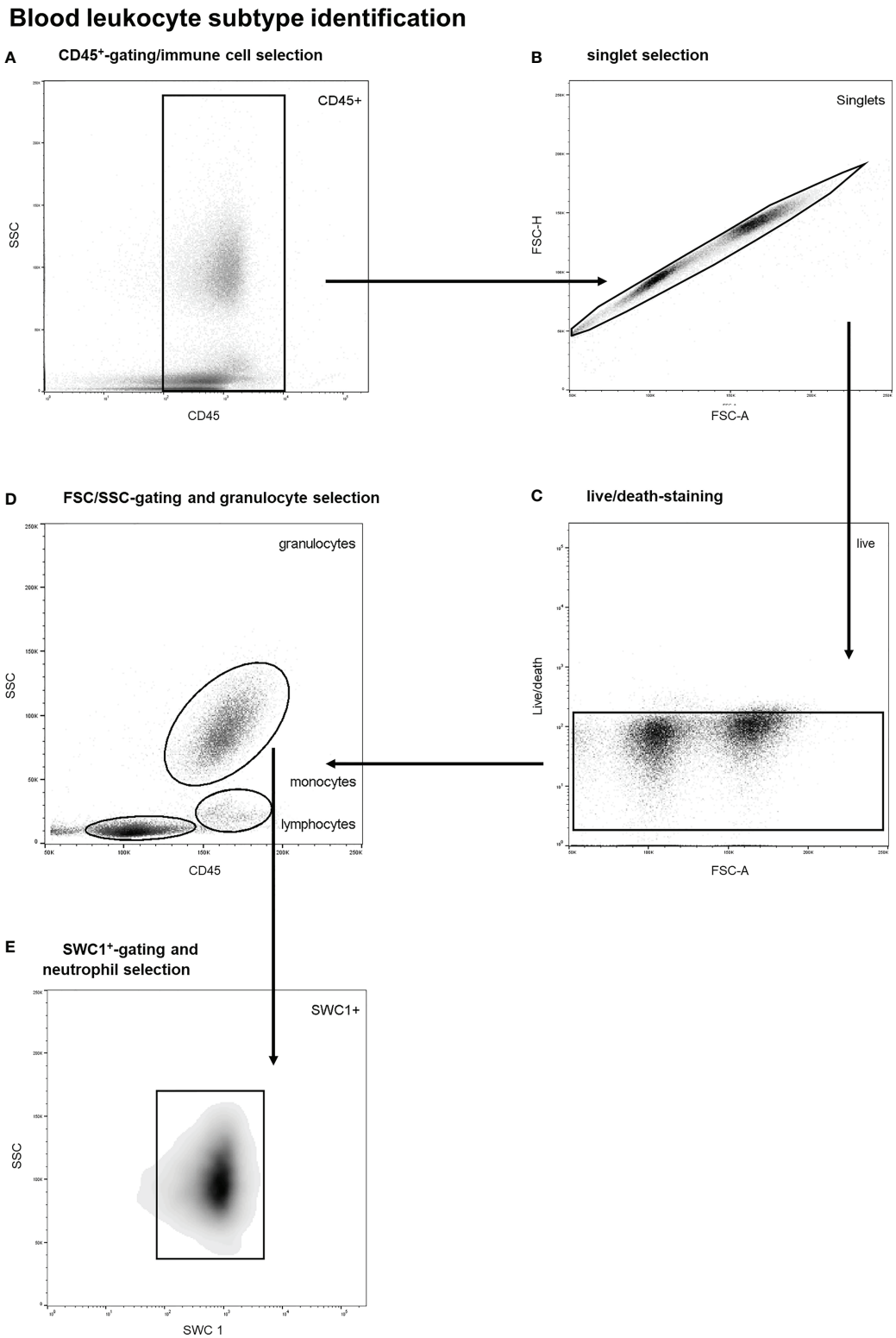

FIGURE 1 | Stepwise neutrophil gating protocol as utilized for identification of circulatory leukocyte subtypes and neutrophils. **(A)** Selection of CD45 positive cells and thereby the exclusion of debris and non-immune cells. **(B)** Exclusion of doublets. **(C)** Life/death-stain and selection of viable immune cells. **(D)** Identification of different leukocyte subtypes and subsequent selection of granulocytes using FSC/SSC-plots. **(E)** Selection of SWC 1^+ cells, and thereby exclusion of eosinophils. SSC, sideward scatter signal; FSC, forward scatter signal.

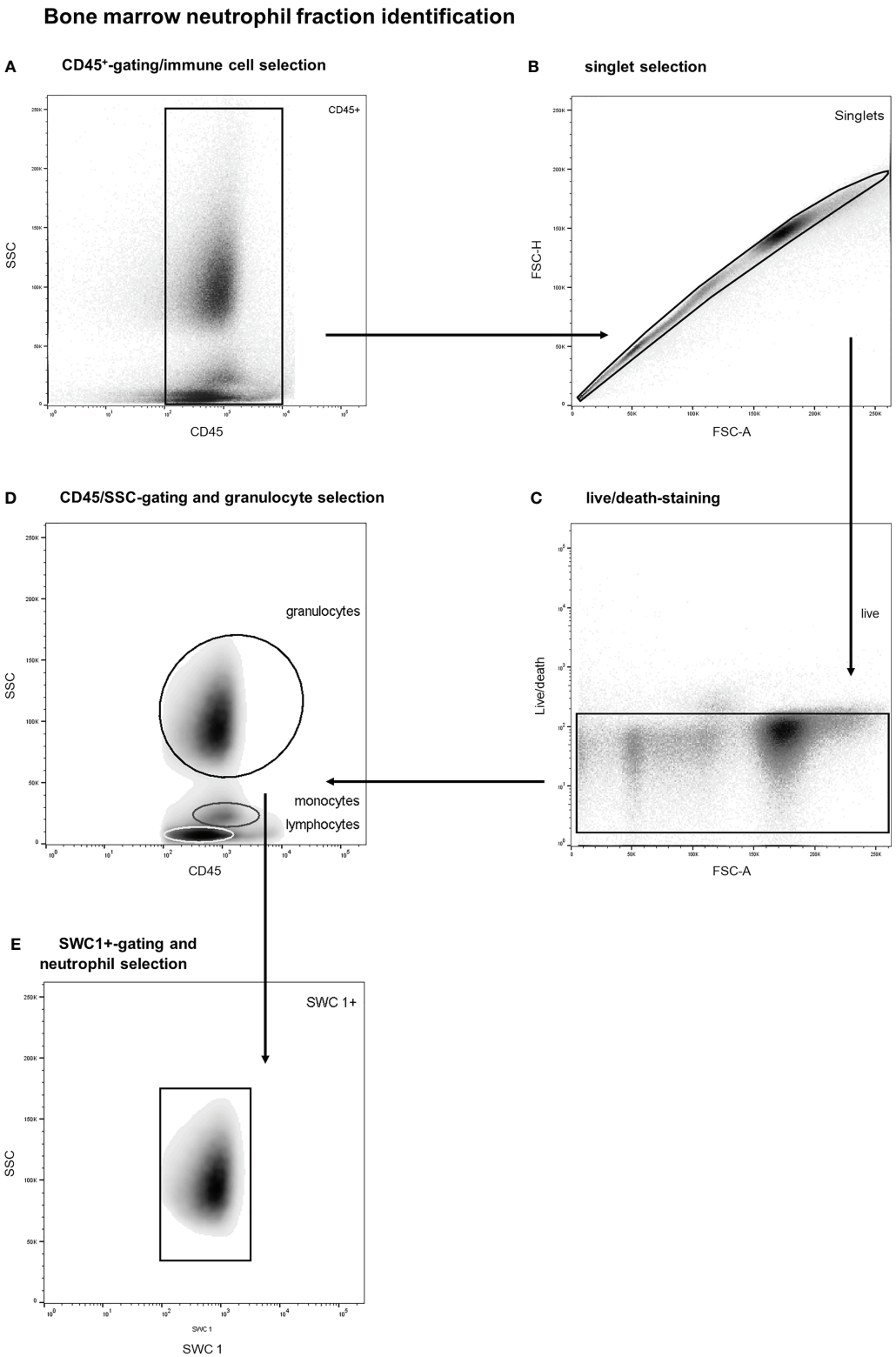

FIGURE 2 | Stepwise neutrophil gating protocol as utilized for identification of the bone marrow neutrophil fraction. **(A)** Selection of CD45 positive cells and thereby the exclusion of debris and non-immune cells. **(B)** Exclusion of doublets. **(C)** Life/death-stain and selection of viable immune cells. **(D)** Identification of different leukocyte subtypes and subsequent selection of granulocytes (of note: basophils are not included in the granulocyte gate due to distinct side scatter signal). **(E)** Selection of SWC 1+ cells, and thereby exclusion of potential contamination by eosinophils. SSC, sideward scatter signal; FSC, forward scatter signal.

Decreased Circulatory Leukocyte Numbers and Altered Relative Presence of Leukocyte Subtypes Following Extensive Trauma Surgery

As shown in **Figure 3** extensive trauma-surgery is associated with a marked and statistically significant drop in leukocyte numbers in peripheral blood. At baseline a mean white blood cell count of 21.3 ± 1.7 x10^6 cells/ml was measured, and after intervention leukocyte numbers reduced to 9.6 ± 1.6 x10^6 cells/ml *(P<0.001)*. The identification of specific white blood cell subtypes is displayed in **Figure 1**. Absolute lymphocyte and neutrophil numbers both dropped significantly over time from 10.3 to 5.9 x10^6 cells/ml *(P=0.01)*, and 9.3 to 3.2 x10^6 cells/ml *(P=0.001)*, respectively. The monocyte population decreased from 1.7 to 0.5 x10^6 cells/ml (*P=0.01*; see **Figure 3**). The mean percentage of blood neutrophils as part of all leukocytes decreased from 43% to 33% *(P=0.07)*, whereas the percentage of blood lymphocytes increased significantly *(P=0.02)*. This shows that extensive trauma surgery causes a shift in the constitution of the blood leukocyte pools characterized by decreased numbers of circulating immune cells and diminished neutrophil presence.

Increase of the Bone Marrow Neutrophil Fraction During Trauma was Associated With a Relative Circulatory Neutropenia

The composition of the bone marrow neutrophil fraction changed strikingly after extensive trauma surgery. Porcine bone marrow neutrophils have been identified according to a multistep gating protocol as described in **Figure 2**. The neutrophil bone marrow fraction increased in 6 out of 7 experimental animals upon insult. Under homeostatic conditions, 63 ± 3 percent of $CD45^+$ nucleated bone marrow cells were identified as neutrophils. However,

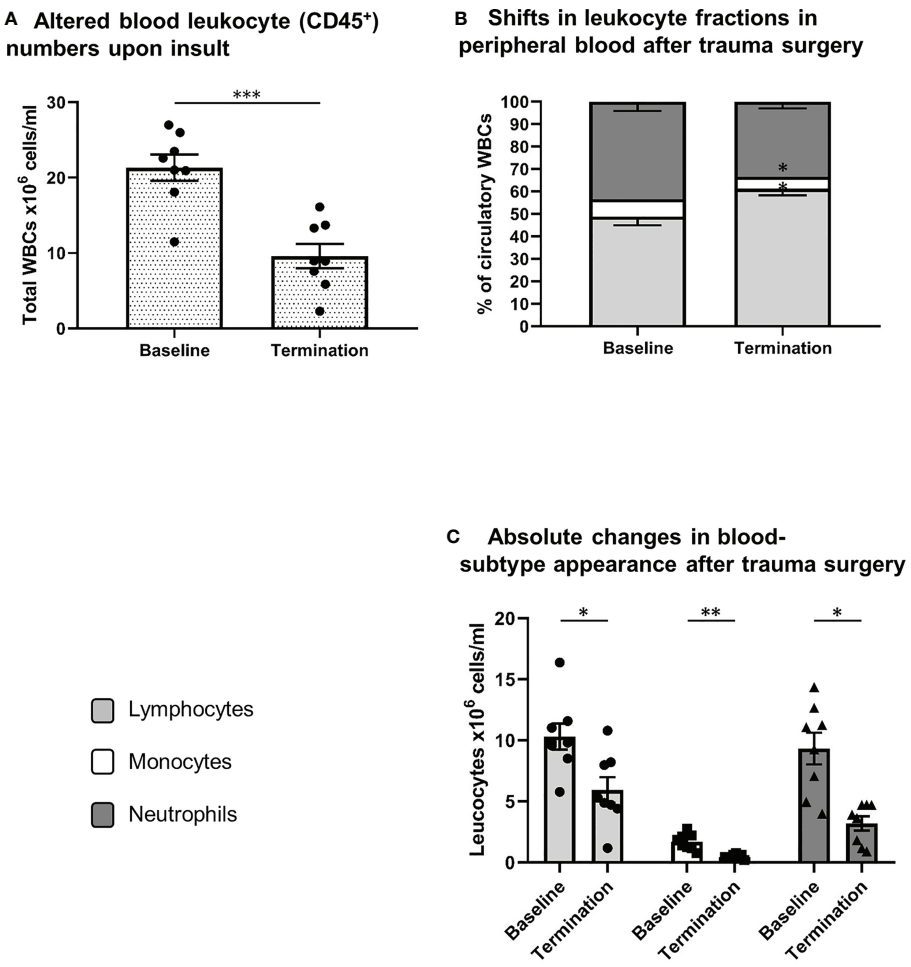

FIGURE 3 | Systemic leukocyte alterations after trauma surgery. **(A)** Difference in white blood cell count between both conditions (baseline vs. termination). Relative **(B)** and absolute **(C)** differences in lymphocyte, monocyte and neutrophil numbers between baseline and termination, reflecting shifts in leukocyte fractions after trauma surgery. S/FSC, sideward/forward scatter signal; N, neutrophils; M, monocytes; L, lymphocytes *P < 0.05, **P < 0.01, ***P < 0.001. Baseline samples were taken prior to intervention and termination sampling was performed directly after the final procedure.

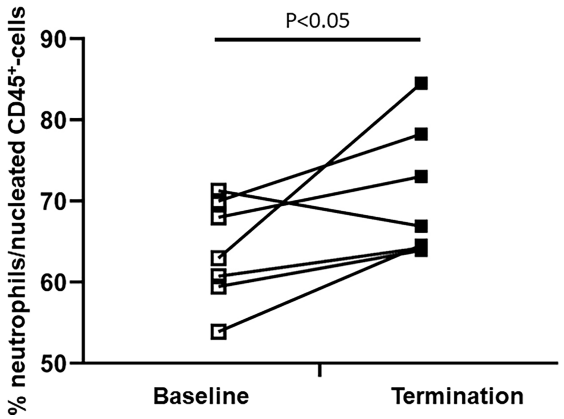

FIGURE 4 | Difference in the bone marrow neutrophil fraction between baseline and termination. The BM-neutrophil pool/fraction has been identified as described in **Figure 2**.

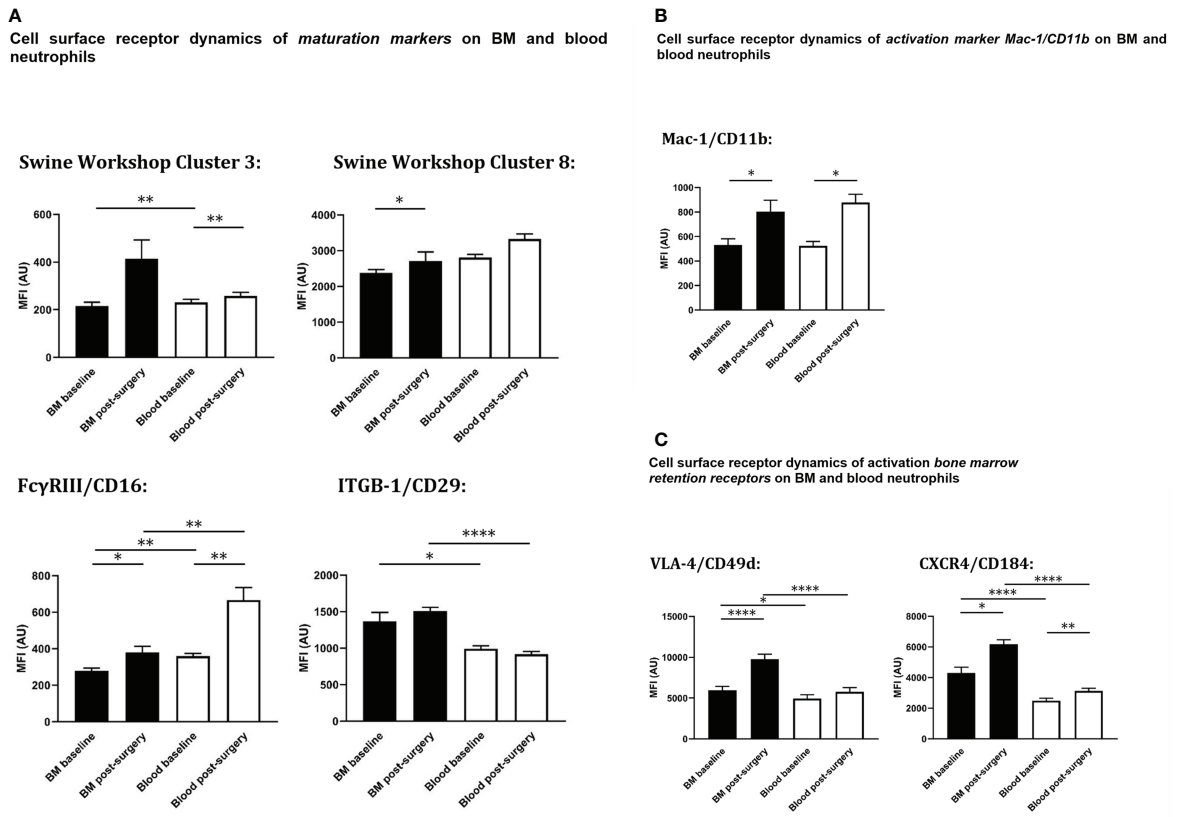

FIGURE 5 | Cell surface expression on circulating and bone marrow neutrophils at baseline and after extensive surgery. **(A)** BM-maturation markers, **(B)** activation markers, **(C)** BM retention receptors. Black bars represent bone marrow samples, white bars represent blood samples. Baseline samples were taken prior to intervention and termination sampling was performed directly after the final procedure. Data are presented as mean ± SEM, MFI, median fluorescence intensity in arbitrary units. *P < 0.05; **P < 0.01; ****P < 0.001.

following extensive surgery, this percentage increased up to 71 ± 3 percent (*P<0.05*, **Figure 4**).

Dynamics in Expression of Cell Surface Receptors Reflect an Instantaneous Shift of Neutrophil Populations From Blood to Bone Marrow After Trauma Surgery

Next to a change in cell numbers of circulatory and bone marrow neutrophils, receptor expression profiles of neutrophils in both compartments changed as well. Changes were homogeneous across the different experimental animals as described in detail hereafter. Relevant receptors involved in porcine neutrophil maturation (**Figure 5A**), activation (**Figure 5B**) and bone marrow retention and homing (**Figure 5C**) were analyzed, using the previously described gating strategy (**Figure 1**) (blood samples) and 2 (bone marrow samples).

At baseline, the population of peripheral blood neutrophils had significantly higher neutrophil surface expression levels of both SWC 3 *(P<0.01)* and CD16 *(P<0.01)* compared with bone marrow neutrophils. After trauma, a statistically significant increase of both neutrophil SWC 3 *(P<0.001)* and CD16 *(P<0.001)* expression was found on circulatory neutrophils, whereas a less prominent increase of SWC 3 (statistically non-significant) and CD16-expression levels *(P<0.05)* was measured on BM-cells. As anticipated, levels of cell surface expression of CD29 (integrin β1-chain) were significantly higher on bone marrow neutrophils than on circulatory neutrophils. No differences were seen between homeostatic and post-insult conditions (**Figure 5A**).

As shown in **Figure 5B**, no statistically significant differences in cell surface expression levels of activation marker CD11b were seen between neutrophils from blood and BM. After extensive surgery, CD11b-expression on circulatory neutrophils significantly increased after insult *(P<0.05)*.

In addition, in homeostasis expression levels of CD184 (CXCR4) and CD49d (VLA4) involved in neutrophil retention in the bone marrow were statistically significantly lower on circulatory neutrophils compared to bone marrow *(P<0.001 and P<0.05, respectively)*. Following intervention, cell surface expression levels of CD184 *(P<0.05)* and CD49d *(P<0.001)* rose on bone marrow neutrophils. CD49d-expression on systemic neutrophils did not change after insult, whereas CD184-expression on circulatory neutrophils increased significantly *(P<0.01)* and VLA-4 on bone marrow neutrophils increased significantly after intervention. Cell surface receptor expression levels of CD49d and CXCR4 on blood and bone marrow neutrophils under different conditions are shown in **Figure 5C**.

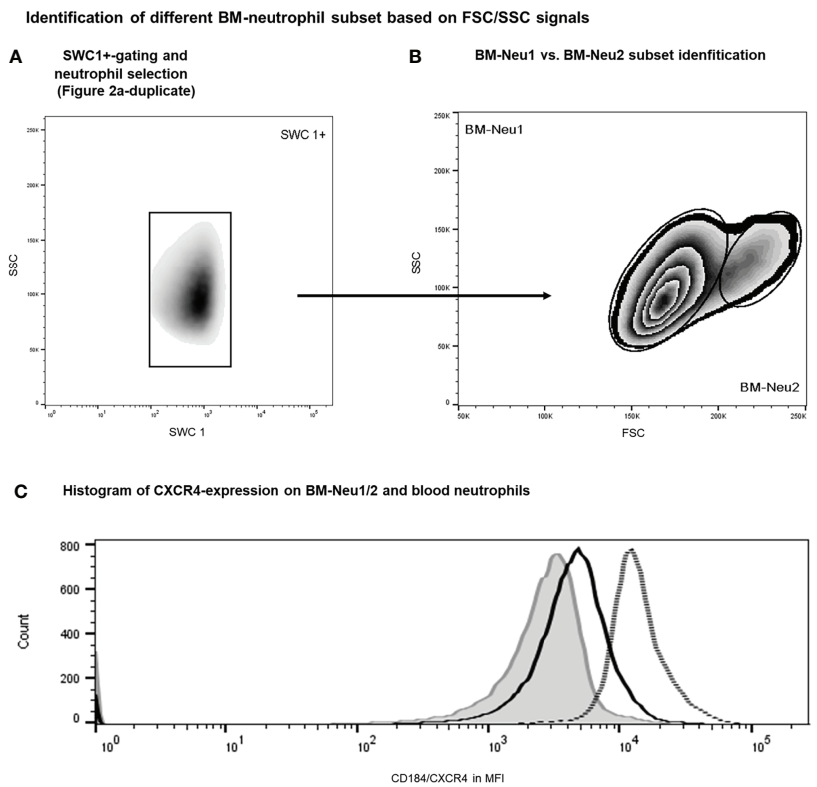

FIGURE 6 | Gating protocol for the identification of BM-neutrophil subsets after intervention. Initial gating steps have been displayed in **Figure 2**. **(A, B)** Representative example of FACS analysis of porcine bone marrow samples after intervention. **(C)** Histograms showing regular neutrophils (BM-Neu1, black line), novel FSC^{high} neutrophils (BM-Neu2, grey line) and reference blood neutrophils at termination (grey filled curve). MFI, median fluorescence intensity.

Increased Heterogeneity of the Bone Marrow Neutrophil Pool and Overrepresentation of an FCS^{high}/CXCR4^{high}-Neutrophil Subset Upon Extensive Porcine Trauma Surgery

As described previously, extensive trauma surgery is associated with striking changes in the cell-surface receptor expression profiles of the BM neutrophil pool (**Figures 5A–C**). Furthermore, the amount of variability of cell surface expression levels of relevant markers (**Figures 5A–C**) on BM neutrophils also increased after intervention, (**Figures 5A–C**), reflecting increased heterogeneity of the bone marrow neutrophil population after trauma.

Additionally, overrepresentation of a specific neutrophil subset of FSC^{high}-neutrophils (BM-Neu2) after insult was demonstrated (**Figures 6A, B**). Forward and side scatter density plots of CD45^{+}/SSC^{high}/SWC 1^{+}- cells (neutrophils) allow for identifying this specific subset (see **Figure 6B**). Under homeostatic conditions this subset (BM-Neu2) is virtually absent in bone marrow and represents 2.7 ± 0.2 percent of bone marrow neutrophils. However, after extensive trauma surgery, BM2-Neu-cells comprise 9.2 ± 1.0 percent of BM-neutrophils (**Figure 6B**). The relative increase of the size of the BM-Neu2 population as fraction of all BM-neutrophils after trauma was statistically significant *(P<0.001)*. BM2-Neu cells were further characterized by a statistically significant higher co-expression of CXCR4/CD184 *(P<0.01)*. A representative example of a histogram of CXCR4 expression on BM-Neu1 (regular neutrophils in BM), BM-Neu2 and a corresponding blood sample is displayed in **Figure 6C**. **Table 1** provides an overview of additional co-expression receptor analyses of both neutrophil subsets.

DISCUSSION

The key findings of the current study can be summarized as follows:

1. Extensive trauma-surgery in a standardized setting in pigs is associated with a prompt (<3hrs) decrease in circulating leukocyte numbers, including neutrophils.
2. Extensive trauma-surgery is associated with shifts in the composition of the bone marrow immune cell pools with an instantaneous relative increase of the BM-neutrophil fraction and an increased expression of neutrophil maturation markers on bone marrow neutrophils.
3. The post-traumatic BM-neutrophil pool is characterized by increased heterogeneity and overrepresentation of a unique CXCR4^{high} neutrophil subset.

TABLE 1 | Comparison of receptor co-expression profiles of BM-Neu1 and BM-Neu2 cells.

	BM-Neu1 (MFI)	BM-Neu2 (MFI)	P-value
SWC3	457 ± 68	356 ± 52	0.20
SWC8	2376 ± 205	2236 ± 806	0.07
FcγRIII/CD16	298 ± 45	385 ± 34	0.16
ITGB-1/CD29	1430 ± 164	902 ± 313	0.31
Mac-1/CD11b	859 ± 130	706 ± 70	0.52
VLA-4/CD49d	8497 ± 940	9777 ± 1156	0.70
CXCR4/CD184	5683 ± 530	14052 ± 1668	**0.0074**

Values in bold indicate statistically significant result. Data are presented as mean ± SEM. MFI, median fluorescence intensity in arbitrary units.

Our study provides essential novel insights into the early cellular immune response to severe trauma surgery within the BM compartment. In line with other studies on extensive trauma surgery, an early increase of activation status (e.g. enhanced neutrophil CD11b/Mac-1 expression) and a systemic neutropenia were demonstrated following insult (30).

It has previously been demonstrated in clinical studies on surgical patients that aberrant circulatory neutrophil/leukocyte numbers after insult are linked to impaired clinical outcome (4, 5, 31–35). Both situations of early decreased circulatory neutrophil numbers (4, 5, 31) as reported in the current study, but also situations of early elevated systemic immune cell numbers (32–35), are associated with inferior clinical outcome. These observations imply that specific patterns of (divergent) circulatory neutrophil kinetics, with either reduced or increased cell numbers, may represent an abnormal cellular immune response. A large number of neutrophils and their progenitors are present in the bone marrow under tight control of their production, differentiation and eventually mobilization (8–10, 17). Therefore, it is key to understand the interplay between the bone marrow, peripheral blood and distant tissues. To our knowledge this is the first study that has investigated the bone marrow's response to extensive trauma surgery and the related relative circulatory neutropenia in a controlled setting. Interestingly, and in contrast to the consensus (13, 14, 16), in the current study a relative increase of the BM-neutrophil fraction upon extensive surgical intervention was demonstrated, rather than depletion of the neutrophil bone marrow population (13, 14, 16).

The production and differentiation of granulocytes (granulopoiesis) mainly takes place in the bone marrow. Granulocytes and precursors make up 60% of BM-leukocytes (12). It is estimated that bone marrow produces approximately 0.5-1.0x 10^{11} neutrophils a day and that there are approximately 50-100 times more neutrophils in the bone marrow than in circulation (12, 36), but these issues are under current debate (37, 38). The bone marrow neutrophil population comprises of cells at different developmental stages. Three specific pools can be distinguished: the stem cell pool with self-renewal cell divisions, the mitotic pool (which includes cells (myeloblasts, (pro) myelocytes) that differentiate during proliferation) and the post-mitotic pool (with non-proliferating but maturing cells). The post-mitotic pool includes differentiated neutrophils (metamyelocytes, banded and mature cells) and forms a large bone marrow pool (39, 40). Mature neutrophils are released into circulation. After mobilization, neutrophils stay in circulation and may migrate into the tissue compartment before cells return to the bone marrow or other poorly defined tissue sites (17, 41). Under

homeostatic conditions systemic neutrophil numbers remain constant due to a balance in production, compartmentalization, and cell death. However, in the case of acute systemic inflammation, neutrophil numbers in different compartments shift markedly (1–5, 42). Our research group has previously shown early neutropenia in a study on experimental extreme trauma surgery in pigs (22), which was reproduced in this study. Interestingly, these novel experiments reveal a simultaneous increase of the bone marrow neutrophil fraction. This is in contrast with several human studies in which the occurrence of an ′empty bone marrow phenomenon′ upon extensive surgery has been suggested (13, 14, 16). In these latter studies a marked decrease of the bone marrow neutrophil pool was seen after insult. This bone marrow neutropenia was explained by a putative exhaustion BM cell production. The differences between our results and these findings may partly be explained by differences in the timing of the different investigations. The current experiment focuses on the acute response to extensive surgery (first 3 hours) only, whereas other studies focus on later time-points (> 24 hours) (13, 14, 16). A similar early relative neutropenia followed by later neutrophilia has been described in a model of human experimental endotoxemia (43).

Besides affecting neutrophil numbers, extensive trauma surgery also led to profound changes in the characteristics of both blood and BM neutrophils. Upon intervention, circulatory neutrophil CD11b expression almost doubled. Similar effects have been described in severe trauma and reflect the marked effect of our extensive surgical model on systemic immune homeostasis (30, 44). In parallel to the relative neutrophilia of the bone marrow, characteristics of the BM-pool, determined by analysis of neutrophil surface expression profiles, changed as well after insult.

More specifically, cell surface expression levels of CD11b, CD16, CD184, SWC 8 on BM-neutrophils increased significantly after trauma-surgery. In addition, a non-statistically significant trend towards increased SWC 3 expression was observed as well after intervention. CD11b, CD16, CD184, SWC 3 and SWC 8 have been identified as maturation markers for bone marrow neutrophils, whose expression levels on neutrophils rise during maturation (29, 29, 45). Therefore, the findings from our study indicate increased overall maturation of the bone marrow neutrophil population (29, 46). Increased expression of CD184 on blood neutrophils after trauma may be secondary due to massive selective tissue migration of young cells under extreme inflammatory conditions. Alternatively, blood may function as a transport medium for tissue neutrophil returning back to the bone marrow. Of note, increased CD11b-expression on BM-neutrophils is most likely mainly due to increased cell activation (30, 44), rather than due to more progressed maturation. Increased bone marrow maturation after surgery can be explained by four processes that are not mutually exclusive:

Firstly, an increase in older neutrophils in the bone marrow might be caused by selective release of young cells into the circulation. This hypothesis is supported by the massive release of banded neutrophils in the first hours after severe trauma (22, 43).

Secondly, selective acceleration of processes of neutrophil proliferation, differentiation and maturation may occur upon extreme conditions; a situation generally coined as emergency granulopoiesis (47, 48). There are, however, no published studies supporting this phenomenon in trauma patients. Also, such emergency granulopoiesis after trauma would result in more immature, rather than aged neutrophils (47, 48). Thirdly, bone marrow neutrophil apoptosis may be affected or postponed after extensive trauma. As mentioned before, aged, but not necessarily apoptotic neutrophils are thought to be cleared in the bone marrow (17, 41). While bone marrow is thought to be involved in clearance of neutrophils, it is also known for its capacity to optimize cell survival by specific BM survival factors (49, 50). In cases of extensive trauma, regulation of cell survival in the bone marrow compartment may differ from regular conditions.

Lastly, enhanced selective influx of aged neutrophils into the bone marrow compartment may occur after trauma. Bone marrow homing of aged but not apoptotic neutrophils in murine models is thought to be a CXCR4 (CD184)-dependent process as cells can respond to stromal derived factor (SDF)-1alpha/CXCL12, the ligand for CXCR4 (45, 51). The bone marrow compartment constitutively expresses SDF-1alpha/CXCL12, and the BM is considered as the preferred homing compartment of $CXCR4^{high}$-cells (18, 45). As such, increased BM accumulation of aged neutrophils, which have been trafficking back from circulation after extensive trauma surgery likely contribute to overall aging of the BM neutrophil population. Additionally, the current study is the first to describe prominent increase of a specific $CXCR4^{high}$-neutrophil subset (termed BM-Neu2) in bone marrow after trauma. This increased population likely reflects returning neutrophils from circulation and has previously been described in non-trauma conditions as well (51, 52). The role and capacities of this subset are currently unclear.

Limitations

Humoral factors upon standardized porcine trauma have been described in detail before and were not analyzed in the current study (53, 54). According to literature, systemic leukocyte neutrophil numbers in pigs range between 10 and 22 $x10^9$/L and are higher than in humans (55). Baseline leukocyte numbers in the current study were within ranges as described in literature. Therefore, we do not believe that stress-induced neutrophilia due to transportation or handling of the pigs played a relevant role (56). Furthermore, as neutrophil subsets were identified after interpretation of the experiments, we were not able to perform *in vitro* studies on the novel BM-subset. For the current study we decided to utilize female subjects only. This should be considered when extrapolating of our findings to male trauma. Female animals were utilized as relevant hormonal fluctuations were unlikely to affect outcome in an extensive trauma study with a short observation period. Furthermore, it has been shown before in multiple species that utilization of female animals is not associated with increased

variability of findings (57, 58). Moreover, housing of female animals is less challenging as they do not engage in hierarchy fights and female animals are easier to handle in the pre-operative phase than males. As a consequence, stress/cortisol-induced `baseline` alterations and subsequent increased variability were prevented (59, 60).

CONCLUSION

This study describes the early bone marrow response to extensive trauma surgery in a controlled setting. The current study shows for the first time that during trauma-induced neutropenia, a parallel increase in neutrophil numbers in the bone marrow occurs. This shift is characterized by relative enrichment of the bone marrow neutrophil fraction, increased maturation-status of the bone marrow neutrophils, and an increased number of a specific $CXCR4^{high}$-neutrophil subset in the bone marrow. This study also reveals that in pre-lethal trauma, aberrant neutrophil responses in blood and bone marrow go hand in hand. Hence, in order to design future immunomodulatory interventions for critically ill trauma patients it is important to acquire a better understanding of the pre-lethal bone marrow response. The porcine model is suitable to perform further studies on this issue and may also be utilized to perform future proof-of-principle interventions for pre-lethal trauma situations interventions.

DATA AVAILABILITY STATEMENT

The raw data supporting the conclusions of this article will be made available by the authors, without undue reservation.

ETHICS STATEMENT

The animal study was approved by the Saarland University Hospital Animal Care Committee.

AUTHOR CONTRIBUTIONS

MT, TB, H-CP, LK and LL conceived and designed the project. MT, MH, RS, EK and NV performed the (pilot) experiments and initial data analysis. MT, TB, NV, RP, H-CP, LK and LL contributed to the analysis and the interpretation of the data. MT, NV, RP, H-CP, LK and LL wrote the first draft of the manuscript. MT, MH, TB, RS, EK, NV, RP, H-CP, LK and LL contributed to the final version of the manuscript. All authors contributed to the article and approved the submitted version.

FUNDING

MT is supported by the Alexandre Suerman Stipend from the University Medical Center Utrecht.

REFERENCES

1. Keel M, Trentz O. Pathophysiology of Trauma. *Injury* (2005) 36(6):691–709. doi: 10.1016/j.injury.2004.12.037
2. Lord JM, Midwinter MJ, Chen YF, Belli A, Brohi K, Kovacs EJ, et al. The Systemic Immune Response to Trauma: An Overview of Pathophysiology and Treatment. *Lancet* (2014) 384(9952):1455–65. doi: 10.1016/S0140-6736(14)60687-5
3. Hesselink L, Spijkerman R, Wessem van K, Koenderman L, Leenen L, Huber-Lang M, et al. Neutrophil Heterogeneity and Its Role in Infectious Complications After Severe Trauma. *World J Emerg Surg* (2019) 14(24):1–11. doi: 10.1186/s13017-019-0244-3
4. Pallister I, Dent C, Topley N. Increased Neutrophil Migratory Activity After Major Trauma: A Factor in the Etiology of Acute Respiratory Distress Syndrome? *Crit Care Med* (2002) 30(8):1717–21. doi: 10.1097/00003246-200208000-00007
5. Botha AJ, Moore FA, Moore EE, Sauaia A, Banerjee A, Peterson VM. Early Neutrophil Sequestration After Injury: A Pathogenic Mechanism for Multiple Organ Failure. *J Trauma* (1995) 39:411–7. doi: 10.1097/00005373-199509000-00003
6. Jacobi CA, Ordemann J, Zieren HU, Volk HD, Bauhofer A, Halle E, et al. Increased Systemic Inflammation After Laparotomy vs Laparoscopy in an Animal Model of Peritonitis. *Arch Surg* (1998) 133(3):258–62. doi: 10.1001/archsurg.133.3.258
7. Richardson RP, Rhyne CD, Fong Y, Hesse DG, Tracey KJ, Marano MA, et al. Peripheral Blood Leukocyte Kinetics Following In Vivo Lipopolysaccharide (LPS) Administration to Normal Human Subjects. Influence of Elicited Hormones and Cytokines. *Ann Surg* (1989) 210(2):239–45. doi: 10.1097/00000658-198908000-00018
8. Eash K, Means J, White D, Link D. CXCR4 Is a Key Regulator of Neutrophil Release From the Bone Marrow Under Basal and Stress Granulopoiesis Conditions. *Blood* (2009) 113(19):4711–9. doi: 10.1182/blood-2008-09-177287
9. Furze RC, Rankin SM. Neutrophil Mobilization and Clearance in the Bone Marrow. *Immunology* (2008) 125:281–8. doi: 10.1111/j.1365-2567.2008.02950.x
10. Manz M, Boettcher S. Emergency Granulopoiesis. *Nat Rev Immunol* (2014) 14:302–14. doi: 10.1038/nri3660
11. Athens JW. Blood: Leukocytes. *Annu Rev Physiol* (1963) 25:195–212. doi: 10.1146/annurev.ph.25.030163.001211
12. Dancey JT, Deubelbeiss KA, Harker LA, Finch CA. Neutrophil Kinetics in Man. *J Clin Invest* (1976) 58(3):705–15. doi: 10.1172/JCI108517
13. Livingston D, Anjaria D, Wu J, Hauser C, Chang V, Deitch E, et al. Bone Marrow Failure Following Severe Injury in Humans. *Ann Surg* (2003) 238 (5):748–53. doi: 10.1097/01.sla.0000094441.38807.09
14. Marsh C, Boggs D, Cartwright G, Wintrobe M. Neutrophil Kinetics in Acute Infection. *J Clin Invest* (1967) 46(12):1943–53. doi: 10.1172/JCI105684
15. Rothstein G, Christensen RD, Nielsen BR. Kinetic Evaluation of the Pool Sizes and Proliferative Response of Neutrophils in Bacterially Challenged Aging Mice. *Blood* (1987) 70(6):1836–41. doi: 10.1182/blood.V70.6.1836.1836
16. Amos R, Deane M, Ferguson C, Jeffries G, Hinds C, Amess J. Observations on the Haemopoietic Response to Critical Illness. *J Clin Pathol* (1990) 43 (10):850–6. doi: 10.1136/jcp.43.10.850
17. Rankin S. The Bone Marrow: A Site of Neutrophil Clearance. *J Leukoc Biol* (2010) 88:241–51. doi: 10.1189/jlb.0210112
18. Furze RC, Rankin SM. The Role of the Bone Marrow in Neutrophil Clearance Unter Homeostatic Conditions in Mouse. *FASEB J* (2008) 22(9):3111–9. doi: 10.1096/fj.08-109876
19. Tsukamoto T, Pape HC. Animal Models for Trauma Research: What are the Options? *Shock* (2009) 31(1):3–10. doi: 10.1097/SHK.0b013e31817fdabf
20. Mair K, Sedlak C, Käser T, Pasternak A, Levast B, Gerner W, et al. The Porcine Innate Immune System: An Update. *Dev Comp Immunol* (2014) 45(2):321–43. doi: 10.1016/j.dci.2014.03.022
21. Rotondo MF, Schwab CW, McGonigal MD, Phillips GR, Fruchterman TM, Kauder DR, et al. "Damage Control": An Approach for Improved Survival in

Exsanguinating Penetrating Abdominal Injury. *J Trauma* (1993) 35(3):375–82. doi: 10.1097/00005373-199309000-00008
22. Teuben M, Heeres M, Blokhuis T, Hollman A, Vrisekoop N, Tan E, et al. Instant Intra-Operative Neutropenia Despite the Emergence of Banded ($CD16^{dim}$/$CD62L^{bright}$) Neutrophils in Peripheral Blood - An Observational Study During Extensive Trauma-Surgery in Pigs. *Injury* (2021) 52(3):426–33. doi: 10.1016/j.injury.2020.11.018
23. Schweinberger MH, Roukis TS. Percutaneous Autologous Bone Marrow Harvest From the Calcaneus and Proximal Tibia: Surgical Technique. *J Foot Ankle Surg* (2007) 46(5):411–4. doi: 10.1053/j.jfas.2007.05.009
24. Gillan E, Christensen R, Suen Y, Ellis R, van de Ven C, Cairo M. A Randomized, Placebo-Controlled Trial of Recombinant Human Granulocyte Colony-Stimulating Factor Administration in Newborn Infants With Presumed Sepsis: Significant Induction of Peripheral and Bone Marrow Neutrophilia. *Blood* (1994) 84(5):1427–33. doi: 10.1182/blood.V84.5.1427.1427
25. Bréa D, Meurens F, Dubois AV, Gaillard J, Chevaleyre C, Jourdan ML, et al. The Pig as a Model for Investigating the Role of Neutrophil Serine Proteases in Human Inflammatory Lung Diseases. *Biochem J* (2012) 447(3):363–70. doi: 10.1042/BJ20120818
26. De Ruiter K, Van Staveren S, Hilvering B, Knol E, Vrisekoop N, Koenderman L, et al. A Field-Applicable Method for Flow Cytometric Analysis of Granulocyte Activation: Cryopreservation of Fixed Granulocytes. *Cytometry A* (2018) 93 (5):540–7. doi: 10.1002/cyto.a.23354
27. Eleghetany M, Ge Y, Patel J, Martinez J, Uhrova H. Flow Cytometric Study of Neutrophilic Granulopoiesis in Normal Bone Marrow Using Expanded Panel of Antibodies: Correlation With Morphologic Assessments. *J Clin Lab Anal* (2004) 18:36–41. doi: 10.1002/jcla.20001
28. Van Lochem EG, Van der Velden VH, Wind HK, Te Marvelde JG, Westerdaal NA, Van Dongen JJ. Immunophenotypic Differentiation Patterns of Normal Hematopoiesis in Human Bone Marrow: Reference Patterns for Age-Related Changes and Disease-Induced Shifts. *Cytometry B Clin Cytom* (2004) 60(1):1. doi: 10.1002/cyto.b.20008
29. Summerfield A, McCullough K. Porcine Bone Marrow Myeloid Cells: Phenotype and Adhesion Molecule Expression. *J Leuk Biol* (1997) 62 (2):176–85. doi: 10.1002/jlb.62.2.176
30. Botha AJ, Moore FA, Moore EE, Peterson VM, Goode AW. Base Deficit After Major Trauma Directly Relates to Neutrophil CD11b Expression: A Proposed Mechanism of Shock-Induced Organ Injury. *Intensive Care Med* (1997) 23 (5):504–9. doi: 10.1007/s001340050365
31. Gulack BC, Englum BR, Lo DD, Nussbaum DP, Keenan JE, Scarborough JE, et al. Leukopenia Is Associated With Worse But Not Prohibitive Outcomes Following Emergent Abdominal Surgery. *J Trauma* (2015) 79(3):437–43. doi: 10.1097/TA.0000000000000757
32. Rovlias A, Kotsou S. The Blood Leukocyte Count and Its Prognostic Significance in Severe Head Injury. *Surg Neurol* (2001) 55(4):190–6. doi: 10.1016/S0090-3019(01)00414-1
33. Waheed U, Williams P, Brett S, Baldock G, Soni N. White Cell Count and Intensive Care Unit Outcome. *Anaesth* (2003) 58(2):180–2. doi: 10.1046/j.1365-2044.2003.02964_5.x
34. Lawrence YR, Raveh D, Rudensky B, Munter G. Extreme Leukocytosis in the Emergency Department. *QJM* (2007) 100(4):217–23. doi: 10.1093/qjmed/hcm006
35. Hasjim BJ, Grigorian A, Stopenski S. Moderate to Severe Leucocytosis With Vasopressor Is Associated With Increased Mortality in Trauma Patients. *J Intens Care Soc* (2020) 1–7. doi: 10.1177/1751143720975316
36. Semerad CL, Liu F, Gregory AD, Stumpf K, Link DC. G-CSF is an Essential Regulator of Neutrophil Trafficking From the Bone Marrow to the Blood. *Immunity* (2002) 17(4):413–23. doi: 10.1016/S1074-7613(02)00424-7
37. Pillay J, den Braber I, Vrisekoop N, Kwast LM, de Boer RJ, Borghans JA, et al. *In Vivo* Labeling With 2H2O Reveals a Human Neutrophil Lifespan of 5.4 Days. *Blood* (2010) 116(4):625–7. doi: 10.1182/blood-2010-01-259028
38. Lahoz-Beneytez J, Elemans M, Zhang Y, Ahmed R, Salam A, Block M, et al. Human Neutrophil Kinetics: Modeling of Stable Isotope Labeling Data Supports Short Blood Neutrophil Half-Lives. *Blood* (2016) 127(26):3431–8. doi: 10.1182/blood-2016-03-700336
39. Orr Y, Wilson DP, Taylor JM, Bannon PG, Geczy C, Davenport MP, et al. A Kinetic Model of Bone Marrow Neutrophil Production That Characterizes Late Phenotypic Maturation. *Am J Physiol Regul Integr Comp Physiol* (2007) 292(4):R1707–16. doi: 10.1152/ajpregu.00627.2006
40. Summers C, Rankin SM, Condliffe AM, Singh N, Peters AM, Chilvers ER. Neutrophil Kinetics in Health and Disease. *Trends Immunol* (2010) 31 (8):318–24. doi: 10.1016/j.it.2010.05.006
41. von Vietinghoff S, Ley K. Homeostatic Regulation of Blood Neutrophil Counts. *J Immunol* (2008) 181:5183–8. doi: 10.4049/jimmunol.181.8.5183
42. Wengner A, Pitchford S, Furze R, Rankin S. The Coordinated Action of G-CSF and ELR + CXC Chemokines in Neutrophil Mobilization During Acute Inflammation *Blood* (2008) 181:5183–8. doi: 0.1182/blood-2007-07-0996481
43. Pillay J, Kamp VM, van Hoffen E, Visser T, Tak T, Lammers JW, et al. A Subset of Neutrophils in Human Systemic Inflammation Inhibits T Cell Responses Through Mac-1. *J Clin Invest* (2012) 122(1):327–36. doi: 10.1172/JCI57990
44. Hietbrink F, Koenderman L, Leenen LP. Intramedullary Nailing of the Femur and the Systemic Activation of Monocytes and Neutrophils. *World J Emerg Surg* (2011) 6:34. doi: 10.1186/1749-7922-6-34
45. Lund-Johannsen F, Terstappen L. Cell Adhesion Molecules During Granulopoiesis. *J Leuk Biol* (1993) 54(1):47–55. doi: 10.1002/jlb.54.1.47
46. Leitão L, Alves CJ, Alencastre IS, Sousa DM, Neto E, Conceição F, et al. Bone Marrow Cell Response After Injury and During Early Stage of Regeneration Is Independent of the Tissue-of-Injury in 2 Injury Models. *FASEB J* (2019) 33 (1):857–72. doi: 10.1096/fj.201800610RR
47. Fuchs A, Moonlish D, Ghosh S, Chang S, Bochicchio G, Schuettpelz L, et al. Trauma Induces Emergency Hematopoiesis Through IL-1/MyD88–Dependent Production of G-CSF. *J Immunol* (2019) 202(10):3020–2. doi: 10.4049/jimmunol.1801456
48. Benarafa C, LeCruyer TE, Baumann M, Stolley JM, Cremona TP, Remold-O-Donnell E. SerpinB1 Protects the Mature Neutrophil Reserve in the Bone Marrow. *J Leukoc Biol* (2011) 90:21–9. doi: 10.1189/jlb.0810461
49. Altznauer F, Martinelli S, Yousefi S, Thurig C, Schmid I, Conway EM, et al. Inflammation-Associated Cell Cycle-Independent Block of Apoptosis by Surviving in Terminally Differentiated Neutrophils. *J Exp Med* (2004) 199:1943–54. doi: 10.1084/jem.20032033
50. Nagase H, Miyamasu M, Yamaguchi M, Imanishi M, Tsuno NH, Matsushima K, et al. Cytokine-Mediated Regulation of CXCR4 Expression in Human Neutrophils. *J Leukoc Biol* (2002) 71(4):711–7.
51. Martin C, Burdon PC, Bridger G, Gutierrez-Ramos JC, Williams TJ, Rankin SM. Chemokines Acting *via* CXCR2 and CXCR4 Control the Release of Neutrophils From the Bone Marrow and Their Return Following Senescence. *Immunity* (2003) 19(4):583–93. doi: 10.1016/S1074-7613(03)00263-2
52. De Filipo K, Rankin SM. CXCR4, the Master Regulator of Neutrophil Trafficking in Homeostasis and Disease. *Eur J Clin Invest* (2018) 48 (Suppl.2):e12949. doi: 10.1111/eci.12949
53. Horst K, Eschbach D, Pfeifer R, Hübenthal S, Sassen M, Steinfeldt T, et al. Local Inflammation in Fracture Hematoma: Results From a Combined Trauma Model in Pigs. *Mediators Inflamm* (2015) 2015:126060. doi: 10.1155/2015/126060
54. Horst K, Greven J, Lüken H, Zhi Q, Pfeifer R, Simon TP, et al. Trauma Severity and Its Impact on Local Inflammation in Extremity Injury-Insights From a Combined Trauma Model in Pigs. *Front Immunol* (2020) 10:3028. doi: 10.3389/fimmu.2019.03028
55. Fingerhut L, Dolz G, de Buhr N. What Is the Evolutionary Fingerprint in Neutrophil Granulocytes? *Int J Mol Sci* (2020) 21(12):4523. doi: 10.3390/ijms21124523
56. Dubreuil P, Courure Y, Faermer C, Petitclerc D. Hematological and Biochemical Changes Following an Acute Stress in Control and Somatostatin-Immunized Pigs. *Can J Anim Sc* (1993) 73(2):241–52. doi: 10.4141/cjas93-026
57. Beery AK. Inclusion of Females Does Not Increase Variability in Rodent Research Studies. *Curr Opin Behav Sci* (2018) 23:143–9. doi: 10.1016/j.cobeha.2018.06.016
58. Prendergast BJ, Onishi KG, Zucker I. Female Mice Liberated for Inclusion in Neuroscience and Biomedical Research. *Neurosci Biobehav Rev* (2014) 40:1–5. doi: 10.1016/j.neubiorev.2014.01.001
59. Sutherland MA, Niekamp SR, Rodriguez-Zas SL, Salak-Johnson JL. Impacts of Chronic Stress and Social Status on Various Physiological and Performance Measures in Pigs of Different Breeds. *J Anim Sci* (2006) 84(3):588–96. doi: 10.2527/2006.843588x
60. McGlone JJ, Salak JL, Lumpkin EA, Nicholson RI, Gibson M, Norman RL. Shipping Stress and Social Status Effects on Pig Performance, Plasma Cortisol,

Natural Killer Cell Activity, and Leukocyte Numbers. *J Anim Sci* (1993) 71 (4):888–96. doi: 10.2527/1993.714888x

Conflict of Interest: The authors declare that the research was conducted in the absence of any commercial or financial relationships that could be construed as a potential conflict of interest.

Publisher's Note: All claims expressed in this article are solely those of the authors and do not necessarily represent those of their affiliated organizations, or those of the publisher, the editors and the reviewers. Any product that may be evaluated in this article, or claim that may be made by its manufacturer, is not guaranteed or endorsed by the publisher.

frontiers | Frontiers in Immunology

ORIGINAL RESEARCH
published: 19 May 2022
doi: 10.3389/fimmu.2022.908618

Inferring Tissue-Specific, TLR4-Dependent Type 17 Immune Interactions in Experimental Trauma/Hemorrhagic Shock and Resuscitation Using Computational Modeling

Ashti M. Shah[1‡], Ruben Zamora[1,2‡], Sebastian Korff[1†‡], Derek Barclay[1], Jinling Yin[1], Fayten El-Dehaibi[1], Timothy R. Billiar[1§] and Yoram Vodovotz[1,2,3§]*

[1] Department of Surgery, University of Pittsburgh, Pittsburgh, PA, United States, [2] Center for Inflammation and Regeneration Modeling, McGowan Institute for Regenerative Medicine, Pittsburgh, PA, United States, [3] Center for Systems Immunology, University of Pittsburgh, Pittsburgh, PA, United States

Trauma/hemorrhagic shock followed by resuscitation (T/HS-R) results in multi-system inflammation and organ dysfunction, in part driven by binding of damage-associated molecular pattern molecules to Toll-like Receptor 4 (TLR4). We carried out experimental T/HS-R (pseudo-fracture plus 2 h of shock followed by 0-22 h of resuscitation) in C57BL/6 (wild type [WT]) and TLR4-null ($TLR4^{-/-}$) mice, and then defined the dynamics of 20 protein-level inflammatory mediators in the heart, gut, lung, liver, spleen, kidney, and systemic circulation. Cross-correlation and Principal Component Analysis (PCA) on data from the 7 tissues sampled suggested that $TLR4^{-/-}$ samples express multiple inflammatory mediators in a small subset of tissue compartments as compared to the WT samples, in which many inflammatory mediators were localized non-specifically to nearly all compartments. We and others have previously defined a central role for type 17 immune cells in human trauma. Accordingly, correlations between IL-17A and GM-CSF (indicative of pathogenic Th17 cells); between IL-17A and IL-10 (indicative of non-pathogenic Th17 cells); and IL-17A and TNF (indicative of memory/effector T cells) were assessed across all tissues studied. In both WT and $TLR4^{-/-}$ mice, positive correlations were observed between IL-17A and GM-CSF, IL-10, and TNF in the kidney and gut. In contrast, the variable and dynamic presence of both pathogenic and non-pathogenic Th17 cells was inferred in the systemic circulation of $TLR4^{-/-}$ mice over time, suggesting a role for TLR4 in efflux of these cells into peripheral tissues. Hypergraph analysis – used to define dynamic, cross compartment networks – in concert with PCA-suggested that IL-17A was present persistently in all tissues at all sampled time points except for its absence in the plasma at 0.5h in the WT group, supporting the hypothesis that T/HS-R induces efflux of Th17 cells from the circulation and into specific tissues. These analyses suggest a complex, context-specific role for TLR4 and type 17 immunity following T/HS-R.

Keywords: trauma, hemorrhagic shock, inflammation, systems biology, computational biology, Toll-like 4 receptor

OPEN ACCESS

Edited by:
Klemens Horst, University Hospital RWTH Aachen, Germany

Reviewed by:
Yukihiro Yamaguchi, University of North Carolina at Chapel Hill, United States
Peter A. Ward, University of Michigan, United States

***Correspondence:**
Yoram Vodovotz
vodovotzy@upmc.edu

***Present address:**
Sebastian Korff, Department of Orthopedics and Traumatology, University of Heidelberg, Heidelberg, Germany

*These authors have contributed equally to this work and share first authorship

*These authors have contributed equally to this work and share senior authorship

Specialty section:
This article was submitted to Inflammation, a section of the journal Frontiers in Immunology

Received: *30 March 2022*
Accepted: *21 April 2022*
Published: *19 May 2022*

Citation:
Shah AM, Zamora R, Korff S, Barclay D, Yin J, El-Dehaibi F, Billiar TR and Vodovotz Y (2022) Inferring Tissue-Specific, TLR4-Dependent Type 17 Immune Interactions in Experimental Trauma/Hemorrhagic Shock and Resuscitation Using Computational Modeling. Front. Immunol. 13:908618. doi: 10.3389/fimmu.2022.908618

INTRODUCTION

Trauma, which often co-occurs with severe hemorrhage (1), is one of the leading causes of death and disability worldwide (2). Patients that survive their initial injuries and hypovolemic shock often undergo organ dysfunction that is associated with, and likely driven by, multi-focal inflammation (3, 4). In the context of human trauma, it is often difficult to discern the dynamic flow of inflammation across tissues and organs, with the systemic circulation being the main compartment that is amenable to interrogation. Despite this limitation, an extensive body of literature has documented the impact of trauma/hemorrhage on immune cells (5, 6), inflammatory mediators (7–9), and a large array of cell-derived proteins and metabolites (10, 11) in the systemic circulation. Among a multitude of findings, these studies have suggested a potential role for type 17 immune responses following traumatic injury (7, 12, 13).

A key, unanswered question remains that of how trauma/hemorrhage impact immuno-inflammatory responses in various organs and the systemic circulation. We have recently begun to address this question in the simpler context of experimental endotoxemia in mice, utilizing computational methods aimed at defining the temporal hierarchy of the cross-tissue progression of inflammation, dynamic networks of inflammation, and the hallmarks of pathological systemic spillover of inflammation (14, 15). These studies also implicated type 17 immune responses in the spatiotemporal elaboration of inflammation (15).

The inflammatory response to both traumatic injury and sepsis/endotoxemia involves Toll-like receptor-4 (TLR4). In the context of sepsis, TLR4 transduces signals from pathogen-derived molecular pattern (PAMP) molecules such as endotoxin/lipopolysaccharide (LPS) (16), whereas in the setting of trauma TLR4 mediates signals from damage-associated molecular pattern (DAMP) molecules such as high-mobility group box-1 (HMGB1) (17). Our prior studies on modeling the spatiotemporal dynamics of LPS-induced inflammation suggested distinct, tissue- and time-specific differences in wild type (WT) C57BL/6 mice as compared to TLR4-deficient ($TLR4^{-/-}$) mice (14, 15).

In the present study, our goal was to interrogate the spatiotemporal dynamics of inflammation in the context of experimental trauma/hemorrhagic shock, and the impact of resuscitation on these dynamics. We also sought to define the impact of TLR4 deficiency. Our prior data-driven modeling studies in both experimental (18) and clinical (12, 19–21) settings of trauma/hemorrhage leveraged Principal Component Analysis (PCA) (7, 18, 22), cross-correlation analysis (14), and dynamic network discovery algorithms (4, 8, 15). Here, we utilized PCA along with an emerging multi-dimensional network analysis approach known as hypergraphs (23–26) to define novel DAMP/TLR interactions.

MATERIALS AND METHODS

Experimental Model of T/HS-R in Mice

All procedures involving animals complied with the regulations regarding the care and use of experimental animals published by the National Institutes of Health and were approved by the Institutional Animal Care and Use Committee of the University of Pittsburgh. Male $TLR4^{+/+}$ C57BL/6 mice were purchased from Jackson Laboratory (Bar Harbor, ME, USA). TLR4-null ($TLR4^{-/-}$) mice were bred at the University of Pittsburgh animal facility on a C57BL/6 background (27). Animals were allowed access to rodent chow and water *ad libitum* and used at the age of 8-12 weeks. Both wild type (WT) and $TLR4^{-/-}$ mice were randomly assigned to one of three experimental groups: Control (animals were sacrificed directly after anesthesia to obtain physiological baseline levels, n=4-5), HS (animals were subjected to pseudo-fracture followed by pressure controlled hemorrhagic shock, n=4), and HS/R (animals were subjected to pseudo-fracture and hemorrhagic shock followed by 30 min, 1h, 4h, and 22h resuscitation, n=4 each), as previously described (28). At different time-points, the animals were anesthetized with isoflurane (0.25-2% as needed), cardiac puncture was performed, blood was collected into heparinized tubes, and then centrifuged to obtain plasma; the mice were then euthanized by cervical dislocation while under anesthesia. Mice were then perfused with ice-cold PBS followed by RNALater™ (Thermo Fisher Scientific, Waltham, MA), which we have previously shown to be a preservation method compatible with Luminex™ analysis and equivalent to flash-freezing in liquid nitrogen (29). A small section (approx. 100 mg) of each tissue (liver [left lobe], heart, gut [terminal ileum], lung [left lobe], spleen, and kidney [left]) was collected and stored at -80°C until analysis. Total protein isolation and determination was done as described previously (30).

Assay of Inflammatory Mediators

Mouse inflammatory mediators were measured using a Luminex™ 100 IS apparatus (Luminex, Austin, TX) and the 20-plex mouse cytokine bead kit (MCYTO-70K-20, Millipore, Burlington, MA) as per manufacturer's specifications. The antibody bead kit included: Granulocyte-Macrophage Colony-Stimulating Factor (GM-CSF), Interferon-γ (IFN-γ), Interleukin (IL)-1α, IL-1β, IL-2, IL-4, IL-5, IL-6, IL-10, IL-12p40, IL-12p70, IL-13, IL-17A, Interferon-γ-inducible Protein 10 (IP-10/CXCL10), Keratinocyte-derived Cytokine (KC/CXCL1), Monocyte Chemoattractant Protein-1 (MCP-1/CCL2), Monokine induced by Interferon-γ (MIG/CXCL9), Macrophage Inflammatory Protein-1α (MIP-1α/CCL3), Tumor Necrosis Factor-α (TNF), and Vascular Endothelial Growth Factor (VEGF). The final mediator concentrations are expressed in pg/ml for plasma samples, and in pg/mg total protein for tissue samples. Experimental data are presented as mean ± SEM.

Statistical and Computational Analyses

Two-Way Analysis of Variance (ANOVA) was carried out to analyze the time-dependent changes in inflammatory mediators in C57BL/6 (wild type, WT) vs. $TLR4^{-/-}$ mice in all organs as well as in plasma, using SigmaPlot (Systat Software, San Jose, CA).

Heatmaps and Spearman's correlation carried out to measure the strength of the association between the Luminex™ data for two different mediators were generated using MetaboAnalyst (https://www.metaboanalyst.ca) (31, 32).

Principal component analysis (PCA) was carried out to identify the inflammatory mediators that contributed the most to the overall variance of the response in all organs as well as in plasma of both wild type and TLR4$^{-/-}$ mice with and without HS and HS/R as described above. The algorithm employed was implemented using MATLAB® software (The MathWorks, Inc., Natick, MA) and has been reported previously (18).

Hypergraphs are a computational tool to model how inflammatory mediators move between tissues across time. This form of network analysis can be used to represent edges that connect two or more vertices (23–26). Here, we created a set of hypergraphs to model the inflammatory mediators sampled in the WT and TLR4$^{-/-}$ experimental groups described above. We designated inflammatory mediators as edges and tissue compartments as nodes. As such, we utilized the following nodes/tissue compartments: liver, spleen, gut, lung, kidney, heart, and plasma. A hypergraph was created for each time point at which a tissue sample was drawn (CTRL, HS, HS/R at 0.5h, 1h, 4h, and 22h). An edge is drawn around one or more nodes when the concentration of the cytokine in the tissue/plasma is > 0. The resultant hypergraphs depict which inflammatory mediators are located within a given set of tissues at specific time point. Hypergraphs were created using the open-source package HyperNetX (https://github.com/pnnl/HyperNetX) (33).

To add quantitative analysis to the hypergraph visualizations, we utilized s-betweenness centrality and edge distribution to characterize network complexity. S-betweenness centrality is a measure of the number of times an edge lies on the shortest path between other edges. In essence, s-betweenness centrality is a measure of the extent to which an edge, or inflammatory mediator, acts as a bridge between nodes, or tissue compartments. Here, we focused on 1-betweenness centrality which captures edges that connect one or more nodes. The second quantitative metric used was edge distribution, which simply tallies the number of edges that surround 1, 2, and 3 nodes, respectively. Such a metric quantifies the extent to which inflammatory mediators are grossly disseminated throughout the body.

RESULTS

Differential Dynamic Expression of Inflammatory Mediators in Multiple Tissues of WT vs. TLR4$^{-/-}$ Mice

We first performed Spearman Rank correlation analysis using all experimental data of WT vs. TLR4$^{-/-}$ mice to visualize differences between WT and TLR4$^{-/-}$ mice at baseline (Control), in response to hemorrhagic shock, and following resuscitation. This analysis suggested a generally more robust inflammatory response in WT as compared to TLR4$^{-/-}$ mice (**Figure 1A**). To compare inflammatory profiles of WT vs. TLR4$^{-/-}$mice for the three experimental conditions (Ctrl, HS, and HS/R), we generated 3 individual heatmaps using the average concentration values for each mediator in each group (**Figure 1B**). This analysis suggested that 1) the main tissues in which inflammation evolved following T/HS-R in both WT and TLR4$^{-/-}$ were the gut > kidney > liver > lung, and, to a lesser degree, the systemic circulation; 2) that in both WT and TLR4$^{-/-}$ mice HS resulted in a major impact on the gut, which persisted in WT mice following resuscitation but that was greatly reduced in TLR4$^{-/-}$ mice; and 3) that baseline inflammatory responses in the kidney were reduced following hemorrhage and further reduced following resuscitation in WT mice, while decreasing following hemorrhage but rising substantially following resuscitation in TLR4$^{-/-}$ mice. This analysis pointed to a complex, context-specific role for TLR4 following T-HS/R.

To determine the impact TLR4 status over time, we next carried out Two-Way ANOVA (**Supplementary Figure 1**). Comparison of time-courses (wild type vs. TLR4$^{-/-}$) showed statistically significant changes in several inflammatory mediators (n) as follows: spleen (n=7 [GM-CSF, IL-1α, IL-5, IL-10, IP-10, KC, MIG]), kidney (n=6 [IL-1α, IL-4, IL-5, IL-12p70, KC, MIP-1α]), plasma (n=5 [KC, MCP-1, MIG, MIP-1α, TNFα]), heart (GM-CSF), liver (KC), lung (IL-4), and gut (IL-10). Notably, the absence of TLR4 was not associated simply with reduced levels of inflammatory mediators; rather, we observed complex dynamics in which certain mediators were higher in WT or in TLR4$^{-/-}$ mice in certain tissues at certain time points (**Supplementary Figure 1**).

Hypergraph Analysis Defines Distinct Multi-Organ Inflammation in WT vs. TLR4$^{-/-}$ Mice

We have reported previously that the expression of TLR4 impacts dynamic networks of inflammation induced by LPS in mice (14, 15). We therefore hypothesized that the expression of TLR4 impacts the cross-compartment spread of inflammation, and thus compared the dynamic evolution of inflammation in WT and TLR4$^{-/-}$ mice following T/HS-R. While dynamic network inference algorithms such as Dynamic Network Analysis (18) and Dynamic Bayesian Network (DyBN) inference (20) have both proven useful in identifying novel features of systemic inflammation following trauma/hemorrhage, as well as for defining cross-tissue interactions in other context of inflammation (34), these methods are not designed explicitly for multi-dimensional analysis. Emerging hypergraph methods (23–26) hold the potential for this type of analysis, and therefore we carried out a hypergraph analysis of the multi-tissue dataset at each time point (**Figures 2**–**7**). Prior to injury, despite overall low levels of inflammatory mediators in general, WT mice (**Figure 2A**) expressed a variety of cytokines and chemokines in fewer organs with more mediators present in the systemic circulation vs. TLR4$^{-/-}$ mice (**Figure 2B**), suggesting that TLR4 deficiency mitigated an inherent tendency for pathological systemic inflammation in C57BL/6 mice. Notably, after 2h of hemorrhagic shock, overall tissue distribution of inflammatory mediators was fairly similar in WT and TLR4$^{-/-}$ mice (**Figure 3**). This overall compartmental similarity of inflammation between WT and TLR4$^{-/-}$ mice was preserved following resuscitation at 0.5h (**Figure 4**), 1h (**Figure 5**), and

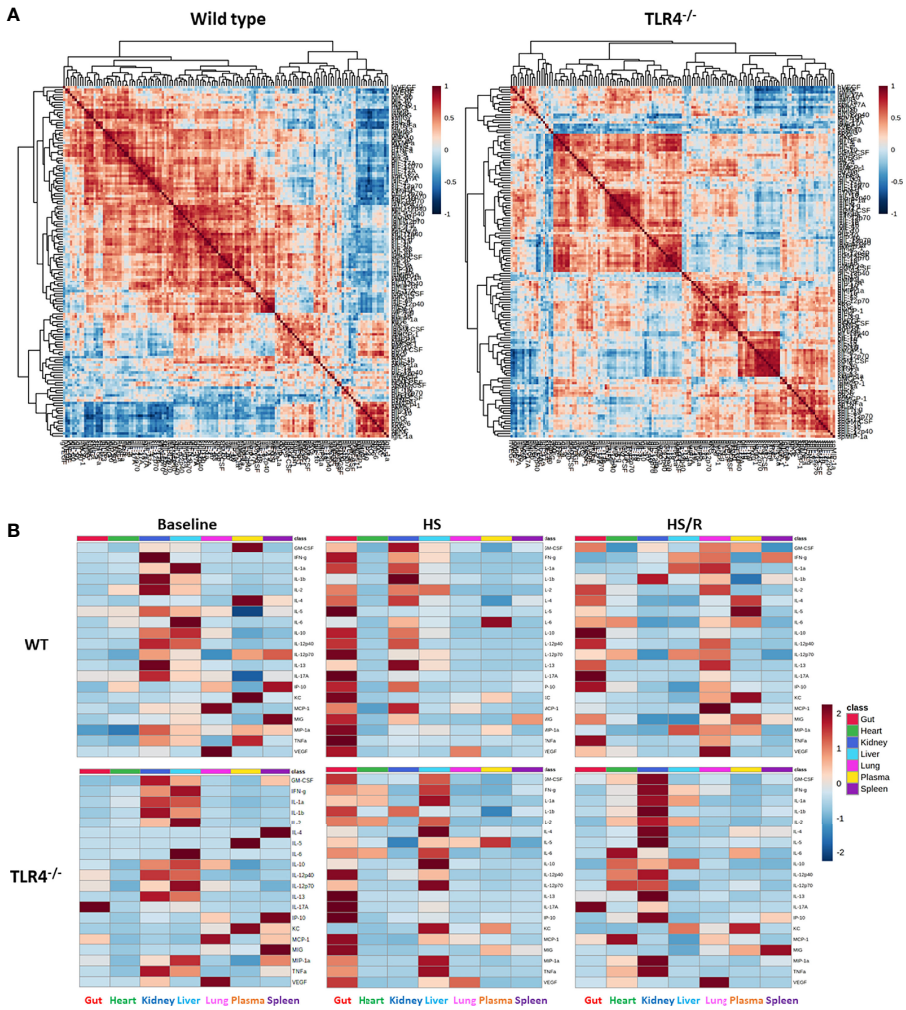

FIGURE 1 | Differential inflammatory correlation patterns in WT vs. TLR4$^{-/-}$ mice. **(A)** Heatmaps show Spearman Rank Correlation patterns using all experimental data (Ctrl + HS + HS/R) in wild type vs. TLR4$^{-/-}$ mice as described in *Materials and Methods*. **(B)** Heatmaps show the average concentration values for each mediator in each experimental group (Ctrl-Baseline, HS, HS/R in wild type vs. TLR4$^{-/-}$ mice as described in Materials and Methods.

4h (**Figure 6**). By 22h following resuscitation, the qualitative pattern of tissue distribution of inflammatory mediators began to resemble that observed prior to the induction of trauma/hemorrhage (**Figure 7**).

Taken together, these results suggest that TLR4 affects baseline inflammatory responses across multiple organs and the systemic circulation. This difference is blurred following severe stress, since inflammation triggered by trauma/hemorrhage and initially following resuscitation was at least qualitatively similar across multiple organs and the systemic circulation in both WT and TLR4$^{-/-}$ mice. By approximately 24h following resuscitated shock, the respective mouse strains appeared to recover toward their original, genetically encoded state.

Despite the overall qualitative similarity, there were different groupings of inflammatory mediators in distinct organ clusters at each time point in WT vs. TLR4$^{-/-}$ mice (**Supplementary Table 1**), suggesting organ-specific roles for TLR4 in regulating post T/HS-R inflammation. Notably, IL-17A was present persistently in all tissues at all sampled time points except for its absence in the systemic circulation following 0.5h of resuscitation in the WT group. Interestingly, TNF was found in all tissues in TLR4$^{-/-}$ mice from 0-4h following resuscitation, but was no longer expressed in the liver, lung, and heart by 22h.

Principal Component Analysis Defines Key Inflammatory Mediators at Baseline and Following Hemorrhagic Shock and Resuscitation in WT and TLR4$^{-/-}$ Mice

We next utilized Principal Component Analysis (70% variance) to better define the principal mediators associated with inflammation at baseline, following hemorrhage, and over time post-resuscitation in WT and TLR4$^{-/-}$ mice. At baseline, inflammation in WT mice was characterized by 4 principal

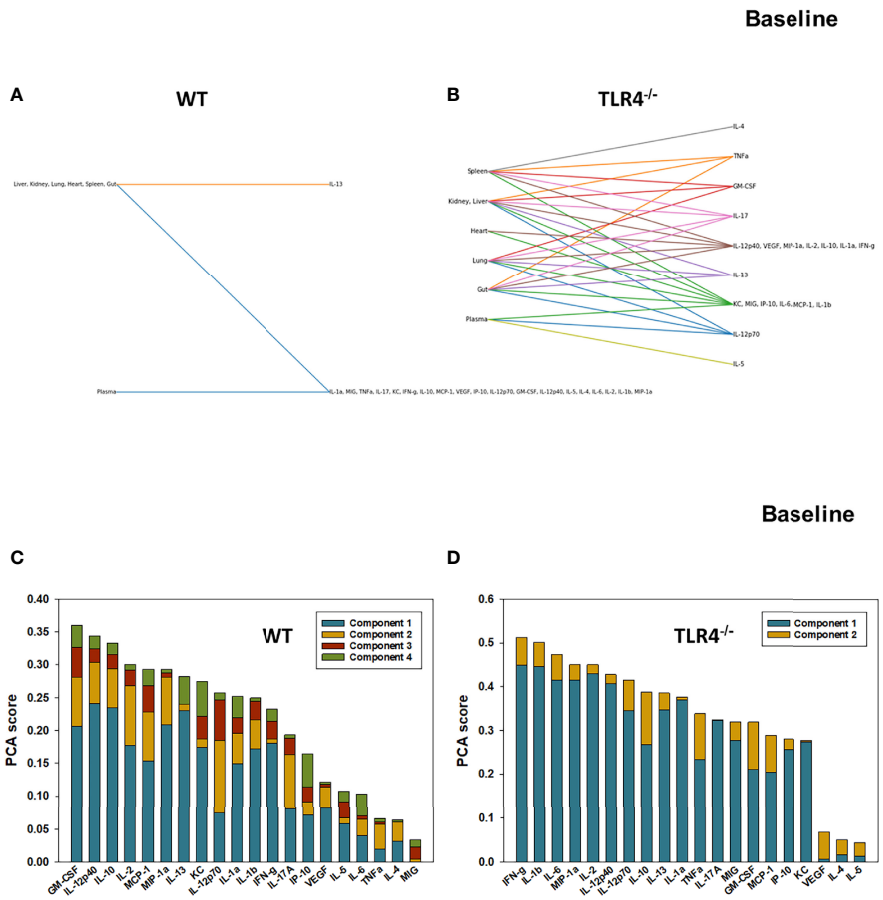

FIGURE 2 | Hypergraphs and Principal Component Analysis suggest differential baseline inflammatory responses in WT and TLR4$^{-/-}$ mice. Plasma and tissue samples from heart, lung, liver, gut, spleen, and kidney were collected from untreated (Ctrl) WT and TLR4$^{-/-}$ mice and analyzed using Luminex^{TM} as described in Materials and Methods. Panels **(A, B)** show the hypergraphs and Panels **(C, D)** show the PCA results (70% variance) in WT and TLR4$^{-/-}$ mice, respectively.

components involving GM-CSF, IL-12p40, and IL-10 among a multitude of other mediators (**Figure 2C**), while in TLR4$^{-/-}$ mice this response was characterized by 2 principal components and IFN-γ and IL-1β along with multiple other mediators. This supports the concept that WT and TLR4$^{-/-}$ differ in the baseline inflammatory propensities. Following hemorrhagic shock, inflammation in WT mice was characterized by 4 principal components involving IL-17A, IL-6, and IL-12p70 among a multitude of other mediators (**Figure 3C**), while in TLR4$^{-/-}$ mice this response was also characterized by 4 principal components and the mediators IL-12p70, IL-5, and MIP-1α among others (**Figure 3D**). This supports the hypothesis that stress in the form of hemorrhagic shock blurs some of the baseline differences between WT and TLR4$^{-/-}$ mice.

The relative similarity between WT and TLR4$^{-/-}$ persisted following resuscitation for 0.5-4h (compare **Figures 4C** vs **4D**, **5C** vs **5C**, and **6C** vs **6C**, respectively). By 22h post-resuscitation, inflammation in WT mice was characterized by 5 principal components involving IL-13, IFN-γ, and IL-17A among others (**Figure 7C**), while in TLR4$^{-/-}$ mice this response was also characterized by 3 principal components and the mediators IFN-γ and IL-12p70 among others (**Figure 7D**), suggesting a return toward baseline inter-strain differences in inflammation.

Taken together, these analyses support the conclusion that TLR4 affects baseline inflammatory responses across multiple compartments, that these differences are blurred somewhat following hemorrhagic shock and resuscitation, and that, with time, these baseline differences re-emerge. Furthermore, the predominance of IL-17A suggests an important role for type 17/type 3 immunity, while the presence of IL-12p40/p70 suggests a role for dendritic cells.

Hypergraph Metrics Yield Insights Into Cross-Compartment Inflammation Following Hemorrhagic Shock and Resuscitation in WT and TLR4$^{-/-}$ Mice

We next sought to better define the compartment-specific role of TLR4 in modulating the spread of inflammation following T/HS-R. Hypergraph Edge Distribution analysis suggested that WT mice had a more robust trans-compartmental inflammatory

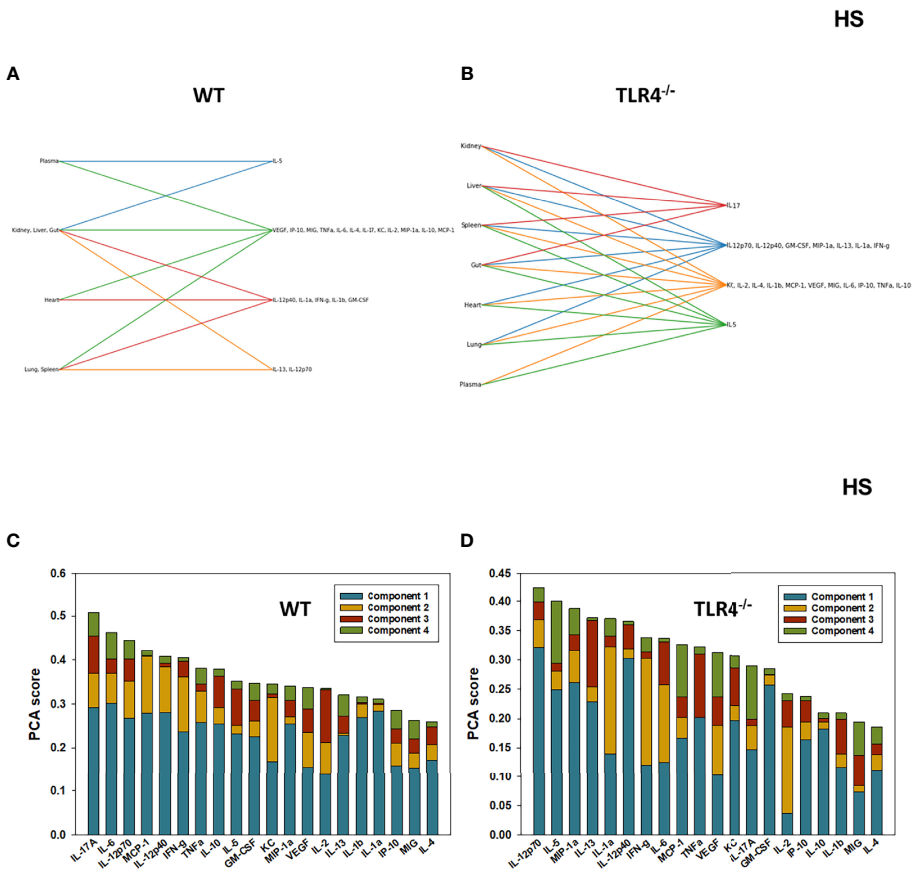

FIGURE 3 | *Hypergraphs and Principal Component Analysis of inflammatory mediators from WT and TLR4$^{-/-}$ mice subjected to HS.* Plasma and tissue samples from heart, lung, liver, gut, spleen, and kidney were collected from WT and TLR4$^{-/-}$ mice subjected to HS and analyzed using Luminex^{TM} as described in Materials and Methods. Panels **(A, B)** show the hypergraphs and Panels **(C, D)** show the PCA results (70% variance) in WT and TLR4$^{-/-}$ mice, respectively.

response at baseline, prior to T/HS-R, as compared to TLR4$^{-/-}$ mice (**Figure 8**). After hemorrhage and prior to resuscitation, WT mice exhibited a decrease in the number of inflammatory mediators there were present in all 7 tissue compartments. By t=1h after resuscitation, the WT group began to express inflammatory mediators in specific tissue compartments as indicated by the bars in the graph, spanning an edge size from 1 to 7. By 22h of resuscitation, the WT group exhibited a generally more limited edge distribution ranging from 6-7 (**Figure 8A**).

In contrast, at pre-hemorrhage baseline, TLR4$^{-/-}$ mice expressed distinct subsets of inflammatory mediators in defined tissue compartments compared to the WT group (**Figure 8B**). The tissue-specific inflammatory responses of TLR4$^{-/-}$ mice to hemorrhage alone were fairly similar to those of WT mice. After resuscitation, TLR4$^{-/-}$ mice exhibited the greatest trans-compartmental inflammation at t = 0.5h and t = 4h, with edge distributions spanning the range of 1-7. By 22h of resuscitation, the edge distribution of TLR4$^{-/-}$ mice was similar to the edge distribution of these mice at baseline, suggesting resolution of cross-compartment inflammation (**Figure 8B**).

As detailed in **Supplementary Table 1**, this homology indicates a similar trans-compartmental distribution of inflammatory mediators in the WT and TLR4$^{-/-}$. Following hemorrhagic shock as well as at 4h and 22h post-resuscitation, the most apparent difference between WT and TLR4$^{-/-}$ mice was that the TLR4$^{-/-}$ mice expressed IL-5 in the spleen, lung, and gut, while WT mice do not. Overall, WT mice expressed a greater number of inflammatory mediators across all compartments and all time points, causing the deceptively different appearing hypergraph structure. However, the graph structures are more similar than different and only differ by more than 50% of the mediators (10/20 inflammatory mediators) in any compartment at baseline.

S-Betweenness centrality, an indicator of the strength by which nodes are connected by a given edge (33) – and inferred as the degree to which inflammation is coordinated – was the greatest at 1h of resuscitation in WT mice. In contrast, S-betweenness centrality was greatest at baseline (Ctrl) in TLR4$^{-/-}$ mice (**Figure 8C**). This result suggests that there may have been a more coordinated inflammatory response to T-HS/R in WT mice, but not so in TLR4$^{-/-}$ mice. In aggregate, our analyses

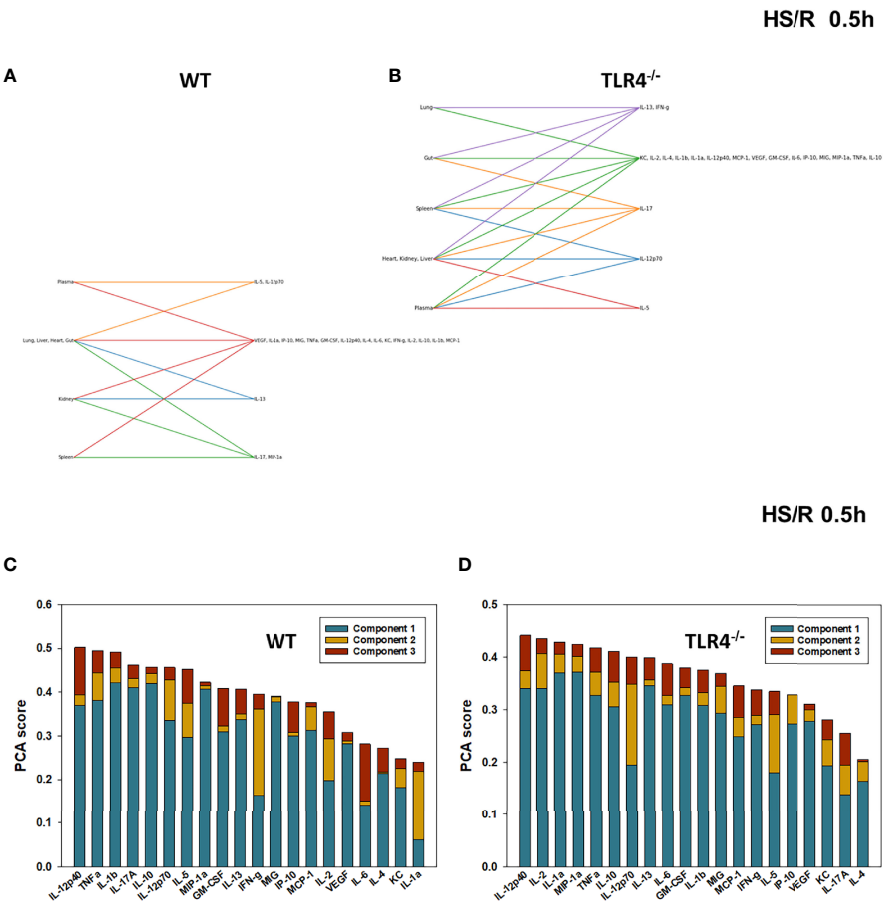

FIGURE 4 | Hypergraphs and Principal Component Analysis of inflammatory mediators from WT and TLR4$^{-/-}$ mice subjected to HS/R (0.5h). Plasma and tissue samples from heart, lung, liver, gut, spleen, and kidney were collected from WT and TLR4$^{-/-}$ mice subjected to HS/R (0.5h) and analyzed using Luminex^{TM} as described in Materials and Methods . Panels **(A, B)** show the hypergraphs and Panels **(C, D)** show the PCA results (70% variance) in WT and TLR4$^{-/-}$ mice, respectively.

suggest that TLR4$^{-/-}$ mice tend to display an inflammatory response that is more diffusely distributed across multiple tissues as compared to WT mice, which display a more restricted tissue distribution pattern of inflammatory mediators.

Inferred Differential Th17 Immune Dynamics in WT vs. TLR4$^{-/-}$ Mice

The cross-correlation and hypergraph analyses pointed to IL-17A in the context of spatiotemporal spread of inflammation following T/HS-R predominantly in WT but also in TLR4$^{-/-}$ mice, in line with our prior studies in trauma patients (7, 12). Interleukin-17A can be produced by a variety of cell types, including Th17 cells, innate lymphoid cells, γδ T cells, and both CD4^{+} and CD8^{+} effector/memory T cells (35–37). Kuchroo et al. have described a sub-population of Th17 cells known as pathogenic Th17 cells, which are implicated in driving pathological inflammatory processes. Pathogenic Th17 cells are characterized by the co-expression of IL-17A and GM-CSF; a reciprocal, non-inflammatory Th17 cell subset expresses IL-17A and IL-10 (38). Furthermore, CD4^{+}/CD8^{+} effector/memory T cells express IL-17A and TNF (39, 40). We have previously utilized Spearman rank correlation analysis of IL-17A vs. GM-CSF, IL-10, or TNF to infer the presence of these three cell subsets (7, 12, 15), with positive and negative correlations being interpreted as increases or decreases, respectively, in these Th17 cell subsets.

We therefore carried out a similar analysis to determine the potential presence of these cells in distinct tissues of WT and TLR4$^{-/-}$ mice. As shown in **Table 1**, pathogenic Th17 cells were inferred in the heart and kidney of WT mice and in the heart, gut, and kidney of TLR4$^{-/-}$ mice. We observed nearly statistically significant Spearman correlations for pathogenic Th17 cells in the lung and gut of WT mice and in the systemic circulation of TLR4$^{-/-}$ mice. Non-pathogenic Th17 cells were inferred in the heart, gut, and kidney of WT mice and in the heart, liver, gut, kidney, and systemic circulation of TLR4$^{-/-}$ mice (**Table 1**).

Finally, memory/effector Th17 cells were inferred in the liver, lung, gut, and kidney of WT mice and in the heart, gut, and kidney of TLR4$^{-/-}$ mice (**Table 1**). Interestingly, we observed a negative correlation for IL-17A and TNF in the spleen of TLR4$^{-/-}$

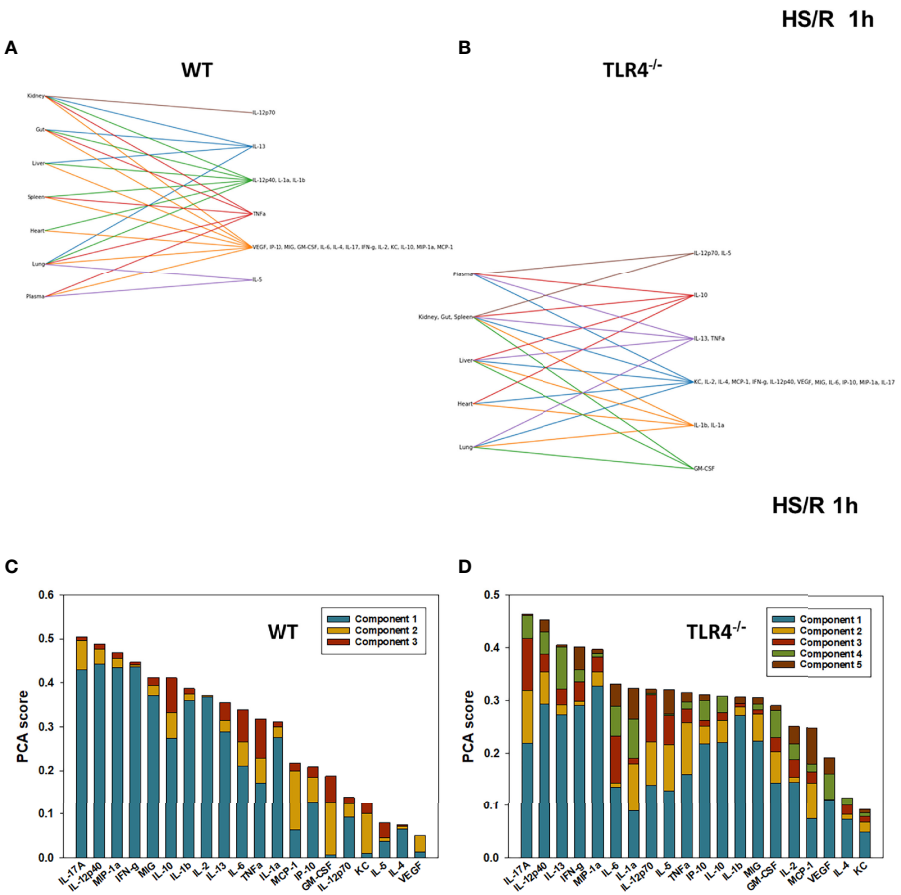

FIGURE 5 | Hypergraphs and Principal Component Analysis of inflammatory mediators from WT and TLR4$^{-/-}$ mice subjected to HS/R (1h). Plasma and tissue samples from heart, lung, liver, gut, spleen, and kidney were collected from WT and TLR4$^{-/-}$ mice subjected to HS/R (1h) and analyzed using Luminex^{TM} as described in Materials and Methods. Panels **(A, B)** show the hypergraphs and Panels **(C, D)** show the PCA results (70% variance) in WT and TLR4$^{-/-}$ mice, respectively.

mice, suggesting that there was a reduction of these cells in that organ. We also observed nearly statistically significant Spearman correlations for memory/effector cells in the heart and systemic of WT mice, suggesting a reduction of this cell subset in these compartments.

Taken together, these results suggest that TLR4 impacts distinct populations of tissue-resident and/or tissue-infiltrating, IL-17A-producing cells following resuscitated hemorrhagic shock.

DISCUSSION

In the present study, we utilized a novel computational pipeline involving hypergraphs as a means of assessing the dynamic, trans-compartment evolution of inflammation subsequent to traumatic injury and resuscitated hemorrhagic shock. These studies extend prior work from our group in which we defined protein-level dynamic networks and principal drivers of inflammation in both experimental (18) and clinical (7, 12, 19–21, 41–46) settings of T/HS-R, as well as in endotoxemia in mice (14, 15).

The inflammatory response to trauma/hemorrhage involves an important role for TLR4 in transducing pro-inflammatory signals from DAMPs such as HMGB1 (17). This includes a variety of functions ranging from cytokine production and organ damage (47–52); intestinal damage/dysfunction and consequent bacterial translocation (52, 53); and coagulation abnormalities (54). These effects require TLR4 expression on both myeloid and dendritic cells (55), and this may explain the inferred role for the dendritic cell-derived cytokine IL-12 (56) in driving Th1 responses (IFN-γ) (56, 57) in our system. Our results also suggest that there are TLR4-dependent differences in resting/baseline inflammatory responses in various tissues, and that these differences are somewhat blurred following T/HS-R and then recover their distinct characteristics following sufficient time post-injury. We speculate that the baseline differences in tissue expression of inflammatory mediators may be related to the reported stable baseline difference in gut microbiome composition between these two mouse strains (58), since enterocyte TLR4 has been implicated in damage/dysfunction in other organs such as the lung (52). Given that T-HS/R

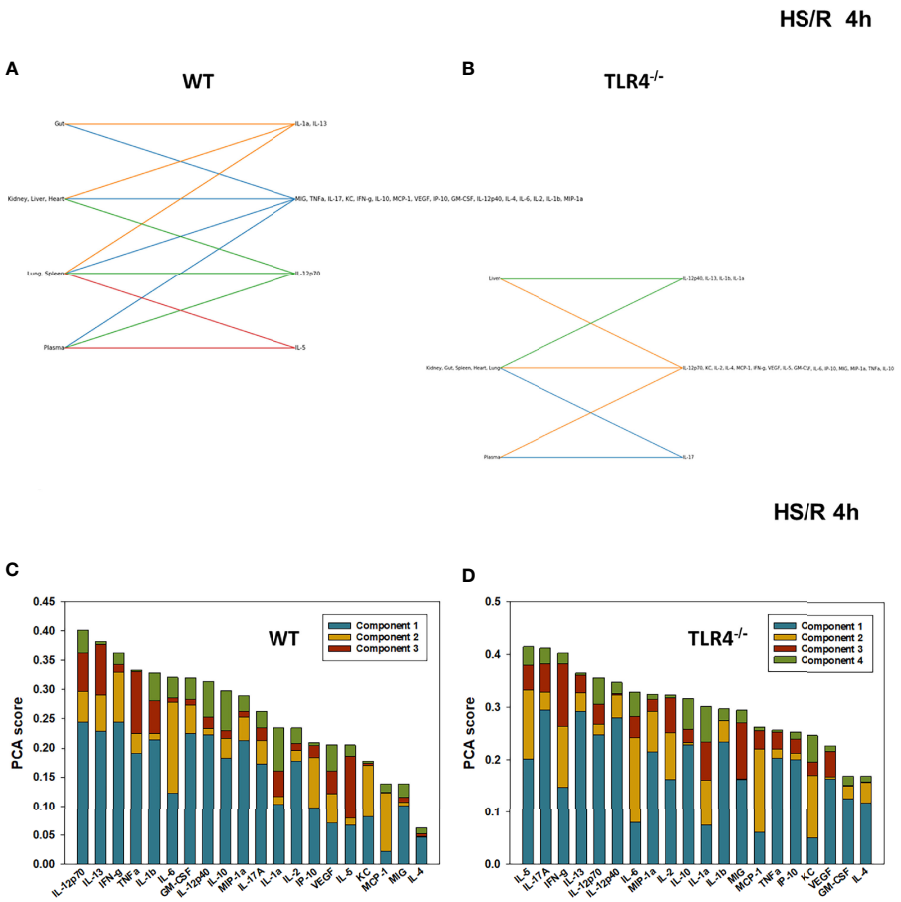

FIGURE 6 | Hypergraphs and Principal Component Analysis of inflammatory mediators from WT and TLR4$^{-/-}$ mice subjected to HS/R (4h). Plasma and tissue samples from heart, lung, liver, gut, spleen, and kidney were collected from WT and TLR4$^{-/-}$ mice subjected to HS/R (4h) and analyzed using Luminex^{TM} as described in Materials and Methods. Panels **(A, B)** show the hypergraphs and Panels **(C, D)** show the PCA results (70% variance) in WT and TLR4$^{-/-}$ mice, respectively.

induces a "genomic storm" (59) and extensive reprogramming of multiple aspects of physiology (11), it is perhaps not surprising that differences between WT and TLR4$^{-/-}$ mice are blurred following injury.

Another key conclusion from our analyses is that TLR4 plays a complex role in regulating distinct inflammatory pathways in different organs/tissues, and this complexity and context dependence may have relevance for critical illness. Specifically, our experimental and computational studies suggest that there is a baseline difference in tissue distribution of multiple cytokines and chemokines between WT and TLR4$^{-/-}$ mice; that surgical cannulation followed by hemorrhagic shock and resuscitation for 0.5-4h tends to reduce those differences; and that the baseline differences between WT and TLR4$^{-/-}$ re-appear by 22h following resuscitation from hemorrhagic shock. Key organs impacted during this complex process appear to be the gut, kidney, liver, and lung; the plasma (systemic circulation) manifested less dramatic differences. The gut has long been implicated as a central driver of inflammatory responses and multiple organ dysfunction following trauma/hemorrhage (60).

Impact of Hemorrhage, Resuscitation, and TLR4 on IL-17A-Related Pathways

Toll-like receptor 4-expressing cells may impact the response to T-HS/R *via* IL-17A, since IL-17A was present persistently at multiple time points across most tissues assessed. Indeed, HMGB1/TLR4-dependent pathways induced subsequent to T-HS/R are tightly intertwined with type 17 (or type 3) immunity. Early studies have suggested that T-HS/R induces neutrophil efflux from the bone marrow *via* IL-17A driven by HMGB1-mediated induction of IL-23 in a TLR4-dependent manner (61). This is likely a broadly conserved inflammatory axis that is not unique to trauma/hemorrhage, since IL-17A production in the context of tuberculosis (62), arthritis (63), and acetaminophen-induced liver inflammation (64). Notably, adenoviral transduction of IL-17A alone was sufficient to induce multi-tissue inflammation, and this required TLR4 (65). The inferred role for IL-12p40/p70 may also implicate Th17 responses (66). It is tempting to speculate that some of these intertwined effects of TLR4 and type 17 immunity ultimately manifest in the clinical outcomes of trauma patients (7, 12, 13).

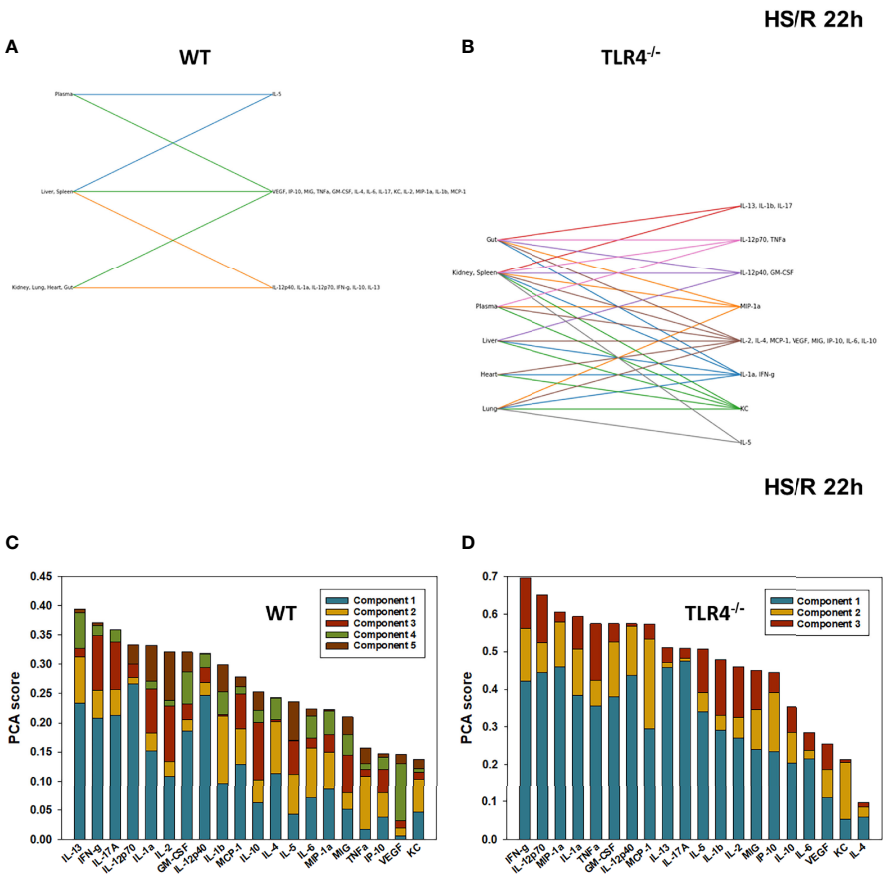

FIGURE 7 | Hypergraphs and Principal Component Analysis of inflammatory mediators from WT and TLR4$^{-/-}$ mice subjected to HS/R (22h). Plasma and tissue samples from heart, lung, liver, gut, spleen, and kidney were collected from WT and TLR4$^{-/-}$ mice subjected to HS/R (22h) and analyzed using Luminex^{TM} as described in Materials and Methods. Panels **(A, B)** show the hypergraphs and Panels **(C, D)** show the PCA results (70% variance) in WT and TLR4$^{-/-}$ mice, respectively.

The finding that IL-5 is present in spleen, lung, and gut of TLR4$^{-/-}$ mice is intriguing in that it suggests a potential role for another IL-17A-producing cell type, namely innate lymphoid cells (ILCs) (67). We have recently reported on a novel pathway of inflammation following T/HS-R in WT mice in which IL-33 induces ILC2 activation in the lung, which in turn induces further IL-5 expression by CXCR2^{+} lung neutrophils and drives early lung injury (68). Our current results suggest the paradoxical possibility that TLR4 deficiency might exacerbate this lung injury; further studies are needed to test this hypothesis.

We also observed TLR4-dependent changes in the post-T/HS-R inflammation in the heart, kidney, liver, lung, TLR4$^{-/-}$ mice exhibited elevated inflammation in the heart following resuscitation, while WT mice had little inflammation at baseline, post-hemorrhage, or following resuscitation in this organ. Renal, hepatic, pulmonary inflammatory responses were elevated at baseline in both mouse strains but diverged following hemorrhagic shock and inflammation. Notably, splenic inflammatory responses were overall low across all treatment groups, and we did not observe any important differences as a function of TLR4.

An important context for the work described herein is the definition of C57BL/6 as a "wild type" strain when comparing to TLR4$^{-/-}$ mice. Notably, the C57BL/6 mouse strain exhibits Th1- (69) and M1- (70) dominant immune responses and has been utilized extensively in studies of experimental T/HS-R (71). Our prior studies suggest that the inflammatory over-responsiveness of this mouse strain – and especially IL-17A-related responses – may reflect the biology of trauma patients that exhibit overly robust, self-sustaining inflammation associated with sub-acute mortality (12) and other adverse clinical outcomes (7). As such, TLR4$^{-/-}$ mice (or other mouse strains that are not explicitly Th1-dominant) may better reflect the responses of trauma survivors. Further comparative studies are needed to address this question.

Novel Insights Into Spatiotemporal Dynamics of Inflammation From Hypergraph Analysis

Our prior work was aimed at defining networks of individual inflammatory mediators interacting over time *within* a given tissue, as well as principal characteristics/drivers of these responses. Here, we utilized hypergraphs to extend prior work

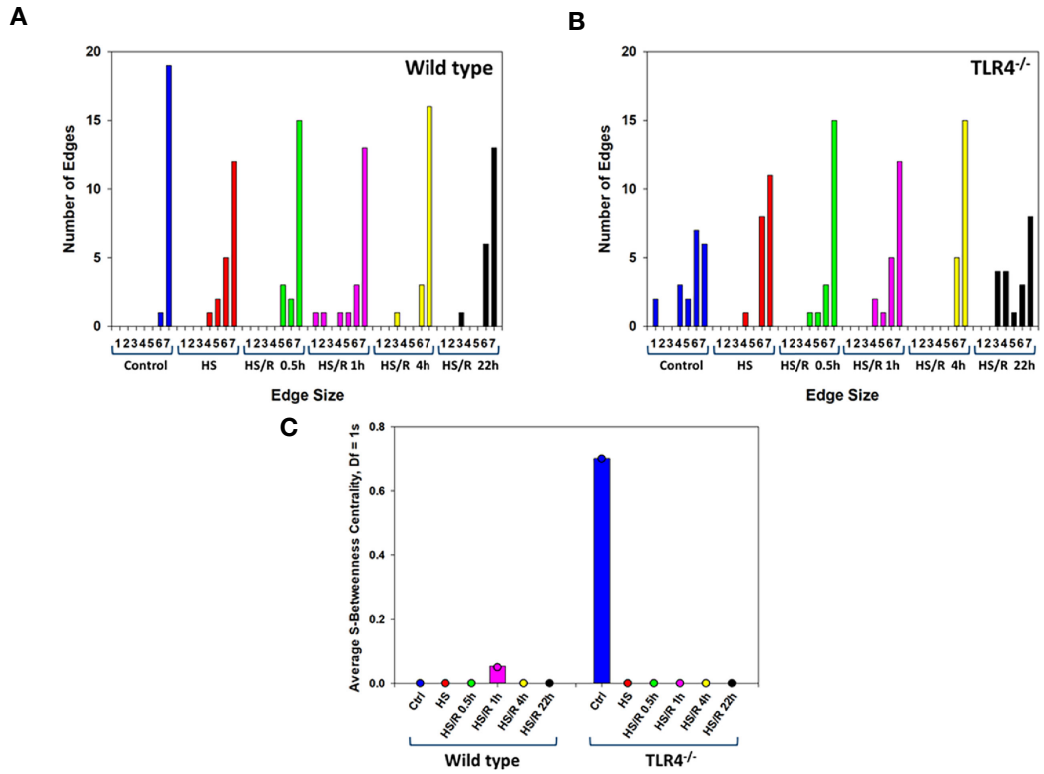

FIGURE 8 | Hypergraph metrics demonstrate differential tissue distribution of inflammatory mediators from WT and TLR4$^{-/-}$ mice. Plasma and tissue samples from heart, lung, liver, gut, spleen, and kidney were collected from Ctrl WT and TLR4$^{-/-}$ mice or mice subjected to HS and HS/R (0.5-22h) and analyzed using Luminex^{TM} as described in Materials and Methods. Panels **(A, B)** show the Hypergraph Edge Distribution analysis in WT and TLR4$^{-/-}$ mice, respectively. Panel **(C)** shows the average S-Betweenness Centrality (Df=1) for each hypergraph as indicated in WT and TLR4$^{-/-}$ mice, respectively.

defining how mediators interact *across* tissues over time (34). Hypergraphs provide several advantages when visualizing and interpreting multi-compartment data, such as that examined in this study. On a basic level, hypergraphs provide a method to visualize inflammatory mediators and their localization to specific tissue compartments across each time point. These visualizations can be simplified to elucidate differences between the localization of key inflammatory mediators at distinct time points between experimental conditions. In conjunction with computational and cross-correlation analyses, hypergraphs provide a spatial map upon which inference on how mediators are interacting within and between tissues may influence the spread of trans-compartmental inflammation. A key quantitative metric of hypergraphs, edge distribution, captures the network complexity of inflammation across tissue samples at a given time point. Changes in edge distribution can highlight important changes in inflammation such as the localization of a few inflammatory mediators to just one compartment or the dispersion of nearly all inflammatory mediators to all tissue compartments. In conjunction with PCA and cross-correlational analyses, hypergraphs provide the ultimate spatial framework upon which analyses regarding how and when inflammatory mediators interact with each to modulate inflammation.

LIMITATIONS

There are several limitations of our study. These include the focus on a subset of inflammatory mediators that broadly interrogate inflammation and immunity but are not a comprehensive set [vs. recent studies that have assessed a broader array of molecules (11)], the absence of cell-level data (5, 72) to validate key hypotheses detailed above, and a lack of validation in human trauma/hemorrhage due to the difficulty in accessing the various tissues (other than the systemic circulation) analysed herein. Key among the inflammatory mediators that could not be assessed across tissue compartments is HMGB1, which is typically found within the nucleus but is secreted in settings of cellular stress and damage (73, 74), since this molecule would be released during the process of tissue homogenization. Another important, related limitation concerns the possibility that some of the phenomena we have described are due to the efflux of bacteria from the gut and PAMPs, rather than DAMPs. Studies in gnotobiotic mice (75) may be needed to address this question. Another important limitation concerns the lack of tissue-specific deletion of TLR4 as a means for directly testing some of the hypotheses raised by our analyses. Finally, it is important to note that all of the analyses presented in this study

TABLE 1 | Spearman Rank Correlations (IL-17A vs. GM-CSF, IL-10 and TNFa) in WT and TLR4-/- mice.

WT	r values	P values	TLR4$^{-/-}$	r values	P values
Plasma	**IL-17A**		**Plasma**	**IL-17A**	
GM-CSF	**-0.150**	0.475	**GM-CSF**	0.420	0.052
IL-10	**-0.085**	0.688	**IL-10**	**0.533**	**0.011**
TNFα	**-0.379**	0.061	**TNFα**	0.105	0.641
Heart	**IL-17A**		**Heart**	**IL-17A**	
GM-CSF	**0.698**	**1.038E-04**	**GM-CSF**	**0.516**	**0.014**
IL-10	**0.906**	**4.458E-10**	**IL-10**	**0.461**	**0.031**
TNFα	0.376	0.064	**TNFα**	**0.5154**	**0.014**
Liver	**IL-17A**		**Liver**	**IL-17A**	
GM-CSF	0.312	0.129	**GM-CSF**	0.313	0.157
IL-10	0.228	0.273	**IL-10**	**0.488**	**0.021**
TNFα	**0.588**	**0.002**	**TNFα**	0.379	0.082
Lung	**IL-17A**		**Lung**	**IL-17A**	
GM-CSF	0.395	0.051	**GM-CSF**	0.289	0.192
IL-10	0.082	0.698	**IL-10**	**-0.158**	0.481
TNFα	**0.597**	**0.002**	**TNFα**	**-0.087**	0.7
Gut	**IL-17A**		**Gut**	**IL-17A**	
GM-CSF	0.392	0.053	**GM-CSF**	**0.632**	**0.002**
IL-10	**0.525**	**0.007**	**IL-10**	**0.513**	**0.015**
TNFα	**0.663**	**0.0003**	**TNFα**	**0.576**	**0.005**
Spleen	**IL-17A**	IL-17A	**Spleen**	**IL-17A**	
GM-CSF	0.231	0.267	**GM-CSF**	**-0.134**	0.552
IL-10	0.340	0.096	**IL-10**	**-0.564**	0.579
TNFα	0.325	0.113	**TNFα**	**-0.438**	**0.042**
Kidney	**IL-17A**		**Kidney**	**IL-17A**	
GM-CSF	**0.571**	**0.003**	**GM-CSF**	**0.622**	**0.002**
IL-10	**0.410**	**0.042**	**IL-10**	**0.56**	**0.007**
TNFα	**0.860**	**3.702E-08**	**TNFα**	**0.558**	**0.007**

Red: Negative correlation coefficient (r) values.
Bold: $p < 0.05$.

are based on statistical correlations, and correlation is not causality. We have shown that it is possible to obtain define potential biological mechanisms related to the response to trauma/hemorrhage *via* a process involving obtaining inflammatory mediator data, carrying out network inference, and then extracting core features into mechanistic computational models that can be interrogated under various conditions to validate and extend the conclusions that can be derived from purely data-driven analyses (76). Future studies will utilize these datasets to carry out this type of iterative, rational process.

CONCLUSIONS

In conclusion, these studies demonstrate multiple novel findings while reinforcing prior conclusions regarding the complex role of TLR4 and type 17 immune responses following trauma/hemorrhage. These studies serve as the basis for future cell-level analyses aimed at yielding an integrated understanding of the spatiotemporal evolution of inflammatory networks in the context of injury and critical illness.

DATA AVAILABILITY STATEMENT

The original contributions presented in the study are included in the article/**Supplementary Material**. Further inquiries can be directed to the corresponding authors.

ETHICS STATEMENT

The animal study was reviewed and approved by IACUC University of Pittsburgh.

AUTHOR CONTRIBUTIONS

AS: analysed data, wrote manuscript. RZ: analysed data, wrote manuscript. SK: obtained data, analysed data, edited manuscript. DB: obtained data. JY: obtained data. FE-D: analysed data. TB: conceived and directed study, analysed data, edited manuscript. YV: conceived and directed study, analysed data, wrote manuscript. All authors contributed to the article and approved the submitted version.

FUNDING

AS: University of Pittsburgh School of Medicine Physician Scientist Training Program.

ACKNOWLEDGMENTS

We would like to thank Brenda Praggastis (Pacific Northwest National Laboratory operated by Battelle for the US Dept. of Energy under contract DE-AC05-76RL01830) for helping with the implementation of hypergraphs.

SUPPLEMENTARY MATERIAL

The Supplementary Material for this article can be found online at: https://www.frontiersin.org/articles/10.3389/fimmu.2022.908618/full#supplementary-material

REFERENCES

1. Peitzman AB, Billiar TR, Harbrecht BG, Kelly E, Udekwu AO, Simmons RL. Hemorrhagic Shock. *Curr Probl Surg* (1995) 32(11):925–1002. doi: 10.1016/S0011-3840(05)80008-5
2. de Munter L, Polinder S, Lansink KW, Cnossen MC, Steyerberg EW, de Jongh MA. Mortality Prediction Models in the General Trauma Population: A Systematic Review. *Injury* (2017) 48(2):221–9. doi: 10.1016/j.injury.2016.12.009
3. Lord JM, Midwinter MJ, Chen YF, Belli A, Brohi K, Kovacs EJ, et al. The Systemic Immune Response to Trauma: An Overview of Pathophysiology and Treatment. *Lancet* (2014) 384(9952):1455–65. doi: 10.1016/s0140-6736(14)60687-5
4. Namas R, Mi Q, Namas R, Almahmoud K, Zaaqoq A, Abdul Malak O, et al. Insights Into the Role of Chemokines, Damage-Associated Molecular Patterns, and Lymphocyte-Derived Mediators From Computational Models of Trauma-Induced Inflammation. *Antiox Redox Signaling* (2015) 10:1370–87. doi: 10.1089/ars.2015.6398
5. Chen T, Delano MJ, Chen K, Sperry JL, Namas RA, Lamparello AJ, et al. A Roadmap From Single-Cell Transcriptome to Patient Classification for the Immune Response to Trauma. *JCI Insight* (2020) 6(2):e145108. doi: 10.1172/jci.insight.145108
6. Billiar TR, Vodovotz Y. Time for Trauma Immunology. *PloS Med* (2017) 14(7):e1002342. doi: 10.1371/journal.pmed.1002342
7. Schimunek L, Lindberg H, Cohen M, Namas RA, Mi Q, Yin J, et al. Computational Derivation of Core, Dynamic Human Blunt Trauma Inflammatory Endotypes. *Front Immunol* (2021) 11:589304(3481). doi: 10.3389/fimmu.2020.589304
8. Bonaroti J, Abdelhamid S, Kar U, Sperry J, Zamora R, Namas RA, et al. The Use of Multiplexing to Identify Cytokine and Chemokine Networks in the Immune-Inflammatory Response to Trauma. *Antioxid Redox Signal* (2021) 35:1393–406. doi: 10.1089/ars.2021.0054
9. Maier B, Lefering R, Lehnert M, Laurer HL, Steudel WI, Neugebauer EA, et al. Early Versus Late Onset of Multiple Organ Failure is Associated With Differing Patterns of Plasma Cytokine Biomarker Expression and Outcome After Severe Trauma. *Shock* (2007) 28(6):668–74. doi: 10.1097/shk.0b013e318123e64e
10. Cyr A, Zhong Y, Reis SE, Namas RA, Amoscato A, Zuckerbraun B, et al. Analysis of the Plasma Metabolome After Trauma, Novel Circulating Sphingolipid Signatures, and in-Hospital Outcomes. *J Am Coll Surg* (2021) 232(3):276–87.e1. doi: 10.1016/j.jamcollsurg.2020.12.022
11. Wu J, Vodovotz Y, Abdelhamid S, Guyette FX, Yaffe MB, Gruen DS, et al. Multi-Omic Analysis in Injured Humans: Patterns Align With Outcomes and Treatment Responses. *Cell Rep Med* (2021) 2(12). doi: 10.1016/j.xcrm.2021.100478
12. Abboud AN, Namas RA, Ramadan M, Mi Q, Almahmoud K, Abdul-Malak O, et al. Computational Analysis Supports an Early, Type 17 Cell-Associated Divergence of Blunt Trauma Survival and Mortality. *Crit Care Med* (2016) 44:e1074–81. doi: 10.1097/CCM.0000000000001951
13. Seshadri A, Brat GA, Yorkgitis BK, Keegan J, Dolan J, Salim A, et al. Phenotyping the Immune Response to Trauma: A Multiparametric Systems Immunology Approach. *Crit Care Med* (2017) 45:1523–30. doi: 10.1097/ccm.0000000000002577
14. Zamora R, Korff S, Mi Q, Barclay D, Yin J, Schimunek L, et al. A Computational Analysis of Dynamic, Multi-Organ Inflammatory Crosstalk Induced by Endotoxin in Mice. *PloS Comput Biol* (2018) 6:e100658. doi: 10.1371/journal.pcbi.1006582
15. Zamora R, Chavan S, Zanos T, Simmons RL, Billiar TR, Vodovotz Y. Spatiotemporally Specific Roles of TLR4, TNF, and IL-17A in Murine Endotoxin-Induced Inflammation Inferred From Analysis of Dynamic Networks. *Mol Med* (2021) 27(1):65. doi: 10.1186/s10020-021-00333-z
16. Beutler B. TLR4 as the Mammalian Endotoxin Sensor. *Curr Top Microbiol Immunol* (2002) 270:109–20. doi: 10.1007/978-3-642-59430-4_7
17. Kaczorowski DJ, Mollen KP, Edmonds R, Billiar TR. Early Events in the Recognition of Danger Signals After Tissue Injury. *J Leukoc Biol* (2008) 83(3):546–52. doi: 10.1189/jlb.0607374
18. Mi Q, Constantine G, Ziraldo C, Solovyev A, Torres A, Namas R, et al. A Dynamic View of Trauma/Hemorrhage-Induced Inflammation in Mice: Principal Drivers and Networks. *PLoS One* (2011) 6(5):e19424. doi: 10.1371/journal.pone.0019424
19. Namas RA, Vodovotz Y, Almahmoud K, Abdul-Malak O, Zaaqoq A, Namas R, et al. Temporal Patterns of Circulating Inflammation Biomarker Networks Differentiate Susceptibility to Nosocomial Infection Following Blunt Trauma in Humans. *Ann Surg* (2016) 263:191–8. doi: 10.1097/sla.0000000000001001
20. Almahmoud K, Namas RA, Zaaqoq AM, Abdul-Malak O, Namas R, Zamora R, et al. Prehospital Hypotension is Associated With Altered Inflammation Dynamics and Worse Outcomes Following Blunt Trauma in Humans. *Crit Care Med* (2015) 43:1395–404. doi: 10.1097/ccm.0000000000000964
21. Almahmoud K, Namas RA, Abdul-Malak O, Zaaqoq AM, Zamora R, Zuckerbraun BS, et al. Impact of Injury Severity on Dynamic Inflammation Networks Following Blunt Trauma. *Shock* (2015) 44:105–9. doi: 10.1097/shk.0000000000000395
22. Namas R, Almahmoud K, Mi Q, Ghuma A, Namas R, Zaaqoq A, et al. Individual-Specific Principal Component Analysis of Circulating Inflammatory Mediators Predicts Early Organ Dysfunction in Trauma Patients. *J Crit Care* (2016) 36:146–53. doi: 10.1016/j.jcrc.2016.07.002
23. Tian Z, Hwang T, Kuang R. A Hypergraph-Based Learning Algorithm for Classifying Gene Expression and arrayCGH Data With Prior Knowledge. *Bioinformatics* (2009) 25(21):2831–8. doi: 10.1093/bioinformatics/btp467
24. Bernal A, Daza E. Metabolic Networks: Beyond the Graph. *Curr Comput Aided Drug Des* (2011) 7(2):122–32. doi: 10.2174/157340911795677611
25. Lugo-Martinez J, Zeiberg D, Gaudelet T, Malod-Dognin N, Pržulj N, Radivojac P. Classification in Biological Networks With Hypergraphlet Kernels. *Bioinformatics* (2020) 37(7):1000–7. doi: 10.1093/bioinformatics/btaa768
26. Gao Y, Zhang Z, Lin H, Zhao X, Du S, Zou C. Hypergraph Learning: Methods and Practices. *IEEE Trans Pattern Anal Mach Intell* (2020) 44(5):2548–66. doi: 10.1109/tpami.2020.3039374
27. Deng M, Scott MJ, Loughran P, Gibson G, Sodhi C, Watkins S, et al. Lipopolysaccharide Clearance, Bacterial Clearance, and Systemic Inflammatory Responses are Regulated by Cell Type-Specific Functions of TLR4 During Sepsis. *J Immunol* (2013) 190(10):5152–60. doi: 10.4049/jimmunol.1300496
28. Pfeifer R, Kobbe P, Darwiche SS, Billiar TR, Pape HC. Role of Hemorrhage in the Induction of Systemic Inflammation and Remote Organ Damage: Analysis of Combined Pseudo-Fracture and Hemorrhagic Shock. *J Orthop Res* (2011) 29(2):270–4. doi: 10.1002/jor.21214
29. Barclay D, Zamora R, Torres A, Namas R, Steed D, Vodovotz Y. A Simple, Rapid, and Convenient Luminex™-Compatible Method of Tissue Isolation. *J Clin Lab Anal* (2008) 22:278–81. doi: 10.1002/jcla.20253

30. Metukuri MR, Beer-Stolz D, Namas RA, Dhupar R, Torres A, Loughran PA, et al. Expression and Subcellular Localization of BNIP3 in Hypoxic Hepatocytes and Liver Stress. *Am J Physiol Gastrointest Liver Physiol* (2009) 296(3):G499–509. doi: 10.1152/ajpgi.90526.2008
31. Chong J, Wishart DS, Xia J. Using MetaboAnalyst 4.0 for Comprehensive and Integrative Metabolomics Data Analysis. *Curr Protoc Bioinf* (2019) 68(1):e86. doi: 10.1002/cpbi.86
32. Chong J, Soufan O, Li C, Caraus I, Li S, Bourque G, et al. MetaboAnalyst 4.0: Towards More Transparent and Integrative Metabolomics Analysis. *Nucleic Acids Res* (2018) 46(W1):W486–94. doi: 10.1093/nar/gky310
33. Feng S, Heath E, Jefferson B, Joslyn C, Kvinge H, Mitchell HD, et al. Hypergraph Models of Biological Networks to Identify Genes Critical to Pathogenic Viral Response. *BMC Bioinf* (2021) 22(1):287. doi: 10.1186/s12859-021-04197-2
34. Aral AM, Zamora R, Barclay D, Yin J, El-Dehaibi F, Erbas VE, et al. The Effects of Tacrolimus on Tissue-Specific, Protein-Level Inflammatory Networks in Vascularized Composite Allotransplantation. *Front Immunol* (2021) 12:591154(1529). doi: 10.3389/fimmu.2021.591154
35. Weaver CT, Hatton RD, Mangan PR, Harrington LE. IL-17 Family Cytokines and the Expanding Diversity of Effector T Cell Lineages. *Annu Rev Immunol* (2007) 25:821–52. doi: 10.1146/annurev.immunol.25.022106.141557
36. Korn T, Bettelli E, Oukka M, Kuchroo VK. IL-17 and Th17 Cells. *Annu Rev Immunol* (2009) 27:485–517. doi: 10.1146/annurev.immunol.021908.132710
37. Cua DJ, Tato CM. Innate IL-17-Producing Cells: The Sentinels of the Immune System. *Nat Rev Immunol* (2010) 10(7):479–89. doi: 10.1038/nri2800
38. Peters A, Lee Y, Kuchroo VK. The Many Faces of Th17 Cells. *Curr Opin Immunol* (2011) 23(6):702–6. doi: 10.1016/j.coi.2011.08.007
39. Langrish CL, Chen Y, Blumenschein WM, Mattson J, Basham B, Sedgwick JD, et al. IL-23 Drives a Pathogenic T Cell Population That Induces Autoimmune Inflammation. *J Exp Med* (2005) 201(2):233–40. doi: 10.1084/jem.20041257
40. McArthur MA, Sztein MB. Unexpected Heterogeneity of Multifunctional T Cells in Response to Superantigen Stimulation in Humans. *Clin Immunol* (2013) 146(2):140–52. doi: 10.1016/j.clim.2012.12.003
41. Zaaqoq AM, Namas R, Almahmoud K, Azhar N, Mi Q, Zamora R, et al. Inducible Protein-10, a Potential Driver of Neurally-Controlled IL-10 and Morbidity in Human Blunt Trauma. *Crit Care Med* (2014) 42:1487–97. doi: 10.1097/CCM.0000000000000248
42. Brown D, Namas RA, Almahmoud K, Zaaqoq A, Sarkar J, Barclay DA, et al. Trauma *in Silico*: Individual-Specific Mathematical Models and Virtual Clinical Populations. *Sci Transl Med* (2015) 7:285ra61. doi: 10.1126/scitranslmed.aaa3636
43. Abdul-Malak O, Vodovotz Y, Zaaqoq A, Guardado J, Almahmoud K, Yin J, et al. Elevated Admission Base Deficit is Associated With a Complex Dynamic Network of Systemic Inflammation Which Drives Clinical Trajectories in Blunt Trauma Patients. *Mediators Inflamm* (2016) 2016:7950374. doi: 10.1155/2016/7950374
44. Lamparello AJ, Namas RA, Abdul-Malak O, Vodovotz Y, Billiar TR. Young and Aged Blunt Trauma Patients Display Major Differences in Circulating Inflammatory Mediator Profiles After Severe Injury. *J Am Coll Surg* (2019) 228:148–60.e7. doi: 10.1016/j.jamcollsurg.2018.10.019
45. Almahmoud K, Abboud A, Namas RA, Zamora R, Sperry J, Peitzman AB, et al. Computational Evidence for an Early, Amplified Systemic Inflammation Program in Polytrauma Patients With Severe Extremity Injuries. *PloS One* (2019) 14(6):e0217577. doi: 10.1371/journal.pone.0217577
46. Zaaqoq AM, Namas RA, Abdul-Malak O, Almahmoud K, Barclay D, Yin J, et al. Diurnal Variation in Systemic Acute Inflammation and Clinical Outcomes Following Severe Blunt Trauma. *Front Immunol* (2019) 10:2699 (2699). doi: 10.3389/fimmu.2019.02699
47. Meng X, Ao L, Song Y, Raeburn CD, Fullerton DA, Harken AH. Signaling for Myocardial Depression in Hemorrhagic Shock: Roles of Toll-Like Receptor 4 and P55 TNF-Alpha Receptor. *Am J Physiol Regul Integr Comp Physiol* (2005) 288(3):R600–6. doi: 10.1152/ajpregu.00182.2004
48. Prince JM, Levy RM, Yang R, Mollen KP, Fink MP, Vodovotz Y, et al. Toll-Like Receptor-4 Signaling Mediates Hepatic Injury and Systemic Inflammation in Hemorrhagic Shock. *J Am Coll Surg* (2006) 202(3):407–17. doi: 10.1016/j.jamcollsurg.2005.11.021
49. Lv T, Shen X, Shi Y, Song Y. TLR4 is Essential in Acute Lung Injury Induced by Unresuscitated Hemorrhagic Shock. *J Trauma* (2009) 66(1):124–31. doi: 10.1097/TA.0b013e318181e555
50. Reino DC, Pisarenko V, Palange D, Doucet D, Bonitz RP, Lu Q, et al. Trauma Hemorrhagic Shock-Induced Lung Injury Involves a Gut-Lymph-Induced TLR4 Pathway in Mice. *PloS One* (2011) 6(8):e14829. doi: 10.1371/journal.pone.0014829
51. Benhamou Y, Favre J, Musette P, Renet S, Thuillez C, Richard V, et al. Toll-Like Receptors 4 Contribute to Endothelial Injury and Inflammation in Hemorrhagic Shock in Mice. *Crit Care Med* (2009) 37(5):1724–8. doi: 10.1097/CCM.0b013e31819da805
52. Sodhi CP, Jia H, Yamaguchi Y, Lu P, Good M, Egan C, et al. Intestinal Epithelial TLR-4 Activation is Required for the Development of Acute Lung Injury After Trauma/Hemorrhagic Shock *via* the Release of HMGB1 From the Gut. *J Immunol* (2015) 194(10):4931–9. doi: 10.4049/jimmunol.1402490
53. Neal MD, Leaphart C, Levy R, Prince J, Billiar TR, Watkins S, et al. Enterocyte TLR4 Mediates Phagocytosis and Translocation of Bacteria Across the Intestinal Barrier. *J Immunol* (2006) 176(5):3070–9. doi: 10.4049/jimmunol.176.5.3070
54. Ding N, Chen G, Hoffman R, Loughran PA, Sodhi CP, Hackam DJ, et al. Toll-Like Receptor 4 Regulates Platelet Function and Contributes to Coagulation Abnormality and Organ Injury in Hemorrhagic Shock and Resuscitation. *Circ Cardiovasc Genet* (2014) 7(5):615–24. doi: 10.1161/circgenetics.113.000398
55. Zettel K, Korff S, Zamora R, Morelli AE, Darwiche S, Loughran PA, et al. Toll-Like Receptor 4 on Both Myeloid Cells and Dendritic Cells is Required for Systemic Inflammation and Organ Damage After Hemorrhagic Shock With Tissue Trauma in Mice. *Front Immunol* (2017) 8:1672(1672). doi: 10.3389/fimmu.2017.01672
56. Trinchieri G. Interleukin-12 and the Regulation of Innate Resistance and Adaptive Immunity. *Nat Rev Immunol* (2003) 3(2):133–46. doi: 10.1038/nri1001
57. Lyakh L, Trinchieri G, Provezza L, Carra G, Gerosa F. Regulation of Interleukin-12/Interleukin-23 Production and the T-Helper 17 Response in Humans. *Immunol Rev* (2008) 226:112–31. doi: 10.1111/j.1600-065X.2008.00700.x
58. Ubeda C, Lipuma L, Gobourne A, Viale A, Leiner I, Equinda M, et al. Familial Transmission Rather Than Defective Innate Immunity Shapes the Distinct Intestinal Microbiota of TLR-Deficient Mice. *J Exp Med* (2012) 209(8):1445–56. doi: 10.1084/jem.20120504
59. Xiao W, Mindrinos MN, Seok J, Cuschieri J, Cuenca AG, Gao H, et al. A Genomic Storm in Critically Injured Humans. *J Exp Med* (2011) 208 (13):2581–90. doi: 10.1084/jem.20111354
60. Deitch EA. Role of the Gut Lymphatic System in Multiple Organ Failure. *Curr Opin Crit Care* (2001) 7(2):92–8. doi: 10.1097/00075198-200104000-00007
61. Liu Y, Yuan Y, Li Y, Zhang J, Xiao G, Vodovotz Y, et al. Interacting Neuroendocrine and Innate and Acquired Immune Pathways Regulate Neutrophil Mobilization From Bone Marrow Following Hemorrhagic Shock. *J Immunol* (2009) 182(1):572–80. doi: 10.4049/jimmunol.182.1.572
62. van de Veerdonk FL, Teirlinck AC, Kleinnijenhuis J, Kullberg BJ, van CR, van der Meer JW, et al. Mycobacterium Tuberculosis Induces IL-17A Responses Through TLR4 and Dectin-1 and is Critically Dependent on Endogenous IL-1. *J Leukoc Biol* (2010) 88(2):227–32. doi: 10.1189/jlb.0809550
63. Pierer M, Wagner U, Rossol M, Ibrahim S. Toll-Like Receptor 4 is Involved in Inflammatory and Joint Destructive Pathways in Collagen-Induced Arthritis in DBA1J Mice. *PloS One* (2011) 6(8):e23539. doi: 10.1371/journal.pone.0023539
64. Wang X, Sun R, Wei H, Tian Z. High-Mobility Group Box 1 (HMGB1)-Toll-Like Receptor (TLR)4-Interleukin (IL)-23-IL-17A Axis in Drug-Induced Damage-Associated Lethal Hepatitis: Interaction of Gammadelta T Cells With Macrophages. *Hepatology* (2013) 57(1):373–84. doi: 10.1002/hep.25982
65. Tang H, Pang S, Wang M, Xiao X, Rong Y, Wang H, et al. TLR4 Activation is Required for IL-17-Induced Multiple Tissue Inflammation and Wasting in Mice. *J Immunol* (2010) 185(4):2563–9. doi: 10.4049/jimmunol.0903664
66. Patel DD, Kuchroo VK. Th17 Cell Pathway in Human Immunity: Lessons From Genetics and Therapeutic Interventions. *Immunity* (2015) 43(6):1040–51. doi: 10.1016/j.immuni.2015.12.003

67. Ebbo M, Crinier A, Vély F, Vivier E. Innate Lymphoid Cells: Major Players in Inflammatory Diseases. *Nat Rev Immunol* (2017) 17(11):665–78. doi: 10.1038/nri.2017.86
68. Xu J, Guardado J, Hoffman R, Xu H, Namas R, Vodovotz Y, et al. IL-33 Drives Lung Injury *via* ILC2 Promotion of Neutrophil IL-5 Production After Polytrauma. *PloS Med* (2017) 14:e1002365.
69. Mosmann TR, Coffman RL. TH1 and TH2 Cells: Different Patterns of Lymphokine Secretion Lead to Different Functional Properties. *Annu Rev Immunol* (1989) 7:145–73. doi: 10.1146/annurev.iy.07.040189.001045
70. Watanabe H, Numata K, Ito T, Takagi K, Matsukawa A. Innate Immune Response in Th1- and Th2-Dominant Mouse Strains. *Shock* (2004) 22(5):460–6. doi: 10.1097/01.shk.0000142249.08135.e9
71. Mira JC, Nacionales DC, Loftus TJ, Ungaro R, Mathias B, Mohr AM, et al. Mouse Injury Model of Polytrauma and Shock. *Methods Mol Biol* (2018) 1717:1–15. doi: 10.1007/978-1-4939-7526-6_1
72. Chen T, Conroy J, Wang X, Situ M, Namas RA, Vodovotz Y, et al. The Independent Prognostic Value of Global Epigenetic Alterations: An Analysis of Single-Cell ATAC-Seq of Circulating Leukocytes From Trauma Patients Followed by Validation in Whole Blood Leukocyte Transcriptomes Across Three Etiologies of Critical Illness. *eBioMedicine* (2022) 76:103860. doi: 10.1016/j.ebiom.2022.103860
73. Czura CJ, Wang H, Tracey KJ. Dual Roles for HMGB1: DNA Binding and Cytokine. *J Endotoxin Res* (2001) 7(4):315–21. doi: 10.1177/09680519010070041401
74. Wang H, Yang H, Tracey KJ. Extracellular Role of HMGB1 in Inflammation and Sepsis. *J Intern Med* (2004) 255(3):320–31. doi: 10.1111/j.1365-2796.2003.01302.x
75. Yang R, Gallo DJ, Baust JJ, Watkins SK, Delude RL, Fink MP. Effect of Hemorrhagic Shock on Gut Barrier Function and Expression of Stress-Related Genes in Normal and Gnotobiotic Mice. *Am J Physiol Regul Integr Comp Physiol* (2002) 283(5):R1263–74. doi: 10.1152/ajpregu.00278.2002
76. Azhar N, Namas RA, Almahmoud K, Zaaqoq A, Malak OA, Barclay D, et al. A Putative "Chemokine Switch" That Regulates Systemic Acute Inflammation in Humans. *Sci Rep* (2021) 11(1):9703. doi: 10.1038/s41598-021-88936-8

Conflict of Interest: YV is a co-founder of, and stakeholder in, Immunetrics, Inc.

The remaining authors declare that the research was conducted in the absence of any commercial or financial relationships that could be construed as a potential conflict of interest.

Publisher's Note: All claims expressed in this article are solely those of the authors and do not necessarily represent those of their affiliated organizations, or those of the publisher, the editors and the reviewers. Any product that may be evaluated in this article, or claim that may be made by its manufacturer, is not guaranteed or endorsed by the publisher.

frontiers | Frontiers in Immunology

ORIGINAL RESEARCH
published: 16 June 2022
doi: 10.3389/fimmu.2022.901005

The H_2S Donor Sodium Thiosulfate ($Na_2S_2O_3$) Does Not Improve Inflammation and Organ Damage After Hemorrhagic Shock in Cardiovascular Healthy Swine

David Alexander Christian Messerer[1,2], Holger Gaessler[3], Andrea Hoffmann[1], Michael Gröger[1], Kathrin Benz[1], Aileen Huhn[1], Felix Hezel[1], Enrico Calzia[1], Peter Radermacher[1] and Thomas Datzmann[1,4]*

[1] Institute for Anesthesiologic Pathophysiology and Process Engineering, Ulm University, Ulm, Germany, [2] Department of Transfusion Medicine and Hemostaseology, Friedrich-Alexander University Erlangen-Nuremberg, University Hospital Erlangen, Erlangen, Germany, [3] Department of Anesthesiology, Intensive Care Medicine, Emergency Medicine and Pain Therapy, German Armed Forces Hospital Ulm, Ulm, Germany, [4] Department of Anesthesiology and Intensive Care Medicine, University Hospital Ulm, Ulm, Germany

OPEN ACCESS

Edited by:
Klemens Horst, University Hospital RWTH Aachen, Germany

Reviewed by:
Rene H. Tolba, University Hospital RWTH Aachen, Germany
William Ottestad, Oslo University Hospital, Norway

***Correspondence:**
David Alexander Christian Messerer
david.messerer@uni-ulm.de

Specialty section:
This article was submitted to Inflammation, a section of the journal Frontiers in Immunology

Received: *21 March 2022*
Accepted: *25 April 2022*
Published: *16 June 2022*

Citation:
Messerer DAC, Gaessler H, Hoffmann A, Gröger M, Benz K, Huhn A, Hezel F, Calzia E, Radermacher P and Datzmann T (2022) The H_2S Donor Sodium Thiosulfate ($Na_2S_2O_3$) Does Not Improve Inflammation and Organ Damage After Hemorrhagic Shock in Cardiovascular Healthy Swine. Front. Immunol. 13:901005. doi: 10.3389/fimmu.2022.901005

We previously demonstrated marked lung-protective properties of the H_2S donor sodium thiosulfate ($Na_2S_2O_3$, STS) in a blinded, randomized, controlled, long-term, resuscitated porcine model of swine with coronary artery disease, i.e., with decreased expression of the H_2S-producing enzyme cystathionine-γ-lyase (CSE). We confirmed these beneficial effects of STS by attenuation of lung, liver and kidney injury in mice with genetic CSE deletion (CSE-ko) undergoing trauma-and-hemorrhage and subsequent intensive care-based resuscitation. However, we had previously also shown that any possible efficacy of a therapeutic intervention in shock states depends both on the severity of shock as well as on the presence or absence of chronic underlying co-morbidity. Therefore, this prospective, randomized, controlled, blinded experimental study investigated the effects of the STS in cardiovascular healthy swine. After anesthesia and surgical instrumentation, 17 adult Bretoncelles-Meishan-Willebrand pigs were subjected to 3 hours of hemorrhage by removal of 30% of the blood volume and titration of the mean arterial pressure (MAP) ≈ 40 ± 5 mmHg. Afterwards, the animals received standardized resuscitation including re-transfusion of shed blood, fluids, and, if needed, continuous i.v. noradrenaline to maintain MAP at pre-shock values. Animals were randomly allocated to either receive $Na_2S_2O_3$ or vehicle control starting 2 hours after initiation of shock until 24 hours of resuscitation. The administration of $Na_2S_2O_3$ did not alter survival during the observation period of 68 hours after the initiation of shock. No differences in cardio-circulatory functions were noted

despite a significantly higher cardiac output, which coincided with significantly more pronounced lactic acidosis at 24 hours of resuscitation in the $Na_2S_2O_3$ group. Parameters of liver, lung, and kidney function and injury were similar in both groups. However, urine output was significantly higher in the $Na_2S_2O_3$ group at 24 hours of treatment. Taken together, this study reports no beneficial effect of $Na_2S_2O_3$ in a clinically relevant model of hemorrhagic shock-and-resuscitation in animals without underlying chronic cardiovascular co-morbidity.

Keywords: physical injuries, hemorrhage, systemic inflammation, hydrogen sulfide, animal model, gaseous mediator

INTRODUCTION

Sodium thiosulfate, $Na_2S_2O_3$, (STS) is an H_2S donor with minimal side effects and clinically approved for the treatment of calciphylaxis, *cis*-Pt toxicity, and cyanide poisoning (1). Along with its sulfide releasing properties it is a known antioxidant. Moreover, STS was shown to be organ-protective in rodent models of acute liver injury (2), endotoxemia (3, 4), bacterial sepsis (3, 5, 6), and, in particular, ischemia/reperfusion (I/R) injury of the brain (7), heart (8–13), and the kidney (14, 15). Organ protective properties had also been demonstrated in larger species, i.e., canine tourniquet-induced limb ischemia and myocardial infarction induced by ligation of the left anterior descending coronary (16). However, none of these models integrated standard intensive care measures into the experimental design, and, moreover, STS was mostly administered as a pre-treatment or virtually simultaneously with the initiation of ischemia.

Hemorrhagic shock and subsequent resuscitation trigger a systemic inflammatory response due to the tissue oxygen deficit and reperfusion (17–21). Therefore, we have recently tested the therapeutic potential of STS using a post-treatment approach in a blinded, randomized, controlled, long-term, resuscitated porcine model of swine with coronary artery disease (22). STS treatment showed marked lung-protective properties, whereas no effects were observed in other organs. We confirmed these beneficial effects of post-treatment STS by attenuation of lung, liver and kidney injury in mice with genetic CSE deletion (CSE-ko) undergoing trauma-and-hemorrhage and subsequent intensive care-based resuscitation (23). However, we had previously shown that any possible efficacy of a therapeutic intervention in shock states not only depends on the severity of shock *per se* (24, 25), but also on the presence or absence of chronic underlying co-morbidity, e.g., atherosclerosis (26, 27), COPD (28), or metabolic derangements (29). In fact, the above-mentioned porcine study on organ-protective effects of STS in porcine hemorrhage-and-resuscitation (22) investigated swine with coronary artery disease, and, hence, decreased expression of the H_2S-producing enzyme cystathionine-γ-lyase (CSE) (30), i.e. an "H_2S-poor condition" that might render exogenous, STS-derived H_2S supplementation particularly promising (31). Based on these considerations, the aim of this study was to investigate the impact of STS on organ function in a randomized, controlled, blinded trial using a long-term, resuscitated model of hemorrhage-and-resuscitation in pigs without preexisting diseases, i.e., without underlying chronic cardiovascular co-morbidity.

METHODS

Animals

Ethical approval was obtained by the local Animal Care Committee of Ulm University and the Federal Authorities (Tuebingen, Germany) for Animal Research (#1341). The experimental protocol was conducted in close adherence to the European Union Directive 2010/63/EU on the protection of animals used for scientific purposes. 18 adult pigs (range body weight 50-78 kg, range age 0.9-1.4 years) were purchased from the Hôpital Lariboisière, Paris, France. Pigs were of the Bretoncelles-Meishan-Willebrand strain. This strain has reduced activity of the von Willebrand Factor (vWF), thereby mimicking the human coagulation system (24, 25, 32, 33), in contrast to the hypercoagulatory state in domestic swine strains (34). Animals were sheltered at Oberberghof, Ulm, Germany, until further use with an acclimatization period of at least two weeks. Animals were kept at a cycle of 12/12 hr light/darkness and were at least monitored daily. Housing was acclimatized at 21-22°C with a humidity of 50-60% The pigs were treated with Ivermectine twice a year. The main outcome variables were 1) kidney function as assessed by creatinine clearance and 2) the noradrenaline infusion rate needed to maintain mean arterial pressure (MAP) at baseline levels. Based on our previous experiments (22, 24, 26), a case number estimation (power 0.8, $\alpha = 0.05$) had yielded a group size of n = 16 (15 animals + 1 reserve animal) with a preset interim analysis after 8 animals. Because that interim analysis suggested futility, the trial was terminated prematurely in accordance with the 3R principles.

Instrumentation and Anesthesia

Prior to instrumentation, animals were sedated by intramuscular injection of 5 mg/kg azaperone and 1-2 mg/kg midazolam followed by an insertion of an intravenous catheter into an ear vein. After pre-oxygenation, total intravenous anesthesia was induced with 1-2 mg/kg propofol and 1-2 mg/kg ketamine

followed by endotracheal intubation and placement of a gastric tube for stomach decompression. Anesthesia was maintained with 6-12 mg/kg/h pentobarbitone and 30 µg/kg buprenorphine with repeated doses of 10-20 µg/kg prior to instrumentation, prior to the initiation of hemorrhagic shock as well as every 8 hours or by signs of additional demand, such as tachycardia and/or an increase in mean arterial blood pressure. Continuous i.v. pancuronium (0.15 mg/kg/h) was used for muscle relaxation. During instrumentation and hemorrhagic shock, animals were ventilated with the following parameters: fraction of inspired O_2 (F_IO_2) 0.21, positive end-expiratory pressure (PEEP) 0 cmH_2O, tidal volume 8 ml/kg, respiratory rate 10 to 12 breaths/min adjusted to maintain arterial PCO_2 = 35 to 40 mmHg, inspiratory (I)/expiratory (E) ratio 1:2. Animals received 10 ml/kg/h Ringer's lactate to maintain fluid balance. A central venous catheter was inserted in the jugular vein to measure central venous pressure (CVP). A thermistor-tipped pulse contour analysis catheter was placed in the femoral artery for mean arterial blood pressure (MAP) recording and trans-pulmonary single indicator thermodilution-cardiac output (CO) measurement. In the contralateral femoral artery, a 10F catheter was inserted for rapid passive blood removal to induce hemorrhagic shock. Urine was collected by a suprapubic catheter. Body temperature was assessed by a rectal probe. Animals were kept at a temperature of 37-38°C.

Porcine Hemorrhagic Shock and Thiosulfate Regimen

The experimental procedure and treatment regimen is summarized in **Figure 1A** and closely mimics previously described experiments (22, 24, 32, 35). Prior to the initiation of hemorrhagic shock after the instrumentation (1-2 h) and a resting period (total of 4 h), baseline data was collected (−0.5 h in **Figure 1**). Hemorrhagic shock was initiated by passive blood removal of 30% of the calculated total blood volume (calculated as bodyweight × 8.8%) with a target mean arterial pressure of 40 ± 5 mmHg for 3 h. Removal of the calculated blood volume was achieved within 30 min in all pigs. Every 15 min, 50 ml of blood were removed or retransfused to maintain target MAP.

Blood was stored in acid-citrate-dextrose solution until re-transfusion. 2 h after the initiation of hemorrhagic shock, animals were randomly allocated to either receive sodium STS (0.025 g/kg/h for two hours followed by 0.1 g/kg/h for 23 h) or the respective vehicle control. The lower initial infusion rate was chosen in order to take into account the reduced volume of distribution during and immediately after the hemorrhage phase. The higher infusion rate during the rest of the treatment phase was used in accordance with our previous study (22). During hemorrhagic shock, maintenance fluid was reduced to 100 ml/h. After the 3 h period, animals were treated by re-transfusion of shed blood, 10 ml/kg/h Ringer's lactate, and continuous i.v.

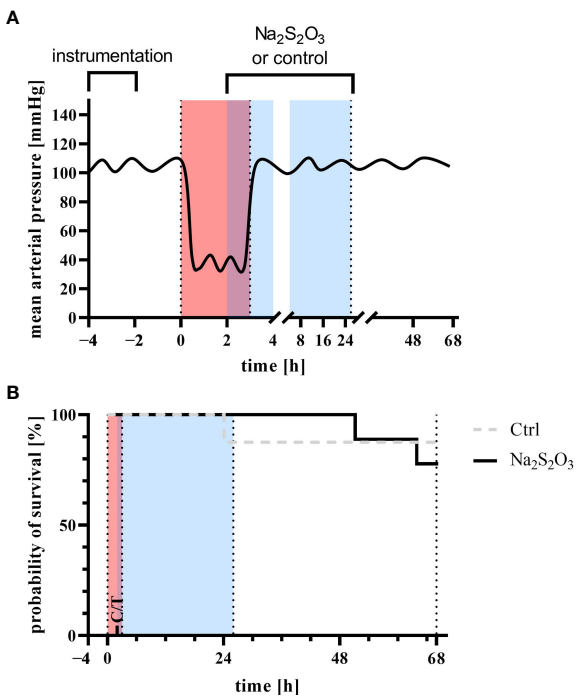

FIGURE 1 | **(A)** Experimental setup and **(B)** survival analysis Log-rank Kaplan-Meyer survival analysis of animals receiving sodium thiosulfate ($Na_2S_2O_3$, n = 9) or vehicle control (Ctrl, n = 8) for the experiment (p = 0.66, Mantel-Cox test). Red indicates the phase of hemorrhagic shock, blue indicates the phase of treatment with $Na_2S_2O_3$ (STS, 0.025 g/kg/h for two hours followed by 0.1 g/kg/h for 23 h) or vehicle control. Instrumentation and resting period was during −4 h and 0 h, hemorrhagic shock with a target mean arterial pressure of 40 ± 5 mmHg during 0 h and 3 h (red), treatment with sodium thiosulfate or vehicle control during 2 h and 25 h (blue) with a total duration of observation and intensive care therapy of 68 h.

noradrenaline if necessary to achieve a mean arterial pressure with a target of 90-100% of the baseline. After hemorrhagic shock, ventilator settings were adjusted as follows: fraction of inspired O_2 (F_IO_2) 0.35, positive end-expiratory pressure (PEEP) 10 cmH_2O, tidal volume 8 ml/kg, respiratory rate 10 to 12 breaths/min adjusted to maintain arterial PCO_2 = 35 to 40 mmHg, inspiratory (I)/expiratory, (E) ratio 1:1.5, peak airway pressure <40 cmH_2O, and modified to I/E ratio 1:1 and PEEP 12 or 15 cmH_2O, respectively, if the ratio of arterial O_2 partial pressure (PaO_2)/FiO_2 was <300 or <200. The STS group consisted of 4/5 male-castrated/female pigs (62 kg; 54-71 kg), the vehicle control groups of 3/5 male-castrated/female animals (61 kg; 56-64 kg). The difference in sample size is explained by a drop out prior to the induction of hemorrhagic shock.

After the treatment and observation period (68 h after the induction of hemorrhagic shock), anesthesia was deepened and animals were sacrificed by an injection of potassium chloride. At the end of the experiment, immediate postmortem tissue sampling of lung and kidney was performed. The trial was terminated earlier if one of the following criteria were fulfilled: A) mean arterial pressure less than < 65 mmHg despite vasopressors (dosing limited to a heart rate of ≥ 160/min in order to prevent tachycardia-induced myocardial infarction); B) failure to sustain arterial PO_2 > 60 mmHg and/or arterial Hb saturation > 90% despite maximum invasive ventilation (acute respiratory distress syndrome, ARDS); and C) acute anuric kidney failure with consecutive hyperkalemia (blood potassium > 6 mmol/L) and cardiac arrhythmia.

Blood and Plasma Measurements

Hemodynamics, gas exchange (calorimetric O_2 uptake and CO_2 production), arterial blood gas tensions, acid-base status, glucose, lactate, creatinine, neutrophil gelatinase-associated lipocalin (NGAL), aspartate transaminase (AST), alanine transaminase (ALT), 8-Isoprostane, bilirubin, and troponin were determined as described previously (32, 35–37). In brief, blood gas analysis, glucose, and lactate levels were measured using a standard blood gas analyzer (ABL 800 Flex, Radiometer GmbH, Krefeld, Germany). Creatinine (#KIT044, BioPorto, Hellerup, Denmark), AST (#AS 1204, Randox, Crumlin, Northern Ireland), ALT (#AL 1205, Randox), 8-Isoprostane (#516351, Cayman Chemical, Ann Arbor, USA), bilirubin (#BR 2361, Randox), and troponin (#2010-4-HSP, Life Diagnostics, West Chester, USA), tumor necrosis factor (TNF, #PTA00, R&D Systems, Minneapolis, USA), interleukin 6 (IL6, #P6000B, R&D Systems), interleukin 10 (IL10, #P1000, R&D Systems), and super oxide dismutase (SOD, #S311, Dojindo Molecular Technologies, Rockville, USA) were determined as recommended by the manufacturer.

Western Blot

Immediately after ending the experiment, postmortem heart, kidney, liver, and lung specimen were analyzed for Caspase-3 (#9661, Cell Signaling Technology, Danvers, USA), inducible nitric oxide synthase (iNOS, PA1-039, Thermo Fisher Scientific, Waltham, USA), heme oxygenase 1 (HO-1, #ADI-OSA-111, Enzo Life Sciences, Farmingdale, USA), nuclear factor of kappa light polypeptide gene enhancer in B-cells inhibitor, alpha (IκBα, #9242, Cell Signaling Technology), cystathionine-β-synthase (CBS, #14782, Cell Signaling Technology), Cystathionine-γ-lyase (CSE, #12217-1-AP, Rosemont), and glucocorticoid receptor (GCR, #3660, Cell Signaling Technology) as described previously (24, 26). Secondary antibodies were anti-rabbit (#7074, Cell Signaling Technology) and anti-mouse (#7076, Cell Signaling Technology) IgG, respectively. Anti-Actin (#sc-1615, Santa Cruz Biotechnology, Dallas, USA) and anti-Vinculin (#sc-73614, Santa Cruz Biotechnology) antibodies were used as loading controls. For quantitative analysis, the mean value of the individual gels from at least two gels for each animal was used. Expression of proteins was normalized to signals from two pigs (both female, 85 and 89 kg) of the same strains without further instrumentation.

Data Analysis

Survival was analyzed using a Kaplan-Meyer-graph followed by Log-rank (Mantel-Cox) Test. Experimental data were considered to be non-parametric. The comparison of treatment and vehicle group was conducted by means of Mann-Whitney U test. Data is graphed in boxplots with median, 25^{th} and 75^{th} quantiles. Whiskers indicate upper and lower extremes, respectively. In the manuscript, data is reported as median in conjunction with 25^{th} quantile and 75^{th} quantile. Statistical analysis was conducted with GraphPad Prism9 (GraphPad Software, Inc., San Diego, California, USA). Because of non-paired testing and similar survival, missing data due to premature deaths does not largely affect the statistical analysis. We chose intentionally to not extrapolate missing data since the distance of measurement time points precluded to reliable the biological course of the variables.

RESULTS

Survival

Survival did not significantly differ between the two groups (**Figure 1B**). In the STS group, two experiments had to be terminated early: one after 51 h due to refractory respiratory failure (ARDS) and another one after 64 h due to a sudden drop in MAP unresponsive to vasopressors infusion. In the vehicle control group, one animal had to be euthanized after 24 h due to ARDS.

Parameters of Hemodynamics, Gas Exchange, Acid-Base Status, and Metabolism

Neither the amount of blood removed to induced hemorrhagic shock (fraction of the calculated total blood volume 39% (38; 46) vs. 32% (28; 44) in the vehicle control and STS groups, respectively, p = 0.13, Mann-Whitney U test), nor the noradrenaline infusion rates needed to achieve hemodynamic targets (0.8 μg/kg/min (0.1; 1.8) vs. 0.9 μg/kg/min (0.5; 1.1), in the vehicle control and STS groups, respectively, p = 0.81, Mann-Whitney U test) differed between the STS and vehicle group.

Tables 1, **2** as well as **Figure 2** summarize the parameters of hemodynamics, gas exchange, acid-base status, and metabolism. There was a small but significant difference in baseline heart rate between the two groups (**Figure 2**). MAP, stroke volume, stroke volume variance, heart rate, and arterial pH did not show any significant intergroup difference, whereas cardiac output and arterial lactate levels were significantly higher and arterial base excess significantly lower in the STS group at 24 hours after shock. Of note, the peak increase of lactate within the first 24 hours after resuscitation in comparison to baseline levels

TABLE 1 | Systemic and respiratory parameters before (pre) and after 3 h of hemorrhagic shock (post) as well as 24 h, 48 h, and 68 h after resuscitation.

Parameter		pre	post	24 h	48 h	68 h
Body Temperature (°C)	C	36.0 (35.3; 36.4)	36.6 (35.7; 37.1)	37.9 (37.5; 38.2)	37.9 (37.9; 38.3)	38.1 (37.6; 38.4)
	T	35.8 (35.4; 37.0)	35.9 (35.0; 36.7)	38.2 (37.7; 38.4)	38.5 (37.8; 39.2)	38.3 (37.9; 38.6)
Central Venous Pressure (mmHg)	C	3 (1; 4)	–4 (–7; –2)	12 (9; 13)	11 (9; 17)	10 (8; 14)
	T	3 (1; 4)	–3 (–5; 1)	10 (8; 14)	11 (5; 14)	8 (4; 11)
Positive end-expiratory pressure (cmH_2O)	C	0 (0; 0)	0 (0; 0)	10 (10; 10)	10 (10; 10)	10 (10; 12)
	T	0 (0; 0)	0 (0; 0)	10 (10; 10)	10 (10; 13)	11 (10; 13)
Respiratory Minute Volume ($l \times min^{-1}$)	C	5.0 (4.3; 5.2)	4.9 (4.3; 5.4)	6.0 (5.2; 6.3)	5.9 (4.8; 6.0)	5.8 (5.3; 7.0)
	T	4.8 (3.9; 5.4)	4.7 (3.9; 5.6)	5.7 (5.1; 6.6)	5.6 (4.7; 6.4)	6.6 (4.5; 7.3)
Arterial PO_2 (mmHg)	C	75 (62; 88)	81 (71; 86)	127 (98; 133)	104 (89; 110)	101 (90; 119)
	T	82 (70; 89)	85 (69; 92)	124 (105; 128)	105 (75; 121)	116 (66; 125)
PaO_2/F_IO_2 ratio (mmHg)	C	357 (292; 419)	387 (340; 408)	422 (326; 442)	347 (297; 367)	337 (300; 397)
	T	390 (335; 424)	404 (327; 438)	413 (340; 425)	350 (228; 402)	317 (216; 396)
Arterial PCO_2 (mmHg)	C	37 (36; 39)	39 (34; 39)	37 (36; 40)	39 (36; 44)	37 (36; 38)
	T	35.5 (32.7; 39.9)	38.2 (31.3; 39.7)	36.4 (35.2; 40.9)	38.9 (38.1; 43.3)	37.7 (35.4; 39.2)
Oxygen Consumption ($ml \times min^{-1}$)	C	209 (197; 257)	200 (175; 236)	310 (300; 339)	308 (286; 339)	327 (284; 380)
	T	206 (188; 222)	185 (153; 227)	327 (276; 372)	361 (291; 398)	380 (301; 470)
Carbon Dioxide Elimination ($ml \times min^{-1}$)	C	159 (138; 205)	142 (139; 183)	190 (163; 221)	176 (160; 191)	184 (149; 218)
	T	145 (114; 175)	121 (108; 186)	206 (171; 225)	208 (164; 251)	202 (164; 251)

n = 8/9 before shock, 8/9 after shock, 8/9 at 24 h, 7/9 at 48 h, and 7/8 at 68 h animals per group for vehicle control (yellow, C) and thiosulfate (purple, T), respectively. Table reports median and interquartile range.

TABLE 2 | Blood glucose, hemoglobin, thrombocyte and leukocyte cell count before (pre) and after 3 h of hemorrhagic shock (post) as well as 24 h, 48 h, and 68 h after resuscitation.

Parameter		pre	post	24 h	48 h	68 h
Arterial Glucose ($mmol \times l^{-1}$)	C	98 (91; 108)	109 (98; 118)	94 (72; 135)	67 (60; 83)	69 (58; 64)
	T	109 (89; 115)	108 (99; 132)	98 (83; 125)	71 (67; 84)	70 (56; 75)
Hemoglobin ($g \times l^{-1}$)	C	79 (69; 81)	93 (83; 100)	95 (84; 99)	73 (69; 92)	84 (71; 91)
	T	83 (78; 88)	93 (82; 102)	107 * (101; 116)	97 * (92; 109)	90 (82; 95)
Thrombocytes ($\times 10^9 \times l^{-1}$)	C	235 (193; 271)	226 (211; 269)	221 (170; 268)	268 (129; 315)	250 (83; 330)
	T	238 (169; 340)	251 (215; 316)	248 (181; 311)	169 (112; 267)	157 (76; 222)
Leukocytes ($\times 10^{12} \times l^{-1}$)	C	15.8 (8.3; 18.6)	14.4 (12.4; 18.5)	14.9 (9.0; 16.0)	11.1 (7.6; 14.4)	11.6 (4.8; 18.2)
	T	13.7 (11.8; 17.2)	18.7 (14.4; 19.7)	20.5 ** (16.2; 28.4)	12.7 (11.1; 13.3)	10.2 (9.1; 16.3)

*n = 8/9 before shock, 8/9 after shock, 8/9 at 24 h, 7/9 at 48 h, and 7/8 at 68 h animals per group for vehicle control (yellow, C) and thiosulfate (purple, T), respectively. * = $p < 0.05$, ** = $p < 0.01$, Mann-Whitney U test. Table reports median and interquartile range.*

measured in a 2 hour interval was 4.0 mmol/l (0.9; 4.3) in the vehicle control group and 2.8 mmol/l (1.9; 7.7) in the STS group ($p > 0.99$). In parallel, there was a decrease in base excess in comparison to baseline levels of −10.7 mmol/l (−16.4; 3.5) in the vehicle control group and −7.0 mmol/l (−13.0; −4.7) in the STS group ($p = 0.96$). Animals receiving STS had similar P_aO_2/F_IO_2 ratios and required ventilator settings to maintain target PO_2 and PCO_2 levels. Likewise, O_2 uptake and CO_2 production were similar in the two groups. Glucose levels were not affected by STS treatment either (**Table 2**).

Parameters of Heart, Kidney, and Liver Function and Organ Injury

There were no significant intergroup differences in troponin, AST, ALT, and bilirubin (**Figure 3**). Of note, baseline bilirubin concentrations were slightly, but significantly higher in the vehicle group, which coincided with a non-significant trend towards higher AST levels in these animals. While urine output was significantly higher in the STS group at 24 h of resuscitation, parameters of kidney (dys)function (NGAL, creatinine) did not differ between the two groups.

Inflammation

Last, the impact of STS treatment on inflammation was assessed during and after hemorrhagic shock. Animals receiving STS had significant higher leukocyte counts 24 h after hemorrhagic shock (**Table 2**). In contrast, systemic levels of TNF, IL6, IL10, 8-isoprostanes, and SOD activity were comparable in the two groups (**Figure 4**). Of note, there was a significant increase in catalase activity 24 h after shock, likely due to the pre-existing, non-significant difference already at baseline.

To further characterize the impact of STS on protein levels in kidney and lung, western blot analysis was conducted (**Figure 5**). No significant alterations for caspase 3, iNOS, HO-1, IκBα, CBS and CSE (the last two only analyzed in the kidney due to technical reasons) were detected. However, there was a significant decrease in GCR protein levels in the STS group. The original western blot captures are presented in **Supplementary Figures 1, 2**.

DISCUSSION

Using a long-term, resuscitated, porcine model of hemorrhage-and-resuscitation, the present randomized, controlled, blinded trial was to test the hypothesis whether STS would attenuate organ dysfunction in adult animals with normal CSE expression, and, consequently, well-maintained endogenous H_2S availability. This study therefore expands the knowledge on STS as therapeutic option in systemic inflammation in addition to "H_2S-poor conditions", e.g. as a result of underlying coronary artery disease (22, 30) or even genetic CSE deletion (CSE-ko) (23) that might enhance STS efficacy (31). The main findings were that *i)* STS did not beneficially affect any variable measured of hemodynamics, lung mechanics and gas exchange, or organ (dys)function and injury, nor *ii)* any of the parameters of systemic and organ inflammation or oxidative and nitrosative stress.

Possible organ-protective effects of STS have been referred to attenuated activation of nuclear transcription factor-κB, hyper-

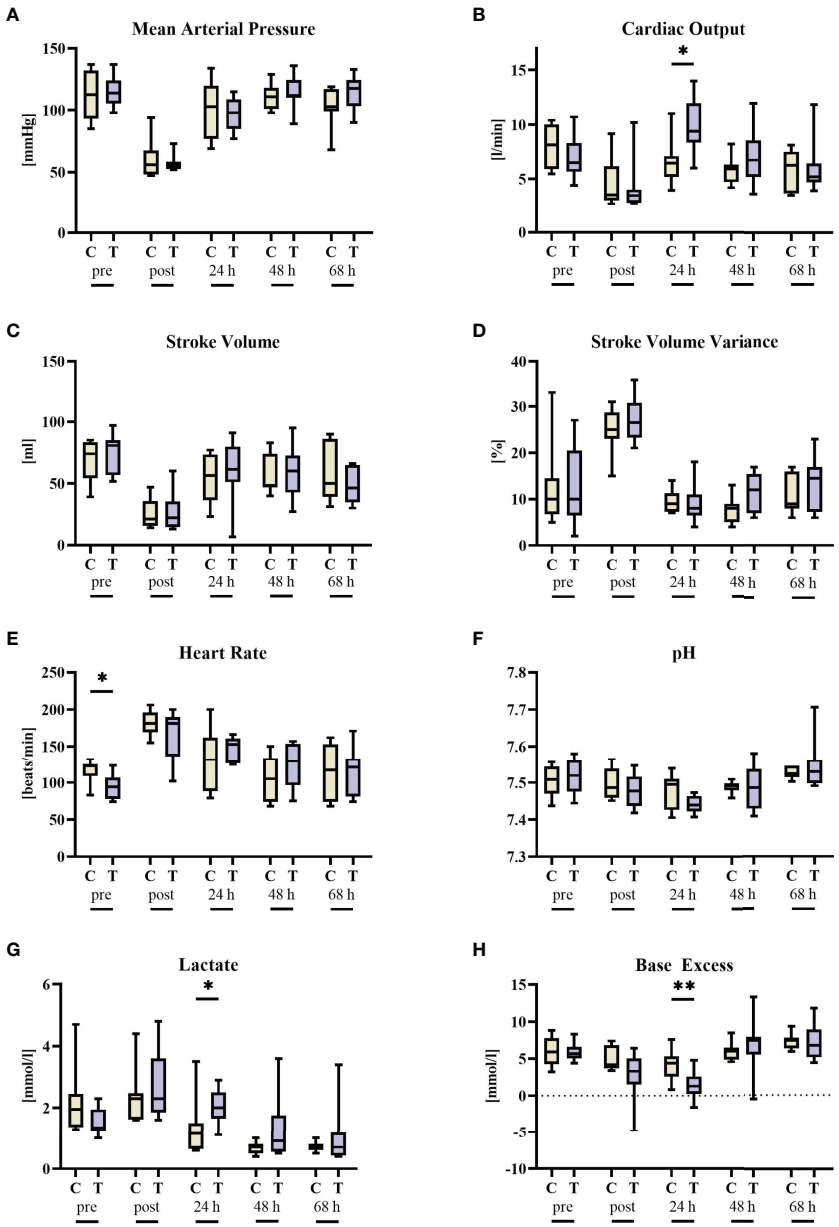

FIGURE 2 | Cardiocirculatory parameters before (pre) and after 3 h of hemorrhagic shock (post) as well as 24 h, 48 h, and 68 h after resuscitation. **(A)** mean arterial pressure, **(B)** cardiac output, **(C)** stroke volume, **(D)** stroke volume variance, **(E)** heart rate, **(F)** blood pH, **(G)** blood lactate, and **(H)** blood base excess. n = 8/9 before shock, 8/9 after shock, 8/9 at 24 h, 7/9 at 48 h, and 7/8 at 68 h animals per group for vehicle control (yellow, C) and thiosulfate (purple, T), respectively. * = $p < 0.05$, ** = $p < 0.01$, Mann-Whitney U test. Box plots report median, interquartile range, minimum, and maximum.

inflammation and oxidative stress (2, 3) and reduced apoptosis (9–11, 13). In addition, we had demonstrated that the marked lung-protective effect of STS in swine with coronary artery disease and, hence, reduced CSE expression coincided with significantly higher tissue glucocorticoid receptor (GR) expression. We had confirmed this finding otherwise healthy, CSE-ko mice receiving STS in addition to standard ICU care during resuscitation from trauma-and-hemorrhage (23). In sharp contrast to these previous results, lung tissue GR expression was even significantly lower in the STS-treated swine than in the vehicle group in the present study. We can only speculate regarding this different result, but the reduced activity of the von Willebrand Factor (vWF) in our Bretoncelles-Meishan-Willebrand pigs may assume importance in this context. We studied heterozygous individuals of this swine strain, because they closely mimic the human coagulation system (24, 25, 32, 33), in contrast to the hypercoagulatory state in other domestic swine strains (34). We cannot exclude, however, that this "vWF-disease", albeit not

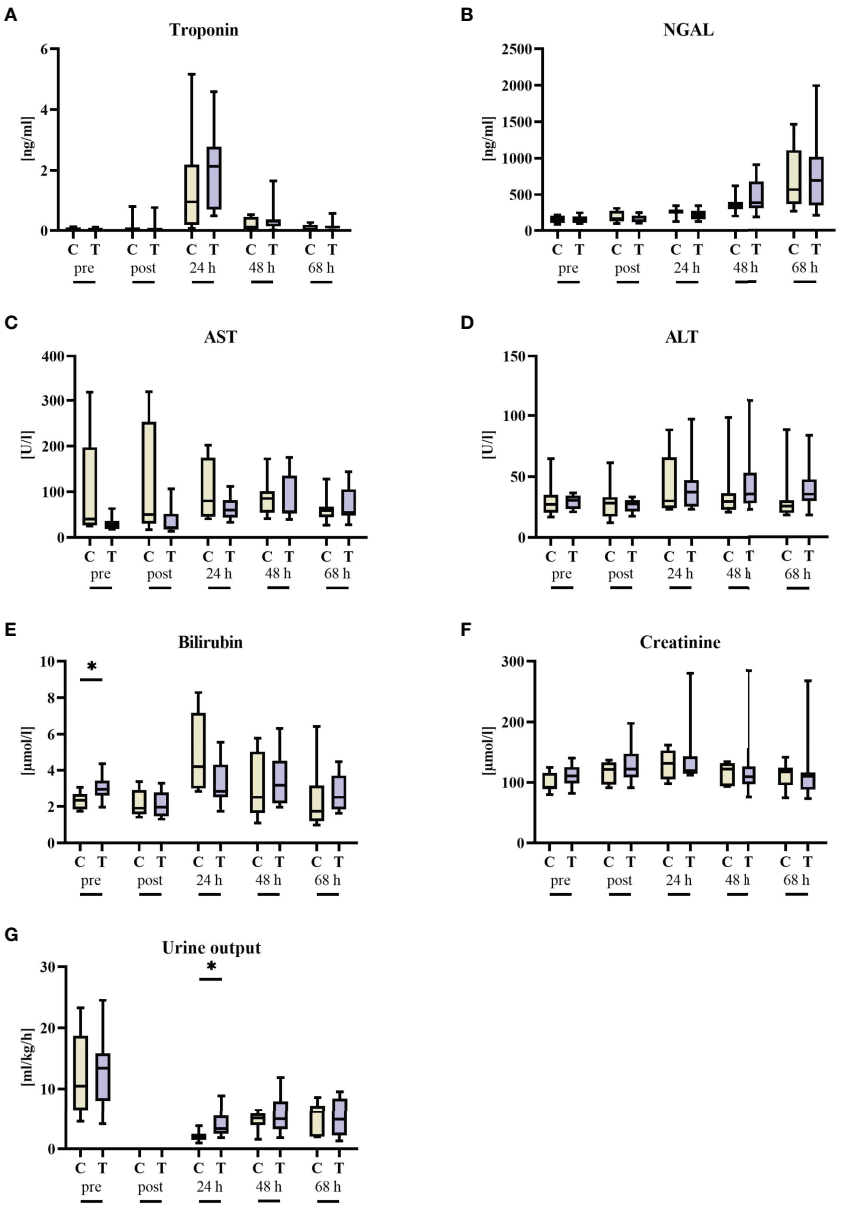

FIGURE 3 | Organ function parameters before (pre) and after 3 h of hemorrhagic shock (post) as well as 24 h, 48 h, and 68 h after resuscitation. **(A)** Troponin, **(B)** neutrophil gelatinase-associated lipocalin (NGAL), **(C)** aspartate transaminase (AST), **(D)** alanine transaminase (ALT), **(E)** bilirubin, **(F)** creatinine, and **(G)** urine output. n = 8/9 before shock, 8/9 after shock, 8/9 at 24 h, 7/9 at 48 h, and 7/8 at 68 h animals per group for vehicle control (yellow, C) and thiosulfate (purple, T), respectively. * = $p < 0.05$, Mann-Whitney U test. Box plots report median, interquartile range, minimum, and maximum.

presenting with any clinically relevant bleeding disorder, may have altered the STS effect on the GR expression: ACTH secreting bronchial carcinoid cells were shown to present with significant glucocorticoid receptor expression (38), and high glucocorticoid levels due to Cushing's disease are associated with increased vWF-activity (39). Exogenous glucocorticoid administration produced less consistent results: in healthy subjects, oral steroids also *increased* vWF activity (40), while under hyper-inflammatory conditions the opposite effect was reported (41). To the best of our knowledge, however, no data are available on the reverse relation, i.e. on the effect of reduced vWF activity *per se* on cortisol concentrations and/or GR expression.

At the end of the treatment phase, i.e., at 24 h of resuscitation, STS was associated with statistically significantly lower arterial base excess levels (STS 1.3 mmol/l (0.3; 2.6) vs. vehicle control 4.4 mmol/l (2.6; 5.3), $p < 0.01$, Mann-Whitney U test). This difference in the acid-base status disappeared until the end of the experiment. The lower base excess is well in line with case reports on i.v. STS (42, 43) as well as in our previous study in swine with coronary artery disease (22). Of note, the arterial base

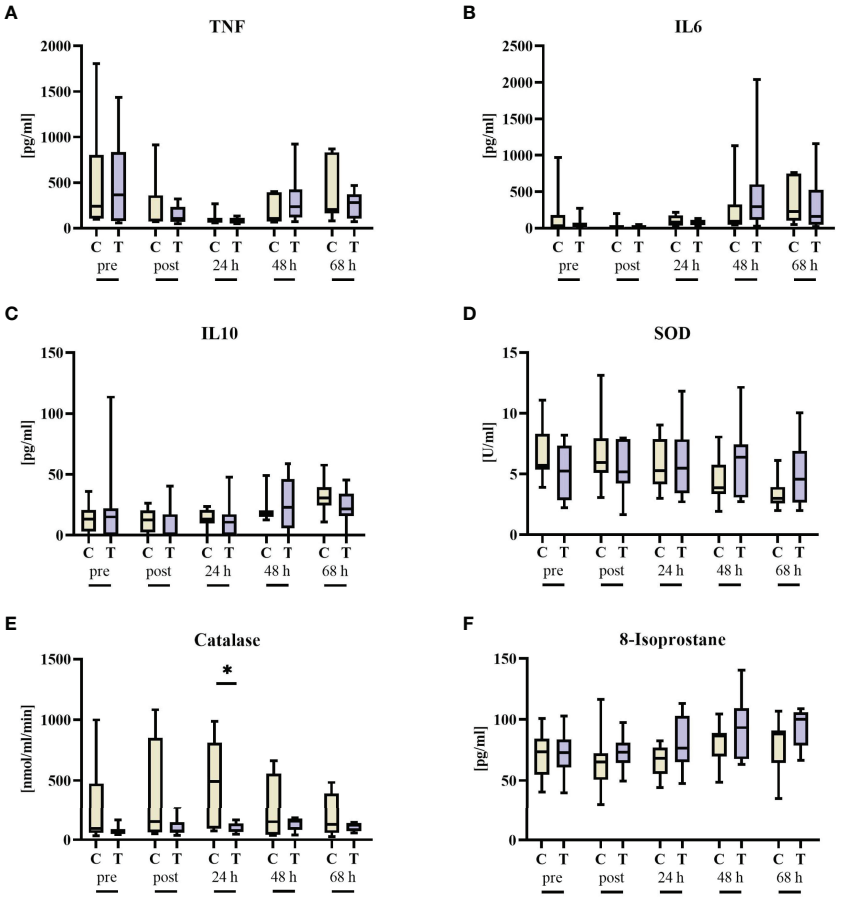

FIGURE 4 | Inflammation parameters before (pre) and after 3 h of hemorrhagic shock (post) as well as 24 h, 48 h, and 68 h after resuscitation. **(A)** TNF, **(B)** IL6, **(C)** IL10, **(D)** superoxide dismutase (SOD), **(E)** catalase, and **(F)** 8-isoprostane. n = 8/9 before shock, 8/9 after shock, 8/9 at 24 h, 7/9 at 48 h, and 7/8 at 68 h animals per group for vehicle control (yellow, C) and thiosulfate (purple, T), respectively. * = $p < 0.05$, Mann-Whitney U test. Box plots report median, interquartile range, minimum, and maximum.

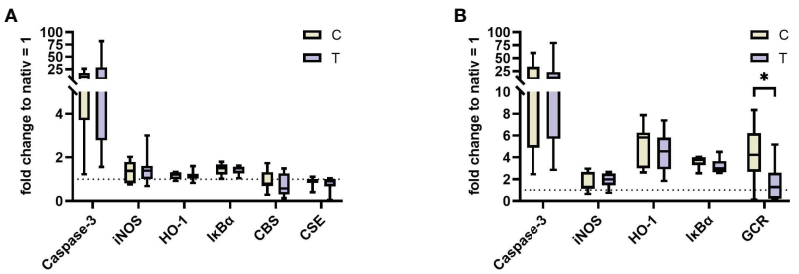

FIGURE 5 | Western Blot analysis of kidney **(A)** and lung **(B)** at the end of the trial for n = 7/8 animals per group for vehicle control (yellow, C) and thiosulfate (purple, T), respectively. Results are normalized to protein levels from two untreated animals. iNOS, inducible nitric oxide synthase; HO-1, heme oxygenase 1; IκBα, nuclear factor of kappa light polypeptide gene enhancer in B-cells inhibitor, alpha; CBS, cystathionine-β-synthase; CSE, Cystathionine-γ-lyase; GCR, glucocorticoid receptor. * = $p < 0.05$, Mann-Whitney U test. Box plots report median, interquartile range, minimum, and maximum.

excess tended to be lower in the STS-treated animals at the end of the shock-phase (STS 3.3 mmol/l (1.5; 5.1) vs. vehicle control 4.2 mmol/l (3.7; 6.8), p = 0.12, Mann-Whitney U test), most likely as a result of the fact that the STS-infusion was already started at 2 h of hemorrhage, i.e. 1 h prior to the initiation of re-transfusion of shed blood, fluid resuscitation, and continuous i.v. noradrenaline. Nevertheless, the fact that this fall in base excess was not associated with a pH < 7.4, any acidosis-related

lung protection may have been prevented: acidosis-related lung-protection *in vivo* was reported at pH ≈ 7.00-7.25 (44).

Limitations

We might have missed a putative therapeutic benefit due to an unbalanced shock severity: Albeit not statistically significant, the amount of blood removed to induced hemorrhagic shock, tended to be higher in the vehicle group (p = 0.13, see above, "*Results*" section). However, not only tended arterial base excess to be lower (see above), but also arterial lactatemia to be slightly higher (STS 2.3 mmol/l (1.9; 3.6) vs. vehicle control 2.3 mmol/l (1.6; 2.5), p = 0.65, Mann-Whitney U test) in the STS-treated animals already at the end of the shock phase. In addition, heart rate in the STS-group had shown a significantly higher baseline value, i.e., the relative heart increase was more severe, possibly suggesting a more pronounced activation of the sympathetic system. Clearly, any difference in shock severity was due to chance, because we used a blinded, random and controlled experimental design. Another limitation is that we might have missed a temporary effect of STS on organ function due to the distance between measurement time points, e.g., a change in organ function after 6 h of treatment. However, based on the similar survival between the groups, there is no hint for such an issue.

CONCLUSION

Altogether, in contrast to our previous study in swine with coronary artery disease, this study reports no beneficial effect of STS using a blinded, randomized controlled trial design in a clinically relevant, long-term porcine model of hemorrhagic shock-and-resuscitation in animals devoid of underlying chronic cardiovascular co-morbidity. We cannot exclude that studying adult animals with heterozygous "vWF" disease may have influenced this result. Nevertheless, the current study highlights the impact of the severity of shock *per se* as well as the investigation of chronic underlying co-morbidities on the possible efficacy of therapeutic interventions in pre-clinical shock research.

DATA AVAILABILITY STATEMENT

The original contributions presented in the study are included in the article/**Supplementary Material**. Further inquiries can be directed to the corresponding author.

ETHICS STATEMENT

The animal study was reviewed and approved by local Animal Care Committee of Ulm University and the Federal Authorities (Tuebingen, Germany) for Animal Research (#1341).

AUTHOR CONTRIBUTIONS

Conceptualization: PR; methodology: DM, AnH, and PR; formal analysis: DM and PR; investigation: DM, HG, AnH, MG, KB, AiH, MG, KB, FH, EC, PR, and TD, resources: PR; writing – original draft: DM and PR; writing – review and editing: DM, HG, AnH, MG, KB, AiH, FH, EC, PR, and TD; visualization: DM; supervision: PR. All authors have read and approved the final version of the article.

FUNDING

DM received funding by means of a "Gerok Rotation" (rotation as clinician scientist) by the Collaborative Research Center 1149 (project number 251293561), German Research Foundation. PR received funding from the Collaborative Research Center 1149 (project number 251293561), German Research Foundation, and the German Ministry of Defense (project E/U2AD/ID013/IF564). The funders had no role in the design of this study, data collection, or interpretation, or the decision to submit the results.

ACKNOWLEDGMENTS

The authors are indebted to Tanja Schulz, Sandra Kress, Andrea Seifritz, Rosemarie Mayer, and Bettina Stahl for skillful technical assistance.

SUPPLEMENTARY MATERIAL

The Supplementary Material for this article can be found online at: https://www.frontiersin.org/articles/10.3389/fimmu.2022.901005/full#supplementary-material

REFERENCES

1. McGeer P. Medical Uses of Sodium Thiosulfate. *J Neurol Neuromedicine* (2016) 1:28–30. doi: 10.29245/2572.942X/2016/3.1032
2. Shirozu K, Tokuda K, Marutani E, Lefer D, Wang R, Ichinose F. Cystathionine γ-Lyase Deficiency Protects Mice From Galactosamine/Lipopolysaccharide-Induced Acute Liver Failure. *Antioxidants Redox Signaling* (2014) 20:204–16. doi: 10.1089/ars.2013.5354
3. Sakaguchi M, Marutani E, Shin H, Chen W, Hanaoka K, Xian M, et al. Sodium Thiosulfate Attenuates Acute Lung Injury in Mice. *Anesthesiology* (2014) 121:1248–57. doi: 10.1097/ALN.0000000000000456
4. Acero G, Nava Catorce M, González-Mendoza R, Meraz-Rodríguez MA, Hernández-Zimbron LF, González-Salinas R, et al. Sodium Thiosulphate Attenuates Brain Inflammation Induced by Systemic Lipopolysaccharide Administration in C57BL/6J Mice. *Inflammopharmacology* (2017) 25:585–93. doi: 10.1007/s10787-017-0355-y
5. Broner CW, Shenep JL, Stidham GL, Stokes DC, Fairclough D, Schonbaum GR, et al. Effect of Antioxidants in Experimental Escherichia Coli Septicemia. *Circ Shock* (1989) 29:77–92.
6. Renieris G, Droggiti D-E, Katrini K, Koufargyris P, Gkavogianni T, Karakike E, et al. Host Cystathionine-γ Lyase Derived Hydrogen Sulfide Protects Against Pseudomonas Aeruginosa Sepsis. *PloS Pathog* (2021) 17:e1009473. doi: 10.1371/journal.ppat.1009473
7. Marutani E, Yamada M, Ida T, Tokuda K, Ikeda K, Kai S, et al. Thiosulfate Mediates Cytoprotective Effects of Hydrogen Sulfide Against Neuronal Ischemia. *JAHA* (2015) 4. doi: 10.1161/JAHA.115.002125

8. Ravindran S, Gopalakrishnan S, Kurian GA. Beneficial Effect of Sodium Thiosulfate Extends Beyond Myocardial Tissue in Isoproterenol Model of Infarction: Implication for Nootropic Effects. *J Biochem Mol Toxicol* (2020) 34. doi: 10.1002/jbt.22606
9. Ravindran S, Ramachandran K, Kurian GA. Sodium Thiosulfate Mediated Cardioprotection Against Myocardial Ischemia-Reperfusion Injury Is Defunct in Rat Heart With Co-Morbidity of Vascular Calcification. *Biochimie* (2018) 147:80–8. doi: 10.1016/j.biochi.2018.01.004
10. Ravindran S, Boovarahan SR, Shanmugam K, Vedarathinam RC, Kurian GA. Sodium Thiosulfate Preconditioning Ameliorates Ischemia/Reperfusion Injury in Rat Hearts *Via* Reduction of Oxidative Stress and Apoptosis. *Cardiovasc Drugs Ther* (2017) 31:511–24. doi: 10.1007/s10557-017-6751-0
11. Ravindran S, Jahir Hussain S, Boovarahan SR, Kurian GA. Sodium Thiosulfate Post-Conditioning Protects Rat Hearts Against Ischemia Reperfusion Injury *via* Reduction of Apoptosis and Oxidative Stress. *Chem Biol Interact* (2017) 274:24–34. doi: 10.1016/j.cbi.2017.07.002
12. Ravindran S, Kurian GA. Preconditioning the Rat Heart With Sodium Thiosulfate Preserved the Mitochondria in Response to Ischemia-Reperfusion Injury. *J Bioenerg Biomembr* (2019) 51:189–201. doi: 10.1007/s10863-019-09794-8
13. Ravindran S, Kurian GA. Effect of Sodium Thiosulfate Postconditioning on Ischemia-Reperfusion Injury Induced Mitochondrial Dysfunction in Rat Heart. *J Cardiovasc Transl Res* (2018) 11:246–58. doi: 10.1007/s12265-018-9808-y
14. Zhang MY, Dugbartey GJ, Juriasingani S, Sener A. Hydrogen Sulfide Metabolite, Sodium Thiosulfate: Clinical Applications and Underlying Molecular Mechanisms. *Int J Mol Sci* (2021) 22:6452. doi: 10.3390/ijms22126452
15. Zhang MY, Dugbartey GJ, Juriasingani S, Akbari M, Liu W, Haig A, et al. Sodium Thiosulfate-Supplemented UW Solution Protects Renal Grafts Against Prolonged Cold Ischemia-Reperfusion Injury in a Murine Model of Syngeneic Kidney Transplantation. *BioMed Pharmacother* (2022) 145:112435. doi: 10.1016/j.biopha.2021.112435
16. Oksman TM, Levandovskiĭ IV, Epishin IN, Vrana M, Blazhek Z. [Sodium Thiosulfate in the Treatment of Early Postischemic Disorders]. *Biull Eksp Biol Med* (1981) 92:275–8. doi: 10.1007/BF00829520
17. Cannon JW. Hemorrhagic Shock. *N Engl J Med* (2018) 378:370–9. doi: 10.1056/NEJMra1705649
18. Angele MK, Schneider CP, Chaudry IH. Bench-To-Bedside Review: Latest Results in Hemorrhagic Shock. *Crit Care* (2008) 12:218. doi: 10.1186/cc6919
19. Messerer DAC, Halbgebauer R, Nilsson B, Pavenstädt H, Radermacher P, Huber-Lang M. Immunopathophysiology of Trauma-Related Acute Kidney Injury. *Nat Rev Nephrol* (2021) 17:91–111. doi: 10.1038/s41581-020-00344-9
20. Eltzschig HK, Carmeliet P. Hypoxia and Inflammation. *N Engl J Med* (2011) 364:656–65. doi: 10.1056/NEJMra0910283
21. Eltzschig HK, Eckle T. Ischemia and Reperfusion–From Mechanism to Translation. *Nat Med* (2011) 17:1391–401. doi: 10.1038/nm.2507
22. Datzmann T, Hoffmann A, McCook O, Merz T, Wachter U, Preuss J, et al. Effects of Sodium Thiosulfate (Na2S2O3) During Resuscitation From Hemorrhagic Shock in Swine With Preexisting Atherosclerosis. *Pharmacol Res* (2020) 151:104536. doi: 10.1016/j.phrs.2019.104536
23. Gröger M, Hogg M, Abdelsalam E, Kress S, Hoffmann A, Stahl B, et al. Effects of Sodium Thiosulfate During Resuscitation From Trauma-And-Hemorrhage in Cystathionine Gamma Lyase (CSE) Knockout Mice. *Shock* (2022) 57:131–9. doi: 10.1097/SHK.0000000000001828
24. Knöller E, Stenzel T, Broeskamp F, Hornung R, Scheuerle A, McCook O, et al. Effects of Hyperoxia and Mild Therapeutic Hypothermia During Resuscitation From Porcine Hemorrhagic Shock. *Crit Care Med* (2016) 44: e264–277. doi: 10.1097/CCM.0000000000001412
25. Nussbaum BL, Stenzel T, Merz T, Scheuerle A, McCook O, Wachter U, et al. Hyperoxia or Therapeutic Hypothermia During Resuscitation From Non-Lethal Hemorrhagic Shock in Swine. *Shock* (2017) 48:564–70. doi: 10.1097/SHK.0000000000000884
26. Hartmann C, Loconte M, Antonucci E, Holzhauser M, Hölle T, Katzsch D, et al. Effects of Hyperoxia During Resuscitation From Hemorrhagic Shock in Swine With Preexisting Coronary Artery Disease. *Crit Care Med* (2017) 45: e1270–9. doi: 10.1097/CCM.0000000000002767
27. Datzmann T, Wepler M, Wachter U, Vogt JA, McCook O, Merz T, et al. Cardiac Effects of Hyperoxia During Resuscitation From Hemorrhagic Shock in Swine. *Shock* (2019) 52:e52–9. doi: 10.1097/SHK.0000000000001283
28. Wagner K, Gröger M, McCook O, Scheuerle A, Asfar P, Stahl B, et al. Blunt Chest Trauma in Mice After Cigarette Smoke-Exposure: Effects of Mechanical Ventilation With 100% O2. *PloS One* (2015) 10:e0132810. doi: 10.1371/journal.pone.0132810
29. Vogt JA, Wachter U, Wagner K, Calzia E, Gröger M, Weber S, et al. Effects of Glycemic Control on Glucose Utilization and Mitochondrial Respiration During Resuscitated Murine Septic Shock. *Intensive Care Med Exp* (2014) 2:19. doi: 10.1186/2197-425X-2-19
30. Merz T, Stenzel T, Nußbaum B, Wepler M, Szabo C, Wang R, et al. Cardiovascular Disease and Resuscitated Septic Shock Lead to the Downregulation of the H2S-Producing Enzyme Cystathionine-γ-Lyase in the Porcine Coronary Artery. *Intensive Care Med Exp* (2017) 5:17. doi: 10.1186/s40635-017-0131-8
31. Szabo C, Papapetropoulos A. International Union of Basic and Clinical Pharmacology. CII: Pharmacological Modulation of H2S Levels: H2S Donors and H2S Biosynthesis Inhibitors. *Pharmacol Rev* (2017) 69:497–564. doi: 10.1124/pr.117.014050
32. Messerer DAC, Datzmann T, Baranowsky A, Peschel L, Hoffmann A, Gröger M, Amling M, Wepler M, Nussbaum BL, Jiang S, et al. Systemic Calcitonin Gene-Related Peptide Receptor Antagonism Decreases Survival in a Large Animal Model of Polymicrobial Sepsis: Blinded Randomised Controlled Laboratory Trial. *Br J Anaesth* (2022) 128:864–73. S0007-0912(21)00860–6. doi: 10.1016/j.bja.2021.11.042
33. Datzmann T, Kapapa T, Scheuerle A, McCook O, Merz T, Unmuth S, Hoffmann A, Mathieu R, Mayer S, Mauer UM, et al. In-Depth Characterization of a Long-Term, Resuscitated Model of Acute Subdural Hematoma–Induced Brain Injury. *J Neurosurg* (2021), 134:223–34. doi: 10.3171/2019.9.JNS191789
34. Read MS, Potter JY, Brinkhous KM. Venom Coagglutinin for Detection of Von Willebrand Factor Activity in Animal Plasmas. *J Lab Clin Med* (1983) 101:74–82.
35. Nußbaum BL, Vogt J, Wachter U, McCook O, Wepler M, Matallo J, et al. Metabolic, Cardiac, and Renal Effects of the Slow Hydrogen Sulfide-Releasing Molecule GYY4137 During Resuscitated Septic Shock in Swine With Pre-Existing Coronary Artery Disease. *Shock* (2017) 48:175–84. doi: 10.1097/SHK.0000000000000834
36. Hauser B, Barth E, Bassi G, Simon F, Gröger M, Oter S, et al. Hemodynamic, Metabolic, and Organ Function Effects of Pure Oxygen Ventilation During Established Fecal Peritonitis-Induced Septic Shock. *Crit Care Med* (2009) 37:2465–9. doi: 10.1097/CCM.0b013e3181aee8ad
37. Wepler M, Hafner S, Scheuerle A, Reize M, Gröger M, Wagner F, et al. Effects of the PPAR-β/δ Agonist GW0742 During Resuscitated Porcine Septic Shock. *Intensive Care Med Exp* (2013) 1. doi: 10.1186/2197-425X-1-9
38. Florkowski CM, Wittert GA, Lewis JG, Donald RA, Espiner EA. Glucocorticoid Responsive ACTH Secreting Bronchial Carcinoid Tumours Contain High Concentrations of Glucocorticoid Receptors. *Clin Endocrinol* (1994) 40:269–74. doi: 10.1111/j.1365-2265.1994.tb02479.x
39. Miljic P, Miljic D, Cain JW, Korbonits M, Popovic V. Pathogenesis of Vascular Complications in Cushing's Syndrome. *Hormones (Athens)* (2012) 11:21–30. doi: 10.1007/BF03401535
40. Majoor CJ, Sneeboer MMS, de Kievit A, Meijers JCM, van der Poll T, Lutter R, et al. The Influence of Corticosteroids on Hemostasis in Healthy Subjects. *J Thromb Haemost* (2016) 14:716–23. doi: 10.1111/jth.13265
41. van Zaane B, Nur E, Squizzato A, Gerdes VEA, Büller HR, Dekkers OM, et al. Systematic Review on the Effect of Glucocorticoid Use on Procoagulant, Anti-Coagulant and Fibrinolytic Factors. *J Thromb Haemost* (2010) 8:2483–93. doi: 10.1111/j.1538-7836.2010.04034.x
42. Mao M, Lee S, Kashani K, Albright R, Qian Q. Severe Anion Gap Acidosis Associated With Intravenous Sodium Thiosulfate Administration. *J Med Toxicol* (2013) 9:274–7. doi: 10.1007/s13181-013-0305-z
43. Selk N, Rodby RA. Unexpectedly Severe Metabolic Acidosis Associated With Sodium Thiosulfate Therapy in a Patient With Calcific Uremic Arteriolopathy. *Semin Dial* (2011) 24:85–8. doi: 10.1111/j.1525-139X.2011.00848.x

44. Sinclair SE, Kregenow DA, Lamm WJE, Starr IR, Chi EY, Hlastala MP. Hypercapnic Acidosis is Protective in an *In Vivo* Model of Ventilator-Induced Lung Injury. *Am J Respir Crit Care Med* (2002) 166:403–8. doi: 10.1164/rccm.200112-117OC

Conflict of Interest: The authors declare that the research was conducted in the absence of any commercial or financial relationships that could be construed as a potential conflict of interest.

Publisher's Note: All claims expressed in this article are solely those of the authors and do not necessarily represent those of their affiliated organizations, or those of the publisher, the editors and the reviewers. Any product that may be evaluated in this article, or claim that may be made by its manufacturer, is not guaranteed or endorsed by the publisher.

frontiers | Frontiers in Immunology

ORIGINAL RESEARCH
published: 21 June 2022
doi: 10.3389/fimmu.2022.894270

Effects of Occult Hypoperfusion on Local Circulation and Inflammation - An Analysis in a Standardized Polytrauma Model

Sascha Halvachizadeh[1,2], Yannik Kalbas[1,2], Michel Paul Johan Teuben[1], Henrik Teuber[1], Nikola Cesarovic[3], Miriam Weisskopf[4], Paolo Cinelli[1,2], Hans-Christoph Pape[1,2] and Roman Pfeifer[1,2]*

[1] Department of Trauma, University Hospital Zurich, Zurich, Switzerland, [2] Harald Tscherne Research Laboratory, University of Zurich, Zurich, Switzerland, [3] Department of Health Sciences and Technology, Eidgenössische Technische Hochschule (ETH) Zurich, Zurich, Switzerland, [4] Center for Surgical Research, University Hospital Zurich, University Zurich, Zurich, Switzerland

OPEN ACCESS

Edited by:
Tom E. Mollnes, University of Oslo, Norway

Reviewed by:
Matthias Fröhlich, Universitiy Witten/Herdecke, Germany
Erik Waage Nielsen, Nord University, Norway

***Correspondence:**
Sascha Halvachizadeh
Sascha.Halvachizadeh@usz.ch

Specialty section:
This article was submitted to Inflammation, a section of the journal Frontiers in Immunology

Received: *11 March 2022*
Accepted: *25 April 2022*
Published: *21 June 2022*

Citation:
Halvachizadeh S, Kalbas Y, Teuben MPJ, Teuber H, Cesarovic N, Weisskopf M, Cinelli P, Pape H-C and Pfeifer R (2022) Effects of Occult Hypoperfusion on Local Circulation and Inflammation - An Analysis in a Standardized Polytrauma Model. Front. Immunol. 13:894270. doi: 10.3389/fimmu.2022.894270

Introduction: Occult hypoperfusion (OH) is defined as persistent lactic acidosis despite normalization of vital parameters following trauma. The aim of this study was to analyze the association of occult hypoperfusion with local circulation and inflammation of injured soft tissue in a porcine polytrauma model.

Methods: This experimental study was performed with male landrace pigs who suffered a standardized polytrauma, including a femoral fracture, blunt chest trauma, liver laceration and a mean arterial pressure (MAP) controlled hemorrhagic shock. One hour after induction of trauma, the animals were resuscitated with retrograde femoral nailing, liver packing and volume replacement. Animals were stratified into Group Norm (normalizing lactate levels after resuscitation) and Group occult hypoperfusion (OH) (persistent lactate levels above 2 mmol/l with normalizing vital parameters after resuscitation). Local circulation (oxygen saturation, hemoglobin amount, blood flow) was measured with optical sensors at the subcutaneous soft tissue at the fractured extremity as well as at the stomach and colon. Local inflammatory parameters [interleukin (IL) 6, 8, 10, and heat shock protein (HSP)] were analyzed in the subcutaneous tissue of the fractured extremity.

Results: Group Norm (n = 19) and Group OH (n = 5) were comparable in baseline vital and laboratory parameters. The shock severity and total amount of blood loss were comparable among Group Norm and Group OH. Following resuscitation Group OH had significantly lower local relative hemoglobin amount at the injured soft tissue of the fractured extremity when compared with Group Norm (39.4, SD 5.3 vs. 63.9, SD 27.6 A.U., p = 0.031). The local oxygenation was significantly lower in Group OH compared to Group Norm (60.4, SD 4.6 vs. 75.8, SD 12.8, p = 0.049). Local IL-6 in the fatty tissue was

significantly higher in Group OH (318.3, SD 326.6 [pg/ml]) when compared with Group Norm (73.9,SD 96.3[pg/ml], p = 0.03). The local circulation at the abdominal organs was comparable in both groups.

Conclusion: OH is associated with decreased local circulation and increased local inflammation at the injured soft tissue of the extremity in polytrauma. OH might reflect the severity of local soft tissue injuries, and guide treatment strategies.

Keywords: local inflammation, porcine model, standardized polytrauma, occult hypoperfusion, persistent lactic acidosis, treat, perfusion in polytrauma

INTRODUCTION

The initial assessment and surgical strategy in the treatment of polytrauma patients is based on the physiologic reaction to injuries (1). The early polytrauma management focuses on the stabilization of the triad of acidosis, coagulopathy, and hypothermia. This triad, combined with the soft tissue damage are prominent predictors for mortality in polytrauma patients (1). The physiologic stabilization of the patient represents one guide of the surgical strategy after polytrauma (2). Despite standardized and improved resuscitation, selected polytrauma cases present with persistent lactic acidosis even after responding to resuscitation. The presence of elevated lactate levels during the clinical course has been interpreted as a sign of occult hypoperfusion (OH). OH in trauma is associated with increased risk for infections and other complications (3). The outcome of trauma patients improves if OH is detected and treated early (4). Several different definitions of OH exist, most of which describe a persistent elevated lactate level with concomitant normal vital parameters (3, 5). Risk factors for the development of OH include Injury Severity Score (ISS), Glasgow Coma Scale (GCS) at admission, hypotension, and advanced age (4). OH has only been approximated by systemic measures or analysis of CO2-gaps between central veins and arteries (6). In order to evaluate the association of persistent lactic acidosis and occult hypoperfusion this study aimed to investigate the following research questions in a standardized porcine polytrauma model: What is the effect of OH on the local circulation of the injured soft tissue in polytrauma? Is OH associated with the amount of blood loss during hemorrhagic shock? How is the local inflammatory reaction of the soft tissue affected by OH?

METHODS

Study Design

This experimental translational study is based on a previously described standardized porcine polytrauma model (7). Reporting of the results adheres to the ARRIVE Guideline (8).

Ethical Statement and Housing

Animal housing and experimental protocols were approved by the Cantonal Veterinary Office, Zurich, Switzerland, under license no. ZH 138/2017, and were executed in accordance with Swiss Animal Protection Law, following the "The Principles of Laboratory Animal Care". Housing and experimental procedures also conformed to the European Directive 2010/63/EU of the European Parliament and of the Council on the Protection of vertebrate animals used for scientific purposes (Council of Europe no. 123, Strasbourg 1985) and to the Guide for the Care and Use of Laboratory Animals (Institute of Laboratory Animal Resources, National Research Council, National Academy of Sciences, 2011). Castrated male Swiss landrace pigs from a disease-free barrier breeding facility were housed in ventilated rooms at a constant room temperature of 21 ± 3°C and a relative humidity of 50%, with natural daylight. Pigs acclimatize to their surroundings for a minimum of 7 days prior to the experiment. takers. Pigs were fasted for a period of 12 h prior to the experiment, water was available ad libitum.

Animal Care and Monitoring

All pigs were sedated with an intramuscular injection of ketamine (Ketasol®-100 ad us.vet.; Dr. E. Graeub AG, Berne, Switzerland; 15 mg/kg body weight), midazolam (Dormicum®.; Roche Pharma AG, Basel, Switzerland; 0.5 mg/kg body weight) and atropine (Atropinsulfat KA vet 0.1%; Kantonsapotheke, Switzerland; 0.05 mg/kg body weight). Anesthesia was induced by an intravenous administration of propofol (Propofol ®-Lipuro 1%, B. Braun Medical AG; Sempach, Switzerland; 1-2 mg/kg body weight) to achieve relaxation and swallow-reflex diminishment sufficient for intubation. Anesthesia was maintained during the duration of the study with propofol (5-10 mg/kg/h).and Sufentanil (1 µg/kg per hour) under positive pressure ventilation with an FiO2 of 0.3. Following our institutional veterinarian protocol, ventilation was set to maintain an end tidal CO2 (etCO2) of 45-55 mmHg All animals received fluid substitution of 21 ml/h Ringerfundin. Animals were placed in supine position for percutaneous ultrasound guided catheterization of the following vessels: left external jugular vein (6F, Avanti®, Cordis® Corporation, Miami Lakes, FL, USA), right femoral artery (5F, Avanti®, Cordis® Corporation, Miami Lakes, FL, USA) and left femoral vein (HighFlow Dolphin Catheter, 13F, Baxter International, Deerfield IL, USA). Oxygenation and ventilation parameters, inspirational oxygen fraction, and expiratory oxygen fraction, etCO2, positive end-expiratory pressure (PEEP), respiratory

frequency, and tidal volume were continuously monitored. Blood gas analysis was performed to regularly assess pressure of oxygen (paO2) and carbon dioxide (paCO2), Arterial blood pressure and central venous pressure (CVP), as well as heart rate was continuously recorded. A suprapubic catheter was placed in the urinary bladder and diuresis was monitored. During the entire experiment, at least two veterinarians, specialized in anesthesiology were present and monitored the narcosis.

Induction of Trauma and Resuscitation

Trauma was induced and resuscitation procedures performed, based on a well-established, previously described standardized large animal protocol (7). Briefly, the polytrauma model included a standardized left-sided femoral shaft fracture, a right sided blunt thoracic trauma, a standardized liver laceration, and mean arterial pressure (MAP)-controlled hemorrhagic shock as follows:

Fractures and associated soft tissue injuries were induced by a bolt gun (Blitz-Kerner, turbocut JOBB GmbH, Germany) with cartridges (9x17; DynamitNobel AG; Troisdorf, Germany) to a custom made metal chisel which was placed on the mid of the left femur shaft. The fracture was verified *via* fluoroscopy. The blunt chest trauma was introduced with the same bolt gun on the right lateral thorax wall utilizing an additional lead pael (1.0cm thickness) between the chest and the bolt gun. A chest x-ray was performed and in case of pneumothorax a chest tube was inserted in the usual manner. The liver laceration was performed with a cross-like incision through one third of the liver tissue following median laparotomy. Liver packing was performed following 30 seconds of uncontrolled bleeding. Afterwards the animals underwent MAP-controlled hemorrhagic shock for 60 min until they reached a MAP of 25 ± 5 mmHg. During trauma and hemorrhagic shock, FiO2 was reduced to 0.21 and fluid substitution was lowered to 10ml/h.

One hour after induction of trauma animals were resuscitated following the ATLS, AO/OTA, and AWMF-S3 guideline on Treatment of Patients with Severe and Multiple Injuries®) principles (9, 10). Hemorrhagic shock was treated with volume controlled fluid resuscitation (three times the blood loss, Ringerfundin®). Normothermia (38.7–39.8°C) was aimed for with warm pads and blankets. Femoral shaft fractures were treated with retrograde intramedullary nailing utilizing a tailored 120 mm nail (cannulated DFN Ø 10.0 mm, DePuySynthes, Raynham, Massachusetts, United States) in the usual manner. The position of the nail was controlled *via* fluoroscopy.

Measurements of Local Circulation

Local tissue perfusion and microcirculation at the fracture site was assessed using an O2C (Oxygen to see, LEA Medizintechnik GMBH, Giessen, Germany) device. White light spectrometry and laser spectroscopy were used to screen the capillary-venous part of the vascular system (penetration depth of 4–8 mm). Relative local blood flow (flow), flow velocity, local oxygen saturation (sO2) and relative local hemoglobin concentration (rHB) were measured one the vastus lateralis muscle adjacent to the femoral fracture. For this, a 3 cm incision was made on the left lateral thigh and the subcutaneous tissue was exposed by preparation of subcutaneous tissue and incision of the fascia. The measuring probe was placed on the subcutaneous tissue for 1 min above the fracture and measurements were continuously taken every second. Local circulation measurements were further taken at the stomach, and the colon. Data are presented in arbitrary units (A.U.). The reason for the introduction of "Arbitrary Units" is based on the origin of the values. The measured signals are electrical values of frequencies and amplitudes, so that the unit would be a combination of electrical units. Therefore usually a new unit for blood flow is introduced. To calculate the blood flow in ml/min, it would be necessary to compare the electrical signals with a method that measures the blood flow in ml/min (e.g. plethysmography, microspheres) for each organ (or organs with similar optical properties). Then the arbitrary units can be converted in ml/min. This "calibration" has to be done at the measured organ, as there is no artificial model at the moment that simulates tissue in a realistic way.

Local Inflammation

Local inflammation was measured 6 hours after induction of trauma. Quantikine porcine immunoassay kits from R&D Systems (Minneapolis, MN) were used for analyses of IL-6, IL-8, and IL-10 according to the manufacturer's protocol. Prior termination of the experiment local soft tissue including fatty tissue and muscle tissue were taken at the fracture site and stored in RNAlater solution (RNAlater Solutions for RNA Stabilization and Storage, ThermoFisher). After shredding of the tissue, RNA extraction was performed using the RNeasy Mini Kit (Qiagen, Hombrechtikon, Switzerland) according to the manufacturer's protocol. PCR analysis for HSP70, IL-6, IL-8, and IL-10 was performed using the following primer (F forward, R reverse): IL-6 F: 5-GAATCCAGACAAAGCCACCA-3, R: 5-GTGCCCCA GCTACATTATCC-3; IL-8/CXCL8, F: 5-CTTCCAAACTGGC TGTTGCC-3, R: 5-GTTGTTGTTGCTTCTCAGTTCTCT-3; IL-10, F: 5-CGGCGCTGTCATCAATTTCT-3, R: 5-CGGGA ACCTTGGAGCAGATT-3; HSP70, F: 5-GCCCTGAATCC GCAGAATA-3, R: 5-TCCCC ACGGTAGGAAACG-3.

Statistical Methods and Stratification of Animals

Continuous variables are presented with mean and standard deviation (SD), or standard error of the mean (SEM) in graphical presentation, categorical variables as count and percentage. Experimental subjects were stratified according to persistent lactic acidosis as defined by persistent elevated serum lactate level of >2mmol/l (Group OH) despite responding vital signs to resuscitation during the entire observation time. Distribution of data was visualized with histogram and qq-plots. Group comparison on normally distributed continuous variables were performed using the student's t-test, for non-normal distributed variables the Mann-Whitney U test was utilized; for comparisons on categorical variables the Fisher exact test was used. Adjustment for multiple testing with a false discovery rate at 1% was performed with the Benjamini-Hochberg procedure. The p-value reported is the adjusted value. All statistical analyses were performed using R (R Core Team (2021). R: A language and

environment for statistical computing. R Foundation for Statistical Computing, Vienna, Austria. URL https://www.R-project.org/.). GraphPad Prism version 9 for macOS was utilized to print the graphs (GraphPad Software, San Diego, California USA, www.graphpad.com).

RESULTS

This experiment included 27 animals. Out of these 24 (88.9%) survived the experiment and were stratified into Group Norm (n=19, 79.2%) and Group OH (n= 5, 20.8%, **Figure 1**). 3 animals died prematurely and were excluded from analyses.

Baseline Values

The animals had a mean weight of 50.7kg (SD 4.5kg) representing adolescent animals. At baseline the animals had a MAP of 73.3mmHg (SD 14.7mmHg), a heart rate of 91.5bpm (SD 17.0bpm), and a CVP of 10.1mmHg (SD 3.7mmHg). Baseline lactate level was 1.1mmol/l (SD 0.6mmol/l), base excess 6.3mmol/l (SD 2.4mmol/l), and the temperature 37.0°C (SD 0.7°C). The baseline hemoglobin was 9.7g/dl (SD 0.9g/dl), and the calcium 1.34mg/dl (SD 0.06mg/dl). The animals were comparable in baseline values and characteristics (**Table 1**).

Severity of Trauma: Course of MAP and Lactate During Trauma and After Resuscitation

During the hemorrhagic shock, the animals lost a mean of 991.8ml (SD 303.8ml) of blood, and had a MAP of 25mmHg (SD 5mmHg) and a mean heart rate of 94.0bpm (SD 18.9bpm). The lactate level increased to 5.9mmol/l (SD 1.4mmol/l), the temperature was 37.4°C (SD 0.6°C).

Lactate level increased to 6.03mmol/l (SD 0.75mmol/l) in Group OH and remained at a mean of 3.44 mmol/l (SD 1.97mmol/l). The lactate level decreased in Group Norm following resuscitation to baseline values. The temperature remained comparable in both groups throughout the experiment as did the pCO2 levels (**Figure 2**).

Occult Hypoperfusion Is Associated With Reduced Local Circulation in the Soft Tissue of the Extremity

Local soft tissue circulation measurements on the hind extremities have shown a significantly reduced microcirculation in Group OH when compared with Group Norm, with local SpO2 in the vastus muscle being significantly lower (Group OH: 60.4, SD 4.6 A.U. versus Group Norm 75.8 SD 12.8 A.U., p=0.049). Local Hb values were also significantly reduced in the OH group (Group OH: 39.4, SD 5.3 A.U. versus Group Norm 63.9, SD 27.6 A.U., p=0.031). No differences were found between the groups in the microcirculation of the abdominal organs, such as the stomach, colon or liver (**Table 2**).

Occult Hypoperfusion Is Associated With an Increased Local Inflammatory Response

The analysis of local soft tissue inflammation revealed a significantly higher concentration of pro-inflammatory cytokines in animals in Group OH when compared with Group Norm. Interleukin-6 was approximately 3 times higher in the OH group when compared to the Norm group (Group OH: 318.3, SD 326.6 pg/ml versus Group Norm 73.9. SD 96.3 pg/ml, p=0.03). Similarly, IL-8 has shown 4 times higher values (Group OH: 442.9, SD 687.6 pg/ml versus Group Norm 72.3,

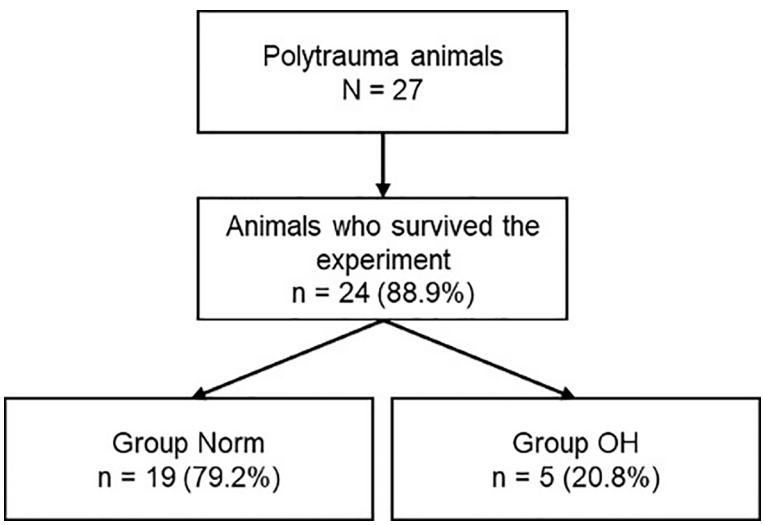

FIGURE 1 | Flowchart and stratification according to occult hypoperfusion (OH) as defined by persistent elevated lactate levels despite responding vital parameters following resuscitation.

TABLE 1 | Baseline characteristics of study animals.

	Group Norm 19	Group OH 5	p-value
MAP [mmHg], mean (SD)	72.91 (15.79)	75.20 (9.50)	0.76
Heart rate [bpm], mean (SD)	93.73 (22.02)	88.80 (14.57)	0.64
CVP [mmHg], mean (SD)	10.11 (4.20)	12.40 (4.98)	0.306
Temperature [°C], mean (SD)	36.82 (0.75)	36.62 (0.70)	0.588
pO2 [kPa], mean (SD)	16.95 (4.05)	13.69 (4.09)	0.117
pCO2 [kPa], mean (SD)	5.86 (0.76)	5.51 (0.72)	0.356
pH, mean (SD)	7.45 (0.05)	7.48 (0.04)	0.192
Lactate [mmol/l], mean (SD)	1.14 (0.60)	0.79 (0.17)	0.217
Local blood flow at extremity [AU], mean (SD)	82.51 (22.35)	81.36 (39.37)	0.936
Local sO2 at extremity [AU], mean (SD)	94.45 (7.46)	93.00 (9.43)	0.737
Local rHb amount at extremity [AU], mean (SD)	68.54 (8.56)	74.60 (13.37)	0.255

MAP, Mean arterial pressure; bpm, beats per minute; CVP, central venous pressure; AU, Arbitrary unit; rHb, relative hemoglobin amount; SD, Standard deviation; p-value after Benjamini-Hochberg adjustment.

SD121.3 pg/ml, p=0.056). Interleukin-10 and HSP were comparable between the groups (**Table 3**).

DISCUSSION

The aim of this study was to analyze the association of OH on the local microcirculation and the local inflammatory of the injured soft tissue reaction following a standardized porcine polytrauma model and found the following points:

- Persistent elevated lactate levels can be present despite standardized trauma and resuscitation protocols.
- Animals in Group OH show reduced local circulation at the injured extremity when compared with Group Norm.
- The local inflammatory reaction of the soft tissue in the injured extremity is significantly higher Group OH when compared with Group Norm.

The identification of multiple injured patients with insufficient response to resuscitation is required to choose an appropriate treatment strategy. Studies have reported a negative outcomes in patients with persistent occult hypoperfusion (OH) (11). There still is, however, a lack of consensus on the definition of OH: Some studies defined OH based on the pH level (pH < 7.25) (12) others described significant hemorrhage despite hemodynamic stability to be associated with occult hypoperfusion (13). A base deficit of less than -4.5mmol/l was further a proposed threshold for OH (14). However, most articles define occult hypoperfusion based on persistent elevated lactate levels, despite normal vital signs (15–17). The range of the cut-off for persistent lactic acidosis varies from 2mmol/l (18), to 2.4 mmol/l (19), 2.5 mmol/l (16), and 3mmol/l (20). The present study has chosen the cut-off of 2mmol/l since this value is clinically one relevant factor in distinguishing between stable and unstable trauma patients (1, 2). This is the first study that provides some evidence for the development of OH despite standardized trauma and standardized treatment protocols. The pathophysiologic cause for OH remains subject of investigations and is hypothesized to be the result of multifactorial pathways. If the oxygen supply decreases other mechanisms attempt to restore oxygenation (21). Hypoxia can induced inflammation and vice versa (22). This association is based on experimental designs that assessed toll-like receptors (TLRs) in kidney or lung transplantation, and the resulting insulin resistance following macrophage migration in adipose tissue (22). The present study provides new data that shows the association of OH with increased inflammation in acute injured soft tissue in a polytrauma model. Ischemia and reperfusion injuries result in sterile inflammation following activation of TLRs, recruitment and activation of immune cells of the innate and adaptive immune system and activation of the complement system (23). This clinically very relevant association has been discussed following biomolecular and histopathologic studies. The present investigation provides a translational approach that introduces standardized quantification methods for OH and local hypoperfusion that might be feasible for routine clinical use. Changes in local circulation depend further on the specific organ of interest (24). The relevance of ischemia-reperfusion injury is further associated with local circulation and represents a challenging condition in trauma patients (25). It has further been shown that the local soft tissue injury serves as a relevant factor for the prediction of mortality in severely injured patients (1, 2). OH and altered microcirculation might be utilized to quantify the severity of the local soft tissue damage. OH might further be associated with persistent centralization. The present study showed that the abdominal organs are not as severely affected by circulatory changes during OH when compared with the extremity. The centralization appears to persist during OH and is an increased risk for complications and mortality (26).

Shock and resuscitation have a substantial impact on the local circulation and the local inflammation (27). Systemic inflammatory response is associated with the severity of trauma and skeletal muscle oxygenation and represents a relevant factor for resuscitation strategies and success (28). The release of damage-associated molecular patterns (DAMPs) following trauma are associated with increased inflammation. Systemic inflammation is increased in polytrauma and the damaged local soft tissue might be responsible for the inflammatory reaction (29). The elevated local inflammation impairs the coagulatory system, increases vascular leakage by

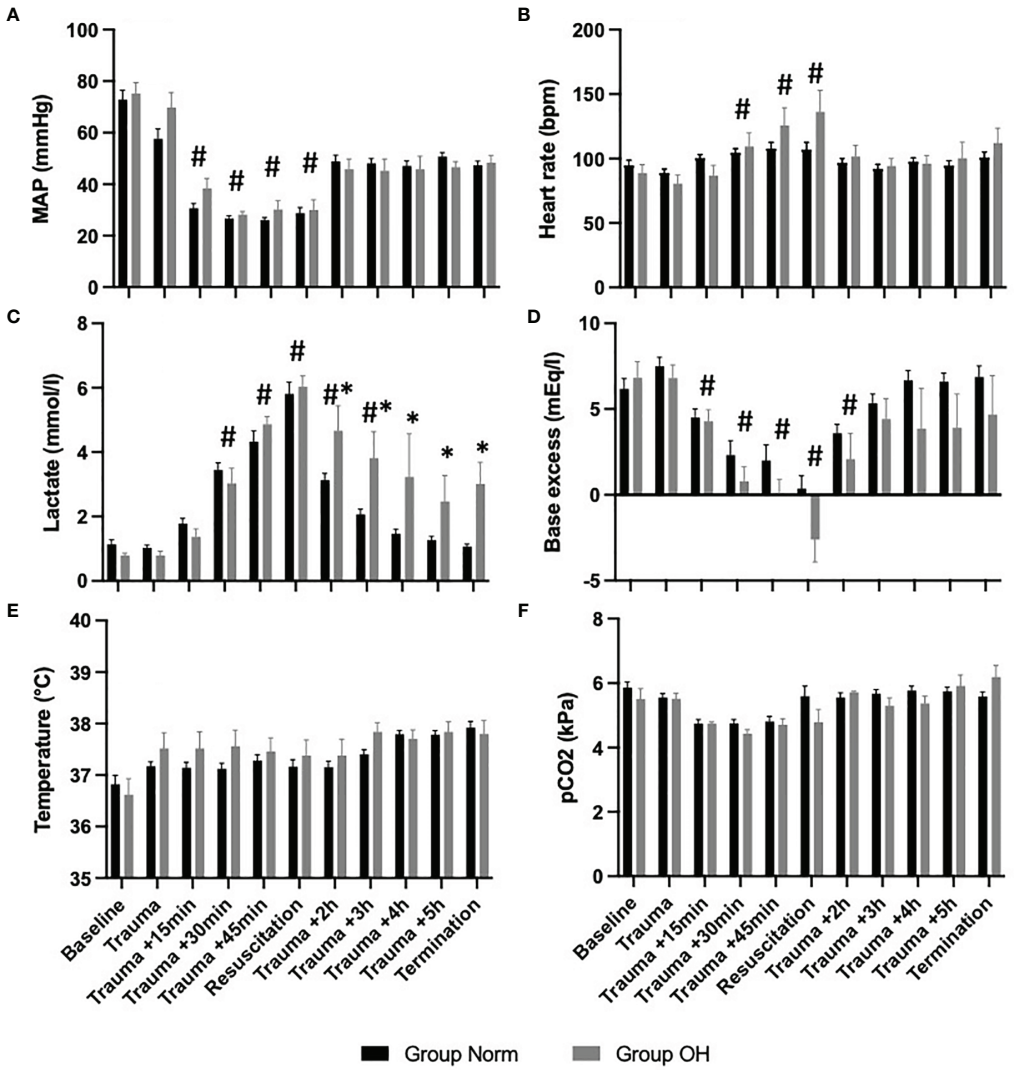

FIGURE 2 | The course of vital parameters, and measures of arterial blood gas analysis during the observational period, presented as mean and standard error of the mean #represents statistical significant difference to baseline, * represents statistical difference among Group Norm and Group OH at the respected timepoint Statistical significance after Benjamini-Hochberg adjustment set at $p < 005$. **(A)** The course of MAP controlled hemorrhagic shock The MAP decreased significantly compared with baseline values, however, the MAP remained comparable among both groups. **(B)** Significant increase of heart rate (compared with baseline) during hemorrhagic shock and return to comparable values. **(C)** The lactate value increased significantly in both Groups when compared to baseline values After the initiation of resuscitation, the lactate value decreased in Group Norm. in Group OH the lactate value remained significantly higher compared to baseline and to Group Norm. **(D)** Base excess decreased significantly in both groups, and remained lower in Group OH (not statistically significant). **(E)** The Temperature was comparable during the experiment, and the animals were warmed throughout. **(F)** The pCO2 level was utilized for ventilation control and remained comparable during the experiment and among both groups.

damaging endothelium and might therefore subsequently damage remote organs (30).

The presented results are in accordance with previously published data that have shown an adequate response to resuscitation within 30 minutes (31). The local circulatory flow rate correlates with the MAP, and following hemorrhagic shock rHB and local O2 measures decreased significantly (27). These data are comparable to the present experiment that shows an effect of the trauma and the hemorrhage to the local circulation. But the present experiment goes one step further, by providing data on an even further effect of OH on the local circulation and inflammation. The systemic response to severe trauma has been shown (31), the effect of polytrauma on local circulation can be quantified (27), and following our results, the severity of decreased local circulation or increased local inflammation of injured soft tissue is further associated with OH.

Experimental studies allow detection of these markers, however, the transfer to human situation remains challenging (32). The present study allows the association of OH, decreased

TABLE 2 | Occult hypoperfusion is associated with reduced local circulation in injured soft tissue 6 hours after trauma.

	Group Norm	Group OH	p-value
Local blood flow at extremity [AU], mean (SD)	75.75 (12.79)	60.38 (4.56)	0.049
Local rHb amount at extremity [AU], mean (SD)	63.92 (27.63)	39.39 (5.33)	0.031
Local sO2 at extremity [AU], mean (SD)	72.02 (6.13)	72.09 (7.84)	0.987
Local blood flow at stomach [AU], mean (SD)	176.23 (14.9)	153.58 (51.3)	0.159
Local rHb amount at stomach [AU], mean (SD)	52.28 (24.08)	58.80 (21.34)	0.674
Local sO2 at stomach [AU], mean (SD)	72.02 (6.13))	72.09 (7.84)	0.987
Local blood flow at colon [AU], mean (SD)	174.66 (34.08)	166.03 (30.51)	0.689
Local rHb amount at colon [AU], mean (SD)	67.02 (4.98)	64.42 (3.89)	0.887
Local sO2 at colon [AU], mean (SD)	53.36 (17.41)	53.60 (18.20)	0.983

AU, Arbitrary units; SD, standard deviation; OH, occult hypoperfusion; p-value after Benjamini-Hochberg adjustment.

TABLE 3 | Occult hypoperfusion is associated with increased local inflammatory response of the injured soft tissue at the fracture.

	Group Norm	Group OH	p-value
HSP fatty tissue [pg/ml], mean (SD)	4.93 (12.68)	5.88 (9.79)	0.892
IL8 fatty tissue[pg/ml], mean (SD)	72.33 (121.31)	442.94 (687.55)	0.056
IL6 fatty tissue [pg/ml], mean (SD)	73.97 (96.29)	318.30 (326.56)	0.03
IL10 fatty tissue [pg/ml], mean (SD)	4.81 (4.29)	3.23 (2.78)	0.558
IL6 muscle [pg/ml], mean (SD)	69215.23 (86342.31)	76003.88 (131083.13)	0.908
IL10 muscle [pg/ml], mean (SD)	1907.29 (3432.24)	286.99 (369.85)	0.435

HSP, Heat shock protein; IL, interleukin; SD, standard deviation; OH, occult hypoperfusion; p-value after Benjamini-Hochberg adjustment.

local circulation, and increased local inflammation and might therefore support the translation of these results to the human situation. The quantification of the local tissue injury is relevant for the risk for complications and for the treatment strategy (33). The local inflammatory response is time-dependent and therefore provides an association of OH and increased local inflammation (34).

Strengths and Limitations

This study is conducted as an experimental study. The strengths of this study are the standardized induction of trauma, and the standardized resuscitation methods. The included study subjects were comparable in baseline characteristics and the observation time were standardized. These conditions are rarely found in clinical trials. OH might be the result of the local microcirculation. Following the present study, we provide data that show a certain association of OH and local microcirculation. Further, this association was measured in a standardized and reproducible manner. However, the reported data cannot prove a cause-relation effect that provides evidence whether the decreased local circulation causes OH or vice versa. Based on the standardized trauma and standardized resuscitation the effect should be investigated on an epigenetic level, since it might be based on an individual reaction to the injury. One might argue that the translation of our results to routine clinical practice might be lacking, however, large animals mirror human physiology better when compared with rodents (35). For those reasons, a certain translation of our results might be feasible. This experiment was designed to analyze the short term effect of trauma on inflammation and circulation. Therefore, long term complications, infections, or mortality were not observed. Albeit this shortcoming, we believe that the presented results might improve the pathophysiologic understanding of OH and its association with decreased local circulation at the extremity and increased local inflammation.

CONCLUSION

OH is associated with decreased local perfusion and increased local inflammation at the injured soft tissue and might serve as a measure for severity of local soft tissue injuries, guide treatment strategies, and measure treatment success.

DATA AVAILABILITY STATEMENT

The raw data supporting the conclusions of this article will be made available by the authors, without undue reservation.

ETHICS STATEMENT

Animal housing and experimental protocols were reviewed and approved by the Cantonal Veterinary Office, Zurich, Switzerland, under license no. ZH 138/2017, and were executed in accordance with Swiss Animal Protection Law, following the "The Principles of Laboratory Animal Care". Housing and experimental procedures also conformed to the European Directive 2010/63/EU of the European Parliament and of the Council on the Protection of vertebrate animals used for scientific purposes (Council of Europe no. 123, Strasbourg 1985) and to the Guide for the Care and Use of Laboratory Animals (Institute of Laboratory Animal Resources, National Research Council, National Academy of Sciences, 2011).

AUTHOR CONTRIBUTIONS

SH and YK contributed equally to this work, conducted the research, collected the data, analysed and interpreted the data, wrote the original draft and critically reviewed the manuscript. MPJT performed the study, was involved in funding acquisition, collected data, interpreted the data and critically reviewed the manuscript. HT interpreted the data, critically reviewed the manuscript. MW and NC conducted the study, performed the anaesthesia on animals, were in charge of housing and animal welfare, collected the data, critically reviewed the manuscript. H-CP and RP supervised the study, were involved in funding acquisition, critically reviewed the manuscript. RP conducted the study, supervised data collection, interpreted the data, developed the study idea, wrote the original draft critically reviewed the manuscript.

FUNDING

This study was supported by the AO Grant S-16–133T: Effects of standard reaming and RIA techniques on local soft tissue and systemic homeostasis in a porcine trauma model.

REFERENCES

1. Pape H-C, Giannoudis PV, Krettek C, Trentz O. Timing of Fixation of Major Fractures in Blunt Polytrauma: Role of Conventional Indicators in Clinical Decision Making. *J Orthop Trauma* (2005) 19(8):551–62. doi: 10.1097/01.bot.0000161712.87129.80
2. Halvachizadeh S, Baradaran L, Cinelli P, Pfeifer R, Sprengel K, Pape H-C. How to Detect a Polytrauma Patient at Risk of Complications: A Validation and Database Analysis of Four Published Scales. *PloS One* (2020) 15(1):e0228082. doi: 10.1371/journal.pone.0228082
3. Claridge JA, Crabtree TD, Pelletier SJ, Butler K, Sawyer RG, Young JS. Persistent Occult Hypoperfusion Is Associated With a Significant Increase in Infection Rate and Mortality in Major Trauma Patients. *J Trauma* (2000) 48(1):8–14. discussion 14–5. doi: 10.1097/00005373-200001000-00003
4. Blow O, Magliore L, Claridge JA, Butler K, Young JS. The Golden Hour and the Silver Day: Detection and Correction of Occult Hypoperfusion Within 24 Hours Improves Outcome From Major Trauma. *J Trauma* (1999) 47(5):964–9. doi: 10.1097/00005373-199911000-00028
5. Martin JT, Alkhoury F, O'Connor JA, Kyriakides TC, Bonadies JA. "Normal" Vital Signs Belie Occult Hypoperfusion in Geriatric Trauma Patients. *Am Surg* (2010) 76(1):65–9. doi: 10.1177/000313481007600113
6. Silbert BI, Litton E, Ho KM. Central Venous-to-Arterial Carbon Dioxide Gradient as a Marker of Occult Tissue Hypoperfusion After Major Surgery. *Anaesth Intensive Care* (2015) 43(5):628–34. doi: 10.1177/0310057X1504300512
7. Hildebrand F, Weuster M, Mommsen P, Mohr J, Fröhlich M, Witte I, et al. A Combined Trauma Model of Chest and Abdominal Trauma With Hemorrhagic Shock–Description of a New Porcine Model. *Shock* (2012) 38(6):664–70. doi: 10.1097/SHK.0b013e3182709c90
8. Percie du Sert N, Hurst V, Ahluwalia A, Alam S, Avey MT, Baker M, et al. The ARRIVE Guidelines 20: Updated Guidelines for Reporting Animal Research. *PloS Biol* (2020) 18(7):e3000410. doi: 10.1371/journal.pbio.3000410
9. ATLS Subcommittee. American College of Surgeons' Committee on Trauma, International ATLS Working Group Advanced Trauma Life Support (ATLS®): The Ninth Edition. *J Trauma Acute Care Surg* (2013) 74(5):1363–6. doi: 10.1097/TA.0b013e31828b82f5
10. Bouillon B, Marzi I. The Updated German "Polytrauma - Guideline": An Extensive Literature Evaluation and Treatment Recommendation for the Care of the Critically Injured Patient. *Eur J Trauma Emerg Surg* (2018) 44(Suppl 1):1. doi: 10.1007/s00068-018-0949-0
11. Meregalli A, Oliveira RP, Friedman G. Occult Hypoperfusion is Associated With Increased Mortality in Hemodynamically Stable, High-Risk, Surgical Patients. *Crit Care* (2004) 8(2):R60–5. doi: 10.1186/cc2423
12. Miami Trauma Clinical Trials Group. Splanchnic Hypoperfusion-Directed Therapies in Trauma: A Prospective, Randomized Trial. *Am Surg* (2005) 71(3):252–60.
13. Brown CVR, Velmahos GC, Neville AL, Rhee P, Salim A, Sangthong B, et al. Hemodynamically "Stable" Patients With Peritonitis After Penetrating Abdominal Trauma: Identifying Those Who Are Bleeding. *Arch Surg* (2005) 140(8):767–72. doi: 10.1001/archsurg.140.8.767
14. Arnold TDW, Miller M, van Wessem KP, Evans JA, Balogh ZJ. Base Deficit From the First Peripheral Venous Sample: A Surrogate for Arterial Base Deficit in the Trauma Bay. *J Trauma* (2011) 71(4):793–7. discussion 797. doi: 10.1097/TA.0b013e31822ad694
15. Salottolo KM, Mains CW, Offner PJ, Bourg PW, Bar-Or D. A Retrospective Analysis of Geriatric Trauma Patients: Venous Lactate Is a Better Predictor of Mortality Than Traditional Vital Signs. *Scand J Trauma Resusc Emerg Med* (2013) 21:7. doi: 10.1186/1757-7241-21-7
16. Bar-Or D, Salottolo KM, Orlando A, Mains CW, Bourg P, Offner PJ. Association Between a Geriatric Trauma Resuscitation Protocol Using Venous Lactate Measurements and Early Trauma Surgeon Involvement and Mortality Risk. *J Am Geriatr Soc* (2013) 61(8):1358–64. doi: 10.1111/jgs.12365
17. Strnad M, Lesjak VB, Vujanović V, Pelcl T, Križmarić M. Predictors of Mortality and Prehospital Monitoring Limitations in Blunt Trauma Patients. *BioMed Res Int* (2015) 2015:983409. doi: 10.1155/2015/983409
18. Caputo N, Reilly J, Kanter M, West J. A Retrospective Analysis of the Respiratory Adjusted Shock Index to Determine the Presence of Occult Shock in Trauma Patients. *J Trauma Acute Care Surg* (2018) 84(4):674–8. doi: 10.1097/TA.0000000000001761
19. Schulman AM, Claridge JA, Carr G, Diesen DL, Young JS. Predictors of Patients Who Will Develop Prolonged Occult Hypoperfusion Following Blunt Trauma. *J Trauma* (2004) 57(4):795–800. doi: 10.1097/01.TA.0000140835.65944.54
20. Radowsky JS, DuBose JJ, Scalea TM, Miller C, Floccare DJ, Sikorski RA, et al. Handheld Tissue Oximetry for the Prehospital Detection of Shock and Need for Lifesaving Interventions: Technology in Search of an Indication? *Air Med J* (2019) 38(4):276–80. doi: 10.1016/j.amj.2019.03.014
21. Semenza GL. Life With Oxygen. *Science* (2007) 318(5847):62–4. doi: 10.1126/science.1147949
22. Eltzschig HK, Carmeliet P. Hypoxia and Inflammation. *N Engl J Med* (2011) 364(7):656–65. doi: 10.1056/NEJMra0910283
23. Eltzschig HK, Eckle T. Ischemia and Reperfusion—From Mechanism to Translation. *Nat Med* (2011) 17(11):1391–401. doi: 10.1038/nm.2507
24. Halvachizadeh S, Mica L, Kalbas Y, Lipiski M, Canic M, Teuben M, et al. Zone-Dependent Acute Circulatory Changes in Abdominal Organs and Extremities After Resuscitative Balloon Occlusion of the Aorta (REBOA): An Experimental Model. *Eur J Med Res* (2021) 26(1):10. doi: 10.1186/s40001-021-00485-y
25. Sönmez TT, Al-Sawaf O, Brandacher G, Kanzler I, Tuchscheerer N, Tohidnezhad M, et al. A Novel Laser-Doppler Flowmetry Assisted Murine Model of Acute Hindlimb Ischemia-Reperfusion for Free Flap Research. *PloS One* (2013) 8(6):e66498. doi:10.1371/journal.pone.0066498
26. Horst K, Hildebrand F, Pfeifer R, Hübenthal S, Almahmoud K, Sassen M, et al. Impact of Haemorrhagic Shock Intensity on the Dynamic of Alarmins Release in Porcine Poly-Trauma Animal Model. *Eur J Trauma Emerg Surg* (2016) 42(1):67–75. doi: 10.1007/s00068-015-0504-1
27. Qiao Z, Horst K, Teuben M, Greven J, Yin L, Kalbas Y, et al. Analysis of Skeletal Muscle Microcirculation in a Porcine Polytrauma Model With Haemorrhagic Shock. *J Orthopaedic Research®* (2018) 36(5):1377–82. doi: 10.1002/jor.23759

28. Dutton RP. Resuscitation From Traumatic Shock. *Curr Opin Anaesthesiol* (2001) 14(2):217–20. doi: 10.1097/00001503-200104000-00014
29. Pfeifer R, Lichte P, Schreiber H, Sellei RM, Dienstknecht T, Sadeghi C, et al. Models of Hemorrhagic Shock: Differences in the Physiological and Inflammatory Response. *Cytokine* (2013) 61(2):585–90. doi: 10.1016/j.cyto.2012.10.022
30. Pfeifer R, Kobbe P, Darwiche SS, Billiar TR, Pape H-C. Role of Hemorrhage in the Induction of Systemic Inflammation and Remote Organ Damage: Analysis of Combined Pseudo-Fracture and Hemorrhagic Shock. *J Orthop Res* (2011) 29(2):270–4. doi: 10.1002/jor.21214
31. Horst K, Simon TP, Pfeifer R, Teuben M, Almahmoud K, Zhi Q, et al. Characterization of Blunt Chest Trauma in a Long-Term Porcine Model of Severe Multiple Trauma. *Sci Rep* (2016) 6:1–13. doi: 10.1038/srep39659
32. Relja B, Land WG. Damage-Associated Molecular Patterns in Trauma. *Eur J Trauma Emerg Surg* (2020) 46(4):751–75. doi: 10.1007/s00068-019-01235-w
33. Pfeifer R, Kalbas Y, Coimbra R, Leenen L, Komadina R, Hildebrand F, et al. Indications and Interventions of Damage Control Orthopedic Surgeries: An Expert Opinion Survey. *Eur J Trauma Emerg Surg* (2020), 47:2081–92. doi: 10.1007/s00068-020-01386-1
34. Horst K, Greven J, Lüken H, Zhi Q, Pfeifer R, Simon TP, et al. Trauma Severity and Its Impact on Local Inflammation in Extremity Injury-Insights From a Combined Trauma Model in Pigs. *Front Immunol* (2019) 10:3028. doi: 10.3389/fimmu.2019.03028
35. Bradley A, Mennie N, Bibby PA, Cassaday HJ. Some Animals are More Equal Than Others: Validation of a New Scale to Measure How Attitudes to Animals Depend on Species and Human Purpose of Use. *PloS One* (2020) 15(1): e0227948. doi: 10.1371/journal.pone.0227948

Conflict of Interest: The authors declare that the research was conducted in the absence of any commercial or financial relationships that could be construed as a potential conflict of interest.

frontiers | Frontiers in Immunology

TYPE Original Research
PUBLISHED 18 August 2022
DOI 10.3389/fimmu.2022.952267

OPEN ACCESS

EDITED BY
Christoph Thiemermann,
Queen Mary University of London,
United Kingdom

REVIEWED BY
Marcin Filip Osuchowski,
Ludwig Boltzmann Institute for
Experimental and Clinical
Traumatology, Austria
Liwu Li,
Virginia Tech, United States

*CORRESPONDENCE
Tom Eirik Mollnes
t.e.mollnes@gmail.com

SPECIALTY SECTION
This article was submitted to
Inflammation,
a section of the journal
Frontiers in Immunology

RECEIVED 24 May 2022
ACCEPTED 28 July 2022
PUBLISHED 18 August 2022

CITATION
Lupu L, Horst K, Greven J, Mert Ü, Ludviksen JAK, Pettersen K, Lau C, Li Y, Palmer A, Qin K, Zhang X, Mayer B, van Griensven M, Huber-Lang M, Hildebrand F and Mollnes TE (2022) Simultaneous C5 and CD14 inhibition limits inflammation and organ dysfunction in pig polytrauma.
Front. Immunol. 13:952267.
doi: 10.3389/fimmu.2022.952267

Simultaneous C5 and CD14 inhibition limits inflammation and organ dysfunction in pig polytrauma

Ludmila Lupu[1], Klemens Horst[2], Johannes Greven[2], Ümit Mert[2], Judith A.K. Ludviksen[3], Kristin Pettersen[3], Corinna Lau[3], Yang Li[1], Annette Palmer[1], Kang Qin[2], Xing Zhang[2], Benjamin Mayer[4], Martijn van Griensven[5], Markus Huber-Lang[1], Frank Hildebrand[2] and Tom Eirik Mollnes[3,6,7]*

[1]Institute of Clinical and Experimental Trauma Immunology, University Hospital Ulm, Ulm, Germany, [2]Department of Orthopedics, Trauma and Reconstructive Surgery, Rheinisch-Westfalische Technische Hochschule (RWTH) Aachen University, Aachen, Germany, [3]Research Laboratory, Nordland Hospital Bodø, Bodø, Norway, [4]Institute of Epidemiology and Medical Biometry, Ulm University, Ulm, Germany, [5]Department Cell Biology-Inspired Tissue Engineering (cBITE), MERLN Institute for Technology-Inspired Regenerative Medicine, Maastricht University, Maastricht, Netherlands, [6]Department of Immunology, Oslo University Hospital, and University of Oslo, Oslo, Norway, [7]Center of Molecular Inflammation Research, Norwegian University of Science and Technology, Trondheim, Norway

Dysfunctional complement activation and Toll-like receptor signaling immediately after trauma are associated with development of trauma-induced coagulopathy and multiple organ dysfunction syndrome. We assessed the efficacy of the combined inhibition therapy of complement factor C5 and the TLR co-receptor CD14 on thrombo-inflammation and organ damage in an exploratory 72-h polytrauma porcine model, conducted under standard surgical and intensive care management procedures. Twelve male pigs were subjected to polytrauma, followed by resuscitation (ATLS® guidelines) and operation of the femur fracture (intramedullary nailing technique). The pigs were allocated to combined C5 and CD14 inhibition therapy group (n=4) and control group (n=8). The therapy group received intravenously C5 inhibitor (RA101295) and anti-CD14 antibody (rMil2) 30 min post-trauma. Controls received saline. Combined C5 and CD14 inhibition reduced the blood levels of the terminal complement complex (TCC) by 70% (p=0.004), CRP by 28% (p=0.004), and IL-6 by 52% (p=0.048). The inhibition therapy prevented the platelet consumption by 18% and TAT formation by 77% (p=0.008). Moreover, the norepinephrine requirements in the treated group were reduced by 88%. The inhibition therapy limited the organ damage, thereby reducing the blood lipase values by 50% (p=0.028), LDH by 30% (p=0.004), AST by 33%, and NGAL by 30%. Immunofluorescent analysis of the lung tissue revealed C5b-9 deposition on blood vessels in five from the

untreated, and in none of the treated animals. In kidney and liver, the C5b-9 deposition was similarly detected mainly the untreated as compared to the treated animals. Combined C5 and CD14 inhibition limited the inflammatory response, the organ damage, and reduced the catecholamine requirements after experimental polytrauma and might be a promising therapeutic approach.

KEYWORDS

complement, CD14, TLR, inflammation, trauma and MODS

Introduction

Severely injured patients frequently develop complications, including coagulopathy, sepsis and multiple organ dysfunction syndrome (MODS) (1). The underlying mechanisms of posttraumatic thrombo-inflammation and organ dysfunction are driven by the trauma-induced immune response (2), which is regulated mainly by the complement cascade and the Toll-like receptor (TLR) signaling pathway (2).

The complement cascade is activated within minutes after trauma (3), and reaches its peak activity within the first 6-h post-injury (4). Complement was reported to be responsible for the oxidative burst in granulocytes and monocytes (5, 6), contributing to development of lung and kidney dysfunction after trauma (7, 8). C5a-primed neutrophils augment their production of reactive oxygen species once exposed to a "second-hit" traumatic event, such as surgery, increasing the risk for thromboembolic events (6).

The CD14 antigen is a cofactor of several TLRs, and plays a crucial role in pathogen-associated molecular patterns (PAMPs) and damage-associated molecular patterns (DAMPs) recognition (9). In a recent study, single-cell mass cytometry analysis applied to blood samples from patients with hip-replacement surgery, revealed that the prolonged postoperative recovery, pain, and functional impairment were strongly correlated with the cell signaling responses of $CD14^+$ cells (10). In trauma settings, the activation of TLRs was associated with prothrombotic events and increased thrombin-antithrombin (TAT) complexes in blood (11). Furthermore, posttraumatic TLRs signaling pathway activation has been associated with lung and kidney dysfunction (12, 13).

Both complement system activation and CD14 antigen expression pattern are associated with monocyte exhaustion in sterile and infection-induced inflammation (14, 15), with life-threatening consequences for the patients. Single-cell RNA-sequencing analysis of murine monocytes revealed that a subclinical LPS dosage could program the monocytes into low-grade inflammatory state, with elevated level of chemokines, chemokines receptors, and C5aR1 expression (16). A subset of $CD14^+$ cells was shown to distinctly change its transcriptional state in bacterial sepsis (17), in severe Covid-19 infection (18), and also in sterile infection caused by trauma, thus delaying the recovery and increasing the likelihood of developing complications (19).

Therefore, inhibition of excessive complement and TLR activation might be beneficial in the posttraumatic immune response. Although, the concept of combined inhibition in sepsis was extensively studied (20–25), this regimen has never been tested in polytrauma. Consequently, the aim of this study was to investigate the effects of simultaneous inhibition of the complement cascade at the C5 level and of the TLR signaling pathway at the CD14 level in a long-term polytrauma porcine model. We hypothesize that combined C5 and CD14 inhibition therapy will improve the systemic inflammatory response, and thus prevent the development of the posttraumatic coagulopathy and MODS.

Materials and methods

Animals and experimental design

The well-established 72-h porcine polytrauma including hemorrhagic shock model (26) was approved by the responsible government authority (Ministry for nature, environment and consumer protection in North Rhine-Westphalia, Recklinghausen, Germany; AZ 81-02.04. 2020.A215). The study was performed in compliance with the German legislation, the Federation of European Laboratory Animal Science Association (FELASA), and the ARRIVE guidelines (27).

Twelve German landrace male pigs (Sus scrofa, aged 12–16 weeks, mean body weight 35 ± 5 kg) from a disease-free barrier breeding facility were housed in ventilated rooms and allowed to acclimatize to their surroundings for a minimum of 7 days before surgery. 12-h before the experiment, the animals were exposed to fasting with water *ad libitum*. Preparation and instrumentation were described in detail by Horst et al. (26).

Briefly, animals were premedicated (Azaperone (Stresnil™, Janssen, Germany) in combination with Ketamine (Ketanest, Pfizer, New York)), intubated and induced in general anesthesia (Propofol (Fresenius, Germany) in combination with Midazolam (Panpharma GmbH, Germany)). Fentanyl (Panpharma GmbH, Germany) was used as a systemic analgesic. The general anesthesia and analgesia, as well as a lung protective ventilation strategy with a tidal volume of 8-12 ml/kg body weight (Evita 4, Draeger, Luebeck, Germany) were maintained throughout the entire experiment. The experimental animals were exposed to polytrauma: blunt chest trauma, laparotomy with liver laceration with a subsequent hemorrhagic shock, and bilateral open shaft femur fracture. The blunt chest trauma was induced using a bolt gun (Dynamit-Nobel, Vienna, Austria). A midline laparotomy was performed to expose the left liver lobe, on which two incisions (4.5cm × 4.5cm) were performed. The bilateral shaft femur fracture was performed using the bolt gun. Meanwhile, the pressure-controlled hemorrhagic shock was initiated by withdrawing blood from the femoral vein until the mean arterial pressure (MAP) fell to 40 ± 5mmHg and maintained for 90 min. Afterwards, the animals were resuscitated according to established trauma guidelines (ATLS® guidelines). Throughout 72-h of experiment, the animals were given fluids (Sterofundin, B. Braun, Germany) at a rate of 0.5-2.0 ml/kg/h and parenteral nutrition (Aminoven, Fresenius Kabi, Germany) 370 kcal/l 50-70 ml/kg body weight and day, under a close monitoring of the fluid balance. The heart rate and MAP were monitored using a Philips patient monitor (Philips Health Systems, Hamburg, Germany). The femur fracture was reduced and fixed by an intramedullary nailing technique (Stryker, Duisburg, Germany). For supporting the respiratory mechanics of pressure-controlled ventilated pigs, the animals were turned every 4-6 hours. If required, norepinephrine was administered i.v. for maintaining the MAP>60 mmHg.

As numerous *in vitro* whole blood studies and *in vivo* mice studies showed the superiority of the combined inhibition therapy over the monotherapy (21–24), for the present study, the decision was taken to proceed only with combined inhibition therapy. This decision was also based on the experience form the previous large animal (pig) study of peritonitis-induced sepsis, where the ethical guidelines (the 3 Rs') were closely followed, including saving the number of animals (25). The experimental animals were allocated to two groups: C5 and CD14 inhibition treated group (n=4) and untreated group (n=8). The treated group included 4 animals due to the limited access to the C5 inhibitor. The combined inhibition therapy included the intravenous (i.v.) administration of the C5 and CD14 inhibitors. One animal from the treated group was given a bolus of C5 inhibitor (3mg/kg) 30 min post-injury with a subsequent continuous infusion (0.55 mg/kg/h) until 64-h after the trauma, and one bolus of anti-CD14 (5mg/kg) at 30 min post-injury. The other three animals of the treated group received higher dosages of the combined inhibition therapy, based on the experiments testing the effects of the two inhibitors in the first animal. The final doses were bolus of C5 inhibitor (5mg/kg) 30 min post-trauma with a subsequent continuous infusion (1.1 mg/kg/h) until 72-h post-injury, and anti-CD14 boluses of 5mg/kg at 30 min, 12-, 30-h and of 2.5 mg/kg at 60-h post-injury. The four pigs were merged to one group since there was negligible variability in the treatment efficacy between the first and the other three pigs ($p<0.05$ for all parameters both for 3 vs 8 and 4 vs 8 pigs).

Interventional drugs

RA101295 (2-kDa peptide) was provided by UCB Pharma (Brussels, Belgium). RA101295 is a C5 inhibitor, with a cross-species activity, that prevents C5 cleavage and the subsequent generation of C5a and formation of the terminal C5b–9 complement complex (TCC), which is present in two forms: as sC5b–9 in the fluid-phase and as the membrane attack complex (MAC) on the cell surface (28).

rMil2 is a recombinant anti-porcine CD14 antibody (clone MIL2; isotype IgG2a), made recombinant as an IgG2/4 chimera in the laboratory of Professor T.E. Mollnes (Norway) (29) and produced largescale by ExcellGene SA (Monthey, Switzerland) according to GMP standards. The anti-CD14 antibody blocks the CD14 antigen and has no effector functions (29). The CD14 antigen in pigs is located mainly on granulocytes and functions as a co-factor for TLR signaling (9, 29, 30).

Immune monitoring of the combined inhibition therapy

The pharmacodynamics of the combined inhibition therapy were assessed every 12-h. The RA101295 pharmacological effect of blocking the classical and alternative complement pathways was evaluated using the Complement System Screen Wieslab (Euro Diagnostica, Malmö, Sweden) according to the manufacturer's instructions. CD14 antigen saturation with the rMil2 anti-CD14 antibody was assessed by flow cytometry analysis using FITC-labelled rMil2 anti-CD14 antibody. Briefly, 75µl of EDTA blood was incubated with anti-CD14-FITC antibody at a concentration of 375 µg/ml. The cells were analyzed using BD FACSCanto™ II. The data are presented as percentage of CD14-FITC positive cells (Figures 1A, B).

TCC measurement

TCC assessment in EDTA-plasma was performed using the ELISA-based technique (lower detection limit: 0.156 CAU/ml) as previously described (31). Briefly, the capture antibody aE11

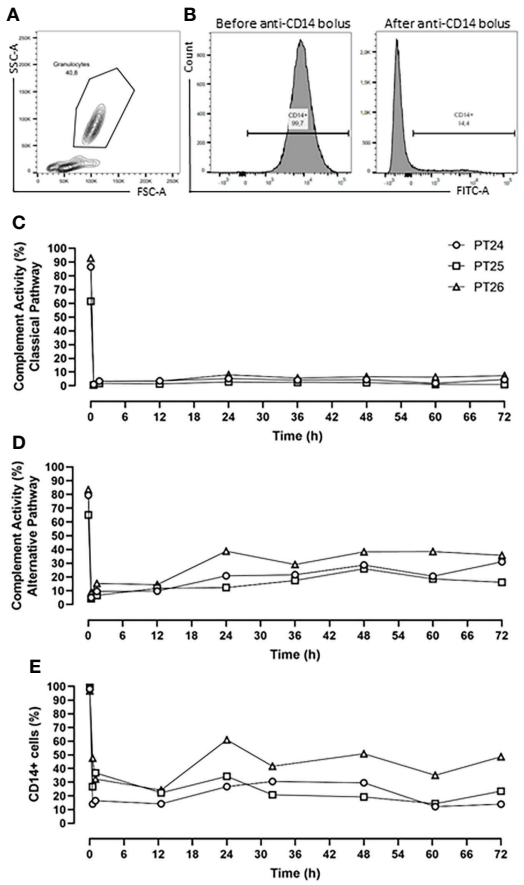

FIGURE 1
Pharmacodynamic analysis. **(A)** Flow Cytometry gating strategy of granulocyte. **(B)** Percentage of CD14+ cells before and after anti-CD14 (rMil2) application. **(C)** RA101295 (5mg/kg bolus, followed by 1.1mg/kg/h continuous infusion) blocked the classical pathway by 96%, and **(D)** the alternative pathway by 81%. **(E)** Simultaneous application of rMil2 (5mg/kg bolus at 30 min, 12-, 30-h, and 2.5mg/kg at 60-h) ensured CD14 antigen saturation of 75%. PT 24, PT25 and PT26 indicate experimental animal code in the treatment group.

(mouse monoclonal anti-C9 neoepitope antibody) reacts with an epitope that is exposed in C9 only when C9 is activated and incorporated into the C5b-9 complex. aE11 has been described previously as an anti-human C9 neoepitope antibody with a strong cross-reactivity to pig (32).

Biochemistry and hematology tests

Complete blood count for the assessment of the white blood cells (WBCs) and platelets (PLTs) was performed using hematology analyzer (Nihon Kohden, Japan). C-reactive protein (CRP), lipase, lactate dehydrogenase (LDH), and aspartate transaminase (AST) analyses were measured in serum by chemistry analyzer (Ortho-Clinical Diagnostics, NJ).

Cytokines, hemostatic and organ damage markers

The immunoassays for these analyses were chosen based on previous assessment of the different commercially available kits (33). Porcine ELISAs were used to quantify the interleukin 6 (IL-6) (lower detection limit: 9.4 pg/ml) and tumor necrosis factor (TNF) (lower detection limit: 11.7 pg/ml) (R&D Systems, MN); plasminogen activator inhibitor-1 (PAI-1) (lower detection limit: 3.1 ng/ml) (Nordic BioSite AB, Taby, Sweden) and neutrophil gelatinase-associated lipocalin (NGAL) (lower detection limit: 4.0 pg/ml) (Abcam, Cambridge, UK). Interleukin 8 (IL-8) was measured in bronchoalveolar lavage fluid (BALF) using Multiplex analysis (lower detection limit: 12.0 pg/ml) (Merck, Darmstadt, Germany). Human ELISA, documented in T.E. Mollnes laboratory to cross-react with pigs, was used to measure the thrombin–antithrombin complex (TAT) (lower detection limit: 2.0 µg/ml) (Siemens Healthineers, Germany). All the assays were performed using snap-frozen EDTA-plasma in accordance with the manufacturers' instructions.

Microscopy analysis

Tissue-Tek OCT (Sakura Finetek, Torrance, CA) embedded lung, kidney, and liver cryosections (7µm) were incubated overnight at 4°C with primary antibody: mouse monoclonal anti-C9 neoepitope exposed in C5b-9, clone aE11 as described above (provided by Professor T.E. Mollnes (Norway)). Goat anti-mouse IgG2a conjugated with Alexa Fluor® 568 (Invitrogen, MA) was used as secondary Ab. The F-actin was stained using Phalloidin Alexa Fluor® 488 (Invitrogen). The slides were mounted with Vectashield mounting medium (Vector Laboratories, Burlingame, CA) containing DAPI for nuclear counterstain. The images were captured using a Zeiss Axio-Imager microscope (Jena, Germany). The images were analyzed based on the presence of absence of the fluorescent signal.

Data presentation and statistics

The results from Wieslab Complement System Screening and Flow Cytometry analysis are given as individual profiles (n=3). GraphPad Prism version 9.2.0 (San Diego, CA) and the R software version 4.1.2 (www.r-project.org) were used for data visualization and statistical analysis. The latter was primarily based on non-parametric approaches because of the low sample sizes. Efficacy of the interventional drugs was evaluated by means of different ancillary approaches:

On the one hand, longitudinal measurements of the outcome parameters were initially summarized by time points and displayed using median values and corresponding interquartile ranges (IQR). The nonparametric Mann-Whitney-U test was used in order to

compare treated and untreated groups at different time points. Further, to account for the repeated measurement structure of the data, a nonparametric approach of longitudinal data analysis in factorial designs was applied (R package nparLD) assessing the difference between treated and untreated animals (group changes over time) for the TCC, lipase, TNF, and NGAL data. Due to missing values, for the remaining variables (WBC, PLT, CRP, AST, LDH, TAT, PAI-1, IL-6) a mixed linear model analysis was applied, since the nparLD approach mentioned above requires complete data.

On the other hand, for each individual trajectory an area under the curve (AUC) was calculated. These individual AUCs reflect the development of each particular outcome parameter over time. All individual AUC values were then summarized using median (IQR) for each group of treated and untreated animals separately. Again, the Mann-Whitney-U test was used to compare the median AUCs between treated and untreated animals. The percentage change of the AUC, reported in the text, represents the difference between the AUC median values of the untreated and the treated group. These AUC results are thought to support the findings from longitudinal data analysis. In the AUC graph representation, the treated pig who received lower medication dosages is depicted as filled black symbol color.

Correlation analysis was performed using nonparametric Spearman rank correlation. For statistical analysis of the immunofluorescence staining results Fisher's exact test was used. Statistical significance was assumed in case of a two-sided P-value < 0.05 (*: $p<0.05$, **: $p<0.01$, ***: $p<0.001$). Because of the study setting, all p-values are interpreted in an exploratory manner, which is why there was no correction of the type 1 error level due to multiple hypothesis testing.

One animal from the untreated group died at 60-h. It was included in the study analysis, while for the time point of 72-h the median of the other seven animals from the untreated group was calculated and used for the statistical analysis.

Results

Defining the dose of the drugs

The C5 inhibitor RA101295 injected i.v. 30 min post-injury as a bolus (3 mg/kg) with a subsequent continuous i.v. administration (0.55 mg/kg/h) until 64-h post-injury, blocked the classical complement pathway by 76% and the alternative pathway by 62% throughout the experiment (Supplementary Figures 1A, B). For optimizing the inhibitory effects, it was decided to increase the RA101295 dosage and duration of the administration for the next three animals. Therefore, RA101295 administration as a bolus of 5 mg/kg (30 min post-injury) with a subsequent continuous i.v. administration (1.1 mg/kg/h) until 72-h post-injury, significantly enhanced the blocking efficacy for the classical complement pathway to 96% and the alternative pathway to 81% throughout the experiment (Figures 1C, D).

Intravenous administration of a single bolus of the anti-CD14 antibody (5mg/kg) 30 min after trauma ensured a saturation of 79% of the CD14 antigen on the granulocytes throughout the experiment (Supplementary Figure 1C). However, the flow-cytometry-based immune monitoring, revealed a high granulocytes turnover after trauma and surgical management, consistent with the slight increase seen during the experiment in the first pig. Therefore, the anti-CD14 regimen was adjusted by giving the anti-CD14 antibody in boluses of 5mg/kg at 30 min, 12-, 30-h and of 2.5 mg/kg at 60-h post-injury, which ensured a continuously stable saturation of 75% of the CD14 antigen throughout the experiment (Figure 1E).

Despite a modest increase in the efficacy after dose adjustments, a substantial inhibition was observed in the first pig and the four pigs were therefore regarded as one single group with very similar treatment efficacy, as described statistically in the Materials and Methods section.

Combined C5 and CD14 inhibition therapy reduced catecholamine requirement

The cardiovascular monitoring did not show any significant differences in MAP and heart rate in the pairwise group comparison per time point (Figures 2A, B), or in the longitudinal mixed model analysis (p=0.716 for MAP, p=0.355 for heart rate). Nonetheless, during the entire experiment, the treated group responded better to the resuscitation therapy, while requiring less norepinephrine for positive ionotropic support therapy compared with the untreated group (p=0.026, mixed model analysis). Therefore, the norepinephrine requirements to maintain the MAP at ≥60mmHg could be reduced by 88% as deduced from the AUC in the treated group, with a statistically significant reduction of the norepinephrine dosage at 72-h timepoint post-injury (p=0.026) (Figures 2C, D).

Combined C5 and CD14 inhibition therapy mitigated the systemic inflammation

A time-dependent generation of TCC was observed in the untreated group (Figure 3). This was significantly reduced in the treated group at 2.5- (p=0.048), 24- (p=0.004), 48- (p=0.004), and 72-h (p=0.008) (Figure 3A). Overall, the

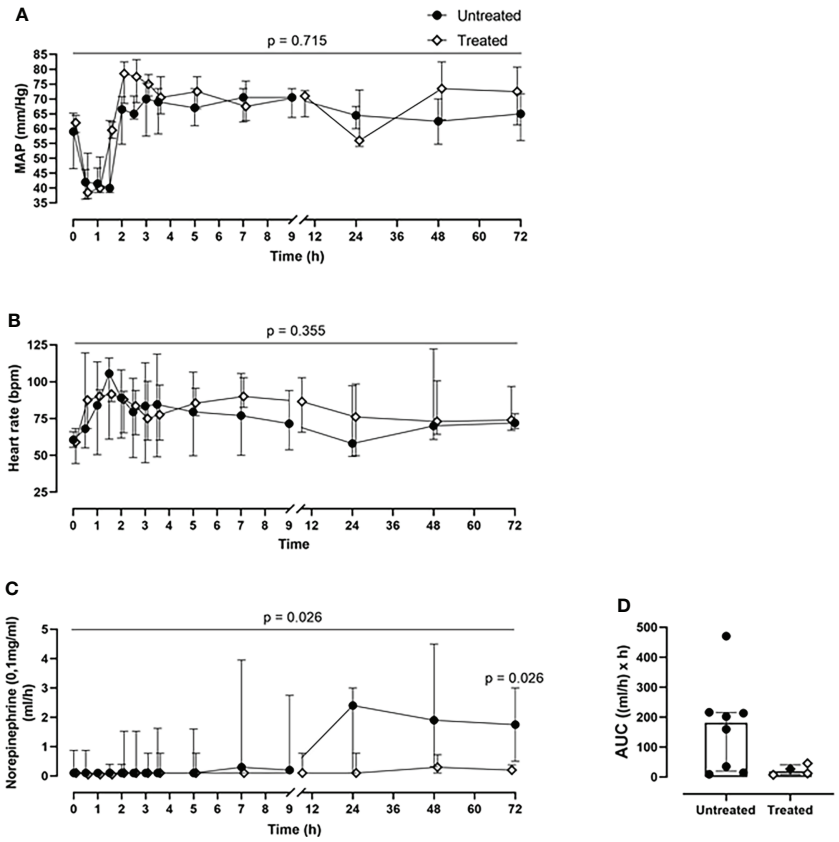

FIGURE 2
Cardiovascular monitoring. **(A)** MAP and **(B)** heart rate monitoring. **(C)** Norepinephrine dosing monitoring and the corresponding **(D)** AUC analysis revealed that the treated group (n=4) required less norepinephrine for maintaining the MAP≥60mmHg, compared to the untreated group (n=8). Overall p-value for group comparison of treated vs. untreated animals over time is displayed above the summary trajectories. In the AUC graphical representation, the first pig, receiving lower inhibitor dosage, is represented as black filled diamond.

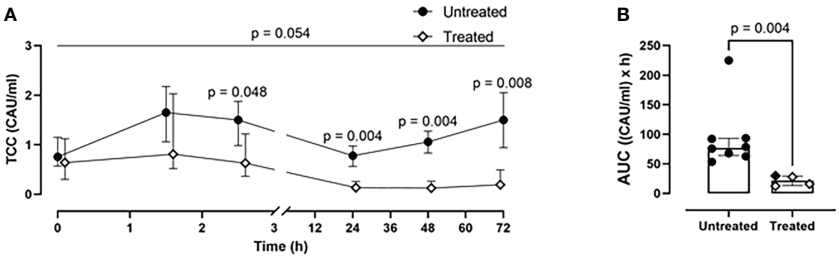

FIGURE 3
Blood TCC measurements. **(A)** TCC formation 2.5-, 24-, 48-, and 72-h after trauma was reduced in the treated group (n=4), compared to the untreated group (n=8). **(B)** Area under the curve analysis showed a statistically significant reduction of TCC in the treated group. Overall p-value for group comparison of treated vs. untreated animals over time is displayed above the summary trajectories. In the AUC graphical representation, the first pig, receiving lower inhibitor dosage, is represented as black filled diamond.

combined blockade therapy effectively reduced complement activation as indicated by significantly reduced TCC formation by 70% (p= 0.004) as measured by AUC throughout the 72-h of the experiment (Figure 3B).

Although the inhibition therapy did not alter the WBC count (Figures 4A, B), it significantly ameliorated the signs of the posttraumatic cytokine storm. The therapy achieved a systemic reduction of the key inflammatory parameters: CRP

10.3389/fimmu.2022.952267

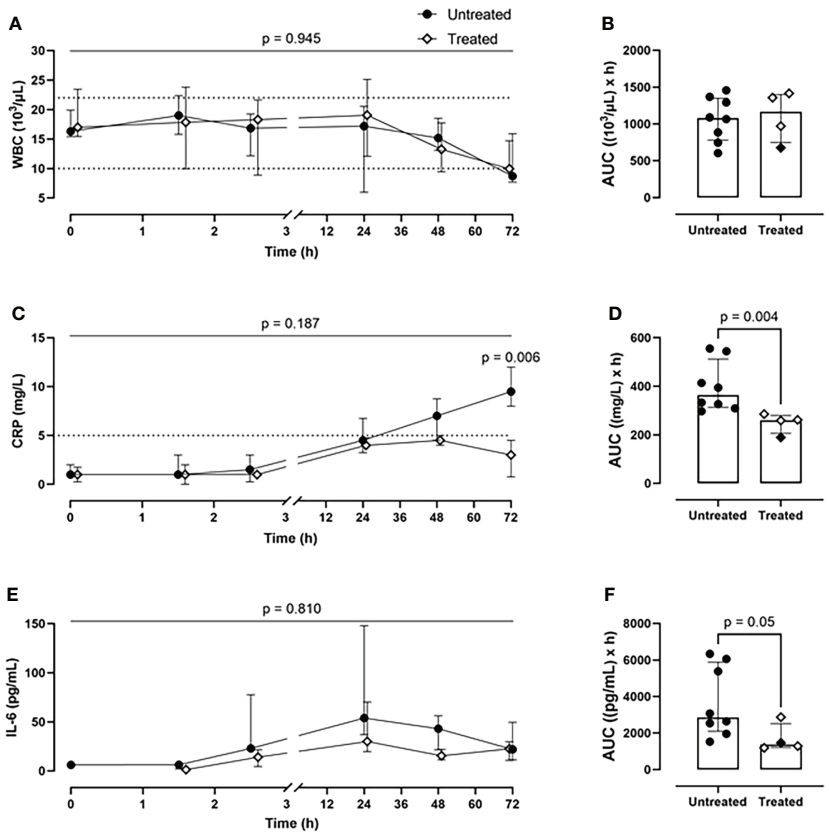

FIGURE 4
Systemic inflammatory parameters. **(A)** WBCs monitoring and **(B)** WBCs AUC analysis showed no difference between the two groups. **(C)** CRP monitoring and **(D)** CRP AUC analysis revealed a significant reduction of CRP values in blood in the treated group (n=4), compared to the untreated group (n=8). **(E)** IL-6 monitoring and **(F)** IL-6 AUC analysis showed a diminished IL-6 expression in the treated group (n=4), compared to the untreated group (n=8). Dotted lines represent the normal reference range. Overall p-value for group comparison of treated vs. untreated animals over time is displayed above the summary trajectories. In the AUC graphical representation, the first pig, receiving lower inhibitor dosage, is represented as black filled diamond.

by 28% (p=0.004) (Figures 4C, D) and IL-6 by 52% (p=0.05) (Figures 4E, F). The therapy had no effect on blood TNF level (Supplementary Figures 2A, B).

Combined C5 and CD14 inhibition therapy prevented the PLT consumption and TAT generation

Over the course of 72-h of monitoring, the treated group showed a greater PLT count (p=0.028, mixed model analysis) and a significant reduction of PLT consumption at the 72-h timepoint (p=0.026) in comparison with the untreated group (Figure 5A). Overall, the combined inhibitory strategy diminished the systemic PLT consumption by 18% during the experiment (Figure 5B). The therapy strongly reduced the TAT formation by 77% (p=0.008) as deduced from AUC (Figures 5C, D). The combined therapy did not affect PAI-1 concentrations (Figures 5E, F).

A significant negative correlation was detected between PLT consumption and TAT formation (r=−0.880; p=0.0003) in both groups (Figure 5G).

Furthermore, the treated group showed lower IL-8 values in BALF compared to the untreated group (Figure 5H).

Combined C5 and CD14 inhibition therapy protected against organ dysfunction

The combined inhibitory therapy was associated with a lower amount of plasma markers reflecting organ damage. The unspecific lipase concentrations were significantly reduced in the treated group at 72-h timepoint (p=0.04) (Figure 6A). Overall, the lipase values were reduced by 50% in the treated group (p=0.03) as seen in the AUC measurement (Figure 6B). Substantially lower LDH blood values were detected in the treated compared to the untreated

10.3389/fimmu.2022.952267

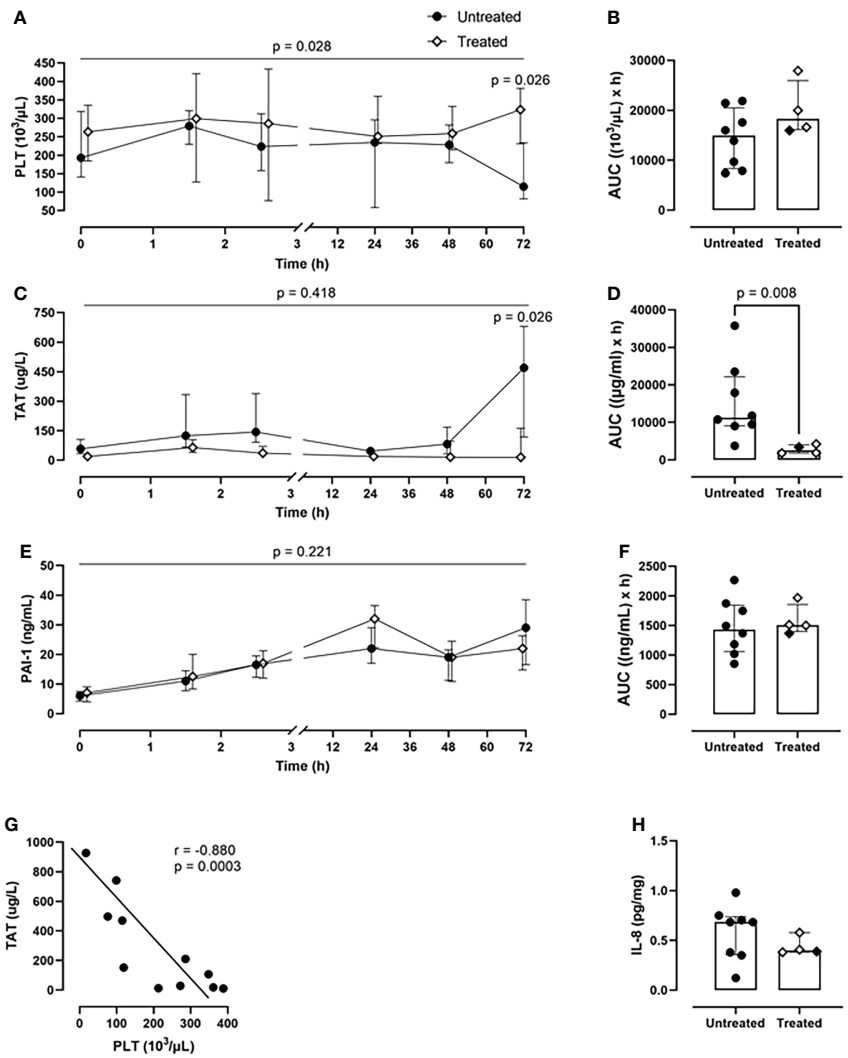

FIGURE 5
Coagulation parameters. **(A)** PLT count monitoring and **(B)** PLT count AUC analysis revealed a reduced PLTs consumption in the treated group (n=4), compared to the untreated group (n=8). **(C)** TAT monitoring and **(D)** TAT AUC analysis showed a significant reduction in TAT complexes formation in the treated group (n=4), but not in the untreated group (n=8). **(E)** PAI-1 monitoring and **(F)** PAI-1 AUC did not differ between the two groups. **(G)** Spearman correlation analysis shows a negative statistically significant correlation between TAT values and PLTs count in blood 72-h post-injury. **(H)** IL-8 measurement in BALF showed a reduction of the IL-8 levels in the treated group (n=4) compared to the untreated group (n=8). Overall p-value for group comparison of treated vs. untreated animals over time is displayed above the summary trajectories. In the AUC graphical representation, the first pig, receiving lower inhibitor dosage, is represented as black filled diamond.

group over 72-h of experiment (p=0.001, mixed model analysis) and specifically at 24- (p=0.028), 48-(p=0.028), and 72-h timepoint (p=0.012) (Figure 6C). Globally, in the treated group, the LDH plasma concentrations were significantly reduced by 30% (p=0.004) (Figure 6D). The therapy reduced the AST values by 33%, with a significant reduction at 72-h (p=0.018) (Figures 6E, F). The treated group displayed a significant decrease in the kidney damage marker NGAL plasma concentrations of 30%, with a significant reduction at 2.5-h post-injury (p=0.016) (Figures 6G, H).

Combined C5 and CD14 inhibition therapy prevented tissue C5b-9 deposition

The immunofluorescent staining of the lung tissue revealed the deposition of C5b-9 on blood vessels in five of the seven animals in the untreated group that lived for 72-h, but in none of the four animals in the treated group (p=0.06) (Figure 7A). In kidney tissue, C5b-9 glomerular deposition was detected in five

10.3389/fimmu.2022.952267

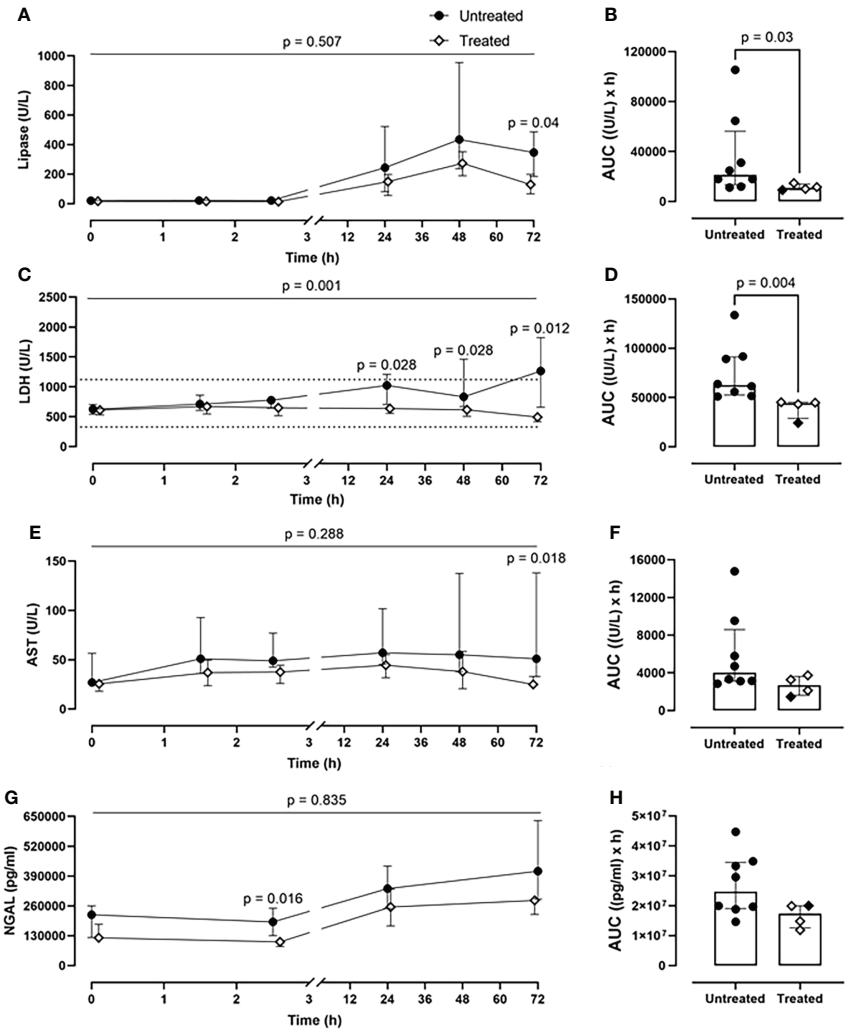

FIGURE 6
Organ damage markers. **(A)** Lipase, **(C)** LDH, **(E)** AST, and **(G)** NGAL monitoring in addition to **(B)** lipase, **(D)** LDH, **(F)** AST, and **(H)** NGAL AUC analysis showed that significantly lower lipase, LHD, AST, and NGAL values were detected in blood in the treated group (n=4), compared to the untreated group (n=8). Dotted lines represent the normal reference range. Overall p-value for group comparison of treated vs. untreated animals over time is displayed above the summary trajectories. In the AUC graphical representation, the first pig, receiving lower inhibitor dosage, is represented as black filled diamond.

from seven untreated animals and in two from four untreated animals (Figure 7B). In the liver tissue, C5b-9 deposition was detected in five from seven untreated animals and in none of the treated animals (p=0.06) (Figure 7C). Moreover, C5b-9 deposition on the liver blood vessels was detected in the untreated compared to the treated animals (Figure 7D).

Discussion

The present study reports the efficacy of a combined C5 and CD14 inhibition therapy in an exploratory study of a long-term large animal polytrauma, with standard surgical and intensive case management. We demonstrated that drug administration given 30 min postinjury strongly attenuated the trauma-induced pro-inflammatory response by diminishing the systemic CRP and IL-6 expression. 30 minutes is within a clinically relevant window since treatment can be given by prehospital personnel if the trauma does not occur close enough to a hospital. Furthermore, the combined therapy successfully prevented classical signs of posttraumatic coagulopathy by reducing the PLT consumption and the formation of TAT complexes. The significant negative correlation between the PLT consumption and TAT formation mirrors the crosstalk among hemostasis, complement and the TLR system, as shown in previous studies

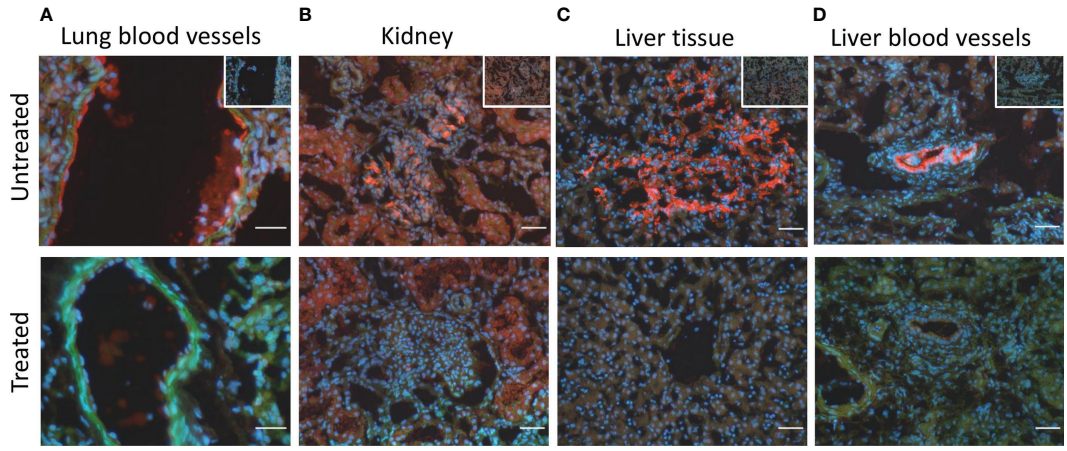

FIGURE 7
C5b-9 immunofluorescent staining showed C5b-9 deposition (red) **(A)** on the blood vessels in lung tissue in 5/7 of the untreated animals and in none of the four treated animals. **(B)** In kidney tissue, C5b-9 glomerular deposition was detected in 5/7 untreated and in 2/4 treated animals. **(C)** In the liver tissue, C5b-9 deposition was detected in 5/7 untreated and in none if the treated animals. **(D)** C5b-9 deposition was also detected in the liver blood vessels in the untreated but not in the treated group. One representative section from each group is shown. To facilitate the recognition of the histological structures the nuclear counterstaining (blue) and F-actin counterstaining (green) have been performed. In the upper panel, in the right upper corner, the respective 'no primary antibody controls' are illustrated. Magnification bars (short white lines bottom right in all panels): 20μm (lung) and 50μm (kidney and liver).

that in trauma settings an increased amount of thrombin is generated by PLTs upon TLR2 and TLR4 activation (34, 35).

Importantly, the treatment reduced organ damage and the need for norepinephrine. The analysis of the organ damage markers clearly showed that the inhibition therapy protected the liver, kidneys, and lungs, minimizing the risk for developing MODS. Thus, the treated group displayed lower blood lipase, LDH, and AST values compared to the untreated group. Moreover, double inhibition therapy reduced C5b-9 deposition in the liver tissue and blood vessels. In the treated group, lower NGAL levels were detected. NGAL as an early marker of acute kidney injury (36), displays an upregulated expression upon TLR stimulation (37). Therefore, blocking CD14, required for several TLRs signaling, can inhibit NGAL overexpression and prevent trauma related acute kidney injury (TRAKI) (8). The double inhibition therapy reduced the C5b-9 deposition in kidney glomeruli, thus minimizing the risk of developing TRAKI. Elevated levels of TCC in plasma of trauma patients were shown to be associated with an increased risk of developing acute lung injury (7). By inhibition of the complement system at the C5 level, we obtained a substantial reduction of TCC in plasma, and a complete abolishment of C5b-9 deposition in the lung blood vessels of the treated animal group. Previously, the polytrauma pig model used in our study was proven to be reliable and clinically relevant for investigating long-term pulmonary consequences of polytrauma (26). In the study conducted by Horst *et al.*, IL-8 measurements in BALF revealed a significant increase of IL-8 at 72-h in the polytrauma group compared to the sham group (26). In the present study, we showed that the combined inhibition therapy strongly reduces the IL-8 values in the BALF in the polytrauma treated compared to the polytrauma untreated group, thus limiting the local pulmonary inflammation.

Substances targeting the complement system or TLR signaling pathways have long been considered potential therapies for various diseases (28, 38). The effectiveness of the complement inhibition therapies at the C3 level (compstatin) and C5 level (RA101295), along with CD14 inhibition monotherapy were already proven to be beneficial in porcine and baboon sepsis models (39–43). In these studies, the complement or CD14 inhibition attenuated the sepsis-induced inflammation and coagulopathy (42, 43), displayed protective effects on the endothelium, and was associated with improved organ performance (39, 40). While the complement or CD14 inhibition monotherapy proved to be effective, the combined inhibition therapy displayed clear enhanced effects. In a polymicrobial sepsis mouse model, the C5 or CD14 inhibition monotherapy strongly reduced the overall inflammation but failed to increase the survival rates, whereas the combined inhibition therapy significantly reduced the inflammation and increased the survival (22), hence proving its therapeutic advantage. A study of experimental porcine sepsis reported an enhanced efficacy of the combined C5 and CD14 inhibition in limiting the thrombo-inflammation and hemodynamic instability over single monotherapies (21). These results were validated in another study of porcine polymicrobial sepsis, where the combined inhibition also significantly improved the survival rates (25). Moreover, the therapeutic efficacy of the C5

and/or CD14 therapy was assessed in a well-established human *ex vivo* whole blood model of inflammation, where it was shown that the combined inhibition therapy exceeded the effects of monotherapies in limiting the inflammation (23, 24). Considering the strong evidence of combined inhibition superiority over the monotherapies, in this study we addressed only the combined inhibition therapy.

Additionally, clinical trials were conducted for efficacy analysis of anti-C5a monoclonal antibody (CaCP29, InflaRx GmbH) (NCT02246595) and of an MD2-TLR4 antagonist (Eritoran, Eisai) in severe sepsis (NCT00334828), but without any clinical effect. We have shown in an *in vitro* human whole blood model that CD14 was substantially more effective in attenuating *Escherichia coli*- and *Staphylococcus aureus*-induced inflammatory reactions than the specific TLR4 inhibitor Eritoran, supporting a broader effect of inhibition of the co-receptor CD14 than that of Eritoran, consistent with CD14 being a co-receptor for several TLRs, including TLR4 and TLR2 (23).

Numerous studies have reported long-term immune dysfunction after sepsis, surgical events, as well as after Covid-19 infection (44, 45), with monocyte exhaustion syndrome being one of the underlying causes (46, 47). Exhausted monocytes are shown to be skewed into the classical monocytes' population (murine $CD11b^{+}CD115^{+}Ly6C^{high}$, human $CD14^{+}CD16^{-}HLA\text{-}DR^{mid}$) (18, 47), and are characterized by cellular NAD^{+} depletion, elevated ROS production, and impaired response to secondary stimuli (47, 48). Mechanistically, exhausted monocytes display an exacerbated activation of signal transducer and activator of transcription 1 (STAT1) and Kruppel-like factor 4 (KLF4). STAT1 involvement in monocytes polarization towards classical and intermediate pro-inflammatory subsets was also confirmed using machine learning methods (16). STAT1 as well as KLF4 can be triggered by interferon-γ (IFN-γ), which will induce a pro-inflammatory cellular response (49, 50). Complement and/or CD14 inhibition successfully reduced the IFN-γ production in mice and baboons' sepsis studies (22, 43), thus preventing STAT1 and KLF4 overactivation. Additionally, interferon gamma-induced protein 10 (IP-10), which expression is dependent on STAT1 signaling (51), was significantly reduced in heart, liver, spleen, and kidney by the combined inhibition therapy in porcine *Escherichia coli* sepsis model (30). Using single-cell RNA-sequencing technique it was showed that persistent low dosed of LPS could induce the generation of two pro-inflammatory subset of monocytes: one subset with a high expression of C5aR1 and interferon activated genes, resembling the human intermediate monocyte subset, and the second subset with high CCR2 expression, resembling the human classical monocyte subset (16). Interestingly, in another study LPS-exhausted monocytes were reposted to increase the expression programmed death-ligand 1 (PD-L1) exhaustion marker, which could be prevented by C5aR1 inhibition (15). TLR4 as well as TLR2 (52) adaptor TRAM was also shown to play a role in monocyte exhaustion generation (47, 53). As CD14 is a co-receptor of TLR2 and TLR4 (9), its inhibition will prevent the overactivation of TRAM to a greater extent than single TLR inhibition. Indeed, in human whole blood model, *Escherichia coli*-induced upregulation of CD11b on monocytes was stronger reduced by CD14 inhibitor alone or in combination with complement inhibition than by a specific TLR4 inhibitor (23). Thus, directly though inhibition of CD14, or indirectly through reduction of cytokine production and release, CD14 inhibition together with complement inhibition can prevent the monocyte exhaustion syndrome and its long-term immune consequences.

Beyond sepsis research, complement antagonists are considered potential therapeutic strategies in severe cases of Covid-19 infections (54, 55). Therefore, ongoing clinical trials are investigating the effectiveness of a C3 inhibitor (AMY-101, Amyndas Pharmaceuticals S.A., PA) in Covid-19-induced acute respiratory distress syndrome (NCT04395456), and of a C5 inhibitor (Zilucoplan, UCB Pharma, Brussels, Belgium) in Covid-19-induced respiratory failure (NCT04382755). Furthermore, several clinical trials are being conducted to assess anti-CD14 monoclonal antibody (IC14, Implicit Bioscience, WA, USA) in patients with Covid-19 infection (NCT04346277; NCT04391309).

The timing rationale of the combined C5 and CD14 inhibition therapy application was based on the data from previous studies (56–58). The complement and coagulation system is activated within minutes after trauma in polytraumatized patients, with the first signs of trauma-induced coagulopathy and complement consumption developing within the first 74 min post-injury (56, 57). The estimated onset of MODS immunopathology was reported to be in the first hours after a traumatic insult (58). The dysregulated immune response post-injury is aggravated by the early total care approach, for example intramedullary nailing surgical strategy (2), as performed in our study. Consequently, it is vital to initiate the immunomodulatory therapy in the first "golden" hour after trauma. Previous studies using the combined C5 and CD14 therapy in pigs undergoing sepsis have been based on the "proof of concept" principle where the drug was given before bacteria administration (20). An *in vitro* study using whole human blood incubated with bacteria and inhibition of complement and CD14 showed that post-challenge inhibition as compared to pre-challenge also attenuated the inflammatory response reasonably well during the first period of time, but the effect was gradually lost (24). In the present study, we took advantage of the clinically relevant therapeutic strategy of post-challenge blocking the immune response, but still before reaching the "point of no return". This timing principle has been previously proposed as an "upstream approach" (59).

In the present study, the low n-size supports the 3Rs' principles (replacement, reduction, refinement), but could be

accompanied with a potential risk for statistical errors. Nevertheless, this did not weaken the robustness of the data, as the difference between the groups was substantial. The unequal sample sizes, due to drug supply shortages, are a limitation of the study. Nevertheless, it was carefully approached in the statistical analysis of the data. Because of the real-time pharmacodynamic analysis, the investigators could not be blinded, and due to drug availability issues, the animals could not be randomized. The performed meticulous monitoring of the pharmacodynamics of C5 and CD14 inhibitors allowed a prompt adjustment of the dosages for accomplishing the study goals. Although the first treatment animal received a lower dosage of the C5 and CD14 inhibitors, its pharmacological efficacy was comparable with the adjusted therapy regimen during the experiments, which included higher dosages of inhibitors and these four animals could therefore be combined as the treatment group. These findings justify the patient-tailored therapeutic approaches. Because the immune response of a multiple trauma patient is unpredictable, it requires close continuous monitoring, with a consequent adjustment of the therapy. The fact that most of the readouts were statistically significant with only four pigs in the treatment group and eight in the control group, underscores the substantial significance between the groups and that type I errors are highly unlikely. However, we cannot exclude that there were some type II errors.

In summary, we demonstrated that the early administration of the combined blockade of C5 and CD14 post-injury, adjusted in response to subsequent immune monitoring, significantly reduced the catecholamine requirements, thrombo-inflammatory response, and organ damage in a 72-h porcine polytrauma model. These data have important implications for future therapeutic strategies in trauma.

Data availability statement

The raw data supporting the conclusions of this article will be made available by the authors, without undue reservation.

Ethics statement

The animal study was reviewed and approved by Ministry for Nature, Environment and Consumer Protection in North Rhine-Westphalia, Recklinghausen, Germany; AZ 81-02.04. 2020.A215.

Author contributions

MH-L, TM, FH, JG, MG, and KH designed the animal study. JG, ÜM, and LL performed the animal study. JG, ÜM, LL, KQ, XZ, AP, and YL collected the data. LL, JL, KP, and CL performed the experiments. BM, TM, and LL analyzed and interpreted the data. LL drafted the manuscript. All authors critically revised the manuscript and approved the final version.

Funding

This research was funded by the Deutsche Forschungsgemeinschaft (DFG, German Research Foundation) – 429837092. RA101295 was provided by UCB Pharma (Brussels, Belgium).

Acknowledgments

The authors would like to thank the Flow Cytometry core facility of University Clinic Aachen, especially Nathalie Steinke and Silke Vaßen for valuable support.

Conflict of interest

The authors declare that the research was conducted in the absence of any commercial or financial relationships that could be construed as a potential conflict of interest.

Publisher's note

Supplementary material

The Supplementary Material for this article can be found online at: https://www.frontiersin.org/articles/10.3389/fimmu.2022.952267/full#supplementary-material

References

1. Teixeira PGR, Inaba K, Hadjizacharia P, Brown C, Salim A, Rhee P, et al. Preventable or potentially preventable mortality at a mature trauma center. *J Trauma* (2007) 63(6):1338–46. doi: 10.1097/TA.0b013e31815078ae

2. Huber-Lang M, Lambris JD, Ward PA. Innate immune responses to trauma. *Nat Immunol* (2018) 19(4):327–41. doi: 10.1038/s41590-018-0064-8

3. Burk AM, Martin M, Flierl MA, Rittirsch D, Helm M, Lampl L, et al. Early complementopathy after multiple injuries in humans. *Shock* (2012) 37(4):348–54. doi: 10.1097/SHK.0b013e3182471795

4. Rognes IN, Pischke SE, Ottestad W, Røislien J, Berg JP, Johnson C, et al. Increased complement activation 3 to 6 h after trauma is a predictor of prolonged mechanical ventilation and multiple organ dysfunction syndrome: a prospective observational study. *Mol Med* (2021) 27(1):35. doi: 10.1186/s10020-021-00286-3

5. Mollnes TE, Brekke OL, Fung M, Fure H, Christiansen D, Bergseth G, et al. Essential role of the C5a receptor in e coli-induced oxidative burst and phagocytosis revealed by a novel lepirudin-based human whole blood model of inflammation. *Blood* (2002) 100(5):1869–77. doi: 10.1182/blood.V100.5.1869.h81702001869_1869_1877

6. Barrett CD, Hsu AT, Ellson CD, Y Miyazawa B, Kong YW, Greenwood JD, et al. Blood clotting and traumatic injury with shock mediates complement-dependent neutrophil priming for extracellular ROS, ROS-dependent organ injury and coagulopathy. *Clin Exp Immunol* (2018) 194(1):103–17. doi: 10.1111/cei.13166

7. Ganter MT, Brohi K, Cohen MJ, Shaffer LA, Walsh MC, Stahl GL, et al. Role of the alternative pathway in the early complement activation following major trauma. *Shock* (2007) 28(1):29–34. doi: 10.1097/shk.0b013e3180342439

8. Messerer DAC, Halbgebauer R, Nilsson B, Pavenstädt H, Radermacher P, Huber-Lang M. Immunopathophysiology of trauma-related acute kidney injury. *Nat Rev Nephrol* (2021) 17(2):91–111. doi: 10.1038/s41581-020-00344-9

9. Lee CC, Avalos AM, Ploegh HL. Accessory molecules for toll-like receptors and their function. *Nat Rev Immunol* (2012) 12(3):168–79. doi: 10.1038/nri3151

10. Gaudillière B, Fragiadakis GK, Bruggner RV, Nicolau M, Finck R, Tingle M, et al. Clinical recovery from surgery correlates with single-cell immune signatures. *Sci Transl Med* (2014) 6(255):255ra131–255ra131. doi: 10.1126/scitranslmed.3009701

11. Eppensteiner J, Kwun J, Scheuermann U, Barbas A, Limkakeng AT, Kuchibhatla M, et al. Damage- and pathogen-associated molecular patterns play differential roles in late mortality after critical illness. *JCI Insight* (2019) 4(16):127925. doi: 10.1172/jci.insight.127925

12. Rani M, Sayyadioskoie SR, Galvan EM, Nicholson SE, Schwacha MG. Trauma-induced lung injury is associated with infiltration of activated TLR expressing myeloid cells. *Cytokine* (2021) 141:155457. doi: 10.1016/j.cyto.2021.155457

13. Paulus P, Rupprecht K, Baer P, Obermüller N, Penzkofer D, Reissig C, et al. The early activation of toll-like receptor (TLR)-3 initiates kidney injury after ischemia and reperfusion. *PloS One* (2014) 9(4):e94366. doi: 10.1371/journal.pone.0094366

14. Gainaru G, Papadopoulos A, Tsangaris I, Lada M, Giamarellos-Bourboulis EJ, Pistiki A. Increases in inflammatory and CD14dim/CD16pos/CD45pos patrolling monocytes in sepsis: correlation with final outcome. *Crit Care* (2018) 22(1):56. doi: 10.1186/s13054-018-1977-1

15. An LL, Gorman JV, Stephens G, Swerdlow B, Warrener P, Bonnell J, et al. Complement C5a induces PD-L1 expression and acts in synergy with LPS through Erk1/2 and JNK signaling pathways. *Sci Rep* (2016) 6:33346. doi: 10.1038/srep33346

16. Lee J, Geng S, Li S, Li L. Single cell RNA-seq and machine learning reveal novel subpopulations in low-grade inflammatory monocytes with unique regulatory circuits. *Front Immunol* (2021) 12:627036. doi: 10.3389/fimmu.2021.627036

17. Reyes M, Filbin MR, Bhattacharyya RP, Billman K, Eisenhaure T, Hung DT, et al. An immune-cell signature of bacterial sepsis. *Nat Med* (2020) 26(3):333–40. doi: 10.1038/s41591-020-0752-4

18. Lee JW, Su Y, Baloni P, Chen D, Pavlovitch-Bedzyk AJ, Yuan D, et al. Integrated analysis of plasma and single immune cells uncovers metabolic changes in individuals with COVID-19. *Nat Biotechnol* (2022) 40(1):110–20. doi: 10.1038/s41587-021-01020-4

19. Chen T, Delano MJ, Chen K, Sperry JL, Namas RA, Lamparello AJ, et al. A road map from single-cell transcriptome to patient classification for the immune response to trauma. *JCI Insight* (2021) 6(2):145108. doi: 10.1172/jci.insight.145108

20. Barratt-Due A, Pischke SE, Nilsson PH, Espevik T, Mollnes TE. Dual inhibition of complement and toll-like receptors as a novel approach to treat inflammatory diseases-C3 or C5 emerge together with CD14 as promising targets. *J Leukoc Biol* (2017) 101(1):193–204. doi: 10.1189/jlb.3VMR0316-132R

21. Barratt-Due A, Thorgersen EB, Egge K, Pischke S, Sokolov A, Hellerud BC, et al. Combined inhibition of complement (C5) and CD14 markedly attenuates inflammation, thrombogenicity, and hemodynamic changes in porcine sepsis. *J Immunol* (2013) 191(2):819–27. doi: 10.4049/jimmunol.1201909

22. Huber-Lang M, Barratt-Due A, Pischke SE, Sandanger Ø, Nilsson PH, Nunn MA, et al. Double blockade of CD14 and complement C5 abolishes the cytokine storm and improves morbidity and survival in polymicrobial sepsis in mice. *J Immunol* (2014) 192(11):5324–31. doi: 10.4049/jimmunol.1400341

23. Gustavsen A, Nymo S, Landsem A, Christiansen D, Ryan L, Husebye H, et al. Combined inhibition of complement and CD14 attenuates bacteria-induced inflammation in human whole blood more efficiently than antagonizing the toll-like receptor 4-MD2 complex. *J Infect Dis* (2016) 214(1):140–50. doi: 10.1093/infdis/jiw100

24. Egge KH, Thorgersen EB, Lindstad JK, Pharo A, Lambris JD, Barratt-Due A, et al. Post challenge inhibition of C3 and CD14 attenuates escherichia coli-induced inflammation in human whole blood. *Innate Immun* (2014) 20(1):68–77. doi: 10.1177/1753425913482993

25. Skjeflo EW, Sagatun C, Dybwik K, Aam S, Urving SH, Nunn MA, et al. Combined inhibition of complement and CD14 improved outcome in porcine polymicrobial sepsis. *Crit Care* (2015) 19:415. doi: 10.1186/s13054-015-1129-9

26. Horst K, Simon TP, Pfeifer R, Teuben M, Almahmoud K, Zhi Q, et al. Characterization of blunt chest trauma in a long-term porcine model of severe multiple trauma. *Sci Rep* (2016) 6(1):39659. doi: 10.1038/srep39659

27. Percie du Sert N, Hurst V, Ahluwalia A, Alam S, Avey MT, Baker M, et al. The ARRIVE guidelines 2.0: Updated guidelines for reporting animal research. *PloS Biol* (2020) 18(7):e3000410. doi: 10.1371/journal.pbio.3000410

28. Garred P, Tenner AJ, Mollnes TE. Therapeutic targeting of the complement system: From rare diseases to pandemics. *Pharmacol Rev* (2021) 73(2):792–827. doi: 10.1124/pharmrev.120.000072

29. Lau C, Gunnarsen KS, Høydahl LS, Andersen JT, Berntzen G, Pharo A, et al. Chimeric anti-CD14 IGG2/4 hybrid antibodies for therapeutic intervention in pig and human models of inflammation. *J Immunol* (2013) 191(9):4769–77. doi: 10.4049/jimmunol.1301653

30. Egge KH, Thorgersen EB, Pischke SE, Lindstad JK, Pharo A, Bongoni AK, et al. Organ inflammation in porcine escherichia coli sepsis is markedly attenuated by combined inhibition of C5 and CD14. *Immunobiology* (2015) 220(8):999–1005. doi: 10.1016/j.imbio.2015.04.002

31. Jansen JH, Høgåsen K, Mollnes TE. Extensive complement activation in hereditary porcine membranoproliferative glomerulonephritis type II (porcine dense deposit disease). *Am J Pathol* (1993) 143(5):1356–65.

32. Mollnes TE, Lea T, Harboe M, Tschopp J. Monoclonal antibodies recognizing a neoantigen of poly(C9) detect the human terminal complement complex in tissue and plasma. *Scand J Immunol* (1985) 22(2):183–95. doi: 10.1111/j.1365-3083.1985.tb01870.x

33. Ueland NL, Ludvigsen JK, Hellerud BC, Mollnes TE, Skjeflo EW. Choice of immunoassay to evaluate porcine cytokine levels. *Vet Immunol Immunopathol* (2020) 230:110129. doi: 10.1016/j.vetimm.2020.110129

34. Vulliamy P, Gillespie S, Armstrong PC, Allan HE, Warner TD, Brohi K. Histone H4 induces platelet ballooning and microparticle release during trauma hemorrhage. *Proc Natl Acad Sci U.S.A.* (2019) 116(35):17444–9. doi: 10.1073/pnas.1904978116

35. Semeraro F, Ammollo CT, Morrissey JH, Dale GL, Friese P, Esmon NL, et al. Extracellular histones promote thrombin generation through platelet-dependent mechanisms: involvement of platelet TLR2 and TLR4. *Blood* (2011) 118(7):1952–61. doi: 10.1182/blood-2011-03-343061

36. Albert C, Zapf A, Haase M, Röver C, Pickering JW, Albert A, et al. Neutrophil gelatinase-associated lipocalin measured on clinical laboratory platforms for the prediction of acute kidney injury and the associated need for dialysis therapy: A systematic review and meta-analysis. *Am J Kidney Dis* (2020) 76(6):826–841.e1. doi: 10.1053/j.ajkd.2020.05.015

37. Cowland JB, Sørensen OE, Sehested M, Borregaard N. Neutrophil gelatinase-associated lipocalin is up-regulated in human epithelial cells by IL-1 beta, but not by TNF-alpha. *J Immunol* (2003) 171(12):6630–9. doi: 10.4049/jimmunol.171.12.6630

38. Hennessy EJ, Parker AE, O'Neill LAJ. Targeting toll-like receptors: emerging therapeutics? *Nat Rev Drug Discovery* (2010) 9(4):293–307. doi: 10.1038/nrd3203

39. Keshari RS, Silasi R, Popescu NI, Patel MM, Chaaban H, Lupu C, et al. Inhibition of complement C5 protects against organ failure and reduces mortality

in a baboon model of escherichia coli sepsis. *Proc Natl Acad Sci U.S.A.* (2017) 114 (31):E6390–9. doi: 10.1073/pnas.1706818114

40. Silasi-Mansat R, Zhu H, Popescu NI, Peer G, Sfyroera G, Magotti P, et al. Complement inhibition decreases the procoagulant response and confers organ protection in a baboon model of escherichia coli sepsis. *Blood* (2010) 116(6):1002–10. doi: 10.1182/blood-2010-02-269746

41. Keshari RS, Popescu NI, Silasi R, Regmi G, Lupu C, Simmons JH, et al. Complement C5 inhibition protects against hemolytic anemia and acute kidney injury in anthrax peptidoglycan-induced sepsis in baboons. *Proc Natl Acad Sci U.S.A.* (2021) 118(37):e2104347118. doi: 10.1073/pnas.2104347118

42. Thorgersen EB, Hellerud BC, Nielsen EW, Barratt-Due A, Fure H, Lindstad JK, et al. CD14 inhibition efficiently attenuates early inflammatory and hemostatic responses in escherichia coli sepsis in pigs. *FASEB J* (2010) 24(3):712–22. doi: 10.1096/fj.09-140798

43. Keshari RS, Silasi R, Popescu NI, Regmi G, Chaaban H, Lambris JD, et al. CD14 inhibition improves survival and attenuates thrombo-inflammation and cardiopulmonary dysfunction in a baboon model of escherichia coli sepsis. *J Thromb Haemost* (2021) 19(2):429–43. doi: 10.1111/jth.15162

44. Gentile LF, Cuenca AG, Efron PA, Ang D, Bihorac A, McKinley BA, et al. Persistent inflammation and immunosuppression: a common syndrome and new horizon for surgical intensive care. *J Trauma Acute Care Surg* (2012) 72(6):1491–501. doi: 10.1097/TA.0b013e318256e000

45. Carfì A, Bernabei R, Landi F. Gemelli against COVID-19 post-acute care study group. persistent symptoms in patients after acute COVID-19. *JAMA* (2020) 324(6):603–5. doi: 10.1001/jama.2020.12603

46. Bohnacker S, Hartung F, Henkel F, Quaranta A, Kolmert J, Priller A, et al. Mild COVID-19 imprints a long-term inflammatory eicosanoid- and chemokine memory in monocyte-derived macrophages. *Mucosal Immunol* (2022) 15(3):515–24. doi: 10.1038/s41385-021-00482-8

47. Pradhan K, Yi Z, Geng S, Li L. Development of exhausted memory monocytes and underlying mechanisms. *Front Immunol* (2021) 12:778830. doi: 10.3389/fimmu.2021.778830

48. Baudesson de Chanville C, Chousterman BG, Hamon P, Laviron M, Guillou N, Loyher PL, et al. Sepsis triggers a late expansion of functionally impaired tissue-vascular inflammatory monocytes during clinical recovery. *Front Immunol* (2020) 11:675. doi: 10.3389/fimmu.2020.00675

49. Herzig D, Fang G, Toliver-Kinsky TE, Guo Y, Bohannon J, Sherwood ER. STAT1-deficient mice are resistant to cecal ligation and puncture-induced septic shock. *Shock* (2012) 38(4):395–402. doi: 10.1097/SHK.0b013e318265a2ab

50. Feinberg MW, Cao Z, Wara AK, Lebedeva MA, Senbanerjee S, Jain MK. Kruppel-like factor 4 is a mediator of proinflammatory signaling in macrophages. *J Biol Chem* (2005) 280(46):38247–58. doi: 10.1074/jbc.M509378200

51. Toshchakov V, Jones BW, Perera PY, Thomas K, Cody MJ, Zhang S, et al. TLR4, but not TLR2, mediates IFN-beta-induced STAT1alpha/beta-dependent gene expression in macrophages. *Nat Immunol* (2002) 3(4):392–8. doi: 10.1038/ni774

52. Stack J, Doyle SL, Connolly DJ, Reinert LS, O'Keeffe KM, McLoughlin RM, et al. TRAM is required for TLR2 endosomal signaling to type I IFN induction. *J Immunol* (2014) 193(12):6090–102. doi: 10.4049/jimmunol.1401605

53. Naler LB, Hsieh YP, Geng S, Zhou Z, Li L, Lu C. Epigenomic and transcriptomic analyses reveal differences between low-grade inflammation and severe exhaustion in LPS-challenged murine monocytes. *Commun Biol* (2022) 5 (1):102. doi: 10.1038/s42003-022-03035-2

54. Risitano AM, Mastellos DC, Huber-Lang M, Yancopoulou D, Garlanda C, Ciceri F, et al. Complement as a target in COVID-19? *Nat Rev Immunol* (2020) 20 (6):343–4. doi: 10.1038/s41577-020-0320-7

55. Holter JC, Pischke SE, de Boer E, Lind A, Jenum S, Holten AR, et al. Systemic complement activation is associated with respiratory failure in COVID-19 hospitalized patients. *Proc Natl Acad Sci U.S.A.* (2020) 117(40):25018–25. doi: 10.1073/pnas.2010540117

56. Brohi K, Singh J, Heron M, Coats T. Acute traumatic coagulopathy. *J Trauma* (2003) 54(6):1127–30. doi: 10.1097/01.TA.0000069184.82147.06

57. Maegele M, Lefering R, Yucel N, Tjardes T, Rixen D, Paffrath T, et al. Early coagulopathy in multiple injury: an analysis from the German trauma registry on 8724 patients. *Injury* (2007) 38(3):298–304. doi: 10.1016/j.injury.2006.10.003

58. Cabrera CP, Manson J, Shepherd JM, Torrance HD, Watson D, Longhi MP, et al. Signatures of inflammation and impending multiple organ dysfunction in the hyperacute phase of trauma: A prospective cohort study. *PloS Med* (2017) 14(7): e1002352. doi: 10.1371/journal.pmed.1002352

59. Mollnes TE, Huber-Lang M. Complement in sepsis-when science meets clinics. *FEBS Lett* (2020) 594(16):2621–32. doi: 10.1002/1873-3468.13881

frontiers | Frontiers in Immunology

TYPE Original Research
PUBLISHED 05 September 2022
DOI 10.3389/fimmu.2022.895888

OPEN ACCESS

EDITED BY
Tom E. Mollnes,
University of Oslo, Norway

REVIEWED BY
Kyuseok Kim,
CHA University, South Korea
Kai O. Böker,
Department of Trauma Surgery, Orthopaedics and Plastic Surgery, University Medical Center Göttingen, Germany

*CORRESPONDENCE
Miriam Kalbitz
miriam.kalbitz@uk-erlangen.de

SPECIALTY SECTION
This article was submitted to Inflammation, a section of the journal Frontiers in Immunology

RECEIVED 14 March 2022
ACCEPTED 08 August 2022
PUBLISHED 05 September 2022

CITATION
Lackner I, Weber B, Pressmar J, Odwarka A, Lam C, Haffner-Luntzer M, Marcucio R, Miclau T and Kalbitz M (2022) Cardiac alterations following experimental hip fracture - inflammaging as independent risk factor. *Front. Immunol.* 13:895888. doi: 10.3389/fimmu.2022.895888

Cardiac alterations following experimental hip fracture - inflammaging as independent risk factor

Ina Lackner[1,2], Birte Weber[2,3,4], Jochen Pressmar[1,2], Anna Odwarka[2], Charles Lam[3], Melanie Haffner-Luntzer[3,5], Ralph Marcucio[3], Theodore Miclau[3] and Miriam Kalbitz[1,2,3]*

[1]Department of Trauma and Orthopedic Surgery, University Hospital Erlangen, Friedrich-Alexander University Erlangen-Nuremberg, Erlangen, Germany, [2]Department of Traumatology, Hand, Plastic, and Reconstructive Surgery, University Medical Center Ulm, Ulm, Germany, [3]Department of Orthopaedic Surgery, Orthopaedic Trauma Institute, Zuckerberg San Francisco General Hospital, University of California, San Francisco, San Francisco, CA, United States, [4]Department of Trauma, Hand and Reconstructive Surgery, Goethe University of Frankfurt, Frankfurt, Germany, [5]Institute of Orthopaedic Research and Biomechanics, University Medical Center Ulm, Ulm, Germany

Background: Cardiac injuries following trauma are associated with a worse clinical outcome. So-called trauma-induced secondary cardiac injuries have been recently described after experimental long bone fracture even in absence of direct heart damage. With the progressive aging of our society, the number of elderly trauma victims rises and therefore the incidence of hip fractures increases. Hip fractures were previously shown to be associated with adverse cardiac events in elderly individuals, which have mainly been attributed to pre-conditioned cardiac diseases. The aim of the present study was to investigate the effect of hip fractures on the heart in healthy young and middle-aged mice.

Materials and Methods: Young (12-week-old) and middle-aged (52-week-old) female C57BL/6 mice either received an intramedullary stabilized proximal femur fracture or sham treatment. The observation time points included 6 and 24 h. Systemic levels of pro-inflammatory mediators as well as local inflammation and alterations in myocardial structure, metabolism and calcium homeostasis in left ventricular tissue was analyzed following hip fracture by multiplex analysis, RT-qPCR and immunohistochemistry.

Results: After hip fracture young and middle-aged mice showed increased systemic IL-6 and KC levels, which were significantly elevated in the middle-aged animals. Furthermore, the middle-aged mice showed enhanced myocardial expression of HMGB1, TLR2/4, TNF, IL1β and NLRP3 as well as considerable alterations in the myocardial expression of glucose- and fatty acid transporters (HFABP, GLUT4), calcium homeostasis proteins (SERCA) and cardiac structure proteins (desmin, troponin I) compared to the young animals following hip fracture.

Conclusion: Young and middle-aged mice showed local myocardial alterations, which might predispose for the development of secondary cardiac injury following hip fracture. Age and the age-associated phenomenon of 'inflammaging' seemed to be an independent risk factor aggravating and accelerating cardiac alterations following hip fracture.

KEYWORDS

proximal femur fracture, hip fracture, secondary cardiac injury, cardiac inflammation, cardiac structure, inflammaging

Introduction

Worldwide, trauma is the leading cause of death and disability within the young population (1, 2). Blunt cardiac injuries following severe trauma were shown to be an independent predictor for a worse clinical outcome and where primarily linked to blunt mechanical myocardial damage (3, 4). Moreover, so-called trauma-induced secondary cardiac injuries (TISCI) have also been described even in absence of direct mechanical heart damage, correlating with long-term morbidity and mortality of the patients (5–7). Trauma-induced secondary cardiac injuries imply the clinical occurrence of adverse cardiac events such as acute coronary syndrome, atrial fibrillation, myocardial depression and ventricular arrhythmia in severely injured patients without mechanical heart damage and are characterized by elevated systemic levels of troponin I and heart fatty acid binding protein (HFABP) (5–7). The development of these secondary cardiac injuries is mostly linked to an exuberant systemic inflammatory response following trauma (5–7).

Recently, our group described secondary cardiac injuries after experimental long bone fracture (8–10). In these studies, pigs showed an impaired cardiac function and valvular insufficiencies 6 h following femur fracture, which was primarily linked to an increased systemic but also local cardiac inflammation, all of which was further observed in mice with isolated diaphyseal femur or tibia fracture (8–10). Cardiac inflammation following bone fracture was mediated *via* damage-associated molecular patterns (DAMPs), toll-like receptor (TLR) signaling as well as by the activation of the complement system and the NLR-pyrin domain containing protein 3 (NLRP3) inflammasome (8–10). Besides inflammation, alterations in cardiac structure, metabolism and calcium handling proteins were considered to contribute to the development of secondary cardiac injuries following long bone fracture (8–10).

With the progressive aging of our society, the number of elderly trauma victims rises correspondingly (11). As a consequence, the incidence of hip fractures increases rapidly (12) and the number of these fractures is expected to reach 4.5 million by the year 2050 (13). Hip fractures primarily occur in elderly individuals aged 70-80 years with low bone mass and are associated with a long-term morbidity and increased mortality. Moreover, distinct age-related co-morbidities were shown to be independent risk factors in elderly hip fracture patients, increasing their in-hospital mortality 3-fold following hip fracture (14). Amongst others, these age-related co-morbidities included several cardiovascular diseases and their development was shown to accelerate with increased aging (15). With respect to secondary cardiac injury, a clinical study showed electrocardiographic abnormalities in patients with traumatic hip fractures, such as atrial fibrillation, abnormal QTc prolongation, sinus tachycardia and sinus bradycardia compared to patients with non-traumatic hip surgery (16). Another clinical study demonstrated the development of major cardiac events (all-cause deaths, heart failure, new-onset atrial fibrillation, myocardial infarction, and cardiovascular re-hospitalization) in elderly patients within 90 days following hip fracture (17). In this study, the patients' age correlated with systemic levels of troponin and brain natriuretic peptide, with reduced ejection fraction and with other major adverse cardiac events (17). In earlier clinical studies, the occurrence of coronary heart disease was shown to be two times more frequent in patients with hip fracture compared to healthy controls (18, 19). However, in all of the above-mentioned studies, the majority of patients suffered from pre-conditioned cardiac diseases such as myocardial infarction and congestive heart failure (16). It was further shown that pre-conditioned cardiac diseases and impaired cardiac function such as a 50% reduced left ventricular ejection fraction (LVEF), increase the occurrence of major adverse cardiac events following hip fracture in elderly individuals and were therefore considered as independent risk factors for a worse clinical outcome in these patients (17, 20, 21). Additionally, age >75 years appeared to be another independent risk factor for an increased mortality (20, 22) but also for the occurrence of major adverse cardiac events following hip fracture (17).

Additionally, several clinical studies showed an increased systemic inflammatory response following hip fracture in elderly

individuals, which was also associated with an increased mortality rate (23). Other studies demonstrated enhanced susceptibility to infections post hip fracture surgery, which was linked to a dysregulated immune response in the elderly patients (24), correlating also with an increased mortality (25).

In conclusion, these clinical studies showed that age is an independent risk factor for an increased mortality following hip fracture in the elderly and that pre-conditioned cardiac diseases aggravate this pathologic condition. With respect to secondary cardiac injury, the occurrence of major cardiac events following hip fracture was mostly linked to pre-conditioned cardiac diseases in combination with an advanced age of the patients. So far, it is unknown whether hip fractures induce myocardial damage in younger individuals, resulting in the pathologic condition of secondary cardiac injuries. Moreover, it remains to be clarified whether age is an independent risk factor aggravating secondary cardiac injuries following hip fracture in absence of pre-conditioned cardiac diseases.

Therefore, we investigated in the present study whether hip fractures induce cardiac inflammation and cardiac alterations in young female mice and whether advanced age is an independent risk factor aggravating these pathologic conditions.

Materials and methods

Animals and experimental design

The animal experiments were conducted in collaboration with the University of California (UCSF), San Francisco Orthopaedic Trauma Institute, San Francisco, California, USA. All animal experiments were approved by the local animal welfare committee (IACUC UCSF AN143402-03B) and were performed in accordance with the international regulations for laboratory animal welfare and handling (ARRIVE guidelines). For the present study, 48 female C57BL/6J mice (The Jackson Laboratory) were used in total. The mice were further divided into two age groups. Twenty-four mice with an age between 10-12 weeks (young) and 24 mice with an age between 52-54 (middle-aged) weeks were used for the experiments. We defined the age of the mice according to the guideline by Jackson Laboratories (https://www.jax.org/research-and-faculty/research-labs/the-harrison-lab/gerontology/life-span-as-a-biomarker). Therefore, 3 months old mice were considered as young mice and 12 months old mice were considered as middle-aged mice (see also Flurkey, K; Currer, J M.; and Harrison, D E., "Mouse models in aging research." (2007). *Faculty Research 2000 - 2009*. 1685.)

Twelve mice of each age group (n=12 young, n=12 middle-aged) received an experimental proximal femur fracture, stabilized by an intramedullary nail, as described previously (26). Control animals of each age group (n=12 young, n=12 middle-aged) underwent sham procedure, including analgesia and anesthesia but without surgical procedure. The animals of each age and treatment group were further randomized into two observation periods of 6 and 24 h, with n=6 animals in each group. Therefore, the following experimental groups were analyzed in the present study: 12-week-old mice after 6 h with proximal femur fracture (n=6) or sham procedure (n=6) and after 24 h with proximal femur fracture (n=6) or sham procedure (n=6). Fifty-two-week-old mice after 6 h with proximal femur fracture (n=6) or sham procedure (n=6) and after 24 h with proximal femur fracture (n=6) or sham procedure (n=6).

Surgical procedure

The surgical procedure was conducted under general anesthesia, using 50 mg/kg ketamine hydrochloride (Henry Schein Animal Health 100 mg/ml) at a ratio of 1:1 with dexmedetomidine hydrochloride (Orion pharma, 0.5 mg/ml) and analgesia, using 0.05 mg/kg buprenorphine (0.03 mg/ml, injection every 6 hours). The experimental proximal femur fracture was applied as described previously (26). Briefly, a 24G cannula was introduced retrograde into the right femur to stabilize the fracture. Afterwards, a 0.5 cm skin incision was made along the femur. The femoral muscles were separated bluntly. Free access to the proximal femur bone was achieved by cutting the tendon insertion at the third trochanter. With a Gigli wire saw of 0.44 mm diameter, an osteotomy was induced between the third and the lesser trochanters, producing an intertrochanteric proximal femur fracture. Afterwards, the muscles were sutured with a Vicryl 5-0 suture. The skin was closed using a non-absorbable Resolon 5-0 suture. After the experimental procedure, mice were allowed to awake and to move freely directly after surgery. The animals were monitored over the entire observation period. After the respective observation periods of 6 and 24 h, the animals were euthanized by using carbon dioxide.

Sample collection

After the follow-up period of either 6 h or 24 h, mice were euthanized using carbon dioxide. Whole blood was taken immediately after euthanasia by cardiac puncture. Plasma samples were collected after centrifugation with 5 min (800 × *g*, 4 °C) and a second centrifugation step for 2 min (13000 × *g*, 4 °C). The plasma samples were stored at −80 °C until analysis. Samples of left ventricular cardiac tissue were taken immediately after euthanasia and either quick-frozen in liquid nitrogen or fixed in 4% paraformaldehyde for 48 h.

Multiplex analysis

To analyze the systemic inflammation after proximal femur fracture in adult and middle-aged mice, a murine ProcartaPlex Immunoassay (ThermoFisher Scientific, Waltham, MA, USA) was used and systemic levels of interleukin-6 (IL-6), keratinocyte chemoattractant (KC) and interferon gamma (IFNγ) were determined in the plasma of the mice. All procedures were performed according to manufacturer's instructions.

Immunohistochemistry (IHC) and immunofluorescence (IF)

For immunohistochemical and immunofluorescence analysis, formalin-fixed and paraffin-embedded tissue sections of the left ventricle were used. Left ventricular tissue sections were dewaxed and rehydrated. Antigen unmasking was performed by boiling the tissue sections in 10 mM citrate buffer (pH 6) at 100°C. Non-specific binding sides were blocked by 10% goat serum. Specific antigen binding was performed by incubating the tissue sections with the respective primary antibodies for C3a receptor (Bioss, Woburn, MA, USA), glutathione peroxidase 4 (GSH) (abcam, Cambridge, UK), High-mobility group box 1 (HMGB1) protein (abcam, Cambridge, UK), desmin (GeneTex, Irvine, CA, USA), α-actinin (GeneTex, Irvine, CA, USA), nitrotyrosine (Merck, Darmstadt, Germany), superoxide dismutase (SOD) (abcam, Cambridge, UK), troponin I (abcam, Cambridge, UK) and tumor necrosis factor (TNF) (abcam, Cambridge, UK) for overnight at 4°C. For immunohistochemical (IHC) staining, a biotin-labelled secondary antibody was used for the detection of specific antibody binding (ThermoFisher, Waltham, MA, USA). Signal amplification was performed by using VECTASTAIN® ABC HRP Kit (Vector Laboratories Inc., Burlingame, CA, USA). Signal development was conducted by using VECTOR® NovaRED™ Peroxidase (HRP) Substrate Kit (Vector Laboratories Inc., Burlingame, CA, USA). Cell nuclei were counterstained with Hematoxylin according to Mayer. For immunofluorescence (IF), an AlexaFluor488®-labelled or an AlexaFluor®647-labelled secondary antibody were used for the detection of specific antibody binding (Jackson ImmunoResearch Laboratories, Inc., West Grove, PA, USA). Cell nuclei were counterstained with Hoechst33342 (ThermoFisher, Waltham, MA, USA). The sections were investigated by bright field microscopy or by fluorescence microscopy using an Axio Imager M.2 microscope (Zeiss, Jena, Germany). To quantify epitope expression, imaging of three distinct, representative fields of view (40x magnification) were examined for each animal. For quantification of immunohistochemical and immunofluorescent staining, the ZEN 2.3 software (Zeiss, Jena, Germany) was used. For imaging, the ZEN 2.3 software was used. Prior to imaging, the optimal exposure time for the respective antibody staining was determined and standardized for the ZEN 2.3 software, to get an optimal image of each stained section. For analysis of protein expression, a specific threshold for pixel density or fluorescence intensity was manually determined and standardized for each antibody staining (C3aR, HMGB1, TNF, nitrotyrosine, SOD, GSH, desmin, α-actinin, troponin I) prior to the quantification. With the ZEN 2.3 software, each picture was analyzed independently with respect to the defined threshold for pixel density or fluorescence intensity. For each picture a specific mean value of pixel density (IHC) or fluorescence intensity (IF) was calculated by the software. Results are presented as mean pixel density (IHC) or mean fluorescence intensity (IF).

Hematoxylin and eosin (H.E.) staining

Formalin-fixed and paraffin embedded tissue sections from left ventricles were used. Tissue sections were dewaxed and rehydrated. Myocardial tissue sections were stained with hematoxylin & eosin staining kit (Morphisto, Frankfurt am Main, Germany). For quantification of myocardial damage, a heart injury score was defined as described previously (27, 28). For determination of the heart injury score, the H.E. sections of myocardial tissue were scored for 1) apoptosis, 2) contraction band necrosis, 3) neutrophil infiltration, 4) intramuscular bleeding, 5) rupture, 6) edema and 7) ischemia.

RNA isolation

RNA was extracted from quick-frozen left ventricular tissue of the mice left ventricle. For this procedure 50 mg of quick-frozen left ventricular tissue was added to 1 ml of Invitrogen TRIzol Reagent (Sigma-Aldrich, St. Louis, MO, USA) and was then homogenized. Left ventricular tissue mRNA was further extracted by using chloroform and purified by using ethanol. mRNA quantity and purity were determined by using Tecan Spark® reader (Tecan Group, Männedorf, Switzerland) and mRNA purity was defined by 260/280 nm ratio.

Reverse transcribed quantitative polymerase chain reaction (RT-qPCR)

The respective RNA samples were reverse transcribed in cDNA using SuperScript™ IV VILO™ MasterMix with ezDNAse (Invitrogen, Carlsbad, CA, USA). For quantitative PCR, the PowerUp™ SYBR™ Green Master Mix (Applied Biosystems, Waltham, MA, USA) was used. For the reverse cDNA transcription, 200 ng of mRNA were used. Then, 20 ng of

cDNA were used for the qPCR. All procedures were performed according to the manufacturer's instructions. For qPCR the QuantStudio3 system (Applied Biosystems, Waltham, MA, USA) was utilized. Quantitative mRNA expression of murine atrial natriuretic peptide (ANP), brain natriuretic peptide (BNP), C3a receptor (C3aR), C5a receptor 1 (C5aR1), fibroblast growth factor 23 (FGF23), glucose transporter 4 (GLUT4), heart fatty acid binding protein (HFABP), interleukin-1β (IL-1β), toll-like receptor (TLR) 2, TLR4, TLR9, tumor necrosis factor (TNF), NLR family pyrin domain containing 3 (NLRP3), sarcoplasmic/endoplasmic reticulum ATPase (SERCA) and troponin I was examined and calculated by the cycle threshold method ΔΔCt. Respective genes were normalized using housekeeping gene glutaraldehyde-phosphate dehydrogenase (GAPDH). Results are presented as mean fold change. The primer sequences of used primers are listed in Table 1.

TABLE 1 Primer sequences.

Gene	Primer sequence
Atrial natriuretic peptide (ANP)	for: 5'-TCCAGGCCATATTGGAGCAA-3' rev: 5'-GTGGTCTAGCAGGTTCTTGAAAT-3'
Brain natriuretic peptide (BNP)	for: 5'-AGCTGCTTTGGGCACAAGATA-3' rev: 5'-CAACAACTTCAGTGCGTTACAG-3'
C3a receptor (C3aR)	for: 5'-CATCGAAACGTGAGAACCGC-3' rev: 5'-CGGGCACACACATCACAAAG-3'
C5a receptor 1 (C5aR1)	for: 5'-CCAGGACATGGACCCCATAG-3' rev: 5'-ATGCCATCCGCAGGTATGTT-3'
Fibroblast growth factor 23 (FGF23)	for: 5'-CAGGAGCCATGACTCGAAGG-3' rev: 5'-CTGGGCTGAAGTGAAGCGAT-3'
Glucose transporter 4 (GLUT4)	for: 5'-TTATTGCAGCGCCTGAGTCT-3' rev: 5'-GGGTTCCCCATCGTCAGAG-3')
Glutaraldehyde-phosphate dehydrogenase (GAPDH)	for: 5'-CTTCAACAGCAACTCCCACTCTTCC-3' rev: 5'-GGTGGTCCAGGGTTTCTTACTCC-3'
Heart fatty acid binding protein (HFABP)	for: 5'-TGACCGGAAGGTCAAGTCAC-3' rev: 5'-TTAGTGTTGTCTCCTGCCCG-3
Interleukin-1β (IL-1β)	for: 5'-GCCACCTTTTGACAGTGATGAG-3' rev: 5'-TGACAGCCCAGGTCAAAGGTT-3'
NLR family pyrin domain containing 3 (NLRP3)	for: 5'-GCTGCTCAGCTCTGACCTCT-3' rev: 5'-AGGTGAGGCTGCAGTTGTCT-3'
Sarcoplasmic/endoplasmic reticulum ATPase (SERCA)	for: 5'-TACCTGGAACAACCCGCAAT-3' rev: 5'-CTAACAACGCACATGCACGC-3'
Toll-like receptor 2 (TLR2)	for: 5'-GAAACCTCAGACAAAGCGTCA-3' rev: 5'-ACAGCGTTTGCTGAAGAGGA-3'
Toll-like receptor 4 (TLR4)	for: 5'-GGACTCTGATCATGGCACTGT-3' rev: 5'-GGAACTACCTCTATGCAGGGAT-3'
Toll-like receptor 9 (TLR9)	for: 5'-GAGAGACCCTGGTGTGGAAC-3' rev: 5'-CCTTCGACGGAGAACCATGT-3'

(Continued)

Statistical analysis

Data were analyzed by using the GraphPad Prism 9.0 software (GraphPad Software, Inc., San Diego, CA, USA). The data were analyzed for normal distribution by using the Shapiro-Wilk test. Unless otherwise indicated, the data were distributed normally. In case of two groups (IHC and IF experiments), data were then analyzed by non-paired student t-test. In case of three or more groups (multiplex and RT-qPCR experiments), data were then analyzed by 2-way Analysis of Variance (ANOVA), followed by Sidak's multiple comparison test. All values are expressed as mean ± SEM. $p \leq 0.05$ was considered as statistically significant. Furthermore, linear regression analysis was performed between the young and the middle-aged animals at the respective time points. The goodness of fit was indicated as R^2.

Results

Systemic inflammation

IL-6, KC and IFNγ

First, we analyzed the systemic levels of specific pro-inflammatory mediators in young and middle-aged mice 6 and 24 h after experimental proximal femur fracture or sham treatment. After 6 and 24 h, the systemic levels of interleukin 6 (IL-6) were significantly elevated in the fractured young as well as in the middle-aged mice, compared to their respective sham control groups (Figure 1A). Furthermore, the systemic IL-6 levels dropped 24 h after fracture compared to 6 h in the respective age groups (Figure 1A). When comparing both age groups, the 52-week-old

TABLE 1 Continued

Gene	Primer sequence
Troponin I	for: 5‘-GATGCGGCTGGGGAACC-3‘ rev: 5‘-ACTTTTTCTTGGCGTGTGGC-3‘
Tumor necrosis factor (TNF)	for: 5‘-GAGAGACCCTGGTGTGGAAC-3‘ rev: 5‘-CCTTCGACGGAGAACCATGT-3‘

Fibroblast growth factor 23 (FGF23) (5’-CAGGAGCCATGACTCGAAGG-3’; 5’-CTGGGCTGAAGTGAAGCGAT-3‘).

mice showed significant higher IL-6 levels 6 and 24 h following fracture, compared to the 12-week-old mice (Figure 1A). Moreover, the middle-aged mice showed enhanced systemic IL-6 levels and a positive linear regression of systemic IL-6 levels 6 h ($R^2 = 0.76$) and 24 h ($R^2 = 0.85$) following hip fracture (Supplemental Figure 2A). Besides systemic IL-6, the systemic levels of keratinocyte chemoattractant (KC) were significantly elevated 6 h after fracture in both age groups, compared to their respective controls (Figure 1B). Furthermore, the systemic KC levels dropped significantly 24 h after fracture compared to 6 h in the young mice, but not in middle-aged animals (Figure 1B). However, in the middle-aged group the systemic KC levels also generally decreased 24 h following fracture compared to 6 h (Figure 1B). Moreover, the systemic levels of interferon gamma (IFNγ) were elevated in the 52-week-old animals 6 and 24 h following fracture compared to the 12-week-old animals (Figure 1C). Therefore, the mice showed increased systemic inflammation 6 and 24 h after proximal femur fracture, which seemed to be enhanced in the middle-aged group.

Cardiac inflammation

HMGB1 and TLR signaling

We further analyzed local cardiac inflammation. We first focused on damage-associated molecular patterns (DAMPs) and toll-like receptor (TLR) signaling. In the 52-week-old mice, the high-mobility group box 1 (HMGB1) protein expression significantly decreased 6 h following fracture but significantly increased after 24 h compared to their respective control groups (Figure 2A). With respect to TLR signaling, the TLR4 mRNA expression was significantly higher 24 h after fracture compared to 6 h in the middle-aged group (Figure 2B). When comparing both age groups, the TLR4 mRNA expression was significantly higher 24 h after fracture in the middle-aged animals compared

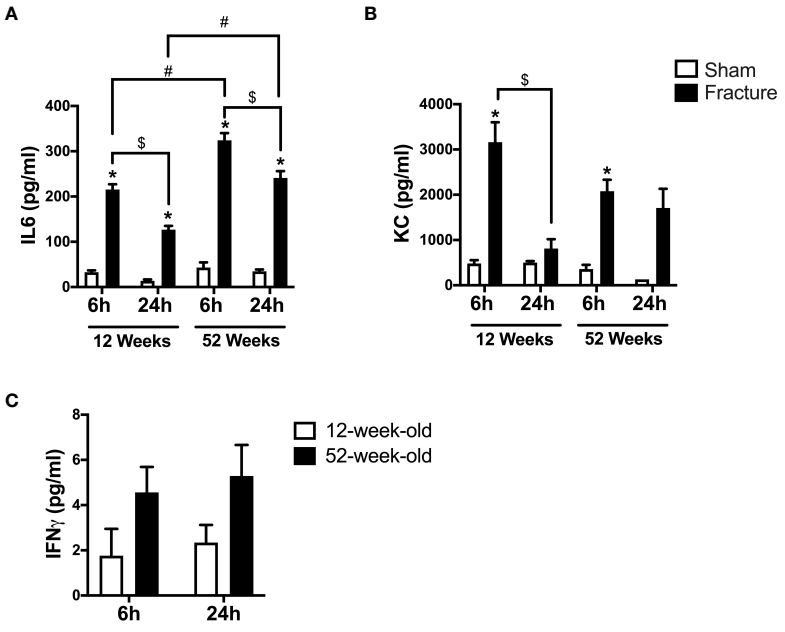

FIGURE 1
Systemic inflammation 6 and 24 h after proximal femur fracture in young and middle-aged mice. Young (12-week-old) and middle-aged (52-week-old) female mice received either sham treatment (white bars) or experimental proximal femur fracture (black bars). Blood plasma was analyzed 6 and 24 h following sham treatment or proximal femur fracture. Systemic levels of interleukin-6 (IL-6) in pg/ml **(A)**, keratinocyte chemoattractant (KC) in pg/ml **(B)** and interferon gamma (IFNγ) in pg/ml **(C)**. Data are presented as mean ± SEM. $p \leq 0.05$ was considered as statistically significant. *$p \leq 0.05$ sham vs. fracture. $$p \leq 0.05$ 6 vs. 24 h after fracture within one age group. #$p \leq 0.05$ 6 vs. 6h and 24 vs. 24 h between two age groups.

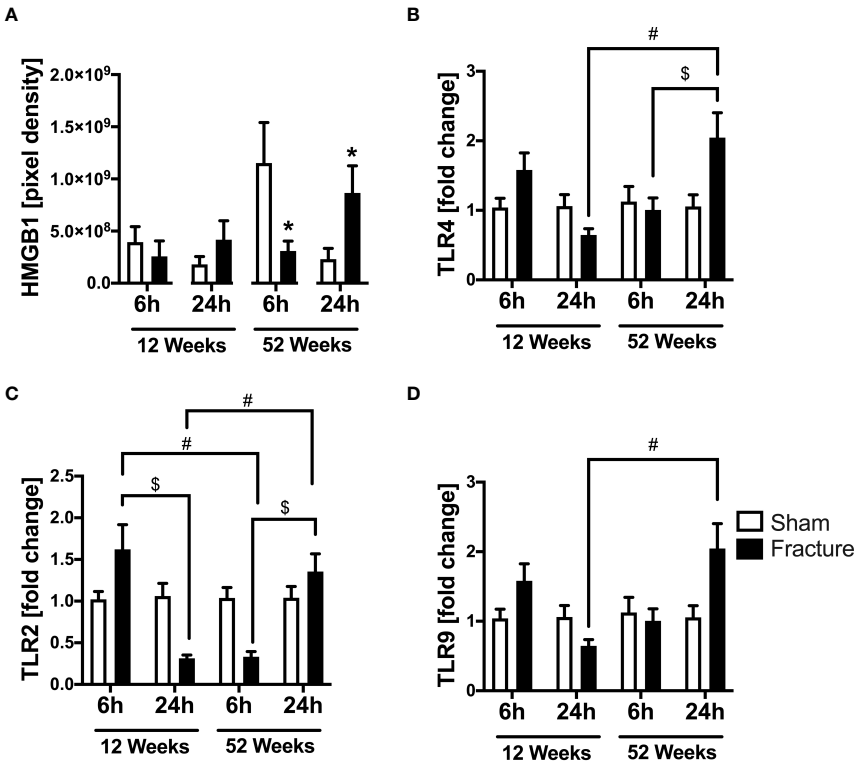

FIGURE 2
Toll-like receptor mediated cardiac inflammation 6 and 24 h after proximal femur fracture in young and middle-aged mice. Young (12-week-old) and middle-aged (52-week-old) female mice received either sham treatment (white bars) or experimental proximal femur fracture (black bars). Left ventricular cardiac tissue was analyzed 6 and 24 h following sham treatment or proximal femur fracture. Local protein expression of high-mobility group box 1 (HMGB1) protein in pixel density **(A)**, mRNA expression of toll-like receptor 4 (TLR4) in fold change **(B)**, mRNA expression of toll-like receptor 2 (TLR2) in fold change **(C)** and mRNA expression of toll-like receptor 9 (TLR9) in fold change **(D)**. Data are presented as mean ± SEM. *p ≤ 0.05 was considered as statistically significant. p ≤ 0.05 sham vs. fracture. $p ≤ 0.05 6 vs. 24 h after fracture within one age group. #p ≤ 0.05 6 vs. 6h and 24 vs. 24 h between two age groups.

to the young animals (Figure 2B). Regarding the TLR2 mRNA expression, the TLR2 mRNA expression was significantly lower 24 h after fracture compared to 6 h in the young group (Figure 2C). In contrast, the TLR2 mRNA expression was significantly higher 24 h following fracture compared to 6 h in the middle-aged group (Figure 2C). When comparing young and middle-aged mice, the TLR2 mRNA expression was significantly lower 6 h following fracture in the middle-aged mice but was significantly higher after 24 h in the middle-aged group when compared to the young animals (Figure 2C). The TLR9 mRNA expression was significantly higher 24 h after fracture in the middle-aged mice compared to young mice (Figure 2D). Additionally, the middle-aged mice showed enhanced levels and a positive linear regression of TLR2 (R^2 = 0.70), TLR4 (R^2= 0.69) and TLR9 (R^2 = 0.53) mRNA expression 24 h following hip fracture (Supplemental Figures 2B–D). Therefore, it seems like hip fracture alters local expression of TLRs in an age-dependent manner with highest expression levels 24h after fracture in middle-aged mice.

Complement system

We analyzed further inflammatory pathways in ventricular tissue. With respect to the complement system, the C3a receptor (C3aR) protein expression was significantly enhanced 6 h after fracture in the young and 24 h after fracture in the middle-aged mice, compared to their respective control groups (Figure 3A). The C3aR mRNA expression did not differ between the respective groups (Figure 3B). The C5a receptor 1 (C5aR1) mRNA expression was significantly reduced 24 h after fracture compared to 6 h in the 12-week-old mice (Figure 3C). Also, the C5aR1 mRNA expression was significantly lower 6 h after fracture in the middle-aged mice compared to the young mice (Figure 3C).

TNF and IL-1β

Regarding pro-inflammatory cytokines, the tumor necrosis factor (TNF) mRNA expression was significantly reduced 24 h after fracture in the young mice compared to sham (Figure 3D). When comparing the two age groups, the TNF mRNA

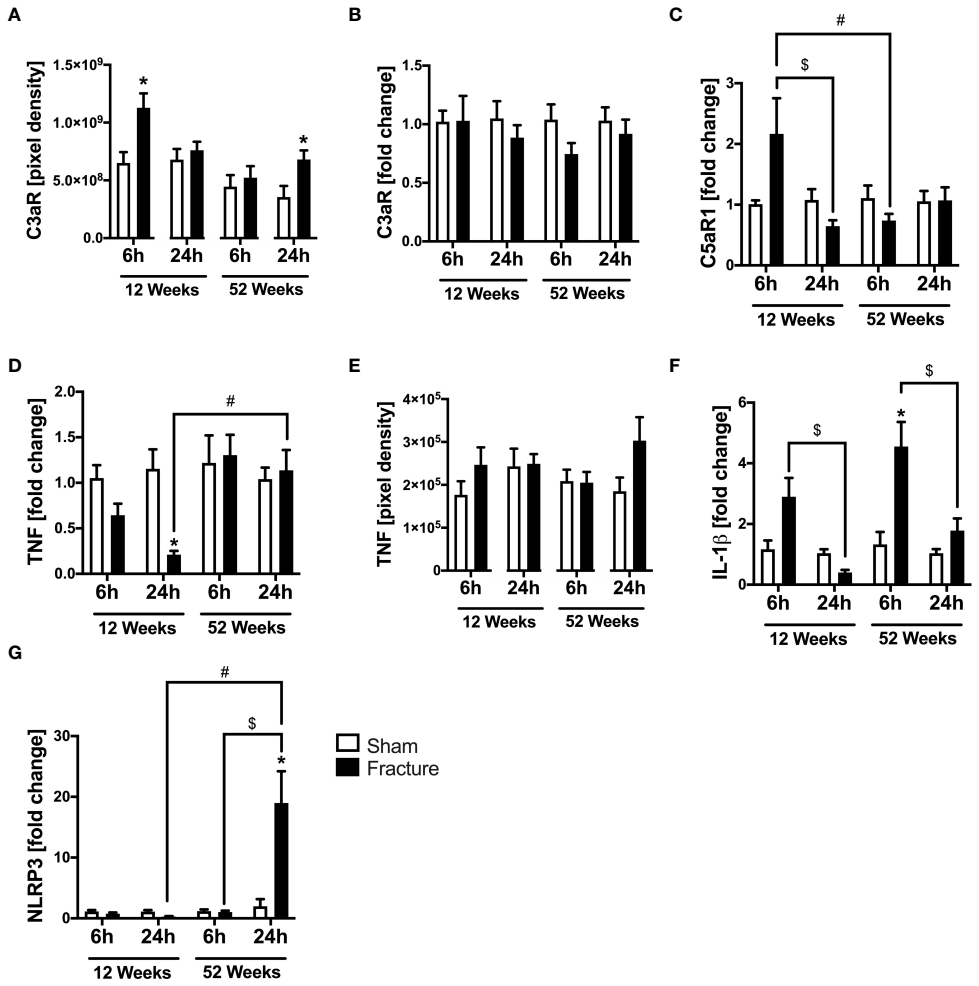

FIGURE 3
Complement system and cytokines mediated cardiac inflammation 6 and 24 h after proximal femur fracture in young and middle-aged mice. Young (12-week-old) and middle-aged (52-week-old) female mice received either sham treatment (white bars) or experimental proximal femur fracture (black bars). Left ventricular cardiac tissue was analyzed 6 and 24 h following sham treatment or proximal femur fracture. Local protein expression of C3a receptor (C3aR) in pixel density **(A)**, mRNA expression of C3a receptor (C3aR) in fold change **(B)**, mRNA expression of C5a receptor 1 (C5aR1) in fold change **(C)**, mRNA expression of tumor necrosis factor (TNF) in fold change **(D)**, protein expression of tumor necrosis factor (TNF) in pixel density **(E)**, mRNA expression of interleukin-1β (IL-1β) in fold change **(F)** and mRNA expression of NLR pyrin domain containing protein 3 (NLRP3) in fold change **(G)**. Data are presented as mean ± SEM. $p \leq 0.05$ was considered as statistically significant. *$p \leq 0.05$ sham vs. fracture. $$p \leq 0.05$ 6 vs. 24 h after fracture within one age group. #$p \leq 0.05$ 6 vs. 6h and 24 vs. 24 h between two age groups.

expression was significantly higher 24 h after fracture in the middle-aged group compared to the young group (Figure 3D). The myocardial TNF protein expression was slightly elevated in the 12-week-old group 6 h after fracture and in the 52-week-old group 24 h after fracture (Figure 3E). The interleukin-1β (IL-1β) mRNA expression was significantly elevated 6 h after fracture in the middle-aged group only compared to sham (Figure 3F) and dropped at 24 h compared to 6 h in the respective age groups (Figure 3F). Moreover, the middle-aged mice showed elevated levels and a positive linear expression of TNF ($R^2 = 0.63$) and IL-1β ($R^2 = 0.53$) mRNA expression 24 h following hip fracture (Supplemental Figures 2E, G).

NLRP3 inflammasome

The NLR pyrin domain containing 3 protein (NLRP3) mRNA expression significantly increased 24 h after fracture in the middle-aged group compared to sham and was also significantly higher compared to 6 h after fracture (Figure 3G). Likewise, the NLRP3 mRNA expression was significantly higher 24 h after fracture in the middle-aged group compared to the young animals (Figure 3G). These data indicate a distinct regulation of inflammatory genes in the heart after hip fracture which might be age-related. The most striking finding is the over 10-fold increase in NLRP3 gene expression 24 h after fracture in the middle-aged mice. Moreover, there were elevated

levels and a positive regression of NLRP3 (R^2 = 0.56) mRNA expression 24 h following hip fracture in the 52-week-old animals (Supplemental Figure 2F).

Cardiac metabolism, oxidative system and calcium handling

HFABP and GLUT4

We further investigated alterations in cardiac metabolism and calcium handling, since these might be caused by enhanced inflammation. With respect to cardiac fatty acid metabolism, the mRNA expression of heart fatty acid binding protein (HFABP) was significantly elevated 6 h following fracture in the young mice compared to sham (Figure 4A). Further, the HFABP mRNA expression was significantly lower 24 h after fracture compared to 6 h in the young mice (Figure 4A). When comparing the young and the middle-aged group, the HFABP mRNA expression was significantly lower 6 h following fracture in the middle-aged group (Figure 4A). The systemic HFABP levels slightly decreased in the middle-aged animals 6 and 24 h following hip fracture (Figure 4B). Regarding the cardiac glucose metabolism, the glucose transporter 4 (GLUT4) mRNA expression was significantly reduced 24 h after fracture compared to sham in both age groups (Figure 4C). Additionally, the GLUT4 mRNA expression was significantly lower after 24 h in the middle-aged group compared to 6 h (Figure 4C).

SERCA

For myocardial calcium handling, the mRNA expression of SERCA significantly increased 24 h following fracture compared to sham in the middle-aged mice (Figure 4D). In the 12-week-old group, the SERCA mRNA expression was significantly lower after 24 h compared to 6 h, whereas in the 52-week-old group the SERCA mRNA expression was significantly higher 24 h

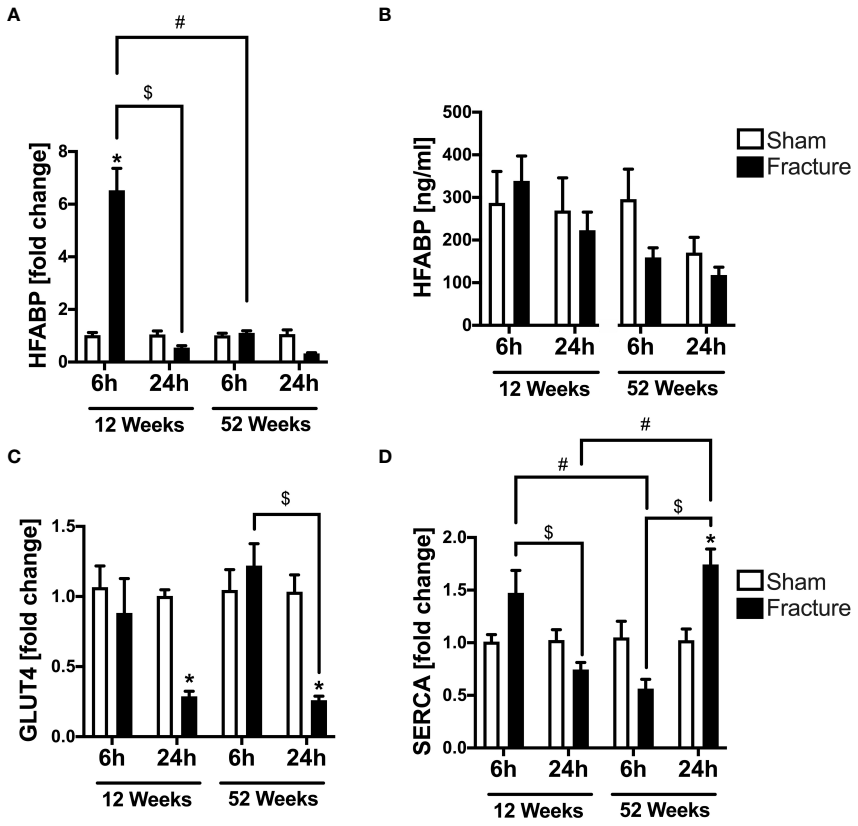

FIGURE 4
Cardiac alterations in metabolism and calcium handling 6 and 24 h after proximal femur fracture in young and middle-aged mice. Young (12-week-old) and middle-aged (52-week-old) female mice received either sham treatment (white bars) or experimental proximal femur fracture (black bars). Left ventricular cardiac tissue was analyzed 6 and 24 h following sham treatment or proximal femur fracture. Local mRNA expression of heart fatty acid binding protein (HFABP) in fold change **(A)**, systemic levels of heart fatty acid binding protein (HFABP) in ng/ml **(B)**, mRNA expression of glucose transporter 4 (GLUT4) in fold change **(C)** and mRNA expression of sarcoplasmic/endoplasmic reticulum ATPase (SERCA) in fold change **(D)**. Data are presented as mean ± SEM. $p \leq 0.05$ was considered as statistically significant. *$p \leq 0.05$ sham vs. fracture. $$p \leq 0.05$ 6 vs. 24 h after fracture within one age group. #$p \leq 0.05$ 6 vs. 6h and 24 vs. 24 h between two age groups.

following fracture compared to 6 h (Figure 4D). When comparing the two age groups, the SERCA mRNA expression 6 h after fracture was significantly lower in the middle-aged mice, whereas after 24 h the SERCA mRNA expression was significantly higher in the middle-aged mice (Figure 4D). Also, there were elevated levels and a positive regression in SERCA (R^2 = 0.80) mRNA expression 24 h following hip fracture in the 52-week-old animals (Supplemental Figure 2H).

Nitrotyrosine, glutathione peroxidase 4 (GSH) and superoxide dismutase (SOD)

We also investigated myocardial nitrosative stress and the myocardial protein expression of anti-oxidative enzymes. With respect to nitrosative stress, the myocardial expression of nitrotyrosine was slightly elevated in the middle-aged groups 6 and 24 h following proximal femur fracture compared to sham (Supplemental Figure 1A). The protein expression of glutathione peroxidase 4 (GSH) in left ventricular tissue did not alter between the respective groups (Supplemental Figure 1B). The expression of superoxide dismutase (SOD) was slightly elevated in the middle-aged group 6 h following fracture (Supplemental Figure 1C).

Atrial natriuretic peptide (ANP), brain natriuretic peptide (BNP) and fibroblast growth factor 23 (FGF23)

We further investigated the myocardial expression of distinct myocardial markers. After 6 h, the young and middle-aged animals showed a slightly elevated myocardial mRNA expression of atrial natriuretic peptide (ANP) compared to their respective controls (Supplemental Figure 1D). Moreover, the brain natriuretic peptide (BNP) mRNA expression was significantly elevated 24 h following hip fracture in the young animals compared to 6 h (Supplemental Figure 1E). The myocardial fibroblast growth factor 23 (FGF23) mRNA expression was slightly elevated 6 and 24 h after fracture in the young and middle-aged animals compared to their respective control groups (Supplemental Figure 1F).

Structural alterations

Heart injury score, desmin, α-actinin and troponin I

We also investigated myocardial structural alterations following hip fracture, since these has been previously linked to enhanced cardiac inflammation. With respect to local myocardial tissue damage, the heart injury score significantly increased 24 h following fracture compared to sham in the middle-aged group only (Figure 5A). Regarding myocardial structure proteins, the desmin protein expression significantly increased 6 h following fracture in the middle-aged group only (Figure 5B). The α-actinin protein expression was significantly elevated 6 h after fracture compared to sham in the young and the middle-aged group, as well as after 24 h in the middle-aged group only (Figure 5C). Additionally, the troponin I protein expression significantly increased 6 h following fracture in the young mice but dropped significantly after 24 h in the middle-aged mice compared to their respective control groups (Figure 5D). The cardiac troponin I mRNA expression was significantly reduced in the 12-week-old group 24 h following fracture compared to sham (Figure 5E). Also, the myocardial troponin I mRNA expression in the young animals was significantly lower 24 h following fracture compared to 6 h (Figure 5E). The troponin I mRNA expression was significantly increased in the middle-aged animals 24 h following fracture compared to the young animals (Figure 5E). Also, there were elevated levels and a positive regression in troponin I (R^2 = 0.83) mRNA expression 24 h following hip fracture in the middle-aged animals (Supplemental Figure 2I). These data indicate that local tissue damage after hip fracture is aggravated in middle-aged mice.

The results are summarized in Table 2.

Discussion

The aim of the present study was to investigate the effect of an experimental proximal femur fracture on the heart with respect to the development of secondary cardiac injury. Furthermore, special attention was given on the co-morbidity factor age as an independent risk factor, possibly aggravating and accelerating the development of this pathologic condition. Therefore, we investigated the systemic as well as the local cardiac inflammation 6 and 24 h following hip fracture in young (12-week-old) and middle-aged (52-week-old) mice. Additionally, local alterations in cardiac structure, metabolism and calcium handling were examined.

The development of secondary cardiac injury following long bone fracture has been recently described; it largely was linked to an immediate activation of the inflammatory response and a subsequent massive systemic release of distinct pro-inflammatory cytokines (8–10). This finding was also confirmed in the present study where mice showed increased systemic levels of IL-6 and KC following hip fracture, which seemed to be higher early after fracture at 6 h, supporting the previous findings of our group (8–10). The systemic IL-6 and KC levels were higher 6 h following fracture in both age groups and showed a slight decrease within 24 h. Both, IL-6 and KC were described as early pro-inflammatory markers following fracture (29), thus supporting the findings in the present study. Interestingly, the systemic IL-6 levels were significantly higher in the middle-aged mice at both time points following hip fracture. Enhanced systemic IL-6 levels have been described after hip fracture, particularly in elderly patients, and has been considered as an independent predictor for adverse

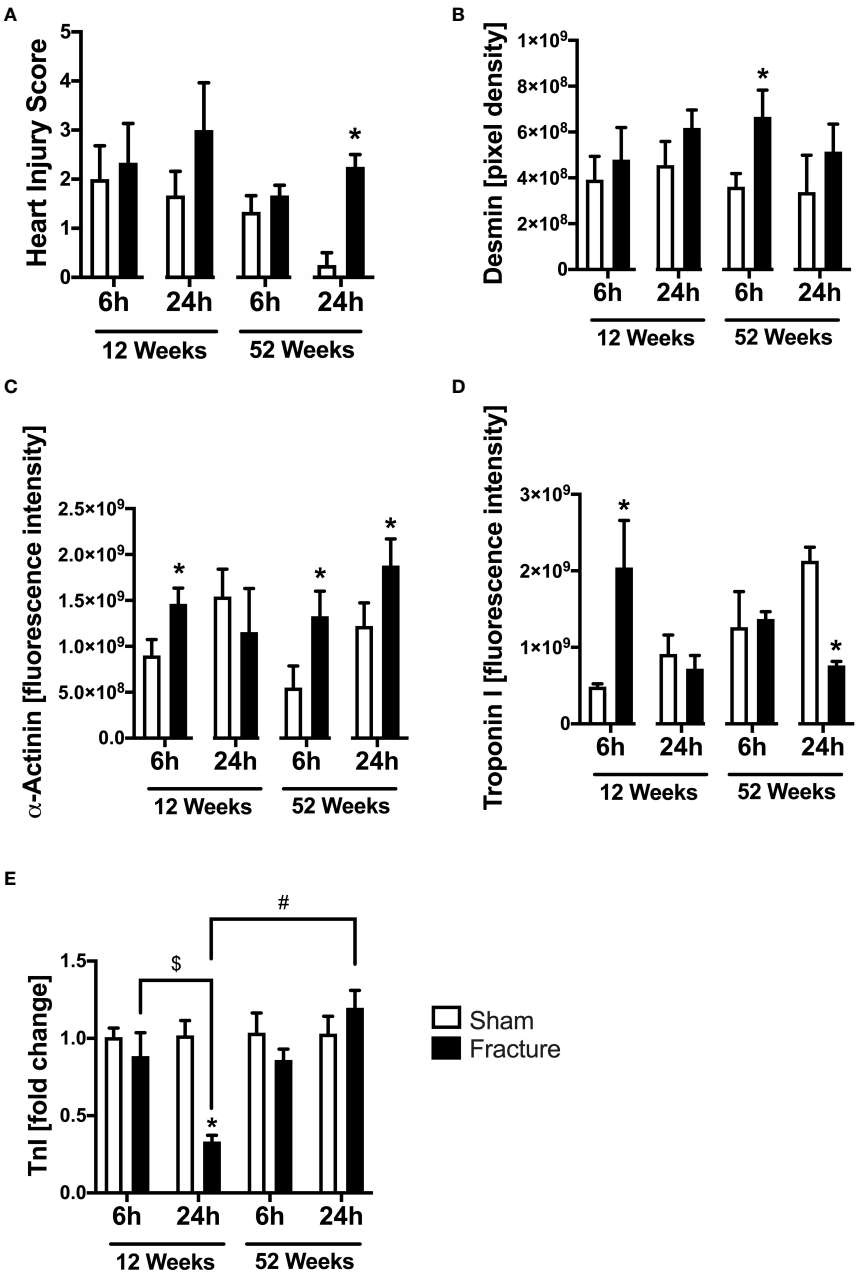

FIGURE 5
Cardiac structural alterations 6 and 24 h after proximal femur fracture in young and middle-aged mice. Young (12-week-old) and middle-aged (52-week-old) female mice received either sham treatment (white bars) or experimental proximal femur fracture (black bars). Left ventricular cardiac tissue was analyzed 6 and 24 h following sham treatment or proximal femur fracture. Myocardial Heart Injury Score **(A)**, local protein expression of Desmin in fluorescence intensity **(B)**, protein expression of α-Actinin in fluorescence intensity **(C)**, protein expression of Troponin I in fluorescence intensity **(D)** and troponin I mRNA expression in fold change **(E)**. Data are presented as mean ± SEM. $p \leq 0.05$ was considered as statistically significant. *$p \leq 0.05$ sham vs. fracture. $$p \leq 0.05$ 6 vs. 24 h after fracture within one age group. #$p \leq 0.05$ 6 vs. 6h and 24 vs. 24 h between two age groups.

postoperative outcomes such as complications and mortality (30). Moreover, older age of the patients was also linked to increased systemic IL-6 levels following hip fracture (31). Age-dependent differences in the pro-inflammatory response following bone fracture were demonstrated in distinct clinical and experimental studies, showing that age itself is an independent predictor for an intensified systemic inflammatory response (32). This was further confirmed in the

TABLE 2 Summary results.

	Sham vs. Fx				Fx 6 h vs. 24 h		Young vs. middle-aged	
	Young 6 h Sham vs. Fx	Young 24 h Sham vs. Fx	Middle-aged 6 h Sham vs. Fx	Middle-aged 24 h Sham vs. Fx	Young 6 h vs. 24 h	Middle-aged 6 h vs. 24 h	6 h Young vs. middle-aged	24 h Young vs. middle-aged
Systemic								
IL-6	↑	↑	↑	↑	↓	↓	↑	↑
KC	↑		↑		↓			
Local								
HMGB1			↑	↑				
TLR2					↓	↑	↓	↑
TLR4						↑		↑
TLR9								↑
C3aR (protein)	↑			↑				
C5aR1					↓		↓	
TNF (mRNA)		↓						↑
IL-1β			↑		↓	↓		
NLRP3				↑		↑		↑
HFABP (mRNA)	↑				↓		↓	
GLUT4		↓		↓		↓		
SERCA				↑	↓	↑	↓	↑
Heart Injury Score				↑				
Desmin			↑					
α-actinin			↑	↑				
TnI (protein)	↑			↓				
TnI (mRNA)		↓			↓			↑
BNP					↑			

↑ significantly increased.
↓ significantly reduced

present study, showing systemically elevated IFNγ levels in the 52-week-old mice 6 and 24 h following fracture compared to the 12-week-old animals. The phenomenon of 'inflammaging' was first described in the year 2000 by Franceschi and colleagues and implies an age-dependent upregulation of the inflammatory response, resulting in a low-grade chronic systemic pro-inflammatory state (33). The state of 'inflammaging' is characterized by enhanced systemic levels of IL-1β, IL-6 and TNF, all of which were further shown to be involved in the pathogenesis of age-associated diseases (34). This chronic pro-inflammatory state results in a vicious cycle of pathophysiological changes, tissue injury and remodeling (35). With respect to the heart, the aging-associated pro-inflammatory response was shown to be a fundamental underlying molecular mechanism for the development of myocardial dysfunction (36). More importantly, 'inflammaging' has been suggested as a major risk factor for the development of heart failure in geriatric patients following hip fracture and has been mostly linked to elevated systemic levels of IL-6 and TNF (32, 37). Furthermore, geriatric patients

suffering from a chronic inflammatory state take longer to resolve this inflammatory response to baseline levels and show an enhanced susceptibility to infections following trauma due to a prolonged immune suppression (38). Interestingly, an enhanced systemic inflammatory response was shown in the present study in middle-aged animals, suggesting that the condition of 'inflammaging' not exclusively appears in geriatric patients but might be just as relevant in a younger, middle-aged population. Summarized, our data showed that experimental hip fracture induces a systemic inflammatory response, which might contribute to the development of secondary cardiac injury following hip fracture in young and middle-aged animals. Additionally, the systemic inflammatory response seemed to be aggravated in the middle-aged animals, suggesting age and the phenomenon of 'inflammaging' as risk factors for the development of this pathologic condition independent from pre-existing cardiac diseases.

Besides systemic inflammation, the development of secondary cardiac injury after bone fracture previously had been linked to an intensified local cardiac inflammation (8–10). To assess the extent of local cardiac inflammation, we analyzed the myocardial expression of HMGB1 as well as of TLR2, TLR4 and TLR9. In accordance with our previous findings, we detected an elevated myocardial expression of HMGB1, TLR2 and TLR4 in the middle-aged mice 24 h following hip fracture, indicating augmented myocardial inflammation after hip fracture, which might be mediated *via* DAMPs and the TLR-signaling pathways (10). Enhanced myocardial expression of HMGB1 was recently demonstrated after experimental multiple trauma in mice (27). Exposure of human and mouse cardiomyocytes (CMs) to HMGB1 *in vitro* reduced their viability and impaired their mitochondrial respiration and calcium signaling, confirming cardio-depressive effects (39). Absence of TLR2 and TLR4 improved cardiac function after ischemia/reperfusion (I/R) injury and during sepsis in mice (40, 41) and ameliorated impaired cardiac calcium handling in presence of extracellular histones (41). In the present study, the myocardial HMGB1 expression dropped significantly in the middle-aged group 6 h following fracture, which might be due to an enhanced systemic elevation of HMGB1, acting as DAMP by recruiting immune cells, thus triggering and aggravating the inflammatory response. Increased systemic HMGB1 levels following experimental hip fracture have been recently described, supporting this hypothesis (42). The significant elevation of the myocardial HMGB1 expression 24 h following hip fracture in the middle-aged group might be a compensatory effect due to enhanced systemic HMGB1 release.

In the present study, the myocardial expression of TLR2, TLR4 and TLR9 was considerably higher in the middle-aged mice compared to the young animals, suggesting that age might aggravate and accelerate myocardial inflammation following hip fracture. Age-dependent differences in TLR-mediated inflammation have already been demonstrated in previous studies. LPS treatment of murine peritoneal macrophages from aged mice showed decreased production of pro-inflammatory cytokines, which were associated with alterations in TLR4 signaling (43). Furthermore, peritoneal macrophages from middle-aged mice demonstrated an impaired ability to develop endotoxin tolerance, which was associated with age-dependent alterations in TLR2 and TLR4 and was further linked to an uncontrollable inflammation (44). Moreover, myocardial macrophages were also shown to play a key role in myocardial inflammation in the condition of 'inflammaging' (45). Taken together, the young and middle-aged mice showed alterations in myocardial TLR expression, suggesting a crucial role of TLR signaling in the heart following hip fracture. As for the systemic inflammation, age as an independent risk factor seemed to have a considerable effect on TLR signaling, provoking myocardial inflammation following hip fracture.

Besides TLR signaling, the development of myocardial injury following trauma has been further associated with an immediate activation of the complement system (8–10, 28, 46–48). In accordance with previous findings, the young and middle-aged mice in the present study showed an increased myocardial expression of the C3aR 6 and 24 h following hip fracture, indicating myocardial complement activation (46, 47). Moreover, the myocardial expression of the C5aR1 was significantly reduced in the middle-aged mice 6 h following hip fracture compared to the young animals. A reduced myocardial expression of the C5aR1 recently has been demonstrated by our group after experimental multiple trauma but also after isolated femur fracture and was associated further to the development of post-traumatic myocardial dysfunction and damage (9, 28).

Age-dependent differences in complement activation have been shown in previous studies. It was demonstrated that the systemic levels of the complement system protein C1q increased with aging, resulting in skeletal muscle aging, muscle fibrosis and in arterial stiffening (49–51). Moreover, the immediate activation of the complement system has been linked to an activation of the myocardial NLRP3 inflammasome, contributing to the development of septic cardiomyopathy (52). The myocardial activation of the NLRP3 inflammasome, inducing the cleavage mature IL-1β was further shown by our group after multiple trauma and isolated bone fracture, and was also considered to contribute to the development of post-traumatic myocardial damage and secondary cardiac injury (9, 10, 28). In the present study, the middle-aged mice demonstrated an increased myocardial IL-1β expression 6 h following hip fracture. Furthermore, the local expression of the NLRP3 inflammasome was strikingly elevated in the middle-aged mice after 24 h, compared to the young animals. Also, the middle-aged mice showed a significantly higher mRNA and protein expression of TNF 24 h following hip fracture compared to the young mice. Both, IL-1β and TNF were shown to act cardio-depressive on human CMs *in vitro*, contributing to the

development of myocardial dysfunction and damage following trauma (9, 28). Age-dependent differences for NLRP3 inflammasome activation have been described in the literature and aged mice showed an enhanced NLRP3 inflammasome activation in alveolar macrophages, contributing to the development of pulmonary fibrosis (53). Summarized, our data showed enhanced myocardial inflammation in the young and middle-aged mice following hip fracture, which was mediated *via* the complement system and the NLRP3 inflammasome, suggesting a crucial role of these inflammatory signaling pathways. Myocardial inflammation seemed to be aggravated in the middle-aged mice, indicating age as independent risk factor, accelerating cardiac inflammation following hip fracture.

Besides myocardial inflammation, the development of secondary cardiac injuries has been further linked to local metabolic alterations following trauma. Alterations in cardiac glucose metabolism were shown during CLP sepsis and linked further to impaired cardiac function (54). Furthermore, alterations in myocardial glucose- and fatty acid transporter expression were demonstrated to be induced by inflammatory mediators (55) and might therefore be an effect of 'inflammaging'. In the present study, the myocardial mRNA expression of HFABP was significantly reduced 6 h following hip fracture in the middle-aged mice compared to the young mice. Moreover, the myocardial GLUT4 expression was diminished 24 h after hip fracture in both young and middle-aged mice. Alterations in myocardial HFABP and GLUT4 expression have been shown by our group after multiple trauma, but also after isolated femur and tibia fracture, and were further associated with the development of post-traumatic myocardial damage (10, 55). Of course, differential oral food intake between the treatment groups cannot be excluded, which possibly influence the myocardial HFABP and GLUT4 expression. However, the alterations in cardiac glucose and fatty acid transporters following bone fracture were recently demonstrated to be induced by pro-inflammatory mediators such as HMGB1, IL-1β, IL-6 and TNF (9, 39, 55), all of which have been shown to be elevated following hip fracture in the present study. Consequently, the alterations in myocardial HFABP and GLUT4 expression in the present study might be caused by pro-inflammatory mediators. To the best of our knowledge age-dependent differences in myocardial glucose- and fatty transporter expression following bone fracture have not yet been demonstrated and might be caused by 'inflammaging'.

Apart from metabolic alterations, the mice showed changes in their myocardial expression of the calcium handling protein SERCA. Alterations in myocardial SERCA expression have been associated with the development of septic cardiomyopathy (56) and post-traumatic myocardial damage (57), which was mediated by pro-inflammatory mediators (46, 57). In the present study, the middle-aged mice showed a significantly reduced SERCA expression 6 h following hip fracture compared to the young animals, whereas after 24 h the myocardial SERCA expression was significantly elevated in the middle-aged animals compared to the young animals. Reduced myocardial SERCA expression and activity have been described in previous studies in mice and has been linked to progressive aging of the heart (58). Furthermore, a diminished SERCA expression was shown in 24-month-old mice after femur fracture and hemorrhage, which was associated with an enhanced mortality rate of the animals following trauma (59). Moreover, alterations in myocardial SERCA expression were shown to be induced by the complement activation products C3a and C5a *in vitro* (46). Consequently, alterations in myocardial SERCA expression might also be caused by 'inflammaging'. To summarize, the mice showed alterations in myocardial expression of glucose- and fatty acid transporters as well as of calcium handling proteins following hip fracture. As for myocardial inflammation, age seemed to be an independent risk factor aggravating the cardiac effects following hip fracture.

Cardiac structural alterations have been associated with the development of post-traumatic myocardial damage and were further linked to inflammation (57). The current study demonstrated that middle-aged mice showed an increased elevation of their heart injury score 24 h after hip fracture, indicating myocardial tissue damage. Moreover, the desmin expression was also significantly elevated in the middle-aged mice after 6 h, whereas the α-actinin expression was increased in the young and middle-aged mice 6 and 24 h following hip fracture. Alterations in myocardial desmin and α-actinin expression were described after severe multiple trauma and isolated long bone fracture, and have been further associated with the development of post-traumatic myocardial dysfunction (9, 10, 28, 57). In different recent experimental studies, age- and gender-related alterations in myocardial desmin expression were demonstrated. Female 14-week-old C57BL/6 wild type mice showed an increased myocardial desmin expression compared to 100-week-old female mice (60). Further, the phosphorylation of desmin in the heart increased with age only in male mice, whereas the troponin phosphorylation only increased in female mice with age, both leading to an impaired calcium signaling of ventricular CMs (61). In the present study, the troponin I expression was significantly elevated in the young mice after 6 h and was reduced in the middle-aged animals 24 h after fracture, indicating an age-dependent effect on myocardial troponin I expression following hip fracture. Interestingly, cardiac troponin T was shown to be expressed in skeletal muscle with age and its mRNA levels were considerably higher in older compared to younger adults (62). Additionally, increased cardiac troponin T expression in skeletal muscle was demonstrated to play a critical role in in mediating neuromuscular junction denervation in skeletal muscle (63), skeletal muscle degeneration and a decline in motor activity in old mice (64). Alterations in myocardial structure protein expression following trauma were also linked to an enhanced

inflammatory response. Treatment of human CMs with a defined polytrauma cocktail induced alterations in cellular troponin I expression (57). As troponin I is an essential protein for cardiomyocyte contraction, the myocardial alterations in troponin I expression in the present study might indicate for adaption of cardiomyocyte contraction proteins, thus maintaining proper cardiac function. Taken together, this study showed alterations in the expression of important myocardial structure proteins, possibly predisposing for the development of secondary cardiac injury following hip fracture. To the best of our knowledge, these age-dependent alterations in myocardial structure following hip fracture have not been demonstrated previously. Moreover, age seemed to be an independent risk factor aggravating and accelerating myocardial damage and structural alterations, consistent contextually in the scope of 'inflammaging'. Besides age, gender differences might additionally play an important role on the heart following hip fracture, which has to be evaluated further in future studies.

There are several limitations in the current study to consider when interpreting the data. One limitation is that relatively short observation time points of 6 and 24 h following hip fracture were studied. These observation time points were chosen to investigate the early myocardial alterations following hip fracture, which is the primary research focus of our group. Therefore, the long-term effects of hip fracture on the heart with respect to age differences were not evaluated. Nevertheless, the linear regression analysis in the present study indicated myocardial alterations mainly 24 h following hip fracture and therefore suggest also later effects on the heart, which has to be included in future studies. Also, the study from De'Ath et al. showed the development of TISCI 72 h following trauma (6), wherefore later timepoints should be considered for future studies to assess the time-dependent development of myocardial alterations following hip fracture in young and middle-aged mice. Another limitation is that the present study only evaluated young (12-week-old) and middle-aged (52-week-old) mice. The middle-aged mice correspond to approximately 60 years of human age. However, the incidence of hip fractures is more commonly seen in elderly individuals greater than 75 years. Moreover, women over the age of 65 years have been shown to be more affected by hip fractures than men due to the onset of osteoporosis (65). To address this impact, elderly animals should be studied in future. Additionally, gender differences should be considered in follow-up studies since age, in combination with gender, seems to affect the clinical outcome of hip fracture patients. Also, osteoporosis should also be evaluated as a co-morbidity factor, since it is known that 52-week-old mice have age-related osteoporosis (66). Moreover, to properly analyze the extent of secondary cardiac injury following hip fracture, cardiac functional analysis by echocardiography or cardio MRI are mandatory for future studies. Finally, the model of proximal femur fracture used in this study possibly induces less soft tissue trauma than a closed fracture and could induce less of an inflammatory response than that seen clinically. Additionally, the experimental fracture was stabilized immediately following fracture, whereas hip fractures typically are stabilized within 24 h. Therefore, the hip fracture model in this study is not completely applicable to the human clinical condition.

Conclusion

In conclusion, young and middle-aged mice showed alterations in myocardial structure, glucose- and fatty acid transport as well as in calcium homeostasis 6 and 24 h following experimental hip fracture, which might predispose for the development of secondary cardiac injury. Also, the young and middle-aged mice demonstrated an elevated systemic and local cardiac inflammatory responses following hip fracture. Interestingly, the myocardial alterations as well as the systemic and local inflammation seemed to be aggravated in the middle-aged mice, indicating age and the age-associated phenomenon of 'inflammaging' as an independent risk factor aggravating and accelerating cardiac alterations and therefore possibly also the development of secondary cardiac injury following hip fracture.

In the present study, we showed for the first time cardiac alterations following hip fracture in young and middle-aged animals in absence of pre-existing cardiac diseases. More importantly, the middle-aged animals demonstrated aggravated systemic and local cardiac inflammation. To the best of our knowledge, we showed for the first time that the condition of 'inflammaging' also occur in middle-aged animals, suggesting even middle age as independent risk factor for cardiac alterations following hip fracture.

Data availability statement

The original contributions presented in the study are included in the article/Supplementary Material. Further inquiries can be directed to the corresponding authors.

Ethics statement

The animal study was reviewed and approved by IACUC UCSF AN143402-03B.

Author contributions

IL, BW, AO, CL, MH-L, and MK, conducting experiments. MK, MH-L, BW, JP, RM, and TM, substantial contributions to research design. MK, RM, JP, and TM, interpretation of data. IL,

drafting and writing the paper. All authors, revising the paper critically and approve the final version of this paper.

Funding

This study was supported by the Hertha-Nathorff program (travel grant to MH-L and MK), the DAAD (travel grant to BW), and the Orthopaedic Trauma Institute at UCSF. This work was conducted in the framework of the CRC1149 funded by the Deutsche Forschungsgemeinschaft (DFG, German Research Foundation) – Project number 251293561.

Conflict of interest

The authors declare that the research was conducted in the absence of any commercial or financial relationships that could be construed as a potential conflict of interest.

Publisher's note

All claims expressed in this article are solely those of the authors and do not necessarily represent those of their affiliated organizations, or those of the publisher, the editors and the reviewers. Any product that may be evaluated in this article, or claim that may be made by its manufacturer, is not guaranteed or endorsed by the publisher.

Supplementary material

The Supplementary Material for this article can be found online at: https://www.frontiersin.org/articles/10.3389/fimmu.2022.895888/full#supplementary-material

SUPPLEMENTARY FIGURE 1
Cardiac nitrosative and oxidative stress and myocardial markers 6 and 24 h after proximal femur fracture in young and middle-aged mice. Young (12-week-old) and middle-aged (52-week-old) female mice received either sham treatment (white bars) or experimental proximal femur fracture (black bars). Left ventricular cardiac tissue was analyzed 6 and 24 h following sham treatment or proximal femur fracture. Myocardial expression of nitrotyrosine in pixel density **(A)**, protein expression of glutathione peroxidase (GSH) in pixel density **(B)**, protein expression of superoxide dismutase (SOD) in pixel density **(C)**, mRNA expression of atrial natriuretic peptide (ANP) in fold change **(D)**, mRNA expression of brain natriuretic peptide (BNP) in fold change **(E)** and fibroblast growth factor 23 (FGF23) in fold change **(F)**. Data are presented as mean ± SEM. $p \leq 0.05$ was considered as statistically significant. *$p \leq 0.05$ sham vs. fracture. $$p \leq 0.05$ 6 vs. 24 h after fracture within one age group. #$p \leq 0.05$ 6 vs. 6h and 24 vs. 24 h between two age groups.

SUPPLEMENTARY FIGURE 2
Regression analysis 6 and 24 h after proximal femur fracture in young and middle-aged mice. Young (12-week-old) and middle-aged (52-week-old) female mice received experimental proximal femur fracture. Regression analysis was performed either after 6 h (blue dots) or after 24 h (green squares) following experimental proximal femur fracture. Linear regression analysis of systemic interleukin-6 (IL-6) levels in pg/ml **(A)**, of cardiac mRNA expression of toll-like receptor 2 (TLR) **(B)**, toll-like receptor 4 (TLR4) **(C)**, toll-like receptor 9 (TLR9) **(D)**, tumor necrosis factor (TNF) **(E)**, NLR pyrin domain containing protein 3 (NLRP3) **(F)**, interleukin-1β (IL-1β) **(G)**, sarcoplasmic/endoplasmic reticulum ATPase (SERCA) **(H)** and troponin I **(I)** in fold change. Data are presented as individual values. Goodness of fit is indicated as R^2.

SUPPLEMENTARY FIGURE 3
Representative images of C3aR and HMGB1 IHC staining of left ventricular tissue from young and middle-aged mice 6 and 24 h following proximal femur fracture. Young (12-week-old) and middle-aged (52-week-old) female mice received experimental proximal femur fracture. Left ventricular cardiac tissue was analyzed 6 and 24 h following sham treatment or proximal femur fracture. Representative images of complement C3a receptor (C3aR) **(A)** and high mobility group box one (HMGB1) protein **(B)**.

SUPPLEMENTARY FIGURE 4
Representative images of TNF IHC and H.E. staining of left ventricular tissue from young and middle-aged mice 6 and 24 h following proximal femur fracture. Young (12-week-old) and middle-aged (52-week-old) female mice received experimental proximal femur fracture. Left ventricular cardiac tissue was analyzed 6 and 24 h following sham treatment or proximal femur fracture. Representative images of tumor necrosis factor (TNF) **(A)** and hematoxylin & eosin (H.E.) staining **(B)**.

SUPPLEMENTARY FIGURE 5
Representative images of α-actinin and desmin IF staining of left ventricular tissue from young and middle-aged mice 6 and 24 h following proximal femur fracture. Young (12-week-old) and middle-aged (52-week-old) female mice received experimental proximal femur fracture. Left ventricular cardiac tissue was analyzed 6 and 24 h following sham treatment or proximal femur fracture. Representative images of α-actinin **(A)** and desmin protein **(B)**.

SUPPLEMENTARY FIGURE 6
Representative images of troponin I IF staining of left ventricular tissue from young and middle-aged mice 6 and 24 h following proximal femur fracture. Young (12-week-old) and middle-aged (52-week-old) female mice received experimental proximal femur fracture. Left ventricular cardiac tissue was analyzed 6 and 24 h following sham treatment or proximal femur fracture. Representative images of troponin I **(A)**.

References

1. Mokdad AH, Forouzanfar MH, Daoud F, Mokdad AA, El Bcheraoui C, Moradi-Lakeh M, et al. Global burden of diseases, injuries, and risk factors for young people's health during 1990-2013: A systematic analysis for the global burden of disease study 2013. *Lancet (London England)* (2016) 387(10036):2383–401. doi: 10.1016/s0140-6736(16)00648-6

2. Alberdi F, García I, Atutxa L, Zabarte M. Epidemiology of severe trauma. *Med Intensiva* (2014) 38(9):580–8. doi: 10.1016/j.medin.2014.06.012

3. Huber S, Biberthaler P, Delhey P, Trentzsch H, Winter H, van Griensven M, et al. Predictors of poor outcomes after significant chest trauma in multiply injured patients: A retrospective analysis from the German trauma registry (Trauma

register dgu®). *Scandinavian J Trauma Resuscitation Emergency Med* (2014) 22:52. doi: 10.1186/s13049-014-0052-4

4. Skinner DL, Laing GL, Rodseth RN, Ryan L, Hardcastle TC, Muckart DJ. Blunt cardiac injury in critically ill trauma patients: A single centre experience. *Injury* (2015) 46(1):66–70. doi: 10.1016/j.injury.2014.08.051

5. De'Ath HD, Manson J, Davenport R, Glasgow S, Renfrew I, Davies LC, et al. Trauma-induced secondary cardiac injury is associated with hyperacute elevations in inflammatory cytokines. *Shock* (2013) 39(5):415–20. doi: 10.1097/SHK.0b013e31828ded41

6. De'Ath HD, Rourke C, Davenport R, Manson J, Renfrew I, Uppal R, et al. Clinical and biomarker profile of trauma-induced secondary cardiac injury. *Br J Surg* (2012) 99(6):789–97. doi: 10.1002/bjs.8728

7. Naganathar S, De'Ath HD, Wall J, Brohi K. Admission biomarkers of trauma-induced secondary cardiac injury predict adverse cardiac events and are associated with plasma catecholamine levels. *J Trauma Acute Care Surg* (2015) 79(1):71–7. doi: 10.1097/ta.0000000000000694

8. Weber B, Lackner I, Miclau T, Stulz J, Gebhard F, Pfeifer R, et al. Early myocardial damage (Emd) and valvular dysfunction after femur fracture in pigs. *Sci Rep* (2021) 11(1):8503. doi: 10.1038/s41598-021-86151-z

9. Weber B, Lackner I, Knecht D, Braun CK, Gebhard F, Huber-Lang M, et al. Systemic and cardiac alterations after long bone fracture. *Shock* (2020) 54(6):761–73. doi: 10.1097/shk.0000000000001536

10. Lackner I, Weber B, Haffner-Luntzer M, Hristova S, Gebhard F, Lam C, et al. Systemic and local cardiac inflammation after experimental long bone fracture, traumatic brain injury and combined trauma in mice. *J Orthop Translat* (2021) 28:39–46. doi: 10.1016/j.jot.2020.12.003

11. Spillman BC, Lubitz J. The effect of longevity on spending for acute and long-term care. *N Engl J Med* (2000) 342(19):1409–15. doi: 10.1056/nejm200005113421906

12. LeBlanc KE, Muncie HLJr., LeBlanc LL. Hip fracture: Diagnosis, treatment, and secondary prevention. *Am Fam Physician* (2014) 89(12):945–51.

13. Cooper C, Cole ZA, Holroyd CR, Earl SC, Harvey NC, Dennison EM, et al. Secular trends in the incidence of hip and other osteoporotic fractures. *Osteoporosis Int J established as result cooperation between Eur Foundation Osteoporosis Natl Osteoporosis Foundation USA* (2011) 22(5):1277–88. doi: 10.1007/s00198-011-1601-6

14. de Luise C, Brimacombe M, Pedersen L, Sørensen HT. Comorbidity and mortality following hip fracture: A population-based cohort study. *Aging Clin Exp Res* (2008) 20(5):412–8. doi: 10.1007/bf03325146

15. Noale M, Limongi F, Maggi S. Epidemiology of cardiovascular diseases in the elderly. *Adv Exp Med Biol* (2020) 1216:29–38. doi: 10.1007/978-3-030-33330-0_4

16. Jansen S, Koster RW, de Lange FJ, Goslings JC, Schafroth MU, de Rooij SE, et al. Electrocardiographic abnormalities in patients admitted for hip fracture. *Neth J Med* (2014) 72(9):455–61.

17. Kim BS, Kim TH, Oh JH, Kwon CH, Kim SH, Kim HJ, et al. Association between preoperative high sensitive troponin I levels and cardiovascular events after hip fracture surgery in the elderly. *J Geriatric Cardiol JGC* (2018) 15(3):215–21. doi: 10.11909/j.issn.1671-5411.2018.03.002

18. Tsai CH, Lin CL, Hsu HC, Chung WS. Increased risk of coronary heart disease in patients with hip fracture: A nationwide cohort study. *Osteoporosis Int J established as result cooperation between Eur Foundation Osteoporosis Natl Osteoporosis Foundation USA* (2015) 26(6):1849–55. doi: 10.1007/s00198-015-3097-y

19. Chiang CH, Liu CJ, Chen PJ, Huang CC, Hsu CY, Chen ZY, et al. Hip fracture and risk of acute myocardial infarction: A nationwide study. *J Bone Mineral Res Off J Am Soc Bone Mineral Res* (2013) 28(2):404–11. doi: 10.1002/jbmr.1714

20. Guzon-Illescas O, Perez Fernandez E, Crespí Villarias N, Quirós Donate FJ, Peña M, Alonso-Blas C, et al. Mortality after osteoporotic hip fracture: Incidence, trends, and associated factors. *J Orthop Surg Res* (2019) 14(1):203. doi: 10.1186/s13018-019-1226-6

21. Cha YH, Ha YC, Ryu HJ, Lee YK, Park SH, Lee KJ, et al. Effect of heart failure on postoperative short and long-term mortality in elderly patients with hip fracture. *Injury* (2020) 51(3):694–8. doi: 10.1016/j.injury.2020.01.004

22. Morri M, Ambrosi E, Chiari P, Orlandi Magli A, Gazineo D, DA F, et al. One-year mortality after hip fracture surgery and prognostic factors: A prospective cohort study. *Sci Rep* (2019) 9(1):18718. doi: 10.1038/s41598-019-55196-6

23. Wang ZC, Jiang W, Chen X, Yang L, Wang H, Liu YH. Systemic immune-inflammation index independently predicts poor survival of older adults with hip fracture: A prospective cohort study. *BMC Geriatr* (2021) 21(1):155. doi: 10.1186/s12877-021-02102-3

24. Weiskopf D, Weinberger B, Grubeck-Loebenstein B. The aging of the immune system. *Transpl Int* (2009) 22(11):1041–50. doi: 10.1111/j.1432-2277.2009.00927.x

25. Kjørholt KE, Kristensen NR, Prieto-Alhambra D, Johnsen SP, Pedersen AB. Increased risk of mortality after postoperative infection in hip fracture patients. *Bone* (2019) 127:563–70. doi: 10.1016/j.bone.2019.07.023

26. Haffner-Luntzer M, Weber B, Lam C, Fischer V, Lackner I, Ignatius A, et al. A novel mouse model to study fracture healing of the proximal femur. *J Orthop Res* (2020) 38(10):2131–8. doi: 10.1002/jor.24677

27. Braun CK, Kalbitz M, Halbgebauer R, Eisele P, Messerer DAC, Weckbach S, et al. Early structural changes of the heart after experimental polytrauma and hemorrhagic shock. *PloS One* (2017) 12(10):e0187327. doi: 10.1371/journal.pone.0187327

28. Kalbitz M, Schwarz S, Weber B, Bosch B, Pressmar J, Hoenes FM, et al. Cardiac depression in pigs after multiple trauma - characterization of posttraumatic structural and functional alterations. *Sci Rep* (2017) 7(1):17861. doi: 10.1038/s41598-017-18088-1

29. Fischer V, Kalbitz M, Muller-Graf F, Gebhard F, Ignatius A, Liedert A, et al. Influence of menopause on inflammatory cytokines during murine and human bone fracture healing. *Int J Mol Sci* (2018) 19(7). doi: 10.3390/ijms19072070

30. Sun T, Wang X, Liu Z, Chen X, Zhang J. Plasma concentrations of pro- and anti-inflammatory cytokines and outcome prediction in elderly hip fracture patients. *Injury* (2011) 42(7):707–13. doi: 10.1016/j.injury.2011.01.010

31. Sedlár M, Kudrnová Z, Erhart D, Trca S, Kvasnicka J, Krska Z, et al. Older age and type of surgery predict the early inflammatory response to hip trauma mediated by interleukin-6 (Il-6). *Arch Gerontol Geriatr* (2010) 51(1):e1–6. doi: 10.1016/j.archger.2009.06.006

32. Vester H, Huber-Lang MS, Kida Q, Scola A, van Griensven M, Gebhard F, et al. The immune response after fracture trauma is different in old compared to young patients. *Immun Ageing* (2014) 11(1):20. doi: 10.1186/s12979-014-0020-x

33. Franceschi C, Bonafè M, Valensin S, Olivieri F, De Luca M, Ottaviani E, et al. Inflamm-aging. an evolutionary perspective on immunosenescence. *Ann New York Acad Sci* (2000) 908:244–54. doi: 10.1111/j.1749-6632.2000.tb06651.x

34. De Martinis M, Franceschi C, Monti D, Ginaldi L. Inflammation markers predicting frailty and mortality in the elderly. *Exp Mol Pathol* (2006) 80(3):219–27. doi: 10.1016/j.yexmp.2005.11.004

35. Baylis D, Bartlett DB, Patel HP, Roberts HC. Understanding how we age: Insights into inflammaging. *Longev Healthspan* (2013) 2(1):8. doi: 10.1186/2046-2395-2-8

36. Wang M, Shah AM. Age-associated pro-inflammatory remodeling and functional phenotype in the heart and Large arteries. *J Mol Cell Cardiol* (2015) 83:101–11. doi: 10.1016/j.yjmcc.2015.02.004

37. Baëhl S, Garneau H, Le Page A, Lorrain D, Viens I, Svotelis A, et al. Altered neutrophil functions in elderly patients during a 6-month follow-up period after a hip fracture. *Exp Gerontol* (2015) 65:58–68. doi: 10.1016/j.exger.2015.03.009

38. Hazeldine J, Lord JM, Hampson P. Immunesenescence and inflammaging: A contributory factor in the poor outcome of the geriatric trauma patient. *Ageing Res Rev* (2015) 24(Pt B):349–57. doi: 10.1016/j.arr.2015.10.003

39. Weber B, Lackner I, Baur M, Fois G, Gebhard F, Marzi I, et al. Effects of circulating hmgb-1 and histones on cardiomyocytes-hemadsorption of these damps as therapeutic strategy after multiple trauma. *J Clin Med* (2020) 9(5). doi: 10.3390/jcm9051421

40. Zhao P, Wang J, He L, Ma H, Zhang X, Zhu X, et al. Deficiency in Tlr4 signal transduction ameliorates cardiac injury and cardiomyocyte contractile dysfunction during ischemia. *J Cell Mol Med* (2009) 13(8a):1513–25. doi: 10.1111/j.1582-4934.2009.00798.x

41. Kalbitz M, Grailer JJ, Fattahi F, Jajou L, Herron TJ, Campbell KF, et al. Role of extracellular histones in the cardiomyopathy of sepsis. *FASEB J Off Publ Fed Am Societies Exp Biol* (2015) 29(5):2185–93. doi: 10.1096/fj.14-268730

42. Yu X, Chen X, Sun T. Microrna-205-5p targets Hmgb1 to suppress inflammatory responses during lung injury after hip fracture. *BioMed Res Int* (2019) 2019:7304895. doi: 10.1155/2019/7304895

43. Boehmer ED, Goral J, Faunce DE, Kovacs EJ. Age-dependent decrease in toll-like receptor 4-mediated proinflammatory cytokine production and mitogen-activated protein kinase expression. *J Leukoc Biol* (2004) 75(2):342–9. doi: 10.1189/jlb.0803389

44. Sun Y, Li H, Yang MF, Shu W, Sun MJ, Xu Y. Effects of aging on endotoxin tolerance induced by lipopolysaccharides derived from porphyromonas gingivalis and escherichia coli. *PloS One* (2012) 7(6):e39224. doi: 10.1371/journal.pone.0039224

45. Chiao YA, Dai Q, Zhang J, Lin J, Lopez EF, Ahuja SS, et al. Multi-analyte profiling reveals matrix metalloproteinase-9 and monocyte chemotactic protein-1 as plasma biomarkers of cardiac aging. *Circ Cardiovasc Genet* (2011) 4(4):455–62. doi: 10.1161/circgenetics.111.959981

46. Lackner I, Weber B, Baur M, Fois G, Gebhard F, Pfeifer R, et al. Complement activation and organ damage after trauma–differential immune response based on surgical treatment strategy. *Front Immunol* (2020) 11:64(64). doi: 10.3389/fimmu.2020.00064

47. Lackner I, Weber B, Miclau T, Holzwarth N, Baur M, Gebhard F, et al. Reaming of femoral fractures with different reaming irrigator aspirator systems shows distinct effects on cardiac function after experimental polytrauma. *J Orthop Res* (2020) 38(12):2608–18. doi: 10.1002/jor.24830

48. Weber B, Mendler MR, Lackner I, Pressmar J, Haffner-Luntzer M, Hofler S, et al. Tissue damage in the heart after cardiac arrest induced by asphyxia and hemorrhage in newborn pigs. *Pediatr Res* (2019) 86(6):709–18. doi: 10.1038/s41390-019-0505-6

49. Naito AT, Sumida T, Nomura S, Liu ML, Higo T, Nakagawa A, et al. Complement C1q activates canonical wnt signaling and promotes aging-related phenotypes. *Cell* (2012) 149(6):1298–313. doi: 10.1016/j.cell.2012.03.047

50. Watanabe S, Sato K, Hasegawa N, Kurihara T, Matsutani K, Sanada K, et al. Serum C1q as a novel biomarker of sarcopenia in older adults. *FASEB J Off Publ Fed Am Societies Exp Biol* (2015) 29(3):1003–10. doi: 10.1096/fj.14-262154

51. Hasegawa N, Fujie S, Horii N, Uchida M, Toyama Y, Inoue K, et al. Aging-induced elevation in circulating complement C1q level is associated with arterial stiffness. *Exp Gerontol* (2019) 124:110650. doi: 10.1016/j.exger.2019.110650

52. Kalbitz M, Fattahi F, Grailer JJ, Jajou L, Malan EA, Zetoune FS, et al. Complement-induced activation of the cardiac Nlrp3 inflammasome in sepsis. *FASEB J Off Publ Fed Am Societies Exp Biol* (2016) 30(12):3997–4006. doi: 10.1096/fj.201600728R

53. Stout-Delgado HW, Cho SJ, Chu SG, Mitzel DN, Villalba J, El-Chemaly S, et al. Age-dependent susceptibility to pulmonary fibrosis is associated with Nlrp3 inflammasome activation. *Am J Respir Cell Mol Biol* (2016) 55(2):252–63. doi: 10.1165/rcmb.2015-0222OC

54. Zheng Z, Ma H, Zhang X, Tu F, Wang X, Ha T, et al. Enhanced glycolytic metabolism contributes to cardiac dysfunction in polymicrobial sepsis. *J Infect Dis* (2017) 215(9):1396–406. doi: 10.1093/infdis/jix138

55. Lackner I, Weber B, Knecht D, Horst K, Relja B, Gebhard F, et al. Cardiac glucose and fatty acid transport after experimental mono- and polytrauma. *Shock* (2020) 53(5):620–9. doi: 10.1097/shk.0000000000001400

56. Kalbitz M, Fattahi F, Herron TJ, Grailer JJ, Jajou L, Lu H, et al. Complement destabilizes cardiomyocyte function in vivo after polymicrobial sepsis and in vitro. *J Immunol (Baltimore Md 1950)* (2016) 197(6):2353–61. doi: 10.4049/jimmunol.1600091

57. Baur M, Weber B, Lackner I, Gebhard F, Pfeifer R, Cinelli P, et al. Structural alterations and inflammation in the heart after multiple trauma followed by reamed versus non-reamed femoral nailing. *PloS One* (2020) 15(6):e0235220. doi: 10.1371/journal.pone.0235220

58. Schmidt U, del Monte F, Miyamoto MI, Matsui T, Gwathmey JK, Rosenzweig A, et al. Restoration of diastolic function in senescent rat hearts through adenoviral gene transfer of sarcoplasmic reticulum Ca(2+)-atpase. *Circulation* (2000) 101(7):790–6. doi: 10.1161/01.cir.101.7.790

59. Horst K, Höfler J, Martin L, Greven J, Schürholz T, Simon TP, et al. Geriatric polytrauma-cardiovascular and immunologic response in a murine two-hit model of trauma. *J Surg Res* (2019) 241:87–94. doi: 10.1016/j.jss.2019.03.053

60. Diedrich M, Tadic J, Mao L, Wacker MA, Nebrich G, Hetzer R, et al. Heart protein expression related to age and sex in mice and humans. *Int J Mol Med* (2007) 20(6):865–74.

61. Kane AE, Bisset ES, Keller KM, Ghimire A, Pyle WG, Howlett SE. Age, sex and overall health, measured as frailty, modify myofilament proteins in hearts from naturally aging mice. *Sci Rep* (2020) 10(1):10052. doi: 10.1038/s41598-020-66903-z

62. Raue U, Trappe TA, Estrem ST, Qian HR, Helvering LM, Smith RC, et al. Transcriptome signature of resistance exercise adaptations: Mixed muscle and fiber type specific profiles in young and old adults. *J Appl Physiol (Bethesda Md 1985)* (2012) 112(10):1625–36. doi: 10.1152/japplphysiol.00435.2011

63. Xu Z, Feng X, Dong J, Wang ZM, Lee J, Furdui C, et al. Cardiac troponin T and fast skeletal muscle denervation in ageing. *J Cachexia Sarcopenia Muscle* (2017) 8(5):808–23. doi: 10.1002/jcsm.12204

64. Zhang T, Feng X, Dong J, Xu Z, Feng B, Haas KM, et al. Cardiac troponin T and autoimmunity in skeletal muscle aging. *Geroscience* (2022). doi: 10.1007/s11357-022-00513-7

65. Rupp M, Walter N, Pfeifer C, Lang S, Kerschbaum M, Krutsch W, et al. The incidence of fractures among the adult population of Germany. *Dtsch Arztebl Int* (2021) 118(40):665–9. doi: 10.3238/arztebl.m2021.0238

66. Wehrle E, Liedert A, Heilmann A, Wehner T, Bindl R, Fischer L, et al. The impact of low-magnitude high-frequency vibration on fracture healing is profoundly influenced by the oestrogen status in mice. *Dis Models Mech* (2015) 8(1):93–104. doi: 10.1242/dmm.018622

frontiers | Frontiers in Immunology

TYPE Original Research
PUBLISHED 12 September 2022
DOI 10.3389/fimmu.2022.980707

OPEN ACCESS

EDITED BY
Tom E. Mollnes,
University of Oslo, Norway

REVIEWED BY
Nikola Cesarovic,
ETH Zürich, Switzerland
Patrick Geraghty,
Downstate Health Sciences University,
United States

*CORRESPONDENCE
Martin Wepler
martin.wepler@uni-ulm.de
Sabine Vettorazzi
sabine.vettorazzi@uni-ulm.de

SPECIALTY SECTION
This article was submitted to Inflammation, a section of the journal Frontiers in Immunology

RECEIVED 28 June 2022
ACCEPTED 23 August 2022
PUBLISHED 12 September 2022

CITATION
Wepler M, Preuss JM, Tilp C, Keck M, Blender J, Wachter U, Merz T, Vogt J, Kress S, Gröger M, Hoffmann A, Fink M, Calzia E, Burret U, Radermacher P, Tuckermann JP and Vettorazzi S (2022) Cigarette smoke exposure reduces hemorrhagic shock induced circulatory dysfunction in mice with attenuated glucocorticoid receptor function.
Front. Immunol. 13:980707.
doi: 10.3389/fimmu.2022.980707

Cigarette smoke exposure reduces hemorrhagic shock induced circulatory dysfunction in mice with attenuated glucocorticoid receptor function

Martin Wepler[1,2]*, Jonathan M. Preuss[3], Cornelia Tilp[4], Martina Keck[4], Jochen Blender[4], Ulrich Wachter[2], Tamara Merz[2], Josef Vogt[2], Sandra Kress[2], Michael Gröger[2], Andrea Hoffmann[2], Marina Fink[2], Enrico Calzia[2], Ute Burret[3], Peter Radermacher[2], Jan P. Tuckermann[3] and Sabine Vettorazzi[3]*

[1]Department of Anesthesiology and Intensive Care Medicine, University Hospital, Ulm, Germany, [2]Institute for Anesthesiologic Pathophysiology and Process Engineering, Ulm University, Ulm, Germany, [3]Institute of Comparative Molecular Endocrinology (CME), Ulm University, Ulm, Germany, [4]Immunology and Respiratory, Boehringer Ingelheim Pharma GmbH & Co KG, Biberach, Germany

Introduction: We previously showed that attenuated glucocorticoid receptor (GR) function in mice ($GR^{dim/dim}$) aggravates systemic hypotension and impairs organ function during endotoxic shock. Hemorrhagic shock (HS) causes impaired organ perfusion, which leads to tissue hypoxia and inflammation with risk of organ failure. Lung co-morbidities like chronic obstructive pulmonary disease (COPD) can aggravate tissue hypoxia *via* alveolar hypoxia. The most common cause for COPD is cigarette smoke (CS) exposure. Therefore, we hypothesized that affecting GR function in mice ($GR^{dim/dim}$) and pre-traumatic CS exposure would further impair hemodynamic stability and organ function after HS.

Methods: After 3 weeks of CS exposure, anesthetized and mechanically ventilated $GR^{dim/dim}$ and $GR^{+/+}$ mice underwent pressure-controlled HS for 1h *via* blood withdrawal (mean arterial pressure (MAP) 35mmHg), followed by 4h of resuscitation with re-transfusion of shed blood, colloid fluid infusion and, if necessary, continuous intravenous norepinephrine. Acid–base status and organ function were assessed together with metabolic pathways. Blood and organs were collected at the end of the experiment for analysis of cytokines, corticosterone level, and mitochondrial respiratory capacity. Data is presented as median and interquartile range.

Results: Nor CS exposure neither attenuated GR function affected survival. Non-CS $GR^{dim/dim}$ mice had a higher need of norepinephrine to keep target hemodynamics compared to $GR^{+/+}$ mice. In contrast, after CS exposure norepinephrine need did not differ significantly between $GR^{dim/dim}$ and $GR^{+/+}$ mice. Non-CS $GR^{dim/dim}$ mice presented with a lower pH and increased blood lactate levels compared to $GR^{+/+}$ mice, but not CS exposed mice. Also, higher plasma concentrations of some pro-inflammatory cytokines were observed in non-CS $GR^{dim/dim}$ compared to $GR^{+/+}$ mice, but not in the CS group. With regards to metabolic measurements, CS exposure led to an increased lipolysis in $GR^{dim/dim}$ compared to $GR^{+/+}$ mice, but not in non-CS exposed animals.

Conclusion: Whether less metabolic acidosis or increased lipolysis is the reason or the consequence for the trend towards lower catecholamine need in CS exposed $GR^{dim/dim}$ mice warrants further investigation.

KEYWORDS

catecholamines, cigarettes smoke exposure, glucocorticoid receptor function, hemodynamic function, hemorrhagic shock, metabolic function, inflammation

Introduction

Hemorrhagic shock (HS) is one of the major mediators of trauma-related mortality (1). During HS as well as during resuscitation from HS impaired organ blood flow may lead to tissue hypoxia, resulting in risk of organ damage (2). Tissue hypoxia itself induces inflammation (3), which in turn aggravates the risk of organ damage. Both, tissue hypoxia and inflammation may lead to enhanced radical formation and mitochondrial dysfunction, altogether leading to multiorgan failure (MOF (1, 2, 4),). During resuscitation after HS, it is important to maintain mean arterial pressure (MAP) to ensure perfusion of the most important organs as heart, kidney, liver, lung, or brain. At best, this hemodynamic state enables microcirculatory perfusion of these important organs to prevent longer impairment of O_2-availability and, thus irreversible organ dysfunction or damage (5). On a cellular level, impaired O_2-availability may lead to mitochondrial dysfunction with uncoupling of mitochondrial respiration and a lack of mitochondrial substrates, resulting in reduced production of adenosine triphosphate (ATP) and increased oxidative stress (5). Besides this mitochondrial dysfunction due to a reduced O_2-availability, during and after shock a hypermetabolic condition with insulin resistance and increased oxygen demands often occurs (6). This, in turn, causes impaired glucose and oxygen availability on a cellular level and, ultimately, lead to metabolic failure. Together with the mitochondrial dysfunction this metabolic failure further impairs organ function after shock (7).

Our group showed already that pre-traumatic cigarette-smoke (CS) exposure enhanced post-traumatic inflammation and radical stress, thereby aggravating lung dysfunction (8). CS is the major risk factor for chronic obstructive pulmonary disease (COPD) (9) and COPD as a lung co-morbidity increases pulmonary and systemic inflammation and might increase tissue hypoxia *via* alveolar hypoxia (10). Furthermore, CS exposure-induced COPD aggravated acute lung injury (ALI) in a murine model of blunt chest trauma (8, 11), causing the strongest inflammatory response in mice after HS and resuscitation under intensive care treatment (12).

Glucocorticoids (GCs) mediate their effects through the glucocorticoid receptor (GR) (13). The GR is an intracellular, ligand-activated transcription factor, which regulates gene transcription by several mechanisms: as a protein dimer it can bind palindromic DNA sequences (glucocorticoid response elements – GREs) or DNA half sites as a monomeric protein (GR monomer (14)). In a non-resuscitated mouse model of endotoxemia, we previously showed that the GR is crucial for the resolution of systemic inflammation (15). In a more recent study, we demonstrated that intact GR dimer also mediates hemodynamic stability in a resuscitated mouse model of endotoxemia, indicated by a higher need of catecholamines in mice with a impaired GR dimerization function ($GR^{dim/dim}$) to keep hemodynamic targets (16). In addition to the mouse model of endotoxemia, we already showed that HS led to impaired lung mechanics and aggravated lung inflammation in $GR^{dim/dim}$ mice compared to littermate control wildtype mice ($GR^{+/+}$) (17). This previous study showed that functional GR signaling plays a

crucial role to attenuate HS-induced lung damage. Based on this study, we hypothesized that an attenuation of GR function together with CS exposure as a lung co-morbidity may lead to organ dysfunctions due to metabolic disturbances and an increased hemodynamic instability during resuscitation from HS with the effects on lung function already published (17). To ensure clinical transferability of the results, we used our murine model of HS with resuscitation similar to intensive care management (infusion of crystalloids and norepinephrine (NE) to achieve hemodynamic targets, lung-protective mechanical ventilation, measurements of gas exchange, and control of body temperature (17–19)) together with a detailed analysis of the metabolic state (18, 20) and mitochondrial function (16, 21) in CS exposed animals (21).

Material and methods

This study was approved by the federal authorities for animal research of the Regierungspräsidium Tübingen, Baden-Wuerttemberg, Germany (approved animal experimentation number: 1359, August 17th, 2017), and performed in adherence with the National Institutes of Health Guidelines on the Use of Laboratory Animals and the European Union "Directive 2010/63 EU on the protection of animals used for scientific purposes." $GR^{dim/dim}$ mice (Nr3c1tm3Gsc) (22) were bred in a mixed background (129/SvEv x C57BL/6) and housed in the animal facility at University Ulm or in the housing facility at Boehringer Ingelheim (Biberach). $GR^{+/+}$ littermate controls were used as wild-type mice. Animals always had free access to food and water, were kept under standardized conditions, and were equally distributed in terms of age (16-26 weeks) and body weight (23-34 g). Groups comprised 7 animals ($GR^{+/+}$ non-CS), 9 animals ($GR^{dim/dim}$ non-CS), 8 animals ($GR^{+/+}$ CS exposure), and 9 animals ($GR^{dim/dim}$ CS exposure) of both gender. Due to the complicated surgery 2 animals in the $GR^{+/+}$ non-CS group and 1 animal in the $GR^{+/+}$ CS group deceased during surgery.

Implementation of general anesthesia and surgery

Anesthesia was induced *via* sevoflurane (2.5%; sevoflurane, Abbott, Wiesbaden, HE, Germany) as described previously (19, 21), followed by intraperitoneal injection (ip) of ketamine ($120\mu g \cdot g^{-1}$; Ketanest-S, Pfizer, New York City, NY), midazolam ($1.25\mu g \cdot g^{-1}$; Midazolam-ratiopharm, Ratiopharm, Ulm, BW, Germany) and fentanyl ($0.25\mu g \cdot g^{-1}$; Fentanyl-hameln, Hameln Pharma Plus GmbH, Hameln, NI, Germany). Afterwards, animals were placed on a closed-loop-system for body temperature control (19, 21). Lung-protective mechanical ventilation using a small animal ventilator (FlexiVent, Scireq, MO, Canada) was performed *via* a tracheostomy (19, 21). Surgical instrumentation comprised catheters in the jugular vein for fluid administration, the carotid artery for hemodynamic measurements, the femoral artery for blood removal, and the bladder to collect urine (19, 21). General anesthesia was titrated to guarantee complete tolerance against noxious stimuli and was sustained by continuous intravenous (iv) administration of ketamine, midazolam, and fentanyl to reach deep sedation (0.85 [0.79; 0.88] $\mu l \cdot g^{-1} \cdot min.^{-1}$ for all animals). Animals were mechanically ventilated with ventilator settings being F_iO_2 0.21%, respiratory rate $150 \cdot min^{-1}$, tidal volume of 6 $mL \cdot kg^{-1}$, and inspiratory/expiratory time ratio 1:2. Ventilation was modified to maintain an arterial $PaCO_2$ between 30 mmHg and 40 mmHg throughout the experiment as described previously (21). Therefore, blood gas analyses were performed before HS, 2h after re-transfusion of shed blood, and at the end of the experiment. However, P_aCO_2 values reported in Table 1 were measured at the end of experiment where adaptation of ventilation was no longer practicable. Therefore, P_aCO_2 values may vary and appear out of that range at the end of the experiment. Positive end-expiratory pressure (PEEP) was adjusted according to the arterial PaO_2 (PaO_2/F_iO_2-ratio>300mmHg: PEEP=3cmH_2O; PaO_2/FiO_2-ratio<300mmHg: PEEP=5cmH_2O; PaO_2/FiO_2-ratio<200mmHg: PEEP=8cmH_2O) (19, 21). Recruitment maneuvers (5s hold at 18 cmH_2O) were repeated hourly to avoid any impairment of thoraco-pulmonary compliance due to anesthesia- and/or supine position-induced atelectasis. A detailed description of the intensive care measures in mice performed in the present study (mouse intensive care unit, MICU) can be found elsewhere (23).

Cigarette smoke inhalation procedure

CS exposure was performed for 5 days per week over a period of 3 weeks using a standardized protocol as described previously (8, 11, 24). Particle concentration was monitored by a real time ambient particle monitor (MicroDust Pro, Casella, Amherst, NH, USA). In pilot experiments, this CS-exposure procedure had not caused any effect on the behavior, body weight, or respiratory pattern. Control animals (non-CS) were exposed to room air. After CS exposure, mice were transported from Boehringer Ingelheim (Biberach) to Ulm University and there were allowed to recover for 1 week to avoid acute stress effects induced by the CS procedure per se (11, 25).

Induction of hemorrhagic shock

After the initiation of lung-protective mechanical ventilation and instrumentation for vascular access, mice underwent 1h of HS. HS was performed by removing blood out of the femoral catheter with citrate-coated syringes (about $30\mu L \cdot g^{-1}$) to titrate mean arterial pressure (MAP) to 35 mmHg. Blood was further

TABLE 1 Hemodynamic and metabolic measurements as well as ventilation parameters in $GR^{dim/dim}$ and $GR^{+/+}$ mice with or without cigarette-smoke (CS) exposure and after hemorrhagic shock(HS) with subsequent resuscitation (4h) at the end of the experiment.

Parameters	Resuscitation (IV colloids and norepinephrine)			
	$GR^{+/+}$+non-CS (n = 7)	$GR^{dim/dim}$+non-CS (n = 9)	$GR^{+/+}$+CS (n = 8)	$GR^{dim/dim}$+CS (n = 9)
Bodyweight [g]	27.5 (25.6; 27.8)	26.7 (25.2; 30.6)	29.2 (26.4; 32.4)	27.3 (25.6; 30.1)
Heart Rate [beats·min^{-1}]	372 (352; 439)	480 (413; 538)	307 (276; 506)	**580 (553; 593)$^{\$}$**
Mean Arterial Pressure [mmHg]	66 (56; 77)	54 (50; 64)	57 (53; 63)	62 (55; 72)
Horovitz Index [mmHg]	486 (386; 490)	356 (348; 457)	460 (358; 525)	322 (293; 384)
$PaCO_2$ [mmHg]	29 (28; 38)	38 (32; 43)	35 (29; 37)	**43 (41; 46)$^{\$}$**
Minute ventilation [mL·kg^{-1}·min^{-1}]	1100 (1040; 1150)	1100 (980; 1150)	1000 (943; 1150)	1070 (1050; 1110)
Glucose [mg·dL^{-1}]	115 (106; 123)	120 (110; 162)	96 (87; 107)	**128 (122; 134)$^{\$}$**
Arterial pH	7.38 (7.33; 7.44)	**7.23 (7.10; 7.31)***	7.35 (7.23; 7.42)	7.26 (7.23; 7.32)
Arterial base excess [mmol·L^{-1}]	-6.4 (-7.4; -5.4)	**-10.2 (-15.7; -8.0)***	-7.1 (-10.4; -5.6)	**-7.6 (-8.9; -4.8)$^{\$}$**
Lactate [mmol·L^{-1}]	1.2 (0.8; 1.5)	**2.3 (1.4; 4.6)***	1.3 (1.1; 1.6)	**1.2 (1.1; 1.7)$^{\$}$**
Hemoglobin [g·dL^{-1}]	8.0 (7.5; 8.4)	7.1 (6.7; 7.6)	8.7 (7.7; 9.2)	**8.7 (7.8; 9.5)$^{\$}$**
Blood volume withdrawn for shock [µl·g^{-1}]	30.0 (30.0; 30.0)	30.0 (27.5; 30.0)	30.0 (30.0; 30.0)	30.0 (23.0; 30.0)
Urinary output [µL]	2235 (1486; 3132)	2118 (1542; 3191)	1760 (1303; 4130)	1945 (1083; 2444)

*P < 0.05 vs. $GR^{+/+}$ non-CS. $^{\$}$P < 0.05 vs. $GR^{+/+}$ CS. $^{\$}$P < 0.05 vs. $GR^{dim/dim}$ non-CS. Data is shown as median (25^{th} and 75^{th} percentile). Significant different values are highlighted bold.

removed or re-transfused to keep MAP at 35 mmHg for 1h. Besides, fluid administration was temporarily stopped. At the start of the resuscitation phase, shed blood was re-transfused, together with the administration of hydroxyethyl starch 6% (10µl·g^{-1} h^{-1}) and NE dissolved in balanced electrolyte solution (≤0.5 ml·h^{-1} for all animals) *via* the jugular vein catheter titrated to maintain MAP≥55 mmHg. The bladder was punctured to collect urine during the experiment. After 4h of resuscitation, animals were exsanguinated, blood and tissue samples were taken immediately thereafter, and prepared for further analyses (19, 21).

Analysis of metabolic pathways and kidney function

Thirty minutes before induction of hemorrhagic shock, mice received a primed continuous infusion of stable, non-radioactive-labeled $^{13}C_6$-glucose, $^{15}N_2$-urea, $^{2}H_5$-glycerol, and 5,5,5–$^{2}H_3$-leucine. Expiratory breath gas was sampled 0.5, 1.5, 2.5, 3.5, 4.5, and 5.5 h (end of experiment) after start of the stable isotope infusion. Arterial blood was sampled at time points 0.5, 2.5, 4.5, and 5.5 h. Together with urine output, gas chromatography/mass spectrometry measurement of plasma und urinary creatinine concentrations using $^{2}H_3$-creatinine as internal standard allowed for calculating creatinine clearance (18). Expiratory gas was analyzed immediately after collection by gas chromatography/mass spectrometry (GC/MS) for total expiratory CO_2 concentration and $^{13}CO_2$ enrichment to assess glucose oxidation rate. Plasma and urine samples were stored at −80°C until sample workup. For metabolic analysis, we only analyzed animals that survived the whole observation period (4 h) in order to guarantee a steady state of isotopes (n=7 for $GR^{dim/dim}$ and $GR^{+/+}$ non-CS, n=8 for $GR^{+/+}$ CS, and n=9 for $GR^{dim/dim}$ CS). For further details see supplemental material.

Parameters of hemodynamics, gas exchange, and metabolism

Systemic hemodynamics and body temperature were recorded hourly. Blood gas tensions, acid-base status, glycaemia, and lactatemia were assessed at the end of the resuscitation period *via* arterial blood gas analysis (ABL800 Felx; Radiometer, Krefeld, Germany) (19, 21).

Mitochondrial respiration

Mitochondrial respiratory capacity was determined *via* high-resolution respirometry with a clark-electrode-based system (Oxygraph 2k, OROBOROS Instruments Corp., Innsbruck, Austria) as described previously (19). Post-mortem muscle, heart, liver, and brain biopsies were mechanically homogenized in Mir05 (respiration medium). Mir05 is composed of 0.5mM EGTA, 3mM MgCl2·6H2O, 60mM Lactobionic acid, 20mM Taurine, 10mM KH2PO4, 20mM HEPES, 110mM Sucrose, 1g·L-1 bovine serum albumin). 1.5-2 mg of tissue (1.5mg: heart, 2mg tissue: muscle, liver, and brain) were added to the Oxygraph chamber. By the addition of a defined sequence of substrates and inhibitors, various states of mitochondrial function could be assessed. Complex I activity was determined after addition of 10mM pyruvate, 10mM glutamate, 5mM malate and 5mM ADP. 10µM cytochrome c was added to check for mitochondrial integrity. Maximum oxidative phosphorylation (OxPhos) was evaluated after subsequent addition of 1mM octanoyl-carnitine and 10mM succinate. Leak compensation was assessed after inhibition of the ATP-synthase by 2.5µM oligomycin, followed by stepwise titration of the uncoupling agent Carbonyl cyanide-4-(trifluoromethoxy)-phenylhydrazone (FCCP, final concentration 1.5µM) to reach maximum respiratory activity of the electron transfer system in the uncoupled state (ETS).

Measurements of cytokine, chemokine, and corticosterone concentrations in plasma

Cytokines, chemokines, and growth factors were measured using Bio-Plex Pro Mouse Cytokine 23-plex Assay (Group I) (Biorad) simultaneously in the plasma according to the manufacturer´s protocol. The multiplex-assay was performed with Bio-Plex 200 machine (Biorad) and the Bio-Plex Manager TM 6.1 software (Biorad). Plasma corticosterone levels were determined with an enzyme linked immunosorbent assay (ELISA) kit (TECAN, IBL international GmbH, RE52211) according to the manufactures protocol. In short, plasma samples were incubated in the anti-corticosterone antibody coated wells alongside with a horse-reddish peroxide (HRP) conjugated corticosterone competitor for one hour at room temperature. After five subsequent washing steps, HRP substrate was added for 15 min followed by stop solution and immediate measure of color intensity at 450 nm using Fluostar OPTIMA plate reader. Corticosterone concentrations were calculated according to the provided standards using a 4-parametric fit.

Statistical analysis

Unless stated otherwise, all data are presented as median (25^{th} and 75^{th} percentile). Data sets were analyzed using non-parametric statistics, i.e. Mann-Whitney U-test (one factor, two independent samples) or Kruskal-Wallis test with *post hoc* Dunn's comparison testing (one factor, four independent samples). P-values <0.05 were considered statistically significant. Quantitative graphical presentations and statistical analyses were accomplished by using GraphPad Prism 9 (GraphPad Software Inc, La Jolla, Calif).

Results

Survival

All CS exposed animals survived to the end of the observation period during resuscitation from $GR^{dim/dim}$ HS (4h). Only two animals with an attenuation of GR function and non-CS exposure did not reach the end of the observation period, however, the survival rates did not show any significant intergroup differences and have been reported previously in the supplementary materials of a publication of our group (17).

Hemodynamics, acid–base balance, parameters of organ (dys)function as well as mitochondrial respiration

To examine the effects of an attenuated GR function as well as exposure of CS on organ function during resuscitation from 1h of HS, hemodynamics, metabolic parameters, and mitochondrial respiration were investigated. Table 1 summarizes the parameters of hemodynamics and acid–base status. Heart rate was significantly higher in $GR^{dim/dim}$ compared to $GR^{+/+}$ mice with CS-exposure, whereas mean arterial pressure (MAP) did not differ between groups. In non-CS exposed mice, $GR^{dim/dim}$ mice had a significantly higher need of catecholamines to keep hemodynamic stability compared to $GR^{+/+}$ mice (Figure 1). In contrast, need of catecholamines did not differ in CS-exposed $GR^{dim/dim}$ and $GR^{+/+}$ mice (Figure 1). After CS exposure, arterial partial pressure of carbon dioxide (P_aCO_2) was significantly higher in $GR^{dim/dim}$ compared to $GR^{+/+}$ mice, whereas minute ventilation did not differ between groups (Table 1). In non-CS exposed mice, pH as well as base excess (BE) were lower and lactate levels were higher in $GR^{dim/dim}$ compared to $GR^{+/+}$ mice (Table 1). Because increased lactate levels may be linked to disturbances in mitochondrial respiration (6, 26), important metabolic organs as muscle, heart, liver and brain were investigated for

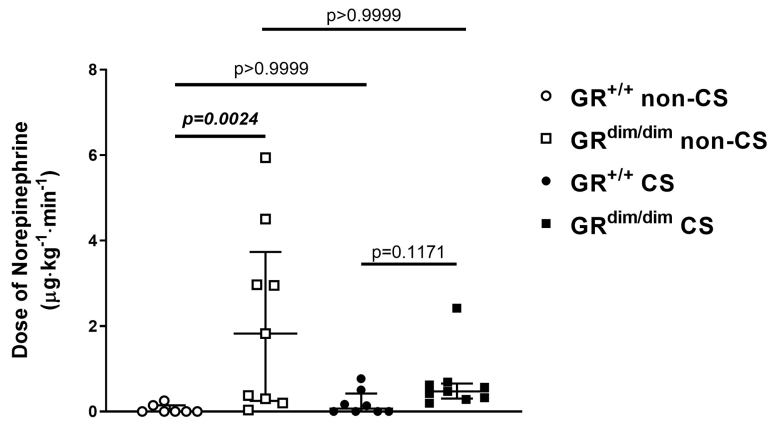

FIGURE 1
Doses of norepinephrine(NE) in mechanically ventilated $GR^{dim/dim}$ and $GR^{+/+}$ mice with or without cigarette-smoke (CS) exposure and after 1 h of hemorrhagic shock (HS, mean arterial pressure (MAP) 35 mmHg) and subsequent resuscitation (colloids, NE) for 4 h. NE was titrated intravenously during resuscitation to keep MAP ≥55mmHg. $GR^{+/+}$ mice non-CS: n = 7, $GR^{dim/dim}$ mice non-CS: n = 9, $GR^{+/+}$ mice CS: n=8, $GR^{dim/dim}$ mice CS: n = 9. Data is presented as median (25^{th} and 75^{th} percentile and minimum/maximum).

mitochondrial respiration in the current study. However, mitochondrial respiration (Figure 2) in tissue from muscle, heart, liver, and brain in $GR^{dim/dim}$ and $GR^{+/+}$ mice with or without CS exposure revealed no intergroup differences in all four organs analyzed in the current study. In summary, after resuscitation from HS, the attenuated function of the GR resulted in a higher need of catecholamines to keep hemodynamic stability and a lower pH together with increased lactate levels. These differences were not present in CS exposed mice.

Measurements of plasma cytokine levels at the end of 4 hours of resuscitation after hemorrhagic shock

To determine effects of an attenuation of GR function and CS exposure on inflammatory parameters, plasma concentration of cytokines and chemokines were determined. In the non-CS group, concentration of interleukine-6 (IL-6), interleukine-12 p40 (IL-12 p40), and Eotaxin were significantly higher in plasma of $GR^{dim/dim}$ mice compared to $GR^{+/+}$ mice (Table 2). Interestingly, there were no intergroup differences for the measured plasma cytokines when animals were exposed to CS before HS. Therefore, only the attenuation of GR function led to an increase in some plasma cytokines, whereas this increase was prevented by CS pre-exposure.

Effects of an attenuation of GR function and CS exposure on metabolic parameters

Despite no differences in minute ventilation during resuscitation (Table 1), $GR^{dim/dim}$ mice showed higher CO_2 values in the exhaled air compared to $GR^{+/+}$ mice, both after CS exposure during the observation period (Figure 3A, together with increased arterial partial pressure of CO_2, see Table 1). The same genotype dependent difference appeared for the concentration of glucose in the plasma, whereas the rate of endogenous glucose production as well as glucose oxidation rate showed no inter-group differences (Figures 3C, D). After CS exposure, rate of appearance for urea (marker for hepatic metabolic capacity as well as kidney function) was significantly lower in $GR^{dim/dim}$ mice compared to $GR^{dim/dim}$ mice with no CS exposure (Figure 4A). Measures of lipolysis (measured *via* rate of appearance for glycerol), protein degradation (rate of appearance for leucine), and kidney function (creatinine clearance, urine output [Table 1]) showed no intergroup differences (Figures 4C, D). Taken together, during resuscitation after HS, CS exposed $GR^{dim/dim}$ mice presented with an increased glucose concentration in plasma (Figure 3B), which does not come from an increase in gluconeogenesis or decrease in glucose oxidation (Figures 3C, D). Furthermore, due to no differences in kidney function (creatinine clearance, Figure 4B) as well as protein breakdown (rate of appearance for leucine, Figure 4D), the reduced rate of appearance of urea in

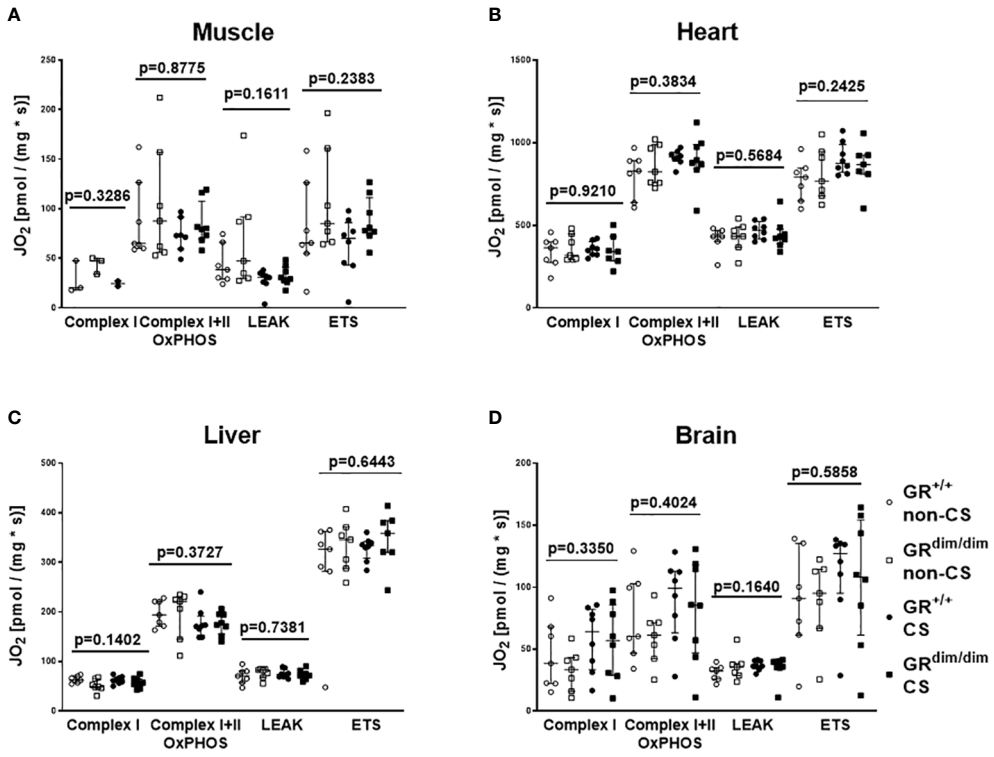

FIGURE 2
Mitochondrial respiration (JO2) in tissue from muscle **(A)**, heart **(B)**, liver **(C)**, and brain **(D)** in $GR^{dim/dim}$ and $GR^{+/+}$ mice with or without cigarette-smoke (CS) exposure and after 1 h of hemorrhagic shock (HS, MAP 35 mmHg) and subsequent resuscitation (colloids, NE) for 4 h. Overall p-values from Kruskal-Wallis-Test are shown above. $GR^{+/+}$ mice non-CS: n = 3-7, $GR^{dim/dim}$ mice non-CS: n = 3-7, $GR^{+/+}$ mice CS: n = 2-8, $GR^{dim/dim}$ mice CS: n=8. For the group $GR^{dim/dim}$ CS in muscle tissue there were no measurements available due to a measurement problem. Data is presented as median (25^{th} and 75^{th} percentile and minimum/maximum).

CS exposed $GR^{dim/dim}$ mice (Figure 4A) is most likely a result of a reduced hepatic synthesis.

Measurements of corticosterone concentration in plasma

As the above measured parameters are well known to be influenced by corticosteroids, we determined the concentration of corticosterone in plasma. Neither an attenuation of GR function nor CS exposure had any effects on plasma corticosterone levels in mice in the present study under intensive care conditions (non-CS $GR^{+/+}$: 112 (78;141), non-CS $GR^{dim/dim}$: 85 (35; 156); CS $GR^{+/+}$: 93 (65; 147), CS $GR^{dim/dim}$: 82 (55; 119), P=0.6852).

Discussion

In the present study, we examined the effects of a dysfunction in the glucocorticoid receptor ($GR^{dim/dim}$) on hemodynamics, metabolic parameters, mitochondrial function, and inflammation during resuscitation from hemorrhagic shock (HS) in mice with pre-traumatic cigarette smoke (CS) exposure with the effects on lung function already published in a previous paper (17).

Neither an attenuation of GR function ($GR^{dim/dim}$) nor CS exposure prior to resuscitation from HS showed an effect on survival rates. However, we found that non-CS exposed $GR^{dim/dim}$ mice needed significantly higher doses of norepinephrine (NE) to keep hemodynamic stability compared to $GR^{+/+}$ mice. Furthermore, lower pH and higher lactate levels as well as an increase in systemic cytokines was present in non-CS $GR^{dim/dim}$ compared to $GR^{+/+}$ mice. Surprisingly, these genotype dependent differences disappeared in CS exposed animals.

Compared to a mouse model based on lipopolysaccharide (LPS)-induced systemic inflammation, we previously reported a significantly increased mortality in $GR^{dim/dim}$ mice compared to $GR^{+/+}$ mice (16). In that LPS model, $GR^{dim/dim}$ mice presented with significant higher need for NE to keep hemodynamic stability, like in the present study the non-CS exposed

TABLE 2 Concentration of cytokines in plasma in $GR^{dim/dim}$ and $GR^{+/+}$ mice with or without cigarette-smoke (CS) exposure and after HS with subsequent resuscitation (4 h) at the end of the experiment.

Concentration of cytokines in plasma	Resuscitation (IV colloids and NE)			
	$GR^{+/+}$+non-CS (n = 1-6)	$GR^{dim/dim}$+non-CS (n = 3-9)	$GR^{+/+}$+CS (n = 1-8)	$GR^{dim/dim}$+CS (n = 1-9)
Interleukine-1 alpha (IL-1 α) [pg·ml^{-1}]	20 (18; 44)	18 (13; 28)	18 (15; 22)	20 (14; 23)
Interleukine-1 beta (IL-1 β) [pg·ml^{-1}]	1.8 (0.6; 6.2)	10.9 (4.1; 15.6)	3.0 (3.0; 5.2)	3.0 (0.6; 7.4)
Interleukine-2 (IL-2) [pg·ml^{-1}]	6.3 (4.7; 7.8)	5.3 (3.4; 13.0)	1.7 (1.7; 1.7)	3.4 (3.4; 3.4)
Interleukine-3 (IL-3) [pg·ml^{-1}]	0.5 (0.1; 1.2)	2.4 (1.0; 2.9)	1.0 (0.3; 7.7)	1.2 (0.5; 2.4)
Interleukine-4 (IL-4) [pg·ml^{-1}]	5.1 (2.9; 7.0)	3.4 (2.3; 4.8)	4.3 (2.0; 5.3)	2.5 (1.4; 3.6)
Interleukine-5 (IL-5) [pg·ml^{-1}]	10.0 (7; 23)	34 (20; 37)	13 (8; 26)	22 (17; 39)
Interleukine-6 (IL-6) [pg·ml^{-1}]	170 (69; 285)	**451 (330; 566)***	297 (205; 393)	327 (212; 405)
Interleukine-9 (IL-9) [pg·ml^{-1}]	11 (9; 13)	6 (5; 8)	25 (3; 41)	86 (66; 106)
Interleukine-10 (IL-10) [pg·ml^{-1}]	10 (10; 22)	22 (13; 47)	16 (8; 20)	9 (8; 23)
Interleukine-12 p40 (IL-12 p40) [pg·ml^{-1}]	142 (103; 191)	**273 (218; 518)***	192 (148; 224)	200 (140; 221)
Interleukine-12 p70 (IL-12 p70) [pg·ml^{-1}]	4 (4; 4)	75 (24; 176)	42 (36; 48)	45 (39; 50)
Interleukine-13 (IL-13) [pg·ml^{-1}]	25 (17; 40)	23 (15; 30)	17 (11; 48)	15 (12; 29)
Interleukine-17 (IL-17) [pg·ml^{-1}]	4.5 (2.5; 7.2)	4.9 (2.5; 15.4)	5.1 (4.1; 5.7)	3.7 (1.0; 4.9)
Eotaxin [pg·ml^{-1}]	1100 (810; 1802)	**2729 (1582; 3275)***	1820 (1563; 2101)	2536 (1782; 2824)
Granulocyte Colony-stimulating Factor (G-CSF) [pg·ml^{-1}]	1042 (704; 1277)	1333 (960; 2310)	1310 (1247; 1344)	879 (830; 1395)
Granulocyte-macrophage Colony-stimulating Factor (GM-CSF) [pg·ml^{-1}]	27 (27; 34)	37 (18; 56)	37 (15; 64)	22 (17; 27)
Interferon gamma (INF-γ) [pg·ml^{-1}]	2.5 (1.6; 3.9)	3.8 (2.9; 6.4)	3.3 (2.9; 10.8)	4.7 (2.9; 7.8)
Keratinocyte Chemoattractant (KC) [pg·ml^{-1}]	20 (17; 28)	18 (13; 22)	25 (19; 34)	28 (19; 57)
Monocyte Chemoattractant Protein-1 (MCP-1) [pg·ml^{-1}]	124 (37; 147)	258 (199; 751)	129 (78; 173)	184 (90; 299)
Macrophage Inflammatory Protein-1 alpha (MIP-1 α) [pg·ml^{-1}]	0.7 (0.3; 0.9)	1.0 (0.7; 1.9)	0.8 (0.7; 1.3)	0.6 (0.3; 0.8)
Macrophage Inflammatoryt Protein-1 beta (MIP-1 β) [pg·ml^{-1}]	5.0 (5.0; 5.0)	7.0 (2.7; 10.8)	5.0 (5.0; 5.0)	46.1 (0.0; 92.1)
Regulated And Normal T-cell Expressed and Secreted (RANTES) [pg·ml^{-1}]	6.2 (5.2; 14.7)	34.6 (10.8; 138.1)	8.0 (5.5; 12.2)	8.3 (6.2; 12.3)
Tumor Necrosis Factor alpha (TNF-α) [pg·ml^{-1}]	21 (14; 47)	34 (11; 38)	15 (9; 26)	14 (14; 14)

*P < 0.05 vs. $GR^{+/+}$ non-CS. Data is shown as median (25^{th} and 75^{th} percentile). Signifiant different values are highlighted bold.

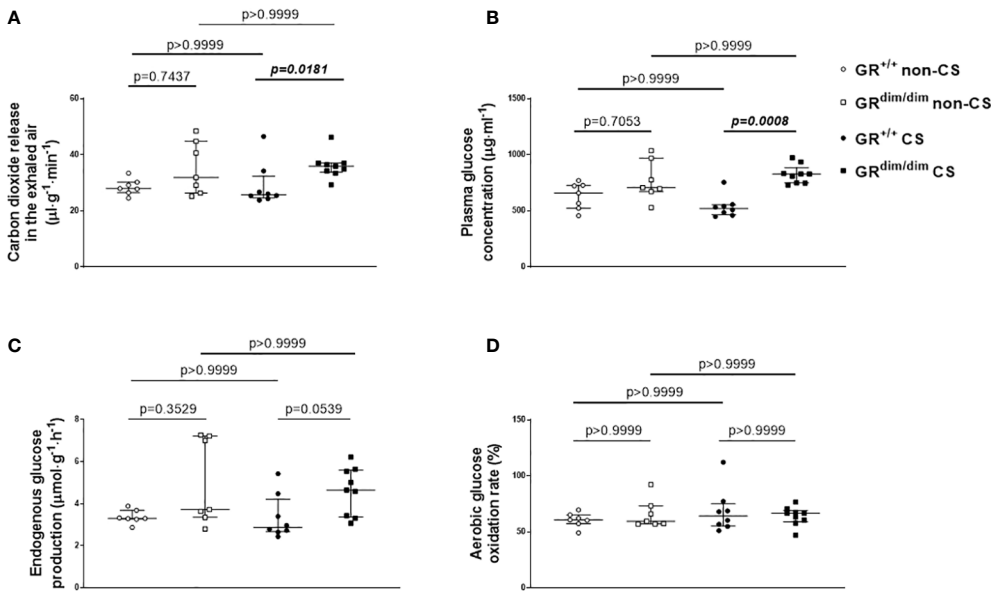

FIGURE 3
Glucose metabolism. **(A)** Carbon dioxide release *via* the exhaled air, **(B)** plasma glucose concentration, **(C)** endogenous glucose production rate, and **(D)** glucose oxidation as percentage of oxidation of infused tracer. $GR^{+/+}$ mice non-CS: n=7, $GR^{dim/dim}$ mice non-CS: n = 7, $GR^{+/+}$ mice CS: n = 8, $GR^{dim/dim}$ mice CS: n = 9. Data is presented as median (25^{th} and 75^{th} percentile and minimum/maximum).

$GR^{dim/dim}$ mice during resuscitation from HS. However, in the present study there was no effect on survival. Although resuscitation manners (except for colloids) as well as definition for hemodynamic stability (MAP≥55mmHg) were similar in both studies, with regards on survival rates it must be considered that the observation time in the LPS study was 6 h and in the present study 4 hours. If the observation time would have been 6 h in the present study, there may would have been more animals not surviving the whole observation period after HS in the non-CS $GR^{dim/dim}$ group with a probably significant effect on survival rates. Interestingly, CS exposure led to a higher hemodynamic stability in $GR^{dim/dim}$ mice following HS shown by a trend towards a decreased dose of NE in the present study. We can only speculate for possible reasons for this effect of CS exposure on hemodynamics. A possible increased sympathetic activity with reduced demand of additional catecholamine support in CS exposed mice during resuscitation from HS has been reported before (21). This may have been the reason for the absolute lower catecholamine need in CS exposed $GR^{dim/dim}$ mice during resuscitation from HS compared to non-CS exposed animals. An interaction of CS exposure and glucocorticoid receptor (GR) function might also be a possible explanation for the lower NE need in CS exposed animals, because one study reported that maternal tobacco smoke exposure increased serum corticosterone levels in adult male rat offspring (27). Another study reported that CS exposure during breastfeeding in rats showed changes in serum corticosterone level in in obese adult offspring (28). However, with the results in the present study, we can only speculate about possible effects of CS exposure on GR function. This needs further investigation.

In a previous study from our group with a similar murine model of resuscitation from HS, subsequent CS exposure per se had the strongest impact on inflammatory responses, shown by an increased systemic inflammation (21). Furthermore, in a murine model of blunt chest trauma (without HS), pre-traumatic CS exposure also enhanced post-traumatic inflammation (8). In the present study, an increased systemic inflammation could only be seen in part due to the attenuation of GR function in non-CS mice (increased plasma IL-6, IL-12 p40, and Eotaxin in non-CS $GR^{dim/dim}$ compared to non-CS $GR^{+/+}$ mice, Table 2), whereas there were no differences in systemic cytokines in CS exposed mice. Although anti-inflammatory effects *via* CS exposure have been reported in a murine model of allergic asthma (29), such protective effects are more unlikely in the present study, because our CS exposure model has, so far, only shown pro-inflammatory effects in our murine trauma models (8, 21). As mentioned above, the short observation time of 4h also might be a reason for the missing inflammatory effect of CS exposure in the present murine trauma model.

With regards to metabolic parameters, in the present study only $GR^{dim/dim}$ mice without a CS exposure presented with a lower pH, a lower base excess (BE), and higher lactate levels compared to $GR^{+/+}$ mice (Table 1). The higher lactate levels are in agreement with the study by Vandewalle and colleagues showing an impaired lactate clearance upon LPS-exposure in

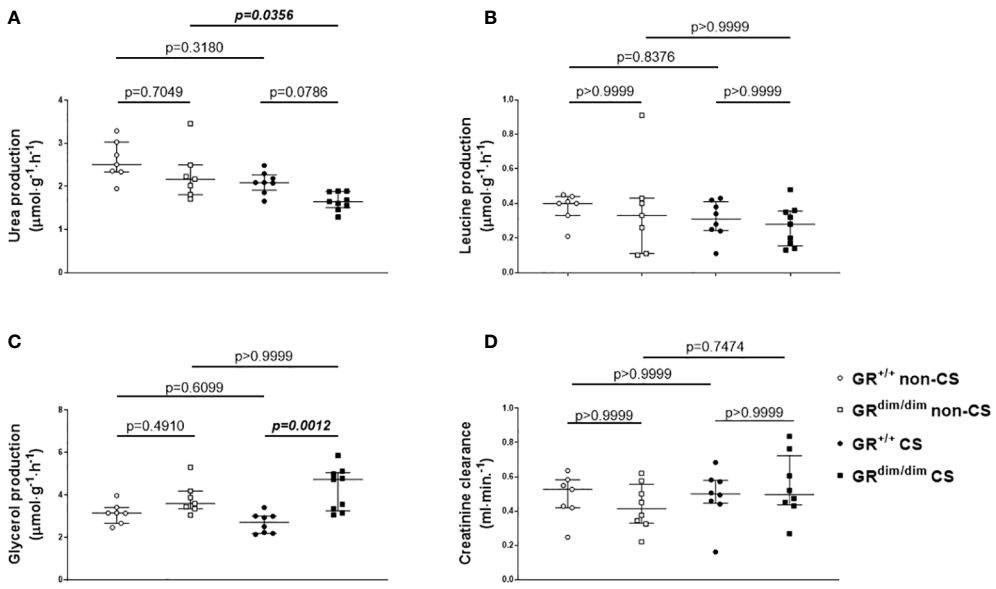

FIGURE 4
Parameters of metabolic and kidney function. Rates of appearance of **(A)** urea, **(B)** leucine, **(C)** glycerol as well as **(D)** creatinine clearance, as measures for hepatic metabolic capacity, protein degradation, lipolysis, and kidney function, respectively. *P < 0.05. #P < 0.01. $GR^{+/+}$ mice non-CS: n = 7, $GR^{dim/dim}$ mice non-CS: n = 7-8, $GR^{+/+}$ mice CS: n=8, $GR^{dim/dim}$ mice CS: n = 8-9. Data is presented as median (25^{th} and 75^{th} percentile and minimum/maximum).

$GR^{dim/dim}$ mice even in the absence of resuscitation (30). With regards to the lower pH and lower BE in non-CS $GR^{dim/dim}$ mice shown in the present study it must be considered that the lactate levels alone cannot be the reason for this metabolic acidosis. A metabolic acidosis in mice due to other fixed acids than lactic acid has been reported before (11, 24). Furthermore, in the present study, pH, BE, and lactate levels were similar in non-CS exposed $GR^{+/+}$ and CS exposed $GR^{+/+}$ and $GR^{dim/dim}$ mice with a trend towards a slightly lower pH in the latter group, which might have been induced by the higher P_aCO_2 values (Table 1). Therefore, CS exposure had no effects on pH, BE, and lactate levels on $GR^{+/+}$ mice in the present study. This is in line with previous studies also showing no effect of CS exposure on pH or lactate levels in a more recent mouse model of HS (21).

Hemodynamic instability coincides with an increased need of catecholamines. It is well known that both, endogenously produced as well as externally administered catecholamines exert non-hemodynamic effects and impact metabolism (31). Vital organs such as heart, brain, and kidney may receive energy under stress situations like HS through release of lactate from skeletal muscle as well as by breaking down amino acids, glycogen, and triglycerides to generate glucose, fatty acids, and ketone bodies, all mediated *via* an increased release of endogenous catecholamines (32, 33). Therefore, the increased glucose level in CS exposed $GR^{dim/dim}$ mice in the present study could have been induced *via* increased doses of catecholamines. However, the need of catecholamines to keep hemodynamic stability was higher in non-CS exposed $GR^{dim/dim}$ mice with no effect on glucose levels compared to $GR^{+/+}$ mice in this group. Furthermore, we found no differences in endogenous glucose production or aerobic glucose oxidation between all groups of mice (Figure 3). Therefore, the increased glucose concentration in CS exposed $GR^{dim/dim}$ mice does not come from an increased dose of catecholamines or an increase in gluconeogenesis or decrease in glucose oxidation. Moreover, it is most likely an effect of a reduced peripheral uptake of glucose in tissue which utilizes glucose in a non-oxidative way in this group of mice. We can only speculate for possible reasons for this effect. On one hand, in our subsequent studies in LPS-challenged $GR^{dim/dim}$ and $GR^{+/+}$ mice we found no differences for glucose concentrations between $GR^{dim/dim}$ and $GR^{+/+}$ mice (16). On the other hand, in previous studies CS exposure in wildtype mice lead to a trend towards lower glucose levels (21, 24). Therefore, the increased glucose level in CS exposed $GR^{dim/dim}$ mice in the present study are more likely related to both, the combination of CS exposure and attenuation of GR function, which warrants further investigation.

Besides a catecholamine-induced energy production *via* increased carbohydrate, catecholamines also mediate energy production *via* a ketotic effect through an increase in fat and protein oxidation (32, 34). The ketotic impacts of both epinephrine and NE are similar at physiologically low concentrations, whereas the ketotic effect of NE predominates at pathophysiological concentrations, possibly due to an

antiketogenic effect resulting from the epinephrine-induced increase of glucose and subsequent insulin concentrations (31), with the latter one may be missing in the present study. With measurements of the rate of appearance of urea in the present study, we were able to determine hepatic metabolic capacity as well as in part kidney function. After CS exposure, $GR^{dim/dim}$ mice produced significantly less urea compared to non-CS $GR^{dim/dim}$ mice and had a trend towards a lower urea production compared to CS exposed $GR^{+/+}$ mice (Figure 4A). With no differences between the groups for kidney function measured *via* plasma creatinine concentration, creatinine clearance, and urine output in the present study we can exclude differences in urea excretion *via* the kidney (Figures 4A, D). With no differences in rate of appearance for leucine (protein degradation, Figure 4B), we can also exclude differences in urea metabolized to amino acids. Therefore, primarily the reduced urea in CS exposed $GR^{dim/dim}$ mice after resuscitation from HS in the present study is most likely a result of a reduced hepatic synthesis. However, this is in contrast with the results of the rate of appearance for glucose, since both, urea and glucose are metabolized in the periportal cells and therefore we should have seen effects on both, rate of appearance in urea and glucose (35).

Last, in CS exposed $GR^{dim/dim}$ mice the rate of appearance for glycerol was higher compared to CS exposed $GR^{+/+}$ mice, which indicates an increase in lipolysis. However, with no differences in plasma corticosterone concentrations in CS exposed $GR^{dim/dim}$ and $GR^{+/+}$ mice in the present study, it is at least less likely that differences in corticosterone concentrations due to an attenuation of GR function might have altered glucose or lipid metabolism in $GR^{dim/dim}$ mice in the present study.

Conclusion

Cigarette smoke (CS) exposure before hemorrhagic shock (HS) led to an increased hemodynamic stability in mice with an attenuated GR function ($GR^{dim/dim}$), indicated by a trend towards an absolute lower norepinephrine (NE) need. CS exposed $GR^{dim/dim}$ mice also presented with less metabolic changes (pH, base excess, and lactate levels), and showed an increase in lipid oxidation compared to non-CS $GR^{dim/dim}$ mice. If the more stable pH and BE values, the lower lactate levels, or the switch to lipid oxidation to possibly increase the efficiency of energy production to may maintain organ function were the reason or the consequence for the lower NE need in these mice warrants further investigation.

Data availability statement

The raw data supporting the conclusions of this article will be made available by the authors, without undue reservation.

Ethics statement

The animal study was reviewed and approved by Regierungspraesidium Tuebingen, Baden-Wuerttemberg, Germany.

Author contributions

MW, JP, PR, JT, and SV conceived and designed the study. MW, JP, TM, UW, CT, MK, JV, SK, MG, MF, EC, UB, PR, and SV performed the experiments and organ analysis. MW, JP, TM, UW, JV, EC, PR, JT, and SV analyzed the data and interpreted the results. MW, JP, and SV prepared the figures. MW, JP, and SV wrote the manuscript. PR and JT revised the manuscript. All authors contributed to the article and approved the submitted version.

Funding

Publication costs are funded by the Deutsche Forschungsgemeinschaft (DFG, German Research Foundation)—Project ID INST 40/600-1—Collaborative Research Center (CRC) Projektnummer 251293561 - SFB 1149 to MW and SV. SV received funding from Deutsche Forschungsgemeinschaft (DFG, German Research Foundation), GRK 2203 and DFG VE 994/2-1. PR and JT received funding from the Deutsche Forschungsgemeinschaft (DFG, German Research Foundation)—Collaborative Research Center (CRC) Projektnummer 251293561 - SFB 1149 and DFG Tu 220/13-1 to JT.

Conflict of interest

Authors CT, MK, and JB are employed by Boehringer Ingelheim Pharma GmbH & Co KG.

The remaining authors declare that the research was conducted in the absence of any commercial or financial relationships that could be construed as a potential conflict of interest.

Publisher's note

Supplementary material

The Supplementary Material for this article can be found online at: https://www.frontiersin.org/articles/10.3389/fimmu.2022.980707/full#supplementary-material

References

1. Angele MK, Schneider CP, Chaudry IH. Bench-to-bedside review: Latest results in hemorrhagic shock. *Crit Care* (2008) 12(4):218. doi: 10.1186/cc6919

2. Denk S, Weckbach S, Eisele P, Braun CK, Wiegner R, Ohmann JJ, et al. Role of hemorrhagic shock in experimental polytrauma. *Shock* (2017) 49(2):154–63. doi: 10.1097/SHK.0000000000000925

3. Eltzschig HK, Carmeliet P. Hypoxia and inflammation. *N Engl J Med* (2011) 364(7):656–65. doi: 10.1056/NEJMra0910283

4. Douzinas EE, Livaditi O, Tasoulis M-K, Prigouris P, Bakos D, Goutas N, et al. Nitrosative and oxidative stresses contribute to post-ischemic liver injury following severe hemorrhagic shock: The role of hypoxemic resuscitation. *PLoS One* (2012) 7 (3):e32968. doi: 10.1371/journal.pone.0032968

5. Merz T, Denoix N, Huber-Lang M, Singer M, Radermacher P, McCook O. Microcirculation vs. mitochondria-what to target? *Front Med (Lausanne)* (2020) 7:416. doi: 10.3389/fmed.2020.00416

6. Barth E, Albuszies G, Baumgart K, Matejovic M, Wachter U, Vogt J, et al. Glucose metabolism and catecholamines. *Crit Care Med* (2007) 35(9 Suppl):S508–18. doi: 10.1097/01.CCM.0000278047.06965.20

7. Vanhorebeek I, Gunst J, Ellger B, Boussemaere M, Lerut E, Debaveye Y, et al. Hyperglycemic kidney damage in an animal model of prolonged critical illness. *Kidney Int* (2009) 76(5):512–20. doi: 10.1038/ki.2009.217

8. Wagner K, Gröger M, McCook O, Scheuerle A, Asfar P, Stahl B, et al. Blunt chest trauma in mice after cigarette smoke-exposure: Effects of mechanical ventilation with 100% O2. *PloS One* (2015) 10(7):e0132810. doi: 10.1371/journal.pone.0132810

9. Geldmacher H, Biller H, Herbst A, Urbanski K, Allison M, Buist AS, et al. Die prävalenz der chronisch obstruktiven lungenerkrankung (COPD) in deutschland. *Ergebnisse der BOLD-Studie Dtsch Med Wochenschr* (2008) 133(50):2609–14. doi: 10.1055/s-0028-1105858

10. Sinden NJ, Stockley RA. Systemic inflammation and comorbidity in COPD: a result of 'overspill' of inflammatory mediators from the lungs? Review of the evidence. *Thorax* (2010) 65(10):930–6. doi: 10.1136/thx.2009.130260

11. Hartmann C, Hafner S, Scheuerle A, Möller P, Huber-Lang M, Jung B, et al. The role of cystathionine-γ-Lyase in blunt chest trauma in cigarette smoke exposed mice. *Shock* (2017) 47(4):491–9. doi: 10.1097/SHK.0000000000000746

12. Minei JP, Cuschieri J, Sperry J, Moore EE, West MA, Harbrecht BG, et al. The changing pattern and implications of multiple organ failure after blunt injury with hemorrhagic shock. *Crit Care Med* (2012) 40(4):1129–35. doi: 10.1097/CCM.0b013e3182376e9f

13. Vettorazzi S, Nalbantoglu D, Gebhardt JCM, Tuckermann J. A guide to changing paradigms of glucocorticoid receptor function-a model system for genome regulation and physiology. *FEBS J* (2021). doi: 10.1111/febs.16100

14. Lim H-W, Uhlenhaut NH, Rauch A, Weiner J, Hübner S, Hübner N, et al. Genomic redistribution of GR monomers and dimers mediates transcriptional response to exogenous glucocorticoid *in vivo*. *Genome Res* (2015) 25(6):836–44. doi: 10.1101/gr.188581.114

15. Vettorazzi S, Bode C, Dejager L, Frappart L, Shelest E, Klaßen C, et al. Glucocorticoids limit acute lung inflammation in concert with inflammatory stimuli by induction of SphK1. *Nat Commun* (2015) 6:7796. doi: 10.1038/ncomms8796

16. Wepler M, Preuss JM, Merz T, Hartmann C, Wachter U, McCook O, et al. Impaired glucocorticoid receptor dimerization aggravates LPS-induced circulatory and pulmonary dysfunction. *Front Immunol* (2019) 10:3152. doi: 10.3389/fimmu.2019.03152

17. Preuss JM, Burret U, Gröger M, Kress S, Scheuerle A, Möller P, et al. Impaired glucocorticoid receptor signaling aggravates lung injury after hemorrhagic shock. *Cells* (2021) 11(1):112. doi: 10.3390/cells11010112

18. Langgartner D, Wachter U, Hartmann C, Gröger M, Vogt J, Merz T, et al. Effects of psychosocial stress on subsequent hemorrhagic shock and resuscitation in Male mice. *Shock* (2019) 51(6):725–30. doi: 10.1097/SHK.0000000000001204

19. Gröger M, Wepler M, Wachter U, Merz T, McCook O, Kress S, et al. The effects of genetic 3-mercaptopyruvate sulfurtransferase deficiency in murine traumatic-hemorrhagic shock. *Shock* (2018) 51(4):472–478. doi: 10.1097/SHK.0000000000001165

20. Gröger M, Hogg M, Abdelsalam E, Kress S, Hoffmann A, Stahl B, et al. Effects of sodium thiosulfate during resuscitation from trauma-and-Hemorrhage in cystathionine gamma lyase (CSE) knockout mice. *Shock* (2022) 57(1):131–9. doi: 10.1097/SHK.0000000000001828

21. Hartmann C, Gröger M, Noirhomme J-P, Scheuerle A, Möller P, Wachter U, et al. In-depth characterization of the effects of cigarette smoke exposure on the acute trauma response and hemorrhage in mice. *Shock* (2018) 51(1):68–77. doi: 10.1097/SHK.0000000000001115

22. Reichardt HM, Kaestner KH, Tuckermann J, Kretz O, Wessely O, Bock R, et al. DNA Binding of the glucocorticoid receptor is not essential for survival. *Cell* (1998) 93(4):531–41. doi: 10.1016/s0092-8674(00)81183-6

23. Merz T, Kress S, Gröger M, Radermacher P, McCook O. Mouse intensive care unit (MICU). *Methods Mol Biol* (2021) 2321:121–35. doi: 10.1007/978-1-0716-1488-4_11

24. Hafner S, Wagner K, Weber S, Gröger M, Wepler M, McCook O, et al. Role of the purinergic receptor P2XR4 after blunt chest trauma in cigarette smoke-exposed mice. *Shock* (2017) 47(2):193–9. doi: 10.1097/SHK.0000000000000726

25. Wollin L, Pieper MP. Tiotropium bromide exerts anti-inflammatory activity in a cigarette smoke mouse model of COPD. *Pulm Pharmacol Ther* (2010) 23 (4):345–54. doi: 10.1016/j.pupt.2010.03.008

26. Vogt JA, Wachter U, Wagner K, Calzia E, Gröger M, Weber S, et al. Effects of glycemic control on glucose utilization and mitochondrial respiration during resuscitated murine septic shock. *Intensive Care Med Exp* (2014) 2(1):19. doi: 10.1186/2197-425X-2-19

27. Zinkhan EK, Lang BY, Yu B, Wang Y, Jiang C, Fitzhugh M, et al. Maternal tobacco smoke increased visceral adiposity and serum corticosterone levels in adult male rat offspring. *Pediatr Res* (2014) 76(1):17–23. doi: 10.1038/pr.2014.58

28. Novaes Soares P, Silva Tavares Rodrigues V, Cherem Peixoto T, Calvino C, Aparecida Miranda R, Pereira Lopes B, et al. Cigarette smoke during breastfeeding in rats changes glucocorticoid and vitamin d status in obese adult offspring. *Int J Mol Sci* (2018) 19(10):3084. doi: 10.3390/ijms19103084

29. Tilp C, Bucher H, Haas H, Duechs MJ, Wex E, Erb KJ. Effects of conventional tobacco smoke and nicotine-free cigarette smoke on airway inflammation, airway remodelling and lung function in a triple allergen model of severe asthma. *Clin Exp Allergy* (2016) 46(7):957–72. doi: 10.1111/cea.12665

30. Vandewalle J, Timmermans S, Paakinaho V, Vancraeynest L, Dewyse L, Vanderhaeghen T, et al. Combined glucocorticoid resistance and hyperlactatemia contributes to lethal shock in sepsis. *Cell Metab* (2021) 33(9):1763–76.e5. doi: 10.1016/j.cmet.2021.07.002

31. Hartmann C, Radermacher P, Wepler M, Nußbaum B. Non-hemodynamic effects of catecholamines. *Shock* (2017) 48(4):390–400. doi: 10.1097/SHK.0000000000000879

32. Gjedsted J, Buhl M, Nielsen S, Schmitz O, Vestergaard ET, Tønnesen E, et al. Effects of adrenaline on lactate, glucose, lipid and protein metabolism in the placebo controlled bilaterally perfused human leg. *Acta Physiol (Oxf)* (2011) 202 (4):641–8. doi: 10.1111/j.1748-1716.2011.02316.x

33. Steinberg D, Nestel PJ, Buskirk ER, Thompson RH. Calorigenic effect of norepinephrine correlated with plasma free fatty acid turnover and oxidation. *J Clin Invest* (1964) 43:167–76. doi: 10.1172/JCI104901

34. Bearn AG, Billing B, Sherlock S. The effect of adrenaline and noradrenaline on hepatic blood flow and splanchnic carbohydrate metabolism in man. *J Physiol* (1951) 115(4):430–41. doi: 10.1113/jphysiol.1951.sp004679

35. Li L, Zhang P, Bao Z, Wang T, Liu S, Huang F. PGC-1α promotes ureagenesis in mouse periportal hepatocytes through SIRT3 and SIRT5 in response to glucagon. *Sci Rep* (2016) 6:24156. doi: 10.1038/srep24156

frontiers | Frontiers in Immunology

TYPE Original Research
PUBLISHED 31 October 2022
DOI 10.3389/fimmu.2022.950646

OPEN ACCESS

EDITED BY
Klemens Horst,
University Hospital RWTH Aachen, Germany

REVIEWED BY
Elen H. Miyabara,
University of São Paulo, Brazil
Archna Sharma,
Feinstein Institute for Medical Research, United States

*CORRESPONDENCE
Shigeaki Inoue
inoues@med.kobe-u.ac.jp

SPECIALTY SECTION
This article was submitted to Inflammation, a section of the journal Frontiers in Immunology

RECEIVED 23 May 2022
ACCEPTED 19 October 2022
PUBLISHED 31 October 2022

CITATION
Nakanishi N, Ono Y, Miyazaki Y, Moriyama N, Fujioka K, Yamashita K, Inoue S and Kotani J (2022) Sepsis causes neutrophil infiltration in muscle leading to muscle atrophy and weakness in mice. *Front. Immunol.* 13:950646. doi: 10.3389/fimmu.2022.950646

Sepsis causes neutrophil infiltration in muscle leading to muscle atrophy and weakness in mice

Nobuto Nakanishi[1], Yuko Ono[1], Yusuke Miyazaki[1], Naoki Moriyama[1], Kazumichi Fujioka[2], Kimihiro Yamashita[3], Shigeaki Inoue[1]* and Joji Kotani[1]

[1]Division of Disaster and Emergency Medicine, Department of Surgery Related, Kobe University Graduate School of Medicine, Kobe, Japan, [2]Department of Pediatrics, Kobe University Graduate School of Medicine, Kobe, Japan, [3]Division of Gastrointestinal Surgery, Department of Surgery, Kobe University Graduate School of Medicine, Kobe, Japan

Background: Sepsis-induced muscle atrophy leads to prolonged physical dysfunction. Although the interaction of muscle atrophy and macrophage has been reported in sepsis, the role of neutrophils in muscle atrophy has not been thoroughly investigated. This study sought to investigate the long-term changes in muscle-localized neutrophils after sepsis induction and their possible role in sepsis.

Methods: Sepsis was induced in seven-week-old male C57BL/6J mice 8-12 (cecal slurry [CS] model) *via* intraperitoneal injection of 1 mg/g cecal slurry. The percentage change in body weight and grip strength was evaluated. The tibialis anterior muscles were dissected for microscopic examination of the cross-sectional area of myofibers or Fluorescence-activated cell sorting (FACS) analysis of immune cells. These changes were evaluated in the following conditions: (1) Longitudinal change until day 61, (2) CS concentration-dependent change on day 14 at the low (0.3 mg/g), middle (1.0 mg/g), and high (2.0 mg/g) concentrations, and (3) CS mice on day 14 treated with an anti-Ly6G antibody that depletes neutrophils.

Results: Body weight and grip strength were significantly lower in the CS model until day 61 (body weight: 123.1% ± 1.8% vs. 130.3% ± 2.5%, p = 0.04; grip strength: 104.5% ± 3.8% vs. 119.3% ± 5.3%, p = 0.04). Likewise, cross-sectional muscle area gradually decreased until day 61 from the CS induction (895.6 [606.0–1304.9] μm^2 vs. 718.8 [536.2–937.0] μm^2, p < 0.01). The number of muscle-localized neutrophils increased from 2.3 ± 0.6 cell/mg on day 0 to 22.2 ± 13.0 cell/mg on day 14, and decreased thereafter. In terms of CS concentration–dependent change, cross-sectional area was smaller (484.4 ± 221.2 vs. 825.8 ± 436.2 μm^2 [p < 0.001]) and grip strength was lower (71.4% ± 12.8% vs. 116.3% ± 7.4%, p = 0.01) in the CS High group compared with the control, with increased neutrophils (p = 0.03). Ly6G-depleted mice

demonstrated significant increase of muscle cross-sectional area and grip strength compared with control mice ($p < 0.01$).

Conclusions: Sepsis causes infiltration of neutrophils in muscles, leading to muscle atrophy and weakness. Depletion of neutrophils in muscle reverses sepsis-induced muscle atrophy and weakness. These results suggest that neutrophils may play a critical role in sepsis-induced muscle atrophy and weakness.

KEYWORDS

muscle atrophy, sepsis, neutrophil, fibrosis, mice

Introduction

Due to advancements in medical treatments, sepsis mortality has decreased by 53% from 1990 to 2017 (1). However, approximately one-third of sepsis survivors have persistent physical impairment 6 months after hospital discharge (2). The loss of skeletal muscle mass during the acute phase is one of the causes of prolonged physical impairment. Sepsis causes skeletal muscle mass loss of 10%–20% in a week, which is associated with functional decline and mortality (3). Although muscle atrophy has been reported in numerous studies, its underlying mechanism has not been elucidated.

One poorly understood field is the interaction between muscle atrophy and the immune system (4). Immune effector cells are involved in muscle tissue destruction and construction (5). While most studies have focused on the role of macrophages in muscle atrophy, neutrophils also play important roles in muscle atrophy (6). Neutrophils are frontline cells that combat microbes by releasing antimicrobial agents and are essential for maintaining tissue homeostasis (7). In exercise- (8) or toxin-induced muscle injuries (9), neutrophil levels were increased in human muscle tissue observed under a microscope. Neutrophil activation can lead to muscle atrophy because neutrophil depletion contributes to reduced skeletal muscle damage and atrophy in a non-sepsis model (10).

However, in sepsis, the interaction between muscles and the immune system is poorly understood. Few previous studies, in our opinion, have investigated the immunologic mechanism in sepsis-induced muscle atrophy or injury. We hypothesized that muscle-localized neutrophils play an important role in sepsis-induced skeletal muscle atrophy. The purpose of the study is to address the longitudinal changes of muscle-localized neutrophils after sepsis and elucidate the interaction between neutrophils and muscle atrophy and weakness.

Material and methods

Ethics

This animal experiment was approved in July 2021 by the Committee on the Ethics of Animal Experiments of Kobe University Graduate School of Medicine (P210704). All experimental procedures were carried out in accordance with the recommendations of the International Expert Consensus Initiative for Improvement of Animal Modeling in Sepsis (11).

Animals

Seven-week-old male C57BL/6J mice were purchased from Charles River (St-Constant, Quebec, Canada). The mice were housed in cages, in groups of five, with a 12-h light-dark cycle and a temperature of 22°C, with water and food ad libitum. Before beginning the test, the mice were acclimatized for a week.

Preparation of cecal slurry

As previously reported, cecal slurry (CS) was prepared (12). To induce polymicrobial sepsis, male Institute for Cancer Research mice aged 8 to 12 weeks were intraperitoneally injected with CS (13). After the mice were sacrificed, the cecum was harvested and ground through a 70 µm mesh cell strainer (EASYstrainer™, Greiner Bio-One, Kremsmünster, Austria). The sample was combined with 1–2 mL of sterile phosphate-buffered saline (PBS, Wako, Osaka, Japan) and filtered twice. Following this, the mixture was centrifuged at 11,000 rpm for 1 min. After removing the supernatant, the residue was mixed with 15% glycerol-PBS to achieve a

concentration of 500 mg/mL. The sample (400–500 μL) was then transferred to cryogenic biobanking tubes (Greiner Bio-one, Kremsmünster, Austria) and stored at −80°C until use.

Sepsis model by CS injection

For the controls, intraperitoneal injection of 1 mg/g bodyweight CS or an equal volume of vehicle (15% glycerol-PBS) was administered to induce sepsis. Mice were anesthetized with isoflurane inhalation and sacrificed on the days specified after CS injection (Figure 1A). Flow cytometry and histology were performed on the right or left tibialis anterior muscle samples, respectively.

To investigate the CS concentration-dependent change, CS was intraperitoneally injected at three different concentrations: 0.3 mg/g (n = 3), 1.0 mg/g (n = 3), 2.0 mg/g bodyweight (n = 4), and vehicle (n = 3). On day 14 after CS induction, we compared the percentage and the number of neutrophil, monocyte, and macrophage in the right tibialis anterior muscle; grip strength; and the cross-sectional area of the left tibialis anterior muscle.

Grip strength

A grip strength meter was used to measure grip strength (MK-380Si; Muromachi Kikai, Tokyo, Japan). As previously described, the grip strength test was carried out with minor modifications (14, 15). In brief, mice were allowed to use their front paws to grab a horizontal bar mounted on the gage, and their tails were pulled back. Grip strength was measured three times before and after CS injection, and the highest value was recorded.

Muscle histology

Tibialis anterior muscles were carefully dissected from both legs of five CS and two control mice on days 7, 14, 20, 35, and 61 following sepsis induction. For at least one day, the tibialis anterior muscle in the left leg was immersed in 4% paraformaldehyde containing 0.2% picric acid. The tibialis anterior muscle was paraffin-embedded and sectioned at a thickness of 5 μm. The section was then stained with a hematoxylin and eosin (H & E) solution (Wako, Osaka, Japan). The specimen was examined with a light microscope equipped with a camera (Olympus BX43, Tokyo,

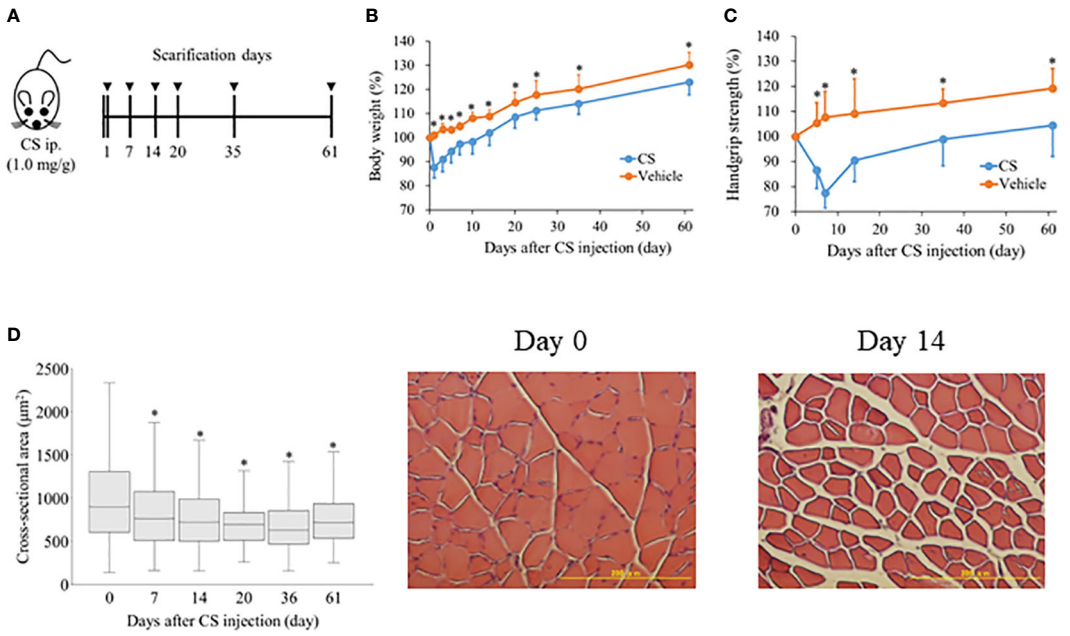

FIGURE 1
Sepsis decreases body weight, grip strength, and muscle atrophy in mice. **(A)** Shema showing study design. Mice were injected 1.0 mg/g of CS intraperitoneally and body weight, grip strength were evaluated from day 1 to 61 (n = 9 in control, n = 22 in CS). To measure cross-sectional area of the anterior tibialis, mice were sacrificed on days 7, 14, 20, 35, and 61 after CS injection. **(B)** Body weight was measured with the sample size (CS/control) at day 0 (22/9), 1 (22/9), 3 (19/8), 5 (19/8), 7 (19/8), 10 (16/7), 14 (16/7), 20 (13/6), 25 (13/6), 35 (13/6), and 61 (10/5). **(C)** Grip strength was measured with the sample size (CS/control) at 0 (20/8), 5 (20/8), 7 (20/8), 14 (17/8), 35 (11/6), and 61 (8/5). **(D)** Histological change in the cross-sectional area of anterior tibialis following sepsis induction. Cross-sectional area of the anterior tibialis decreased after sepsis induction. * Statistical significance at $p < 0.05$ versus control.

Japan) (Olympus DP70, Tokyo, Japan). Next, ImageJ software was used to quantify the captured image at 20 times magnification (National Institutes of Health, Bethesda, MD, USA). To calculate the median myofiber cross-sectional area, approximately 300 myofibers were measured in at least five fields of view per group.

Identification of immune cells in muscle

The right leg's sectioned anterior tibialis muscle was minced with scissors. The minced muscle was combined with 10 mL of RPMI containing 1 mg/mL collagenase type 2 and 0.1 mg/mL Deoxyribonuclease 1. (Worthington, Lakewood, New Zealand). In a shaking incubator, the sample was shaken at 200 rpm for 30 min at 37°C (BR-13FP, Taitec Co, Saitama, Japan). Following the addition of PBS containing 0.1% bovine serum albumin (BSA), the digested tissue was filtered through a 70 µm mesh (EASYstrainer™, Greiner Bio-One, Kremsmünster, Austria). A Countess II FL cell counter was used to count the cells (Thermo Fisher, Waltham, MA, USA). The following antibodies were used in this study: anti-CD45, anti-CD11b, anti-F4/80, anti-GR1, anti-Ly6G, anti-Ly6C, anti-CCR2 anti-CXCR2 (Table S1 in the supplemental file). The gating strategy is shown in Figure S1, and individual immune cell subtypes were identified by the following combinations. Neutrophil: $CD45^+$, $CD11b^+$, $F4/80^-$, $GR1^+$, $Ly6G^+$, $Ly6C^{Int}$; Monocyte: $CD45^+$, $CD11b^+$, $F4/80^-$, $GR1^+$, $Ly6G^-$, $Ly6C^+$; Macrophage: $CD45^+$, $CD11b^+$, $F4/80^+$. Flow cytometry was performed using FACS Verse (BD Biosciences, San Jose, CA, USA), and the data were analyzed using Flow Jo software v10 (Tree Star Inc, Ashland, OR, USA).

Blood sampling and measurements of immune cells

Blood samples were collected from three CS mice and one control mouse on days 0.5, 3, 8, 15, 21, and 30 following CS injection. Flow cytometry was used to count neutrophils, monocytes, and macrophages in blood. Blood was drawn from the inferior vena cava with a heparinized syringe and deposited into a tube using a 23G needle (Terumo, Tokyo, Japan). Blood samples were layered on Histopaque-1119 (Sigma Aldrich, St Louis, MO, USA) to isolate peripheral blood mononuclear cells after being diluted with 0.1% BSA in PBS (PBMCs). The samples were centrifuged at 2000 rpm for 20 minutes to collect PBMCs. Incubation was conducted in a hemolysis buffer at 37°C for 10 min (139.5 mM NH_4Cl and 1.7 mM Tris-HCl). The PBMCs were washed in PBS containing 0.1% BSA, blocked with mouse Fc-blocker (Miltenyi Biotec, Bergisch Gladbach, Germany), and incubated with the Abs mixture for 20 minutes at 4°C. The same gating strategy was used with the muscle tissue. Flow cytometry and analysis were then carried out using FACS Verse and Flow Jo software v10, respectively.

Neutrophil depletion

Five mice were intraperitoneally administered with either 200 µg of Ly6G-specific monoclonal antibody to deplete Ly6G+ cells or IgG2a isotype control antibodies (InVivoPlus anti-mouse Ly6G, Bioxcell, St Louis, NH, USA) 5, 8, 11, 13 days after CS induction. One mouse on each side was cheek bled one day after the first Ly6G-specific monoclonal antibody induction and on the day of scarifice at day 14 to confirm the depletion of $Ly6G^+$ cells *via* flow cytometry. On day 14, after CS induction, we compared the percentage of neutrophils in right tibialis anterior muscle, grip strength, and the cross-sectional area of left tibialis anterior muscle.

Immunohistochemistry

Immunohistochemistry was used to investigate neutrophil localization and the presence of NETs. The sections were deparaffinized with xylenes, rehydrated with graded ethanol, and briefly washed in distilled water. Then, for 30 min, it was blocked with PBS containing 10% BSA to prevent nonspecific immunoglobulin binding. The section was stained for 1 hour at room temperature with a rabbit anti-citrullinated-histone H3 antibody (1:1000, ab5103; Abcam, Cambridge, UK), followed by one-hour incubation with a second antibody (green, 1:500, goat anti-rabbit Alexa 488, Cell Signaling Technology, Danvers, MA, USA). Another antibody, anti-Ly-6G (Gr-1) (red, 1:200, RB6-8C5, Merck, Darmstadt, Germany), was used for 1 hour. Finally, the sections were stained for 30 minutes with 4, 6-diamidino-2-phenylindole (DAPI, blue, 1:500, Dojin, Kumamoto, Japan). Three representative images (20× magnification) were taken in a muscle section using the BZ-X100 microscope (Keyence, Tokyo, Japan). Colocalization of Gr-1, histone H3, and DAPI was considered for NETs.

Statistical analysis

Continuous data were expressed as the mean ± standard deviation or medians (interquartile range), and compared using the t-test or Mann-Whitney U test, as appropriate. All statistical tests were two-tailed, and statistical significance was defined as a p-value <0.05. For statistical analysis, we used JMP statistical software version 13.1.0 (SAS Institute Inc., Cary, NC, USA).

Results

Sepsis decreases body weight, grip strength, and muscle cross-sectional area

After CS injection, we investigated these changes to confirm the longitudinal change in body weight, hand grip strength, and

muscle mass. Following CS induction, body weight decreased considerably (CS model vs. control; 87.7% ± 4.4% vs. 101.1% ± 1.2%, $p < 0.01$) (Figure 1B), and remained significantly lower in the CS model until day 61 (CS model vs. control; 123.1% ± 1.8% vs. 130.3% ± 2.5%, $p = 0.04$). In contrast, hand grip strength in the CS model decreased until day 7 (CS model vs. control; 77.5% ± 1.8% vs. 107.7% ± 2.8%, $p < 0.01$) (Figure 1C), and gradually increased. Until day 61, the hand grip strength was statistically significantly lower in the CS model than control (CS model vs. control; 104.5% ± 3.8% vs. 119.3% ± 5.3%, $p = 0.04$). The cross-sectional area of the anterior tibialis was 895.6 (606.0–1304.9) μm^2 at day 0 (Figure 1D). On day 7, the cross-sectional area was significantly reduced (762.5 [510.2–1076.1] μm^2, $p < 0.01$) until day 61 (718.8 [536.2–937.0] μm^2, $p < 0.01$). The typical histologic change in the muscle tissue is shown in Figure 1D. These results suggest that that muscle atrophy and weakness lasted one to two months after sepsis.

Neutrophils infiltrate muscles during the subacute phase after sepsis

We investigated immune effector cells in the muscle and blood to determine the longitudinal change in immune effector cells and the difference between muscles and blood. A typical depiction of flow cytometry is shown in Figure S4 in which muscle-localized Gr-1^+ cells were compared between naive and CS models 14 days after injection. Gr-1^+ cells, as well as CD11b^+ CD45$^+$ cells, were detected in high numbers in the CS model. On day 14 of the CS model, immunohistochemistry detected several Gr-1^+ cells (Figure S5). The percentage or number of cells displaying the trend of muscle-localized immune effector cells was shown in Figure 2A. The neutrophil ratio per CD45$^+$ CD11b^+ cells increased from 1.0% ± 0.5% on day 0 to 22.2% ± 13.0% on day 14 and 15.5% ± 3.9% on day 20. Likewise, the number of neutrophils per muscle increased from 2.3 ± 0.6 cell/mg on day 0 to 22.2 ± 13.0 cell/mg on day 14 and 15.5 ± 3.9 cell/mg on day 20. Contrary to the number of neutrophils, the number of monocytes and macrophages did not peak on day 14 (4.1 ± 2.1 cell/mg and 13.3 ± 8.8 cell/mg, respectively). Unlike the muscle-localized immune effector cells, the neutrophil ratio per CD45$^+$ CD11b^+ in the blood peaked at day 0.5 (80.3% ± 2.0%), and gradually decreased until day 30 (47.5% ± 8.9%) (Figure 2B). Until day 35, the number of monocytes slightly increased (37.8% ± 5.6%), and macrophages decreased (1.4% ± 0.1%). These findings suggest that neutrophils infiltrate the muscle during the subacute phase after sepsis, while neutrophils in blood increases during the acute phase after sepsis.

Sepsis induces neutrophil infiltration, muscle atrophy, and weakness in a CS-dose dependent manner

We investigated the influence of CS concentration on body weight (Figure 3A), grip strength, muscle cross-sectional area, and muscle localized immune cells. Half of the mice injected with the CS dose of 2.0 mg/g died until day 14, and two mice remained for comparison. Grip strength dose-dependently decreased in the CS model (Control: 116.3% ± 7.4%; CS-Low: 99.3% ± 7.0% [$p = 0.04$]; CS-Middle: 91.1% ± 11.9% [$p = 0.04$]; and CS-High: 71.4% ± 12.8% [$p = 0.01$], Figure 3B). Cross-sectional area dose-dependently decreased in the CS model (Control: 825.8 ± 436.2 μm^2; CS-Low: 668.5 ± 362.6 μm^2 [$p < 0.001$]; CS-Middle: 591.4 ± 286.1 μm^2 [$p < 0.001$]; and CS-High: 484.4 ± 221.2 μm^2 [$p < 0.001$], Figure 3C). Contrary to monocyte and macrophage, the neutrophil ratio per CD45$^+$ CD11b^+ cells was the highest in CS-High group among concentration-dependent CS mice (CS-High vs. Control; 39.6% ± 21.7% vs. 14.9% ± 8.8%, $p = 0.07$, Figures 3D–F), and the number of neutrophils per muscle was the highest in CS-High (CS-High vs. Control; 31.5 ± 8.3 cell/mg vs. 4.1 ± 3.2 cell/mg, $p = 0.03$, Figures 3G–I).

Neutrophil depletion reverses sepsis-induced muscle atrophy and weakness

We depleted muscle-localized neutrophils by using Ly6G-specific monoclonal antibodies (Figure 4A). Neutrophils in the blood decreased in anti-Ly6G-treated CS mouse in one day after the CS induction (CS vs. CS-Ly6G depletion: 626.1 vs. 95.8 cells/uL, n = 1, 1) and at the time of scarifice (CS vs. CS-Ly6G depletion: 163.9 vs. 19.8 cells/uL, n = 1,1) (Figures 4B, C). In anti-Ly6G-treated CS mice, the percentage of neutrophils in the muscle was lower than in the CS mice (CS vs. CS-Ly6G depletion: 14.5% ± 6.1% vs. 6.1% ± 0.8%, $p = 0.03$, n = 3, 4, Figure 4D) with typical FACS image 14 days after induction (Figures 4E, F). Contrary to body weight (Figure 4G), grip strength was higher at Ly6G-depleted CS mice than CS mice (CS vs. CS-Ly6G depletion: 78.1% ± 3.8% vs. 96.2% ± 3.8%, $p = 0.02$, n = 5, 5, Figure 4H). Muscle atrophy was attenuated in Ly6G-depleted CS mice than CS mice (CS vs. CS-Ly6G depletion: 646.5 ± 327.8 μm^2 vs. 755.6 ± 384.8 μm^2, $p < 0.001$, Figure 4I). No mortality was observed till day 14 in five neutrophil-depleted mice. These results indicate that muscle-localized neutrophils contributed to muscle atrophy.

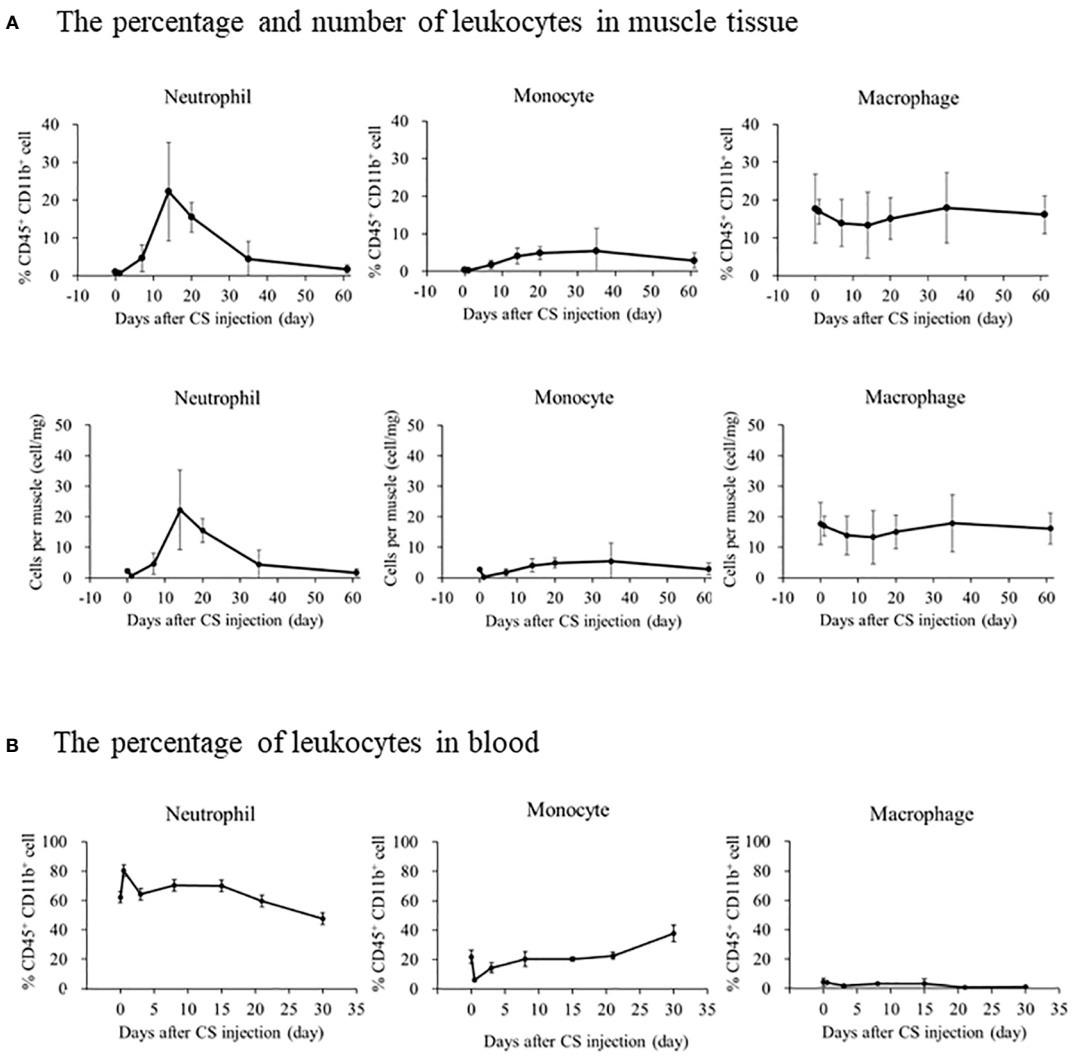

FIGURE 2
The longitudinal change in immune effector cells in muscle or blood after CS injection in mice. **(A)** The upper graph depicts the percentage change in immune effector cells in $CD45^+CD11b^+$ cells in the muscle, and the lower graph depicts the number of immune effector cells identified per muscle. Number of samples were Five CS and two control mice at each measurement day. **(B)** The percentage of immune effector cells in $CD45^+CD11b^+$ cells in the blood. Number of samples were three CS and one control mice at each measurement day.

Sepsis induces NETs in muscle

Finally, we evaluated NETs formation in muscle to determine how neutrophils infiltrating the muscle affect the muscle. We compared the histologic changes in the control and CS-injected mice (Day14) to determine the differences in NETs formation. Gr-1, histone, and DAPI colocalization representing NETs was observed in the muscle in CS-injected mice (day 14), whereas those were not detected in the control (Figure 5).

Discussion

In this study, we reveal that sepsis induces neutrophil infiltration in muscles in the subacute phase, leading to muscle atrophy and weakness in a CS-dose dependent manner. Furthermore, migrated neutrophils form NETs in muscles. We also demonstrated that neutrophil depletion reverses sepsis-induced muscle atrophy and weakness. These findings indicate that infiltrated neutrophils in muscles may play a critical role in sepsis-induced muscle weakness and atrophy.

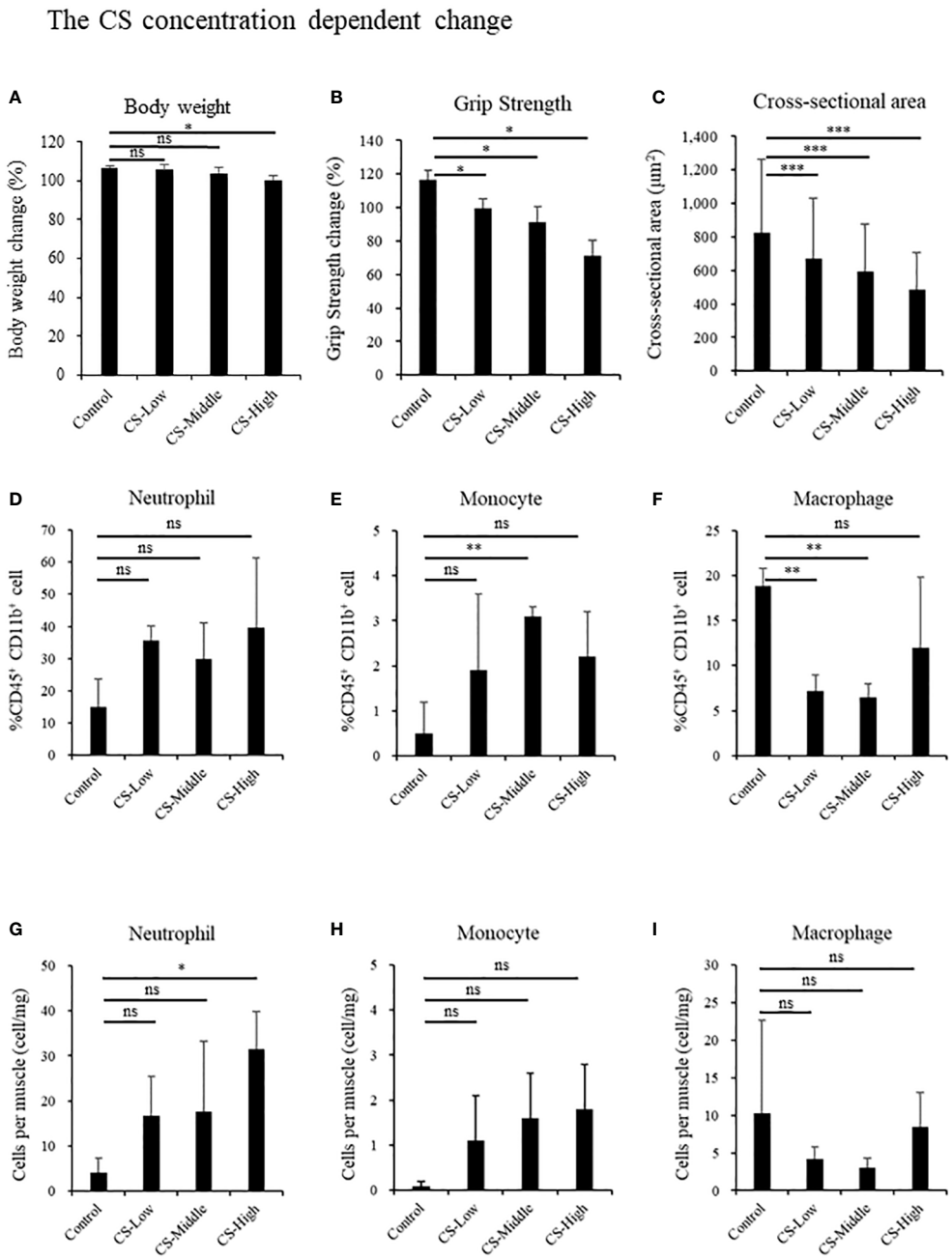

FIGURE 3
Sepsis induces neutrophil infiltration, muscle atrophy, and weakness by CS-dose dependent manner in mice. Body weight, grip strength, and the cross-sectional area of the tibialis anterior muscle, and immune effector cells at day 14 in the different concentrations of low: 0.3 mg/g (n = 3), middle: 1.0 mg/g (n = 3), high: 2.0 mg/g (n = 4). **(A)** Body weight, **(B)** Grip strength, **(C)** Cross-sectional area of the tibialis anterior muscle, percentages of **(D)** Neutrophils, **(E)** Monocyte, **(F)** Macrophage, population of **(G)** Neutrophils, **(H)** Monocyte, **(I)** Macrophage. Statistical significance versus control at $*P < 0.05$, $**p < 0.01$, $***p < 0.001$, ns = not significant ($p > 0.05$).

Muscle-localized neutrophils might be associated with muscle atrophy. In a previous study, neutrophil levels were higher in the skeletal muscle of elderly mice, which was thought to be a cause of muscle atrophy (16). Likewise, previous studies have reported that neutrophil depletion decreased muscle atrophy in a non-sepsis model, such as hindlimb-unloading or cancer-induced muscle atrophy model (10, 17). However, such a relationship in sepsis has not been thoroughly investigated. Even though neutrophils are essential in a host's defense against infection in sepsis, infiltration of

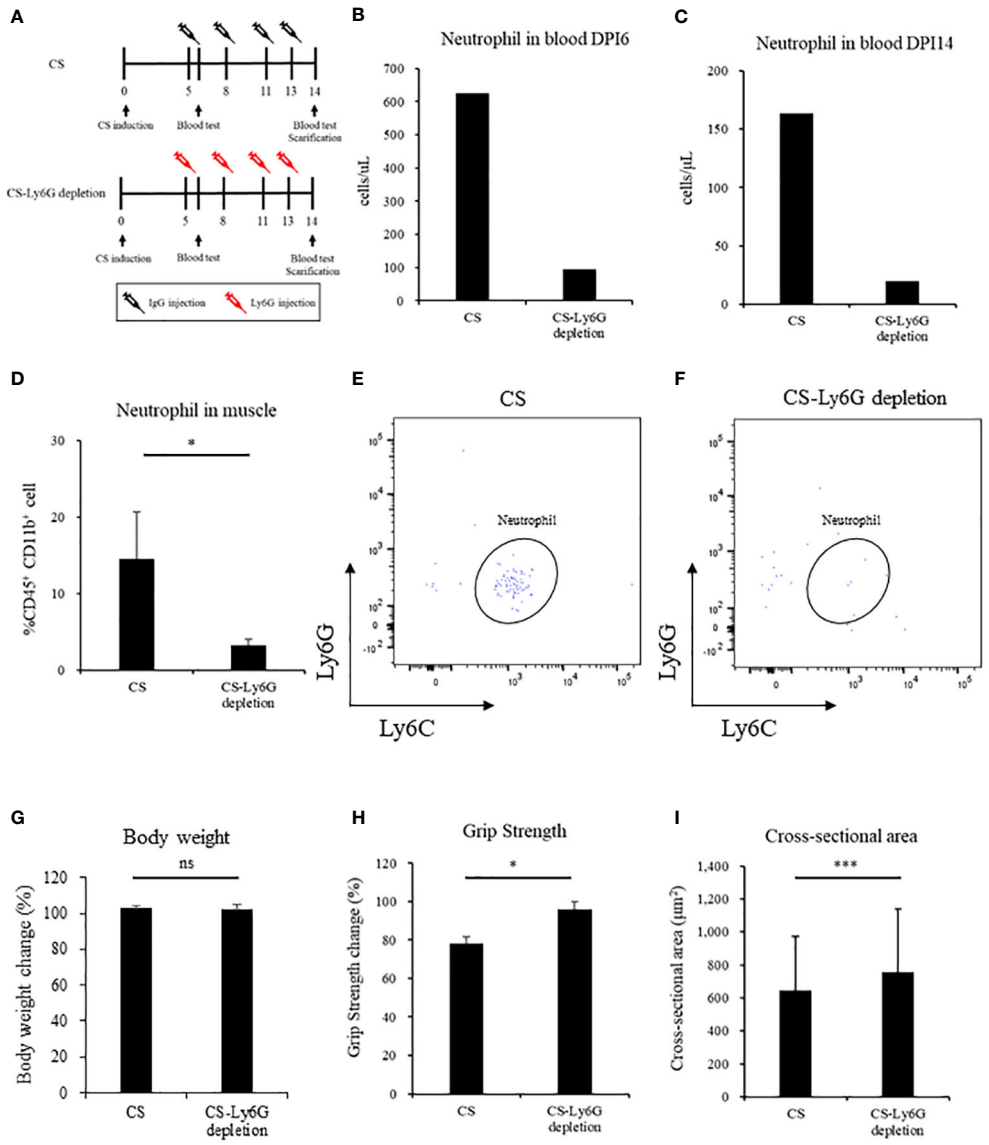

FIGURE 4
Neutrophil depletion reverses sepsis-induced muscle atrophy and weakness in mice. **(A)** Shema showing study design, **(B, C)** Number of neutrophil in blood in Day 6 and Day 14, (n = 1 in each group) **(D)** Percentage of neutrophils in muscle (n = 3–4 in each group), **(E, F)** FACS image 14 days after CS induction and CS-Ly6G depletion (n = 1 in each group) **(G)** Body weight 14 days after CS induction **(H)** Grip strength in 14 days after CS induction **(I)** Muscle cross-sectional area 14 days after CS induction. n = 5 in each group. Statistical significance versus CS at $^{*}P < 0.05$, $^{***}p < 0.001$, ns = not significant ($p > 0.05$).

neutrophils in the muscle is harmful, as it can induce the reduction of muscle volume and strength. This is the first time, to the best of our knowledge, it has been reported that muscle-localized neutrophils are likely contribute to muscle atrophy and weakness following sepsis.

Muscle-localized neutrophils are considered to release inflammatory cytokine, proteases, and free radicals, leading to exacerbated muscle atrophy (18, 19). Furthermore, we found NETs were prominent in muscle on neutrophil-peaked day 14, suggesting that NETs may be associated with muscle atrophy and weakness. NETs play an important role for infection control, but it also causes tissue injuries by increasing pro-inflammatory cytokines (20, 21).

Another new finding in this study is the difference of the timing in neutrophil elevation between blood and muscle tissue. Neutrophils are rapidly elevated in the blood in acute phase after sepsis, while those are elevated in muscle tissue in subacute phase after sepsis in this study. It is reasonable that rapid

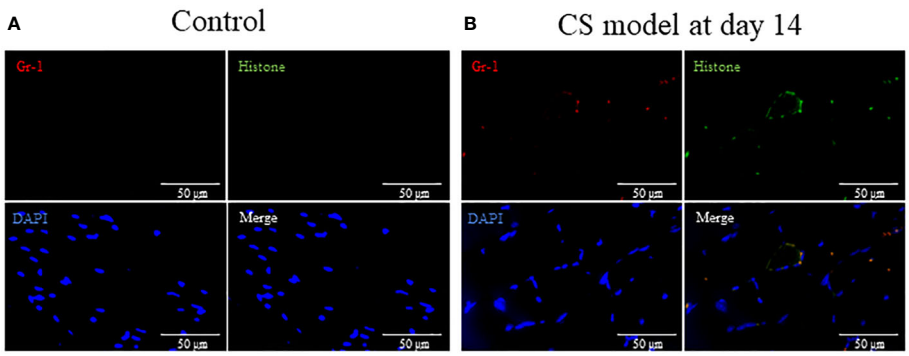

FIGURE 5
Sepsis induces NETs in muscle in mice. **(A)** In tibialis anterior muscle section, neutrophils, degranulation, and the nucleus are stained by Gr-1 (red), histone (green), and DAPI (blue), respectively. Gr-1, histone, and DAPI colocalization represent NETs. **(A)** No NETs were found in the control group. **(B)** At 14 days after CS injection, NETs were visually observed in the CS model. NETs: neutrophil extracellular traps, DAPI: 6-diamidino-2-phenylindole. n = 1 in each group.

increase in neutrophil counts in the blood are equipped with antimicrobial agents to fight microbes on the front lines, however, it is still unclear why and how neutrophils migrated in muscle in the subacute phase of sepsis. Generally, neutrophil survival is usually limited to a few hours (22), therefore, we spectates that there is some mechanisms to extend neutrophil survival including suppression of their apoptosis. In previous study, apoptosis of neutrophils is suppressed in inflammatory tissue (23), and the neutrophils' survival prolongs only for days in inflammation (24), it is unlikely that neutrophils remained for two to three weeks after sepsis was induced. Additionally, some neutrophil attractant cytokines might be released in muscle including chemokines, chemotactic lipids, formyl peptides, and complement anaphylatoxins (7). To address the mechanism of neutrophil migration to muscle, we examined expression of CXCR2 and CCR2 of neutrophils in muscle after sepsis, which are known as neutrophil migration factors. However, we could not find a significant increase of them in subacute phase after sepsis (Data not shown). Further study is needed to address the change and mechanism of neutrophil survival and the mechanism of neutrophil migration to muscles after sepsis.

There are several limitations to our study. First, neutrophil depletion and mortality were not thoroughly investigated. Although no mortality was observed till day 14 in five neutrophil-depleted mice, a previous study reported neutrophil dysfunction increases mortality (25). Second, we did not address the mechanism of neutrophil migration to muscle in sepsis. Third, we did not clarify the interaction of muscle atrophy and NETs. Fourth, we did not examine activation markers of neutrophils in muscle after sepsis. Fifth, we did not evaluate the relationship between neutrophils and other innate immune cells including monocytes and macrophages which also increased in muscle in the subacute phase. Further studies are needed to elucidate these points. Although our study contains several limitations, our finding could help to address the mechanism of this prolonged inflammatory state and muscle atrophy. In the future research to identify a chemoattractant that can orchestrate neutrophils in muscle will lead to a pharmacological intervention to eradicate muscle-specific immune cells.

Conclusions

Sepsis causes infiltration of neutrophils in muscle and muscle atrophy and weakness. Depletion of neutrophils in muscle reverses sepsis-induced muscle atrophy and weakness. These results suggest that neutrophils may play a critical role in sepsis-induced muscle atrophy and weakness.

Data availability statement

The raw data supporting the conclusions of this article will be made available by the authors, without undue reservation.

Ethics statement

The animal study was reviewed and approved by Committee on the Ethics of Animal Experiments of Kobe University Graduate School of Medicine (P210704).

Author contributions

NN and SI took part in study concept. NN, YM, and YO carried out the experiments. NN, KY, SI, and JK obtained

research funding. YO, NM, KF, SI, and JK supervised the project. NN drafted the manuscript and all authors contributed to the revision. All authors contributed to the article and approved the submitted version.

Funding

This study was partially supported by a crowdfunding project entitled the Muscle Atrophy Zero Project using the platform "Otsucle". This study was partially supported by JSPS KAKENHI Grant Numbers JP20K17899.

Acknowledgments

The authors thank people who sup-ported the nonprofit crowdfunding of Muscle Atrophy Zero Project, which aims to prevent muscle atrophy in critically ill patients.

Conflict of interest

The authors declare that the research was conducted in the absence of any commercial or financial relationships that could be construed as a potential conflict of interest.

Publisher's note

Supplementary material

The Supplementary Material for this article can be found online at: https://www.frontiersin.org/articles/10.3389/fimmu.2022.950646/full#supplementary-material

References

1. Rudd KE, Johnson SC, Agesa KM, Shackelford KA, Tsoi D, Kievlan DR, et al. Global, regional, and national sepsis incidence and mortality, 1990–2017: Analysis for the global burden of disease study. *Lancet* (2020) 395(10219):200–11. doi: 10.1016/S0140-6736(19)32989-7

2. Yende S, Austin S, Rhodes A, Finfer S, Opal S, Thompson T, et al. Long-term quality of life among survivors of severe sepsis: Analyses of two international trials. *Crit Care Med* (2016) 44(8):1461–7. doi: 10.1097/ccm.0000000000001658

3. Nakanishi N, Oto J, Tsutsumi R, Akimoto Y, Nakano Y, Nishimura M. Upper limb muscle atrophy associated with in-hospital mortality and physical function impairments in mechanically ventilated critically ill adults: A two-center prospective observational study. *J Intensive Care* (2020) 8(1):87. doi: 10.1186/s40560-020-00507-7

4. Tidball JG. Regulation of muscle growth and regeneration by the immune system. *Nat Rev Immunol* (2017) 17(3):165–78. doi: 10.1038/nri.2016.150

5. Pillon NJ, Bilan PJ, Fink LN, Klip A. Cross-talk between skeletal muscle and immune cells: muscle-derived mediators and metabolic implications. *Am J Physiol Endocrinol Metab* (2013) 304(5):E453–65. doi: 10.1152/ajpendo.00553.2012

6. Hardy D, Besnard A, Latil M, Jouvion G, Briand D, Thépenier C, et al. Comparative study of injury models for studying muscle regeneration in mice. *PLoS One* (2016) 11(1):e0147198. doi: 10.1371/journal.pone.0147198

7. Metzemaekers M, Gouwy M, Proost P. Neutrophil chemoattractant receptors in health and disease: double-edged swords. *Cell Mol Immunol* (2020) 17(5):433–50. doi: 10.1038/s41423-020-0412-0

8. Fielding RA, Manfredi TJ, Ding W, Fiatarone MA, Evans WJ, Cannon JG. Acute phase response in exercise. III. neutrophil and IL-1 beta accumulation in skeletal muscle. *Am J Physiol* (1993) 265(1 Pt 2):R166–72. doi: 10.1152/ajpregu.1993.265.1.R166

9. Cheng M, Nguyen MH, Fantuzzi G, Koh TJ. Endogenous interferon-gamma is required for efficient skeletal muscle regeneration. *Am J Physiol Cell Physiol* (2008) 294(5):C1183–91. doi: 10.1152/ajpcell.00568.2007

10. Dumont N, Bouchard P, Frenette J. Neutrophil-induced skeletal muscle damage: a calculated and controlled response following hindlimb unloading and reloading. *Am J Physiol Regul Integr Comp Physiol* (2008) 295(6):R1831–8. doi: 10.1152/ajpregu.90318.2008

11. Osuchowski MF, Ayala A, Bahrami S, Bauer M, Boros M, Cavaillon JM, et al. Minimum quality threshold in pre-clinical sepsis studies (MQTiPSS): An international expert consensus initiative for improvement of animal modeling in sepsis. *Shock* (2018) 50(4):377–80. doi: 10.1097/shk.0000000000001212

12. Saito M, Inoue S, Yamashita K, Kakeji Y, Fukumoto T, Kotani J. IL-15 improves aging-induced persistent T cell exhaustion in mouse models of repeated sepsis. *Shock* (2020) 53(2):228–35. doi: 10.1097/shk.0000000000001352

13. Starr ME, Steele AM, Saito M, Hacker BJ, Evers BM, Saito H. A new cecal slurry preparation protocol with improved long-term reproducibility for animal models of sepsis. *PLoS One* (2014) 9(12):e115705. doi: 10.1371/journal.pone.0115705

14. Fujinami Y, Hifumi T, Ono Y, Saito M, Okazaki T, Shinohara N, et al. Malocclusion of molar teeth is associated with activities of daily living loss and delirium in dlderly critically ill older patients. *J Clin Med* (2021) 10(10):2157. doi: 10.3390/jcm10102157

15. Ono Y, Maejima Y, Saito M, Sakamoto K, Horita S, Shimomura K, et al. TAK-242, a specific inhibitor of toll-like receptor 4 signalling, prevents endotoxemia-induced skeletal muscle wasting in mice. *Sci Rep* (2020) 10(1):694. doi: 10.1038/s41598-020-57714-3

16. Kawanishi N, Machida S. Alterations of macrophage and neutrophil content in skeletal muscle of aged versus young mice. *Muscle Nerve* (2021) 63(4):600–7. doi: 10.1002/mus.27158

17. Deyhle MR, Callaway CS, Neyroud D, D'Lugos AC, Judge SM, Judge AR. Depleting Ly6G positive myeloid cells reduces pancreatic cancer-induced skeletal muscle atrophy. *Cells* (2022) 11(12):1893. doi: 10.3390/cells11121893

18. You Z, Huang X, Xiang Y, Dai J, Jiang J, Xu J. Molecular feature of neutrophils in immune microenvironment of muscle atrophy. *J Cell Mol Med* (2022) 26(17):4658–65. doi: 10.1111/jcmm.17495

19. Carden DL, Smith JK, Korthuis RJ. Neutrophil-mediated microvascular dysfunction in postischemic canine skeletal muscle. role of granulocyte adherence. *Circ Res* (1990) 66(5):1436–44. doi: 10.1161/01.res.66.5.1436

20. Mutua V, Gershwin LJ. A review of neutrophil extracellular traps (NETs) in disease: Potential anti-NETs therapeutics. *Clin Rev Allergy Immunol* (2021) 61(2):194–211. doi: 10.1007/s12016-020-08804-7

21. Ekaney ML, Otto GP, Sossdorf M, Sponholz C, Boehringer M, Loesche W, et al. Impact of plasma histones in human sepsis and their contribution to cellular injury and inflammation. *Crit Care* (2014) 18(5):543. doi: 10.1186/s13054-014-0543-8

22. Bonilla MC, Fingerhut L, Alfonso-Castro A, Mergani A, Schwennen C, von Köckritz-Blickwede M, et al. How long does a neutrophil live?-the effect of 24 h whole blood storage on neutrophil functions in pigs. *Biomedicines* (2020) 8(8):278. doi: 10.3390/biomedicines8080278

23. Terashima M, Aoyama-Ishikawa M, Ueda T, Hagi A, Usami M, Nakao A, et al. The effects of n-3 polyunsaturated fatty acid-rich total parenteral nutrition on neutrophil apoptosis in a rat endotoxemia. *J Clin Biochem Nutr* (2013) 52(2):154–9. doi: 10.3164/jcbn.12-86

24. Kotani J, Avallone NJ, Lin E, Goshima M, Gandhi K, Lowry SF, et al. Fas-mediated neutrophil apoptosis and associated A1 protein expression during systemic inflammation are regulated independently of both tumor necrosis factor receptors. *Shock* (2003) 19(3):201–7. doi: 10.1097/00024382-200303000-00002

25. Tateda K, Moore TA, Newstead MW, Tsai WC, Zeng X, Deng JC, et al. Chemokine-dependent neutrophil recruitment in a murine model of legionella pneumonia: Potential role of neutrophils as immunoregulatory cells. *Infect Immun* (2001) 69(4):2017–24. doi: 10.1128/iai.69.4.2017-2024.2001

frontiers | Frontiers in Immunology

TYPE Original Research
PUBLISHED 05 January 2023
DOI 10.3389/fimmu.2022.959141

OPEN ACCESS

EDITED BY
Markus Huber-Lang,
Ulm University Medical Center,
Germany

REVIEWED BY
Hayley Louise Letson,
James Cook University, Australia
Yuan Xu,
Tsinghua University, China

*CORRESPONDENCE
Sven Märdian
sven.maerdian@charite.de

SPECIALTY SECTION
This article was submitted to Inflammation, a section of the journal Frontiers in Immunology

RECEIVED 17 June 2022
ACCEPTED 21 November 2022
PUBLISHED 05 January 2023

CITATION
Maleitzke T, Zhou S, Zocholl D, Fleckenstein FN, Back DA, Plewe JM, Weber J, Winkler T, Stöckle U, Tsitsilonis S and Märdian S (2023) Routine laboratory parameters predict intensive care unit admission and hospitalization in patients suffering stab injuries.
Front. Immunol. 13:959141.
doi: 10.3389/fimmu.2022.959141

Routine laboratory parameters predict intensive care unit admission and hospitalization in patients suffering stab injuries

Tazio Maleitzke[1,2,3], Sijia Zhou[2], Dario Zocholl[4], Florian Nima Fleckenstein[5], David Alexander Back[1,6], Julius Maximilian Plewe[7], Jérôme Weber[1,2], Tobias Winkler[1,2,8], Ulrich Stöckle[1], Serafeim Tsitsilonis[1,2] and Sven Märdian[1]*

[1]Center for Musculoskeletal Surgery, Charité – Universitätsmedizin Berlin, Corporate Member of Freie Universität Berlin and Humboldt-Universität zu Berlin, Berlin, Germany, [2]Julius Wolff Institute, Berlin Institute of Health at Charité – Universitätsmedizin Berlin, Berlin, Germany, [3]BIH Charité Clinician Scientist Program, Berlin Institute of Health at Charité – Universitätsmedizin Berlin, BIH Biomedical Innovation Academy, Berlin, Germany, [4]Institute of Biometry and Clinical Epidemiology, Charité – Universitätsmedizin Berlin, Corporate Member of Freie Universität Berlin and Humboldt-Universität zu Berlin, Berlin, Germany, [5]Department of Diagnostic and Interventional Radiology, Charité – Universitätsmedizin Berlin, Corporate Member of Freie Universität Berlin and Humboldt-Universität zu Berlin, Berlin, Germany, [6]Department of Traumatology and Orthopaedics, Septic and Reconstructive Surgery, Bundeswehr Hospital Berlin, Berlin, Germany, [7]Department of Surgery, Charité – Universitätsmedizin Berlin, Corporate Member of Freie Universität Berlin and Humboldt-Universität zu Berlin, Berlin, Germany, [8]Berlin Institute of Health Center for Regenerative Therapies, Berlin Institute of Health at Charité – Universitätsmedizin Berlin, Berlin, Germany

Background: Knife crime has increased considerably in recent years in Northern Europe. Affected patients often require immediate surgical care due to traumatic organ injury. Yet, little is known about clinically relevant routine laboratory parameters in stab injury patients and how these are associated with intensive care unit (ICU) admission, hospitalization and number of surgeries.

Methods: We retrospectively analyzed 258 stab injury cases between July 2015 and December 2021 at an urban Level I Trauma Center. Annual and seasonal incidences, injury site, injury mechanism, Injury Severity Score (ISS), and surgical management were evaluated. First, correlations between routine laboratory parameters for hematology, coagulation, and serum biochemistry (peak, and Δ (change from admission to peak within 3 days following admission)) and length of hospital stay, ICU stay, and number of surgeries were assessed using Spearman's rank correlation coefficients. Second, multivariable Least Absolute Shrinkage and Selection Operator (LASSO) regression analyses were conducted to identify parameters predictive of clinical outcomes. Third, longitudinal developments of routine laboratory parameters were assessed during hospital admission.

Results: In 2021, significantly more stab injuries were recorded compared with previous years and occurred less during winter compared with other seasons.

Mean ISS was 8.3 ± 7.3, and ISS was positively correlated with length of hospital and ICU stay (r = 0.5–0.8, p < 0.001). Aspartate transaminase (AST) (Δ) (r = 0.690), peak C-reactive protein (CrP) (r = 0.573), and erythrocyte count (Δ) (r = 0.526) showed the strongest positive correlations for length of ICU stay for penetrating, thoracoabdominal, and organ injuries, respectively. No correlations were observed between routine laboratory parameters and number of surgeries. For patients with penetrating injuries, LASSO-selected predictors of ICU admission included ISS, pH and lactate at admission, and Δ values for activated partial thromboplastin time (aPTT), K^+, and erythrocyte count. CrP levels on day 3 were significantly higher in patients with penetrating (p = 0.005), thoracoabdominal (p = 0.041), and organ injuries (p < 0.001) compared with those without.

Conclusion: Our data demonstrate an increase in stab injury cases in 2021 and an important link between changes in routine laboratory parameters and ICU admission and hospitalization. Monitoring ISS and changes in AST, CrP, erythrocyte count, pH, lactate, aPTT, and K^+ may be useful to identify patients at risk and adjust surgical and ICU algorithms early on.

KEYWORDS

trauma, knife, penetrating, blood, serum biochemistry, coagulation, hemostasis, inflammation

Introduction

Stab injuries are primarily observed in urban environments and predominantly affect young men between 20 and 30 years of age (1, 2). In a recent retrospective analysis of ~240,000 severely injured patients enrolled in the German Trauma Registry (TraumaRegister DGU®), 4,333 stab injuries (1.8%) were recorded between 2009 and 2018 (3).

While overall patient volumes declined in emergency departments (EDs) during the COVID-19 pandemic, incidences of stabbing trauma increased in both Europe (4, 5) and the United States (6–9). Although most stab injuries are not fatal, thoracoabdominal injuries often require surgery and are associated with postsurgical complications and hospital readmissions (10).

Stab injuries result in the disruption of macro (skin) and micro (cell membranes) barriers, causing the release of damage-associated molecular patterns (DAMPs) into the bloodstream, which leads to an activation of the innate immune system (11). Pathogen-associated molecular patterns (PAMPs) from bacteria, viruses, or fungi are also commonly present at the injury site following penetrating trauma. Both DAMPs and PAMPs cause a rapid immune response, including activation of coagulation and complement cascades and reprioritizing of leukocytes (12). In addition, endothelial damage and platelet activation cause a pro-inflammatory cytokine release, which facilitates neutrophil activation and subsequent tissue damage (13). Therefore, stab injuries are likely to affect multiple-organ systems, both primarily though the injury and secondarily through the concomitant cellular and molecular response.

Various serum laboratory parameters are regularly acquired upon arrival of stab injury patients in the ED to monitor health status and organ functions. Blood tests commonly include hematology, coagulation, and serum biochemistry profiles and may be repeated during later stages of admission depending on the patient's clinical development. How stab injuries alter routine laboratory parameters has not yet been investigated in detail. Knowledge about relevant laboratory parameters to monitor in stab injury patients may however improve assessment and prediction of the clinical course and outcomes early on.

Therefore, this study aimed to describe (i) clinical characteristics of stab injury cases according to the Injury Severity Score (ISS); (ii) explore annual and seasonal differences in monthly stab injury incidences; (iii) evaluate whether peak and Δ (change from admission to peak within 3 days following admission) values of routinely acquired laboratory parameters correlate with clinical outcomes, including length of hospital and ICU stay and number of surgeries performed during admission; and (iv) assess the predictive strength of routinely acquired laboratory parameters for clinical outcomes employing a multivariable regression

analysis approach; and (v) compare the longitudinal course of routine laboratory parameters between patients with different injury characteristics over time.

Materials and methods

Study population and data extraction

All patients admitted to the ED of a Level I Trauma Center (Berlin, Germany) who sustained one or more stab injuries between July 2015 and December 2021 were included and retrospectively reviewed (retrospective chart review employing a convenience sampling approach (14)). All patients were directly admitted to our center (no transfers from other hospitals).

For all patients, the following parameters were extracted: Injury Severity Score (ISS) ((based on injury patterns present at admission); gender; age; time of admission; health insurance status; mental health condition; alcohol consumption; body temperature at admission; injury mechanism; number of stabs; injured body regions; type of injury, X-ray, ultrasonography, and computed tomography (CT) scan reports (acute pathological findings were quantified); trauma team activation (initiated if patients met Grade of Recommendation B-criteria (GoR-B) defined by DGU® (e.g., penetrating injuries) (15)); performed surgeries (including all acute and elective "in house" surgeries and chest drain insertions *via* mini-thoracotomy, whereas simple superficial wound closures in the ED were not included); massive transfusion of blood products (defined as transfusion of ≥10 red blood cell units within 24 h or more than four red blood cell units within 1 h (16)); red blood cell (RBC); fresh frozen plasma (FFP); and platelet units; length of hospital and ICU stay.

As the study population comprised mono- and polytrauma patients, Table 1 categorizes patients based on ISS at admission: minor injuries (ISS of 1–8), moderate injuries (ISS of 9–15), severe injuries (ISS of 16–24), and very severe injuries (ISS ≥25) (17).

According to admission dates, differences in monthly stab injuries between years (2015–2021) and seasons (spring: March–May; summer: June–August; autumn: September–November; winter: December–February) were recorded. As the data set for 2015 only included data for July–December, it was excluded for the assessment of seasonal differences.

Next to demographic data, laboratory values for hematology, coagulation, serum biochemistry, and venous blood gas were recorded. These included hemoglobin, erythrocyte count, leukocyte count, platelet count (all hematology), international normalized ratio (INR), activated partial thromboplastin time (aPTT), fibrinogen (all coagulation), creatinine, urea, total bilirubin, myoglobin, alanine transferase (ALT), aspartate transferase (AST), alkaline phosphatase (ALP), creatine kinase (CK), potassium (K^+), C-reactive protein (CrP) (all serum biochemistry), and pH and lactate at admission (both venous blood gas).

Peak and Δ laboratory parameters

To explore clinically relevant changes in routine laboratory parameters in stab injury patients, Δ and peak values were calculated. Δ values express the difference between admission and peak levels within 3 days of admission (Δ = peak level until day 3-admission level) (18).

Statistical analysis

To test for relationships between groups of different injury severities (according to ISS), chi-square test and Fisher's exact test were employed to analyze variables in contingency Table 1.

The non-parametric Mann–Whitney U test was used to compare continuous or ordinal variables. Due to the asymmetric distribution of laboratory values, the median was reported.

Associations between included laboratory parameters and length of hospital and ICU stay and number of surgeries were evaluated by Spearman's rank correlation coefficients. Following Mukak's guide to the appropriate use of correlation coefficients in medical research, correlation coefficients were categorized as negligible (r = 0–0.3), weak (r = 0.3–0.5), moderate (r = 0.5–0.7), high (r = 0.7–0.9), and very high (r = 0.9–1) (19). Correlation analyses were conducted for patient cohorts with (i) penetrating (all injuries where the visceral or deep fascia was perforated), (ii) thoracoabdominal, and (iii) organ injuries.

To further identify clinically meaningful relationships from the multivariate data set (20), a multivariable selection method was employed to identify potentially predictive sets of variables: LASSO [Least Absolute Shrinkage and Selection Operator (21)] analyses were conducted for each patient cohort of (i) penetrating, (ii) thoracoabdominal, and (iii) organ injuries and each outcome of interest. LASSO models have been commonly used for high-dimensional model selection problems, i.e., if there are numerous predictive factors for a limited sample size. LASSO applies a shrinkage parameter *lambda*, which shrinks some coefficients of a regression model to zero, thus selecting only those variables that are useful for prediction. The specific value of *lambda* determines how many non-zero coefficients are considered. Due to this shrinkage, coefficient estimates are biased by design and p-values or confidence intervals do not have reliable statistical properties (22). Therefore, we report trace plots, showing coefficients of each variable for different

10.3389/fimmu.2022.959141

TABLE 1 Characteristics of patients who suffered stab injuries between July 2015 and December 2021 at a Level I Trauma Center in Berlin, Germany.

ISS		Total	1–8	9–15	16–24	>24	*p* value
n (%)		258 (100)	155 (60.0)	64 (24.8)	28 (10.9)	11 (4.3)	
Gender, n (%)							0.918
Male		235 (91.1)	142 (91.6)	58 (90.6)	25 (89.3)	10 (90.9)	
Female		23 (8.9)	13 (8.4)	6 (9.4)	3 (10.7)	1 (9.1)	
Age, years, median (IQR)		32 (23, 42)	32 (23, 43)	32 (22, 40)	34 (26, 44)	24 (21, 37)	0.530
Time of admission, n (%)							0.215
Daytime (6 a.m.–6 p.m.)		100 (38.8)	53 (34.2)	27 (42.2)	15 (53.6)	5 (45.5)	
Nighttime (6 p.m.–6 a.m.)		158 (61.2)	102 (65.8)	37 (57.8)	13 (46.4)	6 (54.5)	
Health insurance status, n (%)							0.217
Insurance cover		231 (89.5)	135 (87.1)	60 (93.8)	27 (96.4)	9 (81.8)	
No insurance cover		27 (10.5)	20 (12.9)	4 (6.2)	1 (3.6)	2 (18.2)	
Mental health condition, n (%)							0.227
Reported mental illness		45 (17.4)	21 (13.5)	15 (23.4)	7 (25.0)	2 (18.2)	
No reported mental illness		213 (82.6)	134 (86.5)	49 (76.6)	21 (75.0)	9 (81.8)	
Alcohol consumption, n (%)							0.224
Alcohol involved		54 (20.9)	31 (20.0)	11 (17.2)	10 (35.7)	2 (18.2)	
Alcohol not involved		204 (79.1)	124 (80.0)	53 (82.8)	18 (64.3)	9 (81.8)	
Injury mechanism, n (%)							0.330
Self-inflicted		48 (18.6)	25 (16.1)	16 (25.0)	4 (14.3)	3 (27.3)	
Assault-related		210 (81.4)	130 (83.9)	48 (75.0)	24 (85.7)	8 (72.7)	
Injured body region, n (%)							
Head and neck	With	53 (20.5)	32 (20.6)	12 (18.8)	7 (25.0)	2 (18.2)	0.918
	Without	205 (79.5)	123 (79.4)	52 (81.3)	21 (75.0)	9 (81.8)	
Thorax	With	133 (51.6)	58 (37.4)	46 (71.9)	20 (71.4)	9 (81.8)	< 0.001
	Without	125 (48.4)	97 (62.6)	18 (28.1)	8 (28.6)	2 (18.2)	
Abdomen	With	89 (34.5)	46 (29.7)	23 (35.9)	13 (46.4)	7 (63.6)	0.057
	Without	169 (65.5)	109 (70.3)	41 (64.1)	15 (53.6)	4 (36.4)	
Spine	With	9 (3.5)	3 (1.9)	3 (4.7)	3 (10.7)	0 (0)	0.123
	Without	249 (96.5)	152 (98.1)	61 (95.3)	25 (89.3)	11 (100)	
Limbs	With	108 (41.9)	76 (49.0)	20 (31.3)	10 (35.7)	2 (18.2)	0.024
	Without	150 (58.1)	79 (51.0)	44 (68.8)	18 (64.3)	9 (81.8)	
Number of involved body regions, n (%)							0.055
1		161 (62.4)	104 (67.1)	39 (60.9)	12 (42.9)	6 (54.5)	
2–3		92 (35.7)	50 (32.3)	23 (35.9)	15 (53.6)	4 (36.4)	
4–5		5 (1.9)	1 (0.6)	2 (3.1)	1 (3.6)	1 (9.1)	
Type of injury, n (%)							< 0.001
Superficial		64 (24.8)	44 (28.4)	13 (20.3)	5 (17.9)	2 (18.2)	
Penetrating		236 (91.5)	134 (86.5)	63 (98.4)	28 (100)	11 (100)	
Thoracoabdominal		170 (65.9)	78 (50.3)	56 (87.5)	25 (89.3)	11 (100)	
Organ		111 (43.0)	23 (14.8)	52 (81.3)	25 (89.3)	11 (100)	
CT scan, n (%)							0.002
Performed		223 (86.4)	124 (80.0)	62 (96.9)	27 (96.4)	10 (90.9)	
Not performed		35 (13.6)	31 (20.0)	2 (3.1)	1 (3.6)	1 (9.1)	
Trauma team activation, n (%)							0.007
Yes		211 (81.8)	117 (75.5)	60 (93.8)	25 (89.3)	9 (81.8)	
No		47 (18.2)	38 (24.5)	4 (6.2)	3 (10.7)	2 (18.2)	

(Continued)

TABLE 1 Continued

ISS	Total	1–8	9–15	16–24	>24	*p* value
Surgery, n (%)						< 0.001
Yes	183 (70.9)	94 (60.6)	54 (84.4)	24 (85.7)	11 (100)	
No	75 (29.1)	61 (39.4)	10 (15.6)	4 (14.3)	0 (0)	
Massive transfusion, n (%)						< 0.001
Yes	11 (4.3)	0 (0)	0 (0)	6 (21.4)	5 (45.5)	
No	247 (95.7)	155 (100)	64 (100)	22 (78.6)	6 (54.5)	
Blood product, n [median (range)]						-
Red blood cell (RBC) units	25 [6 (1, 46)]	3 [3 (1, 8)]	8 [1 (1, 6)]	8 [11 (2, 14)]	6 [12 (2, 46)]	
Fresh frozen plasma (FFP) units	18 [10 (2, 72)]	2 [5 (3, 6)]	4 [5 (2, 7)]	5 [15 (14, 19)]	7 [10 (3, 72)]	
Platelet units	4 [7 (2, 14)]	0 [0 (0, 0)]	0 [0 (0, 0)]	2 [6 (2, 9)]	2 [9 (4, 14)]	
Length of stay, days, median (IQR)						-
Length of hospital stay	4 (3, 7)	3 (2, 4)	6 (5, 8)	10 (8, 14)	10 (3, 15)	
Length of ICU stay	0 (0, 2)	0 (0, 0)	2 (0, 3)	3 (2, 7)	3 (0, 11)	

Distribution according to ISS.

lambda values. To identify a single model, a suitable value for lambda was determined *via* cross-validation. The identified model was then used to predict admission to ICU, and sensitivity, specificity, and total accuracy of this prediction were assessed as well as the area under the receiver operating characteristic curve (AUC). Since multivariable regression methods require non-missing data on all variables, a subset of patients with most complete data (n = 66) was used and only variables with less than 120 missing values were considered for variable selection.

It should be noted that the models were purely explorative and should be used to identify potentially predictive factors for future research rather than serve as a final predictive model.

Additionally, longitudinal changes of CrP, hemoglobin, erythrocyte, leukocyte, and platelet counts, total bilirubin, ALT, AST, creatinine, urea, CK, INR, and aPTT were recorded for 21 days following admission and the day of discharge.

To compare daily CrP values between patients with different injury characteristics, patient cohorts were compared according to (i) penetrating injuries, (ii) thoracoabdominal injuries, and (iii) organ injuries to those without, as well as in (iv) patients who were admitted to ICU to those who were not. Where less than four data points were available per group, no statistical tests were conducted.

For Spearman correlation, LASSO regression, and longitudinal laboratory parameter analyses, 26 patients were excluded. These included 18 patients who left the hospital against medical advice, five patients who died in hospital due to their injuries, and three patients who were initially transferred to specialized medical departments for further treatment.

A two-tailed p-value <0.05 was considered statistically significant. Data analyses were conducted using SPSS 26.0 (IBM, Chicago, USA) and Prism V.9.0 (GraphPad, California, USA) and R version 4.1.2 [for LASSO analysis: package glmnet (23)].

Ethics

Prior to study initiation, ethical approval (EA1/082/20) was obtained from the local ethics committee, Ethikkommission Charité – Universitätsmedizin Berlin.

Results

Descriptive data of stab injury patients

Between July 2015 and December 2021, 258 stab injuries were identified (23 women, 235 men) with a median age of 32 years (interquartile range (IQR) 23; 42). Most stab injuries occurred between 6 p.m. and 6 a.m. (61.2%) and were due to interpersonal conflicts (81.4%), whereas 18.6% were self-inflicted. In 17.4% of sustained stab injuries, mental illness was recorded, and in 20.9% elevated blood alcohol levels or obvious alcohol intoxication were present.

The trauma team was activated in 81.8% of cases, and 70.9% of patients underwent surgery. More than half of the patients (51.6%) sustained a thorax injury, whereas the limbs and abdomen were affected in 41.9% and 34.5% of cases, respectively. Most patients presented with penetrating injuries (91.5%), and 43.0% sustained organ injuries (Figure 1A; Table 1). The detailed distribution of cases according to ISS is provided in Table 1.

Annual and seasonal differences in monthly stab injuries between 2015 and 2021

We recorded significantly more monthly stab injuries in 2021 compared to 2017 (p = 0.040) and 2018 (p = 0.011) (Figure 1B). Most stabbings occurred during spring, summer,

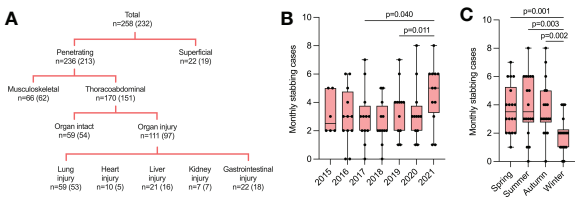

FIGURE 1
Annual and seasonal differences in monthly stab injuries. **(A)** Characteristics of included stab injuries divided by penetrating vs. superficial, thoracoabdominal vs. musculoskeletal, and organ injuries vs. non-organ injuries. Numbers in brackets show the number of cases included in statistical analysis (for details, please see Materials and Methods). **(B)** Monthly stab injury cases between 2015 and 2021. Individual data points represent the number of stabbing cases per month for indicated years. **(C)** Monthly stab injury cases between 2016 and 2021 divided by seasons. Individual data points represent the number of stabbing cases per month for indicated seasons. Data are presented as median box plots with interquartile range and whiskers from minimum to maximum.

and autumn, whereas significantly fewer cases were seen during winter (spring vs. winter, p = 0.001; summer vs. winter, p = 0.003; autumn vs. winter, p = 0.002) (Figure 1C).

Correlations between laboratory parameters and clinical outcomes and predictive variables for ICU admission in penetrating injuries

We next analyzed how injury severity and routine laboratory parameters correlated with length of hospital and ICU stay and number of surgeries in patients with penetrating stab injuries (n = 213). The median time from admission to first blood samples was 35 min (IQR 28–41 min) for blood hematology, biochemistry, and coagulation samples and 10 min (IQR 10–18 min) for venous blood gas samples.

Number of organ injuries, number of pathological CT findings, number of pathological findings in all imaging modalities combined, and ISS were all moderately to highly positively correlated with length of hospital and ICU stay (r = 0.513–0.805, p < 0.001 for all) (Figure 2A).

Further, AST (Δ), CK (Δ), peak CrP, and CrP (Δ) (Figure 2C) were all moderately positively correlated with length of hospital stay (r = 0.510–0.690) and erythrocyte count (Δ) (Figure 2B), peak CrP, and CrP (Δ) (Figure 2C) were also moderately positively correlated with length of ICU stay (r = 0.510–0.558).

The strongest positive correlations were observed between ISS and hospital stay (r = 0.805) and AST (Δ) and ICU stay

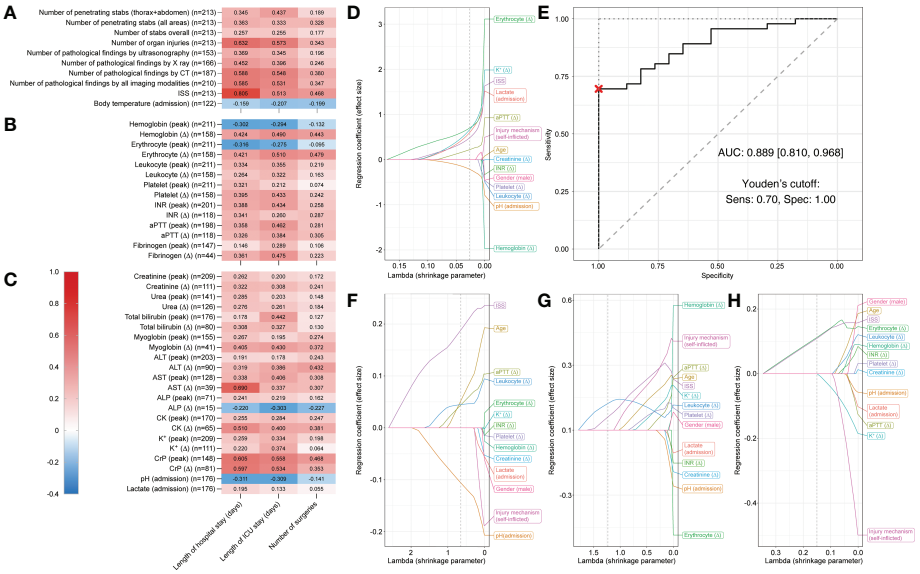

FIGURE 2
Correlation matrix showing Spearman's rank correlation coefficients and Least Absolute Shrinkage and Selection Operator (LASSO) plots showing regression coefficients for patients who suffered penetrating stab injuries. Correlation strength is indicated by color scale on the left. Correlations between three different outcome parameters (length of hospital stay, length of ICU stay, and number of surgeries) and **(A)** injury specifics, **(B)** routine hematology and coagulation, and **(C)** serum biochemistry and venous blood gas laboratory parameters for penetrating injuries (n = 213). Multivariable LASSO trace plots indicate potentially predictive sets of variables for **(D)** ICU admission (yes/no). **(E)** Receiver operating characteristic (ROC) curve for the LASSO model of ICU admission (yes/no). Youden's cutoff indicates the optimal cutoff based on sensitivity (Sens.) and specificity (Spec). **(F)** Further LASSO trace plots for length of hospital stay, **(G)** length of ICU stay, and **(H)** number surgeries. Grey dotted line displays optimal lambda value calculated *via* cross-validation. AUC, area under the curve.

(r = 0.690). For all reported r-values >0.3, p-values were <0.01. Negligible to weak correlations were observed between all assessed parameters and number of surgeries.

For admission to ICU (yes/no), LASSO regression analyses selected the following predictive variables when shrinkage parameter lambda was set to 0.027 (determined *via* cross-validation): pH (admission) (coefficient = -0.213), aPTT (Δ) (coefficient = 0.219), ISS (coefficient = 0.479), lactate (admission) (coefficient = 0.594), K^+ (Δ) (coefficient = 0.657), and erythrocyte count (Δ) (coefficient = 0.696) (Figure 2D).

With these predictive variables, a binary logistic regression model predicting ICU admission had a sensitivity of 73.9% (95% confidence interval [58.7%, 95.7%]), a specificity of 100% [76.5%, 100.0%], and a total accuracy of 81% [69.8%, 92.1%]. The AUC was 0.889 [0.810, 0968] (Figure 2E). Thus, prediction by this model was statistically significantly better than random. In the trace plot, it can be seen that other parameters became dominant with smaller values of lambda. For instance, hemoglobin (Δ) was the largest negative coefficient for lambda values close to zero (Figure 2D).

For length of hospital stay the variable ISS, for length of ICU stay hemoglobin (Δ), and for number of surgeries male gender were the largest coefficients for lambda values close to zero (Figures 2F–H). Details on LASSO-selected variables and their coefficients can be found in Table 2.

Correlations between laboratory parameters and clinical outcomes and predictive variables for ICU admission in thoracoabdominal injuries

Next, we assessed patients who suffered penetrating injuries that affected thoracoabdominal cavities (n = 151).

Number of organ injuries, number of pathological X-ray findings, number of pathological CT findings, and number of pathological findings in all imaging modalities combined, ISS (Figure 3A), AST (Δ), peak CrP, and CrP (Δ) (Figure 3C) were moderately to highly positively correlated with length of hospital stay (r = 0.529–0.821). Similarly, number of organ injuries, number of pathological CT findings, and number of pathological findings in all imaging modalities combined, ISS (Figure 3A), hemoglobin (Δ), erythrocyte count (Δ) (Figure 3B), peak CrP, and CrP (Δ) (Figure 3C) showed moderate to high positive correlations with length of ICU stay (r = 0.520–0.821). The strongest positive correlations were again observed between ISS and hospital stay (r = 0.821) and between peak CrP and ICU stay (r = 0.573). For all reported r-values > 0.3, p-values were <0.01 and only negligible to weak correlations were observed between all assessed parameters and number of surgeries.

For admission to ICU (yes/no), LASSO regression analyses selected variables pH (admission) (coefficient = -0.079), aPPT (Δ) (coefficient 0.175), male gender (coefficient = 0.478), lactate (coefficient = 0.562), erythrocyte count (Δ) (coefficient = 0.564), ISS (coefficient = 0.589), and K^+ (Δ) (coefficient = 0.592) when shrinkage parameter lambda was set to 0.034 (determined *via* cross-validation) (Figure 3D).

The binary logistic regression model predicting ICU admission had a sensitivity of 79.1% (95% confidence interval [62.8%, 93%]), a specificity of 100% [81.2%, 100.0%], and a total accuracy of 84.7% [72.9%, 93.2%]. The AUC was 0.901 [0.825, 0.977] (Figure 3E). Thus, prediction by this model was statistically significantly better than random (Figure 3D).

For length of hospital stay the variable ISS, for length of ICU stay self-inflicted injuries, and for number of surgeries hemoglobin (Δ) were the largest coefficients for lambda values close to zero (Figures 3F–H). Details on LASSO-selected variables and their coefficients can be found in Table 2.

Correlations between laboratory parameters and clinical outcomes and predictive variables for ICU admission in organ injuries

When only analyzing patients who suffered organ injuries (n = 97), length of hospital and ICU stay showed moderate positive correlations with ISS (Figure 4A), hemoglobin (Δ), erythrocyte count (Δ), peak platelet count, platelet count (Δ) (Figure 4B), myoglobin (Δ), AST (Δ), and peak CrP (r = 0.505–0.644) (Figure 4C). The strongest positive correlation was again observed between ISS and hospital stay (r = 0.644) and between erythrocyte count (Δ) and ICU stay (r = 0.526). For all reported r-values > 0.3, p-values were <0.01. Again, only negligible to weak correlations were observed between all assessed parameters and number of surgeries.

For admission to ICU (yes/no), LASSO regression analyses selected variables pH (admission) (coefficient = -0.064), leukocyte count (Δ) (coefficient = 0.088), male gender (coefficient = 0.454), K^+ (Δ) (coefficient = 0.502), creatinine (Δ) (coefficient = 0.643), and erythrocyte count (Δ) (coefficient = 0.911), when shrinkage parameter lambda was set to 0.048 (determined *via* cross-validation) (Figure 4D).

The binary logistic regression model predicting ICU admission showed a sensitivity of 92.1% (95% confidence interval [71.1%, 100%]), a specificity of 100% [75.01%, 100.0%], and a total accuracy of 93.5% [76.1%, 100%]. The AUC was 0.941 [0.884, 1.000] (Figure 4E). Thus, prediction by this model was statistically significantly better than random. In the trace plot, it can be seen that other parameters became dominant with smaller values of lambda. For instance, hemoglobin (Δ) was the largest coefficient for lambda values close to zero (Figure 4D).

For length of hospital stay age, for length of ICU stay hemoglobin (Δ), and for number of surgeries erythrocyte count (Δ) were the largest coefficients for lambda values close

TABLE 2 LASSO-selected predictive variables with corresponding coefficients (n = 66).

	Penetrating injuries				Thoracoabdominal injuries				Organ injuries			
	ICU admission (yes/no)	Length of hospital stay	Length of ICU stay	Number of surgeries	ICU admission (yes/no)	Length of hospital stay	Length of ICU stay	Number of surgeries	ICU admission (yes/no)	Length of hospital stay	Length of ICU stay	Number of surgeries
Lambda (shrinkage parameter)	0.027	1.231	0.647	0.150	0.034	0.311	0.329	0.150	0.048	1.497	0.987	0.212
Selected variables (effect size)												
Gender (male)	–	–	–	–	0.478	–	–	–	0.454	–	–	–
Age	–	–	0.052	–	–	–	–	–	–	–	0.080	–
Injury mechanism (self-inflicted)	–	–	–	–	–	–	0.350	–	–	–	0.282	–
ISS	0.479	0.061	0.188	0.109	0.589	0.277	0.410	0.050	–	0.061	–	0.153
Hemoglobin (Δ)	–	–	–	–	–	–	0.003	0.008	–	–	–	
Erythrocyte count (Δ)	0.696	–	–	0.112	0.564	0.015	0.019	0.153	0.911	–	–	0.069
Leukocyte count (Δ)	–	0.123	0.045	–	–	–	–	0.007	0.088	0.017	0.181	0.003
aPTT (Δ)	0.219	–	0.044	–	0.175	0.026	–	–	–	–	–	–
Creatinine (Δ)	–	–	–	–	–	–	–	–	0.643	–	0.201	–
K^+ (Δ)	0.657	–	–	–	0.592	–	0.096	–	0.502	–	–	–
pH (admission)	-0.213	–	-0.106	–	-0.079	-0.056	-0.097	–	-0.064	-0.033	–	–
Lactate (admission)	0.594	–	–	–	0.562	–	–	–	–	–	–	–

10.3389/fimmu.2022.959141

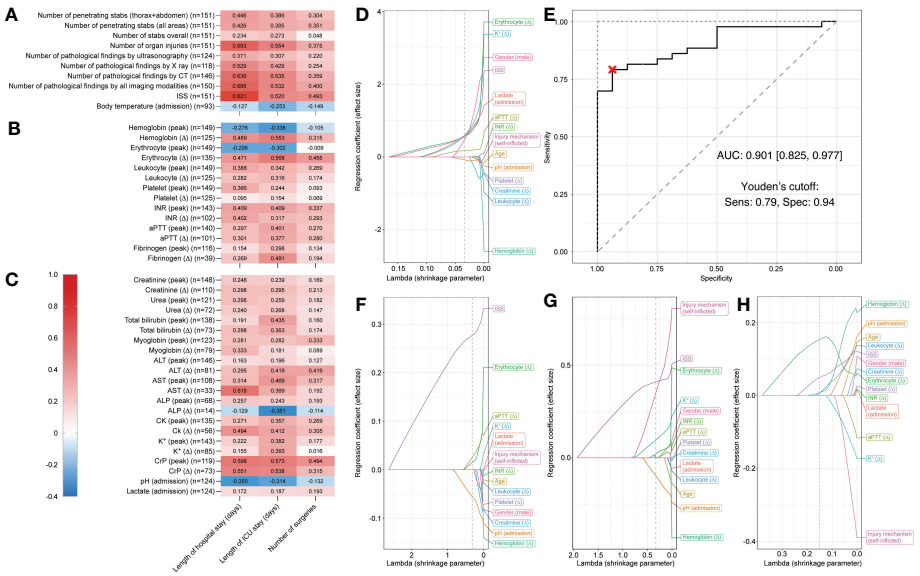

FIGURE 3
Correlation matrix showing Spearman's rank correlation coefficients and Least Absolute Shrinkage and Selection Operator (LASSO) plots showing regression coefficients for patients who suffered thoracoabdominal stab injuries. Correlation strength is indicated by color scale on the left. Correlations between three different outcome parameters (length of hospital stay, length of ICU stay, and number of surgeries) and **(A)** injury specifics, **(B)** routine hematology and coagulation, and **(C)** serum biochemistry and venous blood gas laboratory parameters for penetrating injuries (n = 151). Multivariable LASSO trace plots indicate potentially predictive sets of variables for **(D)** ICU admission (yes/no). **(E)** Receiver operating characteristic (ROC) curve for the LASSO model of ICU admission (yes/no). Youden's cutoff indicates the optimal cutoff based on sensitivity (Sens.) and specificity (Spec). **(F)** Further LASSO trace plots for length of hospital stay, **(G)** length of ICU stay, and **(H)** number surgeries. Grey dotted line displays optimal lambda value calculated *via* cross-validation. AUC, area under the curve.

to zero (Figures 4F–H). Details on LASSO-selected variables and their coefficients can be found in Table 2.

Longitudinal development of daily CrP levels in penetrating, thoracoabdominal, and organ injury cases and in patients admitted to ICU

As a next step, we assessed the longitudinal development of CrP values following stab injuries over time in different patient cohorts.

When assessing all patients (superficial and penetrating injuries combined; patients excluded for correlation and LASSO regression analyses were also excluded here), an increase in CrP levels was observed between admission and day 4. Values then peaked between days 4 and 6 before slowly decreasing again (Figures 5A, B).

When comparing patients with penetrating injuries to those with superficial injuries, CrP levels were significantly higher in the penetrating group on day 3 following admission ($p = 0.005$) (Figure 5C).

Comparing patients with thoracoabdominal injuries to those without, CrP levels were again significantly higher on day 3 following admission ($p = 0.041$) and on the day of discharge ($p = 0.014$) (Figure 5D).

CrP values were also significantly higher on days 2 ($p = 0.046$), 3 ($p < 0.001$), and 4 ($p = 0.003$) following admission, as well as on the day of discharge ($p = 0.001$) in patients with organ injuries compared to those without (Figure 5E).

Finally, in patients admitted to ICU, CrP levels were significantly higher on days 4 ($p = 0.033$) and 5 ($p=0.031$) following admission and on the day of discharge ($p = 0.040$) compared to patients who were not admitted to ICU (Figure 5F).

Longitudinal development of daily laboratory parameters in stab injury patients

To illustrate the longitudinal development of routine laboratory parameters in stab injury patients, we provided an overview for the most relevant parameters, obtained from all patients (superficial and penetrating injuries combined; patients excluded for correlation and LASSO regression analyses were also excluded here).

The longitudinal development of hemoglobin and erythrocyte count over time followed a reversed hockey stick

10.3389/fimmu.2022.959141

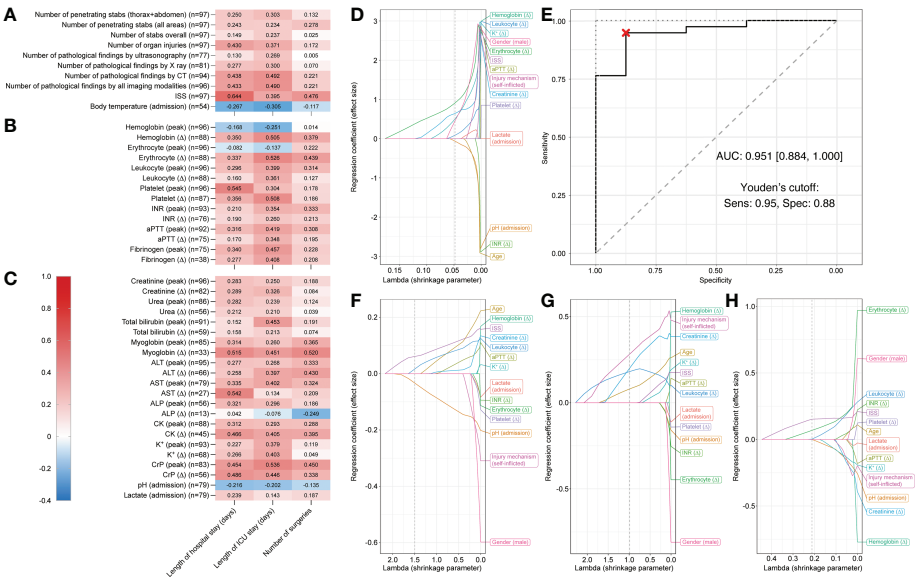

FIGURE 4
Correlation matrix showing Spearman's rank correlation coefficients and Least Absolute Shrinkage and Selection Operator (LASSO) plots showing regression coefficients for patients who suffered organ injuries. Correlations between three different outcome parameters (length of hospital stay, length of ICU stay, and number of surgeries) and **(A)** injury specifics, **(B)** routine hematology and coagulation, and **(C)** serum biochemistry and venous blood gas laboratory parameters for penetrating injuries (n = 97). Multivariable LASSO trace plots indicate potentially predictive sets of variables for **(D)** ICU admission (yes/no). **(E)** Receiver operating characteristic (ROC) curve for the LASSO model of ICU admission (yes/no). Youden's cutoff indicates the optimal cutoff based on sensitivity (Sens.) and specificity (Spec). **(F)** Further LASSO trace plots for length of hospital stay, **(G)** length of ICU stay, and **(H)** number surgeries. Gray dotted line displays optimal lambda value calculated *via* cross-validation. AUC, area under the curve.

pattern, with physiologically high values at admission, followed by a marked decrease on days 1 and 2 and a stable plateau phase until day 21 (Supplementary Figure S1A). Both hemoglobin and erythrocyte count levels were lower on the day of discharge compared to admission.

Leukocyte and platelet counts followed an S-curve over time (Supplementary Figure S1B). Compared to admission, leukocyte levels increased on day 1, then decreased until day 5, and increased again until day 10, before decreasing again until day 21. Platelet levels decreased on day 1 compared to admission but followed a similar pattern to leukocyte counts over time (Supplementary Figure S1B).

Longitudinal development plots for total bilirubin, ALT, AST, creatinine, urea, CK, K^+, hemoglobin, erythrocyte, leukocyte and platelet counts, INR, and aPTT can be found in Supplementary Figures S1C–F.

Discussion

In this retrospective study, annual and seasonal differences in stab injury incidences were assessed at an urban Level I Trauma Center. We further investigated how routine laboratory parameters in stab injury patients correlated with and predicted ICU admission, length of hospital and ICU stay, and number of surgeries performed during admission.

We found that number of organ injuries, the number of acute pathological findings in several imaging modalities, ISS, and Δ values for AST, CK, and CrP correlated moderately to highly with hospitalization length. Only negligible to weak correlations were observed between assessed parameters and number of surgeries. Further, we identified ISS, pH, and lactate at admission, and Δ values for aPPT, K^+, and erythrocyte count as predictors for ICU admission in patients suffering penetrating stab injuries.

ISS and new ISS (NISS) are widely used to predict mortality and morbidity in patients suffering multiple trauma, and both scores correlate with length of hospital stay (24) and can predict ICU admission (25). In this study, we confirmed that ISS may also predict ICU admission and length of hospital stay in patients suffering stab injuries as a higher ISS was associated with longer hospitalization.

The study period in the present study covered more than 20 months during the COVID-19 pandemic (2020/2021), a period that was, to our knowledge, previously not evaluated regarding stab injuries.

Several studies assessed stab injury incidences during the COVID-19 pandemic, and most found a rise in penetrating

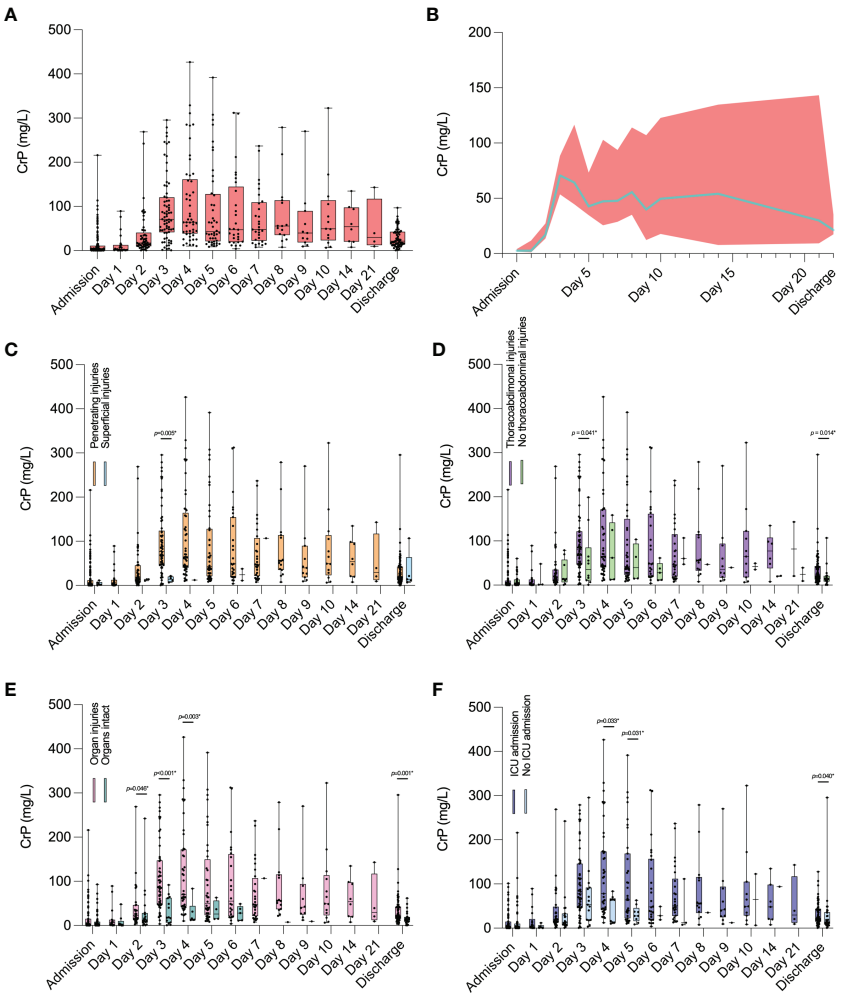

FIGURE 5
Longitudinal development of daily CrP levels in patients who suffered stab injuries. **(A, B)** Values for all patients who suffered stab injuries. **(C)** Comparison of CrP values between penetrating and superficial injuries during hospitalization. **(D)** Comparison of CrP values between patients with and without thoracoabdominal injuries, **(E)** between patients with and without organ injuries, and **(F)** between patients who were admitted to ICU and those who were not. Physiological CrP concentration: <5 mg/l. Data are presented as median box plots with interquartile range and whiskers from minimum to maximum and in **(B)** as median line with 95% confidence intervals displayed as error bands. CrP, C-reactive peptide.

injuries during the first months of 2020 (4–9), but not all (26, 27). Conversely, it was reported that during the first months of the COVID-19 pandemic, crime rates, including assault, decreased globally (28).

We found that stab injuries significantly increased in 2021, i.e., in the later phase of the pandemic and after most COVID-19-related measures had been lifted in Germany. This is congruent with studies demonstrating that several psychological effects occurring after crises (posttraumatic stress disorder, anxiety, fear, and anger) may only be observed with a certain delay (29, 30). A study from Mexico showed that assault and battery numbers decreased in the beginning of the COVID-19 pandemic but increased again when national lockdowns were lifted (31). Congruently, data from the UK showed a return of penetrating injury numbers to pre-pandemic levels, following an initial decline during the first months of the COVID-19 pandemic (27). In line with our findings, observations from natural catastrophes showed a link between length of exposure to natural disasters and increased violence (32, 33), which may explain why significantly more stab injuries were seen during the later phases of the COVID-19 pandemic, in 2021.

We further found that stab injuries occurred less often during winter than during other seasons. This is concordant with data from Ho et al., who reported a positive association between warm weather and penetrating trauma (34). A study from the UK demonstrated that stabbings in young adults mainly occurred

after midnight (35). In accordance, we showed that over 60% of stab injury patients were admitted between 6 p.m. and 6 a.m.

From a clinical and surgical perspective, changes in blood composition are of particular interest in patients suffering penetrating organ injuries. Platelet dysfunction following trauma has previously been linked to increased mortality (36, 37), however, to the best of our knowledge, stab injury-associated thrombocytopenia has not yet been investigated.

In the current study, we found Δ platelet values, which take admission values into account, to be positively correlated with length of ICU stay for patients who suffered organ injuries.

Due to blood loss and dilution following intravenous fluid administration, platelet counts may be reduced in patients suffering stab injuries. In severely injured patients, early administration of platelets is therefore advised, as it was shown to improve hemostasis and reduce mortality (38).

For patients with penetrating and thoracoabdominal injuries, aPTT (Δ) was identified as a predictor for ICU admission. While previous research showed that among other coagulation parameters, aPTT increased significantly during the first hours following trauma (39, 40), we could show that increased aPTT (Δ) values may also predict ICU admission in stab injury patients.

These data underline the importance of monitoring changes in platelet levels and coagulation parameters at and during admission to initiate and adjust early interventions and to avoid prolonged hospitalization.

The acute-phase protein CrP rises in response to trauma and tissue injury. Both penetrating injuries and surgeries disrupt skin barriers and cause an instant and delayed immune response (12). While admission CrP values were generally within the physiological range, we saw that peak CrP values correlated with length of hospital ($r = 0.605$) and ICU stay ($r = 0.558$) in patients suffering penetrating stab injuries. Correlations were similar for Δ values.

In penetrating trauma, prophylactic antibiotic treatment is commonly employed to prevent and treat infectious complications, and strong evidence exists for prophylactic antibiotic treatment for chest wounds that require tube thoracostomy (41).

During the first days of admission, we observed that patients with penetrating stab injuries showed higher CrP values than those without. This also applied to patients with thoracoabdominal injuries, organ injuries, and patients who were admitted to ICU. Similarly, CrP values at discharge were still significantly higher in patients with thoracoabdominal injuries, organ injuries, and ICU admission than in those without.

High CrP concentrations (values higher than 75 mg/l at ICU discharge (42–44) and hospital discharge (45)) were reported as predictors of poor clinical outcomes and increased readmission rates in critically ill patients including multiple trauma, burns, and open heart surgery patients. However, conflicting evidence suggests that CrP values at ICU discharge are unrelated to readmission rates or death (46, 47). Therefore, determining the right time point to discharge a patient requires thorough and repeated clinical assessments in addition to CrP monitoring and must be decided individually.

However, if stab injury patients fall into one of the aforementioned categories (penetrating, thoracoabdominal, organ injuries, or ICU admission), inflammation and sepsis markers including CrP and procalcitonin shall be monitored in addition to the patient's clinical state (48, 49). Further, early admission of prophylactic antibiotics should be considered to potentially reduce hospitalization time.

Tissue damage or hemorrhagic shock commonly cause hyperkalemia in trauma patients (50, 51). Importantly, hyperkalemia is associated with acute kidney injury following severe trauma (52). In our study population, we were able to identify K^+ (Δ) as a predictor of ICU admission in all assessed patient groups (penetrating, thoracoabdominal, and organ injuries).

Hemorrhagic shock and infectious complications can further trigger and exacerbate trauma-related acute kidney injury (53), and elevated CK levels, mainly due to muscle injury, compromise kidney function additionally (54). In line with these findings, we identified creatinine (Δ) as a predictor of ICU admission in patients suffering organ injuries and CK (Δ) correlated with length of hospital stay in patients suffering penetrating stab injuries.

Data from the ongoing UK-based *Activation of Coagulation and Inflammation in Trauma* (ACIT) study showed that trauma-induced acute kidney injury occurred in more than 10% of multiple trauma patients ($n = 1{,}410$) (55). Therefore, monitoring and treating acute kidney injury by avoiding fluid volume deficit, nephrotoxic agents and by facilitating blood pressure support may decrease the risk of complications and mortality (53, 56). Fluid overload, which may worsen acute kidney injury, shall be avoided simultaneously (57, 58).

Prehospital lactate levels were previously shown to predict resuscitative care in trauma patients and may be used to aid triage of normotensive trauma patients (59). High lactate and low pH additionally predicted 72 h mortality in multiple trauma patients (60). Coherently, we identified increased lactate and low pH levels at admission as predictors of ICU admission in penetrating and thoracoabdominal injury patients following stabbing trauma.

Last, we identified Δ values of AST to positively correlate with length of hospital stay in patients with penetrating, thoracoabdominal and organ injuries. Previously, liver transaminase levels were shown to predict liver injury following blunt and penetrating trauma (61, 62).

Our data indicate that even in the absence of organ injuries, monitoring liver and kidney function and adjusting treatment

algorithms early on may help to avoid prolonged hospitalization in stab injury patients.

This study has several limitations. First, this is a retrospective single-center study conducted at an urban Level I Trauma Center, which only allows limited generalization of the findings, especially regarding other geographical regions and countries. These results may also not translate to rural or remote areas where transfers to Level I Trauma Centers commonly cause delayed admissions. These findings should thus be corroborated by further prospective studies from different regions.

Second, the presence of non-medical factors that may have affected ICU admission and discharge could not be taken into consideration in this study (e.g., bed availability due to COVID-19 patients).

Third, due to the observational character of this study, we identified correlations and predictors but can only speculate about causality. Due to the exploratory nature of this study, confounding factors were not included in the analyses and study design.

In summary, we provide solid evidence that routine laboratory parameters have a predictive strength for outcome parameters in patients who suffer stab injuries. Monitoring specific laboratory parameters in stab injury patients may help to identify risk groups and adjust treatment algorithms early on.

Data availability statement

The original contributions presented in the study are included in the article/Supplementary Material. Further inquiries can be directed to the corresponding author.

Ethics statement

The studies involving human participants were reviewed and approved by Ethikkommission Charité – Universitätsmedizin Berlin. Written informed consent from the participants' legal guardian/next of kin was not required to participate in this study in accordance with the national legislation and the institutional requirements.

Author contributions

TM and SM designed and conceived the study. SZ, DZ, TM, FNF, JMP, and JW provided, selected, assembled, analyzed, and interpreted data. Data curation and project administration by DAB, TW, US, and ST. SM provided project supervision and resources. TM drafted the original manuscript. All authors critically reviewed and edited the final manuscript, agreed to be accountable for all aspects of the work and have read and confirmed that they meet ICMJE criteria for authorship.

Acknowledgments

TM is a participant in the BIH Charité Clinician Scientist Program funded by the Charité – Universitätsmedizin Berlin and the Berlin Institute of Health at Charité (BIH).

Conflict of interest

The authors declare that the research was conducted in the absence of any commercial or financial relationships that could be construed as a potential conflict of interest.

Publisher's note

Supplementary material

The Supplementary Material for this article can be found online at: https://www.frontiersin.org/articles/10.3389/fimmu.2022.959141/full#supplementary-material

SUPPLEMENTARY FIGURE S1
Longitudinal development of daily laboratory values in stab injury patients. **(A)** hemoglobin/erythrocyte count, **(B)** leukocyte count/platelet count, **(C)** total bilirubin/ALT/AST, **(D)** creatinine/urea, **(E)** CK/K+, and (F) INR/aPTT. Data are presented as median box plots with interquartile range and whiskers from minimum to maximum. ALT, alanine transaminase; aPTT, activated partial thromboplastin time; AST, aspartate transaminase; CK, creatine kinase; INR, International Normalized Ratio.

References

1. Malik NS, Munoz B, de Courcey C, Imran R, Lee KC, Chernbumroong S, et al. Violence-related knife injuries in a UK city; epidemiology and impact on secondary care resources. *EClinicalMedicine* (2020) 20:100296. doi: 10.1016/j.eclinm.2020.100296

2. Rikken QGH, Chadid A, Peters J, Geeraedts LMG, Giannakopoulos GF, Tan ECTH. Epidemiology of penetrating injury in an urban versus rural level 1 trauma center in the Netherlands. *Hong Kong J Emergency Med* (2020) 29 (1):38–45. doi: 10.1177/1024907920904190

3. Bieler D, Kollig E, Hackenberg L, Rathjen JH, Lefering R, Franke A, et al. Penetrating injuries in Germany - epidemiology, management and outcome an analysis based on the TraumaRegister DGU(R). *Scand J Trauma Resusc Emerg Med* (2021) 29(1):80. doi: 10.1186/s13049-021-00895-1

4. Bäckström D, Wladis A. A cohort study of trauma patients in Sweden during the first months of the COVID-19 pandemic: a small reduction in trauma admissions. *Scand J Trauma Resusc Emergency Med* (2022) 30(1):12. doi: 10.1186/s13049-022-01001-9

5. Sotiropoulou M, Vailas M, Kapiris S. COVID-19 and impact on trauma injuries. a janus facing in opposite directions? *Injury* (2021) 53(7):2671–2. doi: 10.1016/j.injury.2021.02.069

6. Chodos M, Sarani B, Sparks A, Bruns B, Gupta S, Michetti CP, et al. Impact of COVID-19 pandemic on injury prevalence and pattern in the Washington, DC metropolitan region: a multicenter study by the American college of surgeons committee on trauma, Washington, DC. *Trauma Surg Acute Care Open* (2021) 6 (1):e000659. doi: 10.1136/tsaco-2020-000659

7. Ratnasekera AM, Seng SS, Jacovides CL, Kolb R, Hanlon A, Stawicki SP, et al. Rising incidence of interpersonal violence in Pennsylvania during COVID-19 stay-at home order. *Surgery* (2022) 171(2):533–40. doi: 10.1016/j.surg.2021.06.024

8. Ghafil C, Matsushima K, Ding L, Henry R, Inaba K. Trends in trauma admissions during the COVID-19 pandemic in Los Angeles county, California. *JAMA Netw Open* (2021) 4(2):e211320. doi: 10.1001/jamanetworkopen.2021.1320

9. Pelzl CE, Salottolo K, Banton K, Madayag RM, Hamilton D, Duane TM, et al. COVID-19 and trauma: how social distancing orders altered the patient population using trauma services during the 2020 pandemic. *Trauma Surg Acute Care Open* (2021) 6(1):e000645. doi: 10.1136/tsaco-2020-000645

10. Hanna K, Asmar S, Ditillo M, Chehab M, Khurrum M, Bible L, et al. Readmission with major abdominal complications after penetrating abdominal trauma. *J Surg Res* (2021) 257:69–78. doi: 10.1016/j.jss.2020.07.060

11. Zhang Q, Raoof M, Chen Y, Sumi Y, Sursal T, Junger W, et al. Circulating mitochondrial DAMPs cause inflammatory responses to injury. *Nature* (2010) 464 (7285):104–7. doi: 10.1038/nature08780

12. Huber-Lang M, Lambris JD, Ward PA. Innate immune responses to trauma. *Nat Immunol* (2018) 19(4):327–41. doi: 10.1038/s41590-018-0064-8

13. Lord JM, Midwinter MJ, Chen YF, Belli A, Brohi K, Kovacs EJ, et al. The systemic immune response to trauma: an overview of pathophysiology and treatment. *Lancet* (2014) 384(9952):1455–65. doi: 10.1016/S0140-6736(14)60687-5

14. Gearing RE, Mian IA, Barber J, Ickowicz A. A methodology for conducting retrospective chart review research in child and adolescent psychiatry. *J Can Acad Child Adolesc Psychiatry* (2006) 15(3):126–34.

15. Hagebusch P, Faul P, Naujoks F, Klug A, Hoffmann R, Schweigkofler U. Trauma-team-activation in Germany: how do emergency service professionals use the activation due to trauma mechanism? results from a nationwide survey. *Eur J Trauma Emerg Surg* (2022) 48:393–9. doi: 10.1007/s00068-020-01425-x

16. Pham HP, Shaz BH. Update on massive transfusion. *Br J Anaesth.* (2013) 111 Suppl 1:i71–82. doi: 10.1093/bja/aet376

17. VanDerHeyden N, Cox TB. CHAPTER 6 - TRAUMA SCORING. In: Asensio JA, Trunkey DD, editors. *Current therapy of trauma and surgical critical care*. Philadelphia: Mosby (2008). p. 26–32.

18. Brown M, Nassoiy S, Plackett T, Luchette F, Posluszny JJr. Red blood cell distribution width and outcome in trauma patients. *J Osteopath Med* (2021) 121 (2):221–8. doi: 10.1515/jom-2020-0089

19. Mukaka MM. Statistics corner: A guide to appropriate use of correlation coefficient in medical research. *Malawi Med J* (2012) 24(3):69–71.

20. Heinze G, Dunkler D. Five myths about variable selection. *Transpl Int* (2017) 30(1):6–10. doi: 10.1111/tri.12895

21. Tibshirani R. Regression shrinkage and selection *Via* the lasso. *J R Stat Society: Ser B (Methodological).* (1996) 58(1):267–88. doi: 10.1111/j.2517-6161.1996.tb02080.x

22. Heinze G, Wallisch C, Dunkler D. Variable selection - a review and recommendations for the practicing statistician. *Biom J* (2018) 60(3):431–49. doi: 10.1002/bimj.201700067

23. Friedman J, Hastie T, Tibshirani R. Regularization paths for generalized linear models *via* coordinate descent. *J Stat Software* (2010) 33(1):1–22. doi: 10.18637/jss.v033.i01

24. Salehi O, Tabibzadeh Dezfuli SA, Namazi SS, Dehghan Khalili M, Saeedi M. A new injury severity score for predicting the length of hospital stay in multiple trauma patients. *Trauma Mon* (2016) 21(1):e20349. doi: 10.5812/traumamon.20349

25. Lavoie A, Moore L, LeSage N, Liberman M, Sampalis JS. The injury severity score or the new injury severity score for predicting intensive care unit admission and hospital length of stay? *Injury* (2005) 36(4):477–83. doi: 10.1016/j.injury.2004.09.039

26. Pino EC, Gebo E, Dugan E, Jay J. Trends in violent penetrating injuries during the first year of the COVID-19 pandemic. *JAMA Netw Open* (2022) 5(2): e2145708. doi: 10.1001/jamanetworkopen.2021.45708

27. Hickland MM, Massouh P, Sutthakorn RE, Greenslade C, Jennings C, Cantle F, et al. The impact of the COVID-19 pandemic on the number of presentations of penetrating injuries to a UK major trauma centre. *J Public Health (Oxf).* (2022) 44(1):e126–e32. doi: 10.1093/pubmed/fdab333

28. Nivette AE, Zahnow R, Aguilar R, Ahven A, Amram S, Ariel B, et al. A global analysis of the impact of COVID-19 stay-at-home restrictions on crime. *Nat Hum Behav* (2021) 5(7):868–77. doi: 10.1038/s41562-021-01139-z

29. Liao Z, Zhang X, Wang Y, Wang T, Li X, Zhao M, et al. Delayed-onset PTSD and coping strategies of Chinese college students during the COVID-19 pandemic. *Front Sociol* (2021) 6:734738. doi: 10.3389/fsoc.2021.734738

30. Gan Y, Ma J, Wu J, Chen Y, Zhu H, Hall BJ. Immediate and delayed psychological effects of province-wide lockdown and personal quarantine during the COVID-19 outbreak in China. *Psychol Med* (2020), 1–12. doi: 10.1017/S0033291720003116

31. Balmori de la Miyar JR, Hoehn-Velasco L, Silverio-Murillo A. The U-shaped crime recovery during COVID-19: evidence from national crime rates in Mexico. *Crime Sci* (2021) 10(1):14. doi: 10.1186/s40163-021-00147-8

32. Gearhart S, Perez-Patron M, Hammond TA, Goldberg DW, Klein A, Horney JA. The impact of natural disasters on domestic violence: An analysis of reports of simple assault in Florida (1999–2007). *Violence Gender* (2018) 5(2):87–92. doi: 10.1089/vio.2017.0077

33. Thurston AM, Stockl H, Ranganathan M. Natural hazards, disasters and violence against women and girls: a global mixed-methods systematic review. *BMJ Glob Health* (2021) 6(4):e004377. doi: 10.1136/bmjgh-2020-004377

34. Ho VP, Towe CW, Chan J, Barie PS. How's the weather? relationship between weather and trauma admissions at a level I trauma center. *World J Surg* (2015) 39(4):934–9. doi: 10.1007/s00268-014-2881-8

35. Vulliamy P, Faulkner M, Kirkwood G, West A, O'Neill B, Griffiths MP, et al. Temporal and geographic patterns of stab injuries in young people: a retrospective cohort study from a UK major trauma centre. *BMJ Open* (2018) 8(10):e023114. doi: 10.1136/bmjopen-2018-023114

36. Kutcher ME, Redick BJ, McCreery RC, Crane IM, Greenberg MD, Cachola LM, et al. Characterization of platelet dysfunction after trauma. *J Trauma acute Care surg* (2012) 73(1):13–9. doi: 10.1097/TA.0b013e318256deab

37. Jacoby RC, Owings JT, Holmes J, Battistella FD, Gosselin RC, Paglieroni TG. Platelet activation and function after trauma. *J Trauma.* (2001) 51(4):639–47. doi: 10.1097/00005373-200110000-00003

38. Cardenas JC, Zhang X, Fox EE, Cotton BA, Hess JR, Schreiber MA, et al. Platelet transfusions improve hemostasis and survival in a substudy of the prospective, randomized PROPPR trial. *Blood Adv* (2018) 2(14):1696–704. doi: 10.1182/bloodadvances.2018017699

39. Yang Z, Simovic MO, Liu B, Burgess MB, Cap AP, DalleLucca JJ, et al. Indices of complement activation and coagulation changes in trauma patients. *Trauma Surg Acute Care Open* (2022) 7(1):e000927. doi: 10.1136/tsaco-2022-000927

40. Raffee LA, Oteir AO, Alawneh KZ, Alustath AMI. Relationship between initial arterial blood gases and coagulation profiles - analyzing the prognosis and outcomes in patients with multiple Injuries/Trauma. *Open Access Emerg Med* (2020) 12:87–92. doi: 10.2147/OAEM.S244941

41. Kamarova M, Kendall R. 13 prophylactic antibiotics for penetrating injury: a review of practice at a major trauma centre, literature review and recommendations. *Emergency Med J* (2017) 34(12):A869. doi: 10.1136/emermed-2017-207308.13

42. Ho KM, Lee KY, Dobb GJ, Webb SA. C-reactive protein concentration as a predictor of in-hospital mortality after ICU discharge: a prospective cohort study. *Intensive Care Med* (2008) 34(3):481–7. doi: 10.1007/s00134-007-0928-0

43. Kaben A, Correa F, Reinhart K, Settmacher U, Gummert J, Kalff R, et al. Readmission to a surgical intensive care unit: incidence, outcome and risk factors. *Crit Care* (2008) 12(5):R123. doi: 10.1186/cc7023

44. Gulcher SS, Bruins NA, Kingma WP, Boerma EC. Elevated c-reactive protein levels at ICU discharge as a predictor of ICU outcome: a retrospective cohort study. *Ann Intensive Care* (2016) 6(1):5. doi: 10.1186/s13613-016-0105-0

45. Dupre A, Gagniere J, Samba H, Rivoire M, Slim K. CRP predicts safe patient discharge after colorectal surgery. *Ann Surg* (2018) 267(2):e33. doi: 10.1097/SLA.0000000000001983

46. Silvestre J, Coelho L, Povoa P. Should c-reactive protein concentration at ICU discharge be used as a prognostic marker? *BMC Anesthesiol* (2010) 10:17. doi: 10.1186/1471-2253-10-17

47. Al-Subaie N, Reynolds T, Myers A, Sunderland R, Rhodes A, Grounds RM, et al. C-reactive protein as a predictor of outcome after discharge from the intensive care: a prospective observational study. *Br J Anaesth.* (2010) 105(3):318–25. doi: 10.1093/bja/aeq171

48. Simon L, Gauvin F, Amre DK, Saint-Louis P, Lacroix J. Serum procalcitonin and c-reactive protein levels as markers of bacterial infection: a systematic review and meta-analysis. *Clin Infect Dis* (2004) 39(2):206–17. doi: 10.1086/421997

49. Nuutila J, Hohenthal U, Oksi J, Jalava-Karvinen P. Rapid detection of bacterial infection using a novel single-tube, four-colour flow cytometric method: Comparison with PCT and CRP. *EBioMedicine* (2021) 74:103724. doi: 10.1016/j.ebiom.2021.103724

50. Ookuma T, Miyasho K, Kashitani N, Beika N, Ishibashi N, Yamashita T, et al. The clinical relevance of plasma potassium abnormalities on admission in trauma patients: a retrospective observational study. *J Intensive Care* (2015) 3 (1):37. doi: 10.1186/s40560-015-0103-6

51. Perkins RM, Aboudara MC, Abbott KC, Holcomb JB. Resuscitative hyperkalemia in noncrush trauma: a prospective, observational study. *Clin J Am Soc Nephrol.* (2007) 2(2):313–9. doi: 10.2215/CJN.03070906

52. Stewart IJ, Snow BD, Clemens MS, Sosnov JA, Ross JD, Howard JT, et al. Hyperkalemia in combat casualties: Implications for delayed evacuation. *Mil Med* (2017) 182(11):e2046-e51. doi: 10.7205/MILMED-D-17-00119

53. Messerer DAC, Halbgebauer R, Nilsson B, Pavenstadt H, Radermacher P, Huber-Lang M. Immunopathophysiology of trauma-related acute kidney injury. *Nat Rev Nephrol.* (2021) 17(2):91–111. doi: 10.1038/s41581-020-00344-9

54. Assanangkornchai N, Akaraborworn O, Kongkamol C, Kaewsaengrueang K. Characteristics of creatine kinase elevation in trauma patients and predictors of acute kidney injury. *J Acute Med* (2017) 7(2):54–60. doi: 10.6705/j.jacme.2017.0702.002

55. Perkins ZB, Captur G, Bird R, Gleeson L, Singer B, O'Brien B. Trauma induced acute kidney injury. *PloS One* (2019) 14(1):e0211001. doi: 10.1371/journal.pone.0211001

56. Mohsenin V. Practical approach to detection and management of acute kidney injury in critically ill patient. *J Intensive Care* (2017) 5:57. doi: 10.1186/s40560-017-0251-y

57. Alobaidi R, Morgan C, Basu RK, Stenson E, Featherstone R, Majumdar SR, et al. Association between fluid balance and outcomes in critically ill children: A systematic review and meta-analysis. *JAMA Pediatr* (2018) 172(3):257–68. doi: 10.1001/jamapediatrics.2017.4540

58. Payen D, de Pont AC, Sakr Y, Spies C, Reinhart K, Vincent JL, et al. A positive fluid balance is associated with a worse outcome in patients with acute renal failure. *Crit Care* (2008) 12(3):R74. doi: 10.1186/cc6916

59. St John AE, McCoy AM, Moyes AG, Guyette FX, Bulger EM, Sayre MR. Prehospital lactate predicts need for resuscitative care in non-hypotensive trauma patients. *West J Emerg Med* (2018) 19(2):224–31. doi: 10.5811/westjem.2017.10.34674

60. Qi J, Bao L, Yang P, Chen D. Comparison of base excess, lactate and pH predicting 72-h mortality of multiple trauma. *BMC Emerg Med* (2021) 21(1):80. doi: 10.1186/s12873-021-00465-9

61. Bilgic I, Gelecek S, Akgun AE, Ozmen MM. Predictive value of liver transaminases levels in abdominal trauma. *Am J Emerg Med* (2014) 32(7):705–8. doi: 10.1016/j.ajem.2014.03.052

62. Tian Z, Liu H, Su X, Fang Z, Dong Z, Yu C, et al. Role of elevated liver transaminase levels in the diagnosis of liver injury after blunt abdominal trauma. *Exp Ther Med* (2012) 4(2):255–60. doi: 10.3892/etm.2012.575

Frontiers in Immunology

Explores novel approaches and diagnoses to treat immune disorders.

The official journal of the International Union of Immunological Societies (IUIS) and the most cited in its field, leading the way for research across basic, translational and clinical immunology.

Discover the latest Research Topics

See more →

Frontiers

Avenue du Tribunal-Fédéral 34
1005 Lausanne, Switzerland
frontiersin.org

Contact us

+41 (0)21 510 17 00
frontiersin.org/about/contact